THEORETICAL INVESTIGATIONS OF POLYHEDRAL INORGANIC MOLECULES

BODLEIAN LIBRARY OXFORD
DEPOSITED
THESIS
12.1.87.

by

Roy Luigi Johnston

Thesis submitted in part fulfilment of

the requirements for the degree of

Doctor of Philosophy

at the

University of Oxford

St. Catherine's College,

Oxford

July 1986

To my parents

THEORETICAL INVESTIGATIONS OF POLYHEDRAL INORGANIC MOLECULES

Roy L. Johnston **St. Catherine's College**

Doctor of Philosophy **Trinity Term 1986**

ABSTRACT

This Thesis describes some theoretical studies on cluster compounds of the main group and transition metal elements.

Chapter 1 presents a review of the theoretical aspects of cluster chemistry. Three major theoretical approaches are identified, namely the localised, delocalised and free electron models and their historical development is described.

The research described in this Thesis is based on extensions of Stone's Tensor Surface Harmonic (TSH) methodology, supported by Extended Huckel molecular orbital calculations. In **Chapter 2**, the TSH approach is used to describe the skeletal bonding in 3- and 4-connected polyhedral clusters. Like the deltahedral clusters, 4-connected molecules are generally characterised by (n+1) Skeletal Electron Pairs (SEP's). 3-connected clusters, however, possess 3n/2 SEP's. This difference is attributed to the occurrence of additional non-bonding orbitals in the 3-connected case.

In **Chapter 3**, the bonding in a novel class of deltahedral metallaborane clusters is discussed. These hyper-closo or iso-closo species are studied from a fragment orbital viewpoint, regarding the structures as metal-capped fragments of a borane icosahedron. In this way, the problem of whether these clusters possess n or (n+1) SEP's is studied for n=9, 10 and 11.

Although most deltahedral clusters conform to the (n+1) SEP rule, there are a significant number which do not. In **Chapter 4**, these deviations are rationalised from a group theoretical/topological viewpoint. A group theoretical paradigm is developed which simplifies the derivation of the frontier orbitals for these molecules.

Chapter 5 extends the TSH methodology to clusters with bispherical topologies. To discuss these clusters, the TSH wavefunctions are modified to include radial, as well as angular nodes. The methodology is also applied to clusters with toroidal topologies, where the capping atoms form a ring around the equator of the inner cluster sphere.

The bonding in π-donor- and π-acceptor-bridged clusters of the transition metals are compared in **Chapter 6.** Although the symmetry aspects are identical and lead to similar bonding patterns, the π-donor clusters are characterised by a number of unoccupied d^{δ}-based orbitals. The bonding in a series of closo, nido and arachno π-donor clusters, based on edge- and face-bridged octahedral molecules is considered and a relationship between the cluster electron count and the number of unavailable d^{δ}-based orbitals is identified.

The work described in this Thesis was carried out in the Inorganic Chemistry Laboratory, Oxford, from October 1983 to July 1986, under the supervision of Dr. D. Michael P. Mingos. All the work is my own, unless stated to the contrary, and it has not previously been submitted for any degree at this or any other University.

Signature removed from this digital version of the thesis

Roy L. Johnston

ACKNOWLEDGEMENTS

I wish to gratefully acknowledge my supervisor, Dr. Mike Mingos, for his constant help, advice and encouragement throughout the past three years.

I would like to thank my fellow theoreticians, in particular David Evans, David Cox, David Gilmour, Jeremy (David?) Hawes and Kevin Hack, for many stimulating discussions on aspects of theoretical cluster chemistry (i.e. reconstructions at the K.A.). I am especially grateful to David Evans for his help, friendship and catch-phrases.

I am grateful to all those members of the Mingos group, past and present, who have made the lab such an enjoyable place to work in. I would particularly like to acknowledge the following "characters": Mike Luke (for his sparkling wit and repartee), Robert Wardle, Kevin Hall, Zenon (F.K.W.)^3 Demidowicz, Malcolm Hallam, Osayi, all the Part II's and the above mentioned theoreticians.

My deepest thanks are extended to Darren and Susan Sherman for the friendship and encouragement that they have shown me over the years.

Finally, I would like to gratefully acknowledge the patience and diligence (above and beyond the call of duty) of my proof readers, Graham Stringer and Mike (Oz) Watson, who have just about managed to remain sane (I think). In particular, my sincere thanks are extended to Oz for a great deal of help with the production of this Thesis.

ABBREVIATIONS

L	two electron ligand
R	alkyl
Me	methyl
Et	ethyl
Pr^i	iso-propyl
Bu^n	n-butyl
Bu^t	tertiary-butyl
Ph	phenyl
Cp	η^5-C_5H_5
Bz	η^6-C_6H_6
NMR	nuclear magnetic resonance
MO	molecular orbital
hy	hybrid orbital
HOMO	highest occupied molecular orbital
LUMO	lowest unoccupied molecular orbital
SEP	skeletal electron pair
LCAO	linear combination of atomic orbitals
TSH	Tensor Surface Harmonic

CONTENTS

CHAPTER ONE - THEORETICAL MODELS OF CLUSTER BONDING

1.1 Introduction 1

1.2 Localised Cluster Bonding Models 3

1.3 Delocalised Cluster Bonding Models 13

1.4 Free Electron Cluster Bonding Models 45

1.5 Perspective 54

References for Chapter One 59

CHAPTER TWO - GENERAL THEORETICAL ANALYSIS OF THE BONDING IN THREE- AND FOUR-CONNECTED POLYHEDRAL CLUSTERS

2.1 Introduction 73

2.2 Three-Connected Polyhedral Clusters 74

2.2.1 Geometric and electronic features of 3-connected clusters 74

2.2.2 Delocalised treatment of the skeletal bonding in 3-connected clusters 79

2.2.3 Summary 92

2.3 Four-Connected Polyhedral Clusters 94

2.3.1 Geometric features of 4-connected clusters 94

2.3.2 Delocalised treatment of the bonding in 4-connected clusters 96

2.3.3 Summary 104

2.4 Conclusions 106

2.5 Appendix 107

References for Chapter Two 109

CHAPTER THREE - THEORETICAL ANALYSIS OF THE BONDING IN <u>HYPER-CLOSO</u> METALLABORANES AND METALLACARBORANES

3.1 Introduction 113

3.1.1 Metallaborane and metallacarborane clusters 113

3.1.2 Bonding in metallaboranes 114

3.1.3 Anomalies in the borane-metallaborane structural relationship 116

3.2 The <u>Hyper</u>/<u>Iso</u>-<u>Closo</u> Controversy 119

3.2.1 Structural features of <u>hyper</u>-<u>closo</u> metallaboranes 126

3.2.2 The icosahedral fragment approach to <u>hyper</u>-<u>closo</u> structures 127

3.3 Analysis of the Frontier Molecular Orbitals of Borane Fragments Derived from Icosahedral <u>Closo</u>-$[B_{12}H_{12}]^{2-}$ 132

3.4 Ten-Vertex <u>Hyper</u>-<u>Closo</u> Clusters 134

3.4.1 <u>Hyper</u>-<u>closo</u>-$[B_{10}H_{10}]$ 134

3.4.2 <u>Hyper</u>-<u>closo</u>-MB_9 clusters 142

3.5 Nine-Vertex <u>Hyper</u>-<u>Closo</u> Clusters 148

3.5.1 <u>Hyper</u>-<u>closo</u>-$[B_9H_9]$ 148

3.5.2 <u>Hyper</u>-<u>closo</u>-MB_8 clusters 151

3.6 Eleven-Vertex <u>Hyper</u>-<u>Closo</u> Clusters 153

3.6.1 <u>Hyper</u>-<u>closo</u>-$[B_{11}H_{11}]$ 154

3.6.2 <u>Hyper</u>-<u>closo</u>-MB_{10} clusters 156

3.7 Conclusions Concerning the <u>Hyper</u>/<u>Iso</u>-<u>Closo</u> Controversy 160

3.8 Extension to Unusual <u>Nido</u>- and <u>Arachno</u>-Type Geometries 161

3.9 Appendix 164

References for Chapter Three 167

CHAPTER FOUR - A GROUP THEORETICAL PARADIGM FOR RATIONALISING DEPARTURES FROM THE (n+1) SKELETAL ELECTRON PAIR RULE FOR DELTAHEDRAL CLUSTERS

4.1 Introduction 172

4.2 The Four Classes of Deltahedra 173

4.3 The Pairing Principle in Tensor Surface Harmonic Theory 174

4.3.1 Group theoretical aspects of the Pairing Principle 175

4.3.2 Consequences of the Pairing Principle 177

4.3.3 Comments on Fowler's Analysis 180

4.4 Class 1: Centrosymmetric Spherical Deltahedra 186

4.5 Class 2: Polar Deltahedra 187

4.5.1 Sub-class 2(i): C_3-polar deltahedra 188

4.5.2 Sub-class 2(ii): C_2-polar deltahedra 193

4.5.3 Sub-class 2(iii): C_1-polar deltahedra 194

4.6 Class 3: Bipolar deltahedra 196

4.6.1 General topological and group theoretical considerations 196

4.6.2 Sub-class 3(i): D_{nh}-bipyramids 198

4.6.3 Sub-class 3(ii): D_{nd}-bicapped antiprisms 205

4.6.4 Extension to larger bipolar deltahedra 208

4.7 Class 4: Non-Polar Deltahedra 208

4.7.1 Sub-class 4(i): D_{nh}-planar-equatorial deltahedra 209

4.7.1.1 Analysis of the frontier orbital region of tricapped trigonal prismatic clusters 209

4.7.1.2 Consequences of the frontier orbital pattern of tricapped trigonal prismatic clusters 211

4.7.2 Sub-class 4(ii): D_{nd}-puckered-equatorial deltahedra 217

4.7.3 Extension to larger non-polar deltahedra 221

4.8 Summary 222

4.9 Appendix: Symmetry Theorems for Molecular Wavefunctions 229

References for Chapter Four 233

CHAPTER FIVE - APPLICATION OF TENSOR SURFACE HARMONIC THEORY TO THE STUDY OF BONDING IN BISPHERICAL CLUSTER COMPOUNDS

5.1 Introduction 236

5.2 Bispherical Clusters 237

5.3 Topological Features of Bispherical Clusters 238

5.4 Group Theoretical Analysis 243

5.5 Inner Sphere-Outer Sphere Interactions 248

5.6 Bispherical Clusters with Toroidal Topologies 265

5.7 Raft Clusters 270

5.8 Bispherical Clusters with Interstitial Metal Atoms and Cluster Units 272

5.9 Summary 276

References for Chapter Five 279

CHAPTER SIX - π-DONOR-BRIDGED METAL CLUSTERS

6.1 Introduction 282

6.2 Naked Octahedral Metal Clusters 286

6.3 Hydrido-Bridged Octahedral Clusters 289

6.4 π-Donor- and π-Acceptor-Bridged Octahedral Clusters 294

6.4.1 Face-bridged octahedral clusters 295

6.4.2 Edge-bridged octahedral clusters 297

6.4.3 Summary 299

6.5 Nido and Arachno π-Donor-Bridged Clusters 302

6.5.1 The closo, nido, arachno relationship in main group and transition metal carbonyl cluster chemistry 306

6.5.2 Nido and arachno derivatives of the π-donor-face-bridged octahedral clusters 307

6.5.3 Butterfly clusters 314

6.5.4 Nido and arachno derivatives of the π-donor-edge-bridged octahedral clusters 316

6.5.5 Summary 321

6.6 Localised Treatment of the Bonding in Closo, Nido and Arachno π-Donor-Bridged Clusters 321

6.7 π-Donor-Bridged Closo Trigonal Bipyramidal Clusters and their Nido and Arachno Derivatives 324

6.8 Related Systems 326

6.9 Appendix 331

References for Chapter Six 333

APPENDIX I - TENSOR SURFACE HARMONIC THEORY

AI.1 Introduction 339

AI.2 Radial σ-Type Orbitals 340

AI.3 Surface π-Type Orbitals 343

AI.4 Surface δ-Type Orbitals 347

References for Appendix I 348

APPENDIX II - MOLECULAR ORBITAL THEORY AND THE EXTENDED HÜCKEL METHOD

AII.1 Fundamentals of Molecular Orbital Theory 349

AII.2 The Extended Hückel Method 353

AII.3 Description of the Programs used for Performing Extended Hückel Calculations 359

References for Appendix II 361

CHAPTER ONE

THEORETICAL MODELS OF CLUSTER BONDING

1.1 Introduction

The past four decades has seen the development of a major area of chemistry based on polyhedral clusters of the main group and transition metal elements.[1] In the main group area, the foundations were laid with the characterisation of the polyhedral boranes and carboranes,[2] where research was stimulated by the need for alternative rocket fuels.[3] This has been followed by the synthesis of numerous (and at times isoelectronic and isostructural) bare metal cluster cations and anions of bismuth, tin and other B-Group metals.[4] In addition organic chemists have synthesised many polyhedral $(CH)_n$ molecules as part of the development of the alicyclic chemistry of carbon.[5]

In the transition metal field, the unusual catalytic properties of some high nuclearity cluster compounds of rhodium[6] and the belief that transition metal carbonyl clusters[7] could serve as effective models for the chemisorbed state of metal surfaces involved in catalytic processes[8] has led to the study of clusters with up to 55 metal atoms.[9] Cluster compounds of the platinum[10] and coinage metals[11] are generally found to be most stable with ligands (e.g. carbon monoxide, isocyanides and phosphines) which are capable of stabilising low oxidation states. For the earlier transition metals, π-donor ligands such as Cl, S and OR (R = alkyl or aryl group) stabilise clusters with somewhat higher oxidation

states.[12] These clusters have been shown to be of considerable structural interest, forming extended arrays in the solid state,[13] some of which, such as the Chevrel Phases $M_xMo_6S_8$,[14] have been shown to possess unusual magnetic and superconducting properties.[15] The study of molecular sulphido clusters of iron and molybdenum has led to a better understanding of the nature of the active sites in certain electron transfer proteins (such as the ferredoxins) and enzymes (such as nitrogenase).[16]

The characterisation of this wide range of cluster compounds represents a tribute to the power of modern spectroscopic[17] and X-ray crystallographic techniques.[18] These have provided a wealth of spectroscopic and structural data for the theoretical chemist to try and rationalise. Despite the great structural variety exhibited by cluster compounds, patterns have been recognised, which have prompted the development of generalisations which have been used in an attempt to unify the field.

From the earliest days of cluster chemistry, theoretical descriptions of the bonding in polyhedral clusters of the main group and transition metal elements have been divisible into three main types:

(i) Localised Bonding Treatments, where edge (2-centre-2-electron) or face (3-centre-2-electron) localised bonds are invoked to describe bonding in the cluster skeleton. These treatments have their origins in the **Valence Bond** approach developed by Heitler and London[19] and popularised by Pauling.[20]

(ii) Delocalised Bonding Treatments, where the cluster valence electrons occupy **Molecular Orbitals**[21] which are delocalised over the entire cluster framework. These molecular orbitals are often expressed as

linear combinations of orbitals belonging to constituent fragments of the cluster, in order to make the bonding ideas more accessible to chemists.

(iii) Free Electron Treatments, where the cluster electrons are initially free to move over the surface of a sphere which represents the idealised cluster. In this limit the cluster wavefunctions are the solutions of the **Schrödinger Equation** for a particle on a sphere,[22] with energies dependent on their nodal characteristics. Since the cluster atoms define a polyhedron which is not spherical, the orbitals and energies of the real cluster are estimated (from those at the spherical limit) by a perturbation theory analysis[22] which incorporates the actual symmetry of the cluster.

The popularities of these three approaches have waxed and waned as different researchers have espoused the merits of their particular favourites. The characterisation of increasingly complex cluster structures has tested the current bonding theories to the limit and has at times required their substantial revision. The mathematical methodologies of topology, graph theory and group theory have, at one time or another, been incorporated into each of the bonding models, with varying degrees of success.

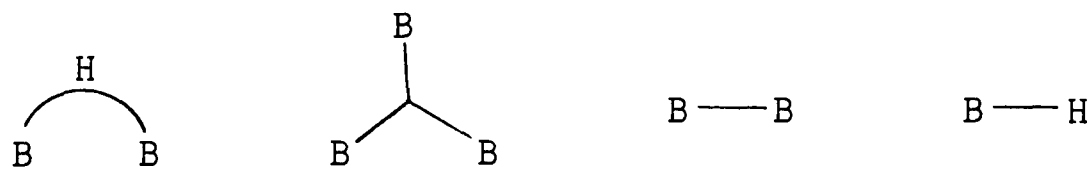
1.2 Localised Cluster Bonding Models

The first clusters to be studied from a localised Valence Bond[19,20] (VB) viewpoint were the boron hydride cage compounds $[B_nH_{n+m}]$ (m = 4 or 6).[2] The VB approach describes bonding in terms of electron pair bonds involving the orbitals of two neighbouring atoms. It was apparent,

however, that the polyhedral boron hydrides were "electron deficient" since they possessed more nearest neighbours (i.e. cluster edges) than bond pairs.[23] In 1949 Longuet-Higgins stated that any localised bonding description of the bonding in such molecules must include 3-centre-2-electron (3c-2e) bonds in addition to the classical 2-centre-2-electron (2c-2e) bonds.[24]

Over the following five years, as more borane clusters were structurally characterised, localised bonding schemes involving 2- and 3-centre bonds (BH, BHB, BB and BBB) were applied to a variety of these molecules by Longuet-Higgins,[25] Duffey[26] and Lipscomb[27]. The **General Valence Orbital** method of Torkington[28] was utilised by Duffey and Lipscomb to generate symmetry adapted hybrid orbitals at each cluster vertex, with the localised orbitals being formed by the interaction of these hybrids. The **Equivalent Orbital** methodology of Lennard-Jones[29] and Pople[30] was also used to transform a basis set of atomic orbitals into a set of edge- or face-localised equivalent orbitals. In this way, the hypothetical tetrahedral species $[B_4H_4]$ was predicted to have 4 bond pairs, residing at the centres of its 4 triangular faces.[26,27]

Lipscomb subsequently developed an elegant topological methodology, involving 2c-2e and 3c-2e bonds, which has proved particularly useful for rationalising the structures of boranes of the type $[B_nH_{n+m}]$. His **styx** formalism[2a] starts from the premise that each boron atom participates in 4 bonds, of the following types:



Description	3c-2e BHB	3c-2e BBB	2c-2e BB	2c-2e BH
Number	**s**	**t**	**y**	**x**

For a general borane $[B_nH_{n+m}]$, possessing n BH units and m <u>endo</u>-terminal or bridging hydrides, the total number (N_T) of bond pairs is:

$$N_T = s + t + y + x = 2n + (m/2)$$

(since each boron atom contributes 3 electrons and each hydrogen atom contributes 1 electron). By enumerating atoms, orbitals and electrons Lipscomb derived the following relationships:[2a]

$$x = m - s \qquad t = n - s \qquad 2y = s - x$$

and assigned each borane cluster a set of <u>styx</u> indices. This method successfully accounted for the geometries and charge distributions in the low symmetry borane cage compounds $[B_nH_{n+m}]$.[2a,31] For the higher symmetry boranes, in particular the deltahedral (i.e. possessing exclusively triangular faces) anions $[B_nH_n]^{2-}$ shown in **Figure 1.1**, the <u>styx</u> formalism led to an unworkable number of resonance forms because the bonding in such clusters can no longer be adequately described within a simple localised framework.[23]

Kettle attempted to circumvent this problem by allowing for overlap between the edge or face-localised cluster bonding orbitals. His **Topological Equivalent Orbital** methodology applied group theoretical labels to cluster orbitals which were constructed as linear combinations of localised orbitals, thereby constituting a compromise between purely localised bonding theories and (delocalised) molecular orbital theory. This analysis was successfully applied to the deltahedral borane anions[32] as well as the more open cage structures.[33]

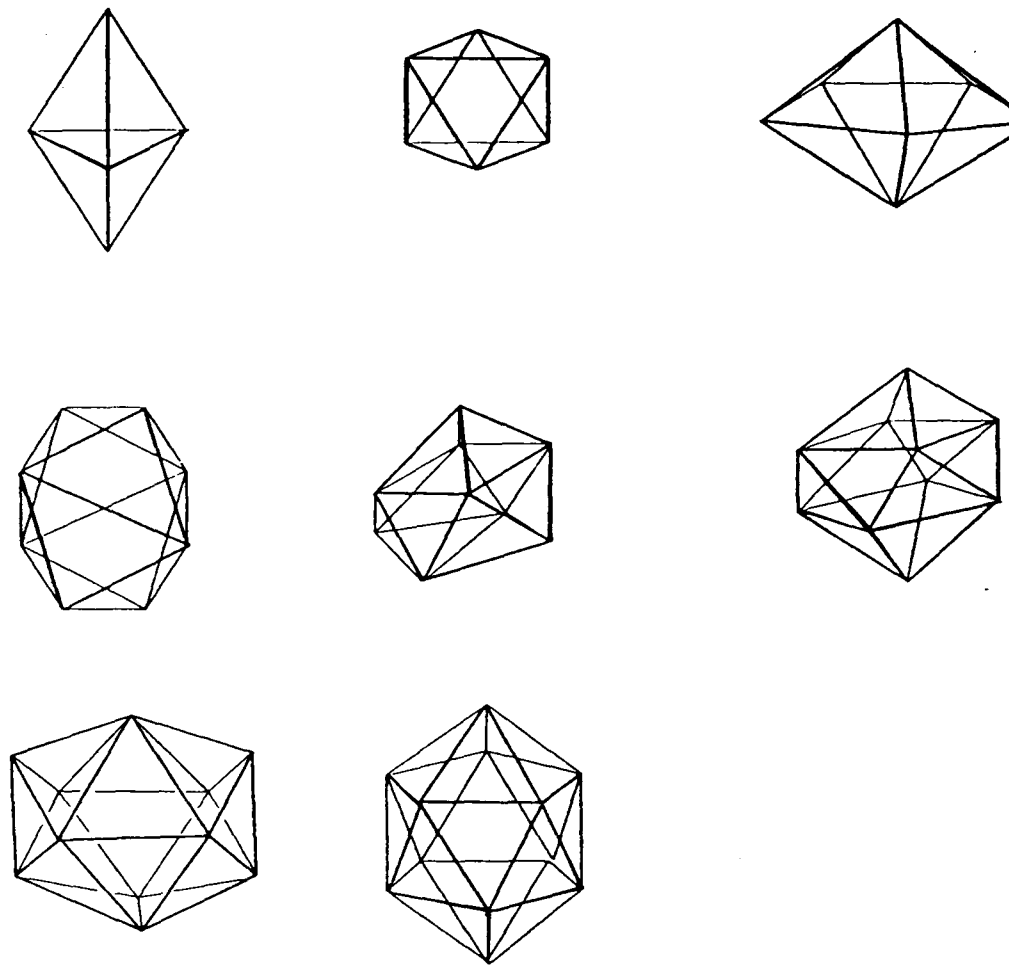


Figure 1.1 Deltahedral geometries adopted by the borane anions $[B_nH_n]^{2-}$.

In the early 1960's the field of transition metal cluster chemistry began to expand rapidly.[34] Some of the first metal clusters to be structurally characterised were the halide bridged clusters of the early transition metals,[12] such as octahedral $[Mo_6Cl_8]^{4+}$ which possesses 8 face-bridging ligands.[35] Sheldon, in a Valence Bond treatment of this cluster, concluded that it possessed 12 discrete 2c-2e bonds, localised along the edges of the metal octahedron.[36] A subsequant qualitative hybrid orbital treatment by Duffey et al. supported this conclusion.[37] Cotton later criticised these Valence Bond treatments on the grounds that they implied the occurrence of significantly bent metal-metal bonds and unrealistically high formal oxidation states for the metal atoms.[34a,38] Kettle subsequently demonstrated that the 12 cluster bonding orbitals of $[Mo_6Cl_8]^{4+}$ (from the Molecular Orbital treatment of Cotton and Haas[38]) are topologically equivalent to symmetry adapted linear combinations of 12 edge-bonding localised orbitals.[39] He also

showed that clusters of the type $[M_6Cl_{12}]^{2+}$ (M = Nb, Ta) (with 12 edge-bridging ligands[40]) possess 8 cluster bonding orbitals[38] which are topologically equivalent to linear combinations of 8 face-bonding (3c-2e) localised orbitals.[39]

Kettle demonstrated that the bonding in small transition metal carbonyl clusters, such as triangular $[M_3(CO)_{12}]$ (M = Fe, Ru, Os) and tetrahedral $[M_4(CO)_{12}]$ (M = Co, Rh, Ir),[7] could also be discussed from a localised viewpoint. He partitioned the cluster valence electrons into those involved in terminal M-CO bonding (including π-back donation from the metal into the vacant π^* orbitals of CO), M-CO (bridging) bonding and those involved in the formation of 2-centre and 3-centre localised metal-metal bonding orbitals.[41] In a study of tetrahedral clusters of the main group and transition metal elements, he noted that the P_4 molecule[42] possesses 6 edge-localised (2c-2e) bonding orbitals.[43] Like $[Mo_6Cl_8]^{4+}$, P_4 is an example of an "electron precise" cluster because there is a one-to-one topological mapping between the edges of the cluster polyhedron and the cluster bond pairs.

The total number of valence electrons in a cluster compound which may be adequately described, in Valence Bond terms, by edge-localised 2c-2e bonds can be calculated on the basis of the **Inert Gas** or **Effective Atomic Number (EAN) Rule**[44] (such that each main group atom in the cluster skeleton has 8 valence electrons and each transition metal atom has 18 valence electrons associated with it). This connection between localised bonding descriptions and the EAN rule can be traced back to the work of Sidgwick[45] and Pauling[20] in the 1930's and '40's. The number of cluster valence electrons (N_e) for "electron precise" main group and transition metal clusters may be calculated from the following

relationships:

main group clusters	$N_e = 8M - 2E$
transition metal clusters	$N_e = 18M - 2E$

where M is the number of atoms in the cluster skeleton and E is the number of edges of the cluster polyhedron.

The EAN rule predicts a valence electron count of 84 for an electron precise octahedral transition metal cluster. It was found, however, that although $[Mo_6Cl_8L_6]^{4+}$ is an 84 electron cluster (including six 2-electron-donating terminal ligands, L), all of the octahedral transition metal carbonyl clusters which had been characterised by the end of the 1960's possess 86 valence electrons (e.g. $[Rh_6(CO)_{16}]^{46}$). Kettle, however, concluded that such clusters are in fact electron deficient, like the isostructural boranes, rather than electron rich as the EAN rule would seem to indicate.[47] Unfortunately, Kettle's Topological Equivalent Orbital treatment of the bonding in $[Rh_6(CO)_{16}]$ suffered from an inability to properly separate metal-metal and metal-carbonyl bonding orbitals so a direct comparison with the bonding in boranes was not possible. As will be shown in the next section, it was the delocalised bonding treatments by Wade and Mingos, based on the earlier anlysis of Longuet-Higgins, which eventually resolved the problem of bonding in electron deficient borane and transition metal carbonyl clusters.

In the past 15 years, the synthesis of a series of 3-connected electron precise hydrocarbon clusters $[C_nH_n]^5$ (see **Figure 1.2** for examples) has renewed interest in localised bonding schemes, since the bonding orbitals in these clusters are topologically equivalent to edge-localised 2c-2e bond pairs in a Valence Bond sense.

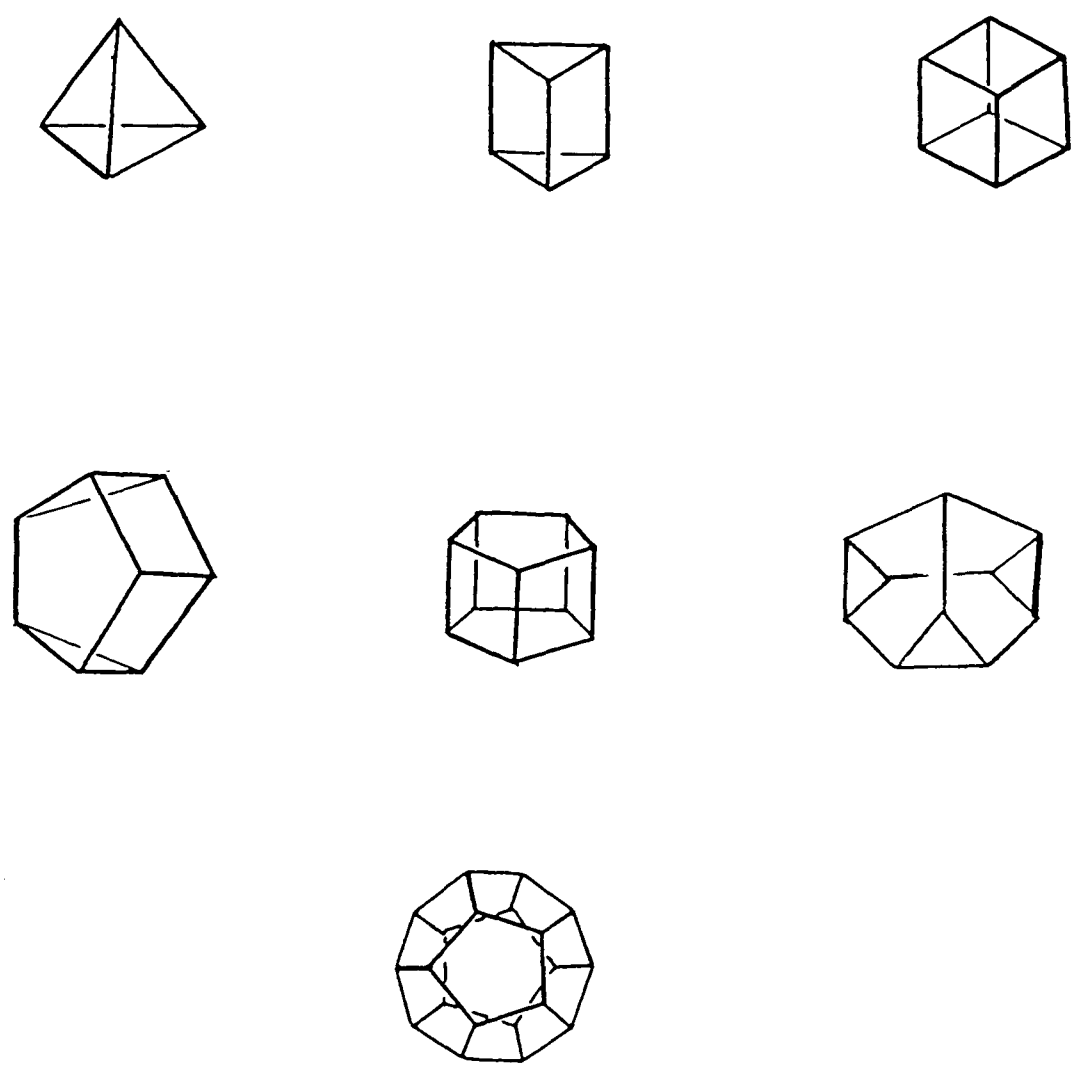


Figure 1.2 3-connected polyhedral geometries adopted by the hydrocarbon clusters $[C_nH_n]$.

Schulman *et al.* performed *ab initio* calculations on cubane $[C_8H_8]$ utilising a basis set of 2c-2e localised C-C and C-H bonding orbitals.[48] The resonance integrals (between localised C-C bonding orbitals) used in these calculations were quite large, thereby giving rise to a wide spectrum of cluster orbitals. Schulman's methodology, which was similar to that employed by Kettle, also included mixing between C-C and C-H bonding orbitals and led to an energy level ordering which was essentially the same as that obtained by delocalised LCAO-MO

treatments.[48] A similar Equivalent Orbital method was applied by Heilbronner et al. to study the bonding in tetrahedrane [C_4H_4].[49]

The formal addition of electron pairs to electron precise clusters generally results in the breaking of cluster bonds (one bond being broken for every electron pair added) with the resulting cluster being termed "electron rich". Mingos showed how this arises from a localised bonding viewpoint, for within such a framework each bond (edge) has associated with it one bonding and one antibonding orbital and the occupation of the latter leads to bond rupture.[50] He gave examples of electron precise (3-connected) and electron rich main group and transition metal clusters and showed how they were related by bond breaking until ultimately ring compounds were obtained. Gillespie subsequently developed this approach, showing that from a Valence Bond standpoint the addition of 2 electrons to a 2c-2e bond results in the cleavage of the bond and the formation of either 2 lone pairs or bonds to 2 additional ligands, as shown in **Figure 1.3.**[51]

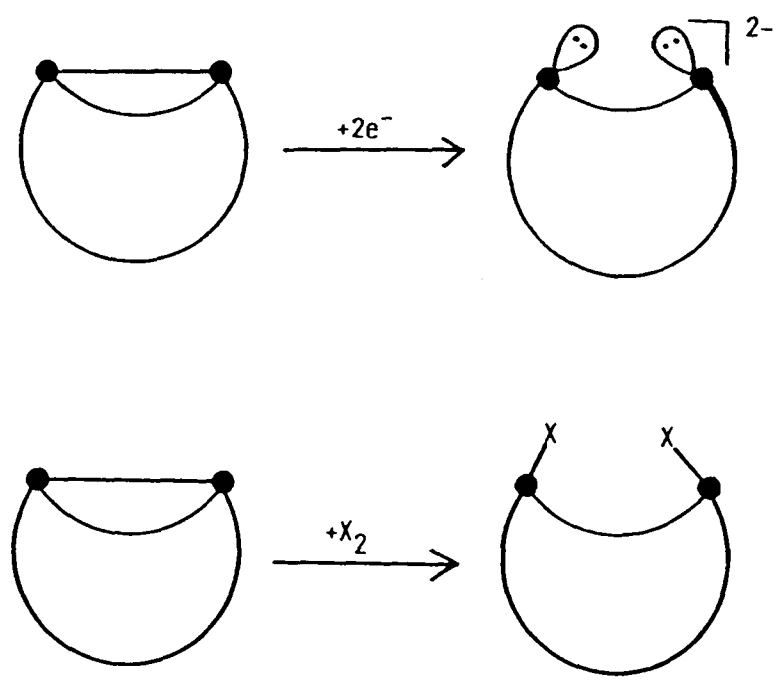


Figure 1.3 Localised view of bond breaking processes.

This methodology was used to rationalise the structures of cluster, cage and ring compounds of the main group elements in terms of electrostatic repulsions between electron pairs (lone pairs and cluster-ligand bond pairs)[51] in an extension of the **Valence Electron Pair Repulsion Theory** developed by Gillespie and Nyholm for main group AB_x molecules.[52] **Figure 1.4** exemplifies these ideas by correlating the structures of some main group 8-atom cage and ring compounds with cuneane [C_8H_8], from which structure they may be derived by cluster bond breaking.

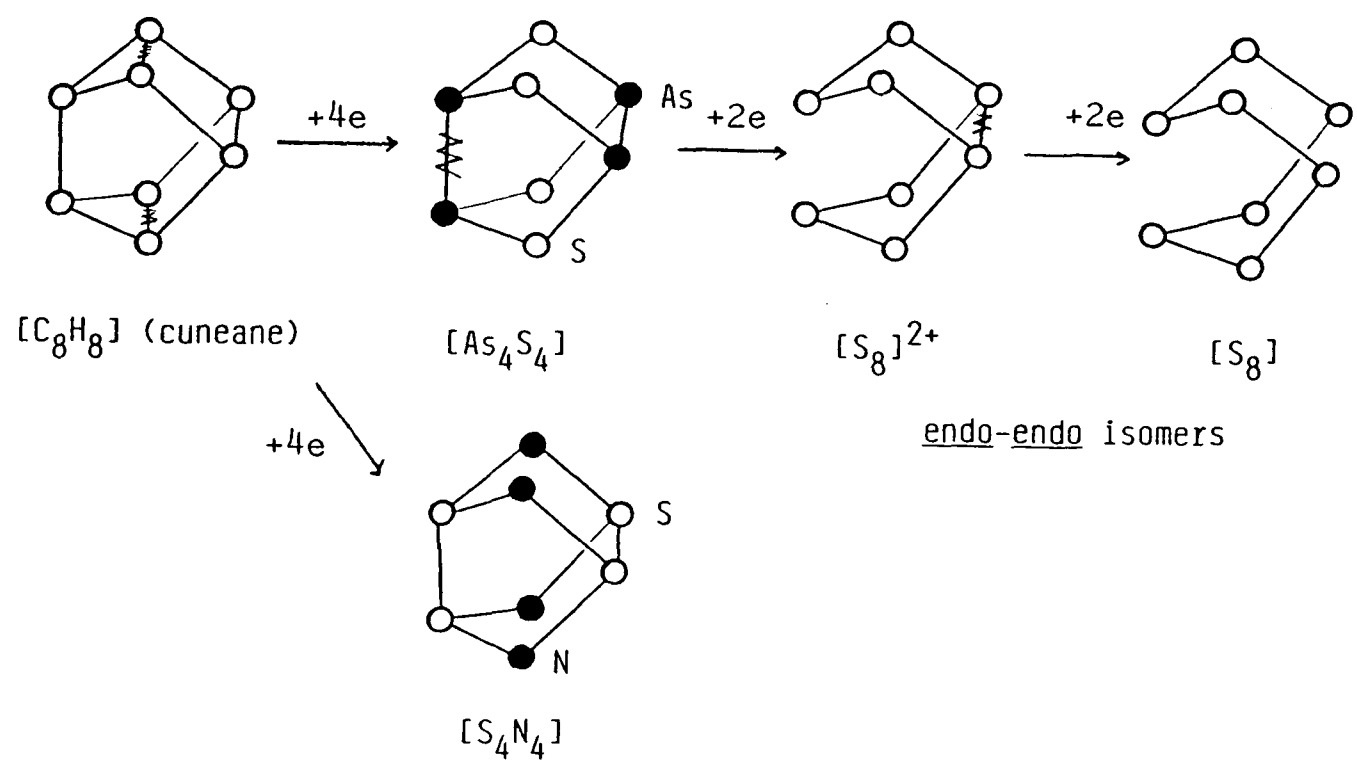


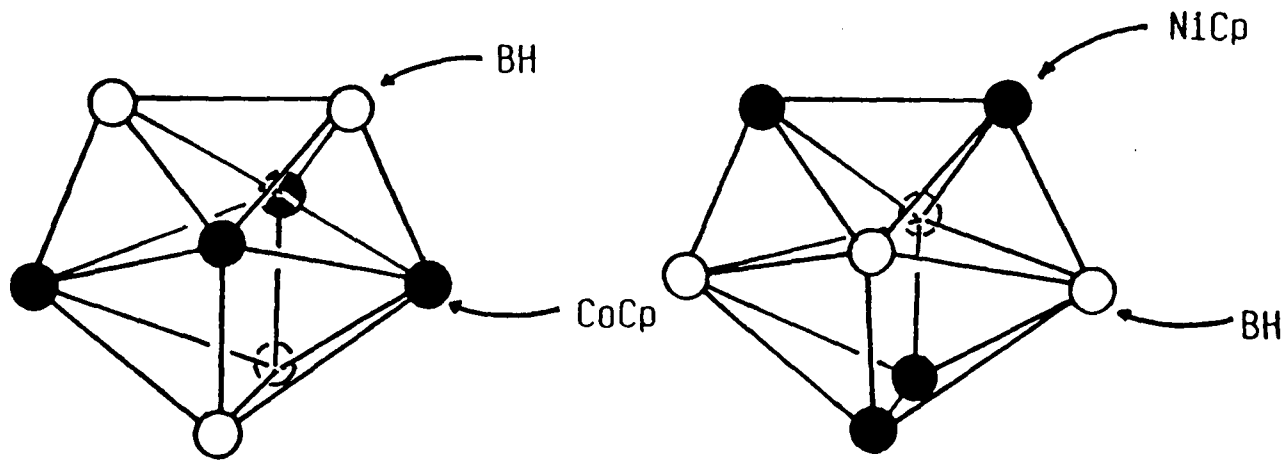
Figure 1.4 Structural correlation of some 8-atom cluster molecules.

Recently, McGlinchey and Tal have developed more topologically based arguments to rationalise and classify the structures adopted by electron rich clusters.[53] Their treatment follows on from the work of

King who, over the past 20 years, has used topology, graph theory and group theory to analyse the bonding in electron deficient, electron precise and electron rich clusters of the main group and transition metal elements[54] as well as coordination compounds.[55] Teo has subsequently proposed a topological electron counting procedure for transition metal clusters.[56] His analysis is performed on the basis of the Effective Atomic Number rule and Euler's theorem (V + F = E + 2), by means of the formula:

$$\text{Number of cluster valence orbitals} = 8V + 2 - F + X$$

where V is the number of cluster vertices, F is the number of faces of the cluster polyhedron and X is the number of "additional" electron pairs required to match the true cluster electron count (thus X=1 for an octahedral metal carbonyl cluster). X reflects the many-centre character of the bonding in cluster compounds and is equal to 0 when the cluster is "electron precise". The method suffers, however, from the empirical way in which X is evaluated. Further recent applications of localised bonding models include studies by King[54c] and Wade[57] (applying Lipscomb's styx methodology) aimed at explaining the different arrangements of metal and boron atoms in the Δ-dodecahedral clusters $[Cp_4Co_4B_4H_4]$ (1)[58] and $[Cp_4Ni_4B_4H_4]$ (2).[59]



$[Cp_4Co_4B_4H_4]$ (1)

$[Cp_4Ni_4B_4H_4]$ (2)

Dahl has performed a series of elegant synthetic and structural studies on transition metal cluster compounds, such as investigating the geometrical consequences of adding and removing electrons.[60] His research has highlighted drawbacks in the localised bonding approach. For example, the formal addition of one electron, on going from $[Co_2Fe(CO)_9S]$ to $[Co_3(CO)_9S]$,[60a,b] leads to an increase of all three metal-metal bond lengths. This indicates the population of an antibonding orbital which is delocalised over the entire triangular cluster, rather than localised between any two metal atoms.[60]

1.3 Delocalised Cluster Bonding Models

The problems associated with the application of localised bonding approaches, described in the previous section, can be conveniently circumvented within the **Molecular Orbital (MO)** framework,[21] where the cluster molecular orbitals ($\Psi_{cluster}$) may be expressed as **linear combinations of atomic orbitals (LCAO's)** (σ_i):[61]

$$\Psi_{cluster} = N \sum_i c_i \sigma_i$$

where N is a normalisation coefficient and c_i is the coefficient of the ith atomic orbital.

The pioneering work of Longuet-Higgins, on the highly symmetrical deltahedral boranes,[62] led to the prediction of icosahedral $[B_{12}H_{12}]^{2-}$ some years before its actual synthesis.[63] He showed that each BH fragment contributes 3 orbitals (one radial sp hybrid and 2 tangential p orbitals) towards the 13 skeletal bonding molecular orbitals of this electron deficient cluster.[63] Lipscomb and Hoffmann performed a series of semi-empirical MO calculations on the polyhedral boranes and

carboranes.[64] They used calculated Mulliken overlap populations[65] and charge distributions to explain bond length and reactivity trends in these "superaromatic" cluster species. Throughout the 1960's Muetterties, Guggenberger and their coworkers used Extended Hückel calculations[64a,66] to evaluate the total energies of borane clusters in order to rationalise their structures in solution and in the solid state.[67] More recently, less empirical (and even ab initio) molecular orbital methods have proved very useful in rationalising the wealth of data arising from experimental investigations of physical properties of specific boranes and carboranes.[68]

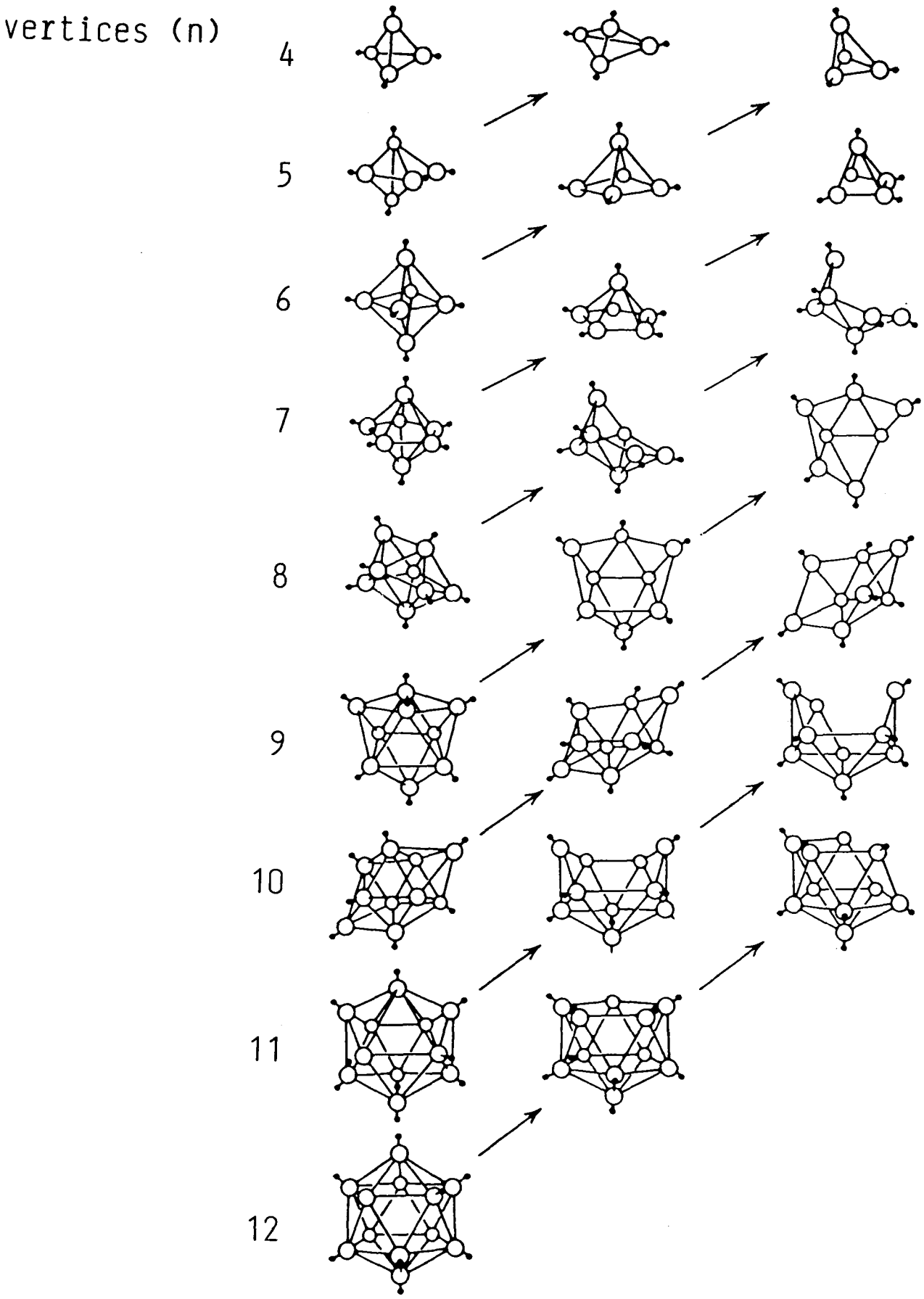
At the beginning of the 1970's, although many molecular orbital calculations had been performed on individual borane and carborane clusters, no generalisations had been made which could allow a theoretical unification of the field. Initially most boranes were thought to adopt stuctures based on fragments of an icosahedron, but it later became apparent, as more borane clusters were structurally characterised, that other deltahedrally based structures were quite common.[69] Williams first elucidated a structural pattern which was based on the recognition of three main structural types.[70] The deltahedral boranes $[B_nH_n]^{2-}$ and carboranes (e.g. $[C_2B_{(n-2)}H_n]$) were given the prefix closo (from the greek for "closed"). The nido (from the greek for "nest-like") structures were defined as being derived from closo clusters by the removal of one (BH) group (i.e. one cluster vertex) and boranes of the type $[B_nH_{n+4}]$ were found to belong to this class of cluster. The arachno (from the greek for "web-like") structures were defined as being derived from closo clusters by the removal of two (BH) cluster vertex units and the boranes $[B_nH_{n+6}]$ were found to belong to

this class.

In a seminal account, Wade exposed the relationship between the structural generalisations of Williams and the number of delocalised (cluster-bonding) **skeletal electron pairs** (SEP's).[71a] He recognised that the (n+1) skeletal electron pairs characteristic of the *closo* boranes $[B_nH_n]^{2-}$ were retained in the *nido* and *arachno* derivatives, $[B_{n-1}H_{(n-1)+4}]$ and $[B_{n-2}H_{(n-2)+6}]$.[71] In *nido* and *arachno* boranes $[B_xH_{x+y}]$ there are x(BH) units and y additional hydrogen atoms which occupy *endo*-terminal or bridging positions around the open face of the cluster. These hydrogen atoms serve to lower the formal negative charge carried by the cluster and to stabilise those cluster molecular orbitals which have large amplitudes around the open face.

Wade pointed out that a convenient way of looking at the *closo*, *nido*, *arachno* pattern is to consider the addition of successive pairs of electrons to an n-atom *closo* cluster with (n+1) SEP's.[71a] This results in an opening out of the structure to yield *nido* and *arachno* structures, characterised by (n+2) and (n+3) SEP's respectively. Rudolph subsequently produced a correlation diagram (reproduced in **Figure 1.5**) which combined the approaches of decapping and electron pair addition.[72]

Wade also recognised the possibility that the bonding pattern observed for *closo*, *nido* and *arachno* boranes may be reproduced by metal carbonyl clusters. He noted that $[H_2Ru_6(CO)_{18}]$ [73] and $[Fe_5C(CO)_{15}]$ [74] constituted a related pair of octahedral (*closo*) and square pyramidal (*nido*) clusters, both possessing 7 skeletal bonding molecular orbitals and that they were, therefore, analogous to $[B_6H_6]^{2-}$ and $[B_5H_9]$.[71a] This conclusion depended on the assumption that each metal tricarbonyl fragment in these clusters (like the BH and CH^+ fragments in boranes and carboranes) contributed 3 orbitals and 2 electrons for skeletal bonding.



Geometry	closo	nido	arachno
No. of SEP's	(n+1)	(n+2)	(n+3)

Figure 1.5 Structure-skeletal electron pair correlation for closo, nido and arachno boranes.

In several subsequent papers Wade[75] and Mingos[50] extended these ideas to electron precise and electron rich clusters and recognised the important bonding similarities between certain main group and transition metal fragments. The term **Polyhedral Skeletal Electron Pair Theory** was introduced by Mason, Thomas and Mingos to cover these theoretical correlations of cluster structure with the number of electrons involved in skeletal bonding.[76] Subsequent Extended Hückel calculations by Evans confirmed the applicability of PSEPT to a wide range of borane cluster geometries.[77]

At about the same time, Braterman rationalised the 86 cluster valence electron count for octahedral metal carbonyl clusters, such as $[Co_6(CO)_{16}]$,[78] $[Ru_6C(CO)_{17}]$ [79] and $[Co_6(CO)_{14}]^{4-}$ [80] in terms of localised M-CO bonds and delocalised skeletal molecular orbitals with predominantly metal d orbital character.[81] Drawing heavily on the molecular orbital calculations of Cotton and Haas, for $[Mo_6Cl_8]^{4+}$ and $[Ta_6Cl_{12}]^{2+}$,[38] he suggested that $[Co_6(CO)_{16}]$, for example, possessed 7 bonding skeletal molecular orbitals derived from the metal d_z2, d_{xz} and d_{yz} orbitals, with all of the linear combinations of the d_{xy} and $d_x2_{-y}2$ orbitals taken to be roughly non-bonding and, therefore, occupied.

Extended Hückel calculations by Mingos, on the octahedral cluster $[Co_6(CO)_{14}]^{4-}$, showed the occurrence of wide bands of orbitals formed from the valence 4s and 4p atomic orbitals on the metal atoms while the 3d-band was calculated to be quite narrow on account of the small 3d-3d overlap integrals.[82] The metal valence s and p orbitals were found to give rise to 11 strongly antibonding cluster molecular orbitals which are "inaccessible" due to their high energies. They are also unsuitable for metal-ligand bonding due to being inwardly hybridised. Mingos

realised that these 11 orbitals have the identical nodal and symmetry properties as the high-lying antibonding orbitals of $[B_6H_6]^{2-}$. The valence electron counts of these two octahedral clusters may be related as shown below:

	$[B_6H_6]^{2-}$	$[Co_6(CO)_{14}]^{4-}$
Valence electron count:	$2 \times \{(4\times6)-11\} = 26$	$2 \times \{(9\times6)-11\} = 86$

(since main group atoms possess 4 valence orbitals and transition metals possess 9 valence orbitals).

Subsequently, Lauher performed Extended Hückel calculations on a wide range of n-atom closo transition metal clusters and confirmed the presence of (2n-1) high-lying "inaccessible" antibonding orbitals, leaving a total of $\{9n - (2n-1)\} = (7n+1)$ occupied cluster valence MO's and an electron count of $(14n+2)$.[83] Lauher's calculations were made on bare metal clusters and the introduction of ligands was considered to constitute only a small perturbation. Calculations on nido and arachno transition metal clusters showed them to be characterised by (14n+4) and (14n+6) valence electrons respectively.[83] The difference in electron count between isostructural (n-atom) main group and transition metal clusters is 10n, corresponding to the occupation of 5 d orbitals per metal atom. These orbitals are either non-bonding (i.e. localised exclusively on the metals) or mix with the s and p orbitals to form inwardly hybridised orbitals which are involved in metal-metal bonding and outwardly hybridised orbitals which are involved in metal-ligand bonding.[50,71]

Wade and Mingos had recognised that the underlying reason for structural similarities between main group and transition metal carbonyl clusters was that the constituent fragments contributed the same number

of electrons and orbitals for cluster bonding and that the orbitals had similar nodal properties.[50,71] Earlier Halpern had noted the electronic equivalence of certain metal fragments and organic groups.[84] Similarities in the reactivity of alkyl radicals and $[Co(CN)_5]^{3-}$, as well as between carbenes and d^8-ML_4 complexes, illustrated this equivalence. Later Dahl drew attention to similarities in the bonding modes of arsenic atoms and conical $Co(CO)_3$ fragments in tetrahedral clusters such as $[As_3Co(CO)_3]$ and $[As_2Co_2(CO)_6]$.[85] Similar features were noted by Ellis.[86] Rudolph rationalised the structures of the hetero-boranes by considering isoelectronic main group fragments.[72] The fact that CH and BH^- are isoelectronic explains why $[C_2B_{(n-2)}H_n]$ and $[B_nH_n]^{2-}$ are isostructural while the icosahedral cluster $[B_{11}H_{11}S]$ [87] is isoelectronic with the isostructural $[B_{12}H_{12}]^{2-}$ molecule, if the sulphur atom is assumed to possess one lone pair instead of a B-H bond pair and 4 electrons in 3 orbitals which are used for cluster bonding, hence making it isoelectronic with BH^{2-}. This approach may be extended to the bare metal (and non-metal) cluster and cage compounds of the post transition elements.[4] As early as 1968, Corbett had pointed out that the trigonal bipyramidal cluster $[Bi_5]^{3+}$ possesses 6 skeletal bond pairs, assuming one lone pair on each bismuth atom[88] (it is therefore isoelectronic with the isostructural $[C_2B_3H_5]$).

Semi-empirical molecular orbital analyses, by Hoffmann and coworkers, of the frontier molecular orbitals of metal carbonyl fragments confirmed that there were definite similarities between the numbers, energies, shapes and nodal characteristics of these orbitals and those of main group fragments EH_n.[89] The term **isolobal** was introduced to describe this relationship[89b] and the **isolobal analogy** has

subsequently been elegantly formulated (for a variety of fragments) by Hoffmann.[90] **Figure 1.6** illustrates the frontier MO's of some isolobal hydrocarbon, CH_n, and ML_m fragments. The isolobal analogy has proved very useful in accounting for structural similarities between main group and transition metal cluster compounds. For example the isolobal nature of CR (R = alkyl or aryl) and conical $Co(CO)_3$ fragments, both presenting 3 orbitals and 3 electrons for cluster bonding, explains the occurrence of a series of tetrahedral clusters $[(Co(CO)_3)_n(CR)_{4-n}]$ (n = 1-4) which all formally possess 6 SEP's.[90] Further examples of isolobal main group and transition metal fragments are given in **Table 1.1** (adapted from Ref. 95).

Figure 1.6 shows that an $M(CO)_3$ fragment has 6 electrons in M-CO (σ) bonding orbitals and 6 electrons in a roughly non-bonding set of metal d orbitals. These orbitals are analogous to the t_{2g} orbitals of the octahedral complex from which the fragment is formally derived (as Wade and Mingos had previously concluded).[90] An alternative expression for the number of valence electrons (N_e) of an n-atom transition metal cluster may, therefore, be written:

$$N_e = 12n + 2S$$

where S is the number of skeletal electron pairs. This equation can then be used to calculate the number of SEP's of a cluster of known formula (and hence known valence electron count).

The semi-empirical arguments upon which the isolobal analogy is based have recently been corroborated by Fehlner and DeKock,[91] who performed LCAO-MO-SCF Fenske-Hall calculations on the nido square pyramidal clusters $[Fe(CO)_3B_4H_8]$,[92] $[CoCpB_4H_8]$ [93] and $[B_5H_9]$. In contrast to an earlier Self Consistent Charge-Extended Hückel study by

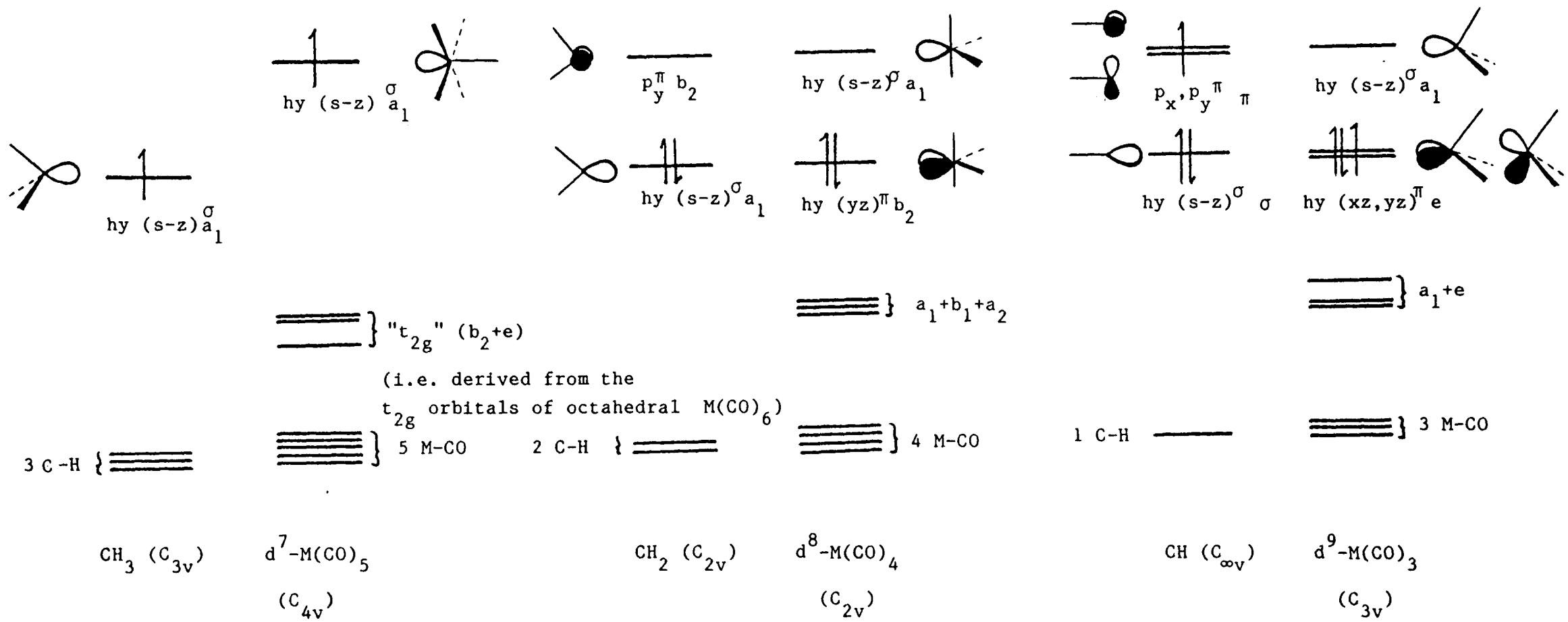


Figure 1.6 Examples of <u>isolobal</u> CH_n and $M(CO)_m$ fragments.

Table 1.1 Examples of isolobal main group and transition metal fragments[a]

CH_3	CH_2	CH
H	S (2 lone pairs)[b]	P, As (1 lone pair)[c]
$M(CO)_5$ (Mn, Tc, Re)	$M(CO)_4$ (Fe, Ru, Os)	$M(CO)_3$ (Co, Rh, Ir)
$Fe(CO)_2Cp$	$Rh(CO)Cp$	$NiCp$
$Mo(CO)_3Cp$	$Re(CO)_2Cp$	$W(CO)_2Cp$
	$Cr(CO)(NO)Cp$	$[Mn(CO)_2Cp]^-$
$Co(CO)_4$	$Cr(CO)_5$	$Re(CO)_4$
$PtH(PR_3)_2$[d]	$Pt(PR_3)_2$[e]	
$ZnCp$	$CuCp$	$RhBz$
$Au(PR_3)$	$IrCl(CO)_2$	$Re(CO)_3Br_2$
$Rh(PR_3)_2(\eta^5\text{-}C_2B_9H_{11})$	$Fe(CO)_2(\eta^5\text{-}C_2B_9H_{11})$	$Mn(CO)_2(\eta^5\text{-}C_2B_9H_{11})$
	$TaMeCp_2$	$TaCl(PR_3)_2Cp$
CH_3^+	CH_2^+	CH^+
BH_3	BH_2, P (2 lone pairs)	BH, Sn (1 lone pair)
$M(CO)_5$ (Cr, Mo, W)	$M(CO)_4$ (Mn, Tc, Re)	$M(CO)_3$ (Fe, Ru, Os)
$Mn(CO)_2Cp$	$Fe(CO)Cp$	MCp (Co, Rh, Ir)

a Isolobal relationships are not one-to-one mappings, so the same metal fragment may (depending on what it is coordinated to) be effectively isolobal with more than one main group fragment. The frontier orbital properties of metal fragments (ML_n) depend critically on the nature of the ligands (L) and the geometry of the fragment. Although metal fragments are generally regarded as being derived from octahedral complexes, other "starting" geometries are possible (e.g. a $d^1\text{-}ML_8$ fragment, with a geometry based on the $[ReH_9]^{2-}$ molecule, is isolobal with CH_3; R. Hoffmann, Angew. Chem. Int. Edn. Engl., 1982, **21**, 711). **b** i.e. a 2-coordinated sulphur atom. **c** i.e. an n-connected phosphorous (or arsenic) atom (n>2). **d** T-shaped ML_3 fragment. **e** Bent ML_2 fragment.

Brint and Spalding,[94] their calculations showed that the 3, supposedly isolobal, fragments ($Fe(CO)_3$, CoCp and BH) do indeed contribute 3 orbitals (one radial nodeless orbital and two tangential singly noded orbitals) and 3 electrons for cluster bonding. Woolley has stated that, although the isolobal analogy does successfully rationalise transition metal cluster geometries and is a useful tool for the synthetic chemist,[95] the detailed electronic structures of main group and transition metal clusters are quite different.[96] In particular, he has criticised some of the early semi-empirical treatments (notably that of Mingos[82]) for underestimating the d-band width in transition metal clusters and underplaying the important contribution to metal-metal bonding made by the d orbitals. In fact, Woolley has stated that d orbital interactions dominate the metal-metal bonding.[96,97]

In the 1970's, the only known large transition metal clusters (n>6) with (borane-like) deltahedrally based (closo, nido and arachno) skeletal geometries were those possessing interstitial main group atoms (see **Table 1.2** for examples).[98] The majority of large metal clusters were found, instead, to have structures corresponding to capped polyhedra (generally capped tetrahedra and octahedra). Mingos introduced the **Capping Principle**[50,76,99] to deal with these clusters (such as the capped octahedron $[Rh_7(CO)_{10}]^{3-}$ [100] and the bicapped tetrahedron $[Os_6(CO)_{16}]$ [76]). He demonstrated that capping a face of a polyhedron leads to no change in the number of skeletal bonding MO's. This is because the frontier orbitals of the capping fragment are matched in symmetry by orbitals, of the parent cluster, which are already bonding.[99] Capping with a conical $M(CO)_3$ fragment, therefore, leads to an increase in cluster valence electron count of 12 (since the fragment

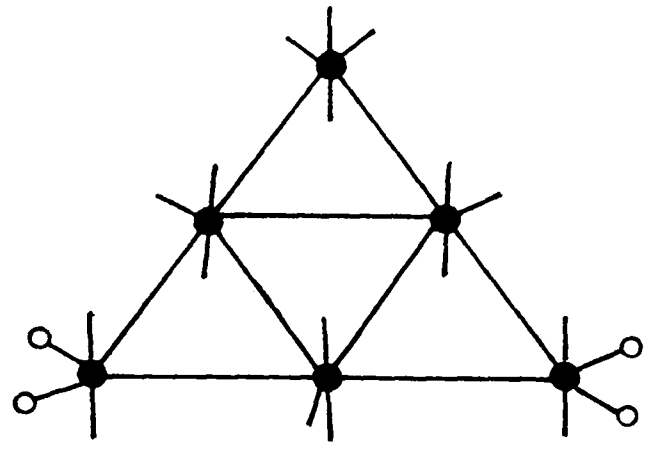
Table 1.2 Closo-, nido- and arachno- transition metal clusters (based on deltahedra with more than 6 skeletal atoms) possessing interstitial main group atoms

Compound	Ref.	Metal Skeletal Geometry	No. of SEP's
$[Os_5C(CO)_{16}]$	**a**	arachno-pentagonal bipyramid	8 (n+3)
$[Co_8C(CO)_{18}]^{2-}$	**b**	square antiprism (arachno)	9 (n+1) **h**
$[Ni_8C(CO)_{16}]^{2-}$	**c**		11 (n+3)
$[Ni_9C(CO)_{17}]^{2-}$	**c**	capped square antiprism (nido)	11 (n+2)
$[Rh_9P(CO)_{21}]^{2-}$	**d**		
$[Rh_{10}S(CO)_{22}]^{2-}$	**e**	closo-bicapped square antiprism	11 (n+1)
$[Rh_{10}E(CO)_{22}]^{3-}$	**f**		
$[Rh_{12}Sb(CO)_{27}]^{3-}$	**g**	closo-icosahedron	13 (n+1)

a B.F.G. Johnson, J. Lewis, J.N. Nicholls, W.J.H. Nelson, J. Puga, P.R. Raithby and M.D. Vargas, J. Chem. Soc., Dalton Trans., 1983, 2447. **b** V.G. Albano, P. Chini, G. Ciani, S. Martinengo and M. Sansoni, J. Chem. Soc., Dalton Trans., 1978, 463. **c** G. Longoni, A. Ceriotti, R. Della Pergola, M. Manassero, M. Perego, G. Piro and M. Sansoni, Phil. Trans. R. Soc. Lond., 1982, **A308**, 47. **d** J.L. Vidal, W.E. Walker, R.L. Pruett and R.C. Schoening, Inorg. Chem., 1979, **18**, 129. **e** G. Ciani, L. Garlaschelli, A. Sironi and S. Martinengo, J. Chem. Soc., Chem. Commun., 1981, 563. **f** (E = P or As) J.L. Vidal, W.E. Walker and R.C. Schoening, Inorg. Chem., 1981, **20**, 238, 243. **g** J.L. Vidal and J.M. Troup, J. Organomet. Chem., 1981, **213**, 351. **h** This cluster has a closo electron count, but the skeletal geometry is intermediate between the square antiprism (arachno) and the triangulated dodecahedron (closo).

has 12 electrons in non-bonding and metal-ligand bonding orbitals). Thus, capped deltahedral clusters are characterised by $\{(14n+2) + 12m\}$ valence electrons, where n is the number of metal atoms in the parent deltahedron and m is the number of capping metal fragments. This leads to electron counts of $14n_t$ and $(14n_t-2)$ for monocapped and bicapped deltahedra respectively (where n_t is the total number (n+m) of metal atoms in the cluster).

Evans and Mingos have subsequently extended the Capping Principle to include edge-bridging C_{2v} ML_4 fragments.[101] Hoffmann had earlier shown that d^8-ML_4 (C_{2v}) fragments are <u>isolobal</u> with carbene (CH_2) units,[90] which explains their tendency to form ring compounds (e.g. $[Os_3(CO)_{12}]$ [7]) and planar raft clusters (e.g. $[Os_6(CO)_{17}(P(OMe)_3)_4]$ (<u>3</u>)).[102]



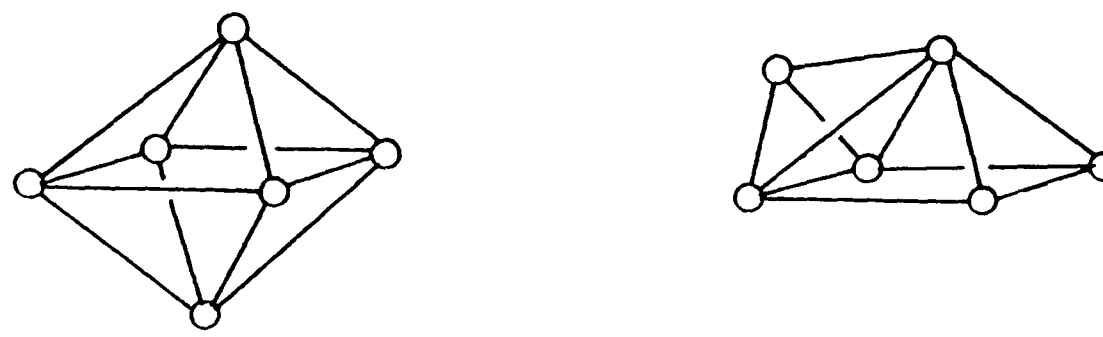
$[Os_6(CO)_{17}\ P(OMe)_3\ _4]$

(<u>3</u>)

As **Figure 1.6** shows, an $Os(CO)_4$ fragment has 14 electrons in non-bonding (metal) and metal-ligand bonding orbitals, so that bridging the edge of a cluster with m of these groups leads to an increase in the cluster valence electron count of 14m. For example, edge-bridged deltahedra are characterised by $\{(14n+2) + 14m\}$ electrons.[101] This again depends on the fact that the frontier orbitals of the bridging group generally interact

with the bonding orbitals of the parent cluster. Mingos has shown, however, that when there are a large number of capping or bridging groups, some linear combinations may be generated which have the correct energy and symmetry to interact strongly with antibonding orbitals of the parent polyhedron. This generates additional cluster bonding MO's, thereby leading to an increase in the number of SEP's.[99,101] The electronic requirements of main group and transition metal cluster and ring compounds (obtained from Polyhedral Skeletal Electron Pair Theory) are summarised in **Table 1.3,** which has been adapted from Ref. 101.

A combination of the Capping Principle and the **Debor Principle** (i.e. that there is no change in the number of SEP's on removing a vertex from a borane, or transition metal cluster)[50,71,72] leads to some interesting structural possibilities. **Figure 1.7** depicts two isoelectronic Os_6 clusters which have different cluster geometries.



$[Os_6(CO)_{18}]^{2-}$ $[H_2Os_6(CO)_{18}]$

Figure 1.7 Alternative skeletal geometries for 86 electron Os_6 clusters.

The <u>closo</u> octahedral cluster $[Os_6(CO)_{18}]^{2-}$ has 86 cluster valence electrons (86 = 14n+2, n=6) as does the Δ-capped <u>nido</u> square pyramidal cluster $[H_2Os_6(CO)_{18}]$ (86 = (14n+4)+12m, n=5, m=1).[103] Diagrams

Table 1.3 Summary of cluster valence electron counts from the Polyhedral Skeletal Electron Pair approach

Polyhedral type	**Main Group**	**Example**	**Transition Metal**	**Example**
Deltahedra (closo)	4n+2	$[B_nH_n]^{2-}$	14n+2	$[Os_5(CO)_{16}]$
nido	4n+4	$[B_nH_{n+4}]$	14n+4	$[Ru_5C(CO)_{15}]$
arachno	4n+6	$[B_nH_{n+6}]$	14n+6	$[Os_4H_3I(CO)_{12}]$
3-connected polyhedra	5n	$[C_nH_n]$	15n	$[Ir_4(CO)_{12}]$
Rings	6n	$[C_nH_{2n}]$	16n	$[Os_3(CO)_{12}]$
Capped deltahedra (m capping groups)	4n+2+2m	-	14n+2+12m	$[Os_6(CO)_{18}]$
Edge-bridged deltahedra (m edge-bridging groups).	4n+2+4m	-	14n+2+14m	-

correlating skeletal geometries and numbers of cluster valence electrons, making use of the Capping and Debor principles, have been constructed by Evans and Mingos[101] and McPartlin.[104] An example of such a correlation diagram is reproduced in **Figure 1.8.**

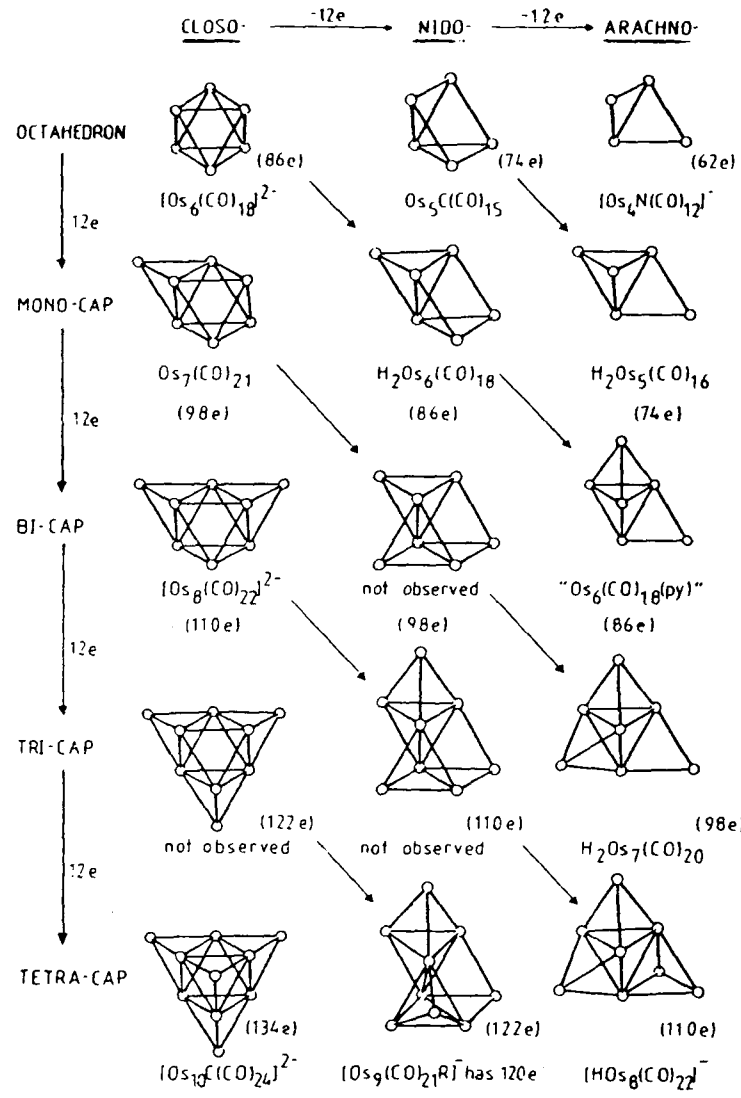


Figure 1.8 Correlation of structure with valence electron count for transition metal clusters, utilising the Capping and Debor principles.

For the later transition metals, the d-p promotion energies are large, which in mononuclear compounds leads to a large number of stable 16 and 14 electron complexes. Over the past ten years a number of platinum clusters, usually with phosphine ligands, have been structurally characterised.[10] These clusters (examples of which are listed in **Table 1.4**) generally possess fewer electrons than would be

Table 1.4 Examples of platinum cluster compounds[a]

Skeletal Geometry	Example	Electron Count	
Triangle	$[Pt_3(CO)_3(PR_3)_3]$	42	(48)[b]
	$[Pt_3(CO)_3(PR_3)_4]$	44	
Tetrahedron	$[Pt_4H_8(PR_3)_4]$	56	(60)
Butterfly	$[Pt_4(CO)_5(PR_3)_4]$	58	(62)
Trigonal Bipyramid	$[Pt_5H_8(PR_3)_5]$	68	(72)
Edge-bridged Tetrahedron	$[Pt_5(CO)_6(PR_3)_4]$	70	(74)
Trigonal Prism	$[Pt_6(CO)_{12}]^{2-}$	86	(90)

a D.M.P. Mingos and R.W.M. Wardle, Transition Met. Chem., 1985, **10**, 441.

b Numbers in parentheses are valence electron counts for clusters of the manganese, iron and cobalt groups.

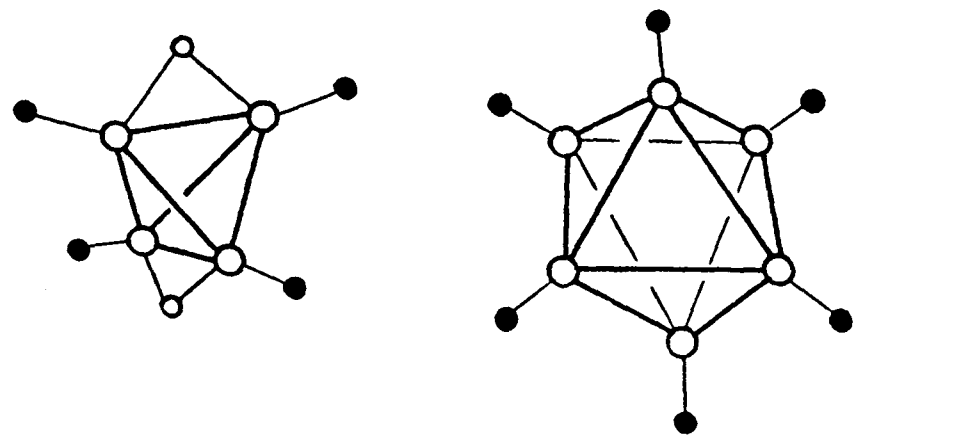
expected on the basis of the Polyhedral Skeletal Electron Pair Theory. Evans and Mingos have presented a detailed analysis of the bonding in clusters of this type, concluding that the high energy of the atomic p orbitals and the deficiency of ligands, leads to some of the cluster MO's with predominantly p^{π} orbital character being unoccupied (in addition to those previously described as "inaccessible" due to being strongly metal-metal antibonding).[105] Their analysis involved the extension of the isolobal analogy to include PtL_2 fragments, the bonding capabilities of which Mingos had studied several years earlier in his theoretical treatment of platinacarboranes.[106]

Relative to those of the earlier transition metals, the d orbitals of the coinage metals (Cu, Ag and Au), are contracted and low lying. Thus, they make only a small contribution to cluster bonding.[107] Since the s-p promotion energy is very large,[108] the valence p orbitals also do not play a large part in metal-metal bonding. Instead, bonding occurs primarily through the valence s orbitals.[107] A large number of gold-phosphine clusters have been structurally characterised[11] and several copper clusters are known (usually with bridging hydride, alkyl or aryl ligands supporting the weak metal-metal bonding),[109] while cluster compounds of silver are rare.[110]

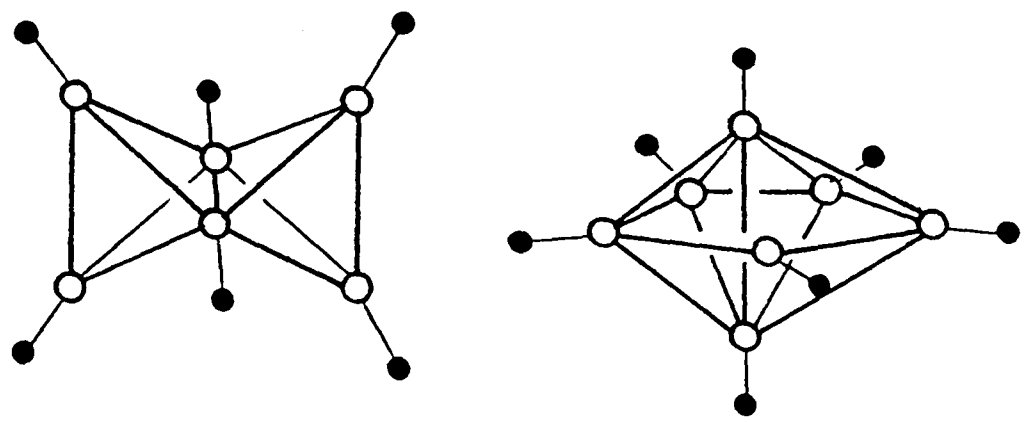
Evans and Mingos have shown that the $Au(PR_3)$ fragment has a low-lying singly occupied sp hybrid orbital (with predominantly s character) and two empty tangential p orbitals, which are too high-lying to become involved in cluster bonding.[111] The fragment is, therefore, effectively isolobal with, for example, H, CH_3 and $Mn(CO)_5$, an analogy which has been synthetically exploited by Lewis, Stone and others.[112]

There are a number of gold clusters with the general formula $[Au_m(PR_3)_m]^{x+}$ (see **Figure 1.9** for examples) whose electron counts are

critically dependent on the cluster geometry.[11]



$[Au_4I_2(PPh_3)_4]$ $[Au_6(Ptol_3)_6]^{2+}$



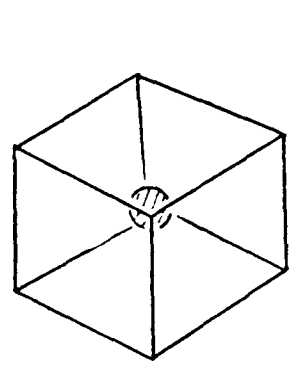
$[Au_6(PPh_3)_6]^{2+}$ $[Au_7(PPh_3)_7]^{+}$

Figure 1.9 Examples of gold clusters of the form $[Au_m(PR_3)_m]^{x+}$.

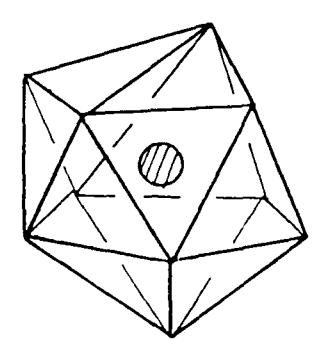
Evans and Mingos have concluded that the occupied skeletal MO's, in these clusters, are low lying (nodeless or singly noded) linear combinations of Au sp hybrid orbitals.[111] Many of the higher nuclearity gold clusters possess structures consisting of a gold atom in the centre of a cage, which is a fragment of an icosahedron.[107] This led Mingos to predict the possibility of synthesising a centred-icosahedral $[Au_{13}]$ cluster,[107,113] a prediction which was subsequently borne out with the characterisation of $[Au_{13}(PMe_2Ph)_{10}Cl_2]^{3+}$.[114]

High nuclearity gold clusters have the general formula $[Au\{Au(PR_3)\}_m]^{x+}$ and may be divided into two sub-classes, according to

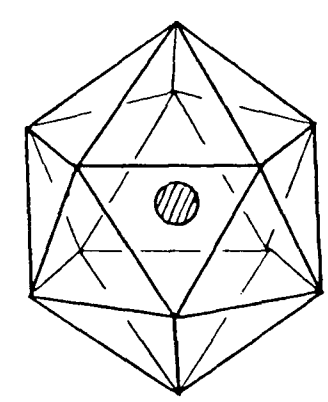
(a) Spherical Clusters: (12m+18) valence electrons



$[Au_9(PR_3)_8]^+$

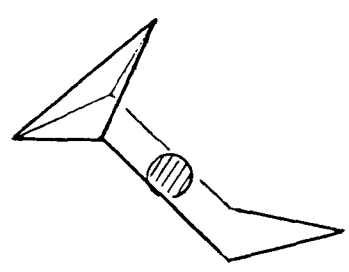


$[Au_{11}I_3(PR_3)_7]$

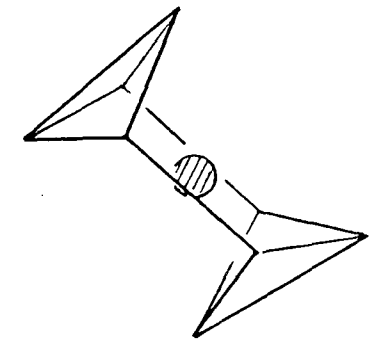


$[Au_{13}Cl_2(PR_3)_{10}]^{3+}$

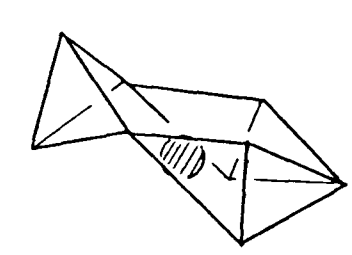
(b) Toroidal Clusters: (12m+16) valence electrons



$[Au_8(PR_3)_7]^{2+}$



$[Au_9(PR_3)_8]^{3+}$



$[Au_{10}Cl_3(PR_3)_6]^+$

Figure 1.10 Examples of high nuclearity gold clusters, $[Au\{Au(PR_3)\}_m]^{x+}$, with spherical and toroidal topologies.

whether the outer gold atoms adopt a spherical or toroidal topology.[115] "Spherical" clusters (see **Figure 1.10a** for examples) are characterised by (12m + 18) cluster valence electrons. Thus, all 9 valence orbitals of the central gold atom are involved in bonding with the radial sp hybrids of the outer AuL groups, which each contribute 2 metal-ligand bonding and 10 non-bonding (d) electrons to the total count. "Toroidal" clusters (see **Figure 1.10b** for examples) are characterised by (12m + 16) cluster valence electrons, since one of the p orbitals on the central gold atom finds no low lying symmetry-matched cluster orbital.[115]

In recent years a large number of high nuclearity transition metal-carbonyl clusters have been synthesised, most of which have structures corresponding to the condensation of smaller tetrahedral, octahedral and trigonal prismatic cluster fragments.[7b] Mingos has recently developed a methodology which has enabled him to formulate rules to account for the cluster valence electron counts in these molecules. In his **Polyhedral Fusion** formalism, the condensed cluster is regarded as the product of two polyhedra sharing a vertex, edge or face.[116,117] In this way Mingos derived the rule that **"the total electron count in a condensed cluster is equal to the sum of the electron counts for the parent polyhedra (A) and (B) minus the electron count (Δ_c) characteristic of the shared unit (atom, pair of atoms etc.)".**[116] Thus if polyhedron (A) is characterised by a electrons and polyhedron (B) by b electrons the condensed cluster (C) has a total of ($a+b-\Delta_c$) electrons (see **Figure 1.11**). **Table 1.5** lists the characteristic electron counts (Δ_c) for various shared units, based on the 18 electron rule, and examples of this analysis of condensed clusters are presented in **Figure 1.12.** Mingos and Evans have subsequently extended the Polyhedral Fusion approach to include

Table 1.5 Characteristic electron counts (Δ_c) for shared units in fused transition metal polyhedra

Shared unit	Δ_c	Molecular analogue
Vertex	18	$[Mo(CO)_6]$
Edge	34	$[Mn_2(CO)_{10}]$
Triangular Face	48[a]	$[Os_3(CO)_{12}]$
	50[b]	-
Square Face	62[b]	$[Ru_4(CO)_{11}(\mu_4\text{-PPh})_2]$
	64[a]	$[Fe_4(CO)_{12}(\mu_4\text{-PPh})_2]$
Butterfly	62	$[Os_4N(CO)_{12}]^-$

[a] These values are used when the fused polyhedra are both 3-connected.

[b] These values are used when one, or both, of the fused polyhedra are not 3-connected (D.M.P. Mingos, Acc. Chem. Res., 1984, **17**, 311).

condensed platinum clusters where the parent clusters and shared units are characterised by fewer electrons than in the previously mentioned examples (16 electrons for a single Pt atom, 30 electrons for a dimer, 42 or 44 electrons for a triangle etc.).[118]

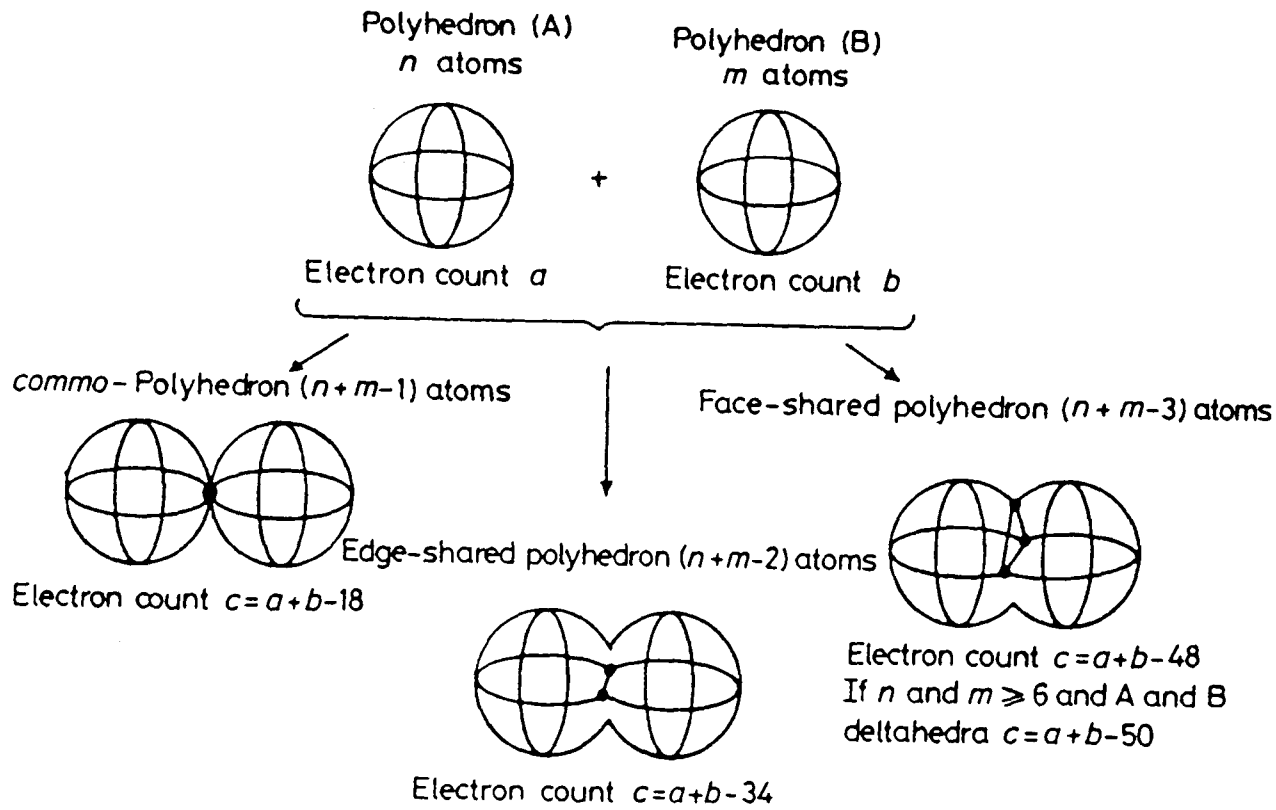
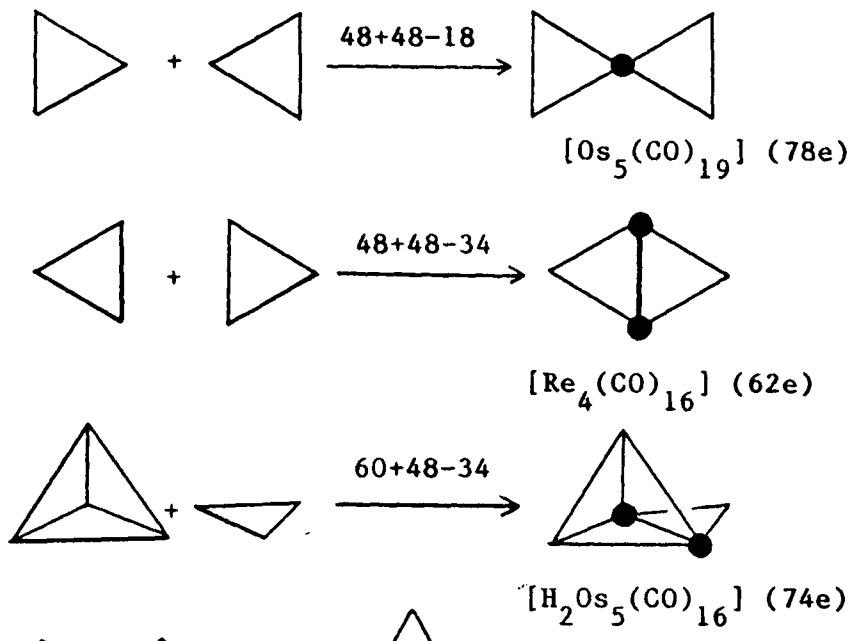
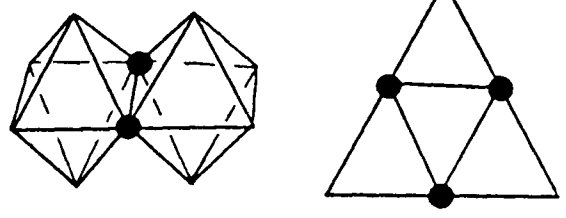


Figure 1.11 Schematic representation of the principle of Polyhedral Fusion.

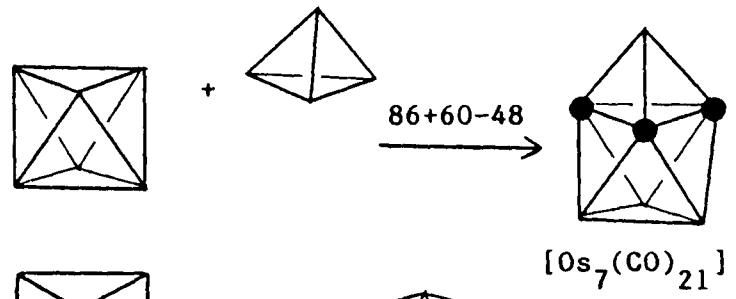
The methodology has also been applied to condensed mixed main group-transition metal clusters.[117]

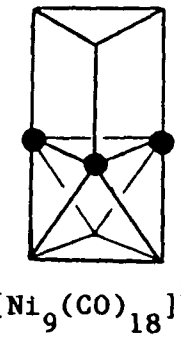
In the 1970's, the idea that discrete transition metal clusters could serve as good models for chemisorption onto bulk metal surfaces was elegantly formulated by Muetterties.[8] Subsequently, a large number of high nuclearity clusters, with structures resembling fragments of bulk metal lattices (i.e. body centred cubic (b.c.c.), cubic close packed (c.c.p.) and hexagonal close packed (h.c.p.)), have been characterised, notably by Chini and coworkers.[119]

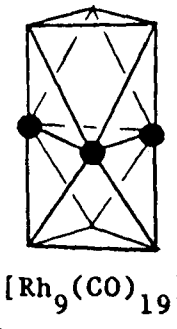


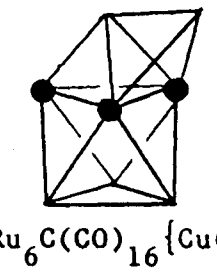

$[Ru_{10}C_2(CO)_{24}]^{2-}$
(138e=86+86-34)

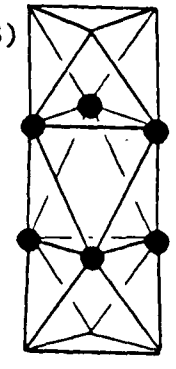
$[Os_6(CO)_{21}]$
(90e=(4x48)-(3x34))

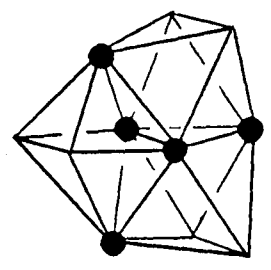



$[Ni_9(CO)_{18}]^{2-}$
(128e=90+86-48)


$[Rh_9(CO)_{19}]^{3-}$
(122e=86+86-50)


$[Ru_6C(CO)_{16}\{Cu(NCMe)\}_2]$
(110e=86+72-48)


$[Rh_{12}(CO)_{25}]$
(158e=(3x86)-(2x50))


$[Rh_{11}(CO)_{23}]^{3-}$
(148e=(3x86)-62-48)

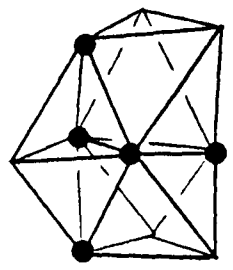

$[Rh_{10}(CO)_{21}]^{2-}$
(134e=(2x86)+72
-62-48)

Figure 1.12 Applications of the principle of Polyhedral Fusion.

Lauher (in 1979) performed Extended Hückel calculations on a series of bare metal close packed clusters, partitioning the cluster valence MO's into those involved in metal-metal bonding and those which can act as acceptor orbitals towards ligands or substrates bound to the surface of a metal.[120] In 1980, Ciani and Sironi published an Extended Hückel analysis of a wider selection of bare metal condensed clusters with known and hypothetical skeletal geometries.[121] They concluded, on the basis of Lauher's criteria, that the majority of these clusters are characterised by (6n+7) cluster valence MO's. This has been rationalised in terms of the Capping Principle by recognising that most of these structures are based on a central octahedron which possesses 7 SEP's.[122]

Recently, Teo has used an extended form of the Hume-Rothery rule (developed for intermetallic alloys)[123] to account for the structures adopted by pseudo-close packed clusters.[124] His conclusions are in agreement with the earlier work of Johnson, Messmer et al. who found that the density of states of a bare metal cluster rapidly converges to that of the bulk metal for as few as 13 (f.c.c.) or 15 (b.c.c.) metal atoms.[125]

Mingos has recently developed an electron counting procedure for these clusters based on the formal division of the high nuclearity cluster into an internal (encapsulated) polyhedron and an external (surface) polyhedron.[126] Three sub-classes of "close-packed" cluster have been identified:

(a) Clusters where radial metal-metal bonding predominates

In this case, the surface atoms act as ligands towards the central atom or cluster, to which they are bonded by radial (σ) bonds. There is no direct surface tangential bonding in these clusters. Cluster valence

electron counts (N_e) for such clusters are given by:

$$N_e = 12n_s + \Delta_i$$

where n_s is the number of surface atoms and Δ_i is the electron count characteristic of the central atom or cluster (see **Table 1.6**). Examples of this class of cluster, which includes the centred gold clusters mentioned above (where a $(12n_s+16)$ electron count is possible for toroidal topologies), are listed in **Table 1.7** (taken from Ref. 126b) and some structures are depicted in **Figure 1.13.**

An important feature of these clusters is that their structures are independent of the electron count of the surface polyhedron. Since radial metal-metal bonding predominates, there is a soft potential energy surface for cluster rearrangement. This has been experimentally observed for gold clusters.[127] Theoretical studies of bulk metals have indicated that alternative close packed (and related) structures are also separated by small energy differences.[128]

(b) Clusters with a partial bonding contribution from the surface tangential orbitals

All of the clusters of this type (see **Table 1.8** and **Figure 1.14** for examples) possess a single interstitial atom and are characterised by $(12n_s+18+x)$ cluster valence electrons. These clusters generally have 3 extra occupied skeletal MO's (i.e. x=6), which are exclusively involved in tangential bonding in the external cluster polyhedron.

(c) Clusters with a large bonding contribution from the surface tangential orbitals

The electron count in these clusters (**Figure 1.15**), as for main

Table 1.6 Characteristic electron counts (Δ_i) for interstitial moieties in high nuclearity clusters

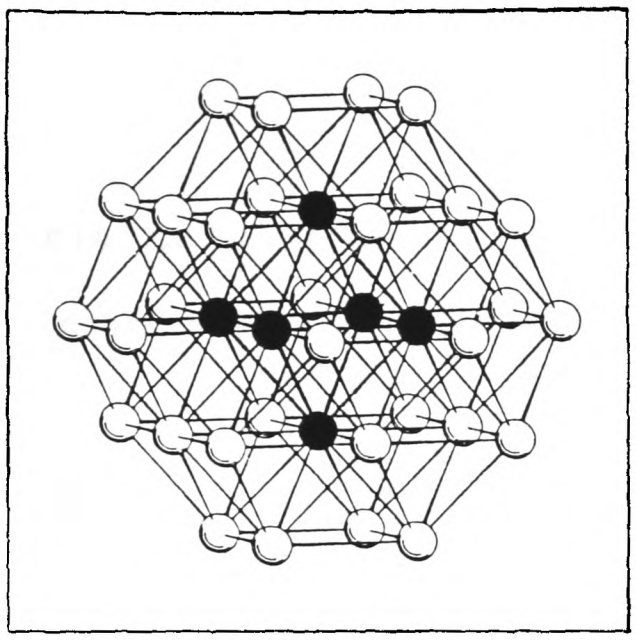
No. of interstitial atoms	Δ_i	**Molecular analogue**
1	18	$[Mo(CO)_6]$
2 (dimer)	34	$[Mn_2(CO)_{10}]$
3 (triangle)	48	$[Os_3(CO)_{12}]$
	50*	-
3 (linear fragment)	50	$[OsRe_2(CO)_{14}]$
4 (tetrahedron)	60	$[Ir_4(CO)_{12}]$
6 (octahedron)	86	$[Rh_6(CO)_{16}]$

* Although isolated triangular clusters are characterised by 48 electrons, the presence of bridging metal atoms can lead to the stabilisation of an a_2' molecular orbital and a valence electron count of 50 for the central triangle (D.G. Evans and D.M.P. Mingos, Organometallics, 1983, **2**, 435).

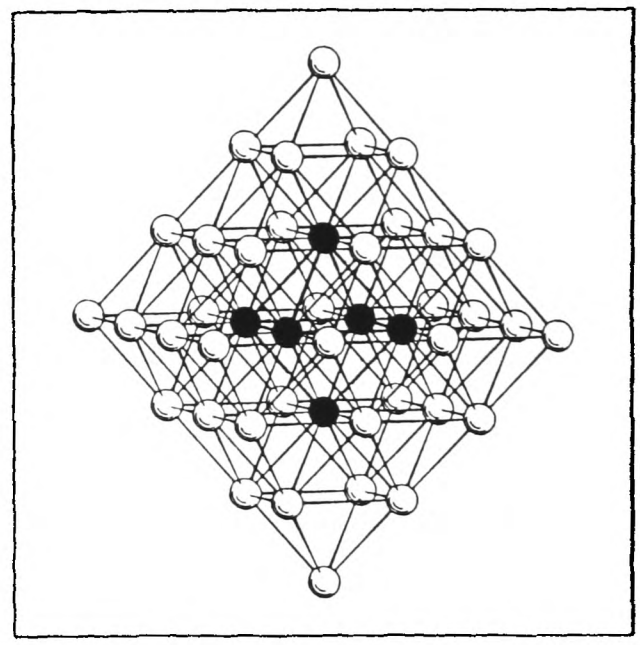
Table 1.7 Examples of high nuclearity cluster compounds where radial metal-metal bonding interactions predominate

Cluster	Ref.	n_i	n_s	Structure	Electron count	
$[Au_9(PPh_3)_8]^+$	**a**	1	8	b.c.c.	114	
$[Au_{11}I_3(PPh_3)_7]$	**b**	1	10	b.c.c./i.c.p.[j]	138	$(12n_s+18)$
$[Au_{13}Cl_2(PMePh_2)_{10}]^{3+}$	**c**	1	12	i.c.p.	162	
$[Pt_{19}(CO)_{22}]^{4-}$	**d**	2	17	i.c.p.	238	
$[Rh_{22}(CO)_{35}H_{(5-q-m)}]^{q-}$	**e**	2	20	c.c.p./b.c.c.	(273+m)[k]	$(12n_s+34)$
$[Au_{13}Ag_{12}Cl_6(PPh_3)_{12}]^{m+}$	**f**	3	22	i.c.p.	(317-m)	$(12n_s+50)$[l]
$[Pt_{26}(CO)_{32}]^{2-}$	**g**	3	23	h.c.p.	326	$(12n_s+50)$[m]
$[Ni_{38}Pt_6(CO)_{48}H_{(6-n)}]^{n-}$	**h**	6	38	c.c.p.	542	$(12n_s+50)$[n]
$[Pt_{38}(CO)_{44}H_m]^{2-}$	**i**	6	32	c.c.p.	(470+m)[o]	

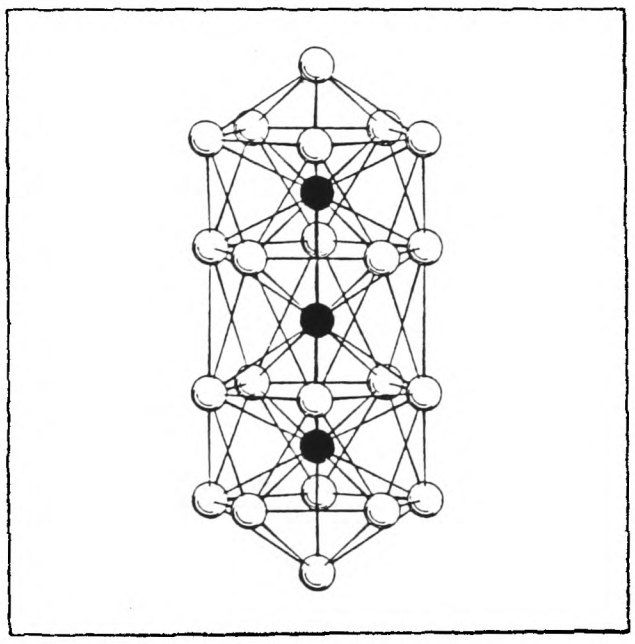
a J.G.M. van der Linden, M.L.H. Paulissen and J.E.J. Schmitz, J. Amer. Chem. Soc., 1983, **105**, 1903. **b** J.M.M. Smits, P.T. Burskens, J.W.A. van der Velden and J.J. Bau, J. Cryst. Spectrosc. Res., 1983, **13**, 373. **c** C.E. Briant, B.R.C. Theobald, J.W. White, L.K. Bell and D.M.P. Mingos, J. Chem. Soc., Chem. Commun., 1981, 201. **d** D.M. Washecheck, E.J. Wucherer, L.F. Dahl, A. Ceriotti, G. Longoni, M. Manassero, M. Sansoni and P. Chini, J. Amer. Chem. Soc., 1979, **101**, 6110. **e** J.L. Vidal, R.C. Schoening and J.M. Troup, Inorg. Chem., 1981, **20**, 227. **f** B.K. Teo and K. Keating, J. Amer. Chem. Soc., 1984, **106**, 2224. **g** D.M. Washecheck, A. Ceriotti, P. Chini, G. Longoni and L.F. Dahl, personal communication. **h** (n = 4 or 5) A. Ceriotti, F. Demartin, G. Longoni, M. Manassero, M. Marchionna, G. Piva and M. Sansoni, Angew. Chem. Int. Edn. Engl., 1985, **24**, 697. **i** D.M. Washecheck, A. Ceriotti, M.A. Murphy, D.A. Nagaki, P. Chini, G. Longoni and L.F. Dahl, personal communication. **j** i.c.p. = "icosahedral close packing", a term used to denote high nuclearity clusters with 5-fold symmetry (D.M.P. Mingos, Chem. Soc. Rev., 1986, **15**, 31. **k** If m=1 this cluster possesses 274 $(12n_s+34)$ valence electrons. **l** Linear trimeric interstitial moiety. If m=3 this cluster possesses 314 $(12n_s+50)$ valence electrons. **m** Triangular interstitial moiety. **n** Octahedral interstitial moiety. **o** If m=0 this cluster possesses 470 $(12n_s+86)$ valence electrons.



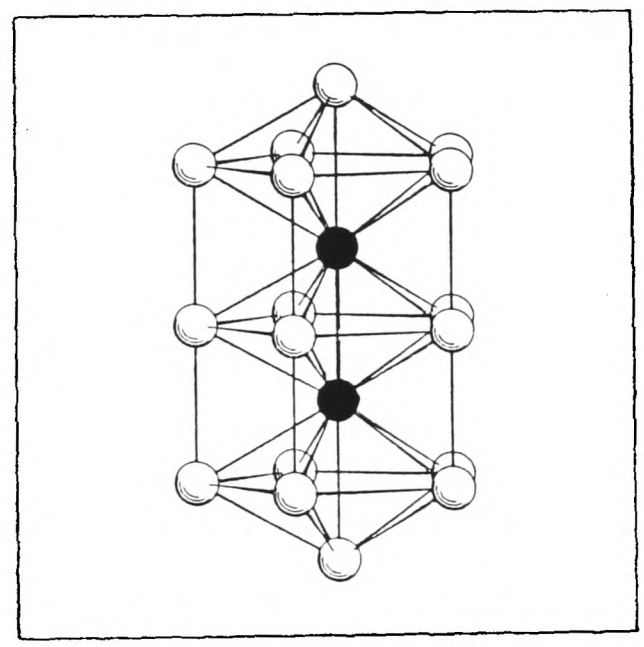
$[Pt_{38}(CO)_{44}H_m]^{2-}$
(c.c.p.)



$[Ni_{38}Pt_6(CO)_{48}H_{(6-n)}]^{n-}$
(c.c.p.)



$[Au_{13}Ag_{12}Cl_6(PPh_3)_{12}]^{m+}$
(i.c.p.)



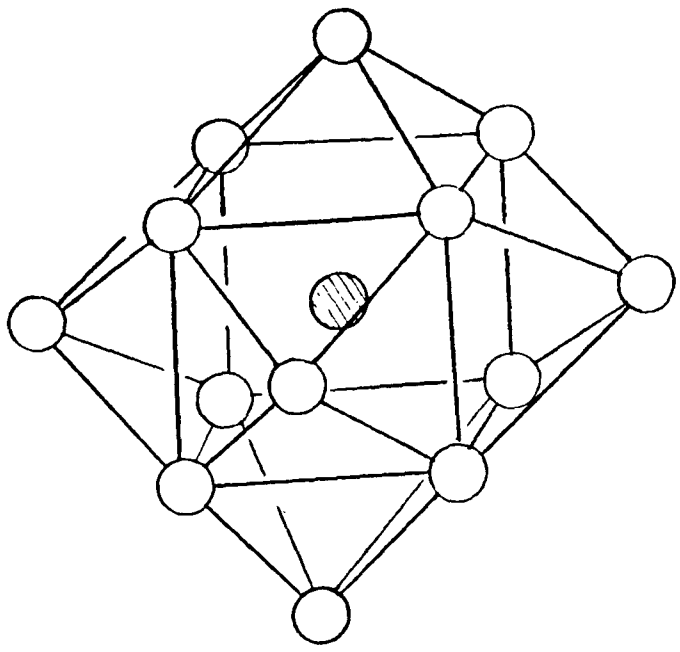
$[Pt_{19}(CO)_{22}]^{4-}$
(i.c.p.)

Figure 1.13 Examples of high nuclearity transition metal clusters, with interstitial metal atoms and cluster fragments, where radial metal-metal bonding predominates.

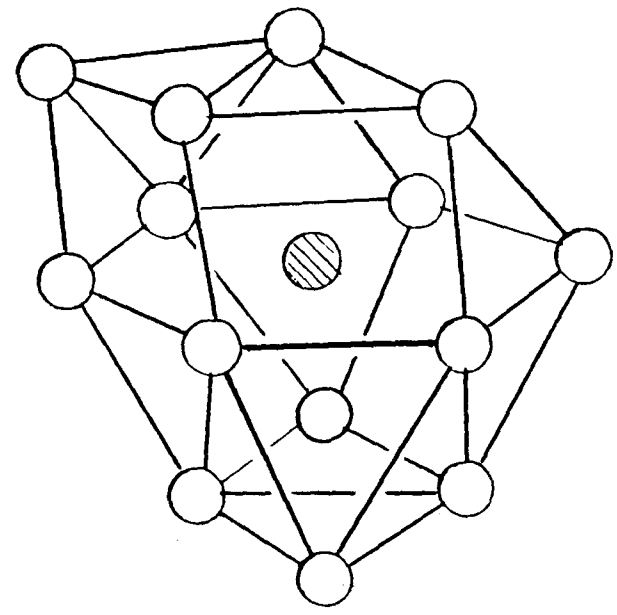
Table 1.8 Examples of high nuclearity cluster compounds where tangential interactions make a partial contribution to metal-metal bonding

Cluster	Ref.	n_i	n_s	Structure	Electron count	
$[Rh_{14}(CO)_{25}]^{4-}$	**a**	1	13	b.c.c.	180	
$[Rh_{14}(CO)_{26}]^{2-}$	**b**	1	13	b.c.c.	180	
$[Rh_{15}(CO)_{27}]^{3-}$	**c**	1	14	b.c.c./h.c.p.	192	$(12n_s+24)$
$[Rh_{17}(CO)_{30}]^{3-}$	**d**	1	16	h.c.p.	216	
$[Rh_{22}(CO)_{37}]^{4-}$	**e**	1	21	c.c.p./h.c.p.	276	
$[Pt_{24}(CO)_{30}]^{2-}$	**f**	1	23	c.c.p.	302	$(12n_s+26)$

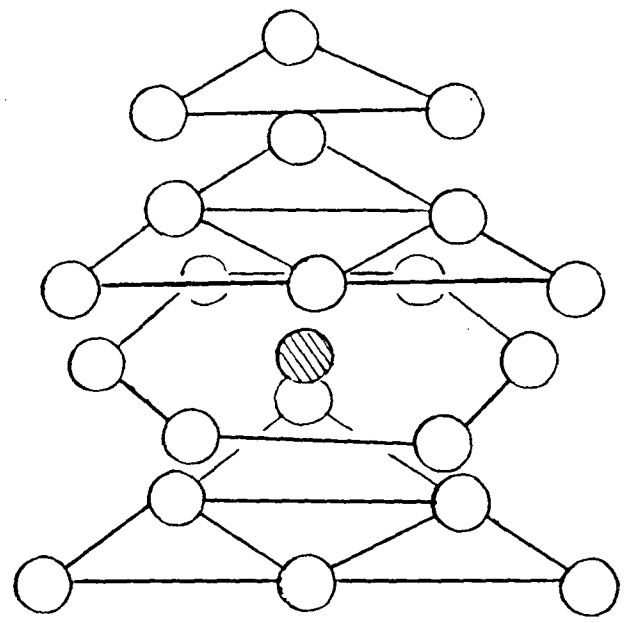
a G. Ciani, A. Sironi and S. Martinengo, J. Organomet. Chem., 1980, **192**, C42. **b** S. Martinengo, G. Ciani and A. Sironi, J. Chem. Soc., Chem. Commun., 1980, 1140. **c** S. Martinengo, G. Ciani, A. Sironi and P. Chini, J. Amer. Chem. Soc., 1978, **100**, 7096. **d** G. Ciani, A. Magni, A. Sironi and S. Martinengo, J. Chem. Soc., Chem. Commun., 1981, 1280. **e** S. Martinengo, G. Ciani and A. Sironi, J. Amer. Chem. Soc., 1980, **102**, 7564. **f** R.A. Montag, A. Ceriotti and L.F. Dahl, personal communication.



$[Rh_{14}(CO)_{26}]^{2-}$ (b.c.c.)



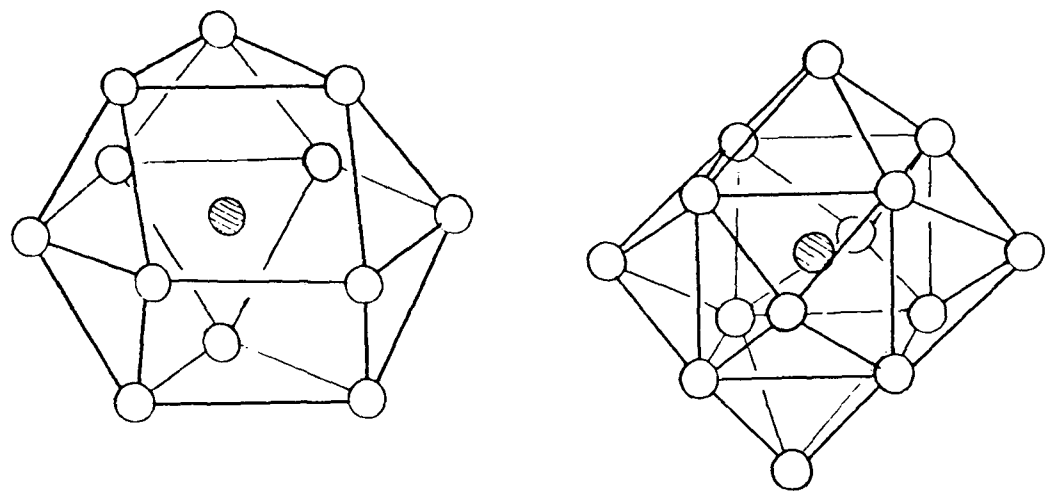
$[Rh_{15}(CO)_{27}]^{3-}$ (b.c.c./h.c.p.)



$[Rh_{22}(CO)_{37}]^{4-}$ (h.c.p./c.c.p.)

Figure 1.14 Examples of high nuclearity transition metal clusters, with interstitial metal atoms, where the surface tangential orbitals make a partial contribution to the metal-metal bonding.

group clusters, is governed by the arrangement of the skeletal (surface) atoms. For closo-type structures the electron count is $14n_s+2$.



$[Rh_{13}(CO)_{24}H_5]$ (h.c.p.) $[Rh_{15}(CO)_{30}]^{3-}$ (b.c.c.)

Figure 1.15 Examples of high nuclearity transition metal clusters, with interstitial metal atoms, where the surface tangential orbitals make a large contribution to the metal-metal bonding.

Woolley has compared the metal-metal bonding in transition metal clusters and bulk metals and concluded that the metal d orbitals contribute significantly to this bonding in both cases.[96,97] He has noted, however, that the presence of ligands in transition metal clusters modifies the bonding properties of the d-band. The idea that the ligands of a cluster effectively insulate the metal atoms has been proposed by Mingos to explain why clusters have so far proved disappointing as regards their catalytic properties.[129] It is, however, still possible that theoretical studies of metal clusters will lead to an increased understanding of reactions on metal surfaces.[130] In addition, the study of large metal cluster compounds may lead to advances in the field of Materials Science, since interesting magnetic

properties have recently been reported for a variety of high nuclearity clusters.[131] These properties have led Benfield to postulate the existence of a new "meta-metallic" state.[132]

1.4 Free Electron Cluster Bonding Models

As early as 1949, Pimental and Pitzer suggested[133] that the skeletal bonding in nido-decaborane [$B_{10}H_{14}$] could be conveniently described in terms of a free electron model similar to those used for bulk metals.[134] Such a method had previously been applied to the study of conjugated polyenes and aromatic hydrocarbons.[135] Subsequently, Chapman and Waddington treated the molecular orbitals of the cage compounds [S_4N_4] and [S_4As_4] [136] in terms of the solution of the Schrödinger Equation for a particle on a sphere[22] (i.e. by allowing full delocalisation of the cluster valence electrons over the surface of a sphere).[137] The cluster molecular orbitals were described, as for atomic orbitals, in terms of the quantum numbers L and M (with L giving the number of angular nodes possessed by the orbital and M = L, L-1, ...0, ...-L).[22] In this simple analysis the (2L+1) components of each L manifold (i.e. orbitals with different M values) were taken to be degenerate, with their energies (E_L) given by the following equation:

$$E_L = h^2L(L+1)/(8\pi^2 \mu a^2)$$

where a is the radius of the cluster sphere. The actual symmetry of the cluster (since the skeletal atoms must define a polyhedron with less than spherical symmetry) was then introduced as a perturbation, thereby breaking the (2L+1)-fold degeneracy of the L manifold. Hoffmann and Gouterman used a similar mode of analysis,[138] but approximated the

perturbation (due to the real cluster geometry) by a Crystal Field[139] expansion. Waddington subsequently adapted his earlier model by constraining the skeletal electrons, in boranes and related species, to move along the edges of the cluster polyhedron (i.e. solving the Schrödinger Equation for a particle on the edges of a box), using topology to factorise the secular equation.[140]

These free electron models were successfully applied to linear and planar hydrocarbon π-systems and spherical aggregates of hydrogen atoms because, in these cases, the nodal characteristics of the molecular orbitals accurately reflect their relative energies. For clusters of real interest it was found, however, that the energy level orderings obtained in this fashion were often different to those obtained by LCAO-MO methods.[138] This is because real clusters possess, in addition to nodeless (σ-type) atomic orbitals, orbitals which are singly (π) or doubly noded (δ) with respect to a plane perpendicular to a radial vector passing through the atom, as shown in **Figure 1.16.**

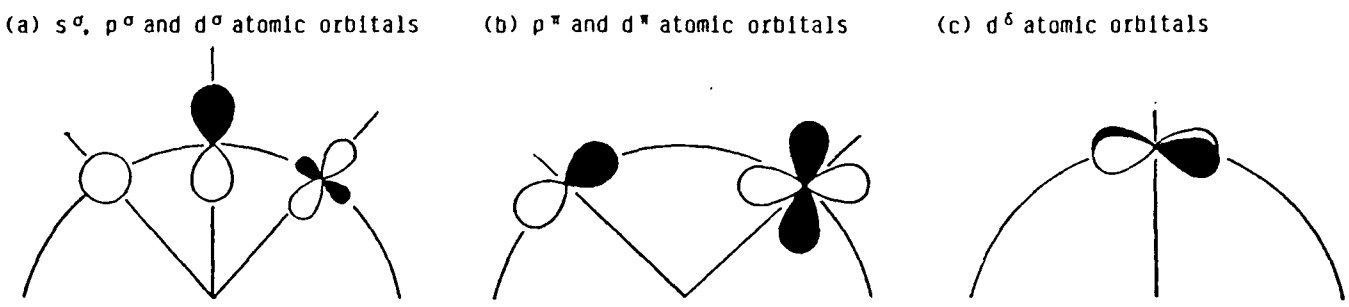


Figure 1.16 σ-, π- and δ-symmetry atomic orbitals.

For linear and planar hydrocarbons, the π-system may be regarded as being topologically equivalent to an arrangement of hydrogen atoms, since the constituent p_z atomic orbitals are nodeless when viewed along an axis perpendicular to the plane of the molecule. Node counting for (3-dimensional) cluster MO's composed of atomic π and δ orbitals is complicated by the fact that these atomic orbitals possess intrinsic nodes which do not contribute to the overall antibonding character of the cluster MO's. Clearly a more sophisticated approach was needed to deal with π and δ as well as σ-type cluster MO's.

The creation of a more sophisticated spherical model for clusters was aided by the work of Hoffman, Ruedenberg and Verkade who developed a pictorial approach to the bonding in main group and transition metal complexes. They used Spherical Harmonic functions, at the centre of the molecule, as Generator Orbitals to create linear combinations of ligand orbitals with the same symmetry and nodal characteristics.[141] These "symmetry orbitals" were then combined with the orbitals of the real central atom of the molecule in order to form localised or delocalised orbitals. The generator orbital was identified with the angular part of a united atom orbital (a concept introduced by Mulliken),[142] where the electrons of a molecule were regarded as being delocalised within a sphere rather than over its surface.

Recently, an elegant approach to the bonding in cluster compounds has been developed by A.J. Stone, whose **Tensor Surface Harmonic (TSH) Theory**[143] derives cluster molecular orbitals from a spherical potential model. All of the cluster atoms are constrained to lie on the surface of a single sphere, of unit radius, with each atom (i) being described by the angular coordinates (θ_i,ϕ_i). The Schrödinger Equation is then solved for a particle on a sphere[22] and the radial part of the solution is

discarded. This yields wavefunctions which are Spherical Harmonic[144] in nature and may (as in the treatment of Chapman and Waddington)[137] be described in terms of the quantum numbers L and M. Stone's method differs from the earlier free electron approaches in that the values of the general Spherical Harmonics $S_{L,M}(\theta,\phi)$ at the cluster atom positions (θ_i,ϕ_i) are used as the coefficients (c_i) in an LCAO expansion of a basis set of atomic orbitals (ρ_i) to yield the cluster MO's $(\Psi_{L,M})$:

$$\Psi_{L,M} = N\ \Sigma_i c_i \rho_i\ = N\ \Sigma_i S_{L,M}(\theta_i,\phi_i)\rho_i$$

For a basis set of atomic (σ) orbitals which are nodeless in the plane perpendicular to the radial vector (see **Figure 1.16a**), the required Harmonics are simply the Scalar Spherical Harmonics $(Y_{L,M}(\theta,\phi))$. The cluster wavefunctions $\Psi^{\sigma}_{L,M} = L^{\sigma}_{M}$ (S^{σ}, P^{σ}, D^{σ}, F^{σ} etc.) are equivalent to the angular parts of the hydrogen-like atomic orbitals.[22] Stone has shown that the energies of the L^{σ}_{M} orbitals rise with increasing L as the increasing number of angular nodes leads to a greater number of antibonding interactions.[143a,b] By making the simple Hückel approximations,[145] assuming an average angle (ω) between neighbouring cluster atoms and taking a weighted average over all (2L+1) values of M for a given L, the following expression was derived for the energies of the L^{σ} orbitals:

$$E^{\sigma}_{L} = \alpha^{\sigma} + (2e/n)\beta^{\sigma}P_L(\cos\omega)$$

(e = number of edges of cluster polyhedron, n = number of cluster vertices, $\alpha^{\sigma} = H_{ii} = \langle\sigma_i|\hat{H}|\sigma_i\rangle$ (Coulomb Integral), $\beta^{\sigma} = H_{ij} = \langle\sigma_i|\hat{H}|\sigma_j\rangle$ if i and j are adjacent (Resonance Integral) and $P_L(\cos\omega)$ is a Legendre polynomial).[144]

The factor (2e/n) was recognised as the average coordination number of the cluster atoms. This number is a maximum for deltahedral structures, which led to the conclusion that (since α^{σ} and β^{σ} are both negative) **if only skeletal bonding molecular orbitals are occupied, the most stable cluster structures are the deltahedra.** In this way Stone rationalised the predominance of such triangulated structures in cluster chemistry.[143a,b]

For a basis set of (π) atomic orbitals which are singly noded in the plane perpendicular to the radial vector (see **Figure 1.16b**), the required Harmonics are the Vector Surface Harmonics,[144] since the atomic orbitals are tangential to the surface of the sphere and have vector properties. Two vector functions may be obtained from each (Scalar) Spherical Harmonic, one by taking its gradient ($\mathbf{V_{L,M}} = \nabla Y_{L,M}$) and the other by forming a vector function which is orthogonal to the first ($\bar{\mathbf{V}}_{\mathbf{L,M}} = \hat{\mathbf{r}} \times \mathbf{V_{L,M}}$). Using these functions to obtain LCAO coefficients, the set of wavefunctions $\Psi^{\pi}_{L,M}$ (= L^{π}_{M}) and $\bar{\Psi}^{\pi}_{L,M}$ (= $\bar{L}^{\pi}_{M}$) are generated. Stone showed that for deltahedral structures, the orbitals L^{π}_{M} are bonding while $\bar{L}^{\pi}_{M}$ are antibonding. L^{π}_{M} and $\bar{L}^{\pi}_{M}$ are related by the Parity Inversion operator ($\hat{P}$) which corresponds to a rotation of 90^{o} about the radial vector of each constituent p^{π} or d^{π} atomic orbital, leading to a reversal of the bonding character of the orbitals:

$$L^{\pi}_{M}\ \text{(bonding)} \xleftrightarrow{\hat{P}} \bar{L}^{\pi}_{M}\ \text{(antibonding)}$$

Stone used the methodology of TSH theory to derive the (n+1) skeletal electron pair count for deltahedral boranes. Each of the (n) BH fragments possesses one σ-type sp hybrid, yielding nL^{σ} cluster MO's in total, one of which (S^{σ}) is strongly bonding because it possesses no

angular nodes. In addition each fragment has two π-type p orbitals which combine to form nL^{π} bonding and $n\bar{L}^{\pi}$ antibonding cluster orbitals. Mixing occurs between L^{σ} and L^{π} orbitals, with the same L values, resulting in one bonding combination and one antibonding combination for every matched pair of L^{σ}/L^{π} orbitals. There is no S^{π} orbital since S^{σ} has no θ or φ dependence and, therefore, no gradient. In total there are (n+1) cluster bonding MO's (S^{σ} and nL^{σ}/L^{π} combinations). More sophisticated MNDO molecular orbital calculations have subsequently been performed by Brint et al., which have confirmed that the qualitative approach of TSH theory leads to a reasonably accurate description of the bonding in deltahedral borane clusters.[146] They concluded that the only significant L^{σ}/L^{π} mixing occurs for the P^{σ} and P^{π} orbitals, since the higher L^{σ} orbitals are strongly antibonding and consequently, the L^{σ}-L^{π} energy separation is large. A qualitative molecular orbital scheme for the deltahedral boranes, based on TSH theory is presented in **Figure 1.17.**

Stone has applied TSH theory to the study of nido and arachno borane clusters, deriving the (n+2) and (n+3) SEP counts for these species.[143c] He has also considered the bonding in transition metal cluster compounds.[143] For these clusters, a new type of Spherical Harmonic with tensor properties is required, since the metal d orbitals have (in addition to 1σ and 2π components) 2δ components (d_{xy} and $d_{x^2-y^2}$) which are doubly noded in the plane perpendicular to the radial vector and hence behave as tensors (see **Figure 1.16c**). Two Tensor Surface Harmonic functions may be obtained from each Scalar Spherical Harmonic as follows:[144]

$$\mathbf{T_{L,M}} = \nabla\nabla Y_{L,M}$$

$$\bar{\mathbf{T}}_{\mathbf{L,M}} = \hat{\mathbf{r}} \times \mathbf{T_{L,M}}$$

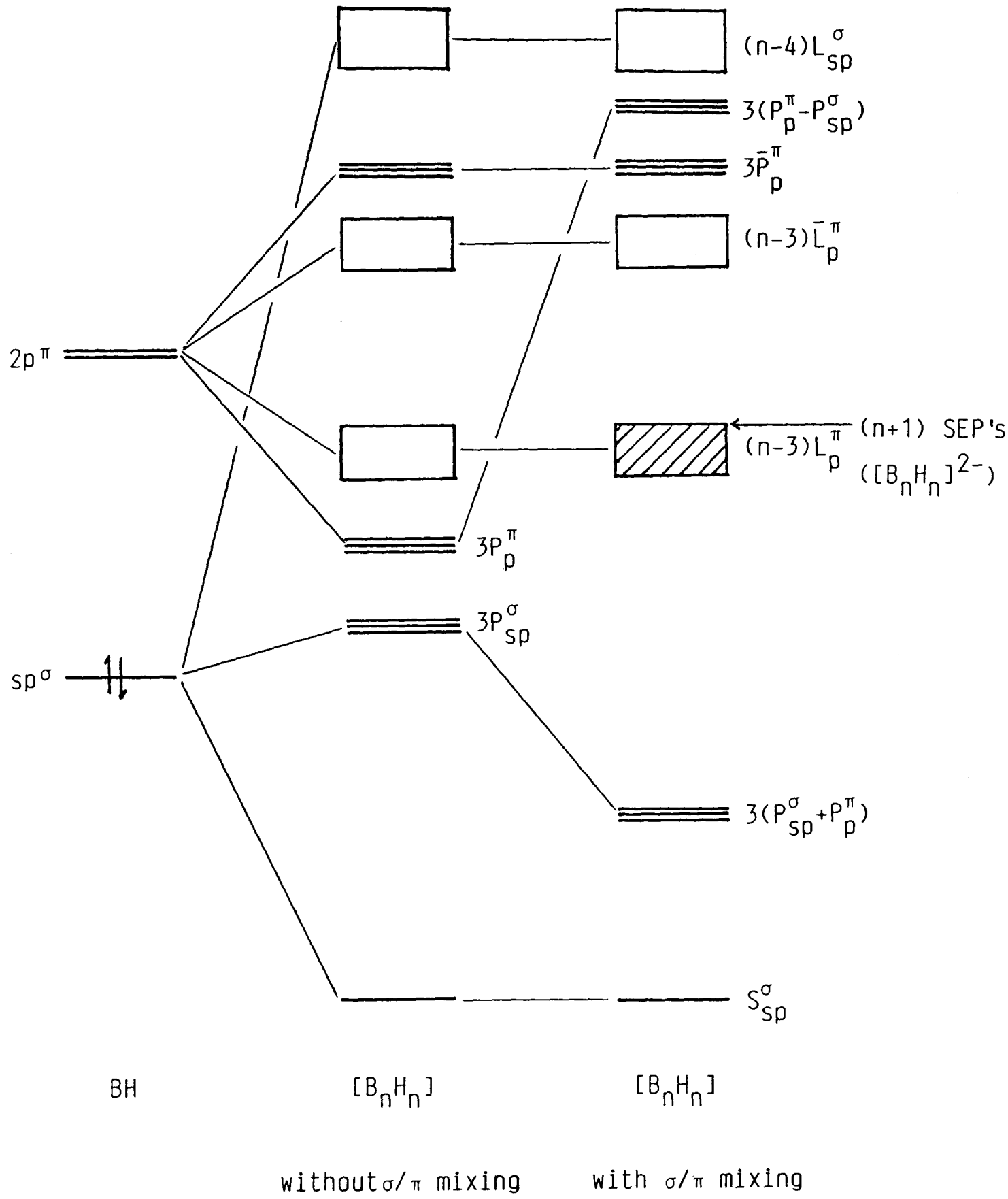


Figure 1.17 Generalised qualitative MO scheme, based on Stone's TSH methodology, for the deltahedral borane anions $[B_nH_n]^{2-}$.

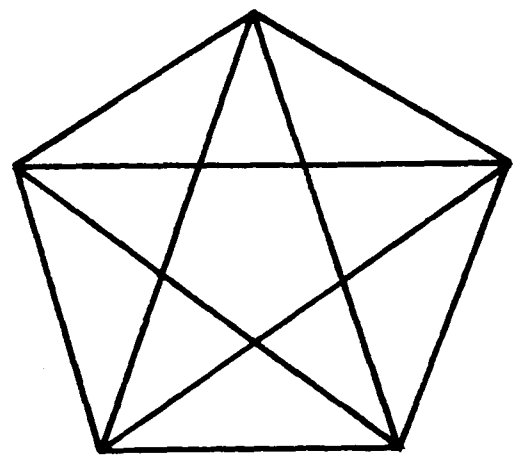
These functions are used to generate LCAO coefficients, yielding the cluster wavefunctions $\Psi^{\delta}_{L,M}$ (= L^{δ}_{M}) and $\bar{\Psi}^{\delta}_{L,M}$ (= $\bar{L}^{\delta}_{M}$) which are generally bonding and antibonding respectively.[143] Since the second derivatives of both S^{σ} and P^{σ} are zero, there are no S^{δ} or P^{δ} functions. By employing Scalar, Vector and Tensor Harmonics, Stone derived the (7n+1) cluster valence MO count for deltahedral transition metal clusters and later developed the model to provide an alternative derivation of Mingos' electron counting rules for condensed metal clusters.[143d]

The most serious drawback to Stone's elementary TSH theory is that all of the (2L+1) cluster MO's of a given L value are taken to be degenerate. For a real cluster, with non-spherical symmetry, the orbital degeneracies are generally lower than (2L+1). Fowler and Porterfield have circumvented this problem by introducing the Extended Hückel parameterisation of the Hamiltonian[64a,66] into the TSH framework, thus creating **Extended Tensor Surface Harmonic (ETSH) Theory.**[147] ETSH theory, which also takes quantitative account of σ-π mixing, leads to the correct orbital degeneracies under the actual point group symmetry of the cluster. The method has been applied to closo boranes in order to rationalise deviations from Wade's (n+1) SEP rule.[147] The analysis of Fowler and Porterfield, together with the earlier studies of Brint et al.,[146] has shown that the strength of TSH theory is that **"its pseudo-spherical symmetry labels give a language for the qualitative discussion of cluster bonding that may still be useful in interpreting more quantitative calculations".**

Several years before the formulation of Tensor Surface Harmonic Theory, King presented a graph theoretical treatment of bonding in borane clusters.[54a] It is instructive to compare this with Stone's

methodology.

King started by representing an n-atom <u>closo</u> cluster by the complete graph K_n, in which all the vertices are connected (for example, K_5 is shown in (<u>4</u>)).



K_5

(<u>4</u>)

By applying algebraic graph theoretical methods,[148] and considering the topology of the bonding interactions of the atomic σ- and π-symmetry orbitals, King derived the eigenvalue spectra of K_n for a set of n radial (σ) atomic orbitals. He showed that the nσ orbitals gave rise to one positive eigenvalue (bonding cluster MO) and (n-1) degenerate negative eigenvalues (antibonding cluster MO's). King also indicated that the 2nπ orbitals give rise to n degenerate bonding cluster MO's and n degenerate cluster antibonding MO's. Wade's (n+1) SEP rule was derived by assuming the occupation of all the bonding cluster MO's.[54a]

King's method (which he also used to derive electron counts for <u>nido</u> and <u>arachno</u> boranes and capped transition metal clusters)[54a] is essentially one step further from the real cluster geometry than TSH

theory. Representing a cluster by the complete graph K_n is equivalent to considering the cluster as hyperspherical (as (n-1) dimensions are required to make the interactions between n atoms equal). This explains why King's analysis leads to higher orbital degeneracies than those obtained from TSH theory.

Recently, Quinn et al. have developed a group theoretical formalism whereby symmetry adapted LCAO ligand functions are generated within the Tensor Surface Harmonic framework.[149] This methodology has been shown to be equally applicable to cluster compounds,[149] enabling the derivation of the L^{σ}, $L^{\pi}/\bar{L}^{\pi}$ and $L^{\delta}/\bar{L}^{\delta}$ orbitals by considering point group symmetries on the spherical shell. This approach also makes use of Mollweide projections (used in cartography)[150] to display the nodal characteristics of the Spherical Harmonics in two dimensions. Fowler has subsequently applied Quinn's group theoretical rules to the study of a variety of main group clusters.[151] A related approach has been used by Ceulemans, who has considered the local site-symmetry of the cluster vertex atoms, as well as the overall symmetry of the cluster.[152]

1.5 Perspective

The preceding sections of this Chapter have outlined the crucial stages in the development of cluster bonding theories. On the whole it has been the qualitative and semi-empirical approaches which have led to the elucidation of patterns and the establishment of bonding models. This is partly because such methods are fast and enable the rapid calculation of the electronic structures of a series of cluster compounds. The success of topological and group theoretical approaches, which concentrate on the cluster polyhedra without being too concerned

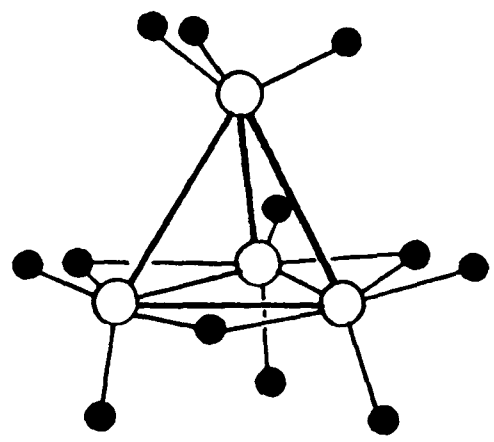
with the actual nature of the cluster atoms, has led to the realisation that most of the cluster structure-electron count correlations are symmetry and topology dependent. This explains the success of symmetry based semi-empirical approaches (such as the Extended Hückel method) in rationalising and predicting cluster geometries and valence electron counts.[153]

As the quantity of spectroscopic data on clusters has grown, however, more sophisticated calculational techniques have been employed in an attempt to reproduce experimental observables and in so doing to gain a more detailed understanding of the electronic structures of these molecules. The electronic structures of bare metal and ligated clusters have been investigated using the theoretical methodologies of solid state physics (e.g. chemical pseudopotential approaches[154a] and Xα methods)[125,154b] in addition to the more familiar (to the chemist) LCAO-MO methods of varying degrees of sophistication (e.g. ab-initio,[155] Fenske-Hall,[156] and CNDO[157]). A comprehensive review of spectroscopic and theoretical studies of transition metal cluster compounds has been published by Manning and Trogler.[158]

In recent years, a considerable amount of synthetic and theoretical attention has been focussed on extended metal-metal bonded systems in the solid state, inspired by the interesting physical properties which some of these compounds exhibit[15] and the wealth of structural data available.[13] Theoretical studies may be divided into those using essentially free electron models (notably by Andersen)[159] and the tight binding calculations favoured by Hoffmann, Burdett and co-workers.[160]

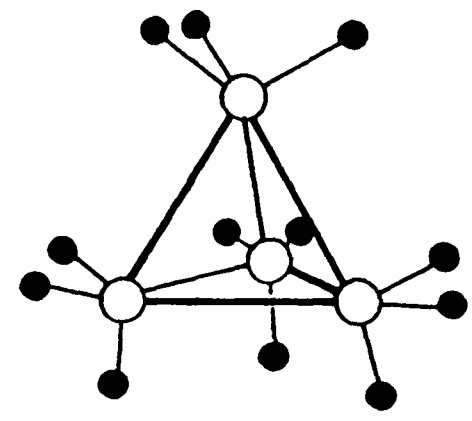
Although most theoretical treatments of transition metal cluster compounds have concentrated on metal skeletal geometry-electron count correlations, an additional (often more difficult) problem concerns the

alternative arrangements adopted by the ligands (especially carbonyl ligands) and ligand fluctionality. Dahl noted that the carbonyl ligands in the triangular cluster $[Fe_3(CO)_{12}]$ adopt an icosahedral arrangement and employed a hard sphere packing model to rationalise this fact.[161] Johnson and Benfield later developed a more elegant methodology for determining the most stable arrangements of ligands in clusters. In their treatment, the cluster and ligand polyhedra are matched in such a way that interligand repulsions are minimised and metal-ligand bonding is maximised.[162] Gillespie likewise analysed the problem in terms of the packing of carbonyl ligands around a cluster core[51] and similar arguments have subsequently been propounded by Keppert[163] and Mingos (who developed the concept of a Cluster Cone Angle in order to analyse steric interactions in gold phosphine clusters).[164] Lauher[165] and Keppert[166] have recently developed Surface Force Field Models for the Molecular Mechanics[167] simulation of ligand arrangements in metal carbonyl clusters. There has been considerable debate as to the relative importance of steric and electronic factors in determining ligand arrangements in clusters.[168] Evans has suggested that electronic features of the constituent ML_n fragments may be used to explain, for example, the different structures adopted by the ligands in the tetrahedral clusters $[Co_4(CO)_{12}]$ **(5)**[168] and $[Ir_4(CO)_{12}]$ **(6)**.[169]



$[Co_4(CO)_{12}]$

(5)



$[Ir_4(CO)_{12}]$

(6)

Minot has used a similar metal fragment approach to analyse the problem of terminal versus bridging coordination of carbonyl ligands.[170]

It is impossible to predict with confidence the ways in which cluster bonding theory will develop in the future, since the theoretical chemist is dependent on synthetic chemists, spectroscopists and crystallographers for raw data. As novel types of clusters are characterised our ideas, concerning the electronic structures of cluster molecules, have to be modified. The increasing availability of larger, faster (and cheaper!) computers should eventually enable the application of ab-initio calculational techniques to even the largest of clusters. Major advances could well be made in the area of rationalising and predicting physical properties of metal clusters (particularly in the solid state) in an effort to aid the synthetic chemist in his endeavour to develop new materials with tailor-made magnetic, conducting and catalytic properties.

The purpose of the work described in this Thesis is to determine, and rationalise, patterns and relationships in the bonding of seemingly disparate cluster molecules of the main group and transition metal elements. Stone's Tensor Surface Harmonic methodology has been used to provide an alternative (to group theory) symmetry labelling of the cluster MO's.[143] Further details of the TSH method are given in **Appendix I.** The Extended Hückel molecular orbital method has been used to determine the cluster MO's and their energies. Details of the Extended Hückel method, and the computer programs used for these calculations, are given in **Appendix II,** along with a brief discussion of the fundamental aspects of Molecular Orbital theory. In addition, group theoretical and topological arguments have been developed to rationalise

some of the successes and failures of the Polyhedral Skeletal Electron Pair approach and to provide general structure-electron count correlations.

References for Chapter One

1. (a) E.L. Muetterties, Chem. Eng. News, 30th. August, 1982, 28; (b) "Transition Metal Clusters", (Ed. B.F.G. Johnson) Wiley, New York, 1981 and references therein.

2. (a) W.N. Lipscomb, "Boron Hydrides", Benjamin, New York, 1963; (b) "Boron Hydride Chemistry" (Ed. E.L. Muetterties), Academic, New York, 1975 and references therein. (c) The first boranes were characterised by Stock and coworkers: A.Stock, "Hydrides of Boron and Silicon", Cornell University Press, Ithaca (New York), 1933 and references therein. (d) For reviews of the related metallaboranes and metallacarboranes see: "Metal Interactions with Boron Clusters", (Ed. R.N. Grimes), Plenum, New York, 1982; R.N. Grimes, Acc. Chem. Res., 1983, **16**, 22.

3. See, for example: E.A. Weilmuenster, Ind. Eng. Chem., 1957, **49**, 1340; D.R. Martin, J. Chem. Educ., 1959, **36**, 208.

4. J.D. Corbett, Prog. Inorg. Chem., 1976, **21**, 129; J.D. Corbett, Chem. Rev., 1985, **85**, 383; H.G. von Schnering, Angew. Chem. Int. Edn. Engl., 1981, **20**, 33 and references therein. For theoretical treatments of naked metal clusters see: C.H.E. Belin, J.D. Corbett and A. Cisar, J. Amer. Chem. Soc, 1977, **99**, 7163; L.L.Lohr, Inorg. Chem., 1981, **20**, 4229; R.C. Burns, R.J. Gillespie, J.A. Barnes and M.J. McGlinchey, Inorg. Chem., 1982, **21**, 799.

5. L.A. Paquette, Acc. Chem. Res., 1971, **4**, 280; T. Clark and M.A. McKervey, Comp. Organic Chem., 1979, **1**, 35; R.J. Ternansky, D.W. Balogh and L.A. Paquette, J. Amer. Chem. Soc., 1982, **104**, 4503 and references therein.

6. For recent reviews of catalytic processes which may involve

transition metal cluster compounds see: R. Whyman, in Ref. 1b, Ch.8 p.545; R. Whyman, Phil. Trans. R. Soc. Lond., 1982, **A308**, 131 and references therein.

7. B.F.G.Johnson and J. Lewis, Adv. Inorg. Chem. Radiochem., 1981, **24**, 225; B.F.G. Johnson and J. Lewis, Phil. Trans. R. Soc. Lond., 1982, **A308**, 5.

8. E.L. Muetterties, T.N. Rhodin, E. Band, C.F. Brucker and W.R. Pretzer, Chem. Rev., 1979, **29**, 91; E.L. Muetterties and R.M. Wexler, Survey Prog. Chem., 1983, **10**, 61.

9. G. Schmid, Struct. Bond., 1985, **62**, 51 and references therein.

10. D.M.P. Mingos and R.W.M. Wardle, Transition Met. Chem., 1985, **10**, 441 and references therein. See also: G. Longoni and P. Chini, J. Amer. Chem. Soc., 1976, **98**, 7225; D. Gregson, J.A.K. Howard, M. Murray and J.L. Spencer, J. Chem. Soc., Chem. Commun., 1981, 716; P.W. Frost, J.A.K. Howard, J.L. Spencer and D.G. Turner, J. Chem. Soc., Chem. Commun., 1981, 1104.

11. K.P. Hall and D.M.P. Mingos, Prog. Inorg. Chem., 1984, **32**, 237 and references therein.

12. H. Schäfer and H.G. von Schnering, Angew. Chem., 1964, **76**, 833; M.C. Baird, Prog. Inorg. Chem., 1968, **9**, 1; R.E. McCarley, Phil. Trans. R. Soc. Lond., 1982, **A308**, 141 and references therein.

13. A. Simon, Angew. Chem. Int. Edn. Engl., 1981, 14, 239; J.D. Corbett, Acc. Chem. Res., 1981, **14**, 239.

14. R. Chevrel, M. Sergent and J. Prigent, J. Solid State Chem., 1971, **3**, 515; R. Chevrel, P. Gougeon, M. Potel and M. Sergent, J. Solid State Chem., 1985, **57**, 25.

15. B.T. Matthias, M. Marezio, E. Corenzwit, A.S. Cooper and H.E. Barz, Science, 1972, **175**, 1465; O. Fischer, Appl. Phys., 1978, **16**, 1.

Topics in Current Physics: "Superconductivity in Ternary Compounds" (Eds. O. Fischer and M.B. Maple), Springer-Verlag, Berlin, 1982, 32.

16. C.D. Garner, in Ref. 1b, Ch. 4 p. 235 and references therein.

17. See, for example: B.T. Heaton, Phil. Trans. R. Soc. Lond., 1982, **A308**, 95; J.C. Green, E.A. Seddon and D.M.P. Mingos, J. Chem. Soc., Chem. Commun., 1979, 94.

18. P.R. Raithby, in Ref. 1b, Ch.2 p.5.

19. H. Heitler and F. London, Z. Phys., 1927, **44**, 455.

20. L. Pauling, "The Nature of the Chemical Bond" (3rd. Edn.), Cornell University Press, Ithaca (New York), 1960.

21. R.S. Mulliken, Phys. Rev., 1932, **41**, 49.

22. L. Pauling and E.B. Wilson, "Introduction to Quantum Mechanics", McGraw-Hill, New York, 1935 and references therein.

23. K. Wade, "Electron Deficient Compounds", Nelson, London, 1971.

24. H.C. Longuet-Higgins, J. Chim. Phys., 1949, **46**, 275.

25. H.C. Longuet-Higgins, J. Roy. Inst. Chem., 1953, **77**, 197.

26. G.H. Duffey, J. Chem. Phys., 1951, **19**, 963; 1952, **20**, 195; 1953, **21**, 761.

27. W.H. Eberhardt, B. Crawford Jr. and W.N. Lipscomb, J. Chem. Phys., 1954, 22, 989.

28. P. Torkington, J. Chem. Phys., 1951, **19**, 528.

29. J.E. Lennard-Jones, Proc. Roy. Soc. A, 1949, **198**, 1, 14.

30. J.A. Pople, Quart. Rev. Chem. Soc, 1957, **11**, 273.

31. E. Switkes, R.M. Stevens, W.N. Lipscomb and M.D. Newton, J. Chem. Phys., 1969, **51**, 2085; E. Switkes, W.N. Lipscomb and M.D. Newton, J. Amer. Chem. Soc., 1970, **92**, 3847; I.R. Epstein, J.A. Tossell,

J.E. Switkes, R.M. Stevens and W.N. Lipscomb, Inorg. Chem., 1971, **10**, 171; D.S. Marynick and W.N. Lipscomb, J. Amer. Chem. Soc., 1972, **94**, 1748; E.A. Laws, R.M. Stevens and W.N. Lipscomb, J. Amer. Chem. Soc., 1972, **94**, 4467.

32. S.F.A. Kettle and V. Tomlinson, J. Chem. Soc. (A), 1969, 2002.

33. S.F.A. Kettle and V. Tomlinson, J. Chem. Soc. (A), 1969, 2007.

34. (a) F.A. Cotton, Quart. Rev. Chem. Soc., 1966, **20**, 389 and references therein. (b) J. Lewis, Pure Appl. Chem., 1965, **10**, 11; P. Chini, Inorg. Chim. Acta. Rev., 1968, **2**, 31; E.W. Abel and F.G.A. Stone, Quart. Rev. Chem. Soc., 1969, **23**, 325.

35. P.A. Vaughan, Proc. Natl. Acad. Sci., 1950, **36**, 461.

36. J.C. Sheldon, J. Chem. Soc., 1960, 1007, 3106.

37. L.D. Crossman, D.P. Olsen and G.H. Duffey, J. Chem. Phys., 1963, **38**, 73.

38. F.A. Cotton and T.E. Haas, Inorg. Chem., 1964, **3**, 10.

39. S.F.A. Kettle, Theor. Chim. Acta., 1965, **3**, 211.

40. A. Simon, H.G. von Schnering and H. Wohrle, Z. Anorg. Allg. Chem., 1965, **339**, 155; A. Simon, H.G. von Schnering and H. Schäfer, Z. Anorg. Allg. Chem., 1968, **361**, 235.

41. S.F.A. Kettle, J. Chem. Soc. (A), 1966, 1013.

42. L.R. Maxwell, S.B. Hendricks and V.M. Mosley, J. Chem. Phys., 1935, **3**, 699.

43. S.F.A. Kettle, Theor. Chim. Acta., 1966, **4**, 150.

44. N.V. Sidgwick, "Electronic Theory and Valence", Clarendon Press, Oxford, 1927; D.P. Craig and G. Doggett, J. Chem. Soc., 1963, 4189; C.A. Tolman, Chem. Soc. Rev., 1972, **1**, 337.

45. N.V. Sidgwick and H.E. Powell, Proc. Roy. Soc. A, 1940, **176**, 153.

46. E.R. Corey, L.F. Dahl and W. Beck, J. Amer. Chem. Soc., 1963, **85**,

1202.

47. S.F.A. Kettle, J. Chem. Soc. (A), 1967, 314.

48. J.M. Schulman, C.R. Fischer, P. Solomon and T.J. Venanzi, J. Amer. Chem. Soc., 1978, **100**, 2949.

49. E. Heilbronner, T.B.Jones, A. Krebs, K.-D. Malsch, G. Maier, J. Pocklington and A. Schmelzer, J. Amer. Chem. Soc., 1980, **102**, 564.

50. D.M.P. Mingos, Nature Phys. Sci., 1972, **236**, 99.

51. R.J. Gillespie, Chem. Soc. Rev., 1979, **8**, 315 and references therein.

52. R.J. Gillespie and R.S. Nyholm, Quart. Rev. Chem. Soc., 1957, **11**, 339; R.J. Gillespie, "Molecular Geometry", Van Nostrand-Reinhold, Princeton (New Jersey), 1972.

53. M.J. McGlinchey and Y. Tal, "Chemical Applications of Topology and Graph Theory", Studies in Phys. and Theor. Chem., 1983, **28**, 124.

54. (a) R.B. King and D.H. Rouvray, J. Amer. Chem. Soc., 1977, **99**, 7834. (b) R.B. King, Inorg. Chim. Acta., 1981, **49**, 237; 1982, **57**, 79; 1986, **116**, 99, 109, 119, 125. (c) R.B. King, Polyhedron, 1982, **1**, 132.

55. R.B. King, J. Amer. Chem. Soc., 1969, **91**, 7211; 1970, **92**, 6455, 6460; 1972, **94**, 95.

56. B.K. Teo, Inorg. Chem., 1984, **23**, 1251; B.K. Teo, G. Longoni and F.R.K. Chung, Inorg. Chem., 1984, **23**, 1258.

57. M.E. O'Neill and K. Wade, Inorg. Chem., 1982, **21**, 461.

58. J.R. Pipal and R.N. Grimes, Inorg. Chem., 1979, **18**, 257.

59. J.R. Bowser, A. Bonny, J.R. Pipal and R.N. Grimes, J. Amer. Chem. Soc., 1979, **101**, 6229.

60. C.-H. Wei and L.F. Dahl, J. Amer. Chem. Soc., 1966, **88**, 1821; C.E.

Strouse and L.F. Dahl, Discuss. Faraday Soc., 1969, **47**, 93; D.L. Stevenson,C.-H. Wei and L.F. Dahl, J. Amer. Chem. Soc., 1971, **93**, 6027; C.E. Strouse and L.F. Dahl, J. Amer. Chem. Soc., 1971, **93**, 6032.

61. R.S. Mulliken, J. Chem. Phys., 1935, **3**, 375.

62. H.C. Longuet-Higgins, Quart. Rev. Chem. Soc., 1957, **11**, 121.

63. H.C. Longuet-Higgins and M. de V. Roberts, Proc. Roy. Soc. A, 1955, **230**, 110.

64. (a) R. Hoffmann and W.N. Lipscomb, J. Chem. Phys., 1962, **36**, 2179. (b) R. Hoffmann and W.N. Lipscomb, J. Chem. Phys., 1962, **36**, 3489; 1962, **37**, 2872.

65. R.S. Mulliken, J. Chem. Phys., 1955, **23**, 1833, 2343.

66. R. Hoffmann, J. Chem. Phys., 1963, **39**, 1397.

67. F. Klanberg and E.L. Muetterties, Inorg. Chem., 1966, **5**, 1955; D.R. Eaton, L.J. Guggenberger and E.L. Muetterties, Inorg. Chem., 1967, **6**, 1271; L.J. Guggenberger, Inorg. Chem., 1968, **7**, 2260; L.J. Guggenberger, Inorg. Chem., 1969, **8**, 2771.

68. D.A. Dixon, D.A. Kleier, T.A. Halgren, J.H. Hall and W.N. Lipscomb, J. Amer. Chem. Soc., 1977, **99**, 6226; M.J.S. Dewar and M.L. McKee, Inorg. Chem., 1978, **17**, 1569; 1980, **19**, 2662; M.F. Guest and I.H. Hillier, Mol. Phys., 1973, **26**, 435.

69. R.E. Williams, Prog. Boron Chem., 1970, **2**, 51.

70. R.E. Williams, Inorg. Chem., 1971, **10**, 210; R.E. Williams, Adv. Inorg. Chem. Radiochem., 1976, **18**, 67.

71. (a) K. Wade, J. Chem. Soc., Chem. Commun., 1971, 792. (b) See also: K. Wade, Adv. Inorg. Chem. Radiochem., 1976, **18**, 1; K. Wade, in Ref. 1b, Ch.3 p.193.

72. R.W. Rudolph and W.R. Pretzer, Inorg. Chem., 1972, **11**, 1974; R.W.

Rudolph, Acc. Chem. Res., 1976, **9**, 446.

73. M.R. Churchill, J. Wormwald, J. Knight and M.J. Mays, J. Chem. Soc., Chem. Commun., 1970, 458.

74. E.H. Braye, L.F. Dahl, W. Hubel and D.L. Wampler, J. Amer. Chem. Soc., 1962, **84**, 4633.

75. K. Wade, Inorg. Nucl. Chem. Lett., 1972, **8**, 559, 563, 823; K.Wade, Nature Phys. Sci., 1972, **240**, 71.

76. R. Mason, K.M. Thomas and D.M.P. Mingos, J. Amer. Chem. Soc., 1973, **95**, 3802.

77. J. Evans, J. Chem. Soc., Dalton Trans., 1978, 18, 35.

78. V. Albano, P. Chini and V. Scatturin, J. Chem. Soc., Chem. Commun., 1968, 163.

79. B.F.G. Johnson, R.D. Johnston and J. Lewis, J. Chem. Soc., Chem. Commun., 1967, 1057; R. Mason and W. Robinson, J. Chem. Soc., Chem. Commun., 1968, 468.

80. V. Albano, P.L. Bellon, P. Chini and V. Scatturin, J. Organomet. Chem., 1969, **16**, 461.

81. P.S. Braterman, Struct. Bond., 1972, **10**, 57.

82. D.M.P. Mingos, J. Chem. Soc., Dalton Trans., 1974, 133.

83. J.W. Lauher, J. Amer. Chem. Soc., 1978, **100**, 5305.

84. J. Halpern, Discuss. Faraday Soc., 1968, **46**, 7.

85. A.S. Foust, M.S. Foster and L.F. Dahl, J. Amer. Chem. Soc., 1969, **91**, 5631.

86. J.E. Ellis, J. Chem. Educ., 1976, **53**, 2.

87. W.R. Hertler, F. Klanberg and E.L. Muetterties, Inorg. Chem., 1967, **6**, 1696.

88. J.D. Corbett, Inorg.Chem., 1968, 7, 198.

89. (a) M. Elian and R. Hoffmann, Inorg. Chem., 1975, **14**, 1058. (b) M. Elian, M.M.L. Chen, D.M.P. Mingos and R. Hoffmann, Inorg. Chem., 1976, **15**, 1148.

90. R. Hoffmann, Nobel Lecture 1981, Science, 1981, **211**, 995; R. Hoffmann, Angew. Chem. Int. Edn. Engl., 1982, **21**, 711.

91. R.L. DeKock and T.P. Fehlner, Polyhedron, 1982, **1**, 521.

92. N.N. Greenwood, C.G. Savory, R.N. Grimes, L.G. Sneddon, A. Davison and S.S. Wreford, J. Chem. Soc., Chem. Commun., 1974, 718.

93. V.R.Miller, R. Weiss and R.N. Grimes, J. Amer. Chem. Soc., 1977, **99**, 5646.

94. R.P. Brint, K. Pelin and T.R. Spalding, Inorg. Nucl. Chem. Lett., 1980, **16**, 391; R.P. Brint and T.R. Spalding, J. Chem. Soc., Dalton Trans., 1980, 1236.

95. F.G.A. Stone, Angew. Chem. Int. Edn. Engl., 1984, **23**, 89 and references therein.

96. R.G. Woolley, Inorg. Chem., 1985, **24**, 3525.

97. R.G. Woolley, Nouv. J. Chim., 1981, **5**, 219, 227, 441; R.G. Woolley, in Ref. 1b, Ch.9 p.607; R.G. Woolley, Inorg. Chem., 1985, **24**, 3519.

98. J.N. Nicholls, Polyhedron, 1984, **3**, 1307; W.A. Herrmann, Angew. Chem. Int. Edn. Engl., 1986, **25**, 56 and references therein.

99. D.M.P. Mingos and M.I. Forsyth, J. Chem. Soc., Dalton Trans., 1977, 610.

100. V.G. Albano, P.L. Bellon and G.F. Ciani, J. Chem. Soc., Chem. Commun., 1969, 1024.

101. D.G. Evans and D.M.P. Mingos, Organometallics, 1983, **2**, 435.

102. R.J. Goudsmit, B.F.G. Johnson, J. Lewis, P.R. Raithby and K.H. Whitmire, J. Chem. Soc., Chem. Commun., 1982, 640.

103. M. McPartlin, C.R. Eady, B.F.G. Johnson and J. Lewis, J. Chem.

Soc., Chem. Commun., 1976, 883.

104. M. McPartlin, Polyhedron, 1984, **3**, 1279; M. McPartlin and D.M.P. Mingos, Polyhedron, 1984, **3**, 1321.

105. D.G. Evans and D.M.P. Mingos, J. Organomet. Chem., 1982, **240**, 321.

106. D.M.P. Mingos, J. Chem. Soc., Dalton Trans., 1977, 601.

107. D.M.P. Mingos, J. Chem. Soc., Dalton Trans., 1976, 1163.

108. R.S. Nyholm, Proc. Chem. Soc. Lond., 1961, 273; P. Pyykkö and J.-P. Desclaux, Acc. Chem. Res., 1979, **12**, 276.

109. G. van Koten and J.G. Noltes, in "Comprehensive Organometallic Chemistry" (Eds. G. Wilkinson, F.G.A. Stone and E. W. Abel), Pergamon, Oxford, 1982, Vol.2 p.709; J.G. Noltes, Phil. Trans. R. Soc. Lond., 1982, **A308**, 35. For a theoretical treat ment of bridged copper clusters see: P.K.Mehrotra and R. Hoffmann, Inorg. Chem., 1978, **17**, 2187.

110. See, for example: C.E. Briant, R.G. Smith and D.M.P. Mingos, J. Chem. Soc., Chem. Commun., 1984, 586.

111. D.G. Evans and D.M.P. Mingos, J. Organomet. Chem., 1982, **232**, 171; 1985, **295**, 389.

112. B.F.G. Johnson, D.A. Kaner, J. Lewis and P.R. Raithby, J. Organomet. Chem., 1981, **215**, C33; B.F.G. Johnson, D.A. Kaner, J. Lewis, P.R. Raithby and M.J. Taylor, J. Chem. Soc., Chem. Commun., 1982, 314; M. Green, A.G. Orpen, I.D. Salter and F.G.A. Stone, J. Chem. Soc., Chem. Commun., 1982, 813; H. Lehrer, D. Matt, P.S. Pregosin, L.M. Venanzi and A.Albinati, J. Amer. Chem. Soc., 1982, **104**, 6825.

113. D.M.P. Mingos, Pure Appl. Chem., 1980, **52**, 705.

114. C.E. Briant, B.R.C. Theobald, J.W. White, L.K. Bell, D.M.P. Mingos

and A.J. Welch, J. Chem. Soc., Chem. Commun., 1981, 201.

115. D.M.P. Mingos, Phil. Trans. R. Soc. Lond., 1982, **A308**, 75; K.P. Hall, D.I. Gilmour and D.M.P. Mingos, J. Organomet. Chem., 1984, **268**, 275; D.M.P. Mingos, Polyhedron, 1984, **3**, 1289.

116. D.M.P. Mingos, J. Chem. Soc., Chem. Commun., 1983, 706.

117. D.M.P. Mingos, Acc. Chem. Res., 1984, **17**, 311.

118. D.M.P. Mingos and D.G. Evans, J. Organomet. Chem., 1983, **251**, C13.

119. P. Chini, J. Organomet. Chem., 1980, **200**, 37.

120. J.W. Lauher, J. Amer. Chem. Soc., 1979, **101**, 2604.

121. G. Ciani and A. Sironi, J. Organomet. Chem., 1980, **197**, 233.

122. Yu. L.Slovokhotov and Yu. T. Struchkov, Russ. Chem. Rev., 1985, **54**, 323.

123. W. Hume-Rothery, "The Metallic State", Oxford University Press, New York, 1931, p.328.

124. B.K. Teo, J. Chem. Soc., Chem. Commun., 1983, 1362.

125. (a) R.P. Messmer, S.K. Knudson, K.H. Johnson, J.B. Diamond and C.Y. Yang, Phys. Rev. B: Solid State, 1976, **13**, 1396. (b) C.Y. Yang, K.H. Johnson, D.R. Salahub, J. Kaspar and R.P. Messmer, Phys. Rev. B: Solid State, 1981, **24**, 5673.

126. (a) D.M.P. Mingos, J. Chem. Soc., Chem. Commun., 1985, 1352. (b) D.M.P. Mingos, Chem. Soc. Rev., 1986, **15**, 31.

127. F.A. Vollenbroek, J.P. van der Berg, J.W.A. van der Velden and J.J. Bour, Inorg. Chem., 1980, **19**, 2685.

128. J.K. Burdett, Prog. Solid State Chem., 1985, **15**, 173.

129. D.M.P. Mingos, Anglo-Japanese Advanced Research Meeting: "Molecular Basis of Transition Metal Catalysis", April 1985, Abstracts, p.9.

130. E. Shustorovich, N.A.T.O. A.S.I. Ser., "Quantum Chemistry: The Challenge of Transition Metals and Coordination Chemistry" (Ed. A.

Veillard), Reidel, Dordrecht (NL), 1986, 445; E. Shustorovich, Surf. Sci. Rep., 1986, **6**, 1.

131. R.E. Benfield, P.P Edwards and A.M. Stacy, J. Chem. Soc., Chem. Commun., 1982, 525; R.E. Benfield, P.P. Edwards, W.J.H. Nelson and M.D. Vargas, D.C. Johnson and M.J. Sienko, Nature, 1985, **314**, 231; B.K. Teo, F.J. DiSalvo, J.V. Waszczak, G. Longoni and A. Ceriotti, Inorg. Chem., 1986, **25**, 2262.

132. R.E. Benfield, unpublished work, mentioned at the Dalton/A.C.S. meeting: "Clusters in the Solid State", Birmingham (U.K.), 1986.

133. G.C. Pimental and K.S. Pitzer, J. Chem. Phys., 1949, **17**, 882.

134. See, for example:R.L. DeKock and H.B. Gray, "Chemical Structure and Bonding", Benjamin/Cummings, Menlo Park (California), 1980, p.419.

135. N.S. Bayliss, J. Chem. Phys., 1948, **16**, 287; H. Kuhn, J. Chem. Phys., 1948,**16**, 840; J.R. Platt, J. Chem. Phys., 1954, 22, 1448; G.R. Wheland, "Resonance in Organic Chemistry", Wiley, New York, 1955.

136. C.-S. Lu and J. Donohue, J. Amer. Chem. Soc., 1944, **66**, 818.

137. D. Chapman and T.C. Waddington, Trans. Faraday Soc., 1962, **58**, 1679.

138. R. Hoffmann and M. Gouterman, J. Chem. Phys., 1962, **36**, 2189.

139. H.A. Bethe, Ann. Physik., 1929, **3**, 133; J.H. Van Vleck, J. Chem. Phys., 1935, **3**, 807; J.S. Griffith, "The Theory of Transition Metal Ions", Cambridge University Press, Cambridge, 1961; C.J. Ballhausen, "Ligand Field Theory", McGraw-Hill, New York, 1962.

140. T.C. Waddington, Trans. Faraday Soc., 1967, **63**, 1313.

141. D.K. Hoffmann, K. Ruedenberg and J.G. Verkade, Struct. Bond.,

1977, **33**, 57.

142. R.S. Mulliken, Rev. Mod. Phys., 1930, **2**, 60, 506; 1932, **4**, 40.

143. (a) A.J. Stone, Mol. Phys., 1980, **41**, 1339. (b) A.J. Stone, Inorg. Chem., 1981, **20**, 563. (c) A.J. Stone and M.J. Stone, Inorg. Chem., 1982, **21**, 2297. (d) A.J. Stone, Polyhedron, 1984, **3**, 2051.

144. D.M. Brink and G.R. Satchler, "Angular Momentum" (2nd. Edn.), Oxford University Press, Oxford, 1971.

145. E. Hückel, Z. Physik., 1931, **70**, 204; 1931, **72**, 310; 1932, **76**, 628.

146. P. Brint, J.P. Cronin and E. Seward, J. Chem. Soc., Dalton Trans., 1983, 675.

147. P.W. Fowler and W.W. Porterfield, Inorg. Chem., 1985, **24**, 3511.

148. N.L. Biggs, "Algebraic Graph Theory", Cambridge University Press, London, 1974.

149. D.B. Redmond, C.M. Quinn and J.G.R. McKiernan, J. Chem. Soc., Faraday Trans. II, 1983, **79**, 1791; Inorg. Chem., 1983, **22**, 2310; J. Chem. Educ., 1984, **61**, 569, 572.

150. P.W. McDonnell Jr., "Introduction to Map Making", Marcell Dekker, New York, 1979.

151. P.W. Fowler, Polyhedron, 1985, **4**, 2051; P.W. Fowler and J. Woolrich, Chem. Phys. Lett., 1986, **127**, 84.

152. A. Ceulemans, Mol. Phys., 1985, **54**, 161.

153. R. Hoffmann, B.E.R. Schilling, R. Bau, H.D. Kaesz and D.M.P. Mingos, J. Amer. Chem. Soc., 1978, **100**, 6088; B.E.R. Schilling and R. Hoffmann, J. Amer. Chem. Soc., 1979, **101**, 3456.

154. (a) D.W. Bullett, Phys. Rev. Lett., 1977, **39**, 664; K.W. Chang and R.G. Woolley, J. Phys. C, 1979, **12**, 2745. (b) G. Seifert, E. Mrosan and H. Müller, Phys. Status Solidi B, 1978, **89**, 553; F.A. Cotton and G.G. Stanley, Chem. Phys. Lett., 1978, **58**, 450; K.H. Johnson,

Crit. Rev. Solid State Mater. Sci., 1978, **7**, 101; R.P. Messmer, Surf. Sci., 1981, **106**, 225; D.A. Case, Annu. Rev. Phys. Chem., 1982, **33**, 151.

155. J. Demuynck, M.-M. Rohmer, A. Strich and A. Veillard, J. Chem. Phys., 1981, **75**, 3443.

156. M.B. Hall and R.F. Fenske, Inorg. Chem., 1972, **11**, 768; B.K. Teo, M.B. Hall, R.F. Fenske and L.F. Dahl, J. Organomet. Chem., 1974, **70**, 413; P.T. Cheskey and M.B. Hall, Inorg. Chem., 1981, **20**, 4419; D.E. Sherwood Jr. and M.B. Hall, Inorg. Chem., 1982, **21**, 3458; D.E. Sherwood Jr. and M.B. Hall, Organometallics, 1982, **1**, 1519.

157. See, for example: D.V. Korol'kov and H. Miessner, Z. Phys. Chem., 1973, **253**, 25.

158. M.C. Manning and W.C. Trogler, Coord. Chem. rev., 1981, **38**, 89.

159. O.K. Andersen and R.G. Woolley, Mol. Phys., 1973, **26**, 905; O.K. Andersen, Phys. Rev. B: Solid State, 1975, **12**, 3060; O.K. Andersen, W. Klose and H. Nohl, Phys. Rev. B: Solid State, 1978, **17**, 1209.

160. See, for example:T.A. Albright, J.K. Burdett and M.-H. Whangbo, "Orbital Interactions in Chemistry", Wiley, New York, 1984, Ch.13 p.229; R. Hoffmann and C. Zheng, N.A.T.O. A.S.I. Ser., "Quantum Chemistry: The Challenge of Transition Metals and Coordination Chemistry" (Ed. A. Veillard), Reidel, Dordrecht (NL), 1986, p.425; J.K. Burdett, E. Canadell and T. Hughbanks, J. Amer. Chem. Soc., 1986, **108**, 3971; J.K. Burdett, Struct. Bond., in press and references therein.

161. C.-H. Wei and L.F. Dahl, J. Amer. Chem. Soc., 1969, **91**, 1351.

162. R.E. Benfield and B.F.G. Johnson, Top. Stereochem., 1981, **12**, 253 and references therein.

163. D.L. Keppert and S.C. Williams, J. Organomet. Chem., 1981, **217**, 235.

164. D.M.P. Mingos, Inorg. Chem., 1982, **21**, 464.

165. J.W. Lauher, J. Amer. Chem. Soc., 1986, **108**, 1521.

166. D.L. Keppert, in "Advances in Dynamic Stereochemistry" (Ed. M.F. Gielen), Freund, London, 1985, Vol.1.

167. U. Berkert and N.L. Allinger, "Molecular Mechanics", American Chemical Society, Washington, 1982.

168. D.G. Evans, D.Phil. Thesis, University of Oxford, 1984 and references therein.

169. D.G. Evans, J. Chem. Soc., Chem. Commun., 1983, 675.

170. C. Minot and M. Criado-Sancho, Nouv. J. Chim., 1984, **8**, 537.

CHAPTER TWO

GENERAL THEORETICAL ANALYSIS OF THE BONDING IN THREE- AND FOUR-CONNECTED POLYHEDRAL CLUSTERS

2.1 Introduction

Stone's Tensor Surface Harmonic approach accounts, in a very general way, for the (4n+2) electron rule for main group deltahedral (triangular-faced) clusters ((14n+2) for the corresponding transition metal compounds).[1] Deltahedral geometries are preferred for these "electron deficient" molecules, because they maximise the number of nearest neighbour bonding interactions. The (n+1) skeletal bonding MO's associated with these "pseudo-spherical" molecules comprise 4 predominantly radial MO's; $S^{\sigma}_{sp} + 3(P^{\sigma}_{sp}+P^{\pi}_{p})$, and (n-3) tangential L^{π}_{p} (L>1) MO's.[1,2]

There are, however, a large number of cluster compounds, of the main group and transition metal elements, which have approximately spherical topologies, but are not deltahedral. The purpose of this Chapter is to analyse, within the Tensor Surface Harmonic framework, the bonding in two types of non-deltahedral molecules, namely **3-connected** and **4-connected polyhedral clusters,** where all of the cluster vertices have either 3 or 4 nearest neighbours respectively. The skeletal MO patterns for these polyhedral types are compared with those of the deltahedra and localised bonding arguments are presented to account for these patterns.

2.2 Three-Connected Polyhedral Clusters

2.2.1 Geometric and electronic features of 3-connected clusters

The number of vertices (V), faces (F) and edges (E) of any convex polyhedron are related by Euler's formula:[3]

$$V + F = E + 2$$

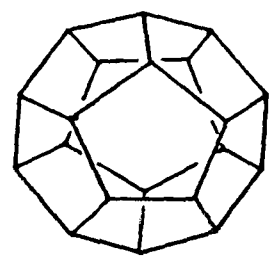
The constraint that each vertex be 3-connected leads to the following relationships (the subscript 3 indicates that the vertex, edge or face belongs to a 3-connected polyhedron):

$$F_3 = (V_3/2)+2$$

$$E_3 = 3V_3/2 = 3(F_3-2)$$

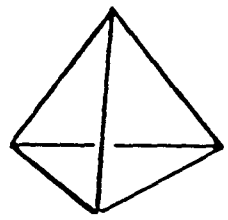
Since the connectivity of all its vertices is odd, a 3-connected polyhedron must possess an even number of vertices. Examples of 3-connected polyhedra are shown in **Figure 2.1**

The archetypal 3-connected main group clusters are the polyhedral alicyclic compounds $[C_nH_n]$,[4] of which dodecahedrane, $[C_{20}H_{20}]$ **(I)**, is probably the most aesthetically pleasing (Paquette has described it as the "Mount Everest of alicyclic chemistry").[4g].

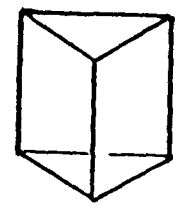


$[C_{20}H_{20}]$ dodecahedrane

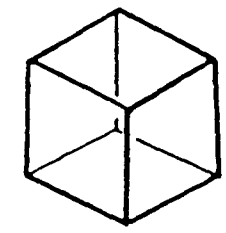
(I)



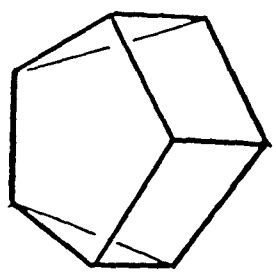
tetrahedron



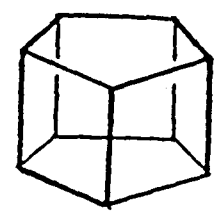
trigonal prism



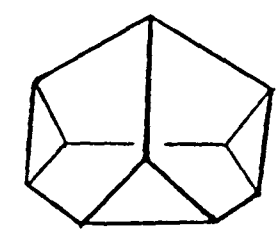
cube



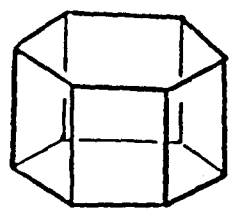
bi-truncated tetrahedron ("cuneane")



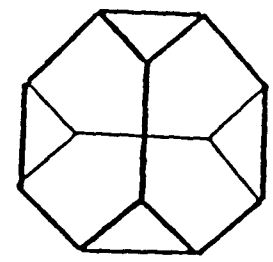
pentagonal prism



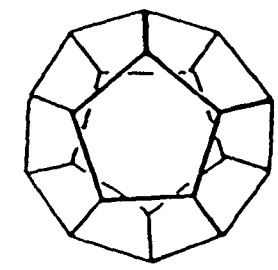
tri-truncated tetrahedron ("diademane")



hexagonal prism



(tetra-) truncated tetrahedron



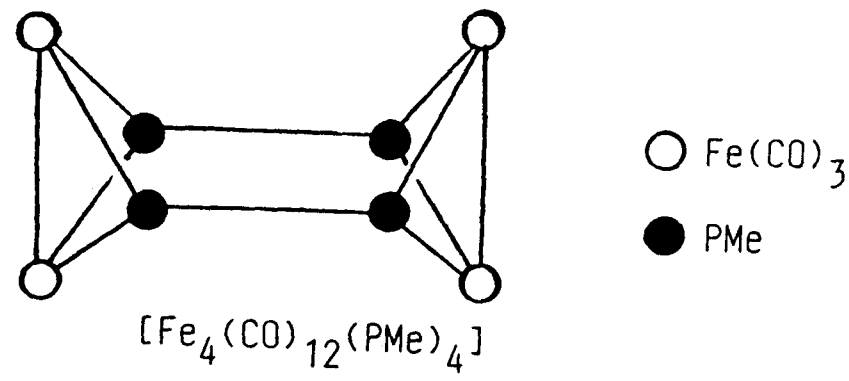
(pentagonal) dodecahedron

Figure 2.1 Examples of 3-connected polyhedra.

The bonding in these 3-connected cluster molecules may be conveniently described in terms of 2-centre-2-electron (2c-2e) bonds which are localised on the edges of the polyhedron.[5] If sp^3 hybridisation of the carbon atoms is assumed, each CH fragment contributes 3 orbitals and 3 electrons for cluster bonding, which is consistent with the formation of 3 localised σ-bonds. Clusters of this type are, therefore, referred to as "electron precise".[6] In terms of the Polyhedral Skeletal Electron Pair approach,[7] a 3-connected hydrocarbon cluster $[C_nH_n]$ is characterised by 3n/2 skeletal electron pairs (one for each of the $3V_3/2$ edges, $n = V_3$) and a total cluster valence electron count of 5n (since there are 2n electrons in the n C-H bonding orbitals).

Apart from these polyhedral alicyclic hydrocarbons, main group 3-connected clusters with 5n electrons are limited to tetrahedral molecules such as $[P_4]$, $[As_4]$ and $[Si_4]^{4-}$.[8] Many transition metal carbonyl clusters with 3-connected skeletal geometries (usually tetrahedral or trigonal prismatic) are known. These clusters possess 15n valence electrons, i.e. 10n electrons more than their main group analogues, due to the effective occupation of the five d orbitals on each metal atom.[7] 3-connected transition metal clusters generally have carbonyl, sulphido, phosphido or related ligands bridging edges or faces of the cluster.[9] There are a number of compounds in which both main group and transition metal atoms go to make up a 3-connected cluster framework. These clusters are characterised by $(15n_1+5n_2)$ valence electrons,[7] where n_1 is the number of transition metal atoms and n_2 is the number of main group atoms in the cluster skeleton. This type of cluster includes some 3-connected polyhedral geometries which have not yet been observed for $[C_nH_n]$ molecules. For example, the structure of

$[Fe_4(CO)_{12}(PMe)_4]$ **(II)**[10] corresponds to the, as yet unknown, octabisvalene isomer of $[C_8H_8]$.



$[Fe_4(CO)_{12}(PMe)_4]$

(II)

Examples of electron precise main group, transition metal and mixed main group/transition metal clusters are listed in **Table 2.1**

The relationship between the electron counts for main group and transition metal 3-connected clusters may be rationalised in terms of the <u>isolobal</u> analogy.[11] The <u>isolobal</u> relationship between $Ir(CO)_3$ and CH, for example, explains the tetrahedral geometry of the cluster $[Ir_4(CO)_{12}]$.[12] In **(II)**, the following <u>isolobal</u> relationships pertain:

$$Fe(CO)_3 \longleftrightarrow_{\sigma} CH^+$$

$$PMe \longleftrightarrow_{\sigma} CH^-$$

(i.e. the conical $Fe(CO)_3$ fragment, like CH^+, contributes 3 orbitals ($1\sigma + 2\pi$) and 2 electrons for cluster bonding, while the PMe fragment contributes 3 orbitals and 4 electrons). Similar <u>isolobal</u> relationships may be used to rationalise the 3-connected polyhedral geometries of main group aggregates such as the series of $[(AlH)(NR)]_x$ compounds, which have alternating aluminium and nitrogen framework atoms.[13] The AlH and

Table 2.1 Examples of 3-connected polyhedral clusters

No. of vertex atoms (n)	Geometry	Example	Valence electron count	Ref.
(a) Main group examples (5n electrons)				
4	Tetrahedron	$[C_4(^tBu)_4]$	20	4a
		$[P_4]$, $[Si_4]^{4-}$, $[Sn_2Bi_2]^{2-}$	20	8
6	Trigonal prism*	$[C_6H_6]$ (prismane)	30	4b
8	Cube	$[C_8H_8]$ (cubane)	40	4c
8	Cuneane*	$[C_8H_8]$ (cuneane)	40	4d
10	Pentagonal prism	$[C_{10}H_{10}]$ (pentaprismane)	50	4e
10	Diademane*	$[C_{10}H_{10}]$ (diademane)	50	4f
20	Dodecahedron	$[C_{20}H_{20}]$ (dodecahedrane)	100	4g
(b) Transition metal examples (15n electrons)				
4	Tetrahedron	$[Ir_4(CO)_{12}]$	60	11
6	Trigonal prism	$[Rh_6C(CO)_{15}]^{2-}$	90	**a**
8	Cube	$[Ni_8(PPh)_6(CO)_8]$	120	**b**
8	Cuneane	$[Co_8S_2(NBu^t)_4(NO)_8]$	120	**c**
(c) Mixed main group/transition metal examples ($15n_1+5n_2$ electrons, $n=n_1+n_2$)**				
4 (n_1=3, n_2=1)	Tetrahedron	$[Co_3(CO)_9CMe]$	50	**d**
4 (n_1=2, n_2=2)	Tetrahedron	$[Cp_2W_2(CO)_4C_2R_2]$	40	**e**
8 (n_1=4, n_2=4)	Cube	$[Fe_4(CO)_{12}As_4Me_4]$	80	**f**
8 (n_1=4, n_2=2)	Octabisvalene	$[Fe_4(CO)_{12}P_4Me_4]$	80	10

* The trigonal prismatic, cuneane and diademane geometries are topologically equivalent to mono-, bi- and tri-truncated tetrahedra respectively. Trishomobenzene, the tetra-truncated tetrahedral isomer of $[C_{12}H_{12}]$, has not been synthesised to date.

** n_1 = no. of transition metal atoms, n_2 = no. of main group atoms

a V.G. Albano, D. Braga and S. Martinengo, J. Chem. Soc., Dalton Trans., 1981, 717. **b** L.D. Lower and L.F. Dahl, J. Amer. Chem. Soc., 1976, **98**, 5046. **c** C.T.W. Chu, PhD thesis, Univ. Wisconsin (Madison), 1977. **d** P.W. Sutton and L.F. Dahl, J. Amer. Chem. Soc., 1967, **89**, 261. **e** D.S. Ginley, C.R. Bock, M.S. Wrighton, B. Fischer, D.L. Tipton and R. Bau, J. Organomet. Chem., 1978, **157**, 41. **f** E. Röttinger and H. Vahrenkamp, J. Organomet. Chem., 1981, **213**, 1.

NR fragments are isolobal with CH^+ and CH^- respectively.

Although the bonding in 3-connected cluster molecules has been described in localised terms,[5] it is instructive to contrast the general bonding features of deltahedral and 3-connected polyhedral clusters within the same delocalised molecular orbital framework.

2.2.2 Delocalised treatment of the skeletal bonding in 3-connected clusters

By inspecting the results of ab initio and semi-empirical molecular orbital calculations on the molecules $[C_nH_n]$,[14] it was observed that 3-connected "spherical" polyhedra have $\{(n/2)+2\}$ skeletal MO's, which are quite strongly bonding, and (n-2) which are effectively non-bonding (or very weakly bonding). This results in a total of 3n/2 SEP's. Extended Hückel calculations were performed on a number of these hydrocarbon molecules, in order to test the validity of this observation for a set of consistent calculations and to assign TSH spherical symmetry labels to the skeletal MO's. Details of the orbital parameters and bond lengths used in these calculations are listed in the **Appendix** to this Chapter (**Section 2.5**).

The results of the Extended Hückel calculations are presented in **Table 2.2.** These confirm the presence of $\{(n/2)+2\}$ skeletal bonding MO's, which may be divided into 4 strongly bonding, predominantly radial, orbitals (S^{σ} + $3P^{\sigma+\pi}$) and $\{(n/2)-2\}$ slightly less bonding tangential (surface) L_p^{π} orbitals. In addition there are (n-2) non-bonding skeletal MO's, of which half $\{(n/2)-1\}$ are L_p^{π} and half are $\bar{L}_p^{\pi}$ tangential orbitals (from this point the p subscript will be dropped as it is implicit in the L^{π} and $\bar{L}^{\pi}$ orbitals of the main group clusters).

Table 2.2 TSH labels and energies of the skeletal MO's of some 3-connected $[C_nH_n]$ molecules, calculated by the Extended Hückel method[a]

$[C_4H_4]$ (T_d)

Orbital(s)	Energy (eV)
$\bar{P}^{\pi}(t_1)$	-4.33
$D_0^{\pi}/\bar{D}_0(e)$	-11.95
$P^{\sigma}(t_2)$	-14.33[b]
$S^{\sigma}(a_1)$	-29.53

$[C_{10}H_{10}]$ (D_{5h})

$\bar{P}^{\pi}_{\pm1}(e_1'')$	-2.10
$\bar{F}^{\pi}_{\pm2}(e_2')$	-11.79
$F^{\pi}_{\pm2}(e_2'')$	-12.50
$D^{\pi}_{\pm1}(e_1'')$	-12.88
$\bar{D}^{\pi}_{\pm1}(e_1')$	-13.12
$D^{\pi}_{\pm2}(e_2')$	-14.81
$D_0^{\pi}(a_1')$	-15.13
$P_0^{\sigma}(a_2'')$	-15.24
$P^{\sigma}_{\pm1}(e_1')$	-15.62
$S^{\sigma}(a_1')$	-31.12

$[C_{20}H_{20}]$ (I_h)[c]

$\bar{P}^{\pi}(t_{1g})$	-1.36
$\bar{F}^{\pi}(g_g)$	-12.64
$\bar{G}^{\pi}(h_u)$	-12.88
$G^{\pi}(h_g)$	-13.28
$F^{\pi}(g_u)$	-13.28
$F^{\pi}(t_{2u})$	-14.35
$D^{\pi}(h_g)$	-15.33
$P^{\sigma}(t_{1u})$	-16.38
$S^{\sigma}(a_{1g})$	-31.22

$[C_6H_6]$ (D_{3h})

$\bar{D}_0^{\pi}(a_1'')$	-1.95
$\bar{P}_0^{\pi}(a_2')$	-6.15
$D^{\pi}_{\pm1}(e'')$	-11.74
$\bar{D}^{\pi}_{\pm1}(e')$	-12.93
$P^{\sigma}_{\pm1}(e')$	-14.74
$P_0^{\sigma}(a_2'')$	-14.77
$D_0^{\pi}(a_1')$	-14.78
$S^{\sigma}(a_1')$	-30.47

$[C_{12}H_{12}]$ (D_{6h})

$\bar{P}^{\pi}_{\pm1}(e_{1g})$	-1.52
$F^{\pi}_{3c}(b_{2u})$	-11.12
$\bar{F}^{\pi}_{\pm2}(e_{2g})$	-11.89
$F^{\pi}_{\pm2}(e_{2u})$	-12.25
$\bar{F}^{\pi}_{3c}(b_{2g})$	-12.94
$D^{\pi}_{\pm1}(e_{1g})$	-13.59
$\bar{D}^{\pi}_{\pm1}(e_{1u})$	-13.68
$D^{\pi}_{\pm2}(e_{2g})$	-14.66
$D_0^{\pi}(a_{1g})$	-15.07
$P_0^{\sigma}(a_{2u})$	-15.21
$F^{\pi}_{3s}(b_{1u})$	-15.25
$P^{\sigma}_{\pm1}(e_{1u})$	-16.01
$S^{\sigma}(a_{1g})$	-31.07

$[C_8H_8]$ (O_h)

$\bar{D}^{\pi}_{0,2s}(e_u)$	+2.79
$\bar{P}^{\pi}(t_{1g})$	-1.67
$D^{\pi}_{\pm1,2c}(t_{2g})$	-12.05
$\bar{D}^{\pi}_{\pm1,2c}(t_{2u})$	-12.61
$D^{\pi}_{0,2s}(e_g)$	-15.10
$P^{\sigma}(t_{1u})$	-15.14
$S^{\sigma}(a_{1g})$	-31.05

$[C_{12}H_{12}]$ (T_d)[c]

$\bar{P}^{\pi}(t_1)$	-4.58
$\bar{D}^{\pi}_{\pm1}(e)$	-11.80
$F^{\pi}(t_1)$	-12.70
$\bar{F}^{\pi}(t_2)$	-13.78[d]
$D^{\pi}_{\pm1}(e)$	-13.99
$D^{\pi}_{0,\pm2}(t_2)$	-14.25[d]
$F_0^{\pi}(a_1)$	-14.93
$P^{\sigma}(t_2)$	-15.86
$S^{\sigma}(a_1)$	-30.56

a For the parameters used in these Extended Hückel calculations see the **Appendix.** The non-bonding level for C 2p-based orbitals corresponds to an energy of -11.4 eV. The non-bonding L^{π} and $\bar{L}^{\pi}$ orbitals are grouped together in boxes. All M quantum numbers are defined relative to the highest C_n rotation axis of the cluster, with the exception of $[C_4H_4]$, where the orbitals are defined relative to a C_2 axis.

b The orbitals denoted P^{σ}, for convenience, are actually $P^{\sigma+\pi}$.

c In cubic (O, O_h, T and T_d) and icosahedral (I and I_h) point groups, due to the high orbital degeneracies, the (normal) General Spherical Harmonics cannot be used for L>2. Instead Cubic and Icosahedral Harmonics, which may be constructed by taking linear combinations of some of the General Harmonics, are used for defining the F, G, H etc. orbitals.

d There is extensive mixing between $D^{\pi}(t_2)$ and $\bar{F}^{\pi}(t_2)$ in this geometry.

The skeletal MO patterns for deltahedral and 3-connected polyhedral clusters are contrasted in **Figure 2.2.** Clearly the deltahedra provide the minimum number of SEP's, and the 3-connected polyhedra the maximum number, consistent with an approximately spherical cluster topology. The deltahedra, therefore, maximise the degree of delocalisation, and the 3-connected polyhedra maximise the extent of localisation, of the SEP's.

The major difference between the two classes of cluster arises from differences of the bonding properties of the L^{π} and $\bar{L}^{\pi}$ surface tangential MO's in the two cases. For illustrative purposes, the bonding $D^{\pi}(t_{2g})$ MO's of an octahedron and their antibonding $\bar{D}^{\pi}(t_{2u})$ counterparts are depicted in **Figure 2.3a,** along with the $D^{\pi}(a_1'+e'')$ and $\bar{D}^{\pi}(a_1''+e')$ MO's of the trigonal prism. In this specific example, rotation of the bottom triangle, so as to eclipse the top triangle of atoms, results in the stabilisation of the e' components of $\bar{D}^{\pi}$ ($\bar{D}^{\pi}_{1s,1c}$) and the destabilisation of the e'' components of D^{π} ($D^{\pi}_{1s,1c}$), as shown in **Figure 2.3b.** These 4 orbitals constitute the (n-2) non-bonding MO's of the trigonal prismatic cluster. Also apparent from **Figure 2.3b** is the fact that the $D^{\pi}_0(a_1')$ and $\bar{D}^{\pi}_0(a_1'')$ orbitals are more strongly bonding and antibonding respectively for the trigonal prism than the octahedron. This splitting of the frontier bonding L^{π} and antibonding $\bar{L}^{\pi}$ orbitals into 3 sets of MO's (one set more strongly bonding, one more strongly antibonding and one non-bonding) is a characteristic feature of the transition from deltahedral to 3-connected polyhedra.

The symmetries and TSH labels for a number of 3-connected polyhedral clusters are listed in **Table 2.3.** In this Table, and in the following discussion, the label $L_{\pm M}$ is used as an abbreviation for $L_{Ms,Mc}$, where these orbitals are degenerate, since linear combinations of the complex (L_{+M} and L_{-M}) functions may be taken to generate the real

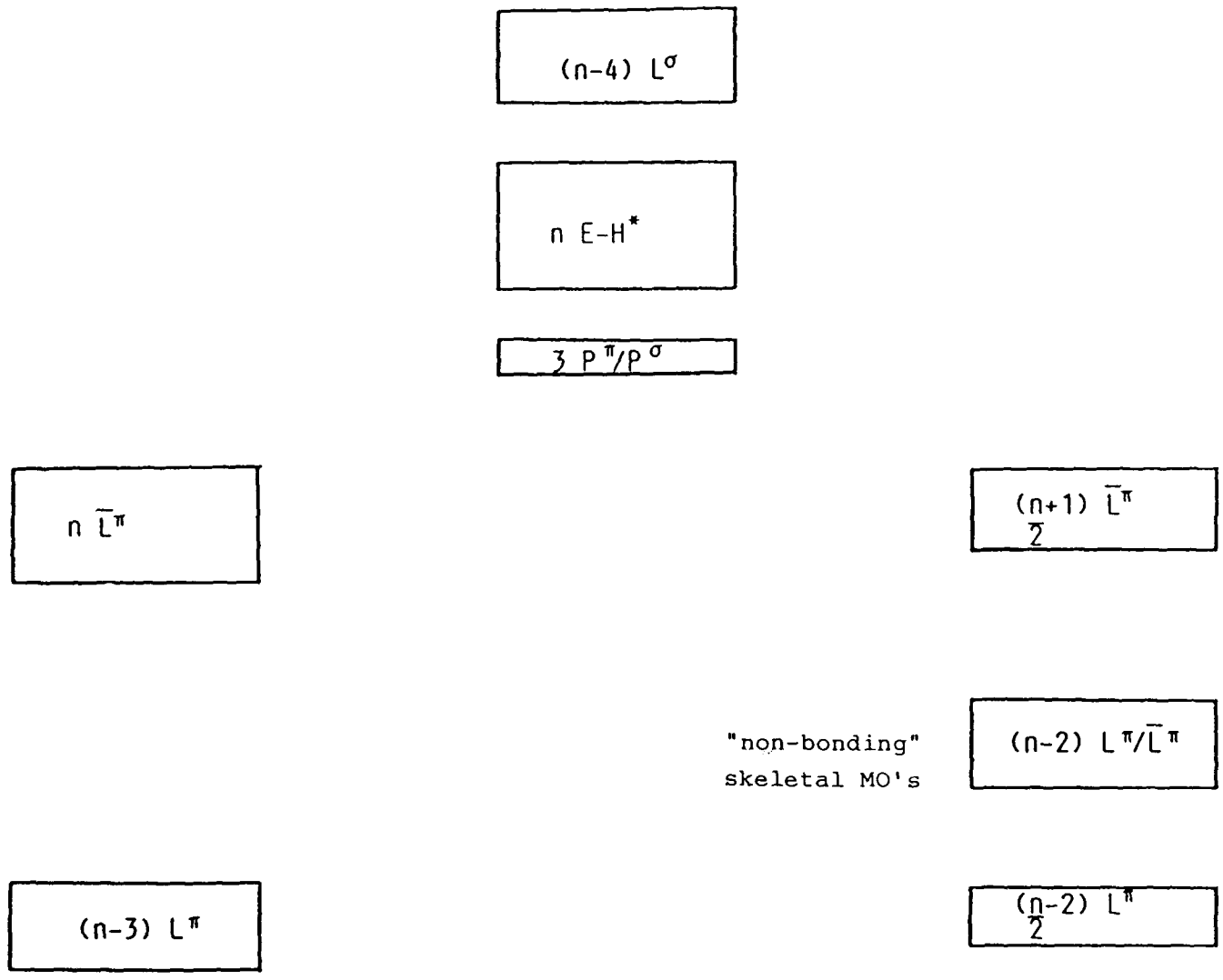


Figure 2.2 A schematic representation of the skeletal MO patterns of deltahedral and 3-connected $[E_nH_n]$ molecules (where E is a main group atom).

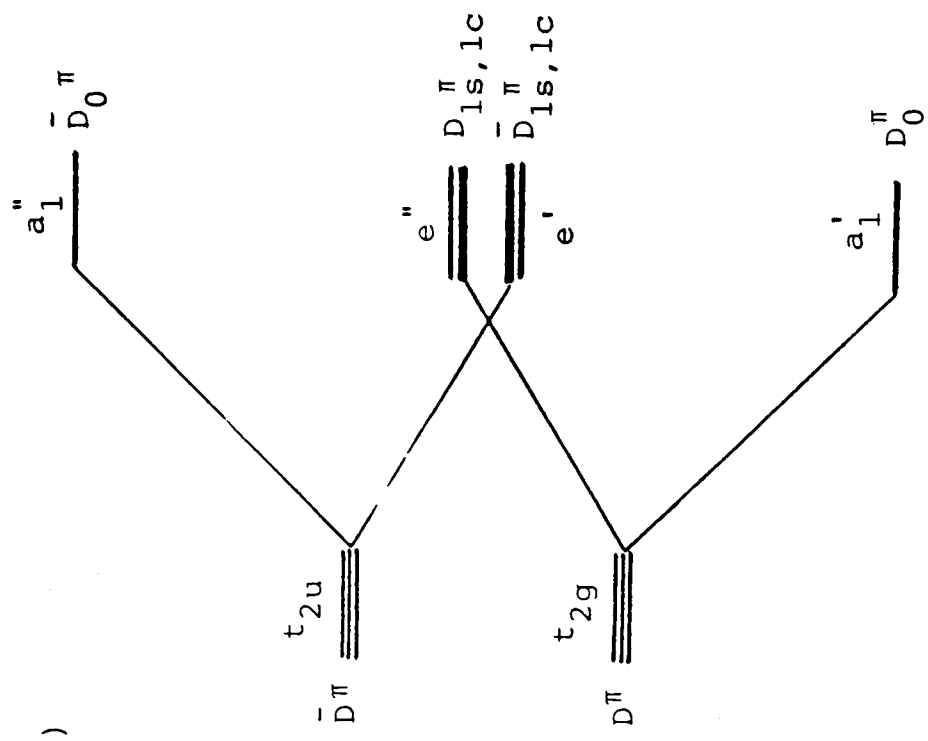


Figure 2.3 Comparison of the D^{π} and $\bar{D}^{\pi}$ skeletal MO's, and their relative energies, of octahedral and trigonal prismatic $[C_6H_6]$.

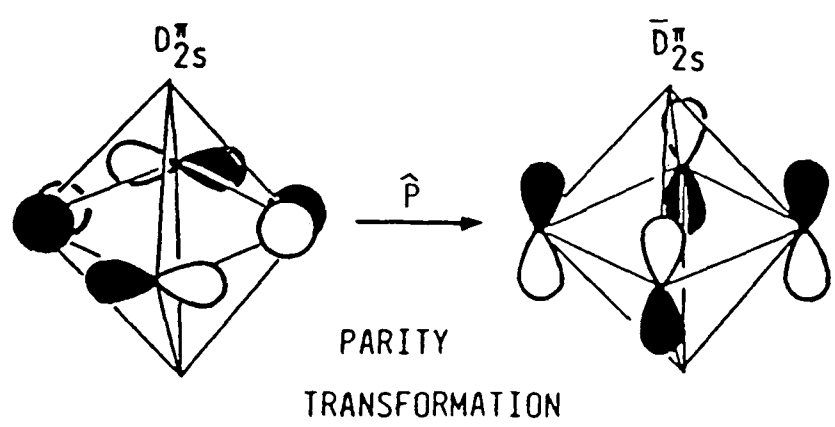
Table 2.3 Bonding and non-bonding skeletal MO's* of some 3-connected polyhedral clusters $[C_nH_n]$

n	Bonding skeletal MO's	Non-bonding skeletal MO's
4 (T_d)	$S^{\sigma}(a_1)$, $P^{\sigma}(t_2)$**	$D_0^{\pi}/\bar{D}_0^{\pi}(e)$
6 (D_{3h})	$S^{\sigma}(a_1')$, $P^{\sigma}(a_2''+e')$, $D_0^{\pi}(a_1')$	$D_{\pm1}^{\pi}(e'')$, $\bar{D}_{\pm1}^{\pi}(e')$
8 (O_h)	$S^{\sigma}(a_{1g})$, $P^{\sigma}(t_{1u})$, $D_{0,2s}^{\pi}(e_g)$	$D_{\pm1,2c}^{\pi}(t_{2g})$, $\bar{D}_{\pm1,2c}^{\pi}(t_{2u})$
10 (D_{5h})	$S^{\sigma}(a_1')$, $P^{\sigma}(a_2''+e_1')$, $D_0^{\pi}(a_1')$, $D_{\pm2}^{\pi}(e_2')$	$D_{\pm1}^{\pi}(e_1'')$, $F_{\pm2}^{\pi}(e_2'')$, $\bar{D}_{\pm1}^{\pi}(e_1')$, $\bar{F}_{\pm2}^{\pi}(e_2'')$
12 (D_{6h})	$S^{\sigma}(a_{1g})$, $P^{\sigma}(a_{2u}+e_{1u})$, $D_0^{\pi}(a_{1g})$, $D_{\pm2}^{\pi}(e_{2g})$, $F_{3s}^{\pi}(b_{1u})$	$D_{\pm1}^{\pi}(e_{1g})$, $F_{\pm2}^{\pi}(e_{2u})$, F_{3c}^{π}(t $\bar{D}_{\pm1}^{\pi}(e_{1u})$, $\bar{F}_{\pm2}^{\pi}(e_{2g})$, $\bar{F}_{3c}^{\pi}$(t
12 (T_d)	$S^{\sigma}(a_1)$, $P^{\sigma}(t_2)$, $D_{0,\pm2}^{\pi}(t_2)$, $F_0^{\pi}(a_1)$	$D_{\pm1}^{\pi}(e)$, $F^{\pi}(t_1)$ $\bar{D}_{\pm1}^{\pi}(e)$, $\bar{F}^{\pi}(t_2)$
20 (I_h)	$S^{\sigma}(a_g)$, $P^{\sigma}(t_{1u})$, $D^{\pi}(h_g)$, $F^{\pi}(t_{2u})$	$F^{\pi}(g_u)$, $G^{\pi}(h_g)$, $\bar{F}^{\pi}(g_g)$, $\bar{G}^{\pi}(h_u)$

* The TSH labels refer to the case where the polar axis is the principal rotation axis, with the exception of the tetrahedron (n=4), where the orbitals are labelled relative to the C_2 axis.

** The orbitals labelled P^{σ}(for convenience) are actually $P^{\sigma+\pi}$.

(L_{Ms} and L_{Mc}) orbitals.[1] In all of the 3-connected examples studied, the $\{(n/2)-1\}$ L^{π} and $\{(n/2)-1\}$ $\bar{L}^{\pi}$ non-bonding skeletal MO's are related by the **Parity Transformation** (or **Parity Inversion Operation**), which involves the rotation (in the same sense) of each atomic p^{π} orbital in an L^{π} MO by 90°, about a radial vector passing through the atom, as shown in (1).[1,15] This transformation results in the cluster $\bar{L}^{\pi}$ MO's having the opposite symmetry under inversion ("parity") to their L^{π} counterparts. It also reverses the bonding characteristics of the cluster MO, so that, for example, strongly bonding L^{π} MO's have matching strongly antibonding $\bar{L}^{\pi}$ MO's.[15]

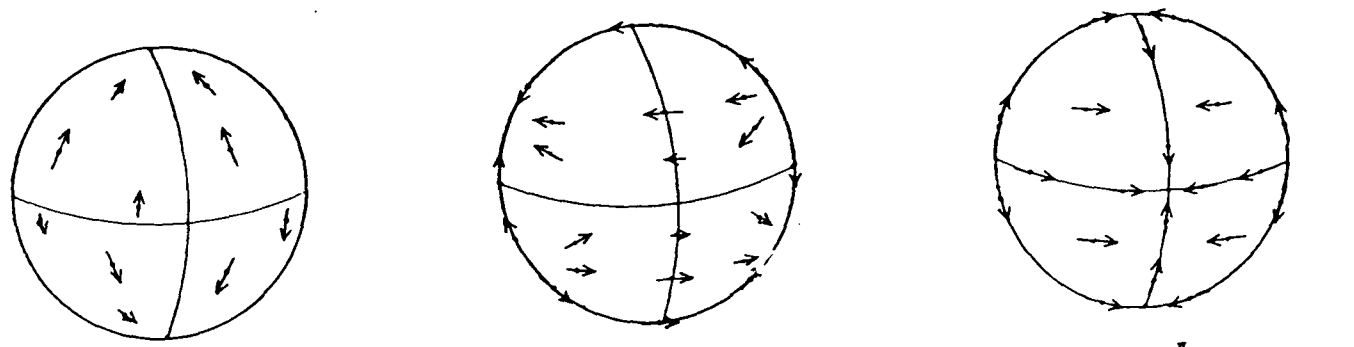


(1)

The occurrence of matching pairs of non-bonding L^{π} and $\bar{L}^{\pi}$ MO's is a consequence of this Parity Transformation, since a non-bonding L^{π} orbital must have a non-bonding $\bar{L}^{\pi}$ counterpart.[15] In the case of the tetrahedron, D_0^{π} and $\bar{D}_0^{\pi}$ are exactly non-bonding and form a degenerate (e) pair of MO's. For higher nuclearities, the (n-2) L^{π} and $\bar{L}^{\pi}$ orbitals are only approximately non-bonding. The non-bonding (or weakly bonding) nature of the (n-2) L^{π} and $\bar{L}^{\pi}$ orbitals, in the frontier region, is

demonstrated by the small contributions which they make to the C-C overlap populations, as indicated in **Table 2.4.**

The geometric feature which most clearly and generally distinguishes deltahedra and 3-connected polyhedral clusters, is the relative disposition of atoms in successive layers. The former have staggered, and the latter eclipsed, arrangements of atoms. 3-connected polyhedra therefore have horizontal pseudo-mirror planes between layers of atoms, whereas deltahedra have no such pseudo-mirror planes. Consequently the different bonding properties of the L^{π} and $\bar{L}^{\pi}$ MO's, in the two structural types, must be related to differences in bonding character across certain horizontal planes of the cluster. When considering prismatic 3-connected clusters, this horizontal plane is that containing the equator of the cluster sphere. **Figure 2.4** illustrates the D^{π} vector surface harmonics in a simplified and general fashion.



(a) D^{π}_{0}

(b) $D^{\pi}_{1s,1c}$

The two components are related by a 90^{o} rotation about the polar axis.

(c) $D^{\pi}_{2s,2c}$

The two components are related by a 45^{o} rotation about the polar axis.

Figure 2.4 The D^{π} vector surface harmonic functions.

Table 2.4 Contributions made to the C-C overlap populations of tetrahedrane and cubane by the "non-bonding" L^{π} and $\bar{L}^{\pi}$ orbitals, and comparison (for cubane) with contributions made by "bonding" L^{π} and "antibonding" $\bar{L}^{\pi}$ MO's*

Cluster	Occupied orbitals	Contribution to C-C overlap popln.**
$[C_4H_4]$ (T_d)	$D^{\pi}/\bar{D}^{\pi}(e)$ (non-bonding)	+0.04 (+0.020)
$[C_8H_8]$ (O_h)	$\bar{P}^{\pi}(t_{1g})$ (antibonding)	-0.35 (-0.117)
	$D^{\pi}(t_{2g})$ (non-bonding)	+0.05 (+0.017)***
	$\bar{D}^{\pi}(t_{2u})$ (non-bonding)	+0.14 (+0.047)***
	$D^{\pi}(e_g)$ (bonding)	+0.13 (+0.065)

* See **Table 2.2** for a list of the skeletal MO's (and their energies) of these molecules.

** Numbers in brackets indicate the average contribution to the C-C overlap population made by a single component of a degenerate set of orbitals.

*** Although the $D^{\pi}(t_{2g})$ orbitals possess very little C-C bonding character, the $\bar{D}^{\pi}(t_{2u})$ orbitals are actually weakly bonding. In this Chapter, however, both sets of orbitals are referred to as non-bonding, indicating that they are the highest-lying occupied skeletal MO's and that they have, at best, weak C-C bonding character.

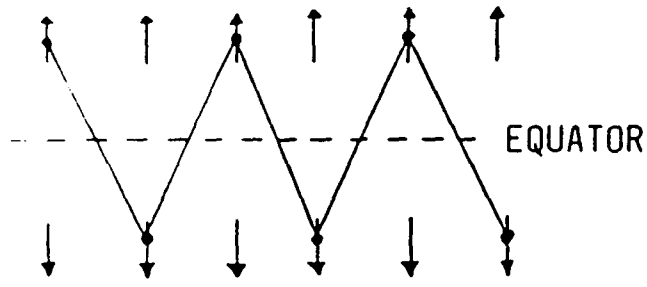
The arrows in the Figure represent the relative phases and magnitudes of the atomic p^{π} orbital contributions to the D^{π} functions. Only one component of $D^{\pi}_{1s,1c}$ is illustrated, as the second component is simply related to that shown by a 90^{o} rotation about the polar axis. Similarly, D^{π}_{2s} and D^{π}_{2c} are related by a 45^{o} rotation about the polar axis. As indicated above, it is only necessary to explain why certain of the D^{π} functions are non-bonding for 3-connected polyhedra, since the corresponding $\bar{D}^{\pi}$ functions are then constrained to be non-bonding, due to the nature of the Parity Transformation.

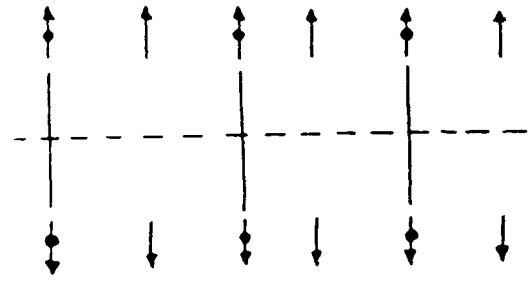
From **Figure 2.4a,** it is apparent that the D^{π}_{0} function is composed entirely of (longitudinal) p^{π} orbitals, i.e those pointing towards the poles of the sphere. Orbital interactions across the equator are bonding, because the function possesses a horizontal mirror plane. The interactions on either side of the equator will also be bonding, because the function is rotationally symmetric about the polar axis. **Figure 2.5a** shows that the bonding interactions will be similar for the D^{π}_{0} MO's of clusters with either staggered or eclipsed geometries and that, in both cases, the cluster orbital will generally be bonding. The only case for which this is not true is the tetrahedron, which is both a 3-connected polyhedron and a deltahedron. The D^{π}_{0} orbital of a tetrahedral cluster takes the form illustrated in **(2a)**. Because the top and bottom layers are staggered by 90^{o}, the cross-equator interaction is π-antibonding and cancels out the bonding interactions on either side of the equator. The $\bar{D}^{\pi}_{0}$ orbital is also non-bonding and forms a degenerate e pair with D^{π}_{0}. In this case, **(2b)**, the cross-equator interactions are bonding and the interactions on either side of the equator are antibonding. The cancelling out of these bonding and antibonding interactions explains

STAGGERED

ECLIPSED

(a) D^{π}_{0}

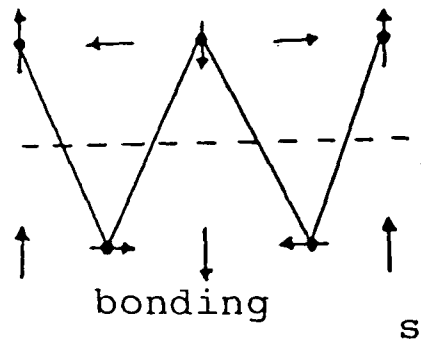


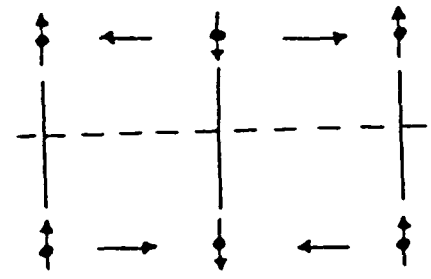


bonding (across equator)

bonding

(b) $D^{\pi}_{1s,1c}$



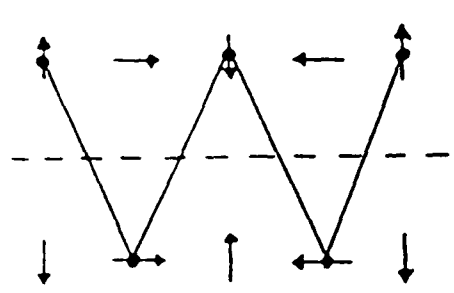


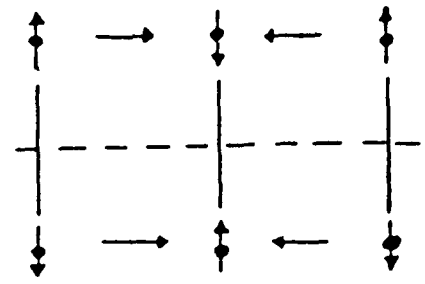
bonding

sign inversion every 180°

antibonding

(c) $D^{\pi}_{2s,2c}$



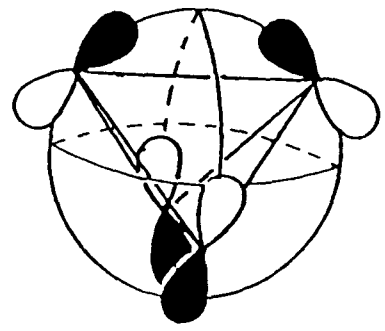


bonding

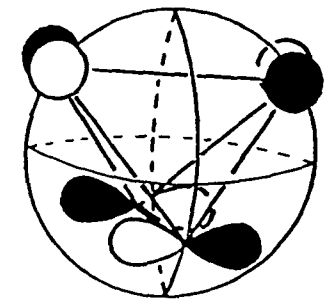
sign inversion every 90°

bonding/antibonding

why the $D_0^{\pi}/\bar{D}_0^{\pi}$ pair are overall non-bonding.



(2a) D_0^{π}



(2b) $\bar{D}_0^{\pi}$

For the $D_{1s,1c}^{\pi}$ functions, there is no mirror plane through the equator, but instead the equator forms a nodal plane (**Figure 2.4b**). Analysis of the bonding characteristics of these functions for staggered and eclipsed geometries (**Figure 2.5b**) reveals that the cross-equator interactions are bonding for the staggered geometry and antibonding for the eclipsed geometry. These $D_{1s,1c}^{\pi}$ MO's are non-bonding for all prismatic clusters, since they are bonding in the planes above and below the equator, and antibonding across the equator. If, however, more layers of atoms are added to the structure, then the $D_{1s,1c}^{\pi}$ orbitals become bonding, because eclipsed atoms on the same side of the equator (**Figure 2.4b**) have their p^{π} orbitals overlapping in-phase.

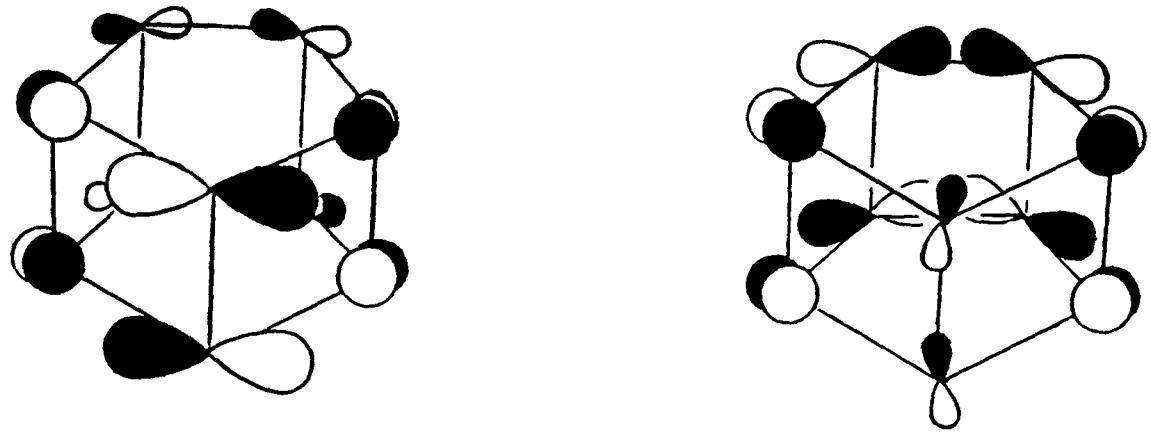
A trigonal prism has 3 D^{π} MO's, $D_0^{\pi}(a_1')$ bonding and $D_{\pm 1}^{\pi}(e'')$ non-bonding. The addition of two atoms, to form a cube, leads to the creation of 2 additional MO's, based on the $D_{2s,2c}^{\pi}$ functions shown in **Figure 2.4c.** The atoms of the cube lie, at 90^{o} intervals, in eclipsed planes on either side of the equator. The $D_{2s,2c}^{\pi}$ functions have (longitudinal) p^{θ} components with maximum in-plane antibonding

interactions at 90° intervals (vertical arrows in **Figure 2.5c**) and (latitudinal) p^{ϕ} components with maximum in-plane bonding character, also at 90° intervals (horizontal arrows in **Figure 2.5c**). These components are spaced 45° apart and both are bonding across the equator. D^{π}_{2c} has pure p^{θ} components at ϕ = 0, 90, 180 and 270°, whereas D^{π}_{2s} (which is rotated by 45°, about the polar axis, relative to D^{π}_{2c}) has pure p^{ϕ} components at these angles. It can, therefore, be seen that D^{π}_{2c} is antibonding within the upper and lower layers, but bonding across the equator and hence is overall non-bonding. In contrast, D^{π}_{2s} is bonding within and between the two layers and is overall bonding. For the square antiprism, which is actually a 4-connected polyhedron rather than a deltahedron (see **Section 2.3**), the two planes of atoms are rotated by 45° relative to each other, so that (**Figure 2.5c**) both the 2s and 2c functions have p^{θ} components only on one side of the equator and p^{ϕ} components on the other, making the interactions antibonding in one layer and bonding in the other. The cross-equator overlaps are in-phase, which makes the $D^{\pi}_{2s,2c}$ orbitals (which form a degenerate e_2 pair under D_{4d} symmetry) overall bonding for the antiprism. The D^{π}_{2c} orbital, which is non-bonding for the prism (cube), becomes more bonding in the antiprism, while the strongly bonding D^{π}_{2s} orbital of the prism becomes slightly less bonding in the antiprism.

For 3-connected polyhedral clusters with more than 8 skeletal atoms, both of the $D^{\pi}_{2s,2c}$ orbitals are bonding. That this should be so may be appreciated by considering the pentagonal and hexagonal prisms. There are now more than 4 atoms in each layer, so their ϕ angles differ by less than 90°. This means that, for the D^{π}_{2c} function, the atoms are not at the correct positions for maximum in-plane antibonding interaction, so the cross-equator bonding interactions win out and the

orbital becomes overall bonding. This orbital becomes degenerate with the D^{π}_{2s} orbital, which becomes slightly less bonding for similar reasons.

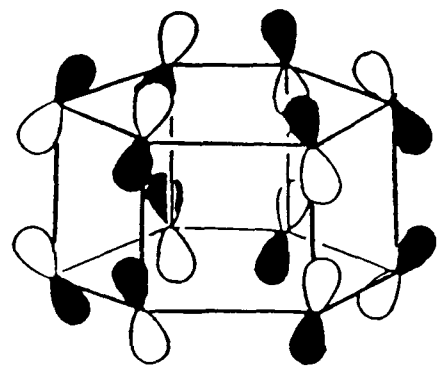
The 4 $\{(n/2)-1\}$ non-bonding L^{π} MO's for the pentagonal prism are $D^{\pi}_{\pm 1}$ and $F^{\pi}_{\pm 2}$ (3).



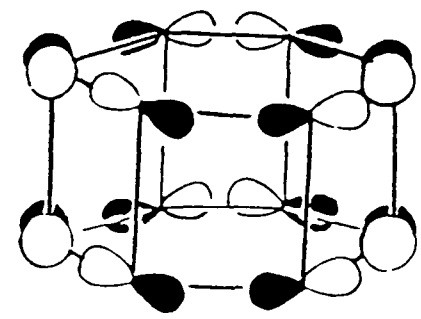
$F^{\pi}_{\pm 2}$ (e''_2)

(3)

The $F^{\pi}_{\pm 2}$ orbitals are similar to $D^{\pi}_{\pm 1}$, in that they possess one horizontal nodal plane (perpendicular to the polar axis) which passes through the equator and, therefore, imparts cross-equator antibonding character. The hexagonal prism has, in addition to these 4 non-bonding orbitals, a non-bonding $F^{\pi}_{3c}(b_{2u})$ orbital **(4a)**, which has similar bonding characteristics to D^{π}_{2c} in the case of the cube. The F^{π}_{3c} orbital has no horizontal nodal planes, but has 3 vertical nodal planes (containing the polar axis) which pass between the cluster atoms and, thereby, impart in-plane antibonding character. In contrast, the $F^{\pi}_{3s}(b_{1u})$ orbital **(4b)** is strongly bonding, because the 3 vertical nodal planes which it possesses pass through the atoms and, due to the singly noded nature of the constituent p^{π} orbitals, impart in-plane bonding character. Like F^{π}_{3c}, this orbital has no horizontal nodal planes, so the cross-equator interaction is bonding.



($\underline{4a}$) F^{π}_{3c} (b_{1u})



($\underline{4b}$) F^{π}_{3s} (b_{2u})

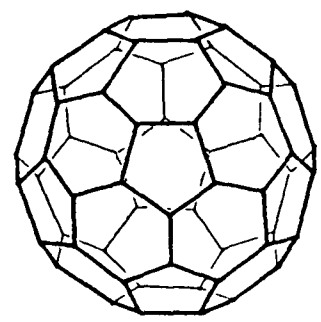
The above discussion has concentrated on 2-layer 3-connected polyhedra (i.e. prisms). In 3-connected clusters which consist of more than 2 layers of atoms (when viewed down the principal rotation axis of the cluster), non-equatorial horizontal nodal planes also become important in determining the bonding characteristics of the cluster L^{π} and $\bar{L}^{\pi}$ orbitals. In such cases the analysis is not as straightforward as for the prisms. It is, however, possible to say that the L values, of the nonbonding L^{π} and $\bar{L}^{\pi}$ MO's, will be larger for those clusters with a greater number of layers of atoms. For these multi-layer clusters, a low value of L means that there are large regions of the cluster which have in-phase orbital overlap, thereby outweighing the antibonding character associated with the (few) nodal planes. For example, when viewed down the C_5 axis, the dodecahedron consists of 4 layers ($5:5:\bar{5}:\bar{5}$) of atoms and its 9 non-bonding L^{π} orbitals are $F^{\pi}(g_u)$ and $G^{\pi}(h_g)$.

2.2.3 Summary

The above analysis has demonstrated the occurrence of the following numbers of non-bonding L^{π} MO's for 3-connected polyhedral clusters: 1-

tetrahedron; 2-trigonal prism; 3-cube; 4-pentagonal prism; 5-hexagonal prism and 9-(pentagonal) dodecahedron. The non-bonding character of these orbitals has been rationalised in terms of the disposition of nodal planes relative to the cluster atom positions. The generalised spectrum of skeletal MO's observed for 3-connected clusters has been contrasted with that of the deltahedra. In general, there are $\{(n/2)-1\}$ non-bonding L^{π} MO's which, due to the nature of the Parity Transformation, are matched by an equal number of non-bonding $\bar{L}^{\pi}$ MO's. The 3n/2 SEP count for these clusters corresponds to the complete occupation of the (n-2) non-bonding MO's, as well as the $\{(n/2)-2\}$ bonding L^{π} and 4 $(S^{\sigma} + 3P^{\sigma+\pi})$ predominantly radial orbitals. The difference in electron count between 3-connected and deltahedral clusters $\{5n-(4n+2) = (n-2)\}$ corresponds to the occupation, in the former, of the $\{(n/2)-1\}$ non-bonding $\bar{L}^{\pi}$ MO's.

Fowler and Porterfield have recently utilised the Extended Tensor Surface Harmonic approach to determine the energies of the skeletal MO's of 3-connected hydrocarbon clusters.[16] Their results support the conclusions presented here. Fowler has also studied the bonding in high nuclearity bare carbon atom clusters, such as $[C_{60}]$ (III),[17] in terms of simple Hückel theory, using TSH labels for the orbitals.[18]



postulated structure of $[C_{60}]$
(truncated icosahedron)

(III)

These molecules are presumed to have 3-connected frameworks, such as those which might reasonably be predicted for high nuclearity [C_nH_n] molecules. In the case of the bare carbon clusters, however, the radial p^σ orbitals, which would otherwise be involved in C-H bonding, constitute a superaromatic π-system. The term "π-system" has been employed, because overlap between the p^σ orbitals on adjacent atoms is very close to being purely π in character, for high nuclearity "spherical" [C_n] clusters.[18]

2.3 Four-Connected Polyhedral Clusters

2.3.1 Geometric features of 4-connected clusters

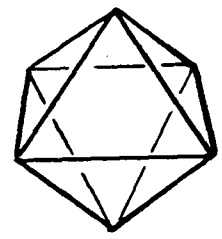
It has recently become apparent that some transition metal clusters adopt structures which are derived neither from deltahedra nor 3-connected polyhedra, but instead are such that each skeletal atom has 4 nearest neighbour cluster atoms.

Figure 2.6 illustrates some examples of 4-connected polyhedra, with 6 to 12 vertices. By applying Euler's relationship, the following vertex-edge-face relationships may be derived:

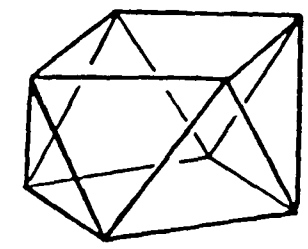
$$F_4 = V_4 + 2$$

$$E_4 = 2V_4 = 2(F_4-2)$$

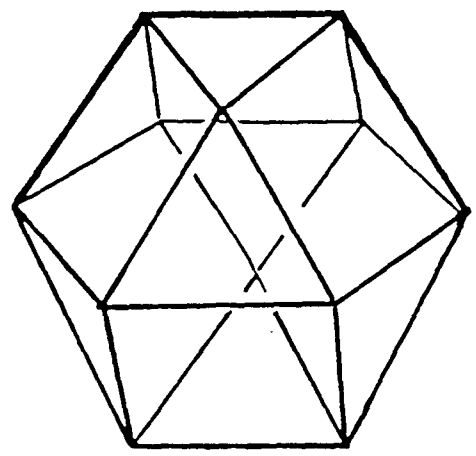
where the subscript 4 indicates a vertex, edge or face belonging to a 4-connected polyhedron. The smallest 4-connected polyhedron is the octahedron (V_4=6) **(a)**, which is also a deltahedron (just as the smallest 3-connected polyhedron, the tetrahedron, is a deltahedron). The polyhedra **(a)-(d)** have all of their vertex atoms lying on the surface of a single sphere. All antiprisms (e.g. **(b)**) are 4-connected and fit into



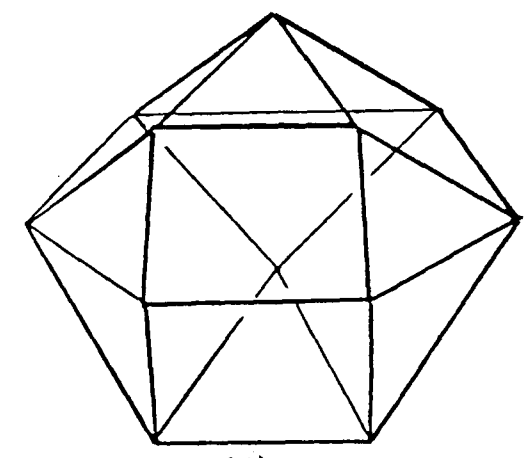
(a) octahedron



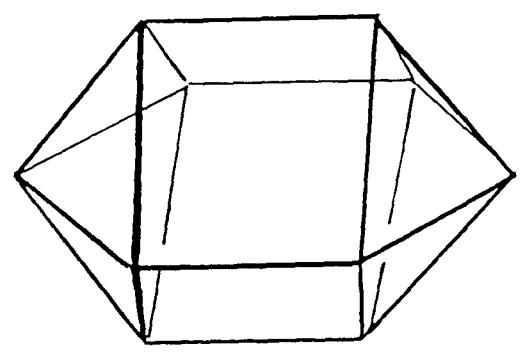
(b) square antiprism



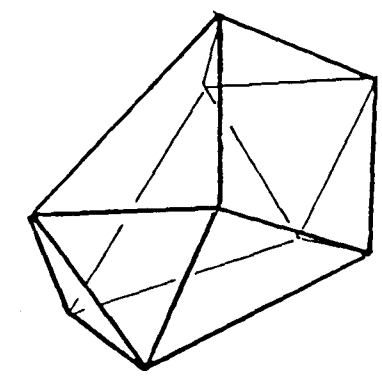
(c) cuboctahedron



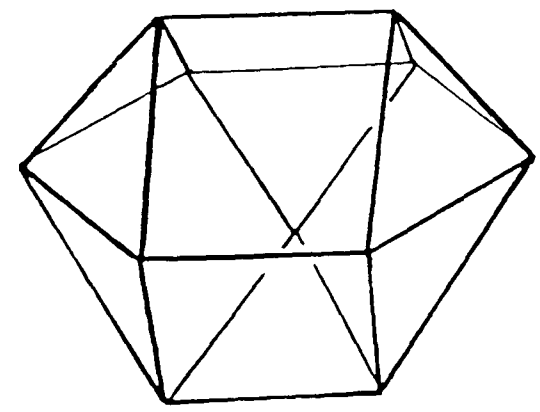
(d) twinned cuboctahedron



(e) bicapped cube



(f) elongated trigonal prism



(g) 4-connected tridecahedron

Figure 2.6 Examples of 4-connected polyhedra.

this "spherical" class. In contrast, **(e)-(g)** are derived by capping 3-connected polyhedra and for **(f)** and **(g)** this requires the simultaneous extension of some of the bonds in the parent polyhedron. For example, **(f)** is an elongated tricapped trigonal prism and **(g)** is a tricapped cube, with 3 bonds of the cube broken. If all the bonds for the polyhedra **(e)-(g)** are constrained to be equal, then the atoms lie on the surface of either oblate or prolate spheroids. For these polyhedra, therefore, a spherical distribution of atoms is only attained if the skeletal bond lengths are unequal.

Since this class of polyhedron has not previously been investigated from a theoretical viewpoint, it was decided to undertake a systematic investigation of its electronic requirements.

2.3.2 Delocalised treatment of the bonding in 4-connected clusters

Extended Hückel calculations were performed on 4-connected and related capped 3-connected clusters, $[B_nH_n]$. The orbital parameters and bond lengths, used in these calculations, are given in the **Appendix.** The bonding and non-bonding (or weakly bonding/antibonding) orbitals of these clusters are listed in **Table 2.5.** The Extended Hückel calculations have suggested the following generalisations:

(i) Spherical 4-connected polyhedral clusters are characterised by a total of (4n+2) valence electrons if the n (= V_4) vertices are main group atoms and (14n+2) if they are transition metal atoms.

(ii) Non-spherical 4-connected polyhedral clusters are associated with variable electron counts of 4n to (4n+4) (main group) and 14n to (14n+4) (transition metal atoms).

Table 2.5 Bonding and non-bonding skeletal MO's of some 4-connected and related capped 3-connected polyhedral clusters $[B_nH_n]$

n	Cluster skeleton	Bonding skeletal MO's	Non-bonding skeletal MO's[a]
6	Octahedron (O_h)	$S^{\sigma}(a_{1g})$, $P^{\sigma}(t_{1u})$, $D^{\pi}_{\pm1,2s}(t_{2g})$	
8	Square-antiprism (D_{4d})	$S^{\sigma}(a_1)$, $P^{\sigma}(b_2+e_1)$, $D^{\pi}_0(a_1)$, $D^{\pi}_{\pm2}(e_2)$	$D^{\pi}_{\pm1}(e_3)$, $\bar{D}^{\pi}_{\pm1}(e_1)$
9	Tricapped trigonal prism (TTP) (D_{3h})	$S^{\sigma}(a_1')$, $P^{\sigma}(a_2''+e')$, $D^{\pi}(a_1'+e'+e'')$	$F^{\pi}_0(a_2'')$, $\bar{F}^{\pi}_0(a_2')$[b]
9	Elongated TTP (D_{3h})	As for TTP but $F^{\pi}_0(a_2'')$ is bonding and $\bar{F}^{\pi}_0(a_2')$ is antibonding.	
10	Bicapped cube (BCC) (D_{4h})	$S^{\sigma}(a_{1g})$, $P^{\sigma}(a_{2u}+e_u)$, $D^{\pi}_0(a_{1g})$, $D^{\pi}_{\pm1}(e_g)$, $D^{\pi}_{2s}(b_{2g})$, $F^{\pi}_{\pm1}(e_u)$	$D^{\pi}_{2c}(b_{1g})$, $\bar{D}^{\pi}_{2c}(b_{1u})$[b]
10	Distorted BCC[c] (D_{4h})	As for BCC but $D^{\pi}_{2c}(b_{1g})$ is bonding ($\bar{D}^{\pi}_{2c}(b_{1u})$ remains effectively non-bonding, however).	
12	Tetracapped cube (D_{4h})	$S^{\sigma}(a_{1g})$, $P^{\sigma}(a_{2u}+e_u)$, $D^{\pi}(a_{1g}+b_{1g}+b_{2g}+e_g)$, $F^{\pi}_{\pm1}(e_u)$, $F^{\pi}_{2c}(b_{1u})$	$F^{\pi}_0(a_{2u})$, $\bar{F}^{\pi}_0(a_{2g})$[b]
12	Cuboctahedron (O_h)[d]	$S^{\sigma}(a_{1g})$, $P^{\sigma}(t_{1u})$, $D^{\pi}(e_g+t_{2g})$, $F^{\pi}(t_{1u}+a_{2u})$	
	(a) defined down C_4	$F^{\pi}(t_{1u})$, $F^{\pi}_0(a_{2u})$	
	(b) defined down C_3	$F^{\pi}(t_{1u})$, $F^{\pi}_{2c}(a_{2u})$	
12	Twinned-cuboctahedron (D_{3h})	$S^{\sigma}(a_1')$, $P^{\sigma}(a_2''+e')$, $D^{\pi}(a_1'+e'+e'')$ $F^{\pi}_0(a_2'')$, $F^{\pi}_{\pm1}(e')$, $F^{\pi}_{3c}(a_1')$	

a Including weakly bonding and weakly antibonding skeletal MO's.

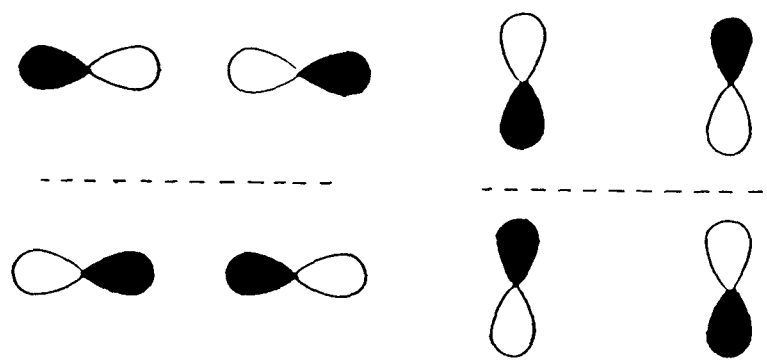
b In these non-spherical cases the (approximately) non-bonding $\bar{L}^{\pi}$ orbital lies at lower energy (is more strongly bonding) than its parity related L^{π} counterpart.

c The (D_{4h})distorted bicapped cube has all of its vertices equidistant from the centre of the polyhedron (i.e. is "spherical") and possesses a regular hexagonal cross section in two perpendicular planes which contain the C_4 axis.

d See footnote **c** to **Table 2.2.**

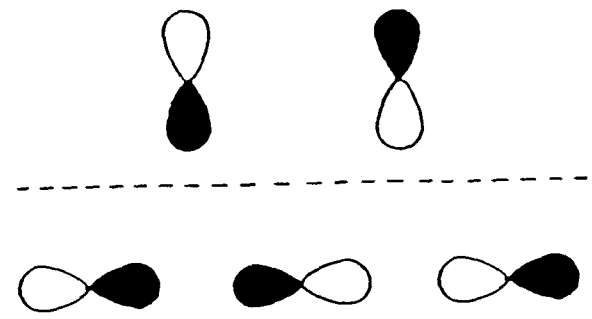
The first generalisation is the most important, because it demonstrates that deltahedral and 4-connected polyhedral clusters have identical electron counts. This may readily be interpreted in terms of the Tensor Surface Harmonic methodology. Both classes of polyhedra have vertex atoms lying on the surface of a sphere and have (n+1) skeletal bonding MO's (S^{σ}, $3P^{\sigma+\pi}$ and $(n-3)L^{\pi}$).

This bonding scheme is in clear contrast with that of the 3-connected polyhedra discussed above which, despite having a pseudo-spherical topology, have 3n/2 occupied skeletal MO's, of which (n-2) are non-bonding. It has already been shown how the eclipsed arrangement of atoms in the 3-connected polyhedra leads to the occurrence of non-bonding cluster MO's, due to the cancelling out of bonding and antibonding in-plane and cross-equator interactions, as summarised in (5).



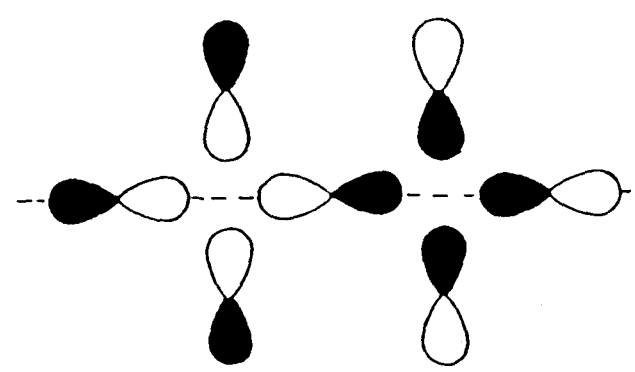
(5)

Those 4-connected polyhedra which are antiprisms and, therefore, have a staggered arrangement of atoms about the equator, may be treated in an analogous fashion to that described above for the deltahedra. In general terms, the L^{π} orbitals which were non-bonding for the prisms become bonding for the antiprisms, due to interactions of the type shown in (6).



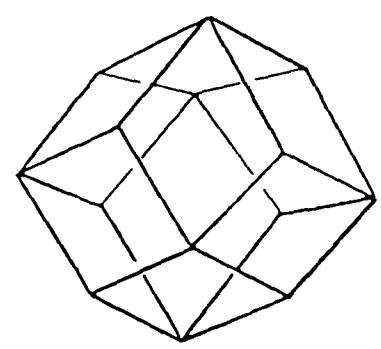
(6)

In clusters which are derived by capping the equatorial faces of a 3-connected polyhedron, the atoms on the equator can stabilise a number of the previously non-bonding MO's (7).



(7)

The rhombic dodecahedron **(IV)**, which has six 4-connected and eight 3-connected vertices, is also predicted to conform to the (4n+2) or (14n+2) rule. This is due to the approximately spherical distribution of the atoms and the staggered arrangement which they adopt.



rhombic dodecahedron

(IV)

The centred rhombic dodecahedral cluster $[Rh_{15}(CO)_{30}]^{3-}$ has the expected 198 valence electron count (n=14, because the interstitial atom contributes all of its electrons to the cluster and only interacts with the skeletal bonding molecular orbitals of the external polyhedron).[19] This cluster may also be regarded as a (centred) hexacapped cube with all of the bonds of the original cube broken.

For the borane anions $[B_nH_n]^{2-}$, deltahedral geometries are favoured because they maximise the number of nearest neighbour resonance integral terms.[1] For transition metal cluster compounds, where the potential energy surfaces connecting alternative polyhedral geometries are softer and ligand-ligand repulsion terms can compete with metal-metal bonding,[20] 4-connected polyhedral structures are also observed.[9] Examples of deltahedral and 4-connected polyhedral transition metal cluster compounds are contrasted in **Table 2.6.** For the 12-vertex situation, both polyhedral types have been characterised, viz. icosahedral $[Rh_{12}Sb(CO)_{27}]^{3-}$ (deltahedral)[21] and twinned-cuboctahedral $[Rh_{13}(CO)_{24}H_{(5-n)}]^{n-}$ (4-connected).[22]

Antiprisms, such as the square antiprism **(b)**, represent a particularly interesting class of molecules. These species are 4-connected polyhedra (and hence expected to conform to the (14n+2) rule), but they are also arachno deltahedra (characterised by (14n+6) electrons).[7] Examples of square antiprismatic transition metal carbonyl clusters with both electron counts have been characterised, i.e. $[Co_8C(CO)_{18}]^{2-}$ (14n+2 = 114e)[23] and $[Ni_8C(CO)_{16}]^{2-}$ (14n+6 = 118e).[24] The cobalt cluster exhibits a slight distortion towards the alternative (deltahedral) dodecahedral structure.[23] The fluctionality of dodecahedral $[B_8H_8]^{2-}$ has also been related to the occurrence of

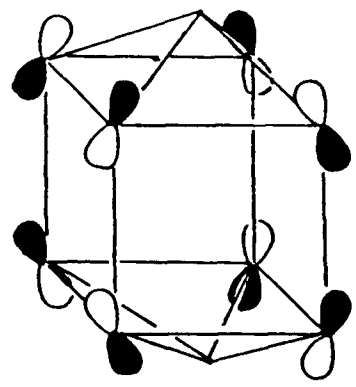
Table 2.6 Examples of deltahedral and 4-connected transition metal clusters with n vertices and (14n+2) cluster valence electrons

		Deltahedral Clusters			4-Connected Clusters		
n	**(14n+2)**	**Geometry**	**Example**	**Ref.**	**Geometry**	**Example**	**Ref.**
6	86	Octahedron	$[Rh_6(CO)_{16}]$	**a**	Octahedron	$[Rh_6(CO)_{16}]$	**a**
7	100	Pentagonal bipyramid					
8	114	(triangular) Dodecahedron			Square anti-prism	$[Co_8C(CO)_{18}]^{2-}$	**b**
9	128	Tricapped trigonal prism (TTP)			Elongated TTP		
10	142	Bicapped square anti-prism	$[Rh_{10}P(CO)_{22}]^{3-}$	**c**	Distorted bicapped cube		
11	156	Octadecahedron					
12	170	Icosahedron	$[Rh_{12}Sb(CO)_{27}]^{3-}$	**d**	(centred) Twinned-cuboctahedron Cuboctahedron	$[Rh_{13}(CO)_{24}H_{(5-n)}]^{n-}$	**e**

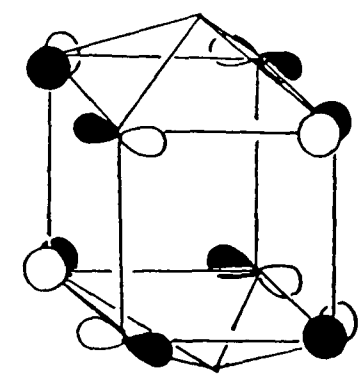
a E.R. Corey, L.F. Dahl and W. Beck, J. Amer. Chem. Soc., 1963, **85**, 1202. **b** V.G. Albano, P. Chini, G. Ciani, S. Martinengo and M. Sansoni, J. Chem. Soc., Dalton. Trans., 1978, 463. **c** J.L. Vidal, W.E. Walker and R.C. Schoening, Inorg. Chem., 1981, **20**, 238. **d** J.L. Vidal and J.M. Troup, J. Organomet. Chem., 1981, **213**, 351. **e** G. Ciani, A. Sironi and S. Martinengo, J. Chem. Soc., Dalton Trans., 1981, 519.

alternative square antiprismatic and bicapped trigonal prismatic structures with similar valence electron requirements and energies.[25] Analysis of the bonding in square antiprismatic $[B_8H_8]^{x-}$ reveals that the HOMO's for the (n+1 = 9) SEP case are the weakly bonding $D^{\pi}_{\pm 1}(e_3)$ orbitals, which correspond to two of the non-bonding D^{π} orbitals of the cube. The LUMO's for this case are the, parity related, weakly antibonding $\bar{D}^{\pi}_{\pm 1}(e_1)$ orbitals, which correspond to two of the non-bonding $\bar{D}^{\pi}$ orbitals of the cube. When these orbitals are occupied, as in the nickel cluster and $[Bi_8]^{2+}$,[26] there are (n+3 = 11) SEP's, corresponding to that expected for an arachno deltahedron. The remaining non-bonding orbitals of the cube, D^{π}_{2c} and $\bar{D}^{\pi}_{2c}$, become quite strongly bonding and antibonding respectively.

The non-spherical 4-connected polyhedral molecules **(e)-(g)** are related by capping processes to the 3-connected polyhedra. In **Section 2.2**, it was shown that the latter have a set of (n-2) non-bonding L^{π} and $\bar{L}^{\pi}$ MO's. The addition of capping atoms can stabilise some or all of these orbitals. For the bicapped cube **(e)**, a pair of parity matched orbitals ($D^{\pi}_{2c}(b_{1g})$ **(8a)** and $\bar{D}^{\pi}_{2c}(b_{1u})$ **(8b)**) are unaffected by the capping process and remain essentially non-bonding.



(8a) D^{π}_{2c} (b_{1g})



(8b) $\bar{D}^{\pi}_{2c}$ (b_{1u})

It is the occurrence of this approximately non-bonding (but non-degenerate) pair of orbitals, which leads to the possibility of electron counts of 14n, (14n+2) or (14n+4) for transition metal clusters with this skeletal geometry, though to date no examples are known. As the cluster is deformed towards a more spherical topology, by simultaneously compressing the capping atoms and expanding the cube, the $D^{\pi}_{2c}(b_{1g})$ orbital becomes bonding, while $\bar{D}^{\pi}_{2c}(b_{1u})$ becomes antibonding, and the (n+1) SEP count is strongly favoured.

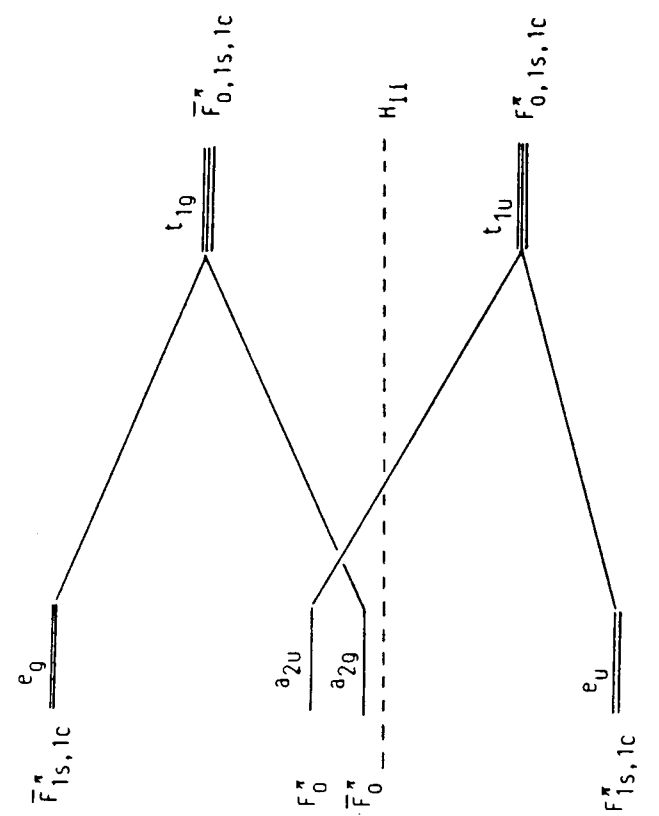
As mentioned above, 4-connected clusters may be formed by capping 3-connected clusters and then breaking some of the bonds of the original polyhedron. In the case of the tricapped trigonal prism, the capping atoms provide orbitals of the correct symmetry to overlap with the 4 non-bonding orbitals, $D^{\pi}_{\pm 1}(e'')$ and $\bar{D}^{\pi}_{\pm 1}(e')$, of the trigonal prism, so that none of the original non-bonding MO's are left in the resulting deltahedron. This cluster does, however, have a pair of orbitals, $\bar{F}^{\pi}_{0}(a_2')$ and $F^{\pi}_{0}(a_2'')$, which are weakly bonding and weakly antibonding respectively and are predominantly localised on the capping atoms. The trigonal prism is characterised by 9 SEP's, so the tricapped trigonal prism could conceivably possess 9 SEP's (n, with neither $\bar{F}^{\pi}_{0}$ nor F^{π}_{0} occupied), 10 SEP's (n+1, when only $\bar{F}^{\pi}_{0}$ is occupied) or 11 SEP's (n+2, when both $\bar{F}^{\pi}_{0}$ and F^{π}_{0} are occupied), i.e. valence electron counts of 4n, (4n+2) or (4n+4). Main group tricapped trigonal prismatic clusters are indeed known with each of these electron counts, e.g. $[B_9Cl_9]$ (36e = 4n),[27] $[B_9H_9]^{2-}$ (38e = 4n+2)[28] and $[Bi_9]^{5+}$ (40e = 4n+4).[29] Wade[30] and Corbett[31] have discussed the geometric consequences of these alternative electron counts. If the polyhedron is distorted from deltahedral to 4-connected **(f)**, by simultaneously breaking the vertical bonds of the trigonal prism

and pulling in the capping atoms, then the frontier orbitals cross over, so that the F_0^{π} orbital becomes bonding and the $\bar{F}_0^{\pi}$ orbital becomes antibonding. The frontier orbitals of the tricapped trigonal prism will be discussed in more detail in **Chapter 4.**

The tetracapped cube (with D_{4h} symmetry) also has a frontier orbital pair consisting of a weakly bonding $\bar{F}_0^{\pi}(a_{2g})$ orbital and a weakly antibonding $F_0^{\pi}(a_{2u})$ orbital (**Figure 2.7a**). The occurrence of these orbitals permits electron counts in the range 4n to (4n+4) for main group clusters (14n to (14n+4) for transition metal clusters). The tetracapped cube has an oblate spheroidal topology, but may be converted into the spherical 4-connected cuboctahedron **(c)** by simultaneously stretching along the fourfold axis and compressing in the equatorial plane. **Figure 2.7b** shows that this distortion results in the stabilisation of F_0^{π} and the destabilisation of $\bar{F}_0^{\pi}$ and a preferred electron count of (4n+2) or (14n+2) for the cuboctahedron.

2.3.3 Summary

In this Section, the bonding in 4-connected polyhedral clusters has been discussed. These clusters fall into two main types, those with approximately spherical topologies and those with grossly non-spherical topologies. The former, like the deltahedra, are generally characterised by (n+1) skeletal bonding MO's, whereas the latter (usually derived from capped 3-connected polyhedra) generally possess n strongly bonding skeletal MO's and 2 parity related orbitals, which are either non-bonding or weakly bonding/antibonding. SEP counts of n, (n+1) or (n+2) are possible for these molecules. The tricapped trigonal prism and tetracapped cube have also been studied, though they are not 4-



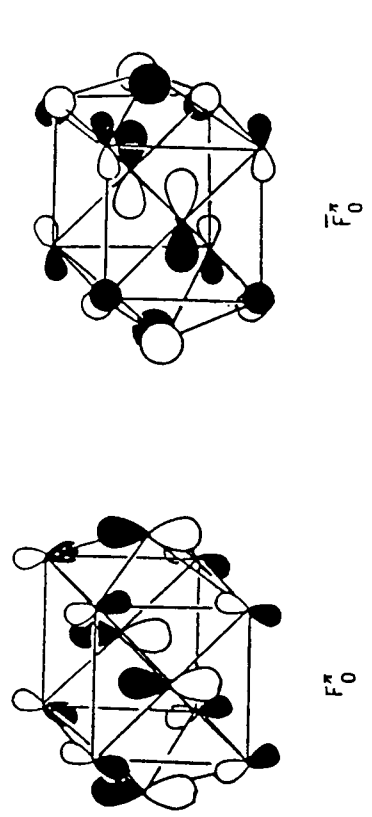


Figure 2.7 (a) The F^{π}_0 and $\bar{F}^{\pi}_0$ orbitals of the tetracapped cube. (b) Correlation of the frontier orbitals of the tetracapped cube and cuboctahedron and illustration of the distortion which interconverts the two geometries.

connected. These polyhedra have oblate-spheroidal topologies and may be distorted to yield spherical 4-connected clusters. There are important general bonding distinctions between clusters with spherical and oblate-spheroidal topologies. Spherical clusters have all the L^{π} orbitals bonding and all the $\bar{L}^{\pi}$ orbitals antibonding, whereas oblate-spheroidal clusters have the bonding nature of some of the L^{π} and $\bar{L}^{\pi}$ orbitals, in the frontier region, reversed (it will be shown in **Chapter 5** that this is a general feature of non-spherical clusters). In all cases, however, it is observed that the (n+1) SEP situation becomes increasingly favoured as the spheroidal cluster is distorted towards a truly spherical topology.

2.4 Conclusions

In Tensor Surface Harmonic theory, the solution of the Schrödinger equation for the particle on a sphere problem generates L^{σ}, L^{π}, $\bar{L}^{\pi}$ etc. functions. For (hypothetical) truly spherical clusters, the L^{π} and $\bar{L}^{\pi}$ functions constitute two sets of orbitals which are strictly bonding and antibonding respectively.[1] An n-vertex spherical cluster, with a basis set of n radial (σ) and 2n tangential (π) orbitals, would be characterised by (n+1) SEP's, corresponding to the occupation of S^{σ} and nL^{π} orbitals (with L^{σ} character mixed in).[1,2]

Previous work has shown that the same bonding scheme may be applied to cluster compounds with deltahedral geometries.[1,2,16] This is because the arrangement of vertices is sufficiently spherical (i.e. represents a fairly good coverage of the spherical surface)[32] for the wavefunctions to represent good approximations to the particle on a sphere solutions. In this Chapter, it has been demonstrated that 4-connected polyhedral

clusters are also characterised by (n+1) SEP's, with the L^{π} and $\bar{L}^{\pi}$ orbitals possessing bonding and antibonding character respectively. 4-connected polyhedra, therefore, also emulate spheres sufficiently well for the spherical limit of TSH theory to be applicable. For both 4-connected and deltahedral geometries (see **Chapter 4**), distortions away from a spherical topology can lead to deviations from the (n+1) rule. This is due to the presence, in the frontier orbital region of these non-spherical clusters, of approximately non-bonding L^{π} and $\bar{L}^{\pi}$ orbitals.

In the case of 3-connected clusters, the situation is completely different. Despite the fact that a 3-connected polyhedron may possess a spherical topology, in that all of its vertices lie on the surface of a single sphere, clusters adopting these geometries do not possess (n+1) SEP's. Instead, these clusters are characterised by (3n/2) SEP's, of which (n-2) correspond to approximately non-bonding parity related L^{π} and $\bar{L}^{\pi}$ MO's. Since the arrangement of their vertices constitutes a poor coverage of a spherical surface,[32] 3-connected polyhedra do not emulate the sphere sufficiently well for their skeletal MO's to be good approximations to the particle on a sphere solution. In particular, the low number of close atom-atom contacts (i.e. cluster edges) is insufficient to enable a distinction to be made, in all cases, of the bonding characteristics of even (L^{π}) and odd parity ($\bar{L}^{\pi}$) tangential orbitals.

2.5 Appendix

The orbital parameters, used in the Extended Hückel calculations on 3-connected $[C_nH_n]$ and 4-connected (and related) $[B_nH_n]^{2-}$ clusters, are listed in **Table 2.7.**

The following bond lengths were used in these calculations: C-C, 1.54Å; C-H, 1.09Å; B-B, 1.70Å; B-H, 1.20Å.

Table 2.7 Extended Hückel parameters

Atom	Orbital	H_{ii} (eV)	Slater exponent (ζ)
B	2s	-15.20	1.300
	2p	-8.50	1.300
C	2s	-21.40	1.625
	2p	-11.40	1.625
H	1s	-13.60	1.300

Wolfsberg-Helmholz constant k = 1.75

References for Chapter Two

1. A.J. Stone, Mol. Phys., 1980, **41**, 1339; Inorg. Chem., 1981, **20**, 563.
2. P. Brint, J.P. Cronin, E. Seward and T. Whelan, J. Chem. Soc., Dalton Trans., 1983, 675.
3. See, for example: H.M. Cundy and A.P. Rollett, "Mathematical Models" (3rd Edn.), Tarquin Pub., U.K., 1981.
4. Synthesis and characterisation of $[C_nH_n]$ clusters and their derivatives: (a) $[C_4Bu^t_4]$; G. Maier, S. Pfriem, U. Schafter and R. Matusch, Angew. Chem., 1978, **90**, 652. (b) $[C_6H_6]$ ("prismane"); T.J. Katz and N. Acton, J. Amer. Chem. Soc., 1973, **95**, 2738. (c) $[C_8H_8]$ ("cubane"); P.E. Eaton and T.V. Cole, J. Amer. Chem. Soc., 1964, **86**, 3157. (d) $[C_8H_8]$ ("cuneane"); L. Cassar, P.E. Eaton and J. Halpern, J. Amer. Chem. Soc., 1970, **92**, 6366 (the octamethyl derivative was reported earlier: R. Criegee and R. Askani, Angew. Chem. Int. Edn. Engl., 1968, **7**, 537). (e) $[C_{10}H_{10}]$ ("pentaprismane"); P.E. Eaton, Y.S. Or and S.J. Branca, J. Amer. Chem. Soc., 1981, **103**, 2134. (f) $[C_{10}H_{10}]$ ("diademane"); A. de Meijnere, D. Kaufmann and O. Schallner, Angew. Chem. Int. Edn. Engl., 1971, **10**, 417. (g) $[C_{20}H_{20}]$ ("dodecahedrane"); R.J. Ternansky, D.W. Balogh and L.A. Paquette, J. Amer. Chem. Soc., 1982, **104**, 4503; 1983, **105**, 5446.
5. (a) S.F.A. Kettle, Theor. Chim. Acta., 1969, **14**, 175. (b) J.M. Schulman,C.R. Fischer, P. Solomon and T.J. Venanzi, J. Amer. Chem. Soc., 1978, **100**, 2949 and references therein.
6. D.M.P. Mingos, Nature Phys. Sci., 1972, **236**, 99.
7. K. Wade, J. Chem. Soc., Chem. Commun., 1971, 792; Adv. Inorg. Chem. Radiochem., 1976, **18**, 1; D.M.P. Mingos, Acc. Chem Res., 1984, **7**, 311.

8. H.G. von Schnering, Angew. Chem. Int. Edn. Engl., 1981, **20**, 33 and references therein.

9. "Transition Metal Clusters" (Ed. B.F.G. Johnson), Wiley, New York, 1980 and references therein.

10. R.L. De and H. Vahrenkamp, Angew. Chem. Int. Edn. Engl., 1984, **23**, 983.

11. R. Hoffmann, Science, 1981, **211**, 995; Angew. Chem. Int. Edn. Engl., 1982, **21**, 711.

12. M.R. Churchill and J.P. Hutchinson, Inorg. Chem., 1978, **17**, 3528.

13. S. Cuccinella, T. Salvatori, C. Busetto and M. Cesari, J. Organomet. Chem., 1976, **121**, 137; G. del Piero, S. Cuccinella and M. Cesari, J. Organomet. Chem., 1979, **173**, 263.

14. MO calculations on $[C_nH_n]$ clusters: (a) $[C_4H_4]$ (tetrahedrane); J.M. Schulman and T.J. Venanzi, J. Amer. Chem. Soc., 1974, **96**, 4739; E. Heilbronner, T.B. Jones, A. Krebs, K.-D. Malsch, G. Maier, J. Pocklington and A. Schmelzer, J. Amer. Chem. Soc., 1980, **102**, 564. (b) $[C_6H_6]$ (prismane); M.D. Newton, J.M. Schulman and M.M. Manus, J. Amer. Chem. Soc., 1974, **96**, 17; J.M. Schulman and R.L. Disch, J. Amer. Chem. Soc., 1985, **107**, 5059. (c) $[C_8H_8]$ (cubane); See Ref. 5b, also: J.M. Schulman and R.L. Disch, J. Amer. Chem. Soc., 1984, **106**, 1202; R.L. Disch, J.M. Schulman and M.L. Sabio, J. Amer. Chem. Soc., 1985, **107**, 1904. (d) $[C_{12}H_{12}]$ (trishomobenzene, truncated tetrahedron); J.M. Schulman, R.L. Disch and M.L. Sabio, J. Amer. Chem. Soc. 1986, **108**, 3258, this isomer of dodecane is calculated (at the 6-31G* level) to be more stable than hexaprismane by 60 kcal/mol, though no $[C_{12}H_{12}]$ clusters have yet been characterised. (e) $[C_{20}H_{20}]$ (dodecahedrane); J.M. Schulman, T.J. Venanzi and R.L.Disch, J. Amer. Chem. Soc., 1975, **97**, 5335. These calculations

include the following types: STO-3G, 4-31G, 6-31G*, SCF-X , MINDO/3 and INDO, using both edge-localised and atomic orbital basis sets. The work cited above includes calculations of heats of formation of polyhedral [C_nH_n] molecules.

15. A.J. Stone and M.J. Alderton, Inorg. Chem., 1982, **21**, 2297.
16. P.W. Fowler and W.W. Porterfield, Inorg. Chem., 1985, **24**, 3511.
17. H.W. Kroto, J.R. Heath, S.C. O'Brien, R.F. Curl and R.E. Smalley, Nature, 1985, **318**, 162; J.R Heath, S.C. O'Brien, Q. Zhang, Y. Liu, R.F. Curl, H.W. Kroto, F.K. Tittel and R.E. Smalley, J. Amer. Chem. Soc., 1985, **107**, 7779.
18. P.W. Fowler and J. Woolrich, Chem. Phys. Lett., 1986, **127**, 84.
19. J.L. Vidal, L.A. Kapicak and J.M. Troup, J. Organomet. Chem., 1981, **215**, C11.
20. For a discussion of the relative merits of steric (mainly ligand-ligand repulsion) and electronic (mainly metal-metal bonding) approaches for rationalising metal cluster geometries see: D.G. Evans, D. Phil. Thesis, University of Oxford, 1984, Ch.3 p.72.
21. J.L. Vidal and J.M. Troup, J. Organomet. Chem., 1981, **213**, 351.
22. G. Ciani, A. Sironi and S. Martinengo, J. Chem. Soc., Dalton Trans., 1981, 519.
23. V.G. Albano, P. Chini, G. Ciani, S. Martinengo and M. Sansoni, J. Chem. Soc., Dalton Trans., 1978, 463.
24. G. Longoni, A. Ceriotti, R. Della Pergola, M. Manassero, M. Perego, G. Piro and M. Sansoni, Phil. Trans. R. Soc. Lond., 1982, **A308**, 47.
25. D.R. Eaton, L.J. Guggenberger and E.L. Muetterties, Inorg. Chem., 1967, **6**, 1271; E.L. Muetterties, R.J. Wiersma and M.F. Hawthorne, J. Amer. Chem. Soc., 1973, **95**, 7520.

26. J.D. Corbett, Inorg. Chem., 1968, **7**, 198; B. Krebs, M. Hucke and C.J. Brendel, Angew. Chem. Int. Edn. Engl., 1982, **21**, 445.

27. M.B. Hursthouse, J. Kane and A.G. Massey, Nature, 1970, **228**, 659.

28. L.J. Guggenberger, Inorg. Chem., 1968, **7**, 2260.

29. R.M. Friedman and J.D. Corbett, Inorg. Chem., 1973, **12**, 1134.

30. M.E. O'Neill and K. Wade, Polyhedron, 1983, **2**, 963.

31. S.C. Critchlow and J.D. Corbett, J. Amer. Chem. Soc., 1983, **105**, 5715; J.D. Corbett, Chem. Rev., 1985, **85**, 383.

32. D.M.P. Mingos and J.C. Hawes, Struct. Bond., 1985, **63**, 1.

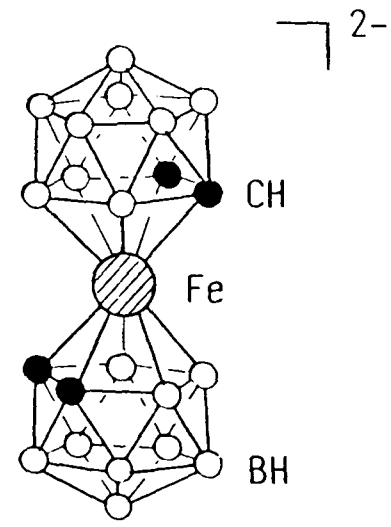
CHAPTER THREE

THEORETICAL ANALYSIS OF THE BONDING IN HYPER-CLOSO-METALLABORANES AND METALLACARBORANES

3.1 Introduction

3.1.1 Metallaborane and metallacarborane clusters

The field of metallaborane $\{M_mB_{(n-m)}\}$ and metallacarborane $\{M_mC_xB_{(n-m-x)}\}$ cluster chemistry (henceforth I shall use the term "metallaborane" to encompass both of these species) was pioneered by Hawthorne in the mid 1960's.[1] In 1965 he noted that the bonding capabilities of the "open" pentagonal face of the nido-$[C_2B_9H_{11}]^{2-}$ anion resemble those of the cyclopentadienyl ion $[C_5H_5]^-$. This observation led to the synthesis of the first transition metallaborane, the "sandwich" compound $[Fe(C_2B_9H_{11})_2]^{2-}$ **(I)**,[2] which is the metallaborane analogue of ferrocene.



$[Fe(C_2B_9H_{11})_2]^{2-}$

(I)

The first metallaborane to be structurally characterised was the "half-sandwich" derivative $[CpFeC_2B_9H_{11}]^-$,[3] which demonstrated that the metal atom occupied the twelfth vertex of an icosahedron.[4] The first structurally characterised metallaborane "sandwich" complex was the anion $[Co(C_2B_9H_{11})_2]^-$,[5] which is isoelectronic with the original ferrocene analogue.

The chemistry of the metallaboranes has been extensively developed, notably by Hawthorne,[1,6] Grimes,[7] Greenwood,[8] and Stone.[9] General synthetic procedures have been developed and cluster reactivity, at both the carborane cage and the metal vertex, has been probed. Hawthorne and coworkers have also described the utilisation of metallaboranes to catalyse olefin hydrogenation and isomerisation.[10]

3.1.2 Bonding in metallaboranes

The majority of metallaboranes adopt structures which are analogous to those of the deltahedrally-based boranes and carboranes.[11] This structural similarity led Wade and Mingos, independently, to conclude that the metal fragments (e.g. $M(CO)_3$ and MCp) in these clusters contribute 3 orbitals for cluster bonding, which are of the same pseudo-symmetry ($1\sigma + 2\pi$) as the frontier orbitals of the BH and CH fragments.[12] This conclusion has subsequently been confirmed with the development of the <u>isolobal</u> analogy.[13] As for borane and carborane clusters, it is the total number of skeletal electron pairs which determines the structure adopted by a metallaborane cluster.[12,14] This results in the occurrence of <u>closo</u>, <u>nido</u>, <u>arachno</u> and <u>hypho</u> geometries for clusters with (n+1), (n+2), (n+3) and (n+4) SEP's respectively, where n is the total number of (main group or transition metal) skeletal

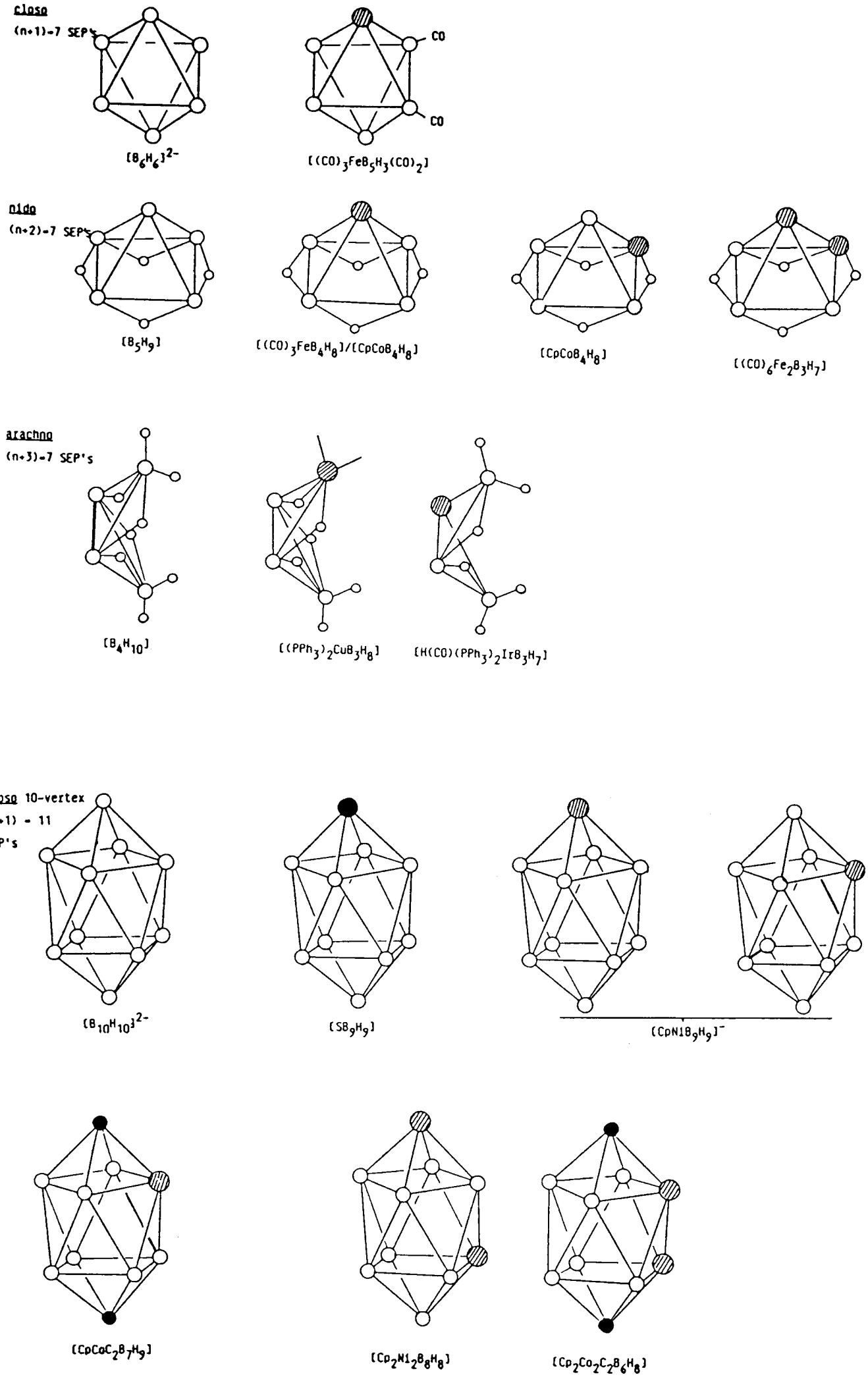


Figure 3.1 Examples of isostructural (and isoelectronic) boranes, metallaboranes and other heteroboranes.

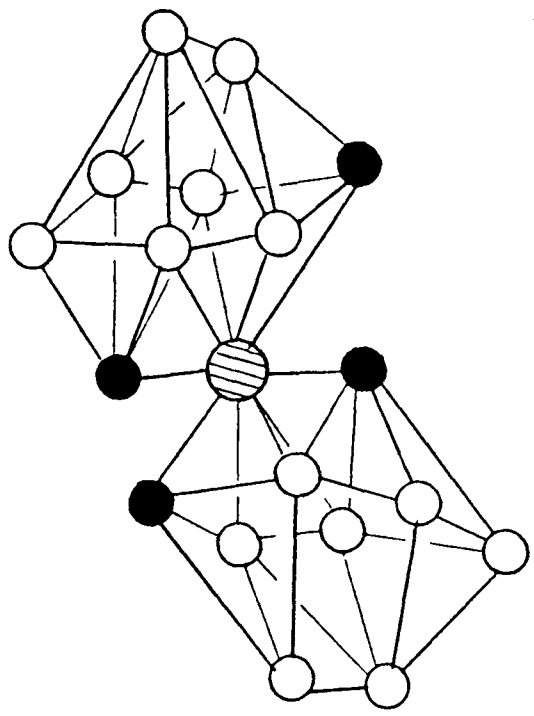
atoms.[12,14] Examples of isoelectronic (and hence isostructural) boranes and heteroboranes (with both main group and transition metal heteroatoms) are shown in **Figure 3.1.**

3.1.3 Anomalies in the borane-metallaborane structural relationship

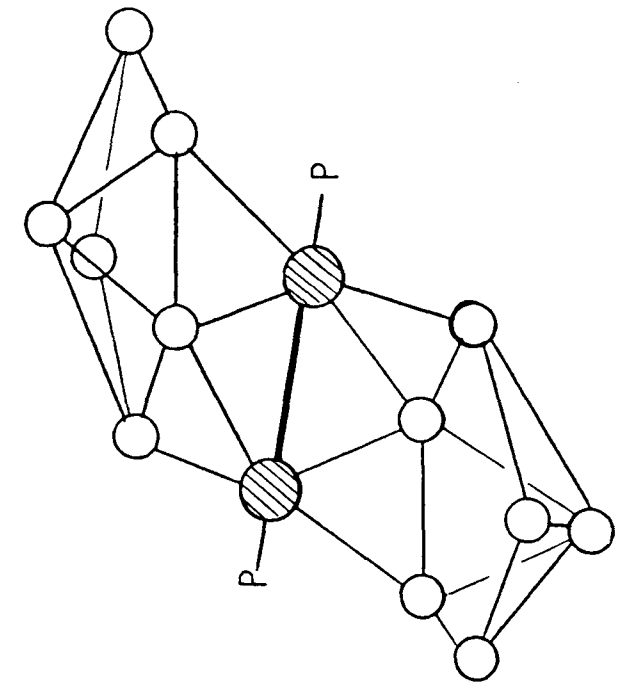
Although the majority of the polyhedral geometries adopted by metallaboranes correspond to known borane (or carborane) structures, there are a growing number of metallaborane compounds whose structures have no borane or carborane counterparts. Examples of such structures are depicted in **Figure 3.2.**

A considerable research effort has been directed towards understanding the ways in which metal fragments stabilise unusual cluster cage geometries.[7c,15] This stabilisation is often due to the ability of metal atoms either to occupy sites of high connectivity, or to act as the fusion points of two cluster polyhedra. The preference shown by metal atoms for high connectivity sites has been related to the relatively high positive charges of these sites in the parent borane anions,[16] since greater stabilisation is achieved when these sites are occupied by electropositive metal atoms. A similar argument has been used to rationalise the greater thermal stability of carboranes where the carbon atoms, being more electronegative than boron, occupy the lower connectivity (more negatively charged) cluster sites.[11,16] The presence of a number of atoms which are more electronegative than boron should also stabilise unusual cluster geometries. Indeed, Grimes has observed unusual structures for a number of carbon rich metallaboranes, in particular those with 4 skeletal carbon atoms.[7c,17]

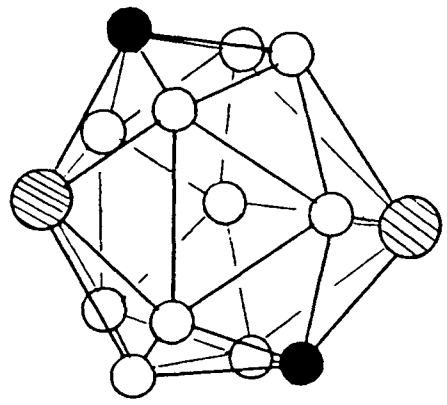
The capped octahedral trimetallaborane $[Cp_3Co_3B_4H_4]$ **(II)**[18]



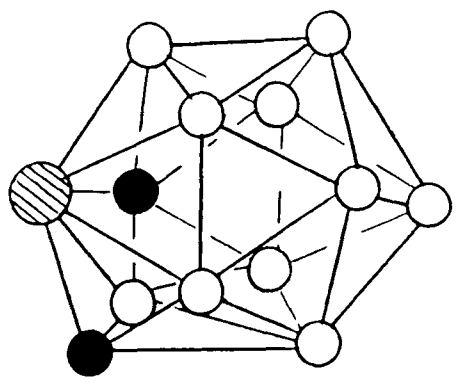
$[Co(C_2B_7H_9)_2]^-$



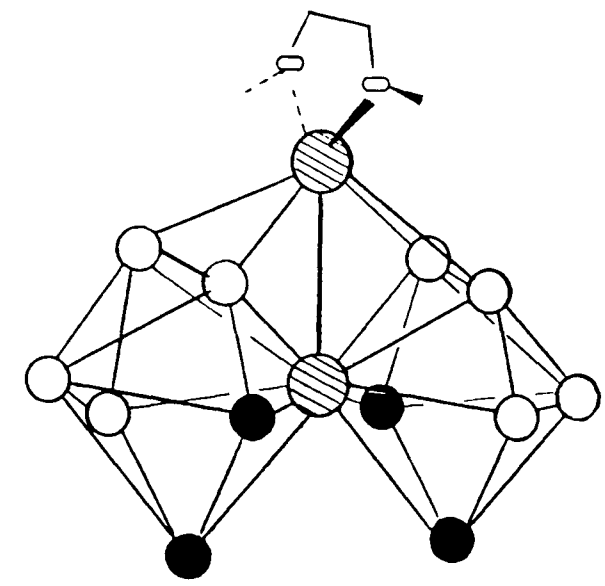
$[\mu\text{-}\{Pt(PMe_2Ph)\}_2(B_6H_9)_2]$



$[Cp_2Co_2C_2B_{10}H_{12}]$



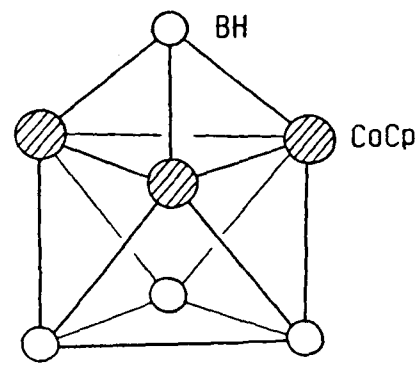
$[CpCoC_2B_{10}H_{12}]$



$[Fe\{(CMe)_2B_4H_4\}Fe\{(OMe)_2C_2H_4\}]$

Figure 3.2 Examples of metallaboranes which have no borane analogues.

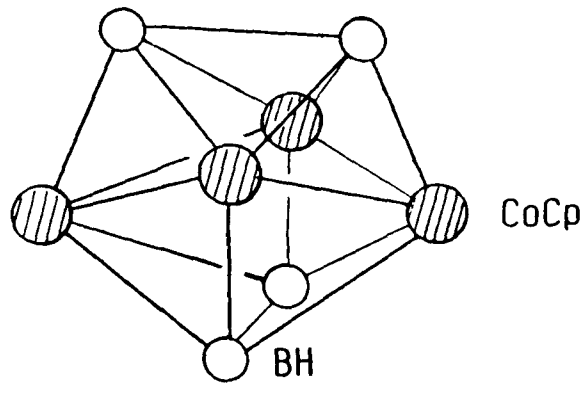
represents an important distinction between borane and metallaborane chemistry. No capped deltahedral boranes are yet known, a fact which Jemmis has attributed to the poor overlap of the valence s and p orbitals of a capping boron atom with a (small) B_3 triangle.[19] In **(II)**, however, the capped triangular face is significantly larger, and the effective overlap between the valence orbitals of the capping boron atom with this triangle is consequently greater.



$[Cp_3Co_3B_4H_4]$

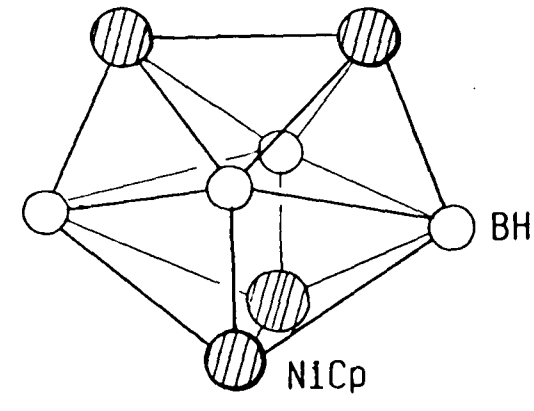
(II)

A different type of anomaly is exemplified by the dodecahedral molecules $[Cp_4Co_4B_4H_4]$ **(IIIa)**[20a] and $[Cp_4Ni_4B_4H_4]$ **(IIIb)**[20b]. These clusters possess the triangulated dodecahedral structure observed for $[B_8H_8]^{2-}$,[21] but they have 8 (n) and 10 (n+2) SEP's respectively, rather than the 9 (n+1) SEP's of the borane analogue.



$[Cp_4Co_4B_4H_4]$

(IIIa)



$[Cp_4Ni_4B_4H_4]$

(IIIb)

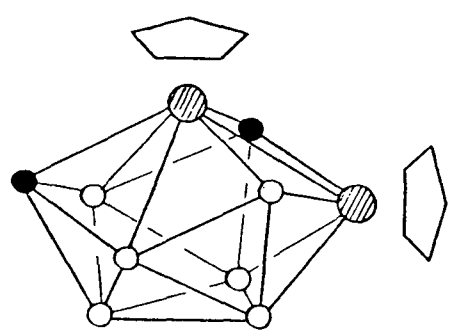
Several theoretical arguments have been put forward to rationalise the electron counts and site preferences in these clusters.[22] Wade has shown that both electron counts are possible for diamagnetic dodecahedral clusters, because both the HOMO and LUMO of $[B_8H_8]^{2-}$ are non-degenerate.[22b] A topologically derived explanation of this frontier orbital pattern, within the framework of Tensor Surface Harmonic theory, is presented in **Chapter 4.**

This Chapter is concerned with a further anomaly in the structural and electronic properties of boranes and metallaboranes. This anomaly is the occurrence of deltahedral geometries (not capped deltahedra) for n-vertex metallaboranes, which are different from those adopted by the n-vertex *closo* boranes and carboranes. There is currently some controversy as to whether these clusters possess n SEP's (i.e. one less than normal *closo* compounds, leading to their description as **"hyper-closo"**)[23] or the normal (n+1) SEP's, with the alternative deltahedral geometry favouring the utilisation of 4, rather than 3, metal orbitals for cluster bonding (i.e. they are merely isomers of the normal *closo* geometries, leading to their description as **"iso-closo"**).[8b,24]

3.2 The *Hyper/Iso-Closo* Controversy

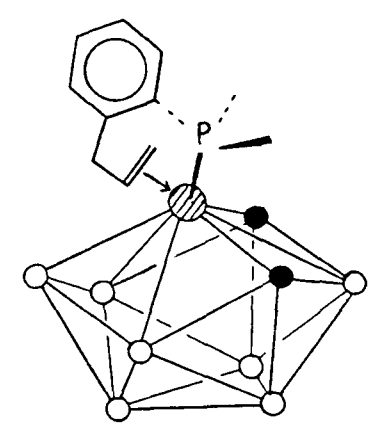
In 1975, Hawthorne and coworkers reported the synthesis and structural characterisation of $[Cp_2Fe_2C_2B_6H_8]$ **(IV)**.[25] They noted that the structure adopted by this metallaborane, although deltahedral, is geometrically distinct from the bicapped square antiprismatic structure, which is generally adopted by 10-vertex *closo* boranes and metallaboranes.[11] It was suggested that this unusual cluster possesses 20, rather than 22, skeletal electrons (i.e. 10 (n) rather than 11 (n+1)

SEP's), with each FeCp fragment contributing 1 electron towards cluster bonding (as they are <u>isolobal</u> with BH^+). This would make the bimetallaborane electronically, as well as structurally, distinct from normal <u>closo</u> clusters. Hawthorne subsequently structurally characterised a monometallic analogue of this cluster, $[\{(\underline{o}\text{-}CH_2{=}CHCH_2C_6H_4)PPh_2\}Ru(CMe)_2B_7H_7]$ **(V)**,[26] in the course of his studies of metallacarborane-catalysed olefin hydrogenation and isomerisation.[10] Taking the RuL_2 fragment as a 2-orbital-0-electron unit,[27] this cluster again has only 10 (n) SEP's.



$[Cp_2Fe_2C_2B_6H_8]$

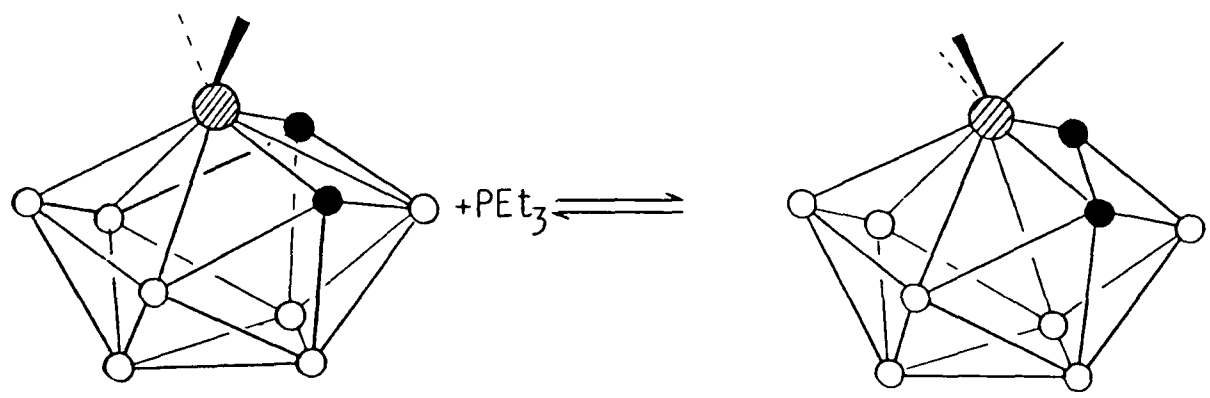
(IV)



$[\{(\underline{o}\text{-}CH_2{=}CHCH_2C_6H_4)PPh_2\}Ru(CMe)_2B_7H_7]$

(V)

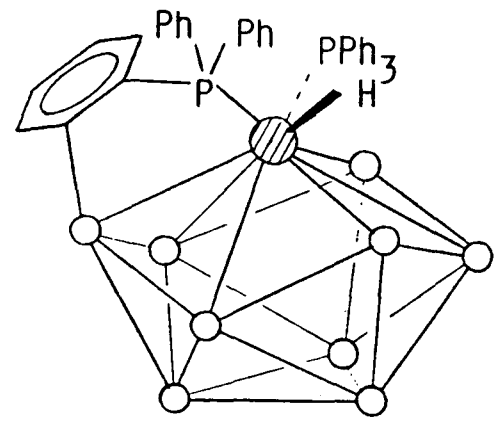
The term "<u>hyper-closo</u>" was introduced to describe this class of n-vertex n-SEP deltahedral clusters. On the basis of ^{11}B NMR data, the following <u>hyper-closo</u> /<u>closo</u> equilibrium was postulated:[28]



$[(PEt_3)_2RuC_2B_7H_9]$
(<u>hyper-closo</u>)

$[(PEt_3)_3RuC_2B_7H_9]$
(<u>closo</u>)

In 1982, Greenwood and Kennedy reported the structure of an analogous 10-vertex iridaborane $[H(PPh_3)(Ph_2\overline{PC_6H_4)IrB_9H_8}]$ **(VI).**[29] The valence electron count for this cluster is 50, i.e. 2 less than predicted for a <u>closo</u> molecule (52 = 14 +{9 x 4} + 2).[12] If the conical IrL_2H fragment is taken as a 3-orbital-2-electron unit (i.e. <u>isolobal</u> with BH), this cluster possesses 10 SEP's and may be classed as <u>hyper-closo</u>.[23]



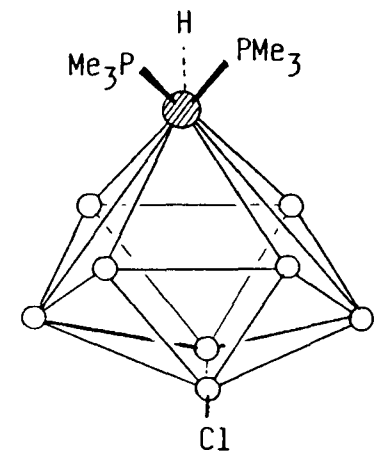
$[H(PPh_3)(Ph_2\overline{PC_6H_4)IrB_9H_8}]$

(VI)

Greenwood and Kennedy, however, considered that the metal fragment contributes 4, rather than 3, orbitals to cluster bonding and, therefore, may be regarded as a 4-electron fragment. Regarding the metal atom as a 4-orbital-4-electron fragment leads to it being designated formally as d^4-Ir(V), rather than d^6-Ir(III) (if it were a 3-orbital-2-electron fragment). In Greenwood and Kennedy's approach, therefore, the electron deficiency of the metallaborane is assumed to be metal-based, so that the cluster has 11 (n+1) SEP's. They have described such clusters as "<u>iso-closo</u>", since, if the skeletal electron pair count is the same, this deltahedral geometry may be regarded as an isomer of the more usual <u>closo</u> deltahedral structure.[8b,24] The concept of metal-localised electron deficiency can be traced back to earlier analyses of electron deficient metallaborane sandwich compounds, where non-bonding d

orbitals on the metal are unoccupied.[30] Nishimura had also previously suggested that the electron deficiency in the hyper-closo-$Fe_2C_2B_6$ cluster **(IV)** could be explained in terms of hyperpolyhedral metal-metal bonding between the iron atoms, with the cluster possessing (n+1), rather than n, SEP's.[30b]

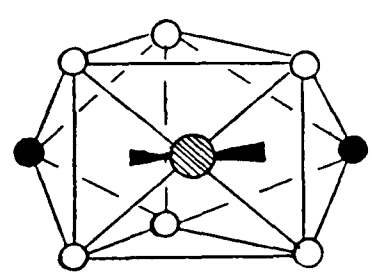
Greenwood and Kennedy, also in 1982, reported the structural characterisation of a novel deltahedral geometry for the 9-vertex iridaborane $[H(PMe_3)_2IrB_8H_7Cl]$ **(VII).**[31]



$[H(PMe_3)_2IrB_8H_7Cl]$

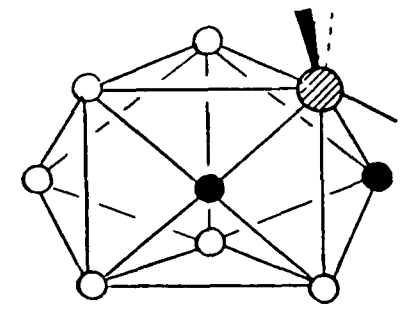
(VII)

The "normal" deltahedral geometry adopted by 9-vertex closo clusters is the tricapped trigonal prism, exemplified by $[(PMe_3)PtC_2B_6H_8]$ **(VIIIa)**[32] and $[(CO)_3MnC_2B_6H_8]^-$ **(VIIIb).**[33]



$[(PMe_3)_2PtC_2B_6H_8]$

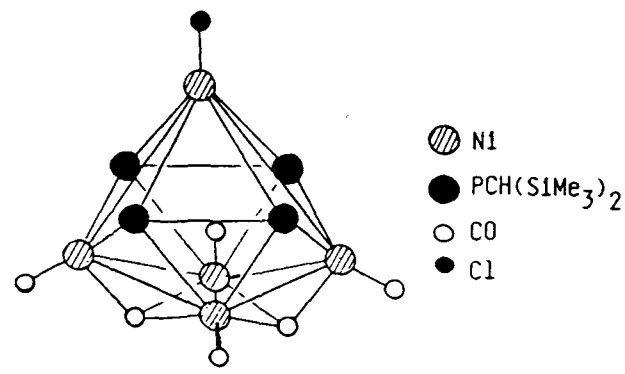
(VIIIa)



$[(CO)_3MnC_2B_6H_8]^-$

(VIIIb)

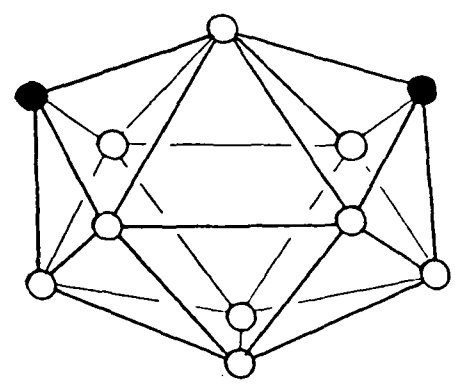
The classification of the IrB_8 compound as hyper- or iso-closo depends upon whether the $Ir(PMe_3)_2H$ moiety is regarded as a 3-orbital-2-electron[23] or 4-orbital-4-electron[24] fragment. Olmstead and Power have subsequently reported an isostructural nickel carbonyl phosphido cluster $[Ni_5(CO)_6(Cl)\{PCH(SiMe_3)_2\}_4]$ **(IX)**,[34] which Baker has classified as hyper-closo .[23] Taking the NiCl, NiCO and PR moieties as -1, 0 and 4 electron fragments respectively, this cluster possesses 19 skeletal electrons, i.e. one more than the number (18 = 2n) predicted for a "hyper-closo" cluster.



$[Ni_5(CO)_6(Cl)\{PCH(SiMe_3)_2\}_4]$

(IX)

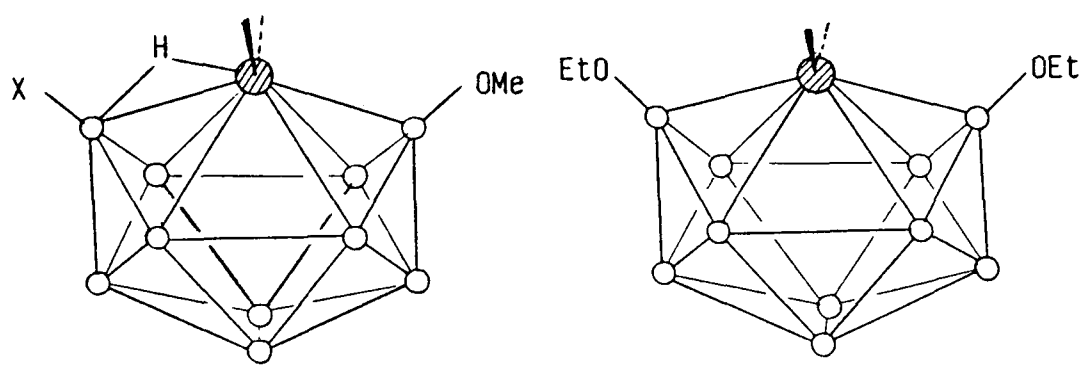
The above mentioned metallaborane clusters are geometrically distinct from the the usual closo structures. In Baker's view they are also electronically distinct, being hyper-electron-deficient.[23] A number of metallaboranes have been characterised, however, which adopt the same polyhedral geometry for what Baker would term the hyper-closo and closo situations. The polyhedron in question is the octadecahedron, which is the structure adopted by closo-$[(CMe)_2B_9H_9]$ **(X)**.[35]



$[(CMe)_2B_9H_9]$

(X)

Greenwood and Kennedy have structurally characterised a number of octadecahedral MB_{10} metallaboranes **(XI)**,[36] which they have classed as "iso-closo", i.e. a 4 orbital contribution from the metal atom to the cluster is invoked.[8b]



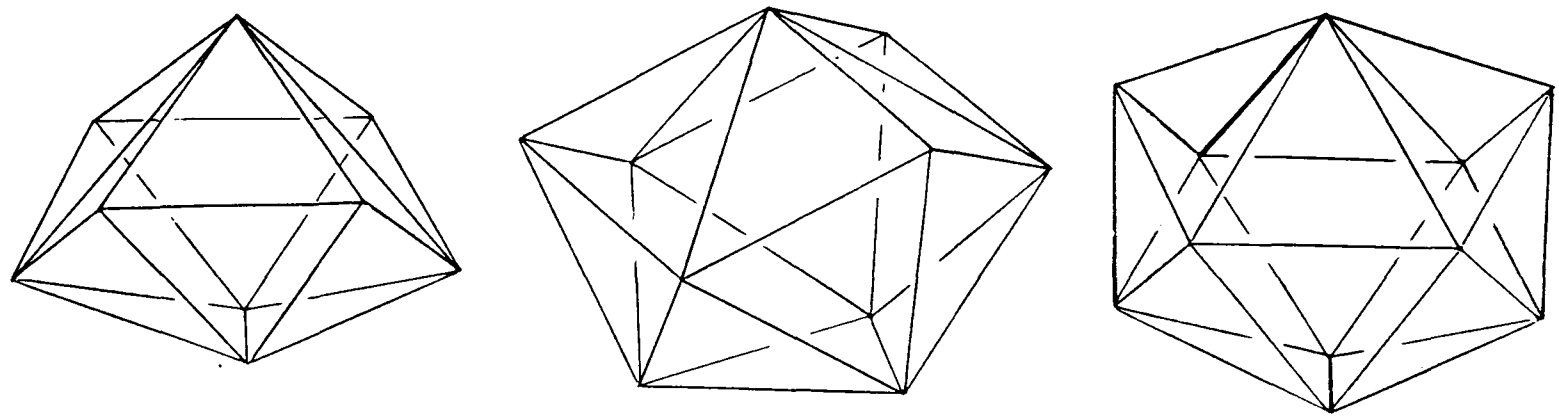
$[(PMe_2Ph)_2RhHB_{10}H_8(OMe)(X)]$
(X = OMe or Cl)

$[(PPh_3)_2RuB_{10}H_8(OEt)_2]$

(XI)

Sneddon has recently reported the characterisation of the π-acid metallaboranes $[(\eta^6\text{-}C_6H_3Me_3)FeB_9H_9]$ and $[(\eta^6\text{-}C_6H_3Me_3)FeB_{10}H_{10}]$. These clusters are believed, on the basis of ^{11}B NMR evidence,[37] to have the same geometries as the 10- and 11-vertex hyper/iso-closo clusters described above. This, together with Greenwood and Kennedy's report of the synthesis of "iso-closo"-$[Cp^*RhB_{10}H_{10}]$,[36b] indicates that this structural type does not require the presence of strong σ-donating ligands (such as phosphines or hydrides) on the metal atom.

Henceforth, the term "hyper-closo" will be used to describe all hyper-electron-deficient deltahedral metallaboranes, though, for the time being, no assumption will be made made as to whether this hyper-electron-deficiency is metal or cluster based. The three types of hyper-closo deltahedra are depicted in **Figure 3.3**, together with examples of clusters adopting these structures. For the octadecahedral structure



Examples

n SEP's*	$[H(PMe_3)_2IrB_8H_7Cl]$[a]	$[H(PPh_3)(Ph_2C_6H_4)IrB_9H_8]$[c]	$[(PPh_3)_2RuB_{10}H_8(OEt)_2]$[d,i]
	$[Ni_5(CO)_6Cl\{PCh(SiMe_3)_2\}_4]$[b]	$[H(PPh_3)ClRuB_9H_7(PPh_3)_2]$[d]	$[H(PMe_2Ph)_2RhB_{10}H_8(OMe)_2]$[j]
		$[Cp_2Fe_2C_2B_6H_8]$[e]	$[(\eta^6\text{-}C_6H_3Me_3)FeB_{10}H_{10}]$[h]
		$[\{(o\text{-}CH_2{=}CHCH_2C_6H_4)PPh_2\}Ru(CMe)_2B_7H_7]$[f]	$[Cp^*RuB_{10}H_{10}]$[d]
		$[(PEt_3)_2RuC_2B_7H_9]$[g]	
		$[(\eta^6\text{-}C_6H_3Me_3)FeB_9H_9]$[h]	
(n+1) SEP's*			$[(CMe)_2B_9H_9]$[k]
			$[H(PEt_3)_2RhC_2B_8H_{10}]$[l]
			$[CpCoC_2B_8H_{10}]$[m]

* n is the number of vertices of the cluster. The hyper-closo clusters have been assigned n SEP's in accordance with Baker's treatment (Ref. 23).

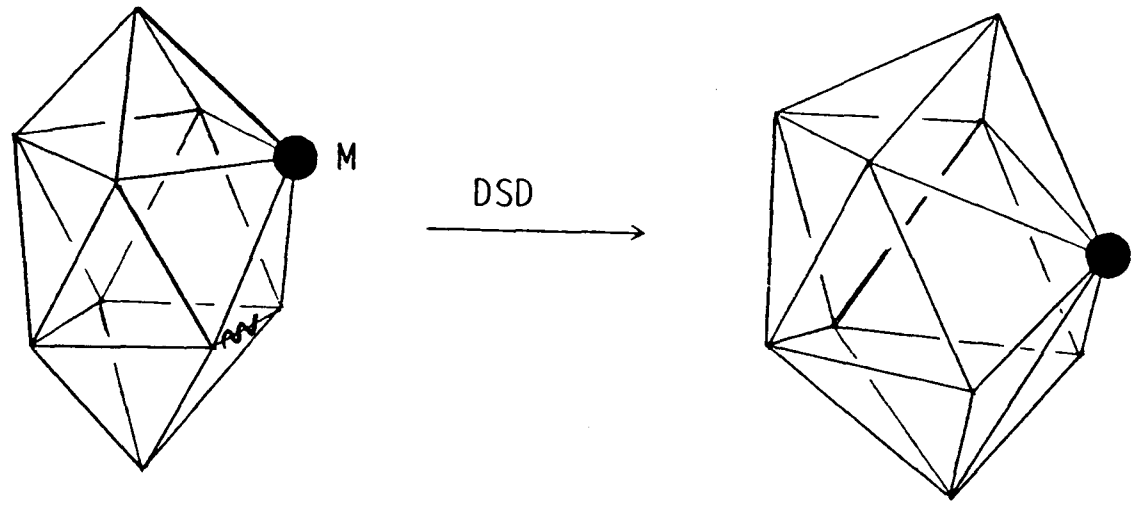
a J. Bould, N.N. Greenwood, J.D. Kennedy and W.S. McDonald, J. Chem. Soc., Dalton Trans., 1985, 1843. **b** M.M. Olmstead and P.P. Power, J. Amer. Chem. Soc., 1984, **106**, 1495. **c** J. Bould, N.N. Greenwood, J.D. Kennedy and W.S. McDonald, J. Chem. Soc., Chem. Commun., 1982, 465. **d** J.E. Crook, M. Elrington, N. Greenwood, J.D. Kennedy, M. Thornton-Pett and J.D. Woolins, J. Chem. Soc., Dalton Trans., 1985, 2407. **e** K.P. Callahan, W.J. Evans, F.Y. Lo, C.E. Strouse and M.F. Hawthorne, J. Amer. Chem. Soc., 1975, **97**, 296. **f** C.W. Jung, R.T. Baker, C.B. Knobler and M.F. Hawthorne, J. Amer. Chem. Soc., 1980, **102**, 5782. **g** C.W. Jung, R.T. Baker and M.F. Hawthorne, J. Amer. Chem. Soc., 1981, **103**, 810. **h** R.P. Micciche, J.J. Briguglio and L.G. Sneddon, Inorg. Chem., 1984, **23**, 3992. J.E. Crook, M. Elrington, N.N. Greenwood, J.D. Kennedy and J.D. Woollins, Polyhedron, 1984, **3**, 901. **j** H. Fowkes, N.N. Greenwood, J.D. Kennedy and M. Thornton-Pett, J. Chem. Soc., Dalton Trans., 1986, 517. **k** C. Tsai and W. Streib, J. Amer. Chem. Soc., 1966, **88**, 4513. **l** C.W. Jung and M.F. Hawthorne, J. Amer. Chem. Soc., 1980, **102**, 3024. **m** D.F. Dustin, G.B. Dunks and M.F. Hawthorne, J. Amer. Chem. Soc., 1973, **95**, 1109.

Figure 3.3 The three types of hyper-closo deltahedra and examples of hyper-closo metallaboranes.

examples of the "normal" closo compounds are also included.

3.2.1 Structural features of hyper-closo metallaboranes

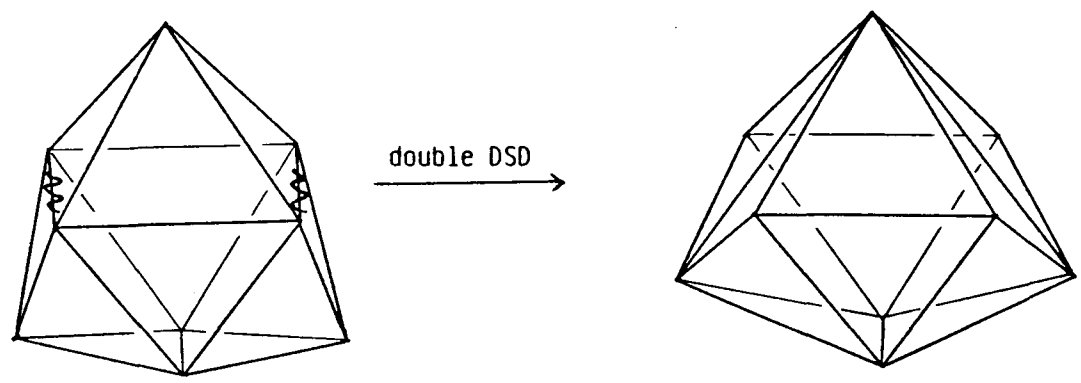
Hawthorne[25,28] and Baker[23] have shown that the alternative 10 vertex deltahedra may be interchanged by altering the bonding characteristics of two adjacent triangular faces. For example, in the MB_9 case, the closo to hyper-closo transformation corresponds to breaking one B-B bond (where both of these atoms are bonded to the metal) and forming an M-B bond, which is perpendicular to the original bond:



closo hyper-closo

They have noted that this process corresponds to the **"diamond-square-diamond"** (DSD) mechanism, proposed by Lipscomb to rationalise borane fluctionality and carborane isomerisation.[38] Evidence for a closo/hyper-closo equilibrium, corresponding to this transformation, has been obtained from NMR studies.[28]

Baker has shown that the 9-vertex hyper-closo deltahedron is related to the closo tricapped trigonal prism by two such DSD transformations:[23]



closo hyper-closo

This hyper-closo geometry was postulated by Lipscomb as an intermediate in a possible "double DSD" mechanism for the isomerisation of 9-vertex carboranes.[38]

Greenwood and Kennedy, while noting the structural and connectivity relationships between closo and hyper-closo geometries, have described an alternative way of deriving the hyper-closo structures.[36a] Just as the usual n-vertex closo metallaborane geometry is formed by capping the open face of an (n-1)-vertex nido borane with a metal atom, an n-vertex hyper-closo metallaborane may be obtained by capping an (n-1)-vertex arachno borane. Thus the n-vertex hyper-closo metallaboranes are seen to be related to the (n+1)-vertex closo boranes by the replacement of a pair of adjacent boron atoms by a single metal atom.

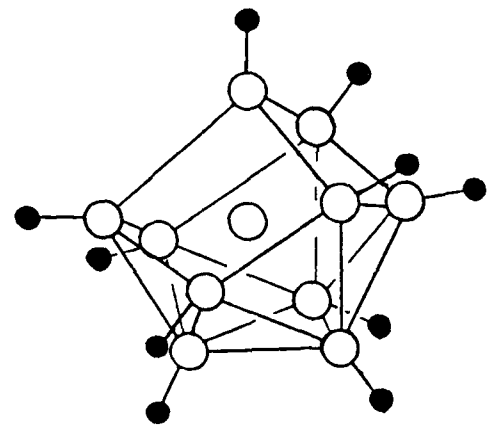
3.2.2 The icosahedral fragment approach to hyper-closo structures

Although Greenwood and Kennedy's structural analysis leads to the derivation of the correct cluster connectivities in hyper-closo

complexes, it does not emphasise the symmetries of these cluster compounds. The borane or carborane cages in these metallaboranes may be considered as fragments of the same polyhedron, namely the closo icosahedron. Thus, as indicated by Greenwood and Kennedy,[8b,24] the MB_{10} hyper-closo species may be regarded as an arachno icosahedron of C_{2v} symmetry, with the open face capped by a single metal atom lying on the C_2 axis.

The hyper-closo-MB_9 polyhedron may be regarded as a hypho icosahedral borane (with C_{3v} symmetry), with the open face capped by a metal atom which lies on the C_3 axis. Greenwood and Kennedy have noted the pseudo-C_{3v} symmetry adopted by the hyper-closo-IrB_9 cluster, which has a $1:3:\bar{3}:3$ arrangement of vertices, 3 short M-B bonds and 3 longer ones (across the rhombic faces of Keppert's polyhedron). **Table 3.1** (taken from Ref. 23) lists the metal-boron (or carbon) bond lengths in the structurally characterised hyper-closo-MB_9 clusters, along with a closo example for comparison. These bond lengths emphasise the pseudo 3-fold symmetry of 10-vertex hyper-closo metallaboranes.

The hyper-closo-MB_9 geometry is identical to that adopted by centred gold clusters of the type $[Au(AuL)_{10}]^{3+}$ **(XII)**,[39] except for the fact that the gold clusters have only 3 bonds from the axial atom to the rest of the cluster (i.e. there are 3 rhombic, rather than 6 triangular faces associated with the axial atom).



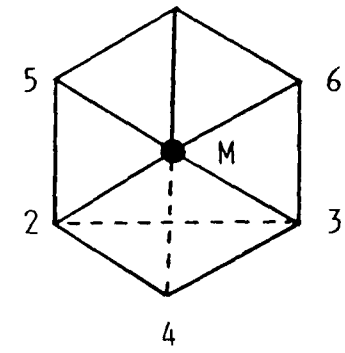
$[Au(AuL)_{10}]^{3+}$

(XII)

Table 3.1 Comparison of skeletal bond lengths in hyper-closo and closo 10-vertex metallacarboranes (adapted from Ref. 23)

Bond	Bond length (Å)				
	IrB_9[a]	RuB_9[b]	RuC_2B_7[c]	$Fe_2C_2B_6$[d]	RhC_2B_7[e]
$M-B_1$	2.16	2.09	2.02	2.10	2.10*
$M-B_2$	2.15	2.09	2.19*	1.99*	2.36*
$M-B_3$	2.19	2.19	2.10*	1.96*	2.21
B_2-B_3**	> 2.95	2.98	2.69*	2.71*	1.79*
$M-B_4$	2.39	2.40	2.49	2.20	3.50
$M-B_5$	2.38	2.35	2.47	2.57***	2.38
$M-B_6$	2.46	2.52	2.34	2.22	2.32

1



* Distances involving carbon atoms.

** Since the hyper-closo-metallacarboranes possess approximately C_{3v} symmetry, the choice of B_2-B_3, to demonstrate the relationship between the hyper-closo and closo geometries, is arbitrary (i.e. B_1-B_2 or B_1-B_3 could equally well have been chosen).

*** In this case "B_5" is actually a second Fe atom.

a hyper-closo-$[H(PPh_3)(Ph_2PC_4H_4)IrB_9H_8]$ **(VI)**; Ref. 29.

b hyper-closo-$[H(PPH_3)ClRuB_9H_7(PPh_3)_2]$; Ref. 36b.

c hyper-closo-[(o-CH_2=$CHCH_2C_6H_4$)PPh_2 $Ru(CMe)_2B_7H_7$] **(V)**; Ref. 26.

d hyper-closo-$[Cp_2Fe_2C_2B_6H_8]$ **(IV)**; Ref. 25.

e closo-$[H(PEt_3)_2RhC_2B_7H_9]$; G.K. Barker, M.P. Garcia, M. Green, F.G.A. Stone, J.-M. Bassett and A.J. Welch, J. Chem. Soc., Chem. Commun., 1981, 653.

Keppert has discussed the (hypothetical) isostructural B_{10} cluster, in his study of the relative energies of borane polyhedra.[40] He concluded that, on the basis of a simple pairwise attractive potential model, the "trirhombohedral" geometry is only slightly less favoured than the bicapped square antiprism. On these grounds, Keppert has postulated the B_{10} trirhombohedron as a possible transition state for the intramolecular rearrangement of $[B_{10}H_{10}]^{2-}$.

Finally, hyper-closo-MB_8 may be regarded as a klado icosahedron (4 missing vertices, C_{2v}) with a metal atom, lying on the C_2 axis, capping the open, inverted boat-like, face.

From these structural relationships, which are summarised in **Figure 3.4**, it is apparent that the topological feature which hyper-closo clusters have in common is that they possess one atom on the principal C_n rotation axis of the molecule (assuming idealised C_{nv} geometries). Defining the principal rotation axis as the **polar axis** leads to the description of these polyhedra as **polar deltahedra.** The class of polar deltahedra will be treated in detail in **Chapter 4,** but for the moment it is only necessary to note that the skeletons of the hyper-closo-MB_8 and MB_{10} clusters may be classed as C_2-polar deltahedra (because the principal C_n axis is a twofold), while the hyper-closo-MB_9 (C_{3v}) cluster may be classified as a C_3-polar deltahedron. The following names may, therefore, be assigned to the hyper-closo type polyhedra:

9 vertices = "C_2-polar tetradeca(delta)hedron"

10 vertices = "C_3-polar hexadecahedron"

11 vertices = "C_2-polar octadecahedron"

Extended Hückel calculations have been used to study the interaction between axial metal fragments (specifically the conical

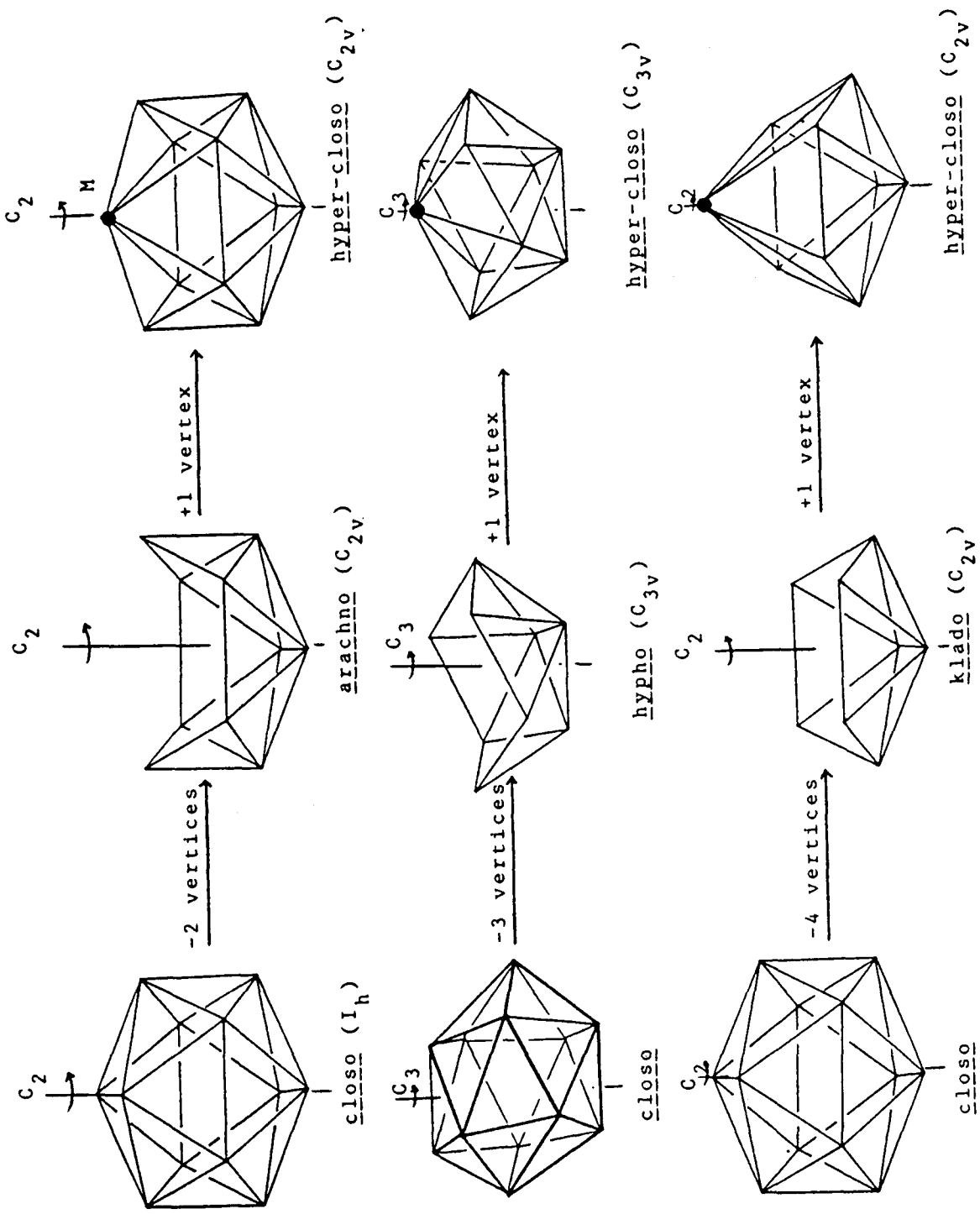


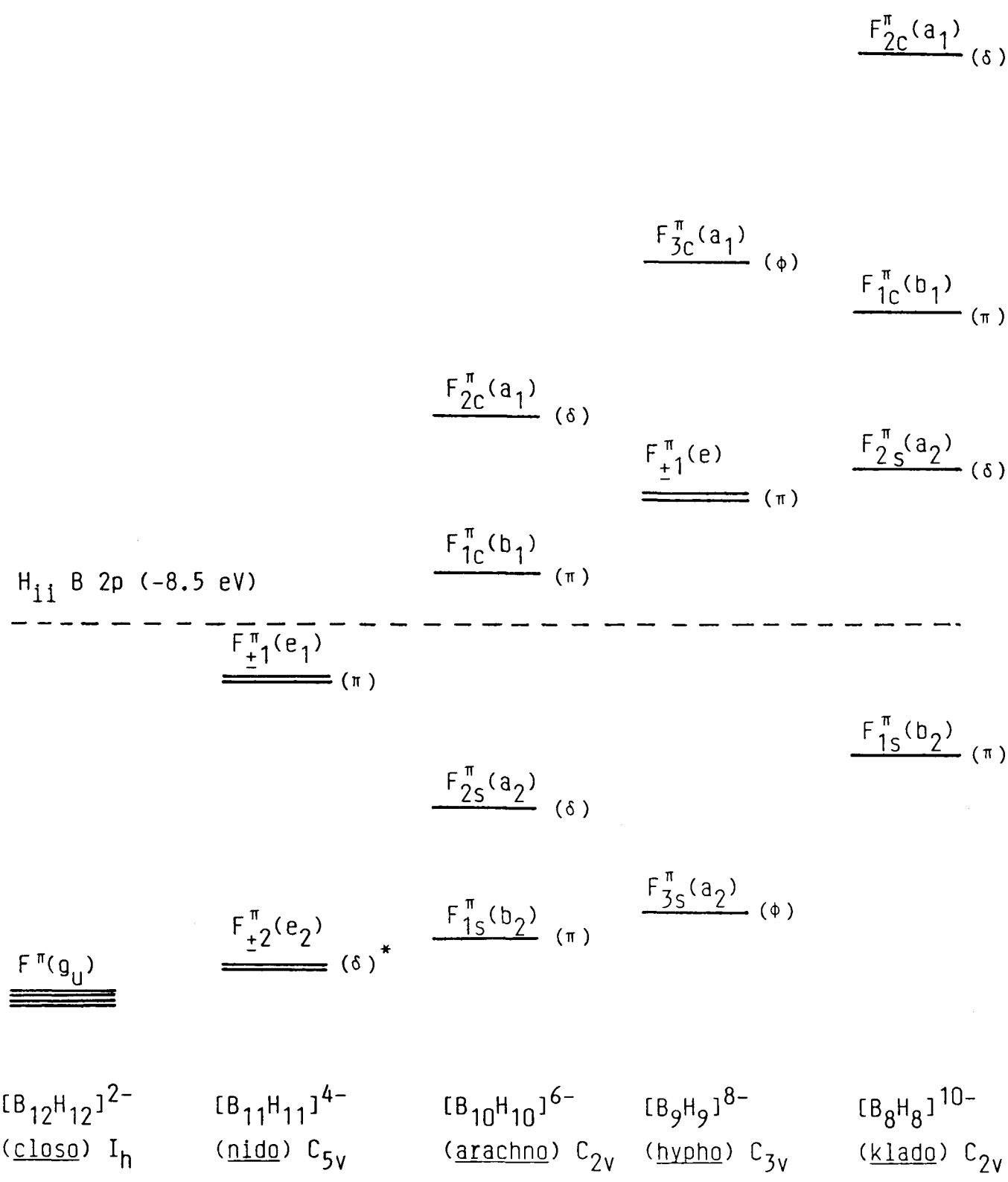
Figure 3.4 Hyper-closo metallaborane structures as metal-capped fragments of icosahedral closo-$[B_{12}H_{12}]^{2-}$.

$Rh(CO)_3$ fragment) and fragments of boron icosahedra. Comparative calculations have also been performed on hyper-closo-$[B_nH_n]$ molecules. The cluster bond lengths and atomic orbital parameters which were used in these calculations are given in the **Appendix** to this Chapter (**Section 3.9**). The Tensor Surface Harmonic methodology[41] has been used to describe the MO's of these borane and metallaborane clusters.

3.3 Analysis of the Frontier Molecular Orbitals of Borane Fragments Derived from Icosahedral Closo-$[B_{12}H_{12}]^{2-}$

The frontier orbitals of major interest, for the nido, arachno, hypho and klado icosahedral fragments, are those derived from the $F^{\pi}(g_u)$ HOMO's of the parent icosahedral borane, since the lower lying skeletal MO's of closo-$[B_{12}H_{12}]^{2-}$ remain essentially bonding upon removing cluster vertices. **Figure 3.5** shows that the degeneracy of the $F^{\pi}(g_u)$ orbitals is lowered as cluster vertices are removed, due to the lowering of symmetry and loss of stabilising overlap with the missing vertices. These orbitals become progressively more antibonding as more vertices are removed. The "F^{π}" label of the parent icosahedron is given to these orbitals, so that this correlation may be made (in terms of the TSH analysis for the individual fragments, some of the frontier orbitals may alternatively be labelled $\bar{D}^{\pi}$ or $\bar{F}^{\pi}$). The axial pseudo-symmetries of the F^{π}-type orbitals are dependent on the number of nodal planes which they possess relative to the principal C_n axis, which is equal to the magnitude of the TSH M quantum number: $F^{\pi}_0 = \sigma$; $F^{\pi}_{\pm 1} = \pi$; $F^{\pi}_{\pm 2} = \delta$; $F^{\pi}_{\pm 3} = \phi$.

In the case of the nido-B_{11} fragment, the $F^{\pi}_{\pm 2}(e_2, \delta)$ orbitals are overall bonding and the non-bonding $F^{\pi}_{\pm 1}(e_1, \pi)$ orbitals are stabilised



* axial pseudo-symmetry of borane fragment MO's, with respect to the open face of the fragment.

Figure 3.5 The effect of removing cluster vertices on the $F^{\pi}(g_u)$ MO's of icosahedral closo-$[B_{12}H_{12}]^{2-}$.

by interaction with the (e_1, π) orbitals of a capping metal atom to generate a closo icosahedral metallaborane with 13 (n+1) SEP's. For the arachno, hypho and klado fragments, however, there are a number of antibonding "F^{π}" orbitals which are high lying and do not possess the correct axial pseudo-symmetry (i.e. possess too many angular nodes relative to the C_n axis) to be stabilised by a single capping metal atom. Thus the polar deltahedral geometries can be seen to be characterised by fewer than 13 SEP's. In order to evaluate the exact number of SEP's which they possess, it is necessary to study each geometry in turn.

3.4 Ten-Vertex Hyper-Closo Clusters

3.4.1 Hyper-closo-$[B_{10}H_{10}]$

From **Figure 3.5**, it is apparent that the hypho-B_9 fragment possesses one "F^{π}" orbital (i.e. $F^{\pi}_{3c}(a_1, \phi)$) which remains innaccessible for the hyper-closo borane, due to its high lying nature and nodal characteristics (i.e. it possesses ϕ-pseudo-symmetry with respect to the C_3 axis). **Figure 3.6** shows the interaction between the skeletal MO's of the hypho fragment and an axial BH group. The radial sp^{σ} hybrid of the BH group interacts mainly with low-lying cluster orbitals of mixed B-B and B-H bonding nature and has, therefore, been omitted from the Figure. The most significant feature of **Figure 3.6** is the three-level interaction between the e symmetry orbitals $F^{\pi}_{\pm 1}$ and $D^{\pi}_{\pm 1}$ of the B_9 cage (both of which possess π-pseudo-symmetry with respect to the C_3 axis) and the $(p_x, p_y)^{\pi}$ e pair of the polar boron atom. This interaction leads to one bonding pair, one antibonding pair and a non-bonding pair of

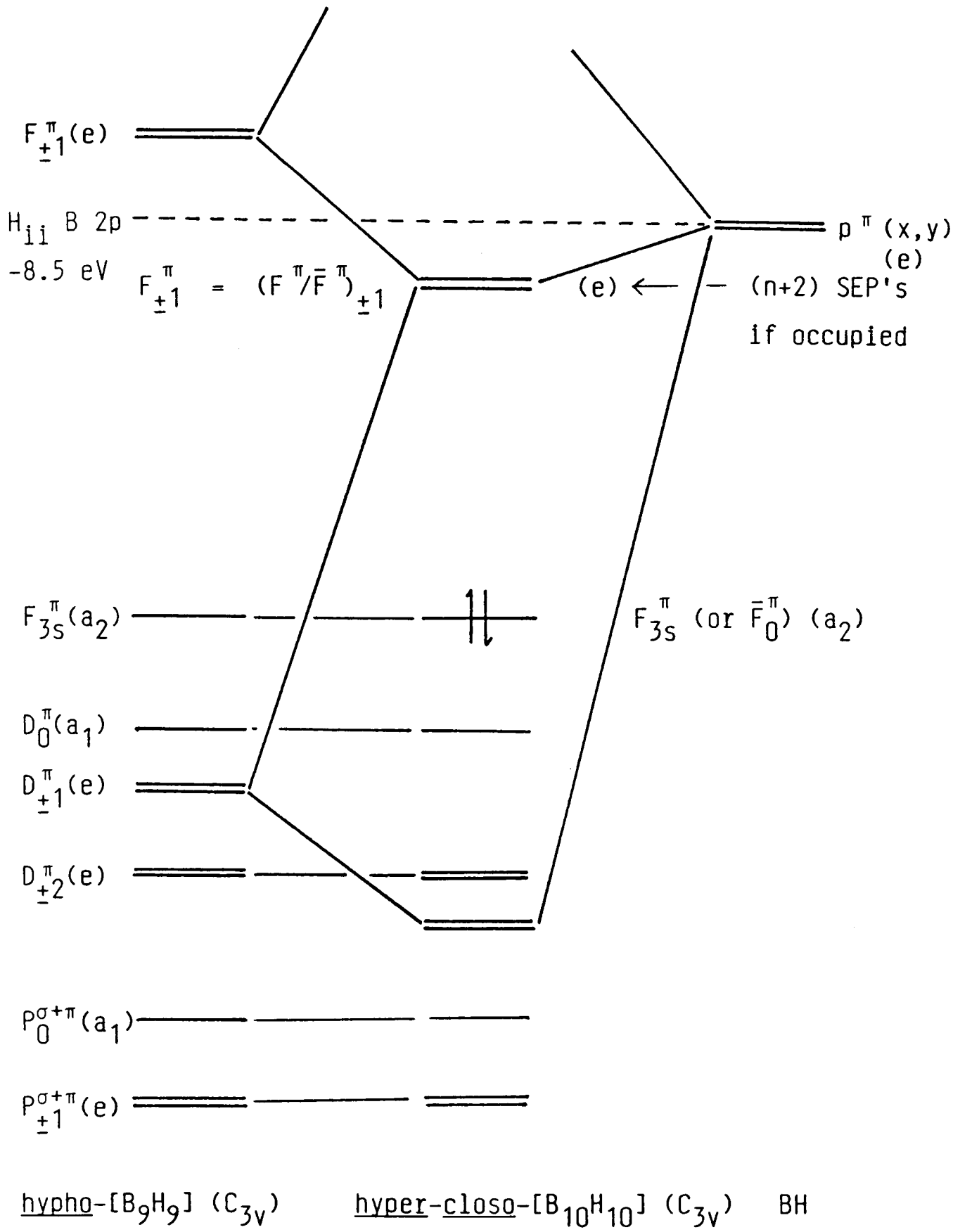
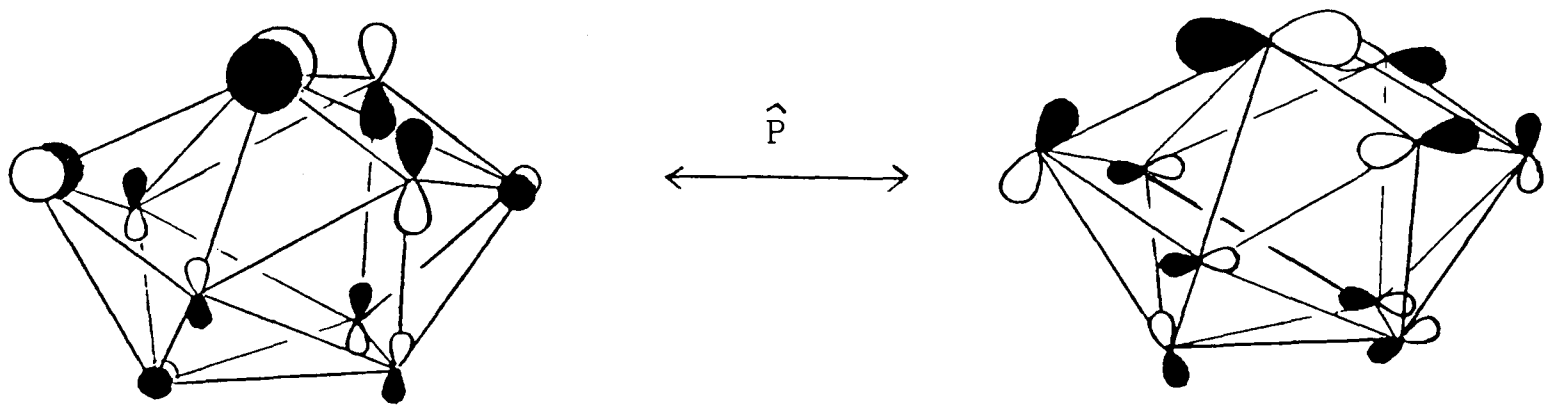


Figure 3.6 Orbital interactions between hypho-[B_9H_9] and a capping BH fragment.

orbitals. This last pair may be identified as $(F^{\pi}/\bar{F}^{\pi})_{\pm 1}$, where this TSH label refers to the hyper-closo deltahedron rather than the icosahedral parent geometry. In this context, it should be noted that the $F_{3s}(a_2)$ orbital of the hypho species is redesignated as $\bar{F}_0^{\pi}$ in the hyper-closo molecule, since these TSH functions are equivalent for both the B_9 and B_{10} geometries and Stone's methodology involves the choice of the lowest possible M quantum number if there are two possibilities. Similarly, the F_{3c}^{π} orbital may be alternatively designated as F_0^{π}.

The pattern of skeletal MO's for hyper-closo-$[B_{10}H_{10}]$ is contrasted with that of the closo bicapped square antiprism on the right-hand side of **Figure 3.7.** The closo bicapped square antiprism is characterised by (n+1) skeletal bonding MO's. In terms of TSH theory, these (n+1) skeletal bonding MO's consist of S^{σ}, $3P^{\sigma+\pi}$ and $(n-3)L^{\pi}$ orbitals. In contrast, the hyper-closo geometry is characterised by n skeletal bonding MO's ($S^{\sigma} + 3P^{\sigma+\pi} + (n-4)L^{\pi}$) and the previously mentioned degenerate (e) pair of non-bonding orbitals, $(F^{\pi}/\bar{F}^{\pi})_{\pm 1}$, which are related by the Parity Inversion operation:



The nature of the Parity Inversion operation ensures that L^{π} and $\bar{L}^{\pi}$ can only be degenerate if they are non-bonding (or approximately non-

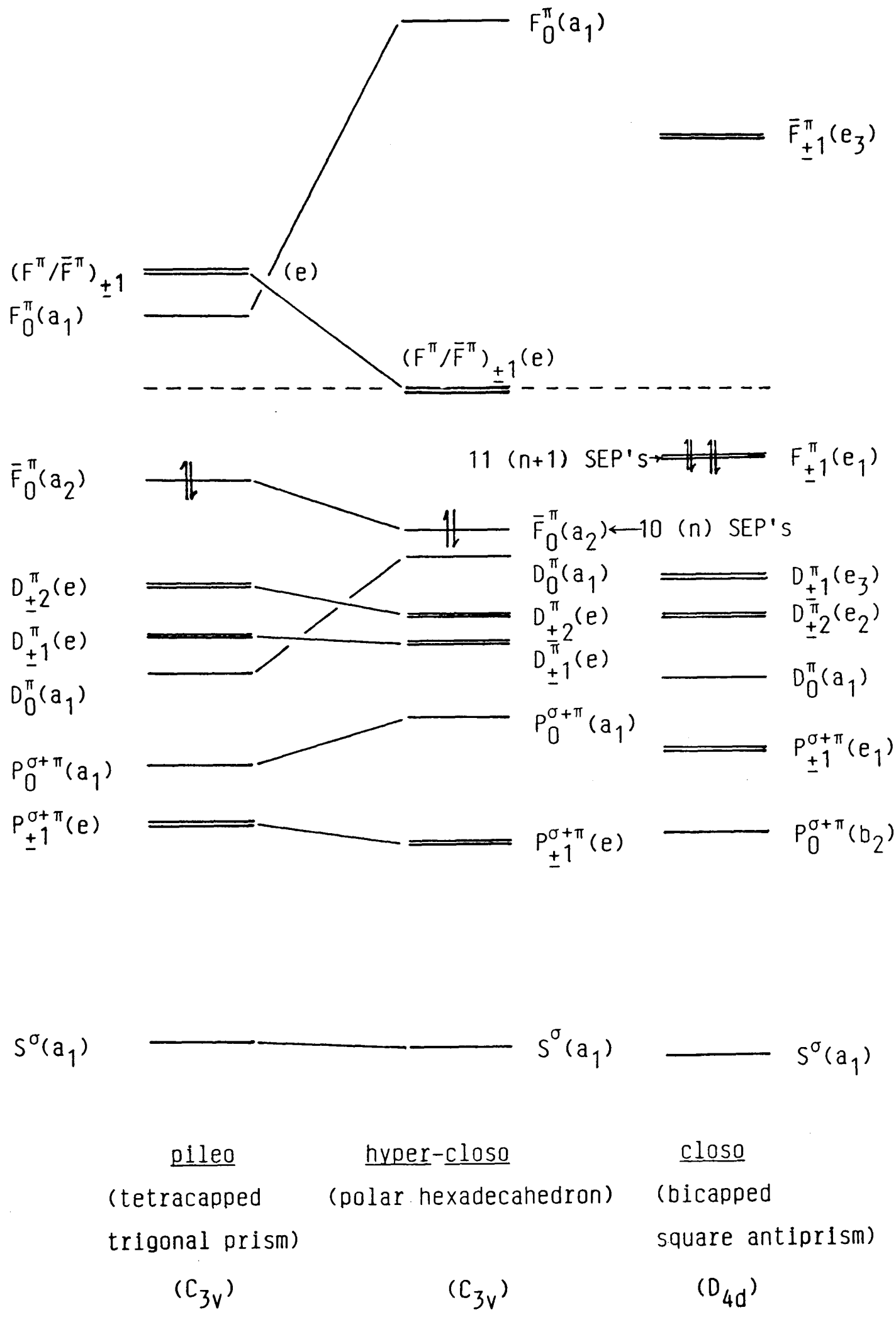
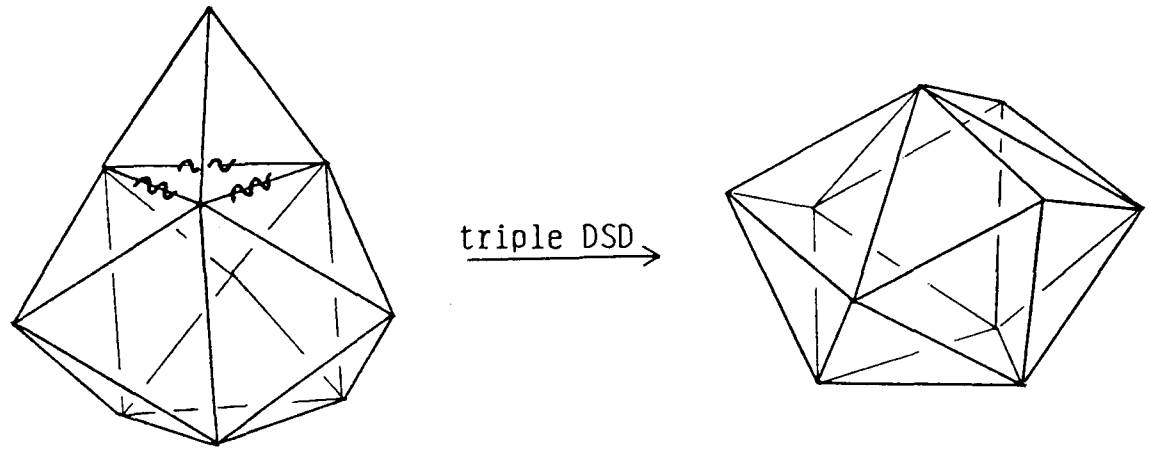


Figure 3.7 Comparison of the skeletal MO pattern of hyper-closo-$[B_{10}H_{10}]$ with those of the pileo and closo clusters.

bonding).[41] Thus the C_3-polar deltahedral B_{10} cluster may be characterised by either n or (n+2), but not (n+1) SEP's. This has relevance to the work of Keppert,[40] since a paramagnetic transition state for the rearrangement of <u>closo</u>-$[B_{10}H_{10}]^{2-}$ is clearly unfavourable on orbital symmetry grounds.

Hawthorne and Baker have noted the similarity between the geometry of the 10-vertex <u>hyper-closo</u> metallaboranes and the tetracapped trigonal prism.[28] The tetracapped trigonal prism (which is also a C_3-polar deltahedron) can be converted into the <u>hyper-closo</u> geometry by breaking the bonds in the capped triangular face and forming bonds between the capping atom and the equatorial atoms. This triple DSD process maintains the C_{3v} symmetry and the 1:3:$\bar{3}$:3 disposition of cluster vertices:

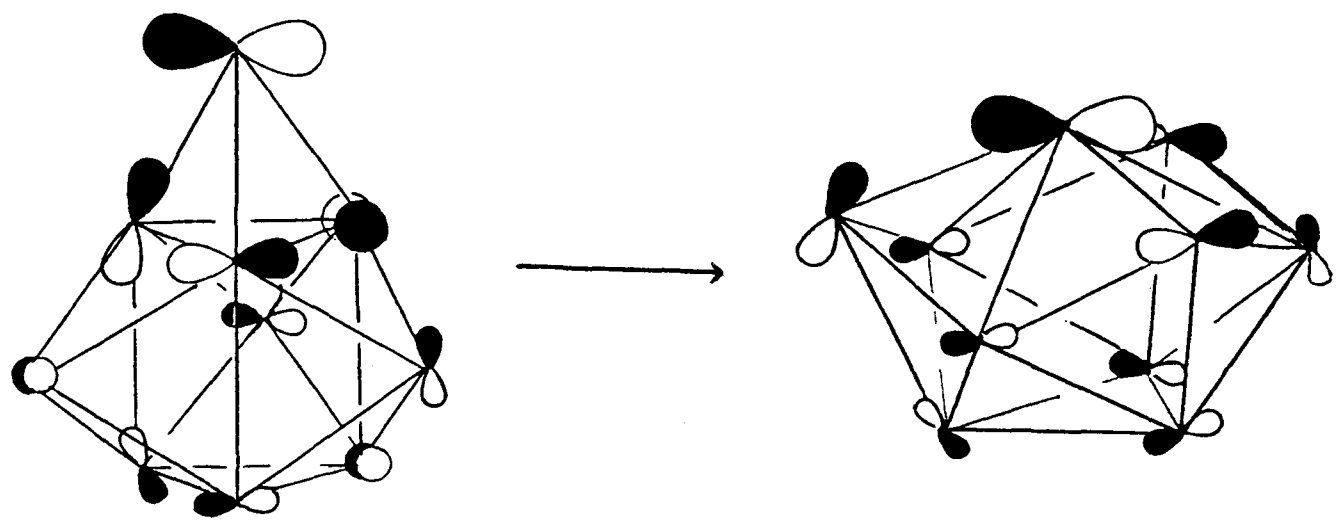


<u>pileo</u> <u>hyper-closo</u>

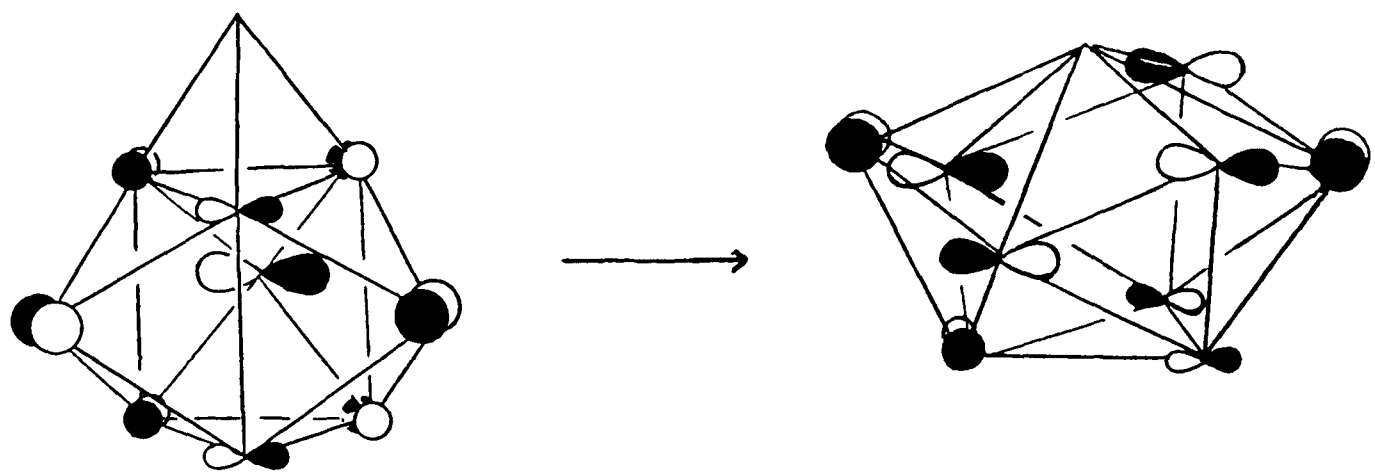
The recognition of this geometric similarity has important electronic consequences, since, on the basis of the Capping Principle,[42] the capped deltahedral structure would be expected to possess n (i.e. 10) SEP's, as postulated for the <u>hyper-closo</u> metallaboranes.[28] The only structurally characterised <u>pileo</u> metallaborane is the capped octahedral cluster

$[Cp_3Co_3B_4H_4]$ **(II)**,[18] which is indeed found to have n (i.e. 7) SEP's.[14c]

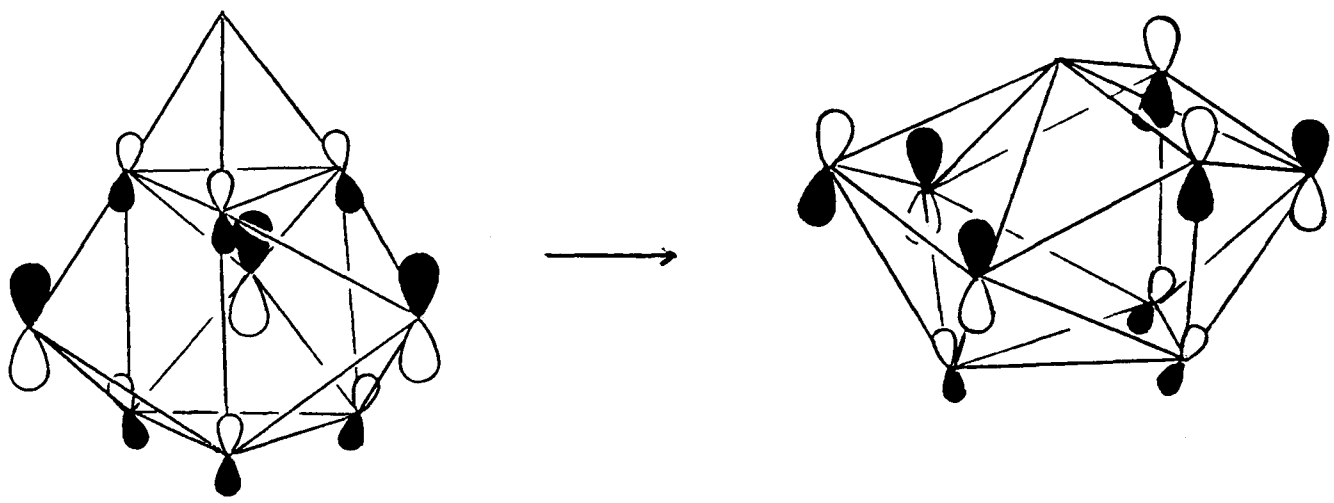
On the left-hand side of **Figure 3.7** the skeletal MO's of the hyper-closo and capped deltahedral ("pileo")[24a] polar deltahedral B_{10} clusters are correlated. The $(F^{\pi}/\bar{F}^{\pi})_{\pm 1}$ pair of orbitals lie at higher energy in the pileo cluster, due to antibonding interactions within the capped triangular face. These interactions are lessened on conversion to the hyper-closo geometry:



The HOMO (for n SEP's) is the same in both geometries, i.e. $\bar{F}^{\pi}_0(a_2)$. This orbital, which possesses no polar atom contribution, becomes more strongly bonding upon deforming the tetracapped trigonal prism into the hyper-closo geometry. This is because the antibonding interactions in the upper triangle are reduced and the bonding interactions between the upper and equatorial triangles of atoms increase as these 6 atoms become more nearly coplanar:



The LUMO (in the n SEP tetracapped trigonal prism) is non-degenerate, $F_0^{\pi}(a_1)$. This means that an (n+1) SEP count is not ruled out, on orbital degeneracy grounds, for this geometry. The F_0^{π} orbital becomes more strongly antibonding, i.e. is no longer in the frontier orbital region, for the hyper-closo geometry, as the π-bonding interactions within the upper triangle are reduced and the π-antibonding interactions between the upper and equatorial triangles increase:

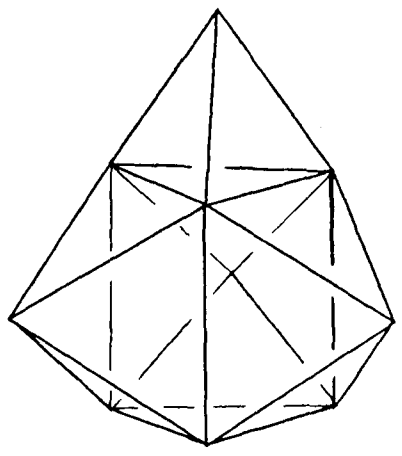


The computed energies (i.e. those obtained by summing the one-electron energies) for the 3 alternative deltahedral geometries of $[B_{10}H_{10}]^{0,2-}$ are presented in **Table 3.2.** The closo bicapped square antiprismatic geometry is favoured for (n+1) SEP's, as all of the occupied skeletal MO's are quite strongly bonding. The hyper-closo geometry is favoured for n SEP's, however, because the $\bar{F}_0^{\pi}(a_2)$ HOMO is more strongly bonding than the $F_{\pm 1}^{\pi}(e_1)$ orbitals of the closo cluster.

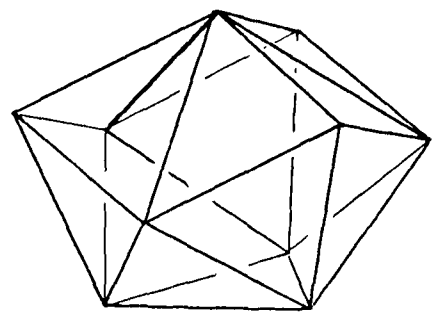
The hyper-closo geometry is energetically favoured over the tetracapped trigonal prismatic geometry for both n and (n+1) SEP's. For n SEP's the difference in energy is almost entirely due to the greater bonding character of the $\bar{F}^{\pi}(a_2)$ HOMO in the hyper-closo case. For (n+1) SEP's the difference in energy is even greater, since the $F_0^{\pi}(a_1)$ LUMO of

Table 3.2 Calculated sum of one electron energies (eV) for pileo-, hyper-closo- and closo-$[B_{10}H_{10}]^{0,2-}$ clusters

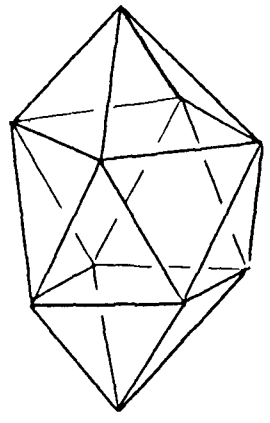
		Cluster geometry		
	No. of SEP's	pileo	hyper-closo	closo
$[B_{10}H_{10}]$	10 (n)	-598.68	-601.76	-600.63
$[B_{10}H_{10}]^{2-}$	11 (n+1)	-613.29	-619.34	-620.37



pileo



hyper-closo



closo

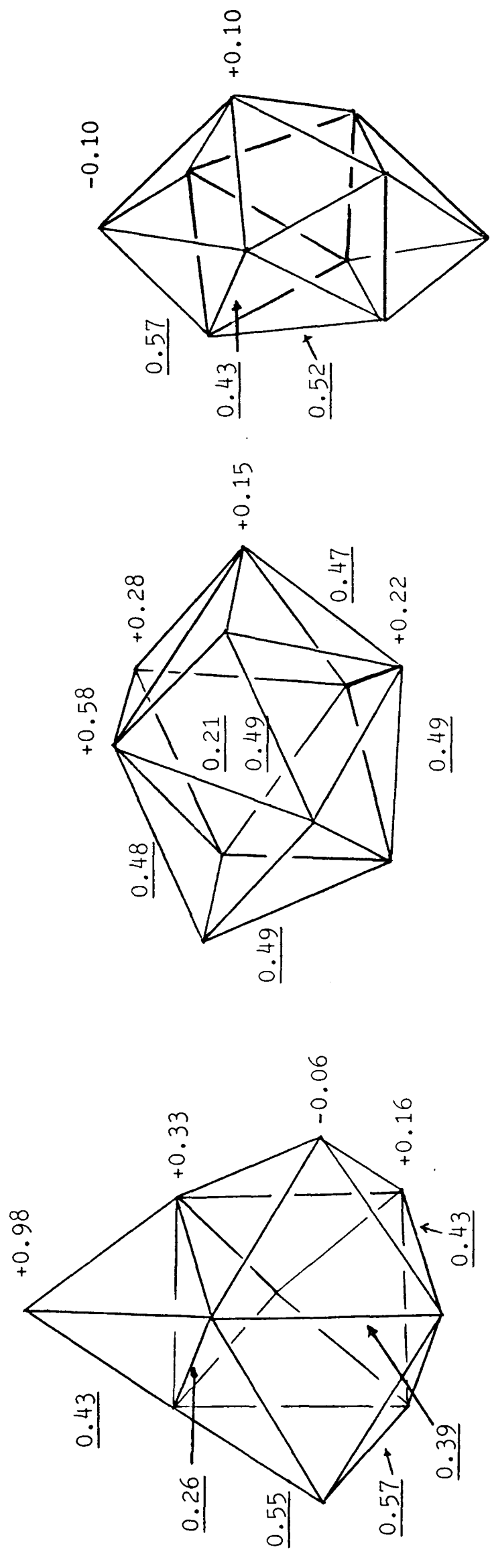
the capped structure is weakly antibonding, while the $(F^{\pi}/\bar{F}^{\pi})_{\pm 1}(e)$ LUMO's of the hyper-closo cluster are non-bonding.

The computed atomic charges and overlap populations for $[B_{10}H_{10}]$ (in both polar deltahedral geometries) and bicapped square antiprismatic $[B_{10}H_{10}]^{2-}$ are presented in **Figure 3.8.** The polar geometries are characterised by large differences in atomic charges and a wide range of B-B overlap populations and will, therefore, be favoured in clusters where the skeletal atoms have differing electronegativities. It is likely that the hyper-closo geometry, in particular, can be stabilised by the introduction of a metal atom at the high connectivity polar site, as the preference of metal atoms for high-connectivity sites is well established.

For the tetracapped trigonal prism, the bonds between the atoms of the capped triangular face are calculated to be weak. This provides an alternative explanation, to that of Jemmis,[18] for the lack of pileo structures in borane and carborane chemistry. Wade has shown that the bonds between highly connected boron vertices are weak because these vertices generally carry the greatest positive charge[16] and hence receive a relatively small share of the skeletal bonding electron density.[12b] These weak bonds favour the transformation, shown above, from the capped deltahedral to the hyper-closo geometry. The idea that the vertices of the capped triangular faces are characterised by the greatest positive charges is supported by the observation that the metal atoms in the pileo-Co_3B_4 cluster **(II)** occupy these sites.[18]

3.4.2 Hyper-closo-MB_9 clusters

Figure 3.9 illustrates the interaction between the frontier



closo-$[B_{10}H_{10}]^{2-}$

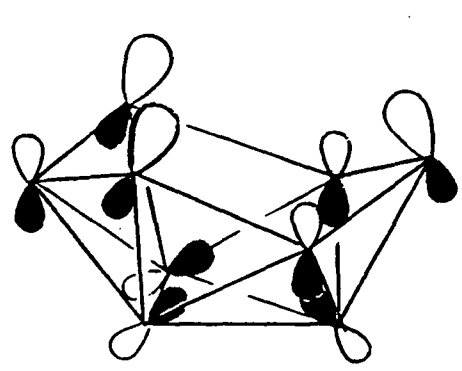
hyper-closo-$[B_{10}H_{10}]$

pileo-$[B_{10}H_{10}]$

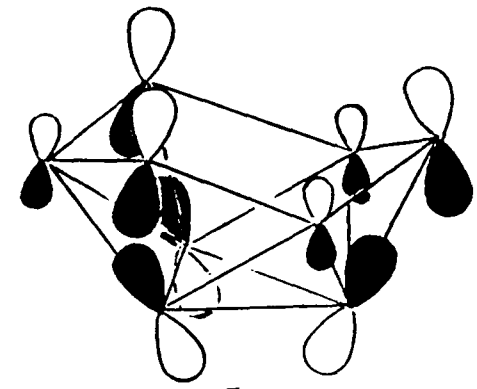
(overlap populations are underlined)

Figure 3.8 Atomic charges and overlap populations for hyper-closo- and pileo-$[B_{10}H_{10}]$ and closo-$[B_{10}H_{10}]^{2-}$.

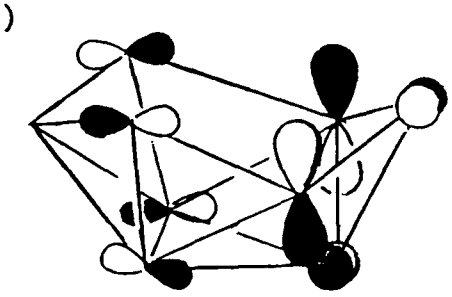
orbitals of $Rh(CO)_3$ and hypho-B_9H_9 fragments. The major bonding interaction occurs between the rhodium dp^{π} (xz,yz) hybrids and the $D^{\pi}_{\pm 1}(e)$ orbitals of the hypho fragment, which are also singly noded with respect to the C_3 axis. The sp^{σ} hybrid of the $Rh(CO)_3$ fragment interacts weakly with the $P^{\sigma+\pi}_0(a_1)$ orbital of the hypho fragment, but there is virtually no interaction with the $D^{\pi}_0(a_1)$ orbital. These various fragment orbitals are depicted below:



$P^{\sigma+\pi}_0(a_1)$



$D^{\pi}_0(a_1)$



$D^{\pi}_{\pm 1}(e)$

The skeletal MO pattern for the hyper-closo-RhB_9 cluster (**Figure 3.9**) is virtually identical to that of hyper-closo-B_{10} (**Figure 3.7**). In this C_{3v} symmetry there are, therefore, a pair of degenerate $(F^{\pi}/\bar{F}^{\pi})_{\pm 1}$ orbitals which are approximately non-bonding. The calculated energies for $[(CO)_3RhB_9H_9]^{+,-}$ in the 3 alternative deltahedral geometries, are presented in **Table 3.3.** The $Rh(CO)_3$ fragment, with C_{3v} geometry, is taken to be staggered with respect to the shorter Rh-B bonds in the two polar structures. The trends in energies are the same as were observed

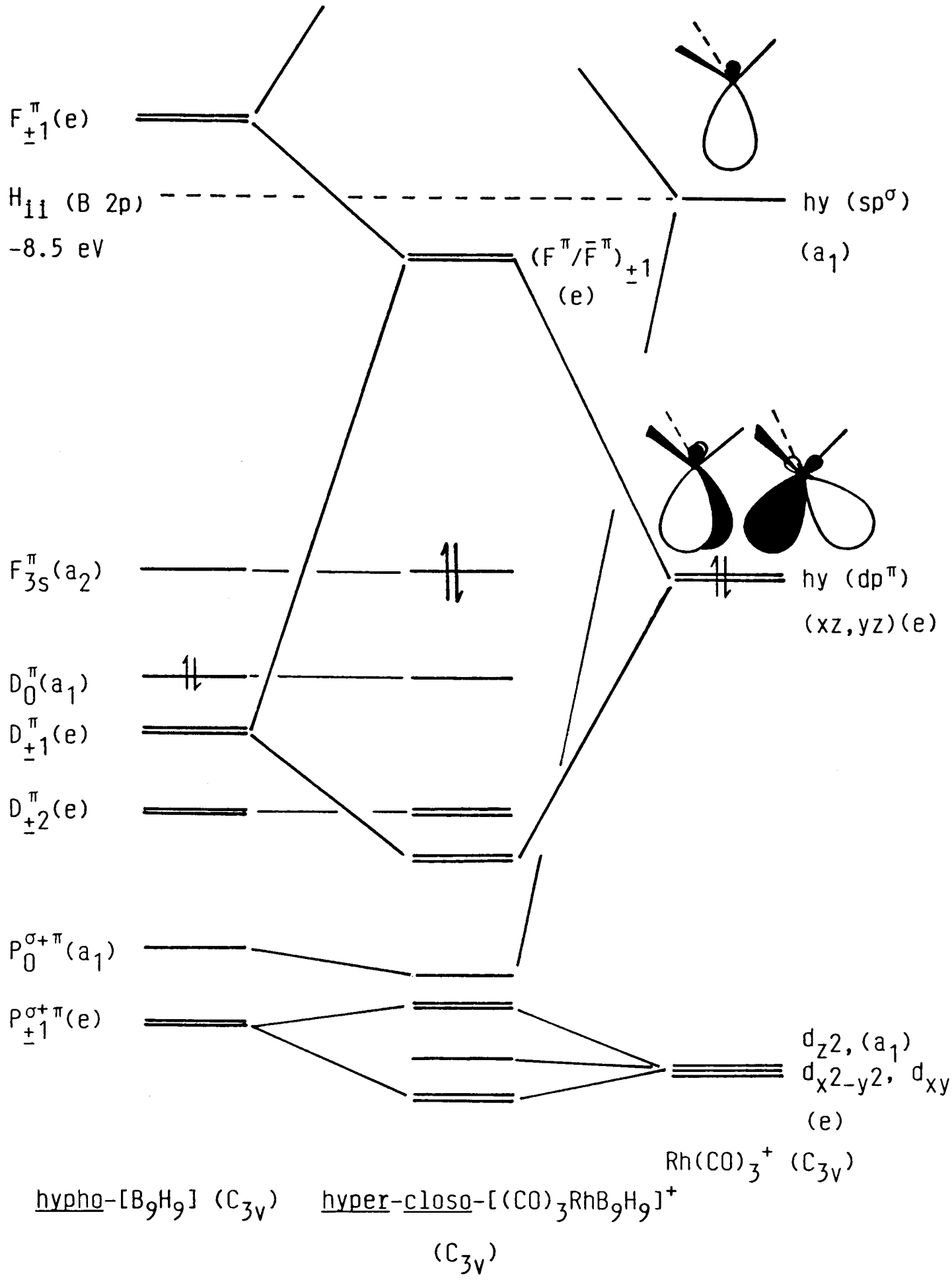
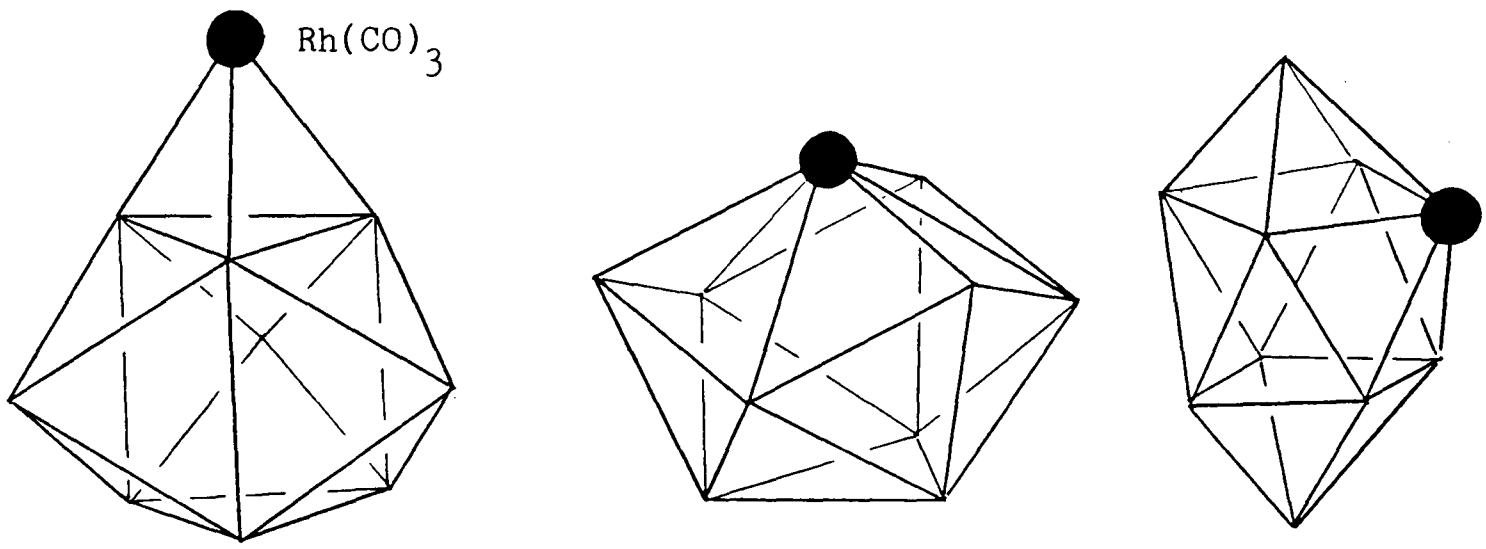


Figure 3.9 Orbital interactions between hypho-$[B_9H_9]$ and a capping $Rh(CO)_3$ fragment.

Table 3.3 Calculated sum of one electron energies (eV) for pileo-, hyper-closo- and closo-$[(CO)_3RhB_9H_9]^{+,-}$ clusters

		Cluster geometry*		
	No. of SEP's	**pileo**	**hyper-closo**	**closo**
$[(CO)_3RhB_9H_9]^+$	10 (n)**	-1248.48	-1253.57	-1253.08
$[(CO)_3RhB_9H_9]^-$	11 (n+1)	-1266.46	-1272.05	-1272.26

* The positions of the metal atoms in these model cluster compounds are indicated below:



pileo hyper-closo closo

** The assignment of the number of SEP's is in accordance with Baker's treatment (Ref. 23).

for the $[B_{10}H_{10}]$ clusters, and predict the hyper-closo geometry for n SEP's and the closo bicapped square antiprismatic structure for (n+1) SEP's.

The calculations described here provide no support for the view, held by Greenwood and Kennedy,[8b,24] that the ML_3 fragment in the hyper-closo-IrB_9 cluster **(VI)**[29] contributes 4, rather than 3, orbitals for cluster bonding. Indeed, on purely symmetry grounds, the C_{3v}-pseudo symmetry of **(VI)** dictates that either both or neither of the $d_{x^2-y^2}$ and d_{xy} orbitals are involved in cluster bonding. As indicated in **Figure 3.9** , in the model RhB_9 cluster, the rhodium $d_{x^2-y^2}$ and d_{xy} orbitals are involved in weak 4-electron interactions and, therefore, contribute very little towards cluster bonding. The $Rh(CO)_3^+$ moiety is, therefore, a 3-orbital-2-electron fragment (i.e. isolobal with BH) and the hypothetical rhodaborane, like $[B_{10}H_{10}]$, is characterised by 10 (n) SEP's.

The IrB_9 cluster **(VI)** actually has an eclipsed arrangement of the IrL_2H fragment and the shorter B-B bonds, because one of the phosphine ligands is also bonded to the borane cage.[29] Our Extended Hückel calculations indicate that there is a very slight energetic preference (approx. 0.05 eV) for the staggered configuration, at least for a conical ML_3 fragment. This small energy difference is confirmed by the fluctionality of the unconstrained hyper-closo species $[(PMe_3)_2HIrB_9H_9]$.[36b] The unconstrained hyper-closo metallaborane, $[(PPh_3)HClRuB_9H_7(PPh_3)_2]$, is, however, non-fluctional.[36b] This cluster also possesses an eclipsed metal geometry. Both of these features may result from an asymmetry in the bonding capabilities of the dp^{π} hybrids, induced by the presence of three quite different substituents on the metal.

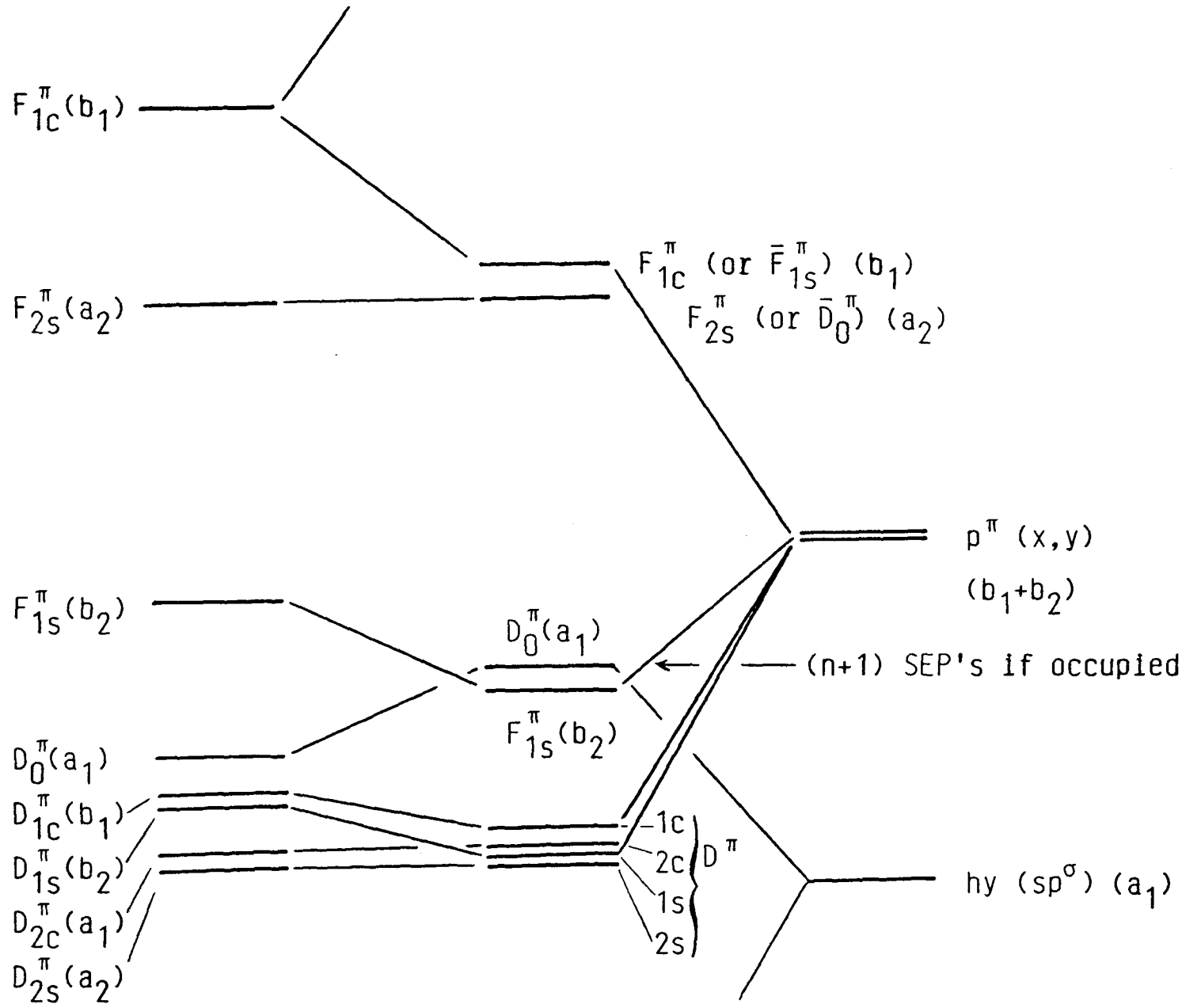
The above results were obtained for an undistorted hypho icosahedral fragment. Constraining the B-B bonds to be 1.70Å and the shorter Rh-B bonds to be 2.17Å, results in the longer Rh-B contacts being 2.62Å. From **Table 3.1**, it can be seen that these longer bonding contacts are generally in the range 2.38-2.50Å. This requires a distortion of the hypho icosahedral B_9 fragment, which corresponds to a slight flattening of the open puckered hexagonal face. Calculations were performed on a distorted $[(CO)_3RhB_9H_9]^+$ model cluster, with Rh-B bond lengths of 2.17Å and 2.40Å. It was found that the flattening distortion results in a significant stabilisation of the hyper-closo structure (approx. 1.7 eV for the n SEP cluster). This difference is attributable to greater bonding interactions between the metal atom and the hypho borane and between the boron atoms of the puckered hexagonal face of the B_9 unit (notably the highest occupied MO's, $\bar{F}^{\pi}_0(a_2)$ and $D^{\pi}_0(a_1)$).

3.5 Nine-Vertex Hyper-Closo Clusters

It can be seen, from **Figure 3.5**, that only one "F^{π}" orbital ($F^{\pi}_{1s}(b_2)$) is sufficiently low lying to be occupied in the klado-B_8 geometry. If none of the other "F^{π}" orbitals is stabilised, by a capping BH or $M(CO)_3$ fragment, then a maximum of 10 (n+1) SEP's is possible.

3.5.1 Hyper-closo-$[B_9H_9]$

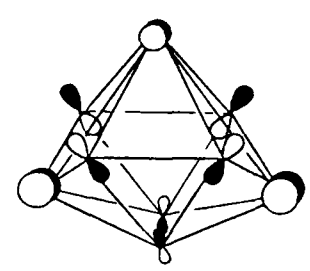
Figure 3.10 shows the interaction between klado-$[B_8H_8]$ and a capping BH fragment. Since they are doubly noded with respect to the C_2 axis, the high-lying $F^{\pi}_{2s}(a_2)$ and $F^{\pi}_{2c}(a_1)$ orbitals of the B_8 entity do not interact with the BH fragment, so they remain inaccessible. The major bonding interactions occur between the p^{π} (b_1+b_2) orbitals of the



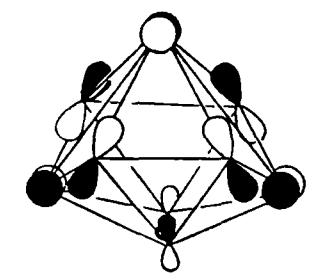
klado-$[B_8H_8]$ (C_{2v}) hyper-closo-$[B_9H_9]$ (C_{2v}) BH

Figure 3.10 Orbital interactions between klado-$[B_8H_8]$ and a capping BH fragment.

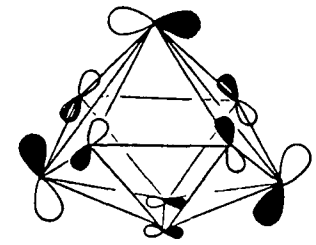
BH moiety and the $D^{\pi}_{1c}(b_1)$, $D^{\pi}_{1s}(b_2)$ and $F^{\pi}_{1s}(b_2)$ orbitals of the B_8 unit. $F^{\pi}_{1c}(b_1)$ is raised in energy, due to a secondary interaction with the BH $p^{\pi}(b_1)$ orbital, and is inaccessible. In terms of the B_9 geometry, this orbital can be redefined as $\bar{F}^{\pi}_{1s}$. The $D^{\pi}_{0}(a_1)$ orbital is also raised in energy slightly, by interacting with the sp^{σ} hybrid of the capping fragment, so that it lies above F^{π}_{1s}. The MO's resulting from these interactions are depicted below:



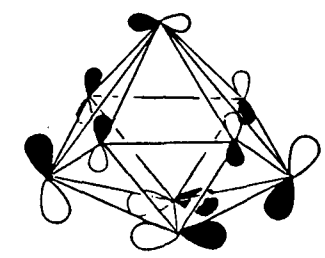
$F^{\pi}_{1s}(b_2)$



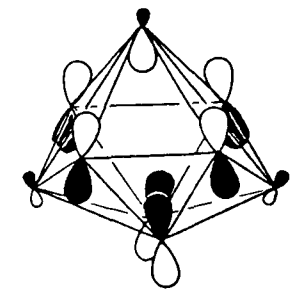
$D^{\pi}_{1s}(b_2)$



$\bar{F}^{\pi}_{1s}(b_1)$



$D^{\pi}_{1c}(b_1)$



$D^{\pi}_{0}(a_1)$

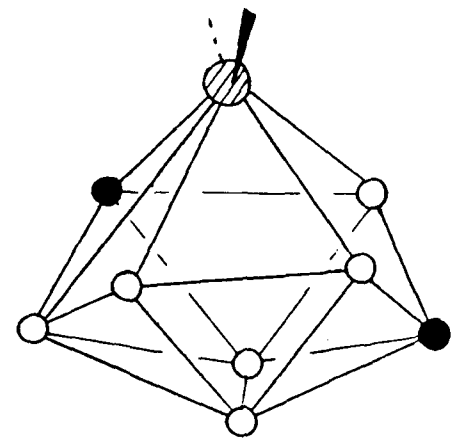
Since there are no e representations in C_{2v} symmetry, there is no symmetry-based reason for the hyper-closo geometry to be characterised by n, rather than (n+1) SEP's. In fact, for $[B_9H_9]$, the Extended Hückel calculations indicate that the cluster would have a small HOMO-LUMO gap (approximately 0.5 eV) for n SEP's, so the (n+1) situation is favoured

in this particular case.

3.5.2 Hyper-closo-MB_8 clusters

Extended Hückel calculations were performed on the model cluster hyper-closo-$[(CO)_3RhB_8H_8]^+$. As for the 10-vertex clusters, these calculations indicate that, when a conical $Rh(CO)_3^+$ fragment occupies the polar position in the 9-vertex hyper-closo polyhedron, the resulting skeletal MO scheme is virtually identical to that obtained for the borane cluster (**Figure 3.10**). Our calculations indicate a small HOMO-LUMO gap for n SEP's (approximately 0.3 eV), as for the B_9 case, with the HOMO and LUMO being F_{1s}^{π} and D_0^{π} respectively. However, by deforming the cluster skeleton (i.e. opening out the klado-B_8 geometry), the D_0^{π}-F_{1s}^{π} separation increases, thereby making the n SEP ("hyper-closo") count more likely.

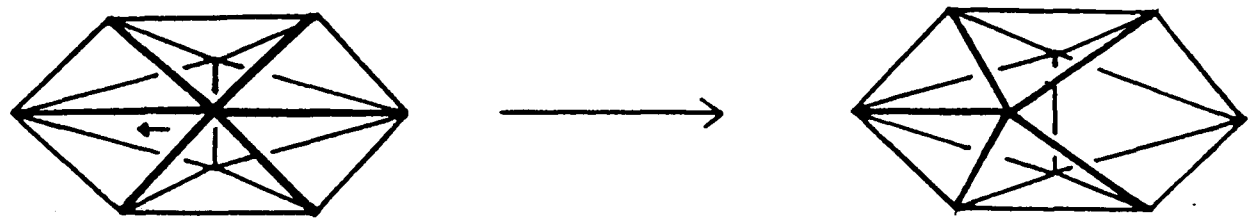
Mingos and Welch have studied the interaction of the PtL_2 fragment with the klado-B_8 cage.[43] They have found that the PtL_2 fragment favours a slip distortion away from the C_2 axis of the B_8 cage, thus accounting for the structure of the unusual open polyhedral isomer **(XIII)** of $[(PMe_3)_2PtC_2B_6H_8]$.[32]



$[(PMe_3)_2PtC_2B_6H_8]$

(XIII)

This structure may be derived from the <u>hyper</u>-<u>closo</u> IrB_8 geometry by breaking one of the longer M-B bonds:



The reason for the slip distortion observed in **(XIII)** is the anisotropic manner in which a V-shaped PtL_2 fragment bonds to a borane cage.[27] The frontier MO's of the PtL_2 fragment are illustrated in **Figure 3.11.**

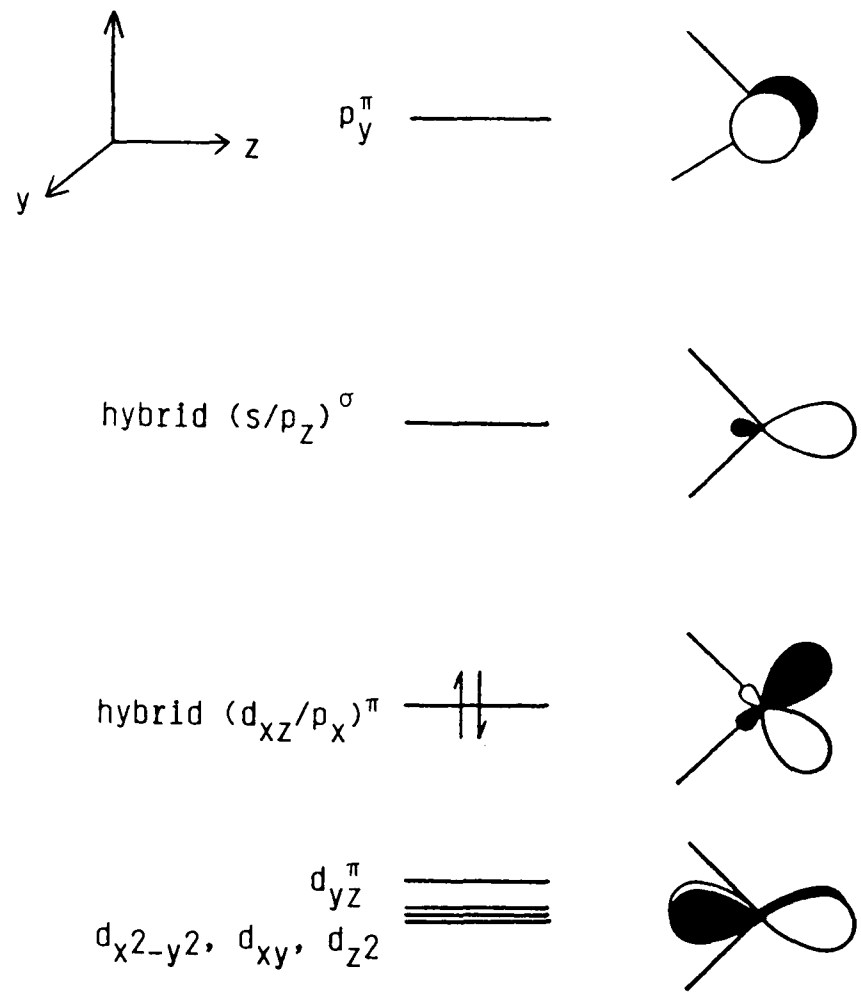


Figure 3.11 Frontier orbitals of a V-shaped PtL_2 fragment.

The most important contribution to cluster bonding comes from the $(d_{xz}/p_x)^{\pi}$ hybrid HOMO, with the higher lying $(s/p_z)^{\sigma}$ hybrid orbital making a fairly small contribution. The metal d_{yz}^{π} orbital remains low lying and unhybridised, because of the angular nature of the PtL_2 fragment. This orbital generally interacts weakly with a borane cage, taking part in 4 electron net non-bonding interactions. The PtL_2 fragment is, therefore, usually considered to act as a 2-orbital-2-electron moiety, isoelectronic (but not isolobal) with BH. Mingos has used these ideas to explain slip distortions and conformational preferences in a range of platinaboranes.[44] Similar arguments have also been used to rationalise electron counts and conformational preferences in platinum clusters.[45]

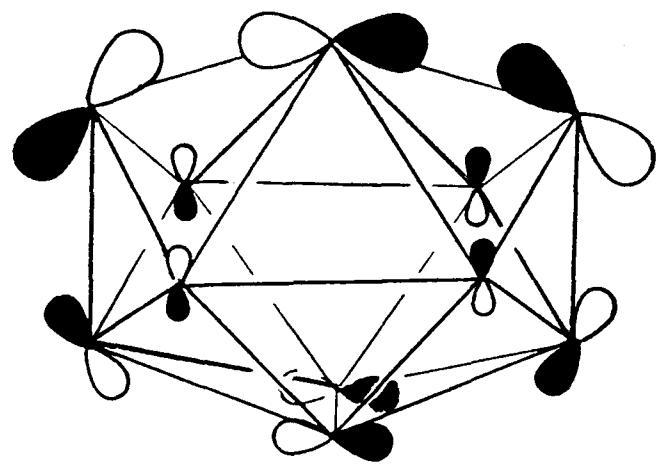
Since conical ML_3 fragments possess 2 dp^{π} hybrids, which are well set up for cluster bonding,[12] they possess more isotropic bonding capabilities. This explains why, with a polar IrL_2H fragment, the hyper-closo-IrB_8 molecule **(VII)** does not undergo a slip distortion.[31]

3.6 Eleven-Vertex Hyper-Closo Clusters

In the case of the 11-vertex clusters, the closo and hyper-closo deltahedral geometries are identical.[36a] Since the C_2-polar octadecahedron possesses C_{2v} symmetry, there are no degenerate representations and, therefore, no symmetry requirement that such a cluster should possess n, rather than (n+1), SEP's. From **Figure 3.5**, the arachno-B_{10} fragment has one high-lying inaccessible "F^{π}" orbital ($F_{2c}^{\pi}(a_1)$), so the capped derivative may possess a maximum of 12 (n+1) SEP's.

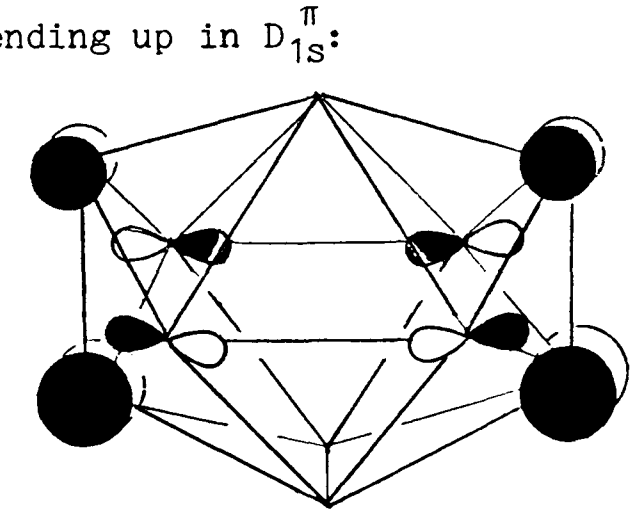
3.6.1 Hyper-closo-$[B_{11}H_{11}]$

The interactions between the orbitals of the arachno-B_{10} fragment and a polar BH unit are illustrated in **Figure 3.12.** From the Figure it is apparent that the major tangential bonding interaction occurs between the p_x^{π} orbital of the polar BH group and the $F_{1c}^{\pi}(b_1)$ orbital of the borane cage:

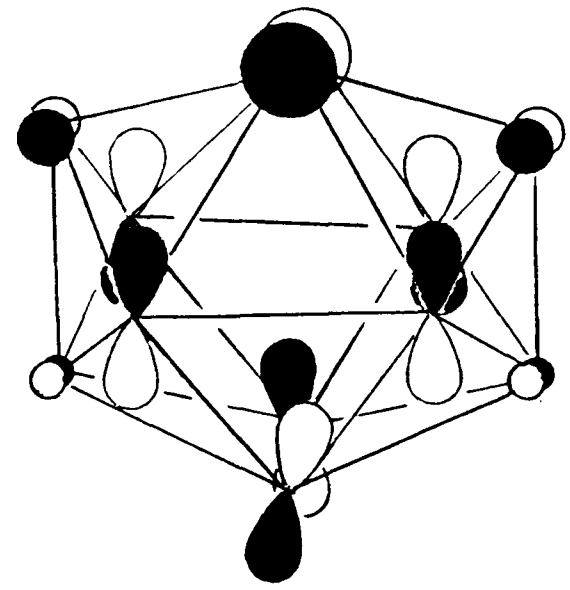


$F_{1c}^{\pi}(b_1)$

The polar p_y^{π} orbital, on the other hand, participates in a three level interaction with $F_{1s}^{\pi}(b_2)$ and $D_{1s}^{\pi}(b_2)$. There is significant $F_{1s}^{\pi}/D_{1s}^{\pi}$ mixing, which results in virtually all of the polar atom p_y^{π} character ending up in D_{1s}^{π}:



$F_{1s}^{\pi}(b_2)$



$D_{1s}^{\pi}(b_2)$

The parity related frontier orbitals in the B_{11} cluster (HOMO-

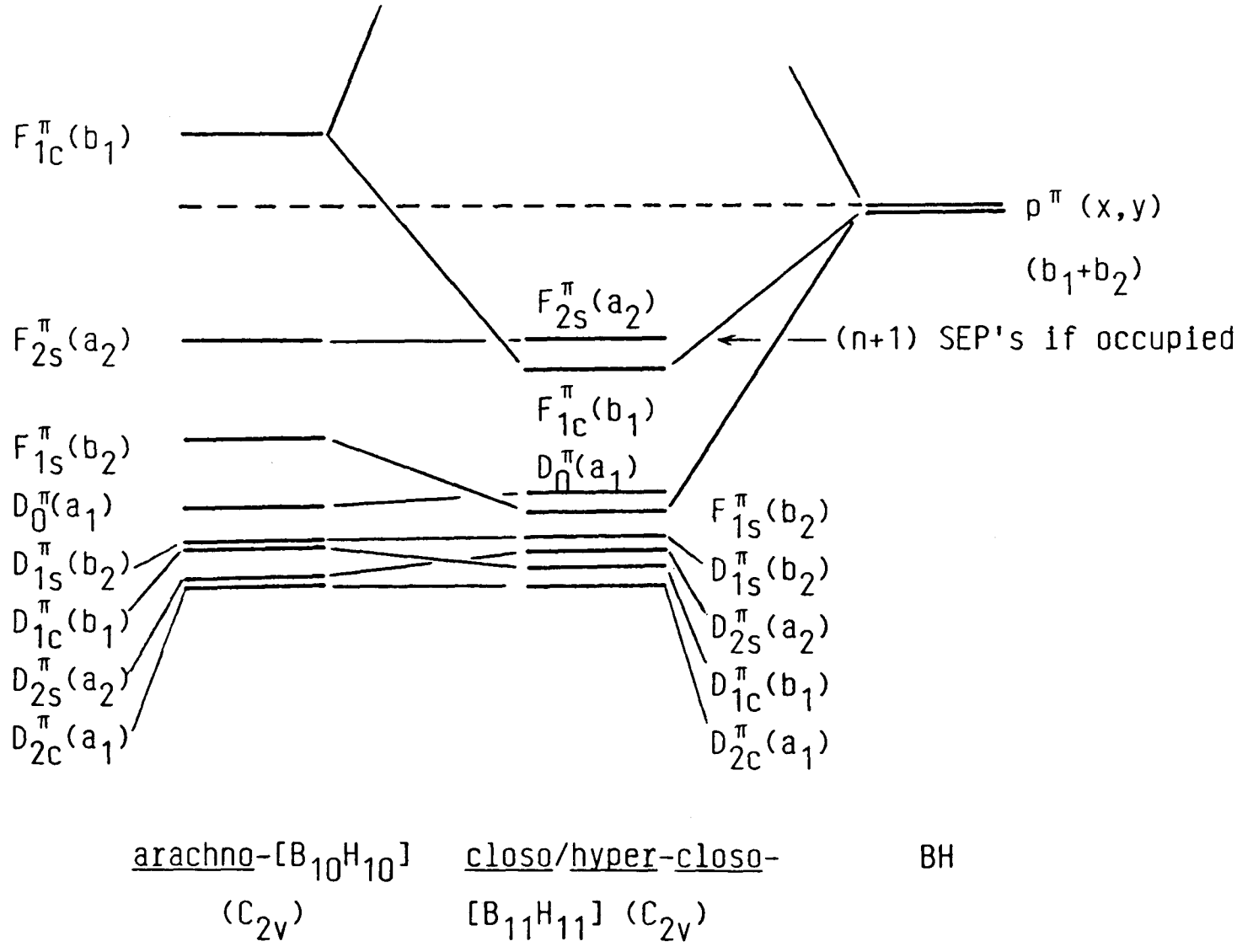
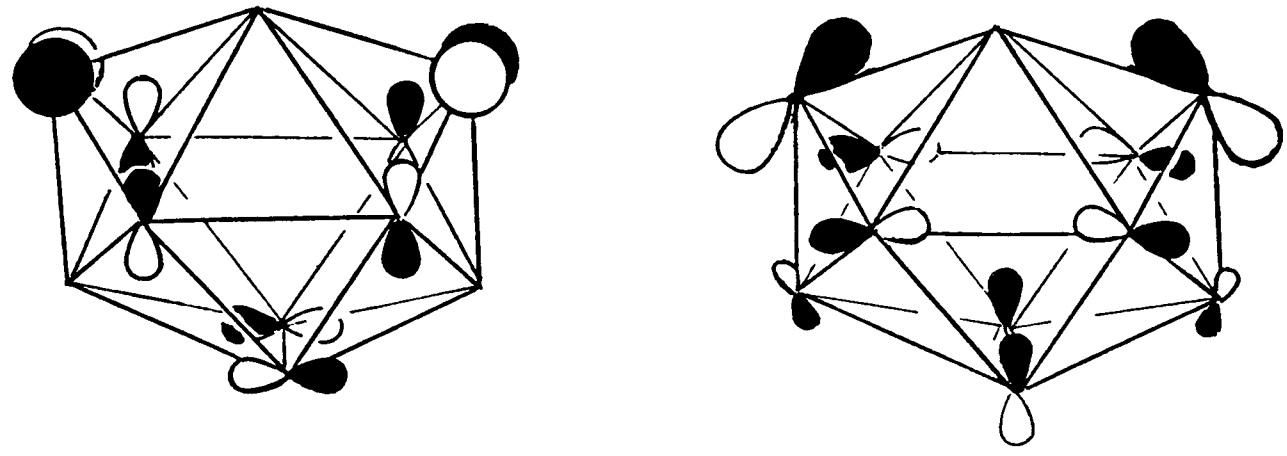


Figure 3.12 Orbital interactions between arachno-$[B_{10}H_{10}]$ and a capping BH fragment.

$F^{\pi}_{2s}(a_2)$; LUMO-$\bar{F}^{\pi}_{2s}(a_1)$) do not possess any contribution from the polar atom, as they are doubly noded with respect to the C_2 (polar) axis:



$F^{\pi}_{2s}(a_2)$ $\bar{F}^{\pi}_{2s}(a_1)$

Inspection of **Figure 3.12** reveals that the (n+1) SEP situation is favoured for boranes and carboranes, because (as in the $[B_9H_9]$ case) the nth and (n+1)th skeletal MO's lie close together in energy, while the (n+1)th and (n+2)th MO's are quite well separated. This accounts for the (n+1) SEP count of, for example, closo-$[(CMe)_2B_9H_9]$ **(X).**[35]

3.6.2 Hyper-closo-MB_{10} clusters

The fragment MO interactions for $[(CO)_3RhB_{10}H_{10}]$ are shown in **Figure 3.13.** Although the $Rh(CO)_3$ fragment lowers the true molecular symmetry to C_s, the spectra of skeletal MO's are very similar for the metallaborane and borane clusters. The lower cluster symmetry leads to no significant changes in the borane cage components of the metallaborane MO's, so C_{2v} symmetry labels have been applied to these MO's, for consistency with the B_{11} clusters.

From **Figure 3.13** the strongest fragment bonding interaction appears to be that between the hybrid $(d_{xz},p_x)^{\pi}$ orbital of $Rh(CO)_3$ and $F^{\pi}_{1c}(b_1)$ of the B_{10} fragment. Other significant bonding interactions occur between

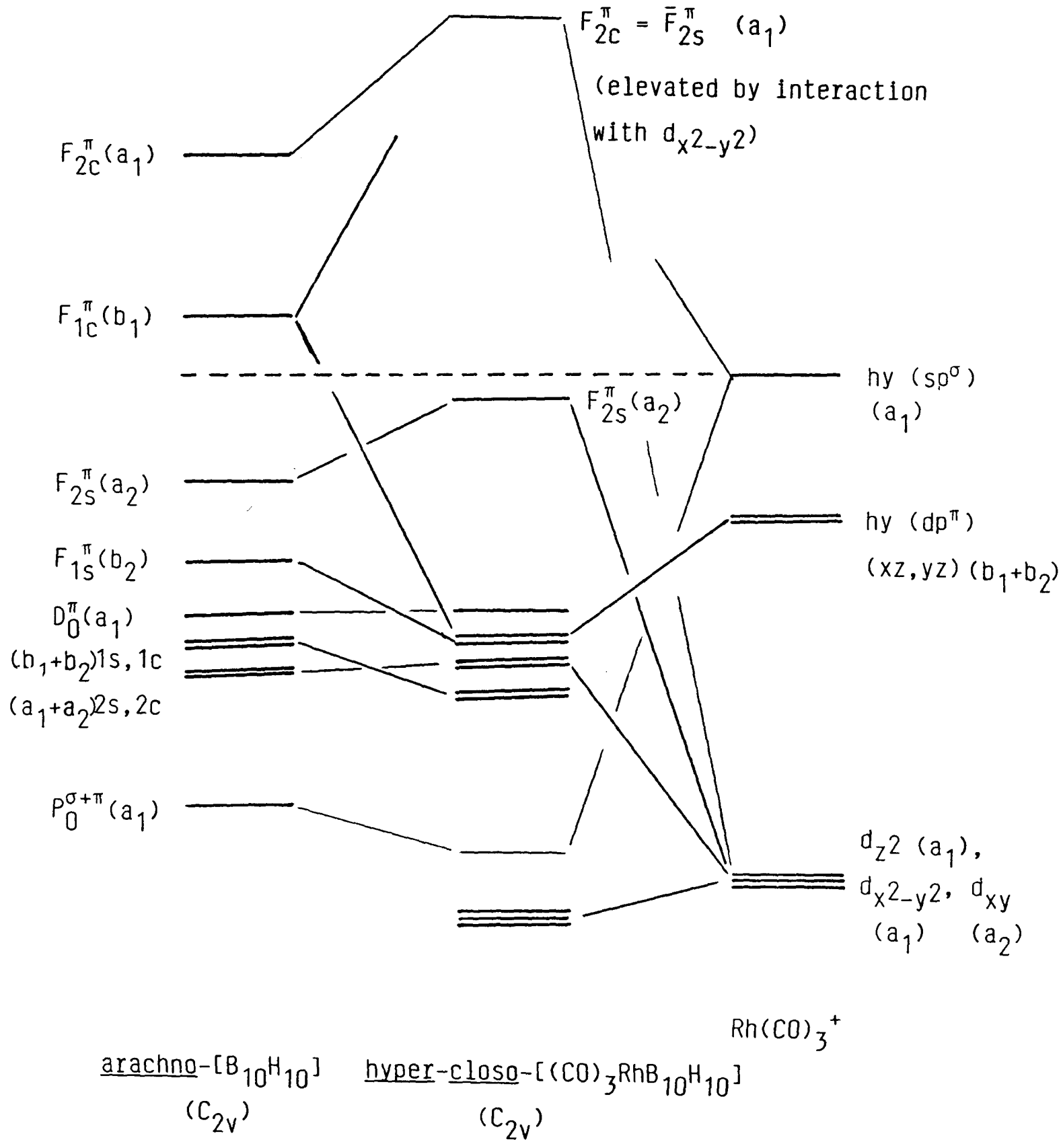
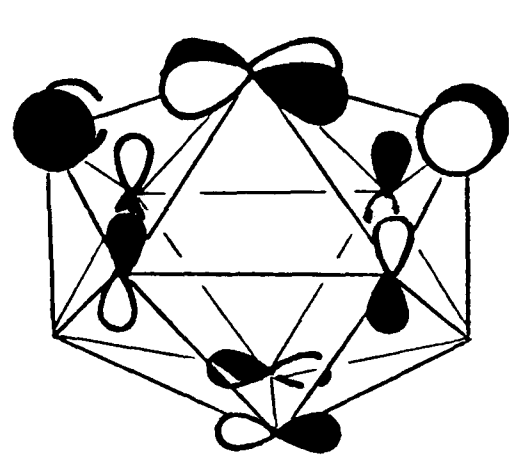
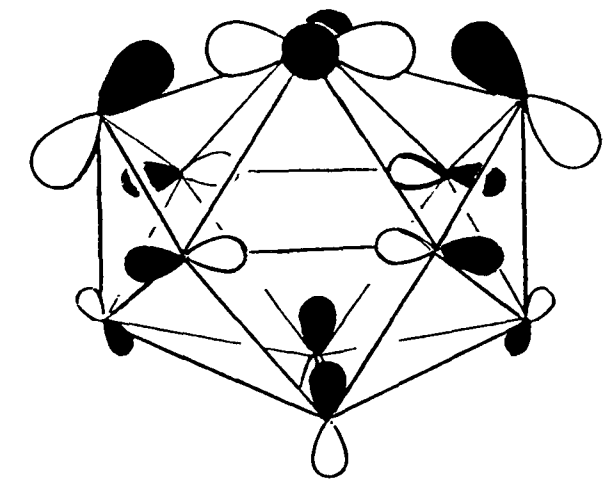


Figure 3.13 Orbital interactions between arachno-$[B_{10}H_{10}]$ and a capping $Rh(CO)_3$ fragment.

the hybrid $(d_{yz},p_y)^{\pi}$ and $F_{1s}^{\pi}(b_2)$ and between the sp^{σ} hybrid and $D_0^{\pi}(a_1)$. A major difference between the skeletal MO patterns of the B_{11} and MB_{10} clusters is that the $F_{2s}^{\pi}(a_2)$ orbital, corresponding to the HOMO in $[B_{11}H_{11}]^{2-}$, is significantly destabilised in the metallaborane. This destabilisation is due to a fairly strong antibonding interaction between the metal d_{xy}^{δ} orbital and the boat-like arrangement of boron atoms on the open face of the B_{10} cage. The relatively high lying antibonding orbital $F_{2c}^{\pi}(a_1)$ is similarly destabilised by interaction with $d_{x^2-y^2}^{\delta}$. In fact, the F_{2c}^{π} orbital may be redefined as $\bar{F}_{2s}^{\pi}$, as it is the parity inverse of F_{2s}^{π}:



$F_{2s}^{\pi}(a_2)$



$\bar{F}_{2s}^{\pi}(a_1)$

The destabilisation of $F_{2s}^{\pi}(a_2)$, along with the significant stabilisation of $F_{1c}^{\pi}(b_1)$, leads to a reasonably large HOMO-LUMO separation (approx. 1.5 eV) for the n SEP situation. However, since the metal d_{xy}^{δ} orbital has been shown to be responsible for destabilising the F_{2s}^{π} orbital, it can be argued that this orbital should be included in the SEP count. In this eventuality, Greenwood and Kennedy's argument, i.e. that the metal fragment in such clusters contributes 4, rather than 3 orbitals and that the clusters possess (n+1), rather than n SEP's[26] is indeed correct for the MB_{10} "iso-closo" clusters.[38]

The net overlap populations between the $Rh(CO)_3$ fragment orbitals and those of the arachno-B_{10} unit are listed in **Table 3.4.**

Table 3.4 Net fragment orbital overlap populations for $[(CO)_3RhB_{10}H_{10}]^+$

	Fragment		
	$Rh(CO)_3^+$	**$[B_{10}H_{10}]$**	**Overlap popln.**
Orbital	$hy(sp)^{\sigma}$	$D_0^{\pi}(a_1)$	+0.15
	$hy(xz,x)^{\pi}$	$F_{1c}^{\pi}(b_1)$	+0.56
	$hy(yz,y)^{\pi}$	$F_{1s}^{\pi}(b_2)$	+0.34
		$D_{1s}^{\pi}(b_2)$	+0.13
	d_{xy}^{δ}	$F_{2s}^{\pi}(a_2)$	+0.13
	$d_{x^2-y^2}^{\delta}$	$F_{2c}^{\pi}(a_1)$	+0.11

These overlap populations confirm the qualitative arguments outlined above concerning the relative strengths of the various inter-fragment bonding interactions. Particularly noteworthy is the significant net bonding interaction between the metal d_{xy}^{δ} orbital and the F_{2s}^{π} orbital of the B_{10} fragment, though this is smaller (by a factor of approximately 4) than the net bonding interactions exhibited by the dp^{π} hybrids. The Table also reveals that there is a net bonding interaction between the metal $d_{x^2-y^2}^{\delta}$ orbital and the relatively high lying $F_{2c}^{\pi}(a_1)$ orbital of the borane fragment.

The net bonding interactions between the metal d^{δ} orbitals (d_{xy},$d_{x^2-y^2}$) and the $F_{2s,2c}^{\pi}$ orbitals of the B_{10} cage means that electrons in these orbitals may indeed be classified as skeletal bonding electrons. In fact, the overlap populations reveal that $d_{x^2-y^2}$ contributesalmost as much as d_{xy} to cluster bonding. There is no

justification in saying, as Greenwood and Kennedy have done,[8b,24] that only one of these orbitals is included in the SEP count, since the calculations indicate that both (or neither) should be included. Since the d^{δ}-borane bonding interactions are weaker than those exhibited by the metal dp^{π} hybrids, however, it is doubtful whether equal weighting should be given to all of the metal-borane cage interactions.

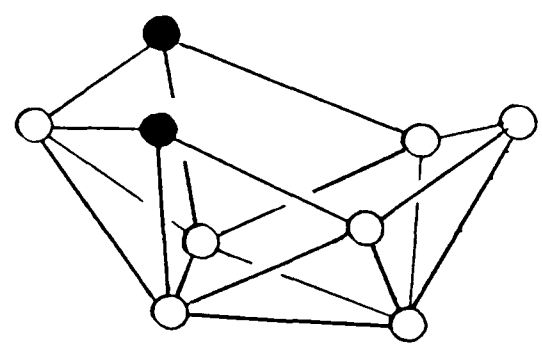
3.7 Conclusions Concerning the Hyper/Iso-Closo Controversy

From the preceding discussion it is clear that, for the 10-vertex hyper-closo deltahedral geometry, Hawthorne and Baker's hyper-closo description is more accurate than Greenwood and Kennedy's iso-closo description. This is because the C_{3v} symmetry of the cluster cage leads to a pair of non-bonding orbitals which are degenerate, so that closed shell molecules are realised for n or (n+2), but not (n+1), SEP's. For the 8 and 11-vertex clusters, however, the situation is not so straightforward. In the lower point group symmetry (C_{2v}) of these cluster cages there are no degenerate representations. This means that there is no symmetry based reason for a cluster to depart from the (n+1) rule. In fact, in the MB_{10} case, the same geometry may be characterised formally by n or (n+1) SEP's, if the hyper-closo description is applied. The (formally) n SEP case arises due to a significant interaction between the metal d^{δ}_{xy} orbital and the HOMO (F^{π}_{2s}) of the borane cage. However, if the bonding component of this interaction (i.e. the orbital with mainly metal d^{δ}_{xy} character) is included in the cluster electron count, then the cluster possesses (n+1) SEP's. There is also a bonding interaction between $d^{\delta}_{x^2-y^2}$ and the LUMO (F^{π}_{2c}), which would lead to an SEP count of (n+2).

The C_2-polar octadecahedral MB_{10} cluster highlights the limitations of electron counting methods in cluster chemistry. It is not always possible to categorise orbitals unambiguously as cluster bonding, cluster-ligand bonding or metal non-bonding. The MB_{10} clusters discussed above lie near the midpoint of the continuum of metal orbital-borane cage bonding interactions, between the limits of complete contribution to the cluster and complete localisation on the metal. In such situations the concept of a certain number of SEP's does not have much meaning. The term "hyper-closo" is more apt than "iso-closo" for these electron deficient MB_{10} clusters, however, since it indicates that a large percentage of the electron deficiency is associated with the cluster skeleton.

3.8 Extension to Unusual Nido- and Arachno-Type Geometries

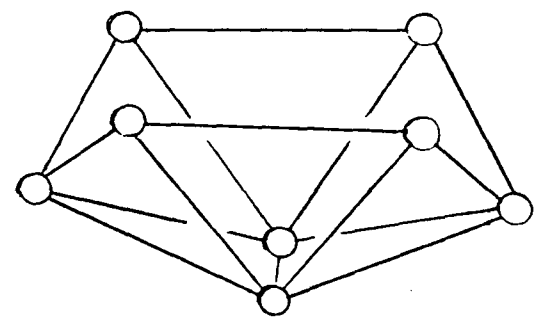
A feature of borane and carborane cluster chemistry, alluded to above, is the possibility of deriving a given open (i.e. vertex deficient) structure from alternative closo polyhedra. For example, $[(CMe)_2B_7H_{11}]$ **(XIV)**,[46] may be regarded, from a geometric point of view, as an arachno structure, derived from $[B_{11}H_{11}]^{2-}$, or a hypho structure, derived from $[B_{12}H_{12}]^{2-}$.



$[(CMe)_2B_7H_{11}]$

(XIV)

The 12 (n+3) SEP count for this molecule means that the former description is generally favoured. There is clearly no distinction, however, if it recognised that there are too few hydrogen atoms to lower all the orbitals required for the hypho electron count, i.e. (n+4) SEP's. Similarly, the structure of the arachno borane $[B_8H_{14}]$ **(XV)**[47] can, as described above, be derived from the icosahedron by the removal of 4 skeletal vertices. The same skeletal geometry is adopted by $[B_8H_{12}]$[48] and $[C_2B_6H_{10}]$[49]. However, although these molecules are formally nido, their skeletal geometry cannot be derived by the removal of a vertex from the closo tricapped trigonal prismatic cluster $[B_9H_9]^{2-}$.

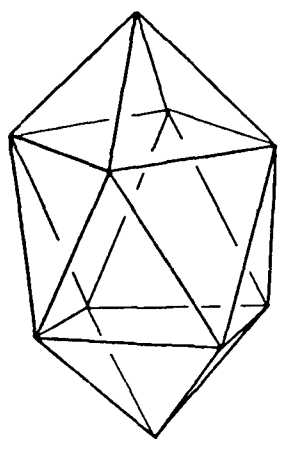


$[B_8H_{14}]$

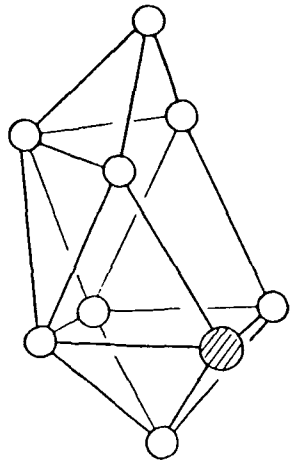
(XV)

Greenwood and Kennedy have noted the occurrence of isomeric nido metallaboranes which may be derived from the same closo parent by the removal of vertices of different connectivities.[8b,24] Examples of the structural relationships between some "iso-nido" metallaboranes are shown in **Figure 3.14.** Williams has noted similar relationships for borane and carborane clusters.[11]

The term "iso-nido" has also been applied to a number of non-deltahedral metallaboranes with unusual skeletal geometries.[8b,24] As for $[B_8H_{12}]$, these compounds do not possess structures which may be

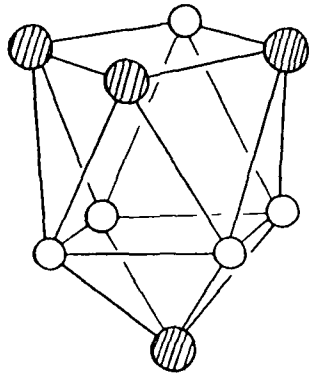


- 5-connected vertex →



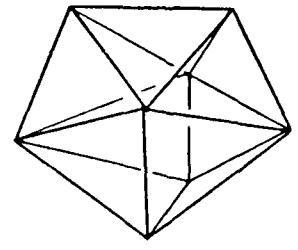
$[(CO)(PMe_3)_2IrB_8H_8]$ [a]

- 4-connected vertex ↘

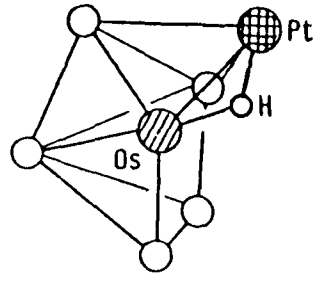


$[Cp_4Ni_4B_5H_5]$ [b]

9-vertex "iso-nido" metallaboranes, with 11 (n+2) SEP's

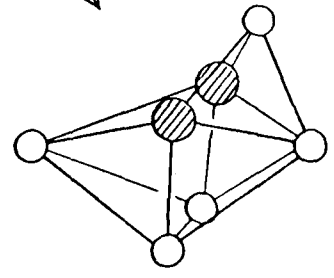


- 5-connected vertex →



$[(CO)(PPh_3)_2Os(\mu\text{-}H)(PMe_2Ph)(Cl)PtB_5H_7]$ [c]

- 4-connected vertex ↘



$[Cp^*_2Co_2B_5H_9]$ [d]

7-vertex "iso-nido" metallaboranes, with 9 (n+2) SEP's

a J. Bould, J.E. Crook, N.N. Greenwood, J.D. Kennedy and W.S. McDonald, J. Chem. Soc., Chem. Commun., 1982, 346.

b J.R. Bowser and R.N. Grimes, J. Amer. Chem. Soc., 1978, 100, 4623; J.R. Pipal and R.N. Grimes, J. Amer. Chem. Soc., 1979, 101, 6229.

c J. Bould, J.E. Crook, N.N. Greenwood and J.D. Kennedy, J. Chem. Soc., Chem. Commun., 1983, 951.

d T.L. Venable and R.N. Grimes, Inorg. Chem., 1982, 21, 887.

Figure 3.14 Examples of "iso-nido" metallaboranes, resulting from the removal of vertices of different connectivities from a common closo precursor.

considered as derived by the removal of one, or more, vertices from a closo deltahedron. For these clusters, as in the "iso-closo" metallaboranes, the normal nido (n+2) SEP count is only attained if a hypervalent metal atom is assumed (e.g. a 4 orbital cluster bonding contribution from ML_3).

Alternatively, these structures may be obtained by removing vertices from hyper-closo , rather than closo, deltahedra. By analogy with the work described above, this would lead to hyper-nido and hyper-arachno metallaboranes, which may be characterised by (n+1) and (n+2) SEP's respectively. A diagram depicting this structural correlation, which is analogous to the closo/nido/arachno correlation diagram of Rudolph,[14d] is shown in **Figure 3.15.** Until calculations are performed on these hyper-nido and hyper-arachno metallaboranes, it is not possible to confirm whether they really possess fewer SEP's than their nido and arachno counterparts, or whether the correlation is merely a structural one.

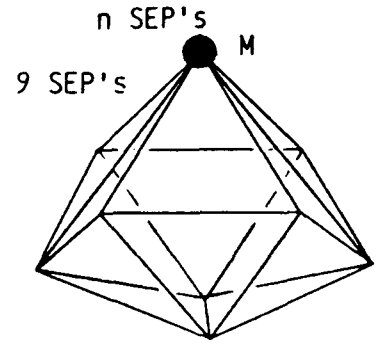
3.9 Appendix

The parameters used in the Extended Hückel calculations, described in this Chapter, are listed in **Table 3.5.**

The following bond lengths were used in these calculations: Rh-B (short contacts), 2.17Å; Rh-B (long contacts), 2.40Å; B-B, 1.70Å; B-H, 1.20Å; Rh-C, 1.80Å; C-O 1.10Å.

"hyper-closo" "hyper-nido" "hyper-arachno"

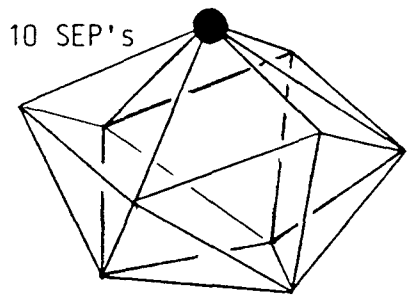
n SEP's (n+1) SEP's (n+2) SEP's



9 SEP's

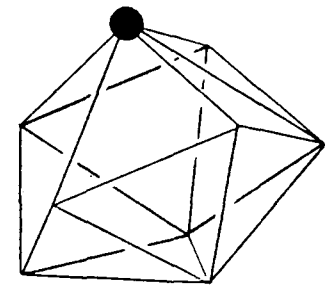
$[H(PMe_3)_2IrB_8H_7Cl]$

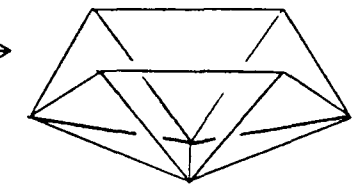
+2e



10 SEP's

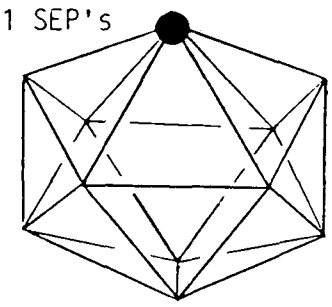
- vertex



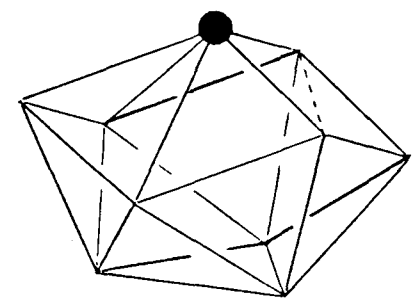


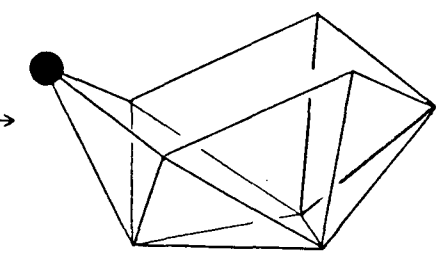
e.g. $[H(PPh_3)(Ph_2C_6H_4)IrB_9H_8]$ $[(PMe_3)_2PtC_2B_6H_8]$ * $[B_8H_{12}]$

+2e +2e



11 SEP's



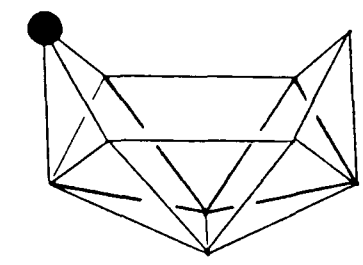


e.g. $[(PPh_3)_2RuB_{10}H_8(OEt)_2]$ $[(PPh_3)_2IrB_9H_{10}(PPh_3)]$ $[(PMe_2Ph)_2PtB_8H_{12}]$ *

$[(PPh_3)(PPh_2C_6H_4)IrB_8H_6(OMe)C(OH)]$

+2e

12 SEP's



$[H(PPh_3)_2IrB_9H_{13}]$

* Assuming the PtL_2 fragment to be a 2-orbital-2-electron moiety.

For references see: N.N. Greenwood and J.D. Kennedy, in "Metal Interactions with Boron Clusters" (Ed. R.N. Grimes), Plenum, New York, 1982, Ch. 2 p.43.

Figure 3.15 Correlation diagram showing how the structures of unusual nido- and arachno-type metallaboranes may be obtained by removing vertices from hyper-closo molecules.

Table 3.5 Extended Hückel parameters

		H_{ii} (eV)	ζ_1[a]	ζ_2[a]	c_1[b]	c_2[b]
Rh	4d	-12.50	4.290	1.970	0.5807	0.5685
	5s	-8.09	2.135			
	5p	-4.57	2.100			
B	2s	-15.20	1.300			
	2p	-8.50	1.300			
C	2s	-21.40	1.625			
	2p	-11.40	1.625			
O	2s	-32.30	2.275			
	2p	-14.80	2.275			
H	1s	-13.60	1.300			

Wolfsberg-Helmholz constant k = 1.75

[a] Slater type orbital exponents

[b] Coefficients used in double-ζ expansion of contracted d orbitals.

References for Chapter Three

1. M.F. Hawthorne, Acc. Chem. Res., 1968, **1**, 281 and references therein.
2. M.F. Hawthorne, D.C. Young and P.A. Wegner, J. Amer. Chem. Soc., 1965, **87**, 1818.
3. M.F. Hawthorne and T.D. Andrews, J. Chem. Soc., Chem. Commun., 1965, 443.
4. A. Zalkin, D.H. Templeton and T.E. Hopkins, J. Amer. Chem. Soc, 1965, **87**, 3988.
5. A. Zalkin, T.E. Hopkins and D.H. Templeton, Inorg. Chem., 1967, **6**, 1911; M.F. Hawthorne, D.C. Young, T.D. Andrews, D.V. Howe, R.L. Pilling, A.D. Pitts, M. Reintjes, L.F. Warren Jr. and P.A. Wegner, J. Amer. Chem. Soc., 1968, **90**, 879.
6. M.F. Hawthorne, J. Organomet. Chem., 1975, **100**, 97; K.P. Callahan and M.F. Hawthorne, Adv. Organomet. Chem., 1976, **14**, 145 and references therein.
7. (a) R.N. Grimes, Acc. Chem. Res., 1978, **11**, 420. (b) R.N. Grimes (Ed.), "Metal Interactions with Boron Clusters", Plenum, New York, 1982. (c) R.N. Grimes, Acc. Chem. Res., 1983, **16**, 22 and references therein.
8. (a) N.N. Greenwood and I.M. Ward, Chem. Soc. Rev., 1974, **3**, 231. (b) N.N. Greenwood and J.D. Kennedy, in Ref. 7b, Ch.2 p.43; N.N. Greenwood, Pure Appl. Chem., 1983, **55**, 77, 1415; N.N. Greenwood, Chem. Soc. Rev., 1984, **13**, 353 and references therein.
9. F.G.A. Stone, J. Organomet. Chem., 1975, **100**, 257 and references therein. The metal atom synthesis of metallaboranes and metallacarboranes has been pioneered by Sneddon and coworkers (see: J.J.

Briguglio and L.G. Sneddon, Organometallics, 1986, 5, 327 and references therein).

10. (a) T.E. Paxson and M.F. Hawthorne, J. Amer. Chem. Soc., 1974, **96**, 4674. (b) C.W. Jung and M.F. Hawthorne, J. Amer. Chem. Soc., 1980, **102**, 3024. (c) R.T. Baker, M.S. Delaney, R.E. King III, C.B. Knobler, J.A. Long, T.B. Marder, T.E. Paxson, R.G. Teller and M.F. Hawthorne, J. Amer. Chem. Soc., 1984, **106**, 2965. (d) J.A. Long, T.B. Marder, P.E. Behnken and M.F. Hawthorne, J. Amer. Chem. Soc., 1984, **106**, 2979. (e)C.B. Knobler, T.B. Marder, E.A. Mizusawa, R.G. Teller, J.A. Long, P.E. Behnken and M.F. Hawthorne, J. Amer. Chem. Soc., 1984, **106**, 2990. (f) J.A. Long, T.B. Marder and M.F. Hawthorne, J. Amer. Chem. Soc., 1984, **106**, 3004. (g) P.E. Behnken, J.A. Belmont, D.C. Busby, M.S. Delaney, R.E. King III, C.W. Kriemendahl, T.B. Marder, J.J. Wilczynski and M.F. Hawthorne, J. Amer. Chem. Soc., 1984, **106**, 3011.
11. R.E. Williams, Adv. Inorg. Chem. Radiochem., 1976, **18**, 67.
12. (a) K. Wade, J. Chem. Soc., Chem. Commun., 1971, 792. (b) D.M.P. Mingos, Nature Phys. Sci., 1972, **236**, 99.
13. R. Hoffmann, Science, 1981, **211**, 995; Angew. Chem. Int. Edn. Engl., 1982, **21**, 711.
14. (a) K. Wade, Inorg. Nucl. Chem. Lett., 1972, **8**, 559, 563, 823. (b) K. Wade, Adv. Chem. Radiochem., 1976, **18**, 1. (c) K. Wade, in "Transition Metal Clusters" (Ed. B.F.G. Johnson), Wiley, New York, 1980, Ch.3 p.195; M.E. O'Neill and K. Wade, in Ref. 7b, Ch.1 p.1. (d) R.W. Rudolph, Acc. Chem. Res., 1976, **9**, 446.
15. C.T. Housecroft and T.P. Fehlner, Adv. Organomet. Chem., 1982, **21**, 57.
16. J.J. Ott and B.M. Gimarc, J. Amer. Chem. Soc., 1986, **108**, 4303.

17. W.M. Maxwell, R.F. Bryan and R.N. Grimes, J. Amer. Chem. Soc, 1977, **99**, 4008; W.M. Maxwell, R. Weiss, E. Sinn and R.N. Grimes, J. Amer. Chem. Soc., 1977, **99**, 4016.

18. J.R. Pipal and R.N. Grimes, Inorg. Chem., 1977, **16**, 3255. The isostructural analogue $[Cp^{*}_{3}Co_{3}B_{4}H_{4}]$ has also been characterised: T.L. Venable and R.N. Grimes, Inorg. Chem., 1982, **21**, 887.

19. E.D. Jemmis, J. Amer. Chem. Soc., 1982, **104**, 7017.

20. (a) J.R.Pipal and R.N. Grimes, Inorg. Chem., 1979, **18**, 257. (b) J.R. Bowser, A. Bonny, J.R. Pipal and R.N. Grimes, J. Amer. Chem. Soc., 1979, **101**, 6229.

21. F. Klanberg, D.R. Eaton, L.J. Guggenberger and E.L. Muetterties, Inorg. Chem., 1967, **6**, 1271; L.J. Guggenberger, Inorg. Chem., 1969, **8**, 2771.

22. (a) D.N.Cox, D.M.P. Mingos and R. Hoffmann, J. Chem. Soc., Dalton Trans., 1981, 1778. (b) M.E. O'Neill and K. Wade, Inorg. Chem., 1982, **21**, 461. (c) R.B. King, Polyhedron, 1982, **1**, 133.

23. R.T. Baker, Inorg. Chem., 1986, **25**, 109.

24. (a) J.D. Kennedy, Prog. Inorg. Chem., 1984, **32**, 519. (b) J.D. Kennedy, Inorg. Chem, 1986, **25**, 111; Prog. Inorg. Chem., in press.

25. K.P. Callahan, W.J. Evans, F.Y. Lo, C.E. Strouse and M.F. Hawthorne, J. Amer. Chem. Soc, 1975, **97**, 296.

26. C.W. Jung, R.T. Baker, C.B. Knobler and M.F. Hawthorne, J. Amer. Chem. Soc., 1980, **102**, 5782.

27. D.M.P. Mingos, J. Chem. Soc., Dalton Trans., 1977, 603.

28. C.W. Jung, R.T. Baker and M.F. Hawthorne, J. Amer. Chem. Soc., 1981, **103**, 810.

29. J. Bould, N.N. Greenwood, J.D. Kennedy and W.S. McDonald, J. Chem.

Soc., Chem. Commun., 1982, 465.

30. (a) D.A.Brown, M.O. Fanning and N.J. Fitzpatrick, Inorg. Chem., 1978, **17**, 1620. (b) E. Nishimura, J. Chem. Soc., Chem. Commun., 1978, 858.

31. J. Bould, J.E. Crook, N.N. Greenwood, J.D. Kennedy and W.S. McDonald, J. Chem. Soc., Chem. Commun., 1982, 346.

32. (a) M. Green, J.L. Spencer, F.G.A. Stone and A.J. Welch, J. Chem. Soc., Chem. Commun., 1974, 794. (b) A.J. Welch, J. Chem. Soc., Dalton Trans., 1976, 225. (c) A.J. Welch, J. Chem. Soc., Dalton Trans., 1977, 962.

33. M.F. Hawthorne and A. Pitts, J. Amer. Chem. Soc., 1967, **89**, 7115; A.D. George and M.F. Hawthorne, Inorg. Chem., 1969, **8**, 1801; F.J. Hollander, D.H. Templeton and A. Zalkin, Inorg. Chem., 1973, **12**, 2262.

34. M.M. Olmstead and P.P. Power, J. Amer. Chem. Soc., 1984, **106**, 1495.

35. C. Tsai and W. Streib, J. Amer. Chem. Soc., 1966, **88**, 4513.

36. (a) J.E. Crook, M. Elrington, N.N. Greenwood, J.D. Kennedy and J.D. Woollins, Polyhedron, 1984, **3**, 901. (b) J.E. Crook, M. Elrington, N.N. Greenwood, J.D. Kennedy, M. Thornton-Pett and J,D, Woollins, J. Chem. Soc., Dalton Trans., 1985, 2407. (c) H. Fowkes, N.N. Greenwood, J.D. Kennedy and M. Thornton-Pett, J. Chem. Soc., Dalton Trans., 1986, 517. (d) M. Elrington, N.N. Greenwood, J.D. Kennedy and M. Thornton-Pett, J. Chem. Soc., Chem. Commun., 1984, 1398.

37. R.P. Micciche, J.J. Briguglio and L.G. Sneddon, Inorg. Chem., 1984, **23**, 3992.

38. W.N. Lipscomb, Science, 1966, **153**, 373.

39. P. Bellon, M. Manassero and M. Sansoni, J. Chem. Soc., Dalton

Trans., 1972, 1481.

40. D.J. Fuller and D.L. Keppert, Polyhedron, 1983, **2**, 749.

41. (a) A.J. Stone, Mol. Phys., 1980, **41**, 1339; Inorg. Chem., 1981, **20**, 563. (b) A.J. Stone and M.J. Alderton, Inorg. Chem., 1982, **21**, 2297.

42. R. Mason, D.M.P. Mingos and K.M. Thomas, J. Amer. Chem. Soc., 1973, **95**, 3802; D.M.P. Mingos and M.I. Forsyth, J. Chem. Soc., Dalton Trans., 1977, 610.

43. D.M.P. Mingos and A.J. Welch, J. Chem. Soc., Dalton Trans., 1980, 1674.

44. D.M.P. Mingos, M.I. Forsyth and A.J. Welch, J. Chem. Soc., Chem. Commun., 1977, 605; J. Chem. Soc., Dalton trans., 1978, 1363; D.M.P. Mingos, P.C. Minshall, M.B. Hursthouse, K.M.A. Malik and S.D. Willoughby, J. Organomet. Chem., 1979, **181**, 169.

45. D.G. Evans and D.M.P. Mingos, J. Organomet. Chem., 1982, **240**, 321.

46. D. Voet and W.N. Lipscomb, Inorg. Chem., 1967, **6**, 113.

47. J. Dobson and R. Schaeffer, Inorg. Chem., 1968, **7**, 402.

48. W.N. Lipscomb, "Boron Hydrides", Benjamin, New York, 1963.

49. A.J. Gotcher, J.F. Ditter and R.E. Williams, J. Amer. Chem. Soc., 1973, **95**, 7514; T. Reilly and A.B. Burg, Inorg. Chem., 1974, **13**, 1250.

CHAPTER FOUR

A GROUP THEORETICAL PARADIGM FOR RATIONALISING DEPARTURES FROM THE (n+1) SKELETAL ELECTRON PAIR RULE FOR DELTAHEDRAL CLUSTERS

4.1 Introduction

A central feature of the Polyhedral Skeletal Electron Pair approach is the (n+1) skeletal electron pair rule for n-vertex closo deltahedra and their (n-1)-vertex (nido) and (n-2)-vertex (arachno) derivatives.[1] The Tensor Surface Harmonic approach has been employed to rationalise this rule in an elegant and general fashion.[2] It has, however, become apparent that for many deltahedra the (n+1) rule is not always strictly adhered to and a significant number of departures from the rule occur. Fowler has suggested that for n=4 the tetrahedron (with 4 or 6 SEP's) represents an "intrinsic" symmetry-induced exception to the (n+1) rule, whereas the halo-boranes, such as $[B_8Cl_8]$ and $[B_9Cl_9]$, represent "accidental" departures. These departures are due to the presence of non-degenerate molecular orbitals in the frontier orbital region.[3]

Wade has determined the degeneracies and symmetries of the frontier orbitals of the closo deltahedral borane clusters, $[B_nH_n]^{2-}$, in order to explain departures from the (n+1) SEP rule.[4] More recently, Fowler and Porterfield have used their Extended Tensor Surface Harmonic method to study the bonding in polyhedral boranes.[5] Since their method does not suffer from the unreal orbital degeneracies inherent in simple TSH theory, they were able to determine spectra of skeletal bonding MO's for

these molecules, while retaining the spherical symmetry labels of TSH theory.

Although the frontier orbital patterns for deltahedral cluster molecules have been elucidated for specific examples, no generalisations have yet been presented to explain these patterns. The purpose of the work described in this Chapter was to provide a fundamental derivation of the frontier orbital patterns of such deltahedral cluster molecules, in order to explain why, and in what fashion, the (n+1) rule comes to be broken. It will be demonstrated that there are four topologically distinct classes of convex deltahedral clusters, with alternative and distinctive modes of departure from the (n+1) rule. The different ways in which these clusters deviate from the (n+1) rule will be rationalised by using group theoretical arguments in conjunction with the **Pairing Principle** inherent in the Tensor Surface Harmonic analysis.[4] The basis for these group theoretical arguments has been discussed previously by Quinn[6] and Ceulemans[7] and some details are presented in the **Appendix** to this Chapter (**Section 4.9**). Extended Hückel calculations, on borane clusters, have been employed to underpin the more qualitative symmetry-based arguments (with orbital parameters and bond lengths as for **Chapter 2**).

4.2 The Four Classes of Deltahedra

The nomenclature and definitions of the four topological classes of deltahedral clusters are presented here along with a hierarchical method for determining to which class a particular cluster belongs. Sub-classes are also indicated where appropriate. Later sections deal with each of these classes and sub-classes in detail.

If a deltahedral cluster is centrosymmetric, with all of its atoms equivalent and lying on the surface of the same sphere, then the cluster belongs to **Class 1 (Centrosymmetric Spherical Deltahedra).** If not, then the disposition of cluster atoms, relative to the principal rotation axis (C_n) of the molecule, must be considered. If only one atom lies on the principal axis the cluster belongs to **Class 2 (Polar Deltahedra).** Subdivision of this class depends on whether the principal axis is a **C_3 (Sub-class 2(i)), C_2 (Sub-class 2(ii))** or **C_1 (Sub-class 2(iii))** (the final case corresponds to no rotational symmetry at all). When there are two atoms on the principal axis the cluster belongs to **Class 3 (Bipolar Deltahedra).** Class 3 may be subdivided into **3(i) Bipyramidal (D_{nh})**, and **3(ii) Bicapped antiprismatic (D_{nd}).** By continuing to stack layers, larger D_{nh} and D_{nd} deltahedra are generated though, in general, these deltahedra are grossly non-spherical and, as such, are beyond the scope of this work. Finally if there are no atoms on the principal axis then the cluster belongs to **Class 4 (Non-Polar Deltahedra).** This class can be subdivided according to whether the atoms around the middle of the cluster lie on the equatorial plane (**4(i) D_{nh}-Planar-Equatorial**) or form a puckered ring around the equator (**4(ii) D_{nd}-Puckered-Equatorial**).

Before considering each of the four deltahedral classes in turn, it is first necessary to establish some group theoretical foundations for the arguments to follow.

4.3 The Pairing Principle in Tensor Surface Harmonic Theory

It has previously been stated that the L^{π} and $\bar{L}^{\pi}$ skeletal MO's of a cluster are related, in a one-to-one fashion, by the Parity Inversion

operation.[2] Fowler has termed this correspondence the "Pairing Principle".[3]

4.3.1 Group theoretical aspects of the Pairing Principle

In group theoretical terms, the Parity Inversion operator ($\hat{P}$), transforms as the odd-parity, pseudo scalar representation Γ_u^0. This is the one dimensional irreducible representation with character +1 under proper operations (i.e. the identity operation and C_n rotations) and -1 under improper operations (i.e. inversion, S_n operations and reflections).[6,7] The irreducible representation, $\Gamma(L^\pi)$, corresponding to a given cluster L^π orbital is converted into that, $\Gamma(\bar{L}^\pi)$ of the parity-related $\bar{L}^\pi$ orbital by multiplication by Γ_u^0:

$$\Gamma(\bar{L}^\pi) = \Gamma(L^\pi) \otimes \Gamma_u^0$$
$$\Gamma(L^\pi) = \Gamma(\bar{L}^\pi) \otimes \Gamma_u^0$$

Henceforth, the symbols Γ_π and $\Gamma_{\bar{\pi}}$ will be used to denote the **reducible** representations spanned by the set of cluster L^π and $\bar{L}^\pi$ orbitals respectively. Since these representations may be expressed as the sum of irreducible $\Gamma(L^\pi)$ and $\Gamma(\bar{L}^\pi)$ representations (e.g. $\Gamma_\pi = \Gamma(L_1^\pi) + \Gamma(L_2^\pi) + \Gamma(L_3^\pi) + \ldots$), the following relationships apply:[3,6]

$$\Gamma_{\bar{\pi}} = \Gamma_\pi \otimes \Gamma_u^0$$
$$\Gamma_\pi = \Gamma_{\bar{\pi}} \otimes \Gamma_u^0$$

Fowler described irreducible representations which are interrelated by Γ_u^0 as **"conjugate".**[3] He noted that in the spherical group (R_{3h}), by definition, the conjugate representations $\Gamma(L^\pi)$ (P_u^π, D_g^π, F_u^π etc.) and $\Gamma(\bar{L}^\pi)$ ($\bar{P}_g^\pi$, $\bar{D}_u^\pi$, $\bar{F}_g^\pi$ etc.) are always symmetrically distinct.

Real cluster molecules, however, cannot actually possess R_{3h} symmetry. Fowler identified three types of finite point groups, with different relationships between conjugate representations (the symbols Γ_A and Γ_B are used to denote generalised congugate representations):[3]

(i) Γ_A is always distinct from its conjugate Γ_B. Groups of this type include C_i, C_s, C_{2v}, $D_{(2n+1)d}$, C_{nh}, $S_{(4n-2)}$, D_{nh}, T_h, O_h, I_h and R_{3h}. The symmetry elements which distinguish the conjugate representations are inversion centres and/or σ_h mirror planes (with the exception of the C_{2v} point group, where there are only σ_v and σ_v' mirror planes). For example, in O_h Γ_A and Γ_B are of opposite parity since $\Gamma_u^0 = A_{1u}$, i.e. if Γ_A has g symmetry (character = +1) under inversion, Γ_B has u symmetry (character = -1). To consider a second example, in D_{3h} $\Gamma_u^0 = A_1''$ so that, if Γ_A has ' symmetry (character = +1) with respect to σ_h, Γ_B has " symmetry (character = -1).

(ii) Γ_A is always **self-conjugate.** Groups of this type describe optically active molecules, e.g. C_n, D_n, T, O and I. In these groups $\Gamma_u^0 = \Gamma_g^0$ (the totally symmetrical one-dimensional irreducible representation, with character +1 under all operations of the group), since they do not possess any improper operations. For example, in D_3 $\Gamma_u^0 = \Gamma_g^0 = A_1$ so $\Gamma_B = \Gamma_A \otimes A_1 = \Gamma_A$. This is always the case, since multiplication by Γ_g^0 leaves any representation unchanged. Therefore, for these groups, $\Gamma(\bar{L}^\pi) = \Gamma(L^\pi)$.

(iii) Some representations, Γ_A, are self-conjugate and some are not. Groups of this type are C_{nv} ($n \geqslant 3$), S_{4n}, D_{2nd} and T_d. The self-conjugate representations are those with zero character under all improper operations of the point group and, as such, must be doubly

degenerate.[8] For example, in T_d, where $\Gamma_u^0 = A_2$, E is self-conjugate ($E \otimes A_2 = E$), wheras T_1 and T_2 are conjugate to each other ($T_1 \otimes A_2 = T_2$, $T_2 \otimes A_2 = T_1$). Not all of the doubly degenerate irreducible representations are necessarily self-conjugate, however. For example, in D_{4d}, E_1 and E_3 constitute a pair of conjugate representations (they have non-zero characters under the improper rotations S_8 and S_8^3), while E_2 is self-conjugate (having zero character under all improper operations).

It will be demonstrated in the next Section that some departures from the (n+1) rule may be rationalised in terms of the number of self-conjugate irreducible representations resulting from a given cluster geometry.

4.3.2 Consequences of the Pairing Principle

In his discussion of the Pairing Principle, Fowler described a group-theoretical analysis of the skeletal MO's of some hypothetical high nuclearity deltahedral boranes, $[B_nH_n]^{q-}$ (n>12).[3] He confirmed Lipscomb's conclusion (based on semi-empirical PRDDO calculations) that a number of these species should be characterised by either n or (n+2) SEP's (i.e. q = 0 or 4), rather than the usual (n+1).[9] It was demonstrated that these unconventional deltahedra did not represent accidental departures from the (n+1) SEP rule, but rather formed the basis of a more general pattern.

Fowler concluded that the group theoretical criterion for symmetry-induced departures from the (n+1) SEP rule is that the reducible representation ($\Gamma_{\pi+\bar{\pi}} = \Gamma_{\pi} + \Gamma_{\bar{\pi}}$), corresponding to the set of cluster L^{π} and $\bar{L}^{\pi}$ orbitals, contains an **odd number of self-conjugate E representations.**[3] The importance of this conclusion relates to the

physical nature of the Parity Inversion operation, which reverses the bonding characteristics of the L^{π} and $\bar{L}^{\pi}$ cluster MO's.[2] If there are an odd number (2m+1) of self-conjugate E representations, then m correspond to bonding L^{π} pairs and m correspond to their (parity-inverted) $\bar{L}^{\pi}$ antibonding counterparts. The remaining E set constitutes a non-bonding degenerate pair of L^{π} and $\bar{L}^{\pi}$ orbitals.[3] Fowler's argument follows from that of Stone who, in his TSH treatment of nido and arachno boranes, demonstrated that L^{π} and $\bar{L}^{\pi}$ orbitals can only be degenerate if they are non-bonding, since constraining one of the pair to be bonding forces the other to be antibonding.[10] In **Chapter 2** similar arguments were used to show that the set of (n-2) approximately degenerate L^{π} and $\bar{L}^{\pi}$ MO's must be reasonably non-bonding.

For those cluster geometries which result in odd numbers of self-conjugate E representations, diamagnetic clusters arise when the non-bonding E pair are either completely empty or fully occupied. This leads to the possibility of alternative SEP counts of n and (n+2), but not (n+1), for such species.

Fowler concluded that, for closo deltahedral geometries, an odd number of self-conjugate E representations only occurs in the following two cases:[3]

(i) T or T_d clusters with an odd number of sets of four equivalent vertices.

(ii) C_m or C_{mv} ($m \geqslant 3$) clusters with an odd number of vertices on the C_m axis.

These conclusions were based upon inspection of the Brester tables of vibrational symmetries for polyhedral molecules,[11] since the

reducible representations corresponding to the stretching and bending modes of a polyhedron are identical to those of the cluster radial (L^{σ}) and tangential ($L^{\pi}/\bar{L}^{\pi}$) MO's respectively:

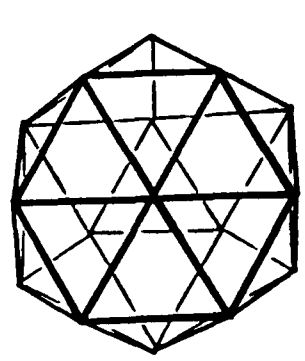
$$\Gamma_{vib}\,(3n) = \Gamma_{stretch}\,(n) + \Gamma_{bend}\,(2n)$$

$$\Gamma_{\sigma} = \Gamma_{stretch}$$

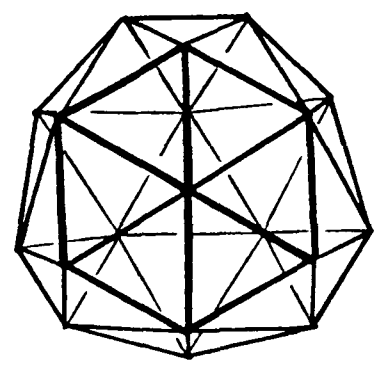
$$\Gamma_{\pi+\bar{\pi}} = \Gamma_{bend}$$

(where n is the number of vertices of the polyhedron). It should be noted that among the vibrations are included the 3 translations $(x,y,z) = P^{\sigma+\pi}$ and 3 rotations $(R_x, R_y, R_z) = \bar{P}^{\pi}$ of the polyhedron as a whole (an n-vertex polyhedron actually has (3n-6) normal vibrational modes).[11]

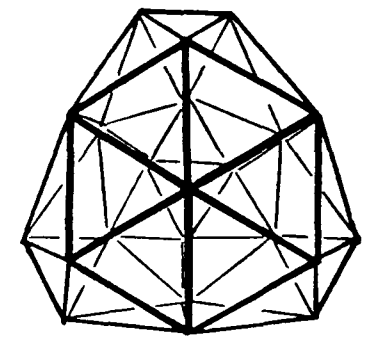
Fowler has used the tetrahedron (belonging to situation (i)) to illustrate his arguments. On the basis of his earlier Extended TSH calculations, the analysis by Stone[2] and the work described in **Chapter 2**, he noted that the tetrahedron has a pair of degenerate non-bonding skeletal MO's, $D_0^{\pi}/\bar{D}_0^{\pi}(e)$. If these orbitals are left unoccupied, the cluster has 4 (n) SEP's, e.g. $[B_4Cl_4]$,[12] whereas their complete occupation leads to a cluster with 6 (n+2) SEP's, e.g. $[C_4Bu^t{}_4]$.[13] For high nuclearity deltahedral boranes Fowler's analysis agrees with the results of Lipscomb's earlier calculations[9] in predicting either n or (n+2) SEP counts, i.e. $[B_nH_n]^{0,4-}$ or isoelectronic analogues, for the molecules (whose skeletal geometries are depicted in **Figure 4.1**) with n = 16 (T_d), 19 (C_{3v}) and 22 (T_d).



$[B_{16}H_{16}]$ (T_d)



$[B_{19}H_{19}]$ (C_{3v})



$[B_{22}H_{22}]$ (T_d)

Figure 4.1 Examples of large deltahedral boranes which are predicted to disobey the (n+1) SEP rule.

4.3.3 Comments on Fowler's Analysis

Fowler has developed an elegant method to explain why certain deltahedral cluster geometries possess a non-bonding degenerate pair of orbitals, in terms of whether they possess an even or odd number of self-conjugate E representations. His treatment does not, however, include a general explanation of why the number of such representations is even or odd. The approach involves the use of published tables of vibrational symmetries (Γ_{vib}) to determine which cluster geometries lead to an odd number of self-conjugate E representations (and hence symmetry-induced deviations from the (n+1) rule). A more general topological/group theoretical derivation of Fowler's rules is presented in **Section 4.5.1.**

Considering Fowler's rules, as to which deltahedral geometries give rise to an odd number of self-conjugate E representations, it is possible to combine them in a simplified version:

"The only deltahedral geometries which give rise to an odd number of self-conjugate E representations are those in which there is (at least) one threefold rotational symmetry axis which passes through a single vertex."

Since they possess single atoms on the principal C_3 rotation axis (axes), these clusters belong to deltahedral **Class 2(i) C_3-Polar Deltahedra,** further discussion of which is given in **Section 4.5.1.**

This simplification of Fowler's rules has been achieved by noting two important topological features of deltahedral clusters:

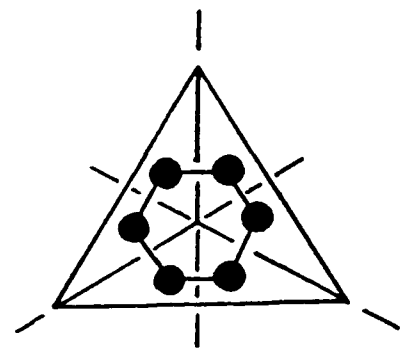
(1) Relating to Fowler's rule **(ii),** it is not feasible to have a closo deltahedron with an odd number of vertices on the principal rotation axis C_m if $m > 3$, since the rotation axis would generate square, pentagonal and larger faces. For $m > 3$, the cluster polyhedra have nido geometries and Stone has demonstrated that such clusters do indeed have a non-bonding degenerate $L^{\pi}/L^{-\pi}$ pair, thereby explaining their (n+2) SEP count.[10] These clusters (of which the C_{mv} pyramids and monocapped antiprisms are the archetypal examples) may be classed as **C_m-polar polyhedra,** though they are clearly not deltahedra.

(2) Relating to Fowler's rule **(i),** it can be shown that those deltahedra, with either T or T_d symmetry, which possess an odd number of sets of four equivalent cage atoms, are actually special examples of the C_3 and C_{3v} deltahedra mentioned in **(1),** if x=1. They are not simple deltahedra if x=3, 5, 7 etc.

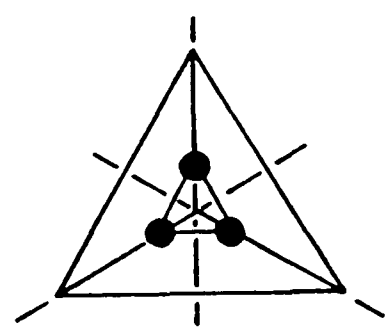
Fowler stated, without derivation, that a cluster belonging to the T_d point group has: m sets of 24; m_d sets of 12 and m_3 sets of 4 equivalent atoms. An explanation of how these sets arise is presented

below.

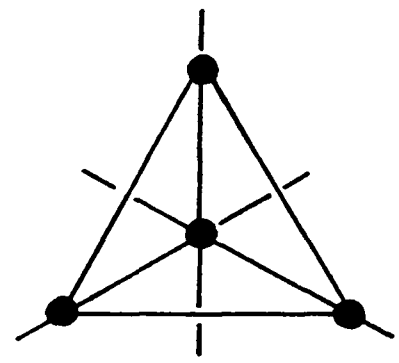
The m sets of 24 atoms correspond to vertices which do not lie on any symmetry elements of the point group, i.e. they occupy **general positions** in the cluster. If one vertex occupies a general position, the symmetry elements of T_d generate another 23. The cluster with m=1, for example, has a regular hexagonal arrangement of atoms around each of the 4 C_3 axes, such that the σ_d mirror planes (which contain the C_3 axis) bisect the edges of the hexagon:



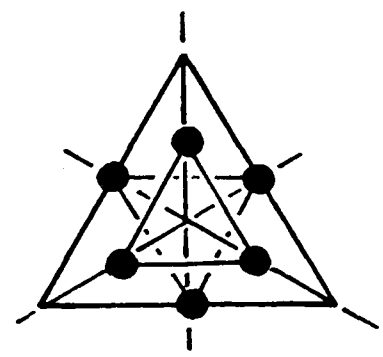
The m_d sets of 12 atoms correspond to vertices which lie on the σ_d mirror planes (but no other symmetry elements) of the cluster, i.e. they occupy **special positions** in the cluster. Constraining one vertex to lie on a mirror plane, the symmetry elements of T_d generate another 11 vertices, provided that the vertex does not lie on any other symmetry elements, such as the C_2 and S_4 axes (where two σ_d planes intersect), or the C_3 axes (where 3 σ_d planes intersect). The polyhedra with m_d=1, for example, have a triangle of vertices around each of the 4 C_3 axes, such that the vertices lie on the 3 σ_d planes which contain the rotation axis:



The m_3 sets of 4 atoms correspond to vertices which lie on the C_3 axes of the tetrahedron. By definition, vertices which lie on these special positions also lie on the σ_d mirror planes. Placing one vertex on a C_3 axis, leads to the generation of another 3 vertices. The polyhedra with m_3=1, for example, have one atom on each C_3 axis:



In addition to the above mentioned general and special cluster atom positions, a tetrahedral cluster may possess m_2 sets of 6 atoms, which lie on the C_2 axes (i.e. special cluster atom positions corresponding to the midpoints of the edges of a tetrahedron). These axes are formed by the intersection of 2 σ_d planes. Since the T_d point group possesses S_4 axes which are colinear with these C_2 axes, if an atom is placed on the C_2 axis (as long as it is not at the centre of the cluster), another 5 vertices are generated:



The total number (n) of atoms in a general tetrahedral cluster is given by the formula:

$$n = 24m + 12m_d + 6m_2 + 4m_3$$

Some examples of T_d polyhedra, with differing values of m, m_d,m_2 and m_3 are illustrated in **Figure 4.2.** Fowler's rule **(i)** follows from the equation which he deduced (from the Brester table of Γ_{vib} for T_d molecules)[11] for the number of (self-conjugate) E representations in $\Gamma_{\pi+\bar{\pi}}$:

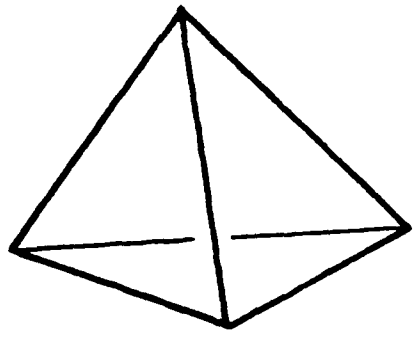
$$no.(E) = 4m + 2m_d + m_3$$

(i.e. the atoms on the C_2 axes contribute no E representations).

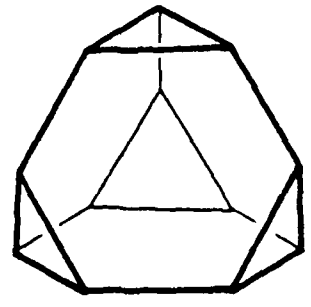
From the above equation, it is apparent that there is only an odd number of E representations if m_3 is odd. The tetrahedron is the simplest example of such a cluster ($m=m_d=0$, $m_3=1$), possessing one non-bonding E pair ($D^{\pi}/\bar{D}^{\pi}$). Since it has one atom on each principal C_3 rotation axis, the tetrahedron may be described as a C_3-polar deltahedron. The only difference between this case and those already mentioned being that T or T_d polyhedra possess 4 of these axes. The three alternative descriptions of the tetrahedron, i.e. as a C_3-polar deltahedron, 3-connected polyhedron (see **Chapter 2**) or <u>nido</u> trigonal bipyramid,[2] are consistent with the occurrence of a non-bonding $L^{\pi}/\bar{L}^{\pi}$ E pair and an (n+2) SEP count (though n SEP clusters are also known). Fowler pointed out that other T_d clusters of this type are the 16 vertex species ($m=0$, $m_d=1$, $m_3=1$) and the 22 vertex molecule ($m=0$, $m_d=1$, $m_2=1$, $m_3=1$), shown in **Figure 4.1.**

If $m_3=2$, there must be 2 atoms on each C_3 axis. For a deltahedron, this results in a bipolar cluster (Class 3), with an even number of E representations and, hence, no symmetry-induced departure from the (n+1) rule.

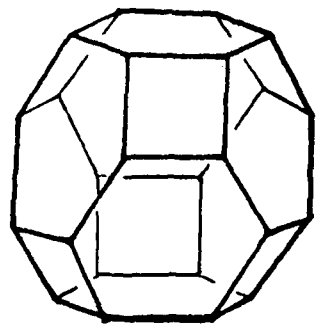
If $m_3=3$, there must be 3 atoms on each C_3 axis. It is impossible, however, for a simple deltahedral cluster to have 3 atoms lying on a



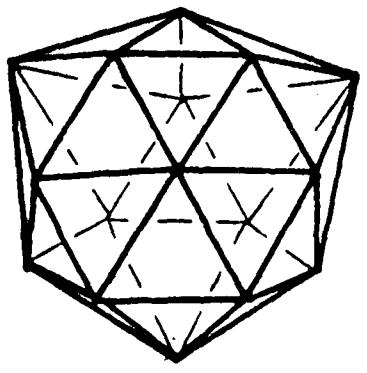
m_3=1 (4 vertices)



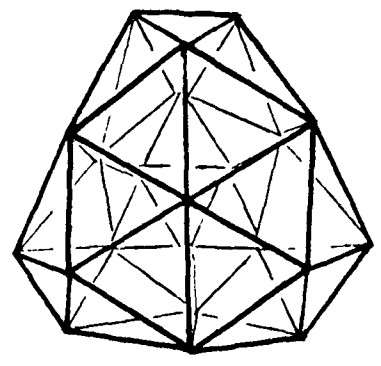
m_d=1 (12)



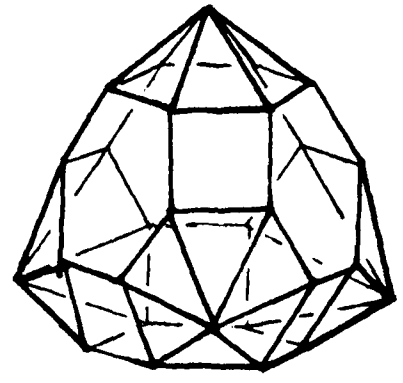
m=1 (24)



m_3=1, m_d=1 (16)



m_3=1, m_d=1, m_2=1 (22)



m_3=1, m=1 (28)

Figure 4.2 Polyhedra, belonging to the T_d point group, with differing numbers of sets of symmetry equivalent atoms.

straight line which passes through the centre of the cluster. This situation may arise, however, when the cluster consists of polyhedra within polyhedra, such as the **Bispherical** and **Multispherical** clusters which will be discussed in **Chapter 5.**

The remainder of this Chapter is concerned with the application of the group theoretical and topological ideas developed above to the four classes of deltahedra previously defined.

4.4 Class 1: Centrosymmetric Spherical Deltahedra

The octahedron (O_h) and icosahedron (I_h) most closely approximate to a spherical pseudo-symmetry. Consequently, TSH theory gives the coefficients of the radial (L^{σ}) and tangential ($L^{\pi}/\bar{L}^{\pi}$) MO's precisely. The centrosymmetric nature of these polyhedra ensures that the odd-parity ($\bar{L}^{\pi}$) orbitals cannot mix with their even-parity (L^{π}) counterparts, because they have opposite symmetry with respect to the inversion operation ($\hat{i}$). As described in **Section 4.1.4**, the L^{π} and $\bar{L}^{\pi}$ functions are related by the Parity Inversion operator ($\hat{P}$), which transforms as Γ^{0}_{u}. This operator interconverts the bonding and antibonding character of the tangential orbitals:[2]

$$
\begin{array}{lll}
L^{\pi} & \Gamma_{\pi} = \Gamma^{L}_{\pi g}\ (L=2n) + \Gamma^{L}_{\pi u}\ (L=2n+1) & \\
\hat{P}\ \downarrow & \otimes\ \Gamma^{0}_{u}\ \downarrow & \\
\bar{L}^{\pi} & \Gamma_{\bar{\pi}} = \Gamma^{L}_{\bar{\pi} u}\ (L=2n) + \Gamma^{L}_{\bar{\pi} g}\ (L=2n+1) &
\end{array}
$$

Thus, the high symmetry of these molecules ensures that the L^{π} and $\bar{L}^{\pi}$ orbitals are symmetrically disposed about the non-bonding energy

line. This situation is illustrated in **Figure 4.3**, for the specific example of an icosahedral cluster, such as <u>closo</u>-$[B_{12}H_{12}]^{2-}$.

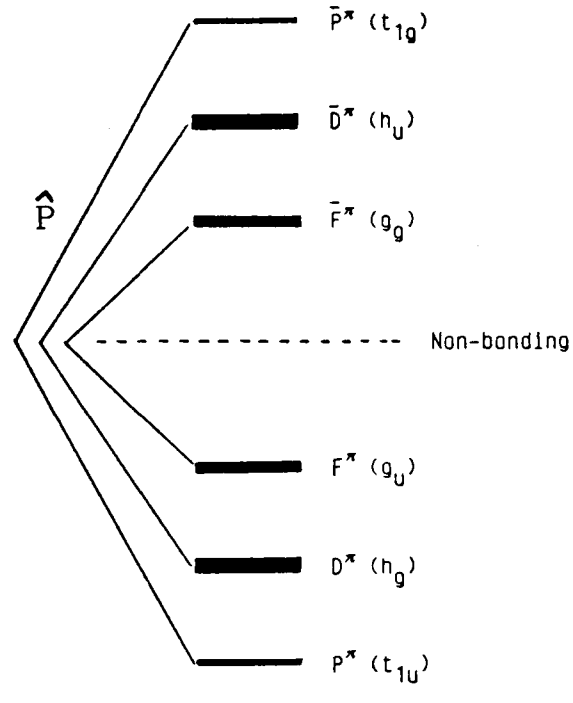


Figure 4.3 The L^{π} and $\bar{L}^{\pi}$ orbitals of an icosahedral cluster, as an example of a "Centrosymmetric Spherical Cluster".

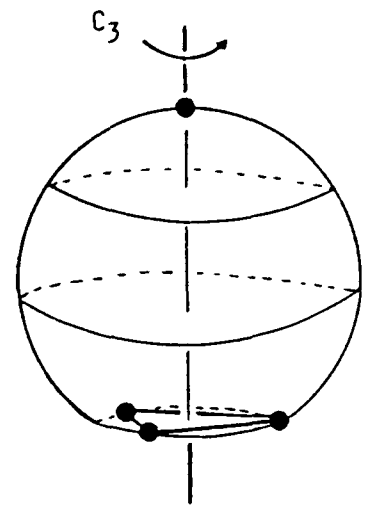
The parity inversion operator in these cases ensures the absence of self-conjugate non-bonding $L^{\pi}/\bar{L}^{\pi}$ E pairs. Consequently, the (n+1) rule is rigorously applicable in such situations. Examples of such clusters include $[B_6H_6]^{2-}$ (octahedral) and $[B_{12}H_{12}]^{2-}$ (icosahedral). Departures from the (n+1) rule will only occur in situations where the clusters are significantly distorted from the idealised geometries.

4.5 Class 2: Polar Deltahedra

Polar deltahedra are defined as possessing one cluster vertex on each principal rotation axis. Three sub-classes may be distinguished, depending on the nature of these rotation axes.

4.5.1 Sub-class 2(i): C_3-polar deltahedra

In this sub-class of polar deltahedra, the axis on which the polar atom lies (polar axis) passes through a triangular face on the other side of the cluster (**1**), thereby making it a C_3 axis.

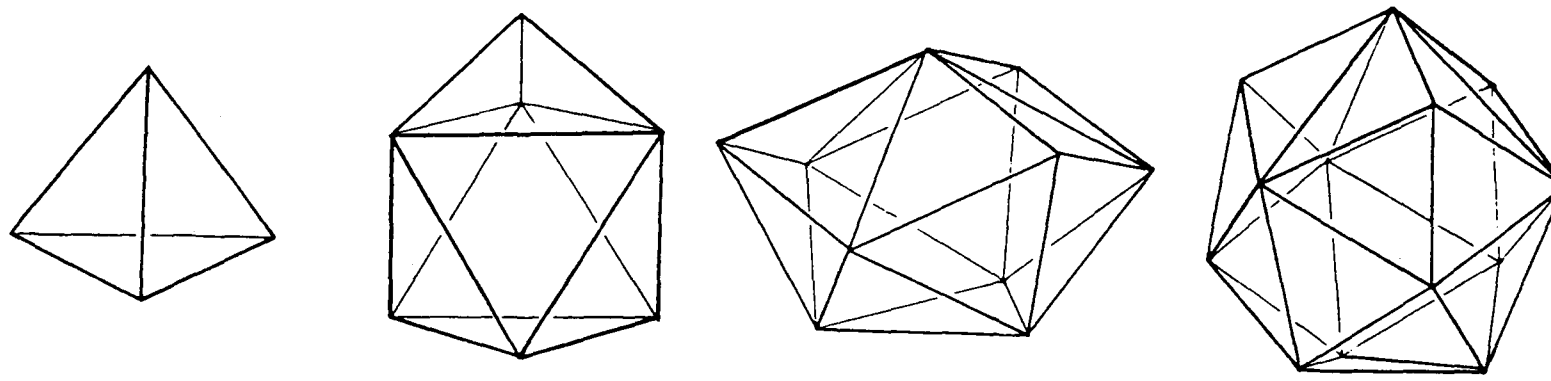


(1)

Such clusters belong to the point groups C_3, C_{3v}, T or T_d, and possess one cluster atom on each principal (C_3) rotation axis.[8] In a C_3 or C_{3v} deltahedron there are p sets (layers) of symmetry related atoms lying in planes perpendicular to the C_3 axis. Consequently, the total number of atoms in C_3-polar deltahedra must be (3p+1). As demonstrated in **Section 4.3.3**, the higher symmetry T and T_d possibilities arise from the occurrence of three additional threefold symmetry axes, but only those polyhedra with (3p+1) atoms have a single atom on each of these axes and may be classified as polar deltahedra.

The polyhedra discussed by Fowler fit into the polar deltahedral scheme and may be classified as follows: p=1 (n=3p+1=4, Td), p=5 (n=3p+1=16, Td), p=6 (n=3p+1=19, C_{3v}) and p=7 (n=3p+1=22, T_d). The analysis described in this Section extends Fowler's treatment to include <u>hyper</u>-<u>closo</u> metallaborane and metallacarborane clusters (such as those described in **Chapter 3**)[14] and capped deltahedra (<u>pileo</u> geometries).

p=1, n=4 p=2, n=7 p=3, n=10 p=4, n=13



Examples

$[B_4Cl_4]$[a] (n SEP's)

$[Re_4H_4(CO)_{12}]$[b]

$[C_4Bu^t_4]$[c] (n+2 SEP's)

$[Ru_4H_4(CO)_{12}]$[d]

$[Cp_3Co_3B_4H_4]$[e] (n)

$[Os_7(CO)_{21}]$[f]

$[H(PPh_3)(Ph_2\overline{C_6H_4})IrB_9H_8]$[g] (n)

$[H(PPh_3)ClRuB_9H_7(PPh_3)_2]$[h]

$[Cp_2Fe_2C_2B_6H_8]$[i]

a M. Atoji and W.N. Lipscomb, Acta Crystallogr., 1953, **6**, 547. **b** R. Saillant, G. Barcelo and H.D. Kaesz, J. Amer. Chem. Soc., 1970, **92**, 5739. **c** G. Maier, S. Pfriem, U. Schafter and R. Matusch, Angew. Chem., 1978, **90**, 652. **d** R.D. Wilson, S.M. Wu, R.A. Love and R. Bau, Inorg. Chem., 1978, **17**, 1271. **e** J.R. Pipal and R.N. Grimes, Inorg. Chem., 1977, **16**, 3255. **f** C.R. Eady, B.F.G. Johnson, J. Lewis, R. Mason, P.B. Hitchcock and K.M. Thomas, J. Chem. Soc., Chem. Commun., 1977, 385. **g** J. Bould, N.N. Greenwood, J.D. Kennedy and W.S. McDonald, J. Chem. Soc., Chem. Commun., 1982, 465. **h** J.E. Crook, M. Elrington, N. Greenwood, J.D. Kennedy, M. Thornton-Pett and J.D. Woolins, J. Chem. Soc., Dalton Trans., 1985, 2407. **i** K.P. Callahan, W.J. Evans, F.Y. Lo, C.E. Strouse and M.F. Hawthorne, J. Amer. Chem. Soc., 1975, **97**, 296.

Figure 4.4 C_3-polar deltahedral clusters, with (3p+1) skeletal atoms.

Some examples of C_3-polar deltahedral clusters (with p = 1, 2, 3 and 4) are shown in **Figure 4.4.** Pileo and hyper-closo polyhedra are topologically equivalent and may be interconverted by an expansion or contraction of the top triangle of atoms, along with movement (in or out) of the polar atom, as shown schematically in **Figure 4.5.**

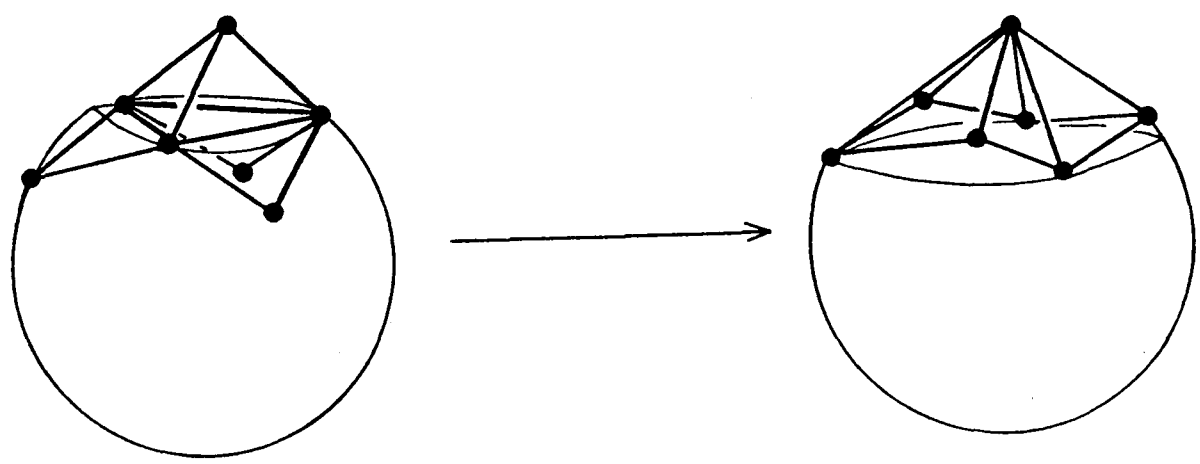


Figure 4.5 Schematic illustration of the geometric relationship between pileo and hyper-closo deltahedral geometries.

For each of the p triangles of symmetry related (non-polar) atoms, the L^{σ} orbitals consist of one A_1 and one E irreducible representation. Quinn has noted that the L^{σ} orbitals of a cluster belonging to an axial point group can be obtained by taking combinations of the L^{σ} orbitals of its constituent **orbits** (i.e. sets of symmetry related atoms).[6] He has also shown that the longitudinal (θ) components of L^{π} and $\bar{L}^{\pi}$ can be derived by using the L^{σ} orbitals as generator functions, with a basis set of tangential p^{θ} orbitals (with the same local

symmetry properties as p_z orbitals) rather than radial orbitals. In group theoretical terms this corresponds to the direct product:

$$\Gamma^{\theta}_{\pi+\bar{\pi}} = \Gamma_{\sigma} \otimes \Gamma_z$$

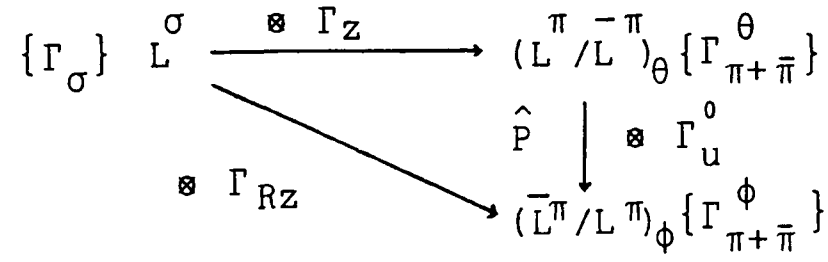
The latitudinal (ϕ) components of L^{π} and $\bar{L}^{\pi}$ are generated by taking the θcomponents and rotating the p^{θ} orbital on each atom by 90^{o} (in the same sense) about the radial vector. This process corresponds to the action of the parity inversion operator ($\hat{P}$). In axial point groups the symmetry of the parity inversion operator (Γ^{0}_{u}) is given by the direct product:

$$\Gamma^{0}_{u} = \Gamma_z \otimes \Gamma_{Rz}$$

Thus, the ϕ components of L^{π} and $\bar{L}^{\pi}$ are obtained from the L^{σ} orbitals by taking the following direct product:

$$\Gamma_{\pi+\bar{\pi}} = \{\Gamma_{\sigma} \otimes \Gamma_z\} \otimes \{\Gamma_z \otimes \Gamma_{Rz}\} = \Gamma_{\sigma} \otimes \Gamma_{Rz}$$

This information is summarised below:



In the C_{3v} point group, for example, $\Gamma_z = A_1$ and $\Gamma_{Rz} = A_2$ (in fact, in axial point-groups, Γ_z and Γ_{Rz} are never part of any multidimensional (E, T etc.) irreducible representations).[8] Since $E \otimes A_1$ or $E \otimes A_2 = E$, for each of the (p) E functions in Γ_{σ} there will be one in $\Gamma^{\theta}_{\pi+\bar{\pi}}$and one in $\Gamma^{\phi}_{\pi+\bar{\pi}}$. The total number of E representations in the tangential cluster orbitals (i.e. the number of E representations in the reducible representation $\Gamma_{\pi+\bar{\pi}}$) is therefore even (2p). When considering polyhedra

with vertices lying on the C_3 axis, the above method for generating the $L^{\pi}/\bar{L}^{\pi}$ orbitals does not work because at the poles of a sphere an atomic p_z orbital has purely radial, rather than tangential, orientation. At any other position, this orbital can be resolved into radial and tangential components. To circumvent this problem, it is merely necessary to evaluate the tangential orbitals for the non-polar structure and add the π-orbitals of the polar atoms. For one polar atom in C_{3v} symmetry, the p^{π} atomic orbitals (p_x and p_y) transform as E, so the polar deltahedron possesses in total an odd number (2p+1) of E representations in the $L^{\pi}/\bar{L}^{\pi}$ orbitals. This results in an equal number (p) of bonding (L^{π}) and antibonding ($\bar{L}^{\pi}$) E functions and one self-conjugate ($L^{\pi}/\bar{L}^{\pi}$) E pair which is non-bonding.

The non-bonding orbitals are singly noded with respect to the polar axis and as such are denoted $(L^{\pi}/\bar{L}^{\pi})_{\pm 1}$, e.g. $(D^{\pi}/\bar{D}^{\pi})_{\pm 1}$ in the case of the tetrahedron (p=1) and $(F^{\pi}/\bar{F}^{\pi})_{\pm 1}$ in the case of the ten-vertex cluster (p=3). In cases other than in T and T_d molecules, where there are four equivalent polar atoms, the non-bonding orbitals are mainly localised on the polar atom. Occupation of these orbitals would lead to a cluster with (n+2) SEP's but (with the exception of the tetrahedron) they are usually unoccupied and an n SEP count is observed.

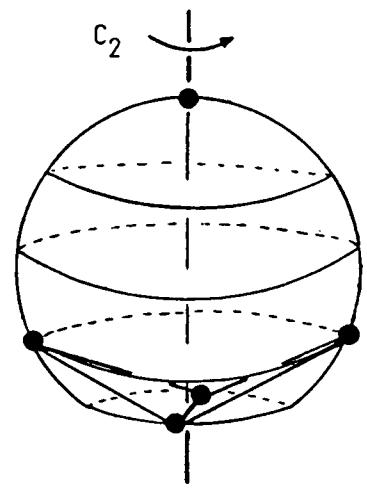
Examples of polar deltahedral clusters possessing C_3 axes and n or (n+2) skeletal electron pairs are given in **Figure 4.4.** The hyper-closo 10-vertex deltahedra have previously been shown to possess 10 (n) SEP's.[14a] Factors governing the stabilisation of these clusters, such as the presence of metal atoms at the higher connectivity sites, have been discussed in **Chapter 3.**

With the exception of tetrahedral molecules (e.g. $[B_4Cl_4]$ and $[P_4]$), polar deltahedral geometries have not been positively identified

for all-main-group clusters. Hyper-closo or capped deltahedral (pileo) geometries may be postulated for the species $[B_7Br_7]$ [16] and $[B_{10}Cl_{10}]$,[17] which have not yet been structurally characterised. These molecules, with n SEP's, are diamagnetic, whereas molecular orbital calculations on the pentagonal bipyramid and bicapped square antiprism indicate (see **Section 4.6.2**) that they would probably be paramagnetic if they adopted the usual closo geometries. This is due to the occurrence of degenerate HOMO's for the (n+1) SEP $[B_nH_n]^{2-}$ species. The n SEP count for monocapped deltahedral clusters, rationalised by Mingos and co-workers in terms of the Capping Principle,[15] is also conveniently explained by recognising these clusters as polar deltahedra.

4.5.2 Sub-class 2(ii): C_2-polar deltahedra

In this sub-class of polar deltahedra the polar axis passes through an edge between two triangular faces of the deltahedron (2), thereby making it a C_2 axis.



(2)

This leads to clusters with C_2 or C_{2v} symmetry. Polar deltahedra with these cluster symmetries are characterised by (2p+1) atoms, where p represents the number of pairs of atoms disposed about the principal

(C_2) axis. Examples of C_2-polar deltahedral clusters (with p = 4, 5 and 6) are given in **Figure 4.6.**

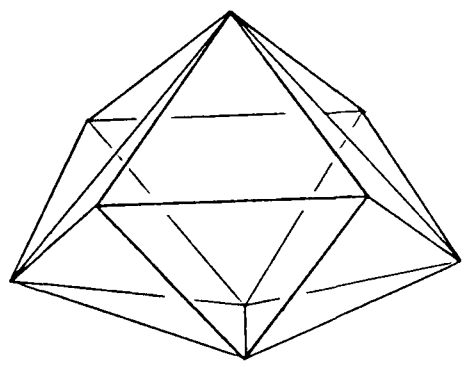
As there are no E representations in C_2 or C_{2v} symmetry, there is no group theoretical restriction opposing the occurrence of clusters with (n+1) skeletal electron pairs. Instead, the electron count depends more critically on the frontier orbital spacings, which in turn depend on the nature of the cluster fragments. As indicated in **Chapter 3,** Extended Hückel calculations have shown that with boron atoms in the polar sites an (n+1) count is favoured, while with metals in these sites, either n or (n+1) skeletal electron pairs is possible.

A number of metallaborane and metallacarborane clusters, with the C_{2v} 11-vertex (p=5) geometry, have been characterised. In agreement with the previous analysis, examples with n (hyper-closo) and (n+1) (closo) SEP's are known, as shown in **Figure 4.6.** Examples of 9 (p=4) and 13 (p=6) C_2-polar deltahedra are also given in the Figure. Lipscomb's calculations on the C_{2v} (p=6) 13-vertex cluster predicted the usual (n+1 = 14) SEP count.[9] This structure, which may be regarded as a distorted edge-bridged icosahedron, was calculated to be the lowest energy geometry for $[B_{13}H_{13}]^{2-}$. For 13 (n) SEP's, however, it is likely that the C_{3v} (p=4) structure (corresponding to a distorted capped icosahedron), shown in **Figure 4.4,** would be favoured.

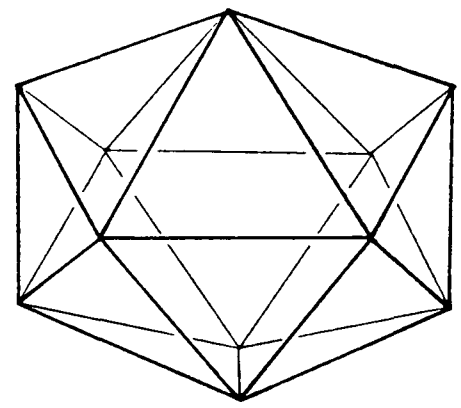
4.5.3 Sub-class 2(iii): C_1-polar deltahedra

In this sub-class of polar deltahedra the polar axis does not pass through the centroid of a face or the middle of an edge of the deltahedron, so that there is no rotational symmetry (only a C_1 axis). This leads to clusters with either C_i or C_s symmetry. As for the C_2-

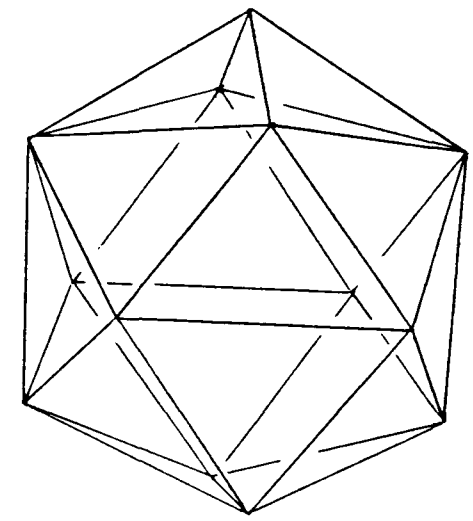
p=4, n=9



p=5, n=11



p=6, n=13



Examples

$[H(PMe_3)_2IrB_8H_7Cl]$[a] (n SEP's)

$[Ni_5(CO)_6Cl\{PCH(SiMe_3)_2\}_4]$[b]

$[(PPh_3)_2RuB_{10}H_8(OEt)_2]$[c] (n)

$[H(PMe_2Ph)_2RhB_{10}H_8(OMe)_2]$[d]

$[(\eta^6\text{-}C_6H_3Me_3)FeB_{10}H_{10}]$[e]

$[(CMe)_2B_9H_9]$[f] (n+1 SEP's)

$[H(PEt_3)_2RhC_2B_8H_{10}]$[g]

$[CpCoC_2B_8H_{10}]$[h]

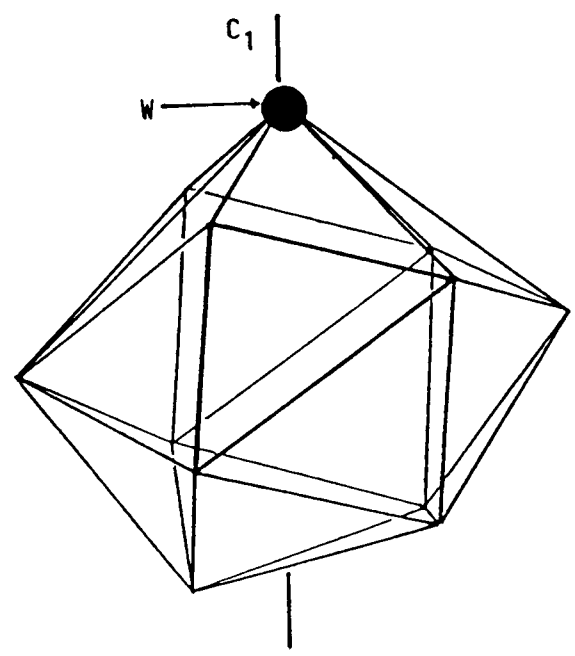
$[CpCoC_2B_{10}H_{12}]$[h,i] (n+1)

$[H(PPh_3)_2RhC_2B_{10}H_{12}]$[j]

a J. Bould, N.N. Greenwood, J.D. Kennedy and W.S. McDonald, J. Chem. Soc., Dalton Trans., 1985, 1843. **b** M.M. Olmstead and P.P. Power, J. Amer. Chem. Soc., 1984, **106**, 1495. **c** J.E. Crook, M. Elrington, N.N. Greenwood, J.D. Kennedy and J.D. Woollins, Polyhedron, 1984, **3**, 901; J.E. Crook, M. Elrington, N.N. Greenwood, J.D. Kennedy, M. Thornton-Pett and J.D. Woollins, J. Chem. Soc., Dalton Trans., 1985, 2407. **d** H. Fowkes, N.N. Greenwood, J.D. Kennedy and M. Thornton-Pett, J. Chem. Soc., Dalton Trans., 1986, 517. **e** R.P. Micciche, J.J. Briguglio and L.G. Sneddon, Inorg. Chem., 1984, **23**, 3992. **f** C. Tsai and W. Streib, J. Amer. Chem. Soc., 1966, **88**, 4513. **g** C.W. Jung and M.F. Hawthorne, J. Amer. Chem. Soc., 1980, **102**, 3024. **h** D.F. Dustin, G.B. Dunks and M.F. Hawthorne, J. Amer. Chem. Soc., 1973, **95**, 1109. **i** M.R. Churchill and B.G. DeBoer, Inorg. Chem., 1974, **13**, 1411. **j** J.D. Hewes, C.B. Knobler and M.F. Hawthorne, J. Chem. Soc., Chem. Commun., 1981, 206.

Figure 4.6 C_2-polar deltahedral clusters, with (2p+1) skeletal atoms.

polar deltahedra, the lack of any E representations in these point groups means that clusters with either n or (n+1) SEP's may be realised. $[(PEt_3)_2Pt(CO)_2W\{\eta^6\text{-}C_2B_9H_8(CH_2R)Me_2\}]$ **(3)** is an example of such a cluster, possessing a 12 atom WC_2B_9 cage, with C_s symmetry, and 12 (n) SEP's.[18]



(3)

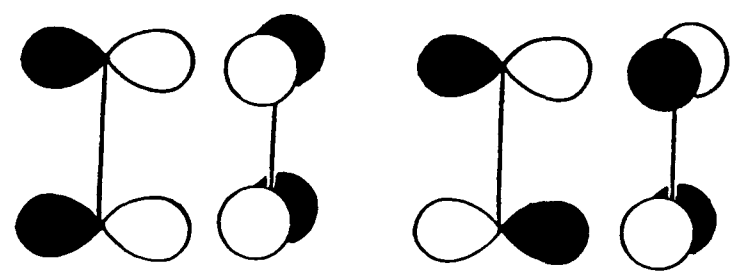
4.6 Class 3: Bipolar Deltahedra

4.6.1 General topological and group theoretical considerations

Bipolar deltahedra have two vertices lying on the principal (C_n) rotation axis. These deltahedra belong to either the D_{nh} (e.g. bipyramids) or D_{nd} (e.g. bicapped antiprisms) types of point group. In such deltahedra there are two (or more) subsets of cluster vertices, which, generally lie on concentric spherical shells of different radii.

Following the analysis presented above for polar deltahedral clusters, the polar atoms are initially ignored and the L^σ orbitals of the component layers (latitudinal orbits) in the cluster are considered. Combinations of these orbitals are taken to generate the L^σ orbitals of the polyhedron (minus polar atoms). As demonstrated in **Section 4.5.1**, in

a generalised axial point group, if Γ_σ contains a certain number (x) of E representations then $\Gamma^{\theta}_{\pi+\bar{\pi}}(=\Gamma_\sigma \otimes \Gamma_z)$ and $\Gamma^{\phi}_{\pi+\bar{\pi}}(=\Gamma_\sigma \otimes \Gamma_{Rz})$ will each contain x E representations. There are, therefore, an even number (2x) of E representations in the $L^{\pi}/L^{-\pi}$ set. Considering the two polar atoms, in phase (Π) and out of phase (Π^*) combinations of the p^{π} orbitals (p_x,p_y) on each atom may be constructed (**4**). In axial point groups these combinations constitute two additional E representations.



$P^{\pi}_{\pm 1}$ (π) $\quad$ $\bar{P}^{\pi}_{\pm 1}$ (π^*)

(4)

The L^{π} and $\bar{L}^{\pi}$ orbitals of the bipolar cluster as a whole are generated by taking combinations of the orbitals of the polar atoms and of the remainder of the polyhedron, so that, in total, there are an even number (2x+2) of E representations within the $L^{\pi}/\bar{L}^{\pi}$ manifold. These are split into (x+1) bonding (L^{π}) and (x+1) anti-bonding ($\bar{L}^{\pi}$) E pairs. There is, therefore, no group theoretical restriction leading to a departure from the (n+1) rule. Consequently, the majority of bipolar clusters obey the rule.

There are, however, a significant number of bipolar clusters which do not obey the (n+1) rule. Deviations arise because bipolar clusters often do not approximate closely enough to a spherical topology. The nature of the variance from the (n+1) rule is best analysed in terms of the interaction between the π orbitals of the various sets of symmetry-

equivalent cluster vertices, which may be regarded as lying on concentric spheres of differing radii. In the case of bipyramidal or bicapped antiprismatic clusters, these two sets of atoms are the polar atoms and the remaining (non-polar) atoms which either lie on the equator (D_{nh}) or are related by an improper rotation axis S_{2n} (D_{nd}).

Since the two polar atoms are not within bonding distance, the spread of L^{π} and $\bar{L}^{\pi}$ orbitals (i.e. $P^{\pi}_{\pm 1}$ and $\bar{P}^{\pi}_{\pm 1}$) for these atoms is much narrower than for the non-polar atoms. The $P^{\pi}_{\pm 1}$ and $\bar{P}^{\pi}_{\pm 1}$ linear combinations of the polar atoms can only interact with the $L^{\pi}_{\pm 1}$ and $\bar{L}^{\pi}_{\pm 1}$ orbitals of the rest of the cluster (ring or antiprism). Two slightly different situations apply for bicapped rings (bipyramids - D_{nh}) and bicapped antiprisms (D_{nd}) and these are described below.

4.6.2 Sub-class 3(i): D_{nh}-bipyramids

Figure 4.7 illustrates the interactions between the L^{π} and L^{π} orbitals of the polar and equatorial (ring) atoms of a trigonal bipyramidal (D_{3h}) cluster. The $\bar{P}^{\pi}_{\pm 1}$ (Π^{*}) polar combination is stabilised by the more strongly antibonding $\bar{P}^{\pi}_{\pm 1}$ pair of the ring, yielding a weakly bonding e'' pair ($D^{\pi}_{\pm 1}$) with a dominant (Π^{*}) polar-atom contribution. In a similar fashion, the $P^{\pi}_{\pm 1}$ (Π) polar combination is destabilised by the more strongly bonding $P^{\pi}_{\pm 1}$ orbitals of the ring, thereby generating a weakly antibonding (parity related) e' pair ($\bar{D}^{\pi}_{\pm 1}$), again with a dominant (Π) polar-atom contribution.

The pentagonal bipyramid (D_{5h} symmetry) shows many of the same features as the trigonal bipyramid, if the polar and equatorial atoms are approximately equidistant from the centre of the cluster (i.e. the cluster topology is closer to spherical). If the polar atoms are

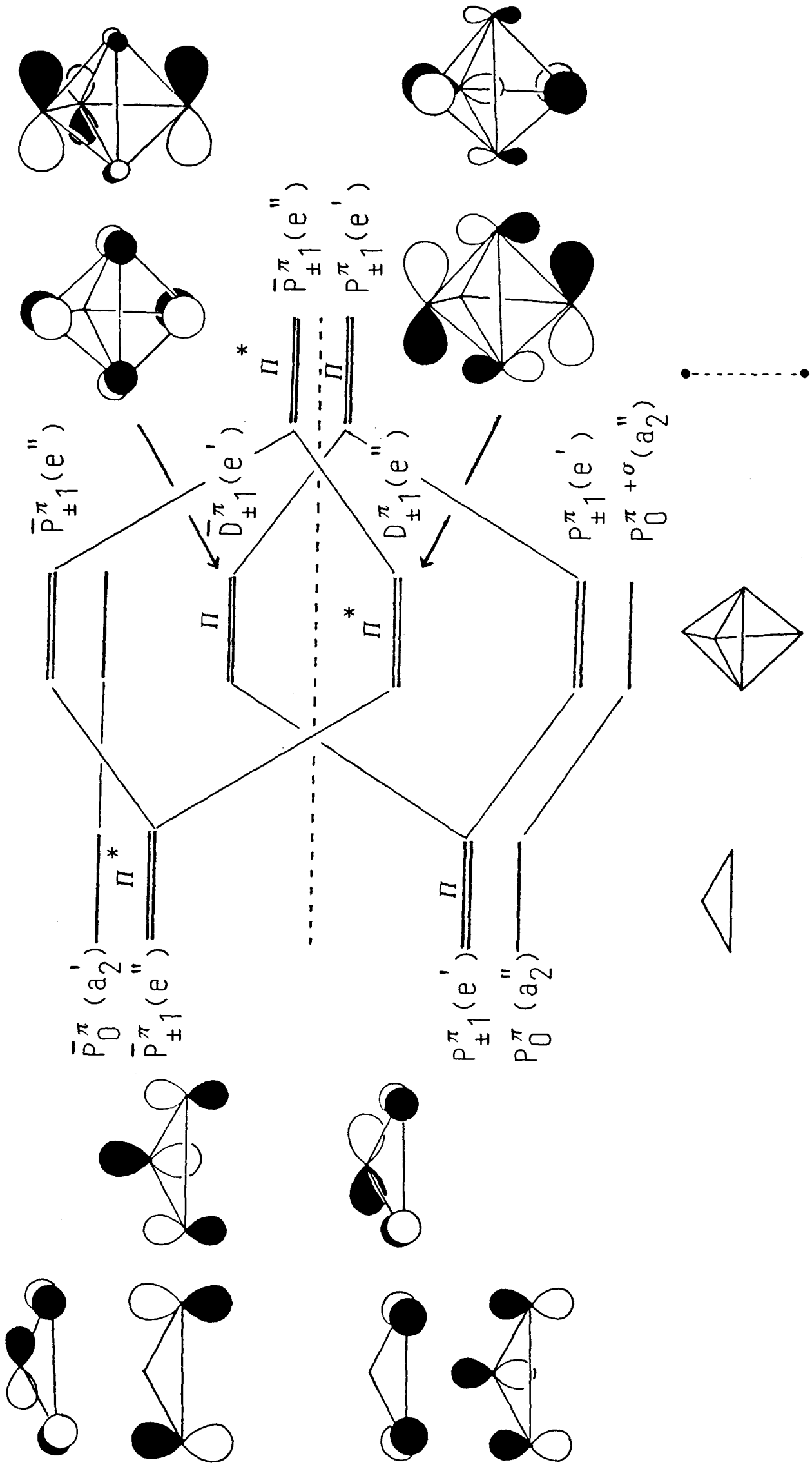
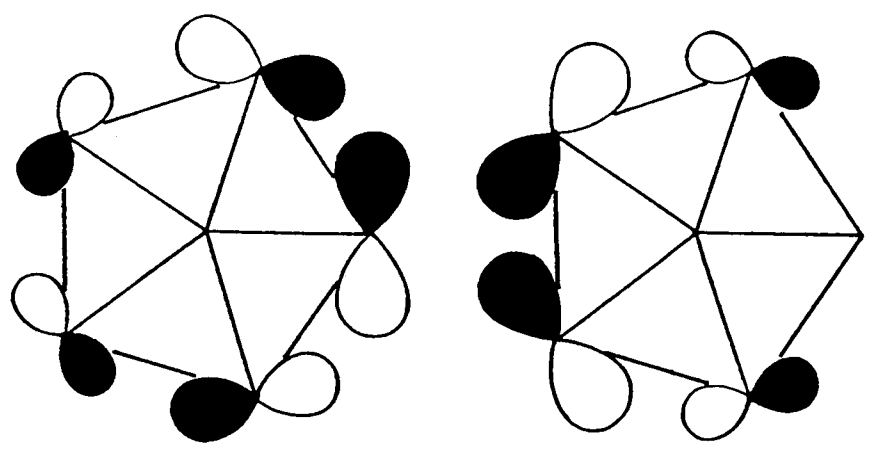


Figure 4.7 Interaction between the L^{π} and $\bar{L}^{\pi}$ orbitals of the ring and polar atoms of a trigonal bipyramidal (D_{3h}) cluster.

displaced towards the centre of the cluster (so as to equalise the skeletal bond lengths), additional electronic effects are observed. Since the pentagonal ring is larger than the trigonal ring, the polar atoms must move closer to the centre of the polyhedron to equalise the skeletal bond lengths. Extended Hückel calculations were performed on pentagonal bipyramidal $[B_7H_7]^{2-}$ clusters: (a) with equal centre-B atom distances (spherical distribution); (b) with equal skeletal bond lengths. The energies of the frontier orbitals, obtained from these calculations, are presented in **Table 4.1.**

In both cases (a) and (b) a stronger interaction occurs between the $\bar{P}^{\pi}$ orbitals of the polar atoms and the ring, for the pentagonal bipyramid than the trigonal bipyramid. This is because the $\bar{P}^{\pi}_{\pm 1}$ orbitals of the pentagonal ring are actually weakly bonding (for instance they constitute the HOMO's in $[C_5H_5]^-$), so the energy match between the ring and polar atoms is better. The resulting $D^{\pi}_{\pm 1}(e''_1)$ orbitals of the pentagonal bipyramid are, therefore, not necessarily the HOMO's. From **Table 4.1** it is apparent that the HOMO's, in both cases (a) and (b), are the ring-localised $D^{\pi}_{\pm 2}(e'_2)$ orbitals **(5)**. For case (a), as for the trigonal bipyramid, the LUMO's are the $\bar{D}^{\pi}_{\pm 1}(e'_1)$ orbitals.



$D^{\pi}_{\pm 2}\ (e'_2)$

(5)

Table 4.1 Calculated energies of the frontier orbitals of pentagonal bipyramidal $[B_7H_7]^{2-}$ and $[B_7Cl_7]$

$[B_7H_7]^{2-}$ a			
(a) All boron atoms equidistant (1.45Å) from the centre of the cluster			
Orbital	**Energy (eV)**	(b) All B-B distances = 1.70Å **b**	
$\bar{D}^{\pi}_{\pm 2}(e''_2)$	-4.44	$\bar{D}^{\pi}_{\pm 1}(e'_1)$	-1.43
$\bar{D}^{\pi}_{\pm 1}(e'_1)$	-4.99	$\bar{D}^{\pi}_{\pm 2}(e''_2)$	-4.44
$D^{\pi}_{\pm 2}(e'_2)$	-10.65	$P^{\sigma+\pi}_{0}(a''_2)$	-10.53
$D^{\pi}_{\pm 1}(e''_1)$	-10.77	$D^{\pi}_{\pm 2}(e'_2)$	-10.60
$P^{\sigma+\pi}_{0}(a''_2)$	-12.65	$D^{\pi}_{\pm 1}(e''_1)$	-10.71

$[B_7Cl_7]$ c (B_7 framework as for (b))	
$\bar{D}^{\pi}_{\pm 1}(e'_1)$	+0.46
$\bar{D}^{\pi}_{\pm 2}(e''_2)$	-3.07
$D^{\pi}_{\pm 1}(e''_1)$	-9.40
$D^{\pi}_{\pm 2}(e'_2)$	-9.50
$P^{\sigma+\pi}_{0}(a''_2)$	-9.85

a Orbital parameters as for **Chapter 2.** Bond lengths: B_{eq}-B_{eq} = 1.70Å; B_{ax}-B_{eq} = 2.05Å; B_{ax}-B_{ax} = 2.90Å and B-H = 1.20Å.

b B_{ax}-B_{ax} = 1.79Å.

c Orbital parameters for Cl: $\zeta(3s) = \zeta(3p) = 2.033$; $H_{ii}(3s) = -26.30$ eV; $H_{ii}(3p) = -14.20$ eV. B-Cl = 1.70Å.

Thus, in case (a), with a large inter-polar distance (2.89Å), the pentagonal bipyramid, like the trigonal bipyramid, is characterised by parity related D^{π} and $\bar{D}^{\pi}$ E pairs in the frontier orbital region. As may be seen from **Table 4.1**, however, the $D^{\pi}_{\pm 1}$-$D^{\pi}_{\pm 2}$ and $\bar{D}^{\pi}_{\pm 1}$-$\bar{D}^{\pi}_{\pm 2}$ energy separations are calculated to be quite small, so that their precise ordering will be sensitive to small changes in internuclear distances, the effects of electron-electron repulsions and other perturbations. Such minor differences apart, both of these bipyramidal clusters have E pairs as their HOMO's and LUMO's. These arguments are also applicable to hexagonal bipyramidal clusters, where g and u symmetry labels distinguish the D^{π} and $\bar{D}^{\pi}$ orbitals. Such bipyramidal clusters are, therefore, capable of supporting (in order to remain diamagnetic), (n-1), (n+1) and (n+3) skeletal electron pairs. Examples of bipyramidal clusters with these alternative SEP counts are listed in **Table 4.2.**

Returning specifically to the pentagonal bipyramid, in case (b), the above generalisation no longer applies. In this case the polar atoms are very close (their separation is as little as 1.79Å if all of the other B-B contacts are constrained to be 1.70Å). This leads to strong inter-polar orbital interactions. One consequence of these interactions, which may be seen from **Table 4.1**, is that the antibonding $\bar{D}^{\pi}_{\pm 1}$ orbitals move to much higher energy, due to the strong π-antibonding interaction between the polar atoms and also the strong antibonding interaction between the polar and ring atoms, so that the LUMO's are now the ring-localised $\bar{D}^{\pi}_{\pm 2}(e''_2)$ orbitals.

A further consequence of the short inter-polar distance, which is potentially more important in terms of changing the spectrum of frontier MO's, is that the $P^{\sigma+\pi}_{0}(a''_2)$ orbital, depicted in **Figure 4.8**, is significantly destabilised because of the strong σ-antibonding

Table 4.2 Examples of bipyramidal clusters

Cluster	Skeletal Electron Pairs	Reference
(a) Trigonal Bipyramidal		
$[C_2B_3H_5]$	6 (n+1)	**a**
$[Os_5(CO)_{16}]$	6	**b**
$[Sn_5]^{2-}$	6	**c**
$[Ni_5(CO)_{12}]^{2-}$	8 (n+3)	**d**
$[Rh_5(CO)_{14}I]^{2-}$	8	**e**
(b) Pentagonal Bipyramidal		
$[B_7H_7]^{2-}$	8 (n+1)	**f**
$[(CO)_3FeC_2B_4H_6]$	8	**g**
$[CpCo(\mu\text{-}C_2B_3MeH_4)CoCp]$	8	**h**
$[CpNi(\mu\text{-}C_5H_5)NiCp]$	10 (n+3)	**i**

a R.E. Williams, Adv. Inorg. Chem. Radiochem., 1976, **18**, 67. **b** C.R. Eady, B.F.G. Johnson, J. Lewis, B.E. Reichert and G.M. Sheldrick, J. Chem. Soc., Chem. Commun., 1976, 271. **c** P.A. Edwards and J.D. Corbett, Inorg. Chem., 1977, **16**, 903. **d** G. Longoni, P. Chini, L.D. Lower and L.F. Dahl, J. Amer. Chem. Soc., 1975, **97**, 5034. **e** S. Martinengo, G. Ciani and A. Sironi, J. Chem. Soc., Chem. Commun., 1979, 1059. **f** W.N. Lipscomb, "Boron Hydrides", Benjamin, New York, 1963. **g** R.N. Grimes, J. Amer. Chem. Soc., 1971, **93**, 261. **h** D.C. Beer, V.R. Miller, L.G. Sneddon, R.N. Grimes, M. Mathew and G.J. Palenik, J. Amer. Chem. Soc., 1973, **95**, 3046. **i** A. Salzer and H. Werner, Angew. Chem. Int. Edn. Engl., 1978, **17**, 869.

interaction between the polar atoms. In fact, as **Table 4.1** indicates, for this compressed geometry, $P_0^{\sigma+\pi}$ is predicted to be the HOMO. The presence of a non-degenerate HOMO gives rise to the possibility of a pentagonal bipyramidal cluster with n SEP's. The alternative frontier orbital patterns which may arise, depending upon the relative radial disposition of the polar and equatorial atoms, for a pentagonal bipyramid are summarised in **Figure 4.8.**

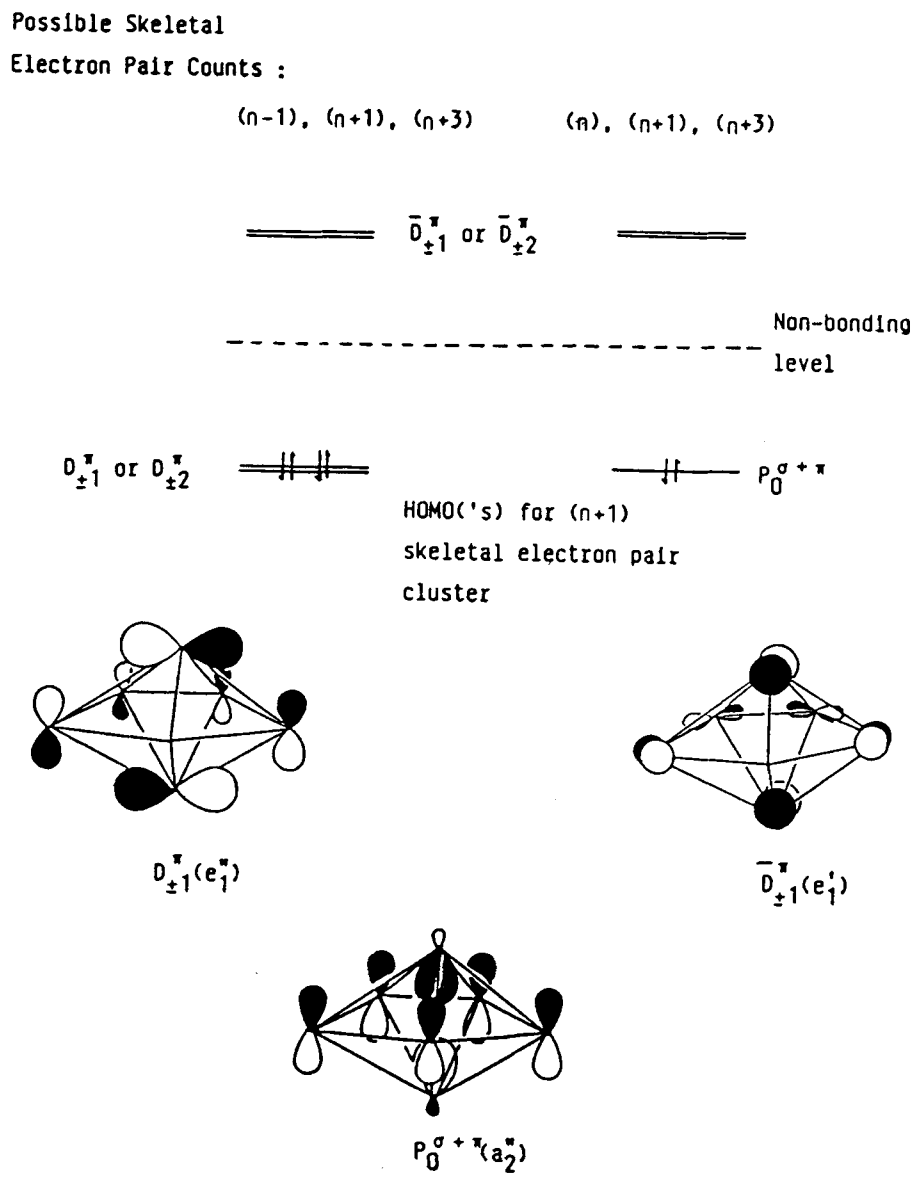


Figure 4.8 Alternative frontier orbital patterns for pentagonal bipyramidal (D_{5h}) clusters.

Fowler, on the basis of Extended Hückel and Extended TSH calculations,[5] has suggested that this second situation (i.e. that $P_0^{\sigma+\pi}$ is unoccupied) may apply in the case of the diamagnetic species

$[B_7Br_7]$.[16] The results of my own Extended Hückel calculations on the related $[B_7Cl_7]$ moiety (in the compressed (b) geometry) seem to oppose this idea, however. As may be seen from **Table 4.1**, the π-symmetry donor orbitals on chlorine raise the energies of the frontier orbitals of the pentagonal bipyramid. The extent to which the bonding orbitals are destabilised is in the order $D^{\pi}_{\pm 1} > D^{\pi}_{\pm 2} > P^{\sigma+\pi}_{0}$, so that (even in the compressed case (b)) the two D^{π} E pairs are predicted to lie above $P^{\sigma+\pi}_{0}$ (a''_2). In **Section 4.5.1** it was suggested that the $[B_7Br_7]$ molecule may, in fact, adopt a C_3-polar deltahedral geometry, which would also explain its n SEP count.

4.6.3 Sub-class 3(ii): D_{nd}-bicapped antiprisms

The frontier orbitals of the square antiprism are shown on the left-hand side of **Figure 4.9.**

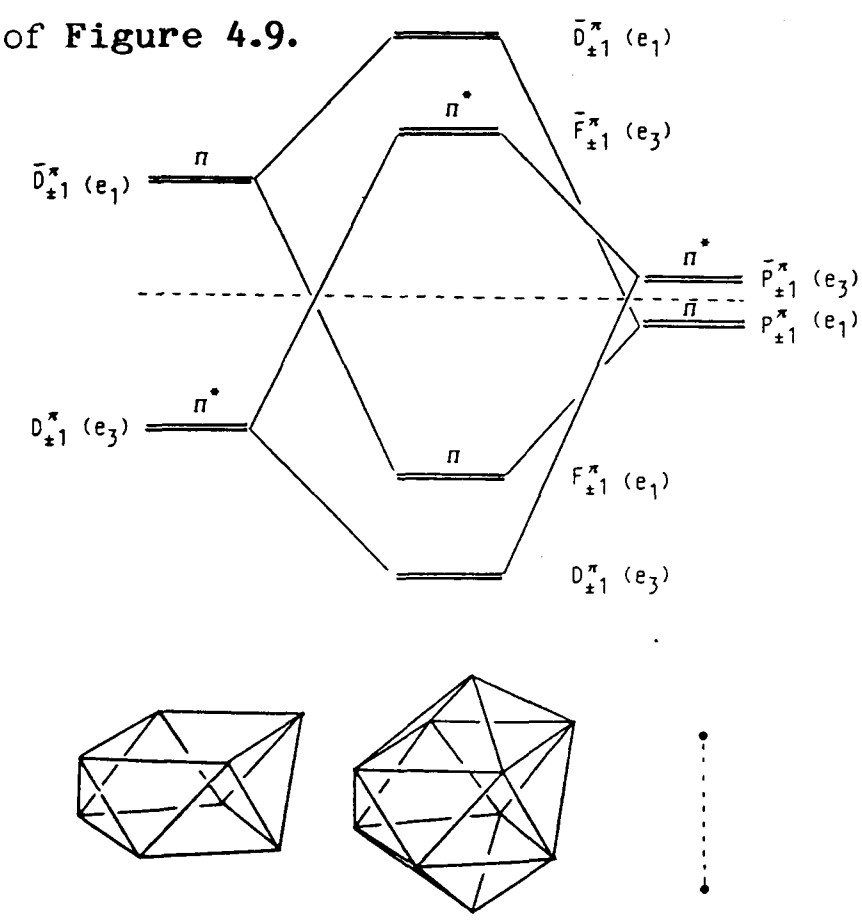


Figure 4.9 Illustration of the interaction between the L^{π} and $\bar{L}^{\pi}$ orbitals of the polar and non-polar atoms of a bicapped square antiprismatic (D_{4d}) cluster.

These orbitals are $D^{\pi}_{\pm 1}/\bar{D}^{\pi}_{\pm 1}$, rather than $P^{\pi}_{\pm 1}/\bar{P}^{\pi}_{\pm 1}$, due to the extra layer of atoms (though, with respect to each of the open faces these functions are singly noded, like $P^{\pi}_{\pm 1}/\bar{P}^{\pi}_{\pm 1}$ in the ring case). Because of the extra node (perpendicular to the principal rotation axis), the $D^{\pi}_{\pm 1}$ pair have Π^{*}, rather than Π character with respect to the polar atoms. **Figure 4.10** shows schematically how the nodal properties (with respect to the polar atoms) of $L^{\pi}_{\pm 1}$ vary with L. In general, $L^{\pi}_{\pm 1}$ orbitals possess Π symmetry with respect to the polar atoms for L = 2n+1 and Π^{*} for L = 2n. The parity inversion operation reverses the bonding characteristics of the cluster tangential orbitals. Thus, if the $L^{\pi}_{\pm 1}$ orbitals possess Π character with respect to the polar atoms, the $\bar{L}^{\pi}_{\pm 1}$ orbitals possess Π^{*} character.

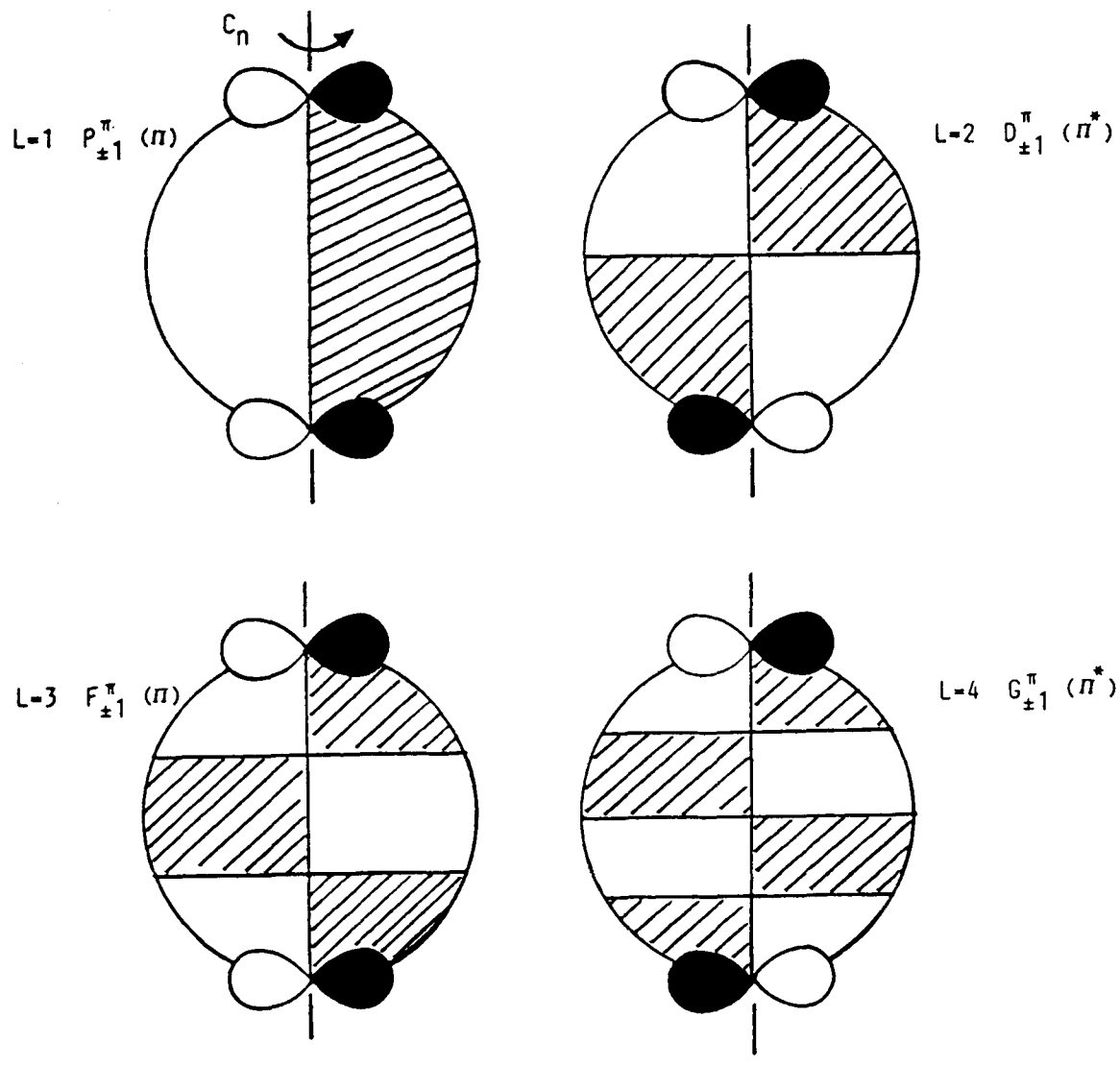
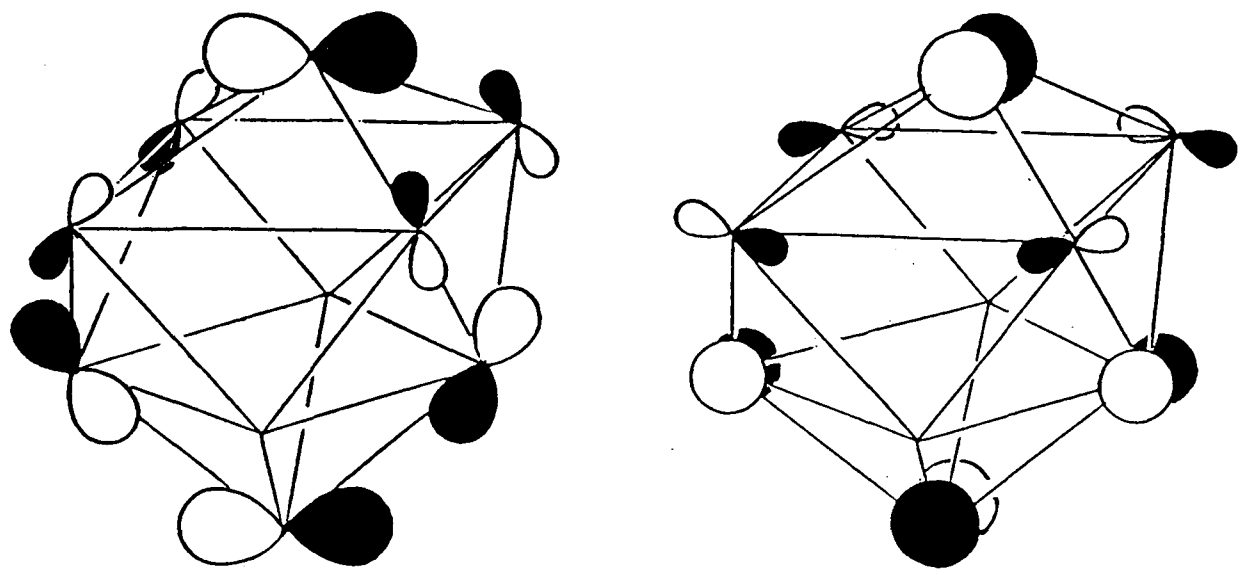


Figure 4.10 Variation of the nodal characteristics (with respect to the polar atoms of a bipolar cluster) of the $L^{\pi}_{\pm 1}$ orbitals, as a function of L.

Interaction of the $P^{\pi}_{\pm 1}$ (Π) and $\bar{P}^{\pi}_{\pm 1}$ (Π^*) orbitals of the polar atoms with the $D^{\pi}_{\pm 1}/\bar{D}^{\pi}_{\pm 1}$ orbitals of the antiprism (as depicted in **Figure 4.9**) generates a bonding pair $\bar{F}^{\pi}_{\pm 1}$ (Π) and an antibonding pair $\bar{F}^{\pi}_{\pm 1}$ (Π^*) of orbitals, which are predominantly localised on the polar atoms **(6)**.



$F^{\pi}_{\pm 1}$ (e_1) (one component) $\bar{F}^{\pi}_{\pm 1}$ (e_3)

(6)

Thus, the HOMO's and LUMO's , as for the trigonal bipyramid discussed above are degenerate E pairs. This gives rise to the possibility of characterising bicapped square antiprismatic clusters with (n-1), (n+1) or (n+3) SEP's. However, on comparing the orbital interaction diagrams for trigonal bipyramids and bicapped antiprisms (**Figures 4.7** and **4.9**) more closely it may be seen that the HOMO-LUMO separation is greater in the latter case. This arises because the Π^* orbitals of the polar atoms interact with strongly bonding orbitals ($D^{\pi}_{\pm 1}$) rather than antibonding ones ($\bar{P}^{\pi}_{\pm 1}$). The result of this is to make the occurrence of bicapped antiprismatic clusters with (n+3) skeletal electron pairs unfavourable on energy grounds and, to date, no such clusters are known. Clusters with (n-1) SEP's would have the $\bar{F}^{\pi}_{\pm 1}$ orbitals unpopulated, which is also

unfavourable because these orbitals have considerable bonding character.

4.6.4 Extension to larger bipolar deltahedra

If another layer of atoms is added to the bicapped antiprisms, bicapped fused-antiprisms are generated. These deltahedra, like the bipyramids, possess D_{nh} symmetry, with a ring of atoms lying on the σ_h mirror plane. By analogy with the cases discussed above, the frontier orbitals of such clusters are expected to be $G^{\pi}_{\pm 1}$ and $\bar{G}^{\pi}_{\pm 1}$, where (as for the bipyramidal clusters) the HOMO's ($G^{\pi}_{\pm 1}$) have Π^* character with respect to the polar atoms and the LUMO's ($\bar{G}^{\pi}_{\pm 1}$) have Π character (see **Figure 4.10**). The addition of further layers of atoms leads to alternating D_{nd} and D_{nh} structures, possessing frontier orbitals ($L^{\pi}_{\pm 1}$) with higher L values. These deltahedra are grossly non-spherical, however, so they will not be considered further.

4.7 Class 4: Non-Polar Deltahedra

Non-polar deltahedra are also non-spherical, with the cluster atoms generally lying on the surfaces of two spheres with different radii. These polyhedra do not possess any atoms on the principal rotation axis, but instead have a ring (planar or puckered) of atoms around the equator of the cluster. Non-polar clusters with a planar arrangement of atoms on the equator generally possess D_{nh} symmetry. It is not, however, feasible to have non-polar deltahedral clusters with D_{nh} symmetry and $n>3$ since this would lead to (open) non-triangular faces. The same restrictions apply to those non-polar clusters with puckered arrangements of atoms about the equator. Thus, non-polar polyhedra of D_{nd} symmetry are not

deltahedra if n>3.

It has been shown above that polyhedra which belong to axial point groups and which have no polar atoms have an even number of E representations in their $L^{\pi}/\bar{L}^{\pi}$ manifolds. Non-polar deltahedral clusters cannot, therefore, have a degenerate $L^{\pi}/\bar{L}^{\pi}$ frontier orbital pair, so there is no symmetry-induced breaking of the (n+1) rule. As for bipolar clusters, however, interactions between the L^{π} and $\bar{L}^{\pi}$ orbitals of the topologically distinct sub-sets (equatorial and non-equatorial) of cluster atoms may be utilised to predict what mode of departure from the rule is likely to occur.

4.7.1 Sub-class 4(i): D_{nh}-planar-equatorial deltahedra

The simplest example of this sub-class of deltahedral clusters is the tricapped trigonal prism. The three capping atoms lie on the equatorial plane and are related by a C_3 axis. The cluster has a horizontal mirror plane passing through the equator and, therefore, has D_{3h} symmetry

4.7.1.1 Analysis of the frontier orbital region of tricapped trigonal prismatic clusters

On the right-hand side of **Figure 4.11**, the P^{π} and $\bar{P}^{\pi}$ orbitals of a three membered ring (i.e. the equatorial subset of the tricapped trigonal prism) are illustrated. These orbitals interact with the L^{π} and $\bar{L}^{\pi}$ orbitals of the trigonal prism. As **Figure 4.11** shows, the e' and e" components ($P^{\pi}_{\pm 1}/\bar{P}^{\pi}_{\pm 1}$) interact with the non-bonding $\bar{D}^{\pi}_{\pm 1}(e')$ and $D^{\pi}_{\pm 1}(e")$ orbitals of the trigonal prism to generate strongly bonding and antibonding combinations. In contrast, the $a"_2$ and a'_2 components ($P^{\pi}_0/\bar{P}^{\pi}_0$)

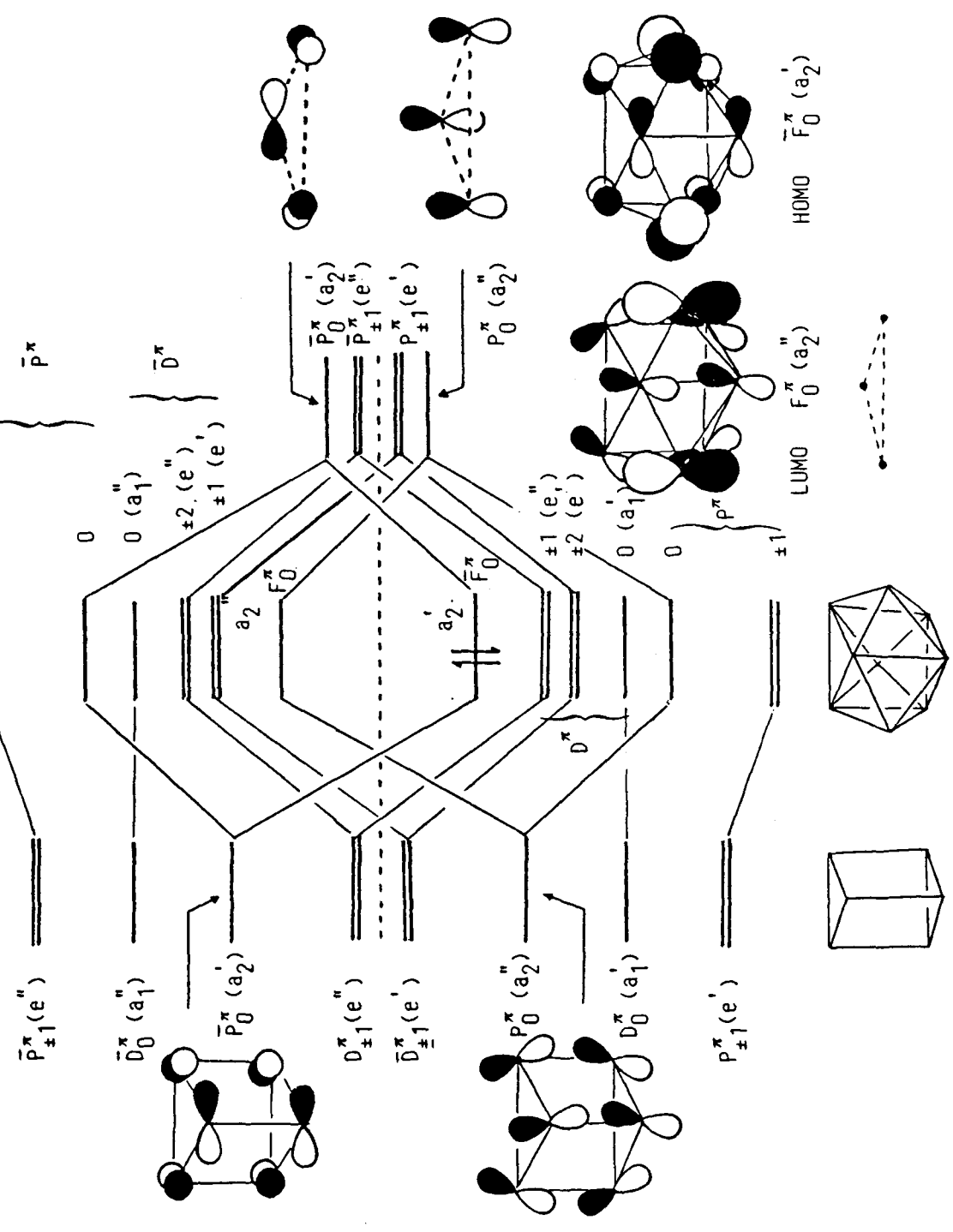
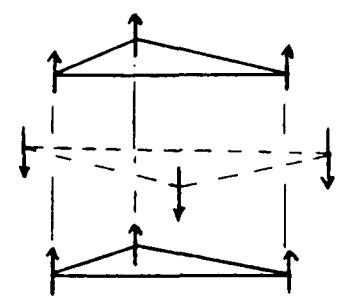


Figure 4.11 Interaction of the L^{π} and $\bar{L}^{\pi}$ orbitals of the two subsets of atoms forming a tricapped trigonal prismatic (D_{3h}) cluster.

interact with the more strongly bonding (P_0^{π}) and antibonding ($\bar{P}_0^{\pi}$) orbitals of the trigonal prism (see **Figure 4.11**) to generate one weakly antibonding orbital (F_0^{π}, a_2'') and one weakly bonding orbital ($\bar{F}_0^{\pi}$, a_2'). Consequently, the frontier orbitals of the non-polar deltahedron consist of a parity related pair of (non-degenerate) orbitals, derived from P_0^{π} and $\bar{P}_0^{\pi}$, which are predominantly localised on the equatorial atoms. As mentioned in **Chapter 2**, Stone's rule for deltahedral clusters (i.e. that the L^{π} orbitals are bonding and the $\bar{L}^{\pi}$ orbitals are antibonding) breaks down in this case because the HOMO has odd parity ($\bar{F}_0^{\pi}$) and the LUMO has even parity (F_0^{π}). Since the frontier orbitals are non-degenerate, this cluster geometry is capable of accomodating n, (n+1) or (n+2) skeletal electron pairs. Examples of clusters with 9 vertex atoms and these alternative electron counts are listed in **Table 4.3.**

4.7.1.2 Consequences of the frontier orbital pattern of tricapped trigonal prismatic clusters

Corbett has made a detailed theoretical and structural study of tricapped trigonal prismatic bare metal clusters.[20] He identified the LUMO for the hypothetical molecule $[Sn_9]^{2-}$ (with 10 = (n+1) SEP's) as possessing a_2'' symmetry. This orbital, which is the HOMO in $[Bi_9]^{5+}$, was shown to have the following topology:[21]



(where the arrows represent p^{π} orbitals). This orbital was said to be

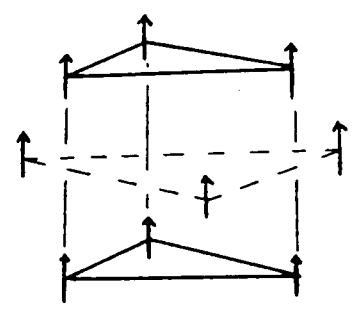
Table 4.3 Examples of tricapped trigonal prismatic clusters

Cluster	No. of SEP's	Reference
$[B_9Cl_9]$	9 (n)	**a**
$[B_9H_9]^{2-}$	10 (n+1)	**b**
$[Ge_9]^{2-}$	10	**c**
$[TlSn_8]^{3-}$	10	**d**
$[CpCoC_2B_6H_8]$	10	**e**
$[(PMe_3)_2PtC_2B_6H_8]$	10	**f**
$[Bi_9]^{5+}$	11 (n+2)	**g**

a M.B. Hursthouse, J. Kane and A.G. Massey, Nature, 1970, **228**, 659. **b** L.J. Guggenberger, Inorg. Chem., 1968, **7**, 2260. **c** C.H.E. Belin, J.D. Corbett and A. Cisar, J. Amer. Chem. Soc., 1977, **99**, 7163. **d** R.C. Burns and J.D. Corbett, J. Amer. Chem. Soc., 1982, **104**, 2804. **e** D.F. Dustin, W.J. Evans, C.J. Jones, R.J. Wiersma, H. Gong, S. Chan and M.F. Hawthorne, J. Amer. Chem. Soc., 1974, **96**, 3085; W.J. Evans, G.B. Dunks and M.F. Hawthorne, J. Amer. Chem. Soc., 1973, **95**, 4565. **f** M. Green, J.L. Spencer, F.G.A. Stone and A.J. Welch, J. Chem. Soc., Chem. Commun., 1974, 794; A.J. Welch, J. Chem. Soc., Dalton Trans., 1976, 225. **g** R.M. Friedman and J.D. Corbett, Inorg. Chem., 1973, **12**, 1134.

π-bonding within the two triangular faces of the trigonal prism and strongly σ-antibonding between them. He also stated that the orbital is weakly bonding between the capping (equatorial) atoms and those of the trigonal prism. This orbital is clearly identical to the F_0^{π} orbital (depicted in **Figure 4.11**) which was identified above as the LUMO in $[B_9H_9]^{2-}$. Corbett demonstrated that the ratio of the vertical height to the edges of the triangular faces of the trigonal prism , in a series of tricapped trigonal prismatic clusters increases on population of the a_2'' orbital. This is in agreement with his assignment of the bonding characteristics of this orbital.[20]

Wade, on the basis of earlier MO calculations on $[B_9H_9]^{2-}$ [22] and $[M_9]^{2-}$,[23] arrived at similar conclusions to those of Corbett.[24] He extended the analysis to include a discussion of the effect of populating the a_2'' orbital on the bond lengths between the trigonal prism and the capping atoms.[24] In this way, Wade showed that these bond lengths are larger when the a_2'' orbital is occupied, an observation which appears to conflict with Corbett's assignment of this orbital. On this basis, Wade proposed that the a_2'' orbital (at least in $[B_9H_9]^{2-}$) actually has all of the p^{π} vectors pointing in the same direction:



If this assignment were correct, then the LUMO in $[B_9H_9]^{2-}$ would be P_0^{π} rather than F_0^{π}, in contradiction to the above analysis. Our own Extended Hückel calculations have indicated that the HOMO and LUMO in

this cluster are indeed $\bar{F}_0^{\pi}$ and F_0^{π} respectively, and that the HOMO has the same topology as that described, for $[Sn_9]^{2-}$, by Corbett. In order to evaluate the bonding characteristics of the frontier orbitals, B-B overlap populations for the clusters $[B_9H_9]^{q-}$ (q = 0, 2, 4), corresponding to the frontier orbital configurations $(\bar{F}_0^{\pi})^0(F_0^{\pi})^0$, $(\bar{F}_0^{\pi})^2(F_0^{\pi})^0$ and $(\bar{F}_0^{\pi})^2(F_0^{\pi})^2$, were calculated. These overlap populations are listed in **Table 4.4**, which includes the contributions made by the individual frontier orbitals.

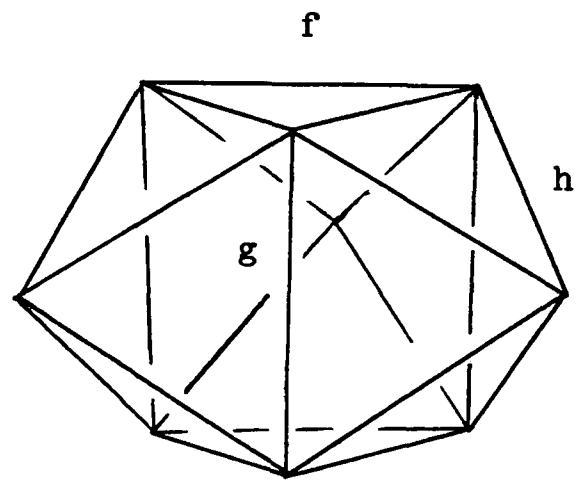
From **Table 4.4** it can be seen that the HOMO ($\bar{F}_0^{\pi}$), depicted in **Figure 4.11**, is antibonding within the triangular faces of the trigonal prism (edge type **f**), but is bonding along the vertical edges of the prism (edge type **g**) and between the prism and capping atoms (edge type **h**). This is in agreement with Wade's conclusions.[24] The LUMO (F_0^{π}), on the other hand, is bonding with respect to the **f**-type edges and antibonding with respect to the **g**- and **h**-type edges. Thus, contrary to Corbett's original analysis for $[Sn_9]^{2-}$,[20] and in agreement with Wade's structural considerations,[24] there should be a lengthening of the prism-cap (**h**) bond length upon occupation of the a_2'' orbital. The reason why this orbital should have prism-cap antibonding character may be appreciated from inspection of **Figure 4.11**. Because of the relative positioning of the prism and capping atoms, the interaction between their p^{π} orbitals is predominantly π, rather than σ, in character. This π-interaction can be seen to be antibonding, in agreement with the frontier orbital analysis described in **Section 4.7.1.1.**

For 9-vertex 11 (n+2) SEP clusters, the usual skeletal geometry is the (nido) monocapped square antiprism. It has been shown, however, that the tricapped trigonal prism can also accomodate 11 SEP's and that the a_2'' orbital which is occupied in such species is only weakly antibonding

Table 4.4 Boron-boron overlap populations for tricapped trigonal prismatic $[B_9H_9]^{q-}$ (q = 0, 2 or 4) and the contributions made by $F_0^{\pi}(a_2'')$ and $\bar{F}_0^{\pi}(a_2')$

	B-B overlap popln.		
Polyhedral edge type:[a]	**f**	**g**	**h**
$[B_9H_9]$	+0.48	+0.36	+0.52
$[B_9H_9]^{2-}$	+0.42	+0.41	+0.57
$[B_9H_9]^{4-}$	+0.48	+0.33	+0.52
Contributions made by individual orbitals			
	f	**g**	**h**
$F_0^{\pi}(a_2')$[b]	-0.06	+0.05	+0.05
$\bar{F}_0^{\pi}(a_2'')$[c]	+0.06	-0.08	-0.05

a Edge types **f**, **g** and **h** (these labels are the ones used in Ref. 24) are illustrated below:



b HOMO for $[B_9H_9]^{2-}$

c LUMO for $[B_9H_9]^{2-}$

(Corbett has calculated a HOMO-LUMO separation of 1.6 eV for D_{3h} $[Sn_9]^{2-}$).[20] The tricapped trigonal prism (D_{3h}) is, therefore, a fairly low energy structural alternative to the monocapped square antiprism (C_{4v}) for 11 SEP's. Iterative Extended Hückel calculations, performed by Corbett, have shown that, for $[Sn_9]^{4-}$ the C_{4v} geometry is favoured over the D_{3h} alternative by 1 eV, whereas, for the paramagnetic species $[Sn_9]^{3-}$ (21 skeletal electrons), the (observed) D_{3h} structure is favoured over C_{4v} by roughly 1.5 eV.[21] For $[Bi_9]^{5+}$, however, the two structural alternatives are essentially isoenergetic. The small calculated difference in energy between the C_{4v} and D_{3h} geometries for $[Bi_9]^{5+}$ is supported by the structural characterisation of a purely D_{3h} ion (in $[Bi_{10}](HfCl_6)_3$)[25] and one which is distorted, by roughly 25%, towards the C_{4v} geometry (in $Bi_{12}Cl_{14}$).[26] Surprisingly, since the D_{3h} geometry is calculated to be considerably more stable than the C_{4v} alternative for 10 (n+1) SEP's,[21] $[Ge_9]^{2-}$ is also observed to be distorted, by 25-30%, along the pathway from D_{3h} to C_{4v}.[27]

It has been observed that the $[Sn_9]^{4-}$ ion, which adopts the C_{4v} geometry in the solid state,[28] is fluctional in solution, such that a single ^{119}Sn NMR signal is observed (even at -40 ^{o}C).[29] Corbett has postulated a $C_{4v} \rightleftharpoons D_{3h}$ interconversion pathway (see **Figure 4.12**) to explain this behaviour.[21] The previous analysis would seem to indicate that the D_{3h} intermediate lies at fairly low energy, which would explain the fact that the $[Sn_9]^{4-}$ anion is fluctional at low temperature. Corbett has also shown that the angles and distances in the two alternative geometries are not very different, so that the interconversion mechanism involves very small movements of the skeletal atoms.[21] The same $C_{4v} \rightleftharpoons D_{3h}$ pathway had previously been suggested by

Guggenberger and Muetterties to account for the observed fluctionality of nido-$[B_9H_9]^{4-}$.[30] This mechanism may also be invoked to explain the fact that $[Rh_9P(CO)_{21}]^{2-}$ (nido , C_{4v})[31] displays only one ^{103}Rh NMR signal at 300 K.[32]

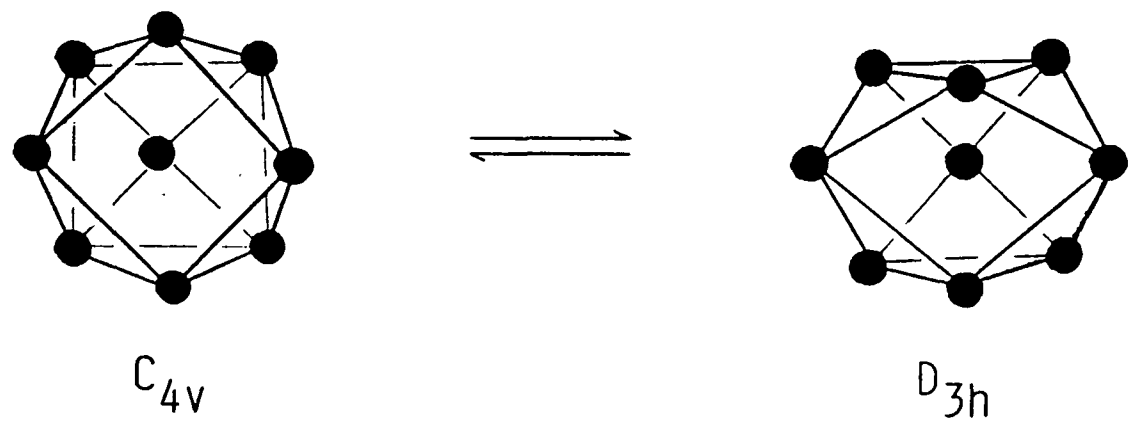


Figure 4.12 The $C_{4v} \rightleftharpoons D_{3h}$ mechanism of cage fluctionality for capped square antiprismatic clusters.

4.7.2 Sub-class 4(ii): D_{nd}-puckered-equatorial deltahedra

The deltahedral dodecahedron (n=8) has a puckered arrangement of four atoms around the equator. The polyhedron has D_{2d} symmetry and the equatorial atoms are related by an S_4 axis (in general an S_{2n} axis would relate the 2n equatorial atoms of a D_{nd} cluster). Larger clusters of D_{2d} or D_{3d} symmetry also belong to this sub-class.

As for the tricapped trigonal prism, the frontier orbitals of the dodecahedron arise from the interaction of the P_0^{π} and $\bar{P}_0^{\pi}$ orbitals (see **Figure 4.13**) of the two subsets of atoms. The two subsets, in this case, may both be considered as distorted tetrahedra, such that the four equatorial vertices define a C_2-flattened tetrahedron and the four non-equatorial vertices define a C_2-elongated tetrahedron.[33] In contrast to

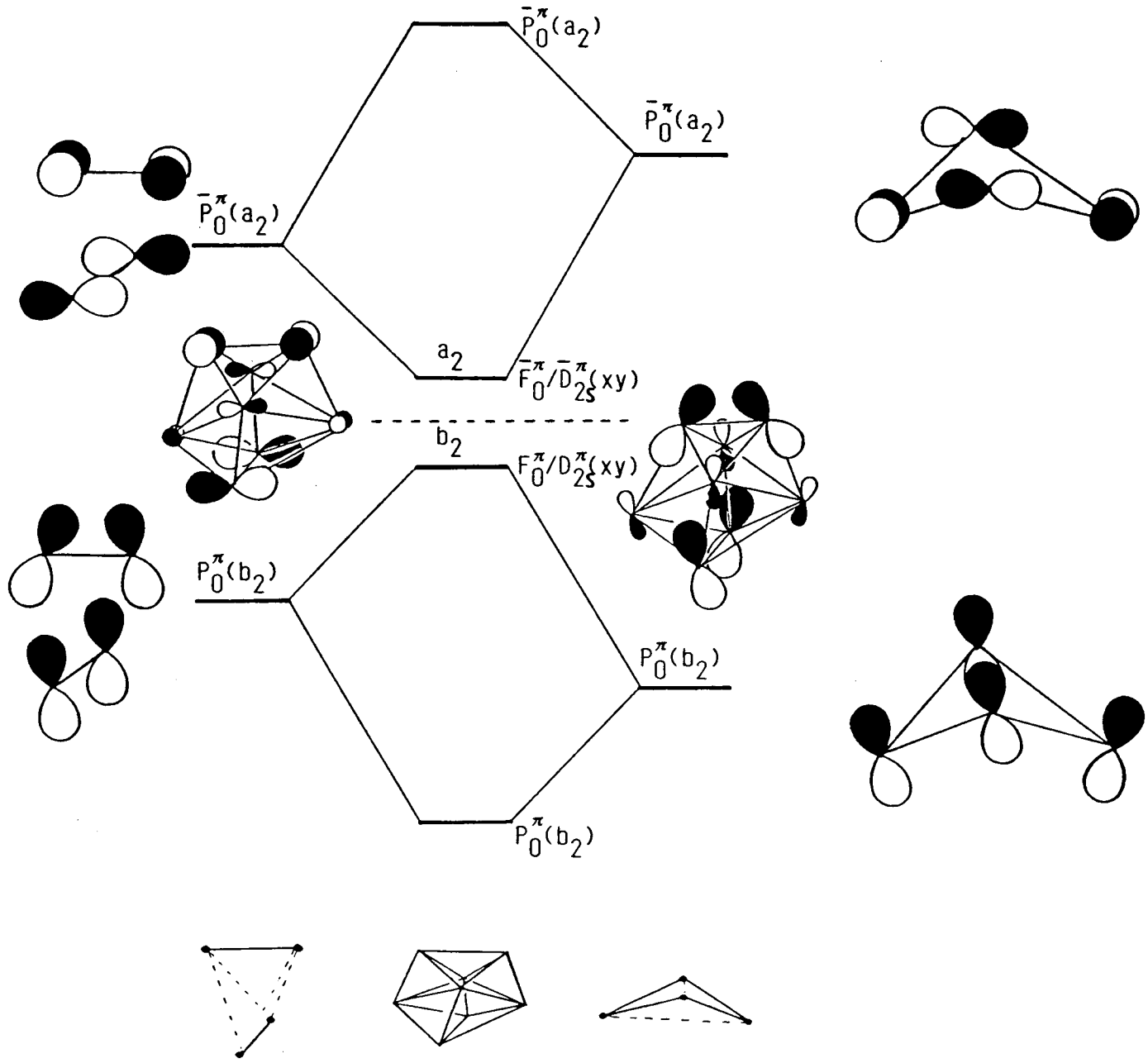
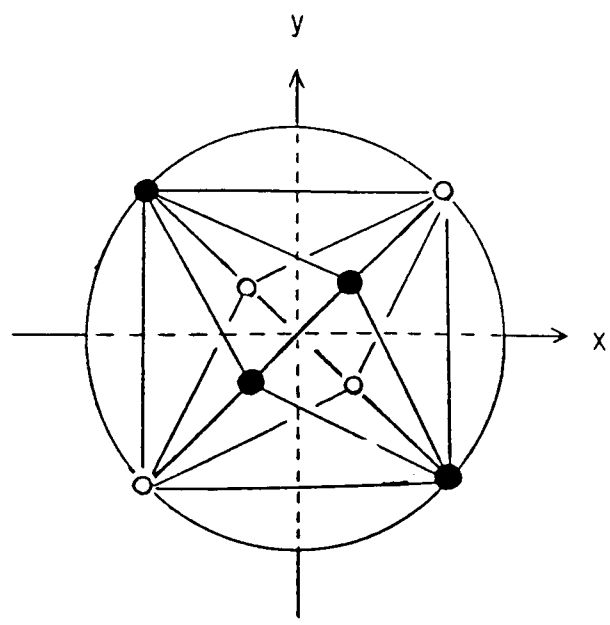


Figure 4.13 Interaction of the L^{π} and $\bar{L}^{\pi}$ orbitals of the two subsets of atoms forming a triangular dodecahedral (D_{2d}) cluster.

the tricapped trigonal prism, however, the equatorial atoms are within bonding distance of each other. This has the effect of making their P_0^{π} combination quite strongly bonding and their $\bar{P}_0^{\pi}$ combination quite strongly antibonding. In this case, the connectivities of the non-equatorial atoms are lower than the equatorial ones so the spread of L^{π} and $\bar{L}^{\pi}$ orbitals is narrower for these non-equatorial atoms. As **Figure 4.13** shows, this results in the (weakly bonding) HOMO and (weakly antibonding) LUMO being predominantly localised on the non-equatorial vertices, in contrast to the tricapped trigonal prism. **Figure 4.13** also shows that the HOMO (with b_2 symmetry) may be identified as F_0^{π} and the (parity related) LUMO (with a_2 symmetry) may be described as $\bar{F}_0^{\pi}$, so that, for the dodecahedron, there is no switching round of bonding character of the frontier L^{π} and $\bar{L}^{\pi}$ orbitals. Moreover, the HOMO and LUMO may be alternatively described as $D_{2s}^{\pi}(xy)$ and $\bar{D}_{2s}^{\pi}(xy)$ respectively (the axis system is depicted in (7)) since these functions are identical to $F_0^{\pi}/\bar{F}_0^{\pi}$ for the D_{2d} dodecahedron.



Dodecahedron viewed down the z axis

● above xy plane

○ below xy plane

(7)

Table 4.5 Examples of (triangulated) dodecahedral clusters

Cluster	No. of SEP's	Reference
$[B_8Cl_8]$	8 (n)	**a**
$[Cp_4Co_4B_4H_4]$	8	**b**
$[B_8H_8]^{2-}$	9 (n+1)	**c**
$[CpCoSn(CMe)_2B_4H_4]$	9	**d**
$[Cp_4Ni_4B_4H_4]$	10 (n+2)	**e**

a R.A. Jacobson and W.N. Lipscomb, J. Chem. Phys., 1959, **31**, 605. **b** J.R. Pipal and R.N. Grimes, Inorg. Chem., 1979, **18**, 257. c L.J. Guggenberger, Inorg. Chem., 1969, **8**, 2771; F. Klanberg, D.R. Eaton, L.J. Guggenberger and E.L. Muetterties, Inorg. Chem., 1967, **6**, 1271. **d** K.S. Wong and R.N. Grimes, Inorg. Chem., 1977, **16**, 2053. **e** J.R. Bowser, A. Bonny, J.R. Pipal and R.N. Grimes, J. Amer. Chem. Soc., 1979, **101**, 6229.

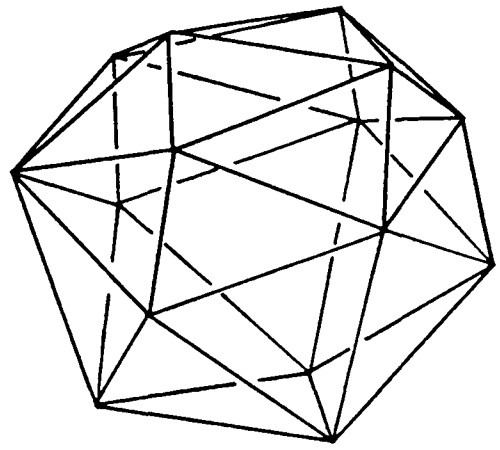
The advantage of the $F_0^{\pi}/\bar{F}_0^{\pi}$ notation is that it emphasises the similarity to the tricapped trigonal prism and also explains why the frontier orbitals are weakly bonding or antibonding whereas the remainder of the D^{π} and $\bar{D}^{\pi}$ functions are strongly bonding and antibonding respectively.[33]

Due to the weakly bonding and antibonding nature of the non-degenerate HOMO and LUMO, the triangular dodecahedron (like the tricapped trigonal prism) can accomodate n, (n+1) or (n+2) skeletal electron pairs.[4,33,34] Examples of clusters with such electron pair counts are given in **Table 4.5.**

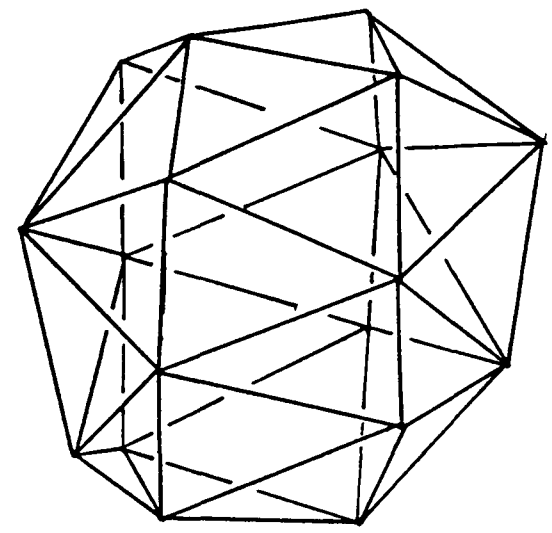
For both the dodecahedron and the tricapped trigonal prism, the stabilisation of n SEP clusters by terminal halide ligands (e.g. $[B_8Cl_8]$ and $[B_9Cl_9]$) is due to the non-degenerate HOMO being raised in energy as a result of the interaction with the low lying halide p^{π} orbitals.[35]

4.7.3 Extension to larger non-polar deltahedra

Larger non-polar (planar-equatorial and puckered-equatorial) deltahedral clusters of this type, i.e. possessing a greater number of layers of atoms, can be postulated. Providing that these clusters are not tremendously non-spherical, the conclusions derived above may equally well be applied to them. What will vary, however, is the L value of the frontier $L^{\pi}/\bar{L}^{\pi}$ orbitals (in this case L_0^{π} and $\bar{L}_0^{\pi}$), as for the multilayer bipolar clusters. Two hypothetical large non-polar deltahedra are the 15-vertex (D_{3h}, planar-equatorial) and 18-vertex (D_{3d}, puckered-equatorial) polyhedra **(8)**, which Lipscomb predicted to be the favoured geometries for $[B_{15}H_{15}]^{2-}$ and $[B_{18}H_{18}]^{2-}$ respectively.[9]



15-vertex, D_{3h}-planar-equatorial deltahedron



18-vertex, D_{3d}-puckered-equatorial deltahedron

($\underline{8}$)

4.8 Summary

The detailed analysis presented above for the four classes of deltahedral cluster can be summarised effectively in terms of the following generalisations derived from group theory and the Pairing Principle inherent in Stone's Tensor Surface Harmonic analysis.

(a) Centrosymmetric Spherical Clusters

The presence of a centre of symmetry in such clusters prevents the occurrence of any self-conjugate irreducible representations. In addition, the highly spherical nature of the clusters ensures that the orbitals are split into strongly bonding (L^{π}) and strongly antibonding ($\bar{L}^{\pi}$) components, so the (n+1) rule is rigorously obeyed.

(b) Polar Deltahedral Clusters

Polar deltahedral clusters with C_3, C_{3v}, T or T_d symmetry possess an odd number of E representations, leading to the occurrence of a non-bonding (self-conjugate) E pair $(L^{\pi}/\bar{L}^{\pi})_{\pm 1}$ of orbitals which are

predominantly localised on the polar atom. The (n+1) rule is broken because the degenerate frontier orbitals give rise to closed shell configurations for (n) and (n+2) skeletal electron pairs. Polar deltahedral clusters with lower symmetry have no such symmetry-based restriction on the number of SEP's and the electron count is dependent on the nature of the atoms occupying the various cluster sites.

(c) Bipolar and Non-Polar Clusters

These clusters consist of two subsets of atoms which lie on the surfaces of concentric spheres of different radii (bispherical deltahedra). This deviation from spherical topology leads to a spectrum of MO's which is intermediate between that anticipated from Stone's particle on a sphere solution and those of the individual subsets (which are themselves solutions to the particle on a sphere problem). If cluster bonding is analysed in terms of the interactions between the two subsets (which may be termed the **inner** and **outer spheres**) then the Parity Transformation (Parity Inversion Operation) is helpful in deciding the symmetries of the frontier orbitals.[2]

In the point groups $D_{(2n+1)d}$ and D_{nh} there are no self-conjugate representations,[4] since in the former case even and odd parity functions are distinguished by their differing behaviour (g or u) under inversion while in the latter case they are distinguished by their differing symmetries (' or ") with respect to the mirror plane (σ_h):

$$L^{\pi}\ (g,u) \xrightarrow{\Gamma^{0}_{u}\ (u)} \bar{L}^{\pi}\ (u,g)$$

$$L^{\pi}\ (',") \xrightarrow{\Gamma^{0}_{u}\ (")} \bar{L}^{\pi}\ (",')$$

Figure 4.14 illustrates the interaction between a pair of parity related sets of orbitals (A and B, with symmetries Γ_A and Γ_B) on the inner sphere and a similar pair of outer sphere orbitals. The spread of orbitals is narrower for the outer sphere than the inner sphere because the atoms are generally further apart on the outer sphere.

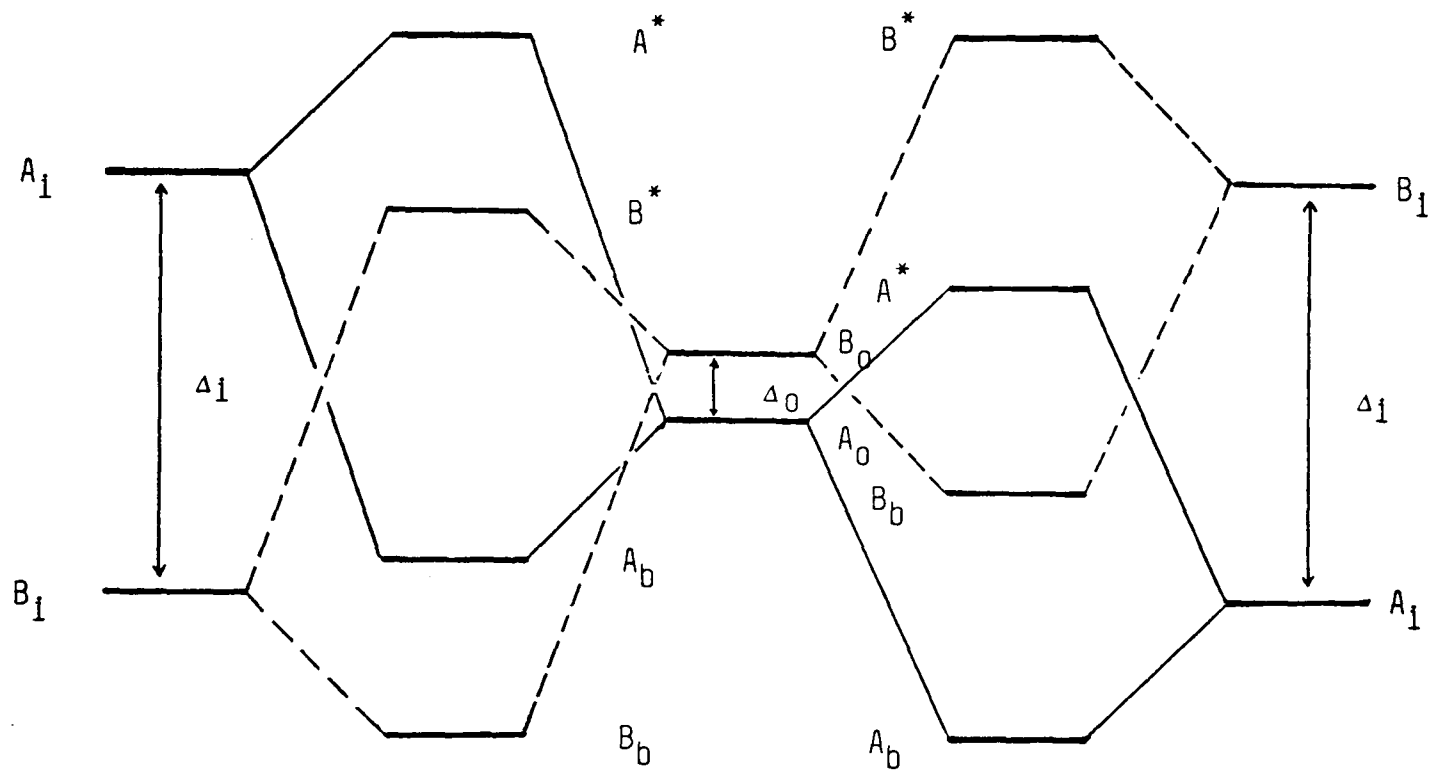


Figure 4.14 Illustration of the alternative ways in which the frontier orbitals of two subsets of atoms may interact to give the orbitals of a bispherical cluster.

The Parity Transformation requires that the MO's of the bispherical cluster are also symmetrically disposed about the non-bonding line.[2,10] The interaction between the orbitals A_i (inner) and A_o (outer) generates a bonding combination (A_b) and an antibonding combination (A^*). Similarly the B orbitals interact to form B_b and B^*. The Parity

Transformation interchanges A and B and also reverses the bonding character of the orbitals as shown below:

$$A_b \xleftrightarrow{\hat{P}} B^*$$

$$B_b \xleftrightarrow{\hat{P}} A^*$$

The orbitals A_b and B_b are no longer related by the Parity Transformation. Although the components from the inner and outer spheres in these MO's undergo parity inversion, the interactions between the two spheres is bonding for both A_b and B_b. Physically this corresponds to a rotation of 90^o (about a radial axis) of each p^{π} component on the inner sphere and an equal rotation, in the opposite sense, of the orbitals on the outer sphere. This operation, though having the same symmetry as the Parity Transformation is clearly distinct as it does not reverse the inner sphere-outer sphere bonding nature of the orbital. The same argument applies to the antibonding orbitals A^* and B^*.

Two alternative situations can be distinguished from **Figure 4.14** because the ordering of orbitals A and B on the inner sphere may either be the same as for the outer sphere or may be inverted. In **Figure 4.14a** the A orbital of the outer sphere and the B orbital of the inner sphere are bonding and a large HOMO-LUMO separation results for the bispherical cluster. In **Figure 4.14b,** however, the A orbitals of both the outer and the inner spheres are bonding and a small HOMO-LUMO separation results. The magnitude of the HOMO-LUMO gap is found to be inversely related to the magnitude of the A-B spacings (Δ_i and Δ_o) for the inner and outer spheres. The Figure also shows that the HOMO and LUMO are predominantly localised on the outer sphere for both situations.

In the class of bipolar deltahedral clusters the orbitals A and B are doubly degenerate E functions with the symmetries of the $P^{\pi}_{\pm 1}$ and $\bar{P}^{\pi}_{\pm 1}$ orbitals of the polar atoms. Bicapped antiprisms and trigonal bipyramids have been shown to belong to the cases illustrated in **Figures 4.14a** and **4.14b** respectively. This explains the larger HOMO-LUMO separation in bicapped square antiprismatic clusters and the fact that the (n+1) rule is adhered to for these clusters. On the other hand, the HOMO-LUMO spacing in trigonal bipyramidal clusters is quite small and clusters with (n+3) SEP's have been characterised. The pentagonal bipyramid differs from the trigonal bipyramid in that its polar atoms lie on the inner rather than the outer sphere. The exact nature of the frontier orbitals in these clusters is very dependent on the relative ratios of the two spheres and the exact nature of the cluster and ligand atoms. The LUMO's are always doubly degenerate ($\bar{D}^{\pi}_{\pm 1}$ or $\bar{D}^{\pi}_{\pm 2}$) whereas the HOMO('s) may be either non-degenerate ($P^{\sigma+\pi}_{0}$) or doubly degenerate ($D^{\pi}_{\pm 1}$ or $D^{\pi}_{\pm 2}$). Since the HOMO-LUMO gap is generally small, skeletal electron pair counts ranging from (n-1) to (n+3) (except (n+2)) are possible. Similar arguments apply to bipyramidal clusters with six or more atoms in the equatorial plane.

Non-polar clusters (e.g. the tricapped trigonal prism and the dodecahedron) belong to the situation illustrated in **Figure 4.14b.** In this case the orbitals A and B are singly degenerate, corresponding to the P^{π}_{0} and $\bar{P}^{\pi}_{0}$ orbitals of the outer sphere. In the dodecahedron the spacing between the A and B orbitals for both spheres is sufficiently large for there to be no cross-over between the bonding component of the B-B interaction (B_b) and the antibonding component of the A-A interaction (A^*). Non-polar clusters (planar-equatorial or puckered-

equatorial) may therefore accomodate n, (n+1) or (n+2) skeletal electron pairs.

Table 4.6 summarises the frontier orbital nature of bipyramidal and non-polar deltahedral clusters in terms of the orbitals of the outer sphere. In both of these classes of cluster the frontier orbitals are derived from components of the P^{π} and $\bar{P}^{\pi}$ orbitals of the outer sphere. For bipolar clusters these components are $P^{\pi}_{\pm 1}$ and $\bar{P}^{\pi}_{\pm 1}$, while for non-polar clusters they are P^{π}_{0} and $\bar{P}^{\pi}_{0}$. Thus, a complementary pattern exists between the frontier orbital patterns of bipolar and non-polar deltahedral clusters. The Table also illustrates that for D_{nh} clusters (e.g. those with bipyramidal or non-polar planar-equatorial geometries) the ordering is B below A, that is the HOMO has outer sphere $\bar{P}^{\pi}$ character and the LUMO has P^{π} character. In contrast, D_{nd} clusters (e.g. those with bicapped antiprismatic or non-polar puckered-equatorial geometries) have this ordering reversed. The symmetries of the P^{π} and $\bar{P}^{\pi}$ orbitals, for several D_{nh} and D_{nd} point groups, are listed in **Table 4.7.**

The arguments developed above are equally applicable to the large (n>12) deltahedral clusters discussed by Lipscomb,[9] provided that they do not deviate too greatly from a spherical topology. Thus the degeneracies and number of nodes in a plane perpendicular to the principal rotation axis (i.e. the magnitudes of the M quantum numbers) of the frontier orbitals should be the same for these large clusters as for the smaller clusters dealt with here. The presence of extra layers of atoms, however, leads to a greater number of nodes parallel to the principal axis (i.e. the L quantum number is higher).

Table 4.6 Outer sphere components of the frontier orbitals of bipolar and non-polar deltahedral clusters

	Cluster Class			
	Bipolar		**Non-Polar**	
	D_{nh}	D_{nd}	D_{nh}	D_{nd}
LUMO('s)*	$P^{\pi}_{\pm 1}$	$\bar{P}^{\pi}_{\pm 1}$	P^{π}_{0}	$\bar{P}^{\pi}_{0}$
HOMO('s)*	$\bar{P}^{\pi}_{\pm 1}$	$P^{\pi}_{\pm 1}$	$\bar{P}^{\pi}_{0}$	P^{π}_{0}

* The HOMO('s) and LUMO('s) refer to those clusters with (n+1) SEP's.

Table 4.7 Symmetries of cluster P^{π} and $\bar{P}^{\pi}$ orbitals in some D_{nh} and D_{nd} point groups

	D_{nh}				D_{nd}			
n	**3**	**4**	**5**	**6**	**2**	**3**	**4**	**5**
P^{π}_{0}	a''_2	a_{2u}	a''_2	a_{2u}	b_2	a_{2u}	b_2	a_{2u}
$P^{\pi}_{\pm 1}$	e'	e_u	e'_1	e_{1u}	e	e_u	e_1	e_{1u}
$\bar{P}^{\pi}_{0}$	a'_2	a_{2g}	a'_2	a_{2g}	a_2	a_{2g}	a_2	a_{2g}
$\bar{P}^{\pi}_{\pm 1}$	e''	e_g	e''_1	e_{1g}	e	e_g	e_3	e_{1g}

4.9 Appendix: Symmetry Theorems for Molecular Wavefunctions

Quinn has developed an elegant methodology for generating ligand (and cluster) linear combinations of orbitals, with local π- and δ-pseudo-symmetry, from the σ-orbitals of the ligand/cluster polyhedron.[6] The following discussion will deal specifically with cluster MO's.

The reducible representations corresponding to linear combinations of s, p, d, f etc. atomic orbitals, located at the cluster vertices, may be denoted Γ_s, Γ_p, Γ_d, Γ_f etc.. Quinn has shown that the reducible representation Γ_l (l=0 (s), 1 (p), 2 (d) etc.) may be generated by multiplying the permutation representation of the cluster (Γ_ρ) by the representations spanned by the $Y_{l,m}$ functions at the origin of the cluster (Γ_l^o):[6]

$$\Gamma_l = \Gamma_\rho \otimes \Gamma_l^o$$

The (reducible) permutation representation (Γ_ρ) is such that the character ($\chi_\rho(R)$) for each operation (R) of the point group is equal to the number of cluster vertices which remain fixed under the operation.[6]

The reducible representation Γ_l is clearly the sum of irreducible representations (Γ^i):

$$\Gamma_l = \sum_i a_i \Gamma^i$$

If the character of R in each irreducible representation is denoted by $\chi^i(R)$, then, by applying the group orthogonality principle,[8] the coefficients (a_i) (i.e. number of times that the ith irreducible representation appears in Γ_l) are given by:

$$a_i = (1/h) \sum_R \chi^i(R)\, \chi_\rho(R)$$

where h is the order of the group.[8]

Because s orbitals are nodeless, their linear combinations generate (in TSH terms) the cluster L^{σ} MO's:[2]

$$\Gamma_s = \Gamma_\rho \otimes \Gamma_s^o = \Gamma_\sigma$$

where Γ_s^o is the totally symmetric irreducible representation, Γ_g^0, with character +1 under all operations. Since multiplication by Γ_g^0 leaves any representation unchanged, $\Gamma_\sigma = \Gamma_\rho$.

At the origin, the p atomic orbitals transform as $\Gamma_{x,y,z}$. Using the above equations, and the fact that $\Gamma_\rho = \Gamma_\sigma$, enables the following relationship to be derived:[6]

$$\Gamma_p = \Gamma_\sigma \otimes \Gamma_p^o = \Gamma_\sigma \otimes \Gamma_{x,y,z}$$

Unlike the s orbitals, the atomic p orbitals possess one angular node. At each cluster vertex, linear combinations of p_x, p_y and p_z may be taken, which generate one radial (p^σ) and two tangential (p^π) orbitals. In terms of TSH theory these orbitals form the basis of the cluster L_p^σ and $L_p^\pi/\bar{L}_p^\pi$ MO's.[2] In group theoretical terms, Γ_p can be divided into radial and tangential parts as follows:

$$\Gamma_p = \Gamma_\sigma + \Gamma_{\pi+\bar{\pi}}$$

Similarly, for the d based cluster MO's the following relationships may be written:[6]

$$\Gamma_d = \Gamma_\sigma \otimes \Gamma_d^o \ (z^2,\ x^2\text{-}y^2,\ xy,\ xz,\ yz)$$

$$= \Gamma_\sigma + \Gamma_{\pi+\bar{\pi}} + \Gamma_{\delta+\bar{\delta}}$$

and for f-based cluster MO's:

$$\Gamma_f = \Gamma_\sigma + \Gamma_{\pi+\bar{\pi}} + \Gamma_{\delta+\bar{\delta}} + \Gamma_{\phi+\bar{\phi}}$$

Quinn has used these relationships to obtain equations for deriving the symmetries of cluster π- and δ-type MO's from those of the L^σ orbitals:[6]

$$\Gamma_{\pi+\bar{\pi}} = \{\Gamma_\sigma \otimes \Gamma_{x,y,z}\} - \Gamma_\sigma$$
$$\Gamma_{\delta+\bar{\delta}} = \{\Gamma_{\pi+\bar{\pi}} \otimes \Gamma_{x,y,z}\} - \{\Gamma_\sigma \otimes \Gamma_u^0\} - \Gamma_{\pi+\bar{\pi}} - \Gamma_\sigma$$

where Γ_u^0 is the totally antisymmetric irreducible representation, with character +1 for proper rotations and -1 for improper rotations, including inversion and reflections.

In general, if l' indicates the number of angular nodes of an atomic orbital (at a cluster vertex) relative to the radial vector, and $\Gamma_{l'}$ is the reducible representation spanned by linear combinations of these orbitals ($\Gamma_0 = \Gamma_\sigma$, $\Gamma_1 = \Gamma_{\pi+\bar{\pi}}$, $\Gamma_2 = \Gamma_{\delta+\bar{\delta}}$ etc.), then the following relationship can be derived:[6]

$$\Gamma_{l'+1} = \{\Gamma_{l'} \otimes \Gamma_{x,y,z}\} - \Gamma_{l'} - \Gamma_{l'-1}$$

This equation is valid for l'>2, e.g. $\Gamma_{\phi+\bar{\phi}} = \{\Gamma_{\delta+\bar{\delta}} \otimes \Gamma_{x,y,z}\} - \Gamma_{\delta+\bar{\delta}} - \Gamma_{\pi+\bar{\pi}}$.

Quinn has derived simplified forms of these equations for axial point groups, where the p^θ and p^ϕ components of the tangential p^π orbitals may be treated separately. The tangential orbitals are merely formed by taking the L^σ MO's with a basis set of p^θ and p^ϕ orbitals, rather than radial orbitals. The p^θ orbitals have the same local symmetry as Γ_z, while the p^ϕ orbitals have the local symmetry of Γ_{Rz}:[6]

$$\Gamma_{\pi+\bar{\pi}} = \Gamma^{\theta}_{\pi+\bar{\pi}} + \Gamma^{\phi}_{\pi+\bar{\pi}}$$
$$= \{\Gamma_{\sigma} \otimes \Gamma_{z}\} + \{\Gamma_{\sigma} \otimes \Gamma_{Rz}\}$$

Similarly, Quinn has shown that, in axial point groups, the L^{δ} and $\bar{L}^{\delta}$ orbitals can be split into their $d^{\theta\theta}$ and $d^{\theta\phi}$ components. The former have the same local symmetry as $\Gamma_{z}2$ (which transforms as Γ^{0}_{g} in axial point groups), while the latter transform as Γ^{0}_{u}:[6]

$$\Gamma_{\delta+\bar{\delta}} = \Gamma^{\theta\theta}_{\delta+\bar{\delta}} + \Gamma^{\theta\phi}_{\delta+\bar{\delta}}$$
$$= \{\Gamma_{\sigma} \otimes \Gamma_{z}2\} + \{\Gamma_{\sigma} \otimes \Gamma^{0}_{u}\}$$
$$= \Gamma_{\sigma} + \{\Gamma_{\sigma} \otimes \Gamma^{0}_{u}\}$$

As indicated in **Chapter 5**, however, these formulae are not valid for atoms lying on the principal rotation axis, where p_z and d_z2 have purely radial character. In these cases, provided there are no atoms lying in the equatorial plane, we have noted that the following equations may be used:

$$\Gamma_{\pi+\bar{\pi}} = \Gamma_{\sigma} \otimes \Gamma_{x,y}$$
$$\Gamma_{\delta+\bar{\delta}} = \Gamma_{\sigma} \otimes \Gamma_{xy,x^2-y^2}$$

These follow because, at all cluster vertex positions (except those in the equatorial plane), linear combinations of p_x and p_y (or d_{xy} and $d_x2_{-y}2$) may be taken to generate two tangential p^{π} (or d^{δ}) orbitals.

References for Chapter Four

1. K. Wade, Adv. Inorg. Chem. Radiochem., 1976, **18**, 1; D.M.P. Mingos, Acc. Chem. Res., 1984, **17**, 311 and references therein.
2. A.J. Stone, Mol. Phys., 1980, **41**, 1339; Inorg. Chem., 1981, **20**, 563.
3. P.W. Fowler, Polyhedron, 1985, **4**, 2051.
4. K. Wade and M.E. O'Neill, Inorg. Chem., 1982, **21**, 461.
5. P.W. Fowler and W.W. Porterfield, Inorg. Chem., 1985, **24**, 3511.
6. D.B. Redmond, C.M. Quinn and J.G.R. McKiernan, J. Chem. Soc., Faraday Trans. II, 1983, 79, 1791; Inorg. Chem., 1983, 22, 2310; J. Chem. Educ., 1984, **61**, 569, 572.
7. A. Ceulemans, Mol. Phys., 1985, **54**, 161.
8. See, for example: F.A. Cotton, "Chemical Applications of Group Theory" (2nd. Edn.), Wiley, New York, 1971.
9. L.D. Brown and W.N. Lipscomb, Inorg. Chem., 1977, **16**, 2989; J. Bicerano, D.S. Marynick and W.N. Lipscomb, Inorg. Chem., 1978, **17**, 2041, 3443.
10. A.J. Stone and M.J. Alderton, Inorg. Chem., 1982, **21**, 2297.
11. See, for example: G. Herzberg, "Infra-Red and Raman Spectra of Polyatomic Molecules", Van Nostrand, New York, 1945.
12. M. Atoji and W.N. Lipscomb, Acta Crystallogr., 1953, **6**, 547.
13. G. Maier, S. Pfriem, U. Schafter and R. Matusch, Angew. Chem., 1978, **90**, 652.
14. (a) R.T. Baker, Inorg. Chem, 1986, **25**, 109 and references therein. (b) J.D. Kennedy, Inorg. Chem., 1986, **25**, 111 and references therein.
15. R. Mason, K.M. Thomas and D.M.P. Mingos, J. Amer. Chem. Soc., 1973, **95**, 3802; D.M.P. Mingos and M.I. Forsyth, J. Chem. Soc., Dalton

Trans., 1977, 610.

16. N.A. Kutz and J.A. Morrison, Inorg. Chem., 1980, **19**, 3295.
17. T. Davan and J.A. Morrison, Inorg. Chem., 1986, **25**, 2366.
18. M.J. Attfield, J.A.K. Howard, A.N. de M. Jelfs, C.M. Nunn and F.G.A. Stone, J. Chem. Soc., Chem. Commun., 1986, 918.
19. A.W. Duff, K. Jonas, R. Goddard, H.-J. Kraus and C. Kruger, J. Amer. Chem. Soc., 1983, **105**, 5479.
20. S.C. Critchlow and J.D. Corbett, J. Amer. Chem. Soc., 1983, **105**, 5715.
21. J.D. Corbett, Chem. Rev., 1985, **85**, 383.
22. L.J. Guggenberger, Inorg. Chem., 1968, **7**, 2260.
23. R.C. Burns, R.J. Gillespie, J.A. Barnes and M.J. McGlinchey, Inorg. Chem., 1982, **21**, 806.
24. M.E. O'Neill and K. Wade, Polyhedron, 1983, **2**, 963.
25. R.M. Friedman and J.D. Corbett, Inorg. Chem., 1973, **12**, 1134.
26. A. Hershaft and J.D. Corbett, Inorg. Chem., 1963, **2**, 979.
27. C.H.E. Belin, J.D. Corbett and A. Cisar, J. Amer. Chem. Soc., 1977, **99**, 7163.
28. J.D. Corbett and P.A. Edwards, J. Amer. Chem. Soc., 1977, **99**, 3313.
29. R.W. Rudolph, W.L. Wilson, F. Parker, R.C. Taylor and D.C. Young, J. Amer. Chem. Soc., 1978, **100**, 4629.
30. L.J. Guggenberger and E.L. Muetterties, J. Amer. Chem. Soc, 1976, **98**, 7221.
31. J.L. Vidal, W.E. Walker, R.L. Pruett and R.C. Schoening, Inorg. Chem., 1979, **18**, 129.
32. B.T. Heaton, L. Strona, R. Della Pergola, J.L. Vidal and R.C. Schoening, J. Chem. Soc., Dalton Trans., 1983, 1941.
33. D.N. Cox, D.M.P. Mingos and R. Hoffmann, J. Chem. Soc., Dalton

Trans., 1981, 1788.

34. R.B. King, Polyhedron, 1982, **1**, 132.

35. P.R. LeBreton, S. Urano, M. Shahbaz, S.L. Emery and J.A. Morrison, J. Amer. Chem. Soc., 1986, **108**, 3937.

CHAPTER FIVE

APPLICATION OF TENSOR SURFACE HARMONIC THEORY TO THE STUDY OF BONDING IN BISPHERICAL CLUSTER COMPOUNDS

5.1 Introduction

Tensor Surface Harmonic theory is based on the assumption that all of the skeletal atoms of a deltahedral cluster lie on the surface of a single sphere, with the ligands lying on a second, concentric, spherical surface.[1] There are, however, a number of deltahedral geometries which are distinctly non-spherical. In **Chapter 4**, it was shown that these polyhedra may be conveniently described in terms of two topologically distinct sets of skeletal atoms, which lie on two concentric spheres. Consideration of the interactions between the orbitals of the "inner sphere" and "outer sphere" atoms were used to rationalise the frontier orbital patterns in these polyhedra.

The aim of the work described in this Chapter was to use Tensor Surface Harmonic theory, together with group theoretical arguments (see **Section 4.9** for further details),[2] to gain an understanding of the bonding in high nuclearity clusters, which have skeletal atoms on two (**"bispherical"**) or more (**"multispherical"**) concentric spheres. In these clusters, the deviation from spherical topology is generally much greater than in the previously mentioned deltahedra. Examples of such molecules include capped clusters, raft clusters and high nuclearity pseudo-close-packed clusters (consisting of an inner sphere polyhedron

which is completely encapsulated by the outer sphere polyhedron).

To describe the bonding in bispherical and multispherical clusters, Stone's original TSH approach has been modified slightly to take into account the radial nodes which the skeletal MO's of such clusters possess. Group theoretical techniques (more details of which have been given in **Section 4.9**) have been used to evaluate the symmetries and L values of the skeletal molecular orbitals of multispherical polyhedral clusters. Relationships between the nodal properties and energies of the skeletal MO's of spherical and multispherical clusters have also been drawn. To aid these arguments, Extended Hückel calculations have been performed on polyhedral boranes, $[B_nH_n]^{q-}$, with parameters as for **Chapter 2.**

5.2 Bispherical Clusters

Bispherical clusters are defined as those clusters having two sets of symmetry equivalent atoms, which lie on the surfaces of two concentric spheres of differing radii. The relationship between spherical (all atoms on the surface of the same sphere) and bispherical clusters may be clearly demonstrated for high symmetry situations, such as that shown in **Figure 5.1.** The rhombic dodecahedron has effectively fourteen atoms lying on a single sphere (actually the polyhedron is not quite spherical, but there is an interior sphere which cuts all of its edges) and, therefore, its bonding can be analysed in terms of the (single sphere) Tensor Surface Harmonic Theory. The analysis is further simplified by the octahedral symmetry of the polyhedron. **Figure 5.1** also illustrates how two bispherical clusters of O_h symmetry can be generated from the rhombic dodecahedron, i.e. the octacapped octahedron and the

hexacapped cube. Both of these bispherical clusters are examples of omnicapped polyhedra and are topologically related by the **dual** nature of the cube and the octahedron.

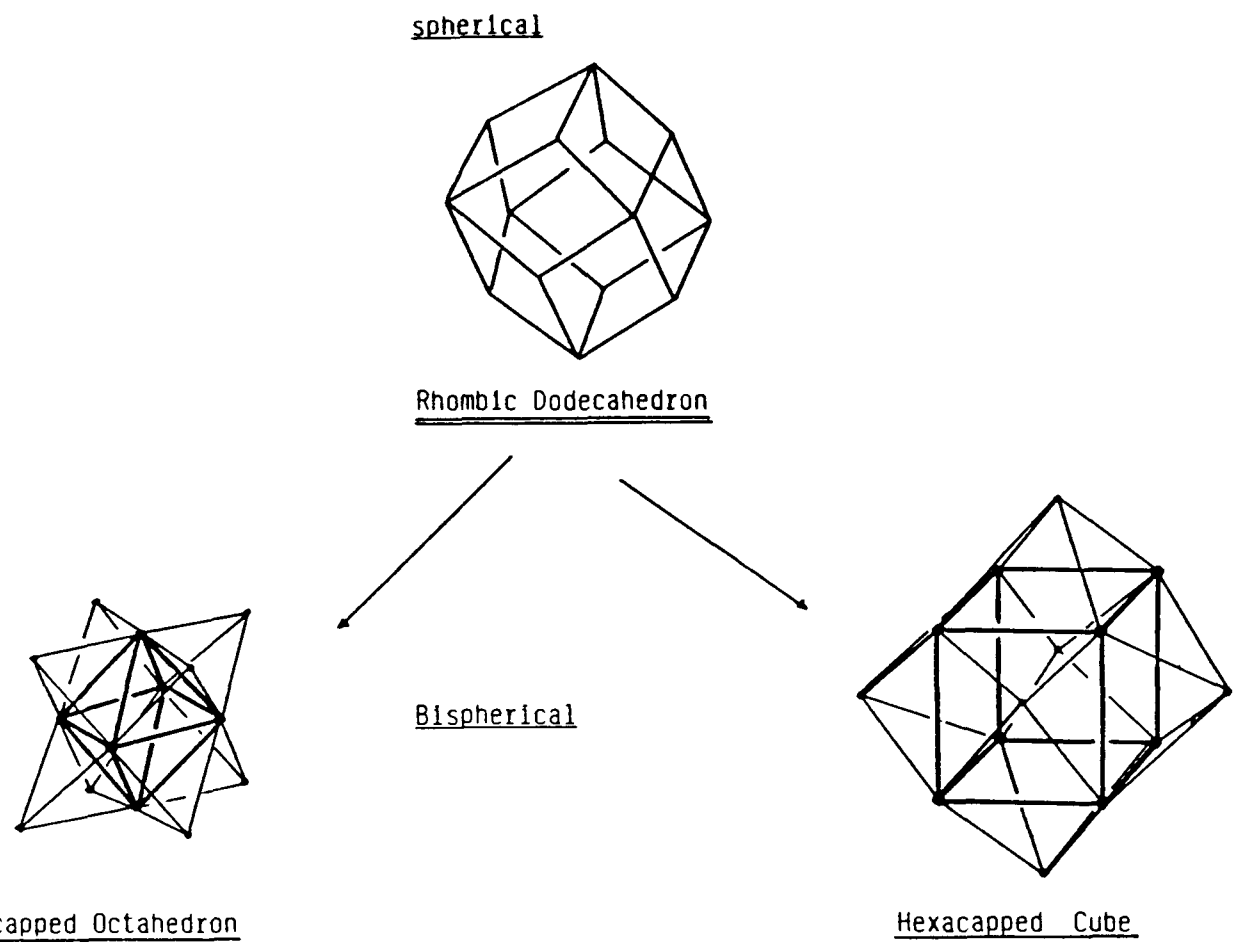


Figure 5.1 14-vertex spherical and bispherical polyhedra with octahedral symmetry.

5.3 Topological Features of Bispherical Clusters

Two polyhedra, A and B, are described as **geometric face-duals**[3] if the faces of A are replaced by vertices in B and vice-versa. The polyhedra A and B belong to the same symmetry point group and the relationships between the numbers of vertices (V), edges (E), and faces (F) of the two dual polyhedra are as follows:

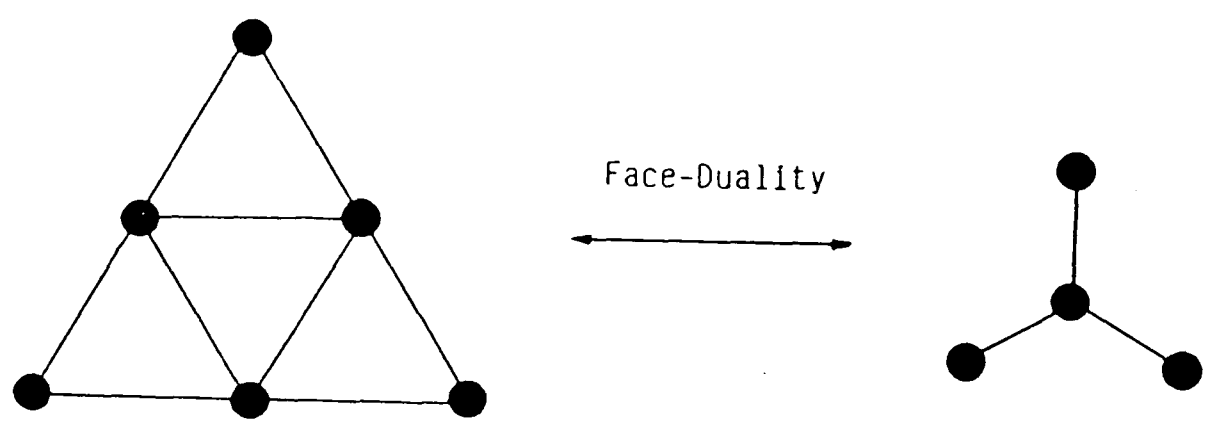
$$V_B = F_A$$

$$F_B = V_A$$

$$E_B = E_A$$

Euler's relationship, $(V+F=E+2)^3$, which applies to all convex polyhedra, may be used to derive more specific topological relationships.

In the case illustrated in **Figure 5.1**, polyhedron A is an octahedron, which is an example of a deltahedron. Its (face-) dual B is a cube, which is a 3-connected polyhedron. The dual of a deltahedron, where each of the triangular faces has three neighbouring faces, is always a 3-connected polyhedron, as shown in **Figure 5.2**. Since the dual relationship is reciprocal, the dual of a 3-connected polyhedron is a deltahedron.



Deltahedron (triangular faces) 3-connected polyhedron (trivalent vertices)

Figure 5.2 The face-duality relationship between deltahedra and 3-connected polyhedra.

Some examples of face-dual deltahedra and 3-connected polyhedra are presented in **Figure 5.3.**

The following topological relationships apply to deltahedra (denoted by subscript Δ) and 3-connected polyhedra (denoted by subscript 3):

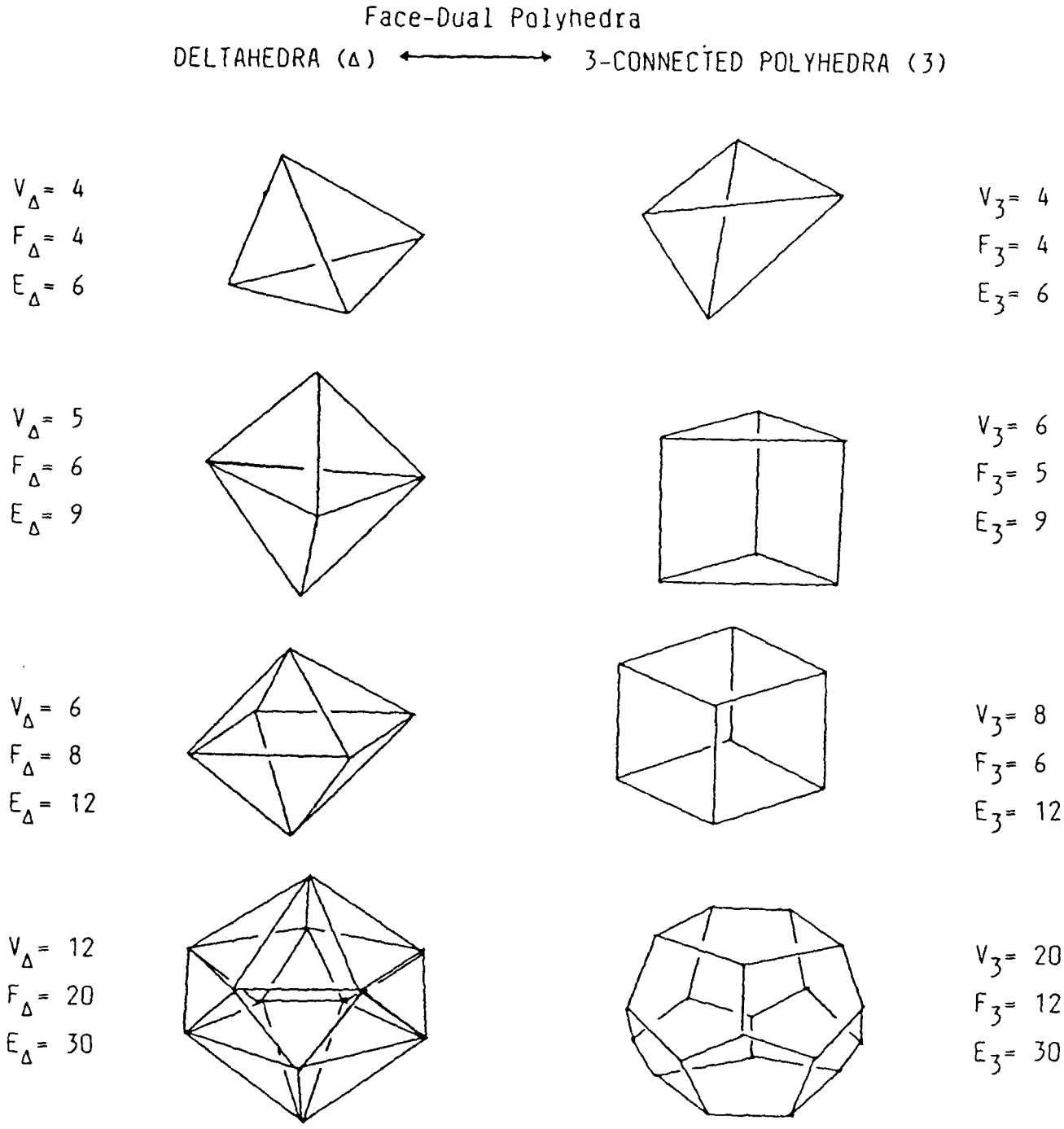


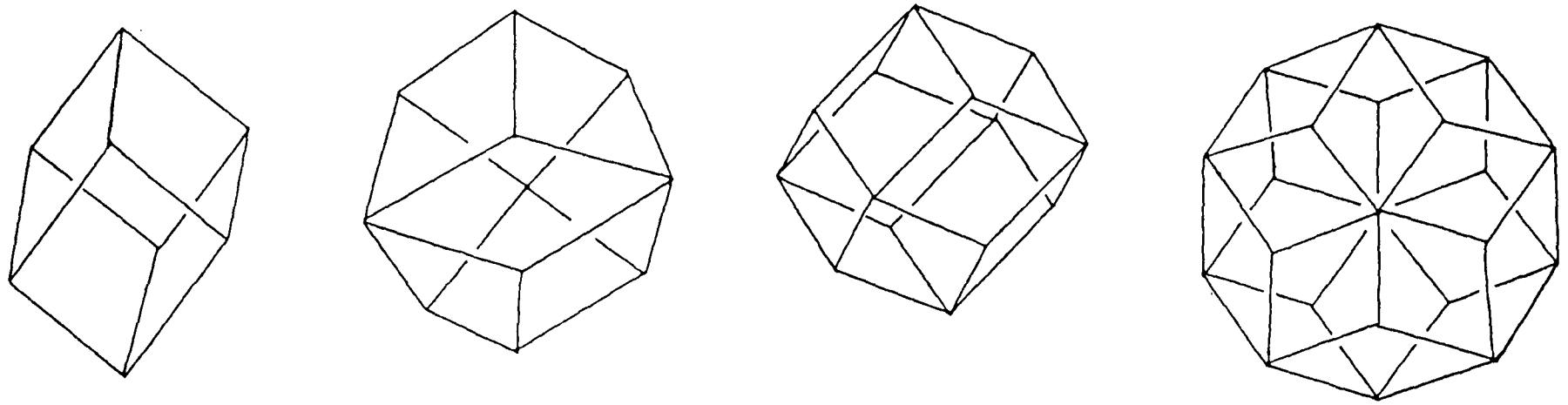
Figure 5.3 Some face-dual deltahedra and 3-connected polyhedra.

Deltahedra	**3-connected polyhedra**
$F_\Delta = 2(V_\Delta-2)$	$F_3 = (V_3/2)+2$
$E_\Delta = 3(V_\Delta-2)$	$E_3 = (3V_3/2)$
$E_\Delta = (3F_\Delta/2)$	$E_3 = 3(F_3-2)$

The number of vertices in an omnicaped deltahedron, or omnicapped 3-connected polyhedron, is obviously the same (V_{omni}) when the deltahedron and 3-connected polyhedron are duals.

$$V_{omni} = V_\Delta + V_3$$
$$= V_\Delta + F_\Delta \quad = F_3 + V_3$$
i.e. $$V_{omni} = 3V_\Delta-4 \quad = (3V_3/2)+2$$

Bispherical omnicapped polyhedra may be converted into spherical polyhedra by simultaneously expanding the inner sphere and contracting the outer sphere until all of the vertices lie on the same sphere. This does not change the point group symmetry of the polyhedron since it is the radial and not the angular disposition of the cluster vertices which is changed by this process. In the spherical limit $V_{omni} = V_{sph}$ and the above relationships apply, with V_{omni} replaced by V_{sph}. Since 3-connected polyhedra must possess an even number of vertices V_3 takes the values 4, 6, 8, 10 etc. which, from the equations above, results in V_{omni} (or V_{sph}) values of 8, 11, 14, 17 etc.. Thus bispherical or spherical clusters, which are composites of a deltahedron and its 3-connected dual, are characterised by (3x+5) atoms (x = 1, 2, 3 etc.). Examples of spherical clusters of this type are given in **Figure 5.4.** It should be noted that these spherical polyhedra are all rhombohedra (possessing square or rhombic faces, $V_{sph}=V_\Diamond$) and as such are the duals of 4-connected polyhedra. The spherical clusters can be distorted in two



Cube (Rhombic Hexahedron)	Rhombic Enneahedron	Rhombic Dodecahedron	Rhombic Triacontahedron
$V_{\diamond} = V_{\Delta}(4)+V_{3}(4) = 8$	$V_{\diamond} = V_{\Delta}(5)+V_{3}(6) = 11$	$V_{\diamond} = V_{\Delta}(6)+V_{3}(8) = 14$	$V_{\diamond} = V_{\Delta}(12)+V_{3}(20) = 32$
$V_{\diamond} = 3X+5$ $(X=1)$	$X=2$	$X=3$	$X=9$
$F_{\diamond} = V-2 = E_{\Delta}=E_{3} = 6$	$F_{\diamond} = 9$	$F_{\diamond} = 12$	$F_{\diamond} = 30$

(N.B. The number of faces ($F_{\diamond}$) of a rhombohedron is equal to the number of edges ($E_{\Delta}=E_{3}$) of its constituent (dual) polyhedra because the rhombohedra are the face-duals of the (4-connected) polyhedra derived by placing a vertex at the midpoint of each edge of the deltahedra or 3-connected polyhedra (i.e. edge-duals)).

$E_{\diamond} = 2F_{\diamond} = E_{\Delta}+E_{3} = 12$	$E_{\diamond} = 18$	$E_{\diamond} = 24$	$E_{\diamond} = 60$

Figure 5.4 "Spherical" rhombohedra as the composites of 3-connected polyhedra and their dual deltahedra.

distinct ways to generate bispherical clusters with either the deltahedron or its 3-connected dual lying on the inner sphere.

5.4 Group Theoretical Analysis

The skeletal MO's of the constituent polyhedral cluster units of a bispherical cluster (i.e. those whose atoms lie on either the inner or the outer sphere) can, by employing the TSH methodology, be expressed as Spherical Harmonic expansions and assigned L^{σ}, L^{π}, $\bar{L}^{\pi}$ etc. quantum numbers. A sequence of steps, based on the group theoretical techniques described in **Section 4.9**,[2] can be followed to obtain the symmetries and TSH labels of these orbitals, as outlined below:

(1) For each constituent polyhedron, the reducible representation (Γ_{σ}) resulting from the permutation of radial (σ) orbitals, under the operations of the cluster point group, is decomposed into its constituent irreducible representations:

$$\Gamma_{\sigma} = a_1\Gamma_1 + a_2\Gamma_2 + a_3\Gamma_3 + \ldots.$$

(2) The L^{σ} labels are obtained by consulting a correlation table (see **Table 5.1** for example) for the descent in symmetry from spherical (R_{3h}) to the appropriate cluster point group symmetry. The lowest L values are chosen which generate all of the irreducible representations of Γ_{σ}.

(3) The irreducible representations spanned by the L^{π} and $\bar{L}^{\pi}$ orbitals are obtained from those of the L^{σ} orbitals by applying the following relationship:[2]

$$\Gamma_{\pi+\bar{\pi}} = \{\Gamma_{\sigma} \otimes \Gamma_{x,y,z}\} - \Gamma_{\sigma}$$

Table 5.1 Symmetries of the Spherical Harmonics in some finite point groups*

R_{3h}	I_h	O_h	T_d	D_3
S_g^σ (Γ_g^0)	A_g	A_{1g}	A_1	A_1
P_u^σ, P_u^π	T_{1u}	T_{1u}	T_2	A_2+E
D_g^σ, D_g^π	H_g	E_g+T_{2g}	$E+T_2$	A_1+2E
F_u^σ, F_u^π	$T_{2u}+G_u$	$A_{2u}+T_{1u}+T_{2u}$	$A_1+T_1+T_2$	A_1+2A_2+2E
G_g^σ, G_g^π	G_g+H_g	$A_{1g}+E_g+T_{1g}+T_{2g}$	$A_1+E+T_1+T_2$	$2A_1+A_2+3E$
Γ_u^0	A_u	A_{1u}	A_2	A_1
$\bar{P}_g^\pi$	T_{1g}	T_{1g}	T_1	A_2+E
$\bar{D}_u^\pi$	H_u	E_u+T_{2u}	$E+T_1$	A_1+2E
$\bar{F}_g^\pi$	$T_{2g}+G_g$	$A_{2g}+T_{1g}+T_{2g}$	$A_2+T_1+T_2$	A_1+2A_2+2E
$\bar{G}_u^\pi$	G_u+H_u	$A_{1u}+E_u+T_{1u}+T_{2u}$	$A_2+E+T_1+T_2$	$2A_1+A_2+3E$

* The representations spanned by the even parity Spherical Harmonics (Y_L, $L\geq 2$), in a given point group, may be obtained from the following recursive formula:

$$\Gamma_{L+1} = \{\Gamma_L \otimes \Gamma_{x,y,z}\} - \{\Gamma_L \otimes \Gamma_u^0\} - \Gamma_{L-1}$$

(e.g. $\Gamma_D = \{\Gamma_P \otimes \Gamma_{x,y,z}\} - \{\Gamma_P \otimes \Gamma_u^0\} - \Gamma_S$). The representations spanned by the odd parity functions are then obtained by multiplying the even parity representations by Γ_u^0:

$$\bar{\Gamma}_{L+1} = \Gamma_{L+1} \otimes \Gamma_u^0$$

This equation is based on the fact that, at any atom position, linear combinations of p_x, p_y and p_z atomic orbitals may be taken so as to generate one radial (p^{σ}) and two tangential ($2p^{\pi} = p^{\theta} + p^{\phi}$) components. In axial point groups the θ and ϕ components of $\Gamma_{\pi+\bar{\pi}}$ may be obtained directly from the following relationships (see **Section 4.9** for the derivation):

$$\Gamma^{\theta}_{\pi+\bar{\pi}} = \Gamma_{\sigma} \otimes \Gamma_{z}$$

$$\Gamma^{\phi}_{\pi+\bar{\pi}} = \{\Gamma_{\sigma} \otimes \Gamma_{z}\} \otimes \Gamma^{0}_{u} = \Gamma_{\sigma} \otimes \Gamma_{Rz}$$

(provided that there are no atoms on the principal rotation axis).

In those cases where there are atoms on the principal rotation axis, the following equation may be used:

$$\Gamma_{\pi+\bar{\pi}} = \Gamma_{\sigma} \otimes \Gamma_{x,y}$$

(provided that there are no atoms in the equatorial plane of the cluster).

(4) Once the irreducible representations spanned by the tangential orbitals ($\Gamma_{\pi+\bar{\pi}}$) are known then the L^{π} and $\bar{L}^{\pi}$ labels may be obtained by consulting a correlation table (e.g. **Table 5.1**), which includes $\bar{L}^{\pi}$ as well as L^{π} ($\Gamma(\bar{L}^{\pi}) = \Gamma(L^{\pi}) \otimes \Gamma^{0}_{u}$). The L^{π} and $\bar{L}^{\pi}$ functions must be equal in number and parity related.

(5) Finally, for bi- or multi-spherical clusters (Z), or spherical clusters consisting of two or more distinct sets of symmetry equivalent atoms (A, B, C...), the irreducible representations spanned by L^{σ} and $L^{\pi}/\bar{L}^{\pi}$ are obtained by summing those of the constituent polyhedra. For example:

$$\Gamma_{\sigma}(Z) = \Gamma_{\sigma}(A) + \Gamma_{\sigma}(B) + \Gamma_{\sigma}(C) + \ldots$$

Again a correlation table, such as **Table 5.1**, may be used to evaluate the L values for the L^{σ}, L^{π} and $\bar{L}^{\pi}$ orbitals of the multi-spherical cluster. The principle of always taking the lowest possible L values may lead to L^{π} orbitals of the multi-spherical cluster which are not symmetry matched by the L^{π} orbitals of its constituent polyhedra. Instead, these orbitals correspond to combinations of $\bar{L}^{\pi}$ orbitals of the constituent polyhedra. The Parity Inversion operation ensures that there are an equal number of parity related combinations of L^{π} orbitals which end up as $\bar{L}^{\pi}$ for the multi-spherical cluster.

Taking the rhombic dodecahedron as an example (the symmetries of the orbitals of the hexacapped cube and the octacapped octahedron will be identical), then the L^{σ}, L^{π} and $L^{-\pi}$ orbitals of its constituent polyhedra (cube and octahedron) may be evaluated in this way.

For the cube:

$$\Gamma_{\sigma}\ \Gamma_{\sigma}(\text{cube}) = a_{1g} + t_{1u} + t_{2g} + a_{2u}$$
$$\Gamma_{\pi+\bar{\pi}}(\text{cube}) = t_{1u} + t_{2g} + e_g + t_{1g} + t_{2u} + e_u$$

The cube has 12 occupied skeletal MO's: $S^{\sigma}(a_{1g}) + P^{\sigma+\pi}(t_{1u}) + D^{\pi}(e_g+t_{2g}) + \bar{D}^{\pi}(t_{2u})$ (see **Table 5.2**), 6 of which are roughly non-bonding orbitals ($D^{\pi}(t_{2g}) + \bar{D}^{\pi}(t_{2u})$). The occupied skeletal MO's are topologically equivalent to the 12 edges of the cluster and can be alternatively generated as linear combinations of edge-bonding (nodeless) localised orbitals.[5] The unoccupied orbitals, on the other hand, may be expressed as linear combinations of edge-antibonding (singly noded) localised orbitals. As concluded in **Chapter 2**, a general

Table 5.2 L^{σ} , L^{π} and $\bar{L}^{\pi}$ orbitals (and their symmetries) of the cube, octahedron and rhombic dodecahedron (O_h symmetry)

	Cube	**Octahedron**	**Rhombic dodecahedron**
L^{σ}			
S^{σ}	A_{1g}	A_{1g}	A_{1g}
P^{σ}	T_{1u}	T_{1u}	T_{1u}
D^{σ}	T_{2g}	E_g	E_g+T_{2g}
F^{σ}	A_{2u}		$A_{2u}+T_{1u}$
G^{σ}			A_{1g}
L^{π}			
P^{π}	T_{1u}	T_{1u}	T_{1u}
D^{π}	E_g+T_{2g}	T_{2g}	E_g+T_{2g}
F^{π}			$T_{1u}+T_{2u}$
$\bar{L}^{\pi}$			
$\bar{P}^{\pi}$	T_{1g}	T_{1g}	T_{1g}
$\bar{D}^{\pi}$	E_u+T_{2u}	T_{2u}	E_u+T_{2u}
$\bar{F}^{\pi}$			$T_{1g}+T_{2g}$

3-connected polyhedron has $3V_3/2$ (= E_3) skeletal electron pairs, (V_3-2) of which are non-bonding (these consist of $\{(V_3/2)-1\}$ L^{π} orbitals and their $\{(V_3/2)-1\}$ $\bar{L}^{\pi}$ parity-inverted counterparts.

For the octahedron:

$$\Gamma_{\sigma} \quad \text{(octahedron)} = a_{1g} + t_{1u} + e_g$$
$$\Gamma_{\pi+\bar{\pi}} \quad \text{(octahedron)} = t_{1u} + t_{2g} + t_{1g} + t_{2u}$$

The octahedron, being a deltahedron, possesses 7 (= $V_{\Delta}+1$) skeletal bonding molecular orbitals:[1,6] $S^{\sigma}(a_{1g}) + P^{\sigma+\pi}(t_{1u}) + D^{\pi}(t_{2g})$ (see **Table 5.2**) and no non-bonding orbitals.

Finally, for the rhombic dodecahedron:

$$\Gamma_{\sigma} \quad \text{(rhombic dodec.)} = 2a_{1g} + 2t_{1u} + t_{2g} + e_g + a_{2u}$$
$$\Gamma_{\pi+\bar{\pi}} \quad \text{(rhombic dodec.)} = 2t_{1u} + 2t_{2g} + 2t_{1g} + 2t_{2u} + e_g + e_u$$

By consulting **Table 5.1**, L values may be assigned to the above orbitals, yielding the results shown in **Table 5.2.** It should be noted that the two sets of $\bar{D}^{\pi}(t_{2u})$ orbitals (one from the cube and one from the octahedron) give rise, in the rhombic dodecahedron, to one set of odd parity ($\bar{D}^{\pi}$) and one set of even parity (F^{π}) orbitals. Similarly, the two sets of $D^{\pi}(t_{2g})$ orbitals give rise to D^{π} and $\bar{F}^{\pi}$ combinations.

5.5 Inner Sphere-Outer Sphere Interactions

In the limit of no interaction between the orbitals of the outer and inner spheres (for instance when the outer sphere radius tends to infinity), the spectrum of skeletal MO's of the bispherical cluster corresponds to that of the isolated inner sphere polyhedron, with

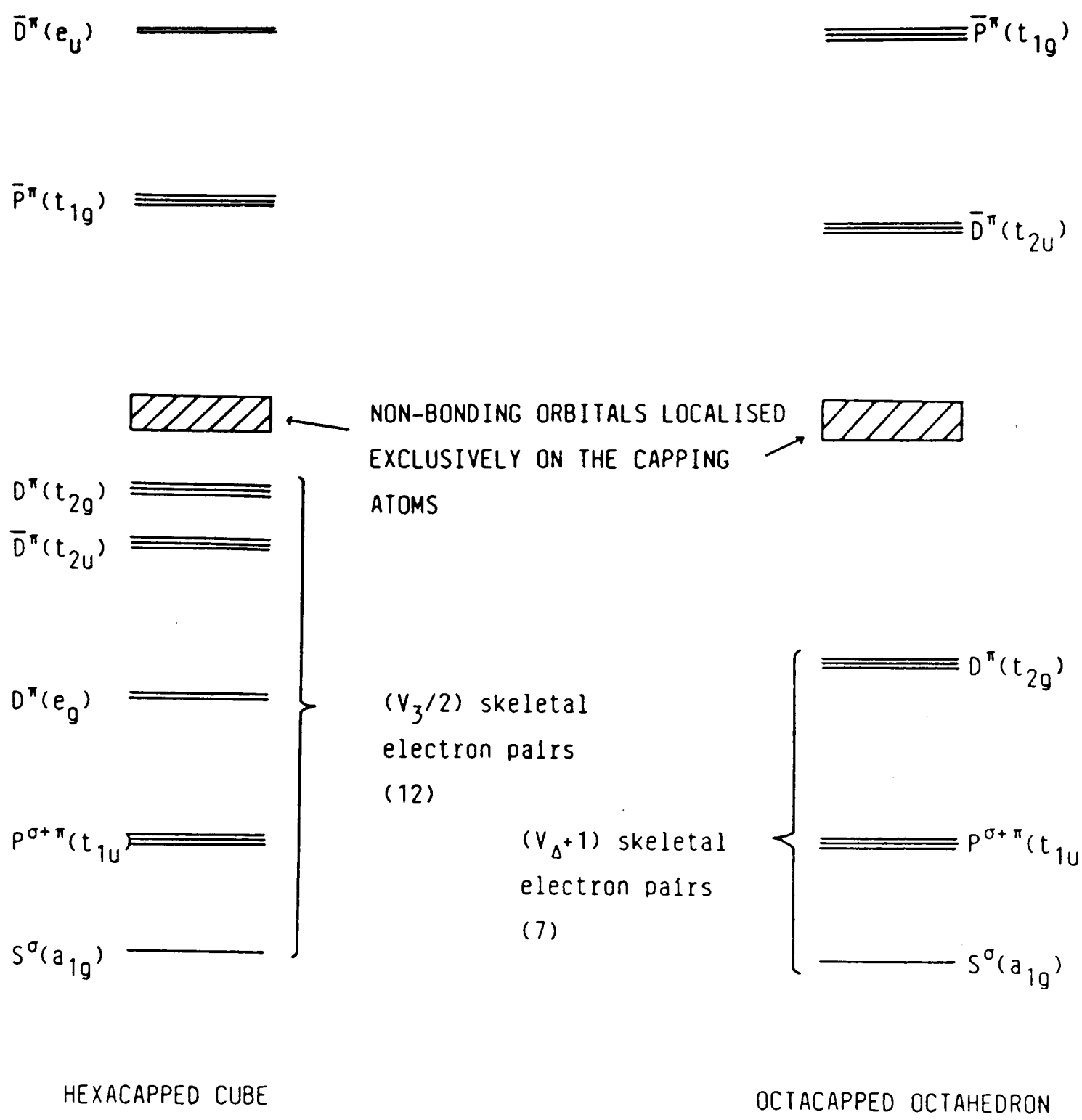


Figure 5.5 Molecular orbital schemes for the bispherical extremes of the hexacapped cube and the octacapped octahedron, with no interaction between the orbitals of the inner and outer sphere polyhedra.

additional, degenerate, non-bonding orbitals belonging to the outer sphere polyhedron. **Figure 5.5** illustrates the non-interacting bispherical extremes for the octacapped octahedron and the hexacapped cube. The cluster atoms possess three valence orbitals (1σ and 2π) which give rise to cluster molecular orbitals of the type L^{σ}, L^{π} and $\bar{L}^{\pi}$. In this limit, the omnicapped deltahedron is characterised by $(V_{\Delta}+1)$ skeletal bonding molecular orbitals and the omnicapped 3-connected polyhedron by $(3V_3/2)$ skeletal bonding molecular orbitals.[6]

As the outer sphere radius is reduced, the MO's of the inner and outer sphere polyhedra (with matching symmetry characteristics) begin to interact. The effect of this interaction is to introduce radial, as well as angular, nodes into the cluster wavefunctions. The primary interactions correspond to the overlap of inner and outer sphere MO's with matching L quantum numbers. **Figure 5.6** illustrates these interactions for L^{σ} and L^{π} orbitals of a generalised bispherical cluster and emphasises how additional radial nodes are introduced.

Generalised molecular orbital interaction diagrams, for L^{σ}, L^{π} and $\bar{L}^{\pi}$ orbitals, are presented in **Figure 5.7.** Since the atoms of the outer sphere polyhedron are further apart than those of the inner sphere, the spread of MO's is narrower for the outer sphere polyhedron. For L^{σ} and L^{π}, this generally results in the in-phase combinations being predominantly localised on the inner sphere, while the radially noded antibonding combinations are predominantly localised on the outer sphere (see **Figure 5.6**). For L^{σ} orbitals with high L values, however, the orbitals of the inner sphere are high in energy due to the large number of angular nodes in the wavefunction. Thus, the in-phase inner sphere-outer sphere combination is predominantly localised on the outer sphere

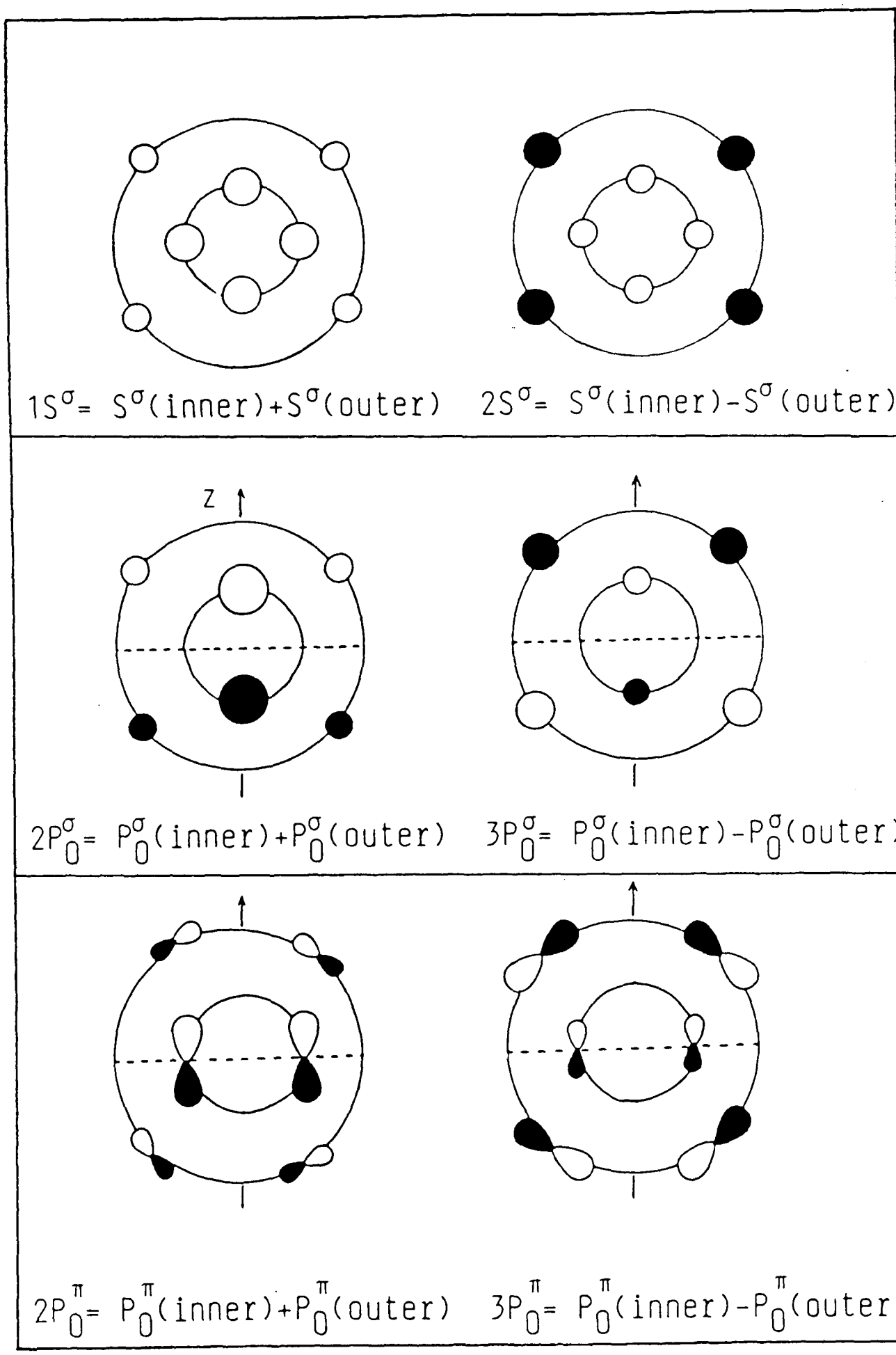
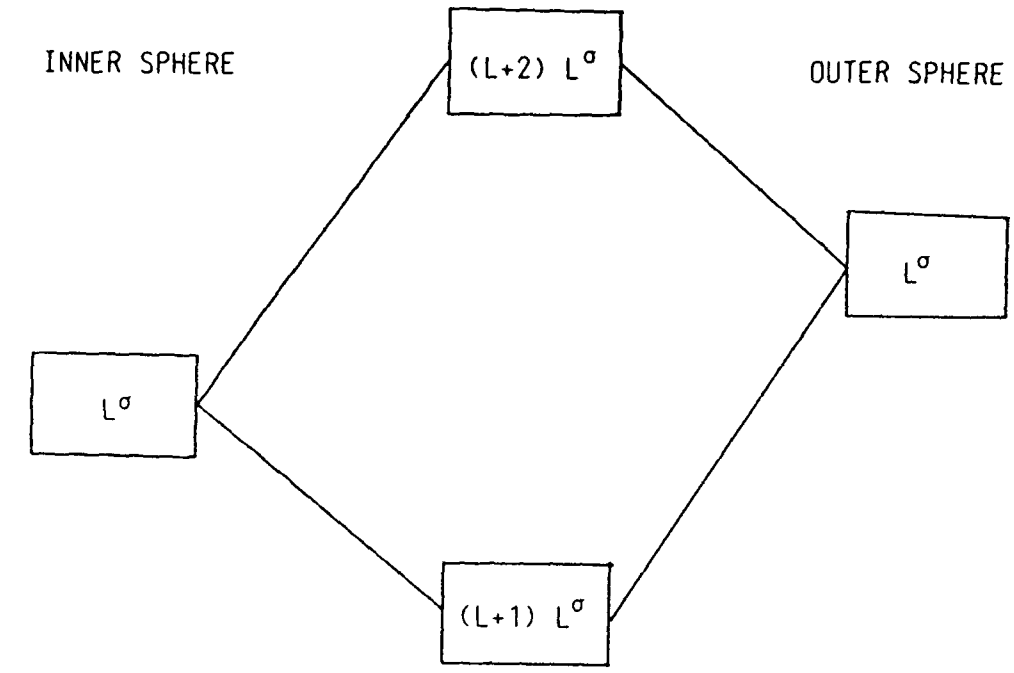


Figure 5.6 Bispherical TSH wavefunctions (nL^{σ} and nL^{π}) possessing radial, as well as angular, nodes.



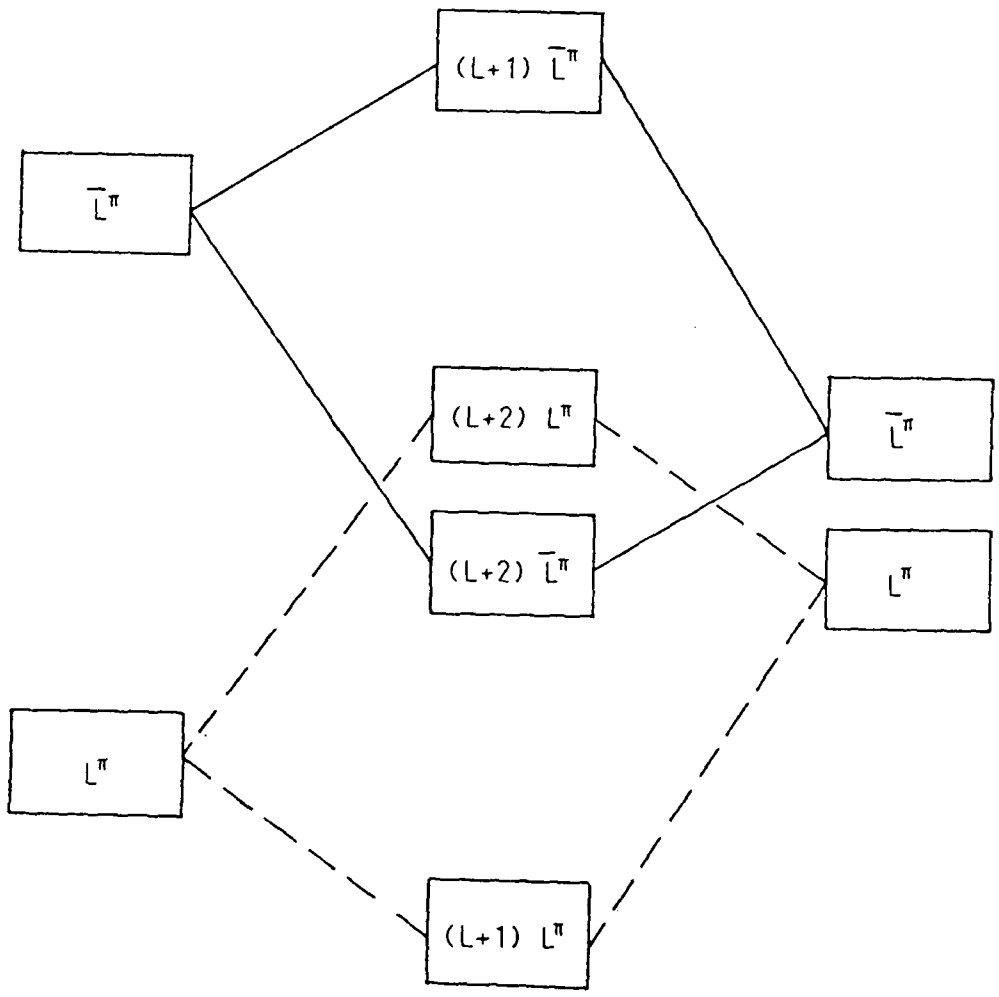


Figure 5.7 Interaction between orbitals of the inner and outer sphere polyhedra in bispherical clusters.

atoms. The $\bar{L}^{\pi}$ orbitals are generally more antibonding for the inner than the outer sphere, so their bonding combinations(see **Figure 5.7**) are mainly localised on the outer sphere.

The nomenclature employed here follows that used for atomic orbitals. Thus, the $1S^{\sigma}$ cluster orbital posesses no radial nodes, while $2S^{\sigma}$ and $3S^{\sigma}$(needed in a trispherical cluster) possess one and two radial nodes respectively. Similarly, $2P^{\sigma}$ and $2P^{\pi}$ possess no radial nodes and $3P^{\sigma}$ and $3P^{\pi}$ possess one radial node. In general, the orbital $nL^{\sigma,\pi,\bar{\pi}}$ possesses (n-L-1) radial nodes, as is the case for atomic orbitals.[7] Another property of atomic orbitals is that the maximum in the radial part of the wavefunction moves to greater radius as n increases. This is neatly mimicked in our model (at least for L^{σ} orbitals with low L values) by the localisation of the maximum of electron density on successively larger spheres as the n quantum number increases (see **Figure 5.6**).

Upon interaction of the L^{σ} and L^{π} orbitals of the inner and outer spheres, the resulting orbital with the fewer radial nodes (lower value of n) is more strongly bonding. As a result of the Parity Inversion operator $(\hat{P})$, which relates L^{π} and $\bar{L}^{\pi}$ and interconverts their bonding characteristics,[1] the reverse situation applies for the $\bar{L}^{\pi}$ orbitals of a bispherical cluster, i.e. the greater the number of radial nodes (higher n) the lower the energy of $n\bar{L}^{\pi}$. These conclusions are summarised in **Figure 5.7.**

The consequences of these inner sphere-outer sphere interactions, for the omnicapped octahedron and the omnicapped cube, are shown in **Figure 5.8.** An important feature to note is that, in both cases, the interaction effectively leads to the stabilisation of the bonding orbitals of the inner sphere polyhedron and the corresponding

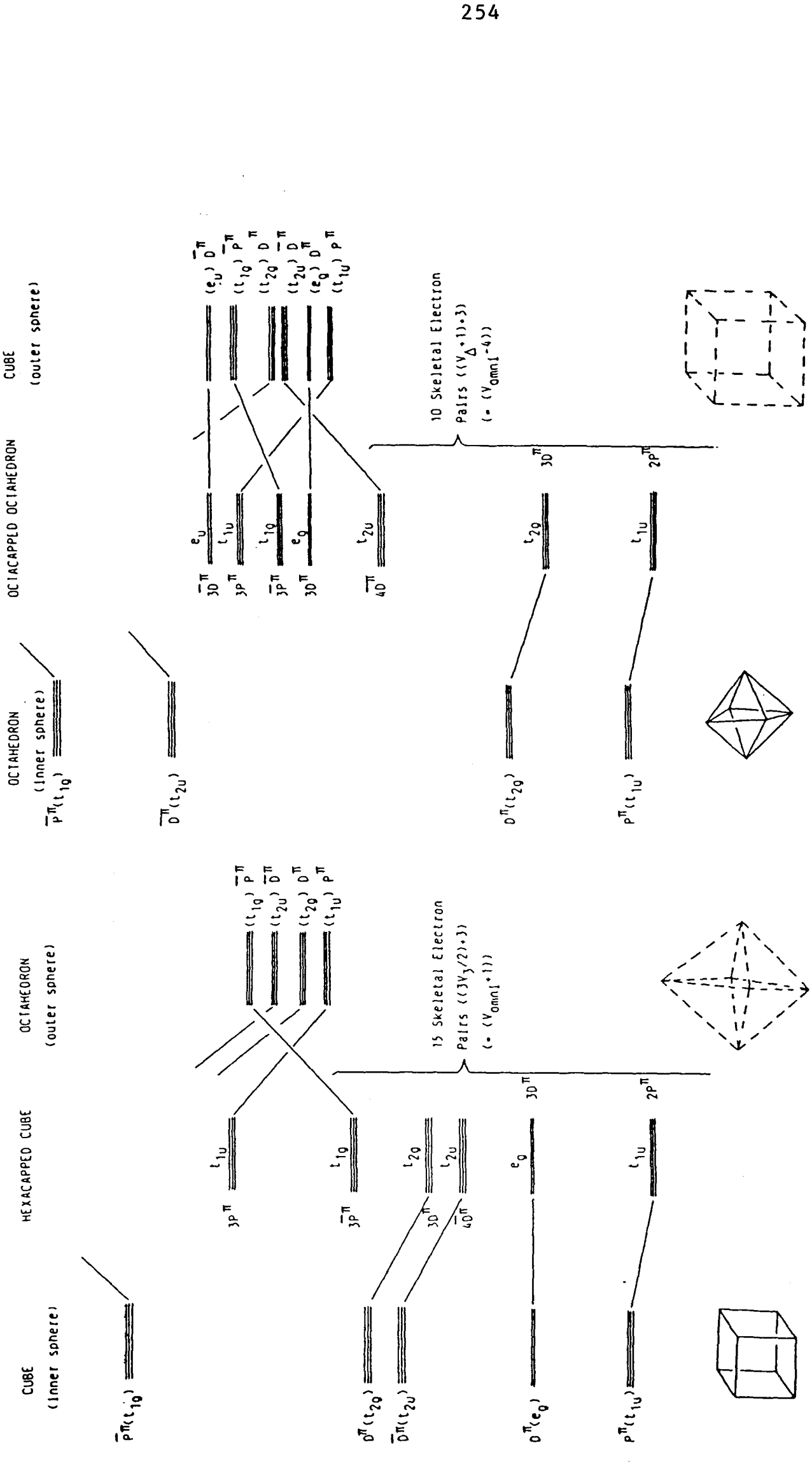


Figure 5.8 Molecular orbital (inner sphere-outer sphere) interaction diagrams for the hexacapped cube and the octacapped octahedron.

destabilisation of those of the outer sphere. In itself this would lead to no change in the number of SEP's, which is indeed observed when polyhedra are capped on only a few of their faces (i.e. when there are not many atoms on the outer sphere). These ideas constitute the basis of the **Capping Principle.**[8] When the capping atoms form a complete, well defined polyhedron, however, certain bonding combinations of L^{π} orbitals may become sufficiently low lying to be occupied.

For 3-connected polyhedra, the $\bar{L}^{\pi}$ orbitals of interest are $\bar{P}^{\pi}$. As shown in **Figure 5.8** the three $3\bar{P}^{\pi}(t_{1g})$ orbitals of the hexacapped cube possess overall bonding character. 3-connected polyhedra, in general, have the $\bar{P}^{\pi}$ orbitals as their LUMO's, because of the π-bonding interaction which they exhibit across three mutually perpendicular cluster planes. **Figure 5.9a** illustrates this bonding interaction for one component of the $\bar{P}^{\pi}$ orbitals ($\bar{P}^{\pi}_{0}$). When a ring of capping atoms (outer sphere) are introduced (creating a toroidal topology for the bispherical cluster), their $\bar{P}^{\pi}_{0}$ combination interacts strongly with that of the 3-connected polyhedron, to create a slightly bonding $3\bar{P}^{\pi}_{0}$ orbital (**Figure 5.9b**). In the case of an omnicapped 3-connected polyhedron, this process is repeated (in three perpendicular planes) for all three $\bar{P}^{\pi}$ orbitals and three extra skeletal bonding MO's result, which constitute the HOMO's of the bispherical cluster. This leads to an SEP count of $(3V_3/2)+3$ for omnicapped 3-connected polyhedra (i.e. 15 SEP's for the hexacapped cube). The parity related $3P^{\pi}$ orbitals (antibonding combination of P^{π} on the two spheres) are the LUMO's. These orbitals are, generally, fairly low lying and, therefore, potentially accessible.

The $\bar{P}^{\pi}$ orbitals are more strongly antibonding for deltahedra than for 3-connected polyhedra because, as shown in **Figure 5.10a**, the

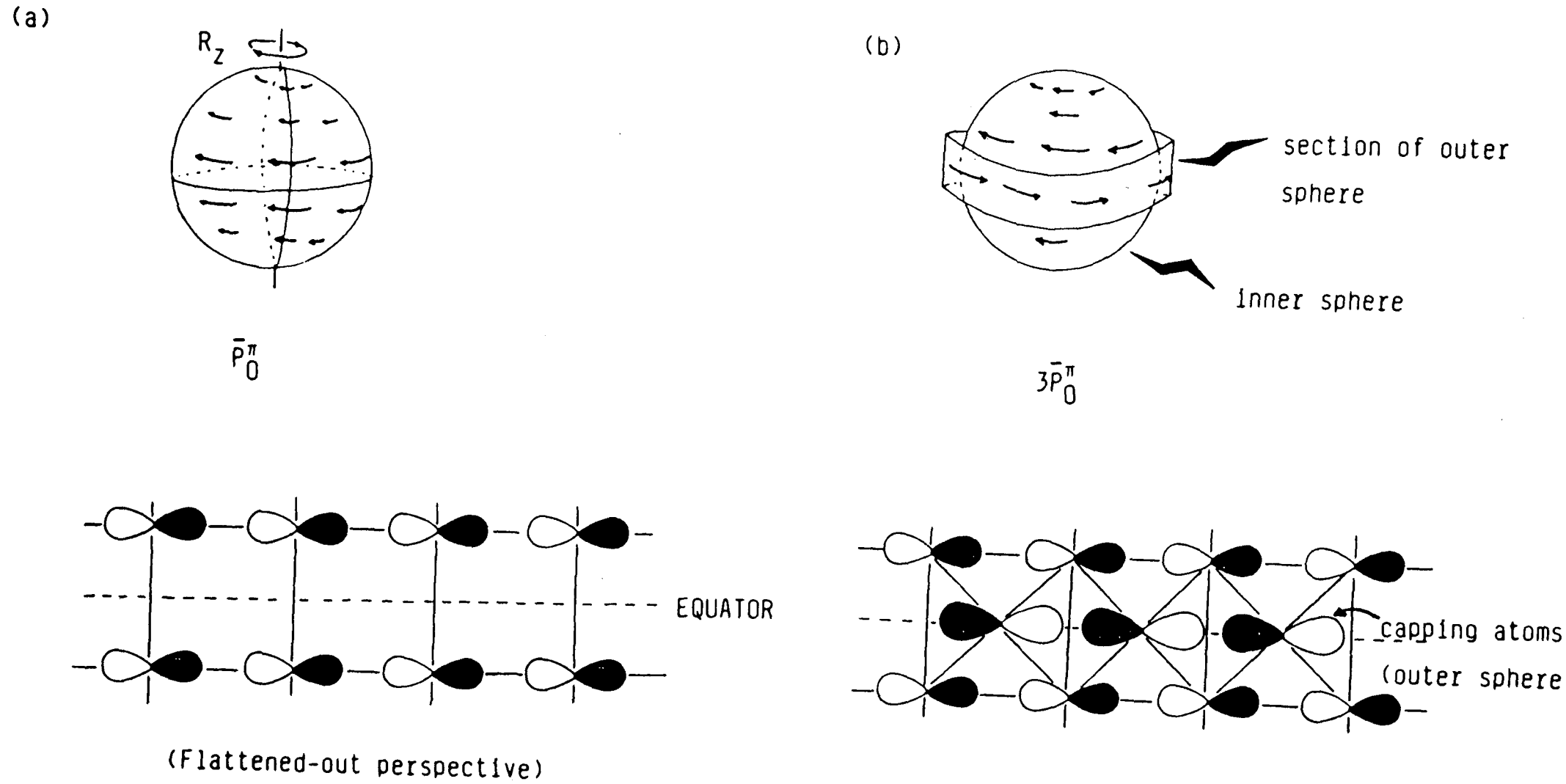


Figure 5.9 $\bar{P}_0^{\pi}$ orbitals for spherical and bispherical clusters based on a prismatic (3-connected) inner sphere polyhedron.

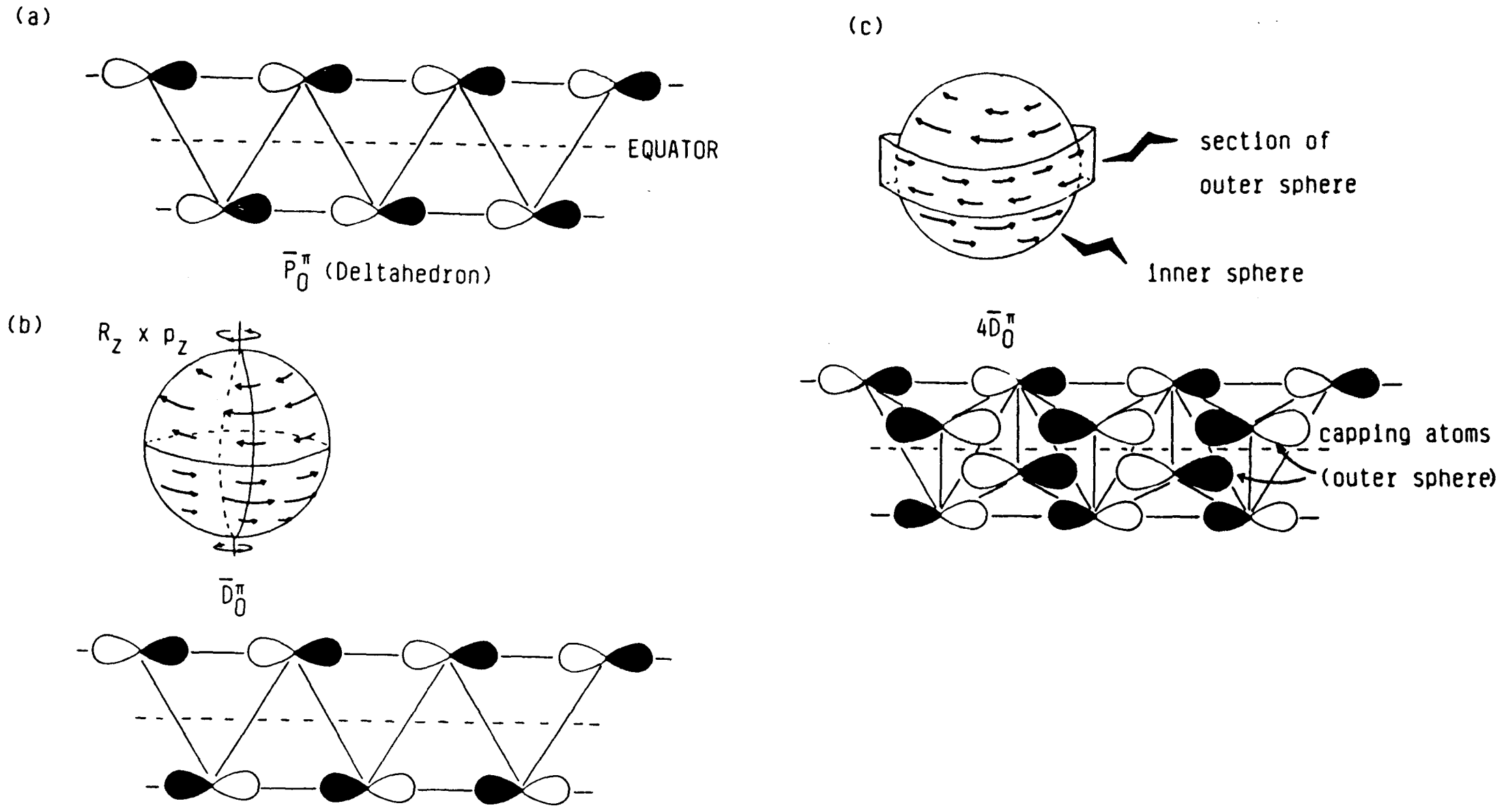


Figure 5.10 $\bar{P}_0^{\pi}$ and $\bar{D}_0^{\pi}$ orbitals for spherical and bispherical clusters based on an antiprismatic (i.e. deltahedral with respect to the equator) inner sphere polyhedron.

interaction across the equator is antibonding, rather than bonding. The LUMO's of the octahedron are $\bar{D}^{\pi}_{0,\pm1}$ (with the octahedron viewed down the threefold axis). **Figure 5.10b** illustrates the $\bar{D}^{\pi}_{0}$ orbital of a deltahedron which is now bonding across the equator (it is strongly antibonding for a 3-connected prism). As **Figure 5.10c** shows, the overlap of this orbital with the $\bar{D}^{\pi}_{0}$ orbital of the outer sphere constitutes a significant bonding interaction. When this interaction is repeated in three dimensions, all three $\bar{D}^{\pi}_{0,\pm1}$ orbitals interact strongly to yield three additional bonding orbitals ($4\bar{D}^{\pi}_{0,\pm1}$ - t_{2u}) and a total of ($V_{\Delta}+4 = 10$) skeletal electron pairs for the octacapped octahedron (see **Figure 5.8**).

Intermediate between the two extremes of bispherical clusters lies the spherical cluster, where all of the cluster atoms lie on the surface of the same sphere. Because the cluster is spherical, its MO's may be adequately described in terms of spherical harmonic functions (L^{σ}, L^{π}, $\bar{L}^{\pi}$ etc.) with no radial nodes.[1] **Figure 5.11** shows that, on merging the inner and outer spheres to create a spherical cluster, the radial nodes are converted into extra angular nodes. The L values of the resulting orbitals depend critically on the disposition of the atoms and, in particular, the number of layers of atoms in the structure.

The L^{π} and $\bar{L}^{\pi}$ skeletal MO's of the octacapped octahedron (bispherical), rhombic dodecahedron (spherical) and hexacapped cube (bispherical) are correlated in **Figure 5.12.** A notable feature of this correlation diagram is the reversal (in both cases) of the bonding character of $3P^{\pi}$ and $3\bar{P}^{\pi}$ on going from the bispherical to the spherical topology. In the spherical cluster, the $3P^{\pi}$ orbitals become bonding (F^{π}), while the $3\bar{P}^{\pi}$ orbitals become antibonding ($\bar{F}^{\pi}$). Going from the hexacapped cube to the rhombic dodecahedron there is, therefore, no

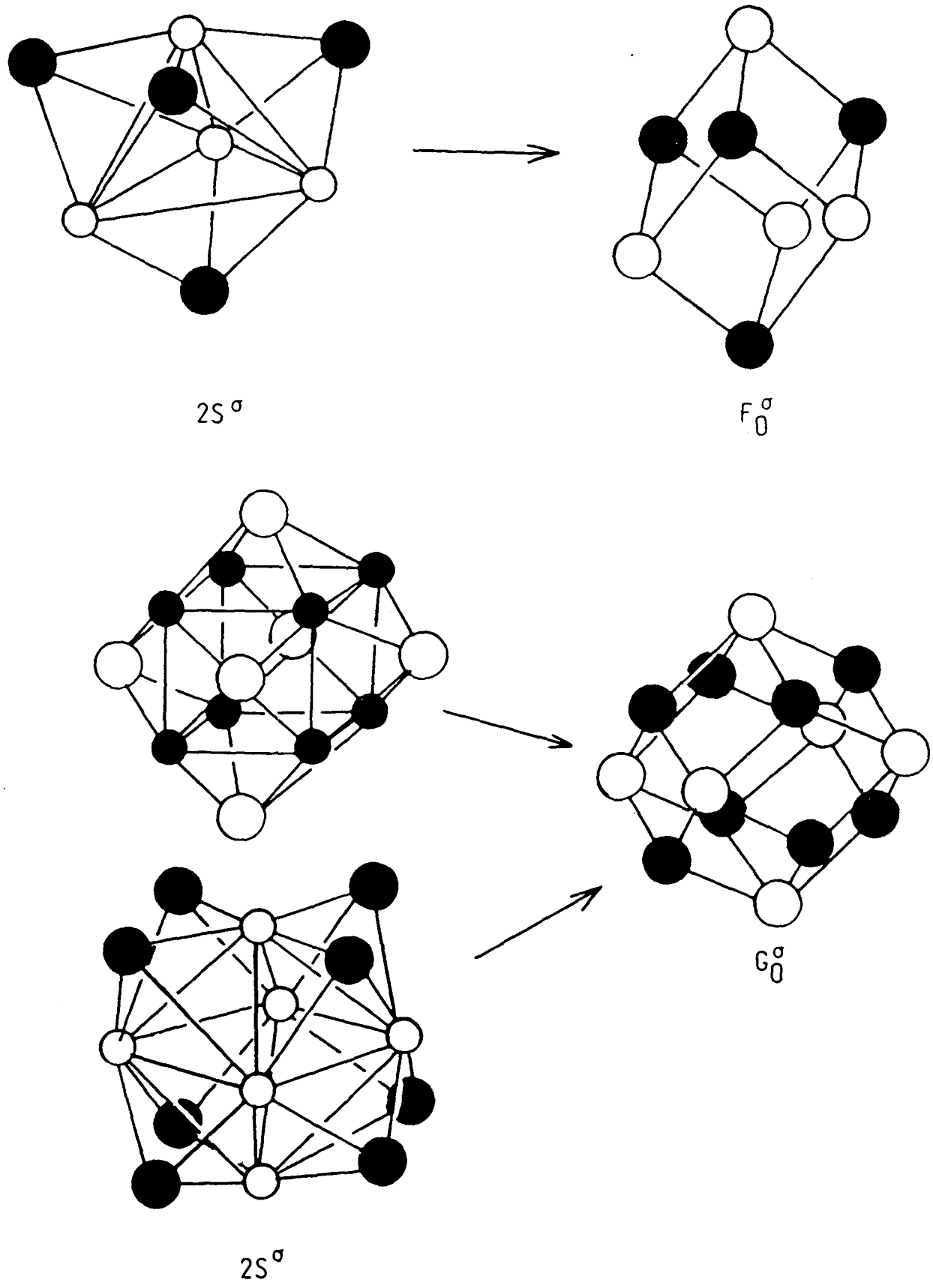


Figure 5.11 The conversion of radial nodes (in cluster MO's) into additional angular nodes on going from bispherical to spherical topology.

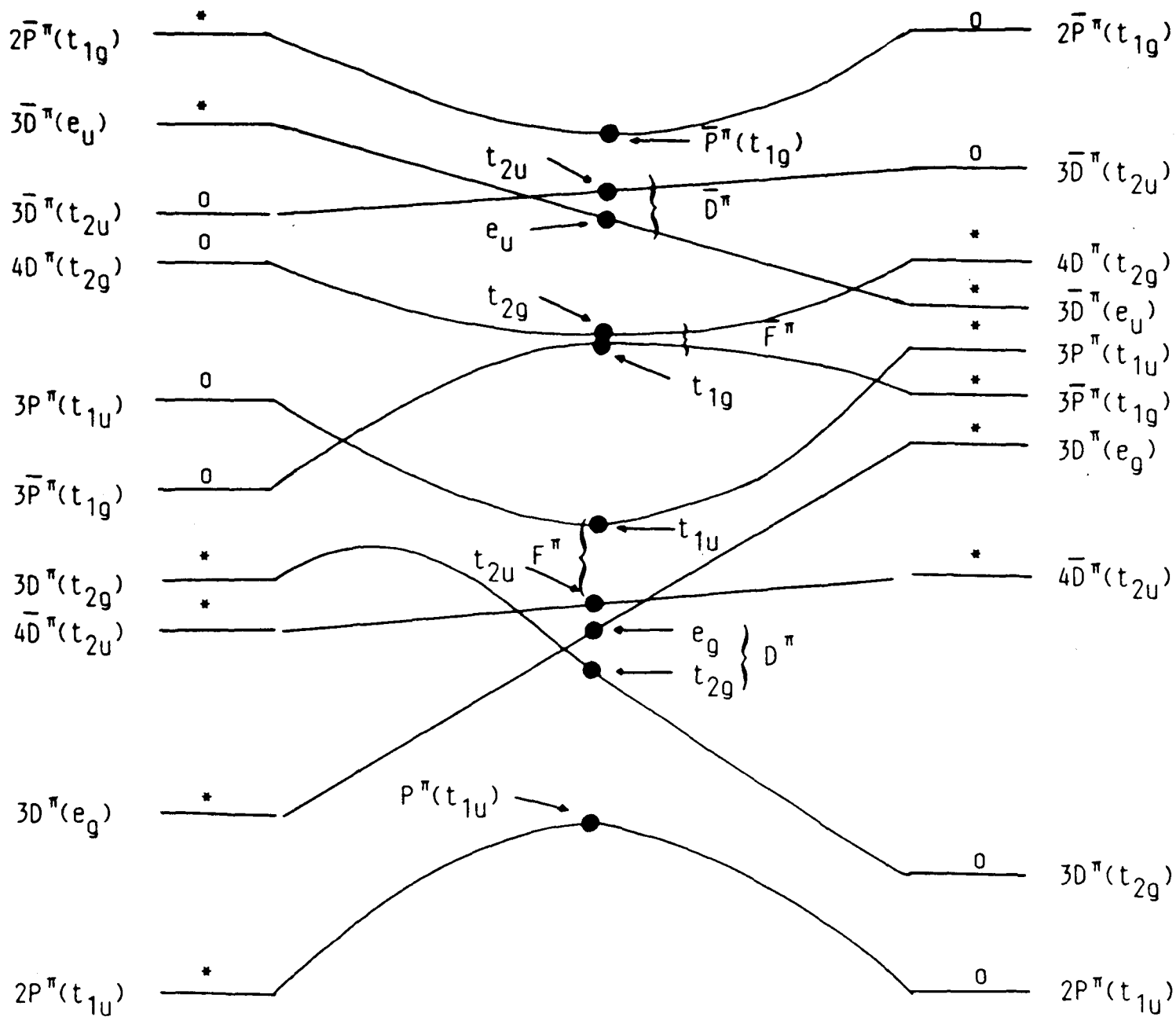


Figure 5.12 Correlation of the L^{π} and $\bar{L}^{\pi}$ skeletal MO's of the (spherical) rhombic dodecahedron with those of the two bispherical extremes (i.e. the hexacapped cube and the octacapped octahedron).

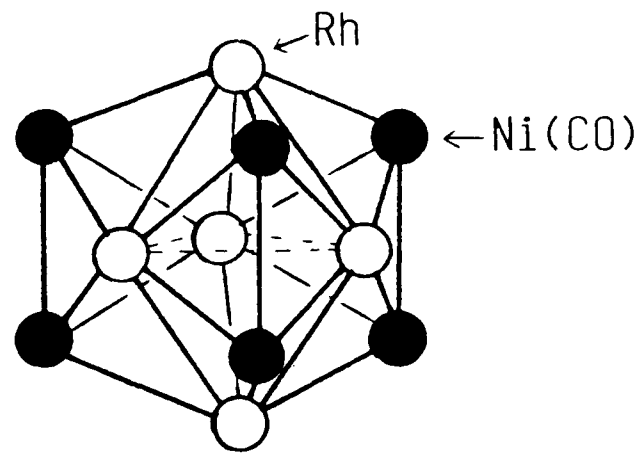
change in the number of skeletal electron pairs: $(3V_3/2)+3 = V_{sph}+1$ (since $V_{sph} = (3V_3/2)+2$) and the spherical polyhedron has the expected (n+1) skeletal electron pair count.[6] On going from the octacapped octahedron to the rhombic dodecahedron five extra orbitals become bonding; $D^{\pi}(e_g$, localised exclusively on the cube atoms) and $3P^{\pi}$ (becoming $F^{\pi}(t_{1u})$).

An example of the spherical situation discussed above is the cluster $[Rh_{15}(CO)_{30}]^{3-}$, which has a rhombic dodecahedral structure, with an additional metal atom at the centre of the cluster.[9] This cluster possesses 198 cluster valence electrons, corresponding to the occupation of 15 (i.e. (n+1), where n is the number of surface atoms) skeletal bonding MO's. The 198 (14n+2) electron count is made up of (2n+2) skeletal bonding electrons and 12 electrons per (outer) metal, which are either non-bonding (localised on the metals), or involved in metal-ligand bonding.[6] The orbitals of the interstitial metal atom interact with those of the cluster in such a way that its electrons are donated to the cluster. The presence of interstitial (main group or transition metal) atoms stabilises more spherical geometries, due to the formation of strong radial bonds.[10]

As mentioned above, omnicapping a 3-connected polyhedron leads to a bispherical cluster with $3P^{\pi}$ and $3\bar{P}^{\pi}$ in the frontier orbital region. On omnicapping a tetrahedral cluster (6 SEP's) and then distorting the bispherical cluster, so that all of the atoms lie on the surface of the same sphere, a cube (rhombic hexahedron) is formed. Cubic clusters (O_h symmetry) are characterised by 12 skeletal electron pairs and the 6 "additional" electron pairs occupy orbitals ($D^{\pi}(t_{2g})$ and $\bar{D}^{\pi}(t_{2u})$), which are roughly non-bonding,[6] and which correspond to the $3P^{\pi}(t_2)$ and

$3\bar{P}^{\pi}(t_1)$ orbitals of the (bispherical) tetracapped tetrahedron (T_d). This should be contrasted with the rhombic dodecahedron which only possesses 3 skeletal electron pairs in excess of the 12 possessed by the cube, from which it is derived. **Table 5.3** gives examples of 3-connected clusters and their (spherical) rhombohedral derivatives, which may be regarded as distorted (bispherical) omnicapped 3-connected polyhedra.

Dahl has recently reported the synthesis and structural characterisation of an unusual bispherical cluster. The paramagnetic anion $[Rh_5Ni_6(CO)_{21}H_x]^{3-}$ (x = odd) has a structure **(1)** which is mid-way between a hexacapped trigonal bipyramid and a pentacapped trigonal prism.[11] This structure is distinct from the the "spherical" rhombic enneahedron illustrated in **Figure 5.4**, since the "vertical" bonds of the original 5-vertex and 6-vertex polyhedra are retained in the 11-vertex polyhedron. This 11-vertex polyhedron is, therefore, a deltahedron with idealised D_{3h} symmetry and two rhodium atoms on the principal (C_3) rotation axis. In terms of the terminology developed in **Chapter 4** the polyhedron **(1)** is a bipolar octadecahedron, i.e. a deltahedral isomer of the more usual C_2-polar octadecahedron discussed in **Chapter 3.**



$[Rh_5Ni_6(CO)_{21}H_x]^{3-}$

(1)

Table 5.3 Rhombohedral clusters as topological composites of 3-connected polyhedra and their deltahedral duals

3-connected polyhedron (3)	**Deltahedron (Δ)**	**Rhombohedron (◇)** *
Tetrahedron (V_3=4)	Tetrahedron (V_Δ=4)	Cube ($V_\diamond$=8)
SEP's = 6 ($3V_3/2$)	SEP's = 6	SEP's = 12 $\{(3V_3/2)+6\}$
e.g. $[Ir_4(CO)_{12}]$ **a**		$[Ni_8(PPh)_6(CO)_8]$ **b**
Trigonal prism (V_3=6)	Trigonal bipyramid (V_Δ=5)	Rhombic enneahedron ($V_\diamond$=11)
SEP's = 9 ($3V_3/2$)	SEP's = 6	SEP's = 12 $\{(3V_3/2)+3\}$?
e.g. $[Rh_6C(CO)_{15}]^{2-}$ **c**	$[Os_5(CO)_{15}]$ **d**	----
Cube (V_3=8)	Octahedron (V_Δ=6)	Rhombic dodecahedron ($V_\diamond$=14)
SEP's = 12 ($3V_3/2$)	SEP's = 7	SEP's = 15 $\{(3V_3/2)+3\}$
e.g. $[Ni_8(PPh)_6(CO)_8]$ **b**	$[Os_6(CO)_{18}]^{2-}$ **e**	$[Rh_{15}(CO)_{30}]^{3-}$ **f**

* Depicted in **Figure 5.4.**

a M.R. Churchill and J.P. Hutchinson, Inorg. Chem., 1978, **17**, 3528.

b L.D. Lower and L.F. Dahl, J. Amer. Chem. Soc., 1976, **98**, 5046.

c V.G. Albano, D. Braga and S. Martinengo, J. Chem. Soc., Dalton Trans., 1981, 717.

d C.R. Eady, B.F.G. Johnson, J. Lewis, B.E. Reichert and G.M. Sheldrick, J. Chem. Soc., Chem. Commun., 1976, 271.

e M. McPartlin, C.R. Eady, B.F.G. Johnson and J. Lewis, J. Chem. Soc., Chem. Commun., 1976, 883.

f J.L. Vidal, L.A. Kapicak and J.M. Troup, J. Organomet. Chem., 1981, **215**, C11.

It is believed that the Rh_5Ni_6 anion has one hydrogen atom (x=1).[11] This would lead to a total of 151 (12n+19) cluster valence electrons, i.e. 9 SEP's. In **Chapter 4** it was concluded that diamagnetic D_{nh} (or D_{nd}) bipolar clusters are generally characterised by (n-1), (n+1) or (n+3) SEP's, so that the Rh_5Ni_6 cluster would appear to have one electron in excess of the (n-1) SEP count.

The 11-vertex polyhedron is significantly distorted from a spherical topology, since the non-bonding Rh-Rh equatorial contacts are quite short (3.103Å), so its description as bispherical is still valid. A more spherical arrangement of atoms would result if these equatorial Rh-Rh contacts were lengthened. **Figure 5.13** indicates that the "spherical" bipolar octadecahedron can be derived from the 15-vertex (D_{3h}) non-polar deltahedron (calculated by Lipscomb to be the favoured structure for the hypothetical borane $[B_{15}H_{15}]^{2-}$),[12] by removing the top and bottom triangles and capping both of the open puckered hexagonal faces.

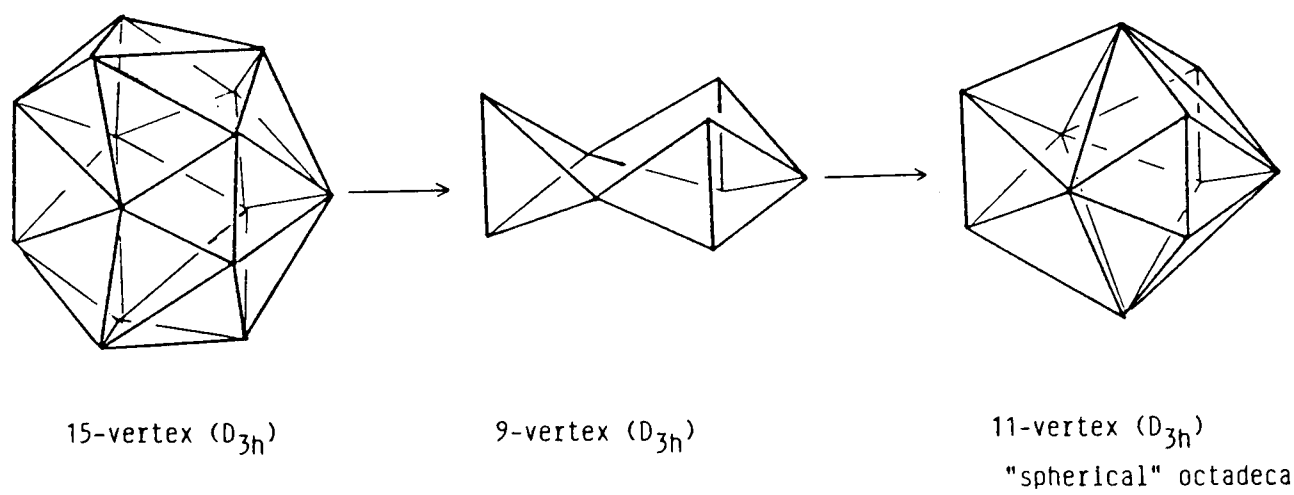


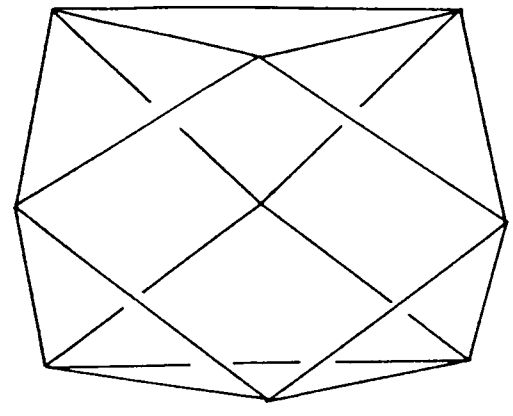
Figure 5.13 Derivation of the "spherical" bipolar octadecahedron from the 15-vertex D_{3h}-deltahedron.

This process is analogous to that described in **Chapter 3,** for obtaining the (hyper-closo) C_3-polar hexadecahedron by capping a hypho-B_9 fragment (derived from the icosahedron).

5.6 Bispherical Clusters with Toroidal Topologies

So far, the discussion has concerned omnicapped polyhedral structures. However, other bispherical polyhedra are known, where the outer sphere consists of a number of atoms which is less than the number of faces of the inner polyhedron. Such examples include edge-bridged polyhedra and capped (but not omnicapped) polyhedra. Bispherical clusters, in which the capping atoms define a planar or puckered ring, may be described as possessing **toroidal** topologies. The non-polar deltahedra discussed in **Chapter 4** belong to this class if they are significantly non-spherical.

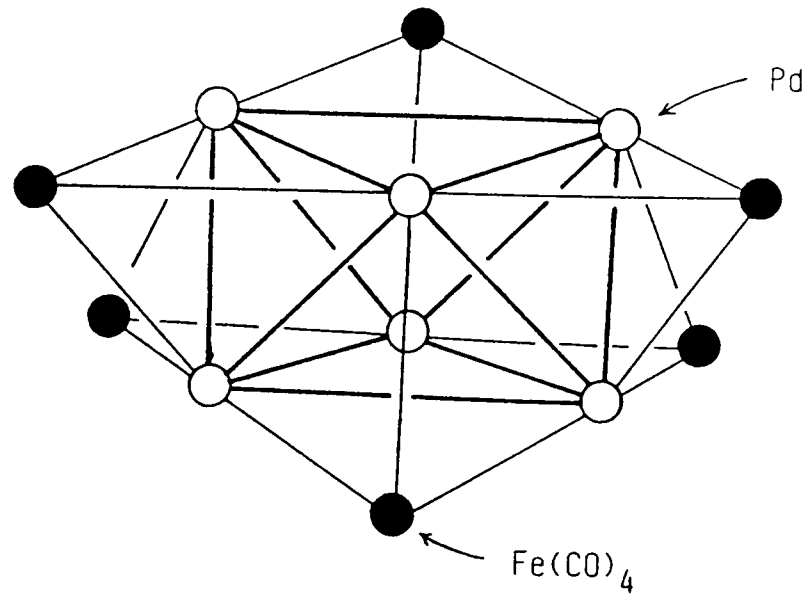
The tricapped trigonal prism is an example of a toroidal bispherical cluster, consisting of a 3-connected inner sphere polyhedron with a planar ring of capping atoms around the equator. In **Chapter 4,** it was shown that the interaction between the $\bar{P}^{\pi}$ orbitals of the two subsets of atoms leads to one component of (what is here defined as) $3\bar{P}^{\pi}$ ($3\bar{P}^{\pi}_0$) becoming weakly bonding while $3P^{\pi}_0$ is weakly antibonding. On forming the spherical (4-connected) polyhedron **(2)** (see **Chapter 2**), by elongating the trigonal prism and drawing in the capping atoms, these two orbitals cross over to make F^{π}_0 (bonding) and $\bar{F}^{\pi}_0$ (antibonding), so that both the bispherical cluster and the spherical cluster possess the same number of skeletal electron pairs; $(3V_3/2)+1 = V_3 + (V_3/2) +1$ (i.e. $V_{sph}+1$), where $(V_3/2)$ is the number of capping atoms around the equator.



(2)

A similar situation pertains to the tetracapped cube, with D_{4h} symmetry, which can be distorted into the 4-connected spherical cuboctahedron (note here the symmetry is actually increased to O_h) with 13 (n+1) skeletal electron pairs, as demonstrated in **Chapter** 2.

Capping an octahedron around the equator yields a bispherical cluster, with an outer sphere of 6 atoms forming a puckered ring. In contrast to the omnicapped octahedron, only one component ($4D_0^{\pi}$) of the $4D^{\pi}$ orbitals is sufficiently bonding to be occupied and a polyhedron with 8 (V_{Δ}+2) skeletal electron pairs results. An example of such a cluster is $[Fe_6Pd_6(CO)_{24}H]^{3-}$ **(3)**.[13]



$[Fe_6Pd_6(CO)_{24}H]^{3-}$

(3)

adopt polyhedral or polygonal (planar or puckered) arrangements and where certain $\bar{L}^{\pi}$ orbitals may be sufficiently stabilised to be occupied, are given in **Table 5.4.** In agreement with the theoretical analysis, those clusters which have an incomplete set of capping atoms either possess the same number of skeletal bonding molecular orbitals as the parent polyhedra, or have an additional electron pair occupying one component of $\bar{L}^{\pi}$.

The only clusters which do not appear to conform to the above analysis are $[Ni_{16}C_4(CO)_{23}]^{4-}$ and $[Pd_{23}(CO)_{22}(PEt_3)_{10}]$ (see **Table 5.4**). The Ni_{16} cluster has a distorted tetracapped cuboctahedral structure[14] and has 4 SEP's in addition to the 13 characteristic of a cuboctahedral cluster. The distortion in this instance may be sufficient for this cluster to be classified as spherical, with (n+1 = 17) SEP's. The Pd_{23} cluster has a trispherical geometry based on a centred cuboctahedron which is capped on all its square faces, so that the capping atoms define an octahedron, and has a set of four edge-bridging PdL_2 groups.[15] If these edge-bridging groups donate 2 electrons to the cluster (thereby forming localised 2-centre-2-electron bonds to the central cuboctahedral unit), then the bispherical cluster which remains would be expected to have 16 SEP's. This electron pair count corresponds to the occupation of the 13 skeletal bonding orbitals of the cuboctahedron and 3 orbitals, which are the bonding combinations of $\bar{D}^{\pi}_{\pm 1,2c}(t_{2u})$ (with the orbitals defined relative to a C_4 axis) on the cuboctahedron and the octahedron $(4\bar{D}^{\pi}_{\pm 1,2c}(t_{2u}))$. The Pd_{23} cluster, however, actually possesses 15 skeletal electron pairs, which is attributable to the lowering of symmetry (to D_{4h}), due to the presence of the four edge-bridging palladium atoms, and the consequent splitting of the $\bar{D}^{\pi}(t_{2u})$ orbitals

Table 5.4 Examples of bispherical clusters (capped structures)

Description	Example	Ref.	n_i	n_o	n_t*	SEP's	Extra SEP's
Octahedron	$[Os_6(CO)_{18}]^{2-}$	**a**	6	0	6	7 (n_i+1)	-
Capped octahedron	$[Os_7(CO)_{21}]$	**b**	6	1	7	7 (n_i+1 = n_t)	0
Bicapped octahedron	$[Os_8(CO)_{22}]^{2-}$	**c**	6	2	8	7 (n_t-1)	0
Tetracapped octahedron	$[Os_{10}C(CO)_{24}]^{2-}$	**d**	6	4	10	7 (n_t-3)	0
	$[Pd_{10}(CO)_{12}(PBu_3)_6]$	**e**	6	4	10	8 (n_i+2)	1
Hexacapped octahedron	$[Pd_6Fe_6(CO)_{23}H]^{3-}$	**f**	6	6	12	8 (n_i+2)	1
Octahedron **	$[Cu_6(PPh_3)_6H_6]$	**g**	6	0	6	6 (n_i)	-
Tetracapped octahedron	$[Cu_6Fe_4(CO)_{16}]^{2-}$	**h**	6	4	10	6 (n_i)	0
	$[Hg_6Rh_4(PMe_3)_{12}]$	**i**	6	4	10	6 (n_i)	0
Cube	$[Ni_8(PPh)_6(CO)_8]$	**j**	8	0	8	12 ($3n_i/2$)	-
Pentacapped cube (centred)	$[Rh_{14}(CO)_{25}]^{4-}$	**k**	8	5	13	12 ($3n_i/2$)	0
	$[Rh_{14}(CO)_{26}]^{2-}$	**l**					
Rhombic dodecahedron/ Hexacapped cube (centred)	$[Rh_{15}(CO)_{30}]^{3-}$	**m**	8	6	14	15 ($\{3n_i/2\}$+3 = n_t+1)	3
Pentagonal prism	$[C_{10}H_{10}]$	**n**	10	0	10	15 ($3n_i/2$)	-
Tetracapped pentagonal prism (centred) *** (2⬡+2◇)	$[Rh_{15}C_2(CO)_{28}]^{-}$	**o**	10	4	14	16 ($\{3n_i/2\}$+1)	1
Square antiprism ****	$[Co_8C(CO)_{18}]^{2-}$	**p**	8	0	8	9 (n_i+1) (closo-)	-
Tetracapped square antiprism (4Δ)	$[Co_3Ni_9C(CO)_{20}]^{3-}$	**q**	8	4	12	10 (n_i+2)	1
Square antiprism	$[Ni_8C(CO)_{16}]^{2-}$	**q**	8	0	8	11 (n_i+3) (arachno-)	-
	$[Bi_8]^{2+}$	**r**	8	0	8	11 (n_i+3) (arachno-)	-
Trigonal prism	$[C_6H_6]$	**s**	6	0	6	9 ($3n_i/2$)	-
	$[Rh_6C(CO)_{15}]^{2-}$	**t**					
Capped (and edge-bridged) trigonal prism (1◇)	$[Rh_8C(CO)_{19}]$	**u**	6	1	7	9 ($3n_i/2$)	0
Bicapped trigonal prism (2Δ)	$[Cu_2Rh_6C(CO)_{15}(NCCH_3)_2]$	**v**	6	2	8	9 ($3n_i/2$)	0
Tricapped trigonal prism (3◇)	$[B_9H_9]^{2-}$	**w**	6	3	9	10 ($\{3n_i/2\}$+1 = n_t+1)	1
	$[TlSn_8]^{3-}$	**x**					
	$[Bi_9]^{5+}$ *****	**y**	6	3	9	11 ($\{3n_i/2\}$+2 = n_t+2)	2
Square-face-sharing fused trigonal prisms (A)	$[Co_6Ni_2C_2(CO)_{16}]^{2-}$	**z**	8	0	8	10	-
Bicapped A	$[Ni_{10}C_2(CO)_{16}]^{2-}$	**aa**	8	2	10	11	1
Twinned-cuboctahedron (centred)	$[Rh_{13}(CO)_{24}H_{(5-n)}]^{n-}$	**bb**	12	0	12	13 (n_i+1)	-
Cuboctahedron			12	0	12	13 (n_i+1)	-
Distorted tetracapped cuboctahedron (4◇)	$[Ni_{16}C_4(CO)_{23}]^{4-}$	**cc**	12	4	16	17 (n_i+5 = n_t+1)	4
Hexacapped (and edge-bridged) cuboctahedron (centred) (6◇)	$[Pd_{23}(CO)_{22}(PEt_3)_{10}]$	**dd**	12	6	18	15 (n_i+3)	2

Table 5.4 (continued)

* n_1 = number of inner sphere atoms (central core)

n_o = number of outer sphere (capping) atoms (not counting edge-bridging groups which form essentially localised 2-centre-2-electron bonds to the inner sphere polyhedron)

n_t = total number of cluster atoms (not counting central/interstitial atoms or edge-bridging atoms, which donate all of their valence electrons to the cluster)

** Polyhedral clusters of the group IB and IIB metals generally have one skeletal electron pair less than normal. Octahedral clusters of this type are therefore characterised by 84 cluster valence electrons. Another example of a bispherical cluster based on an 84 electron octahedron is $[Ag_6\{Fe(CO)_4\}_3(Ph_2P)_3CH]$ which has three faces capped by $Fe(CO)_4$ groups and the other capped by a tripodal phosphine ligand (C.E. Briant, R.G. Smith and D.M.P. Mingos, J. Chem. Soc., Chem. Commun., 1984, 586).

*** The numbers in brackets refer to the number and type of face which is capped, in those cases where the inner sphere polyhedron possesses more than one type of face.

**** The square antiprism (see **Chapter 2**) may be regarded as either a 4-connected polyhedron (in which case it should possess n+1=9 SEP's as for a closo cluster) or an arachno species (characterised by n+3=11 SEP's).

***** For the $[Bi_9]^{5+}$ cluster (see **Chapter 4**) both $3\bar{P}_0^{\pi}$ and $3P_0^{\pi}$ are occupied ($3P_0^{\pi}$ is a fairly low lying LUMO for $[B_9H_9]^{2-}$).

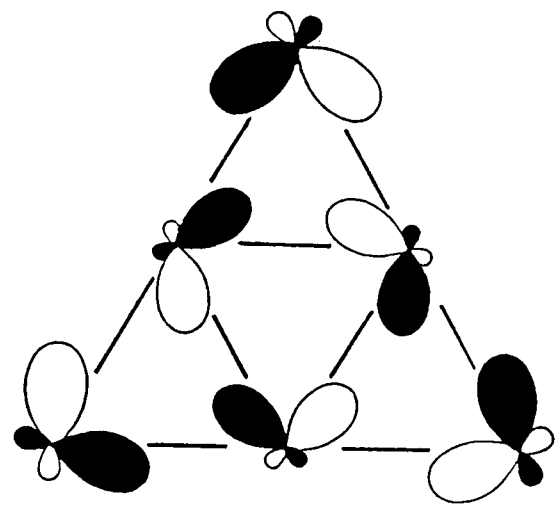
a M. McPartlin, C.R. Eady, B.F.G. Johnson and J. Lewis, J. Chem. Soc., Chem. Commun., 1976, 883. **b** C.R. Eady, B.F.G. Johnson, J. Lewis, R. Mason, P.B. Hitchcock and K.M. Thomas, J. Chem. Soc., Chem. Commun., 1977, 385. **c** P.F. Jackson, B.F.G. Johnson, J. Lewis and P.R. Raithby, J. Chem. Soc., Chem. Commun., 1980, 60. **d** P.F. Jackson, B.F.G. Johnson, J. Lewis, W.J.H. Nelson and M. McPartlin, J. Chem. Soc., Dalton Trans., 1982, 2099. **e** E.G. Mednikov, N.K. Eremenko, S.P. Gubin, Yu.L. Slovokhotov and Yu.T. Struchkov, J. Organomet. Chem., 1982, **239**, 401. **f** G. Longoni, M. Manassero and M. Sansoni, J. Amer. Chem. Soc., 1980, **102**, 3242. **g** M.R. Churchill, S.A. Bezman, J.A. Osborn and J. Wormald, Inorg. Chem., 1972, **11**, 1818. **h** G. Doyle, B.T. Heaton and E. Ochiello, Organometallics, 1985, **4**, 1224; G. Doyle, K.A. Eriksen and D. van Engen, J. Amer. Chem. Soc., 1986, **108**, 445. **i** R.A. Jones, F.M. Real, G. Wilkinson, A.M.R. Galas and M.B. Hursthouse, J. Chem. Soc., Dalton Trans., 1981, 126. **j** L.D. Lower and L.F. Dahl, J. Amer. Chem. Soc., 1976, **98**, 5046. **k** G. Ciani, A. Sironi and S. Martinengo, J. Organomet. Chem., 1980, **192**, C42. **l** S. Martinengo, G. Ciani and A. Sironi, J. Chem. Soc., Chem. Commun., 1980, 1140. **m** J.L. Vidal, L.A. Kapicak and J.M. Troup, J. Organomet. Chem., 1981, **215**, C11. **n** P.E. Eaton, Y.S. Or and S.J. Branca, J. Amer. Chem. Soc., 1981, **103**, 2134. **o** V.G. Albano, M. Sansoni, P. Chini, S. Martinengo and D. Strumulo, J. Chem. Soc., Dalton Trans., 1976, 970. **p** V.G. Albano, P. Chini, G. Ciani, S. Martinengo and M. Sansoni, J. Chem. Soc., Dalton Trans., 1978, 463. **q** G. Longoni, A. Ceriotti, R. Della Pergola, M. Manassero, M. Perego, G. Piro and M. Sansoni, Phil. Trans. R. Soc. Lond., 1982, A308, 47. **r** J.D. Corbett, Inorg. Chem., 1968, **7**, 198; B. Krebs, M. Hucke and C.J. Brendel, Angew. Chem. Int. Edn. Engl., 1982, **21**, 445. **s** T.J. Katz and N. Acton, J. Amer. Chem. Soc., 1973, **95**, 2738. **t** V.G. Albano, D. Braga and S. Martinengo, J. Chem. Soc., Dalton Trans., 1981, 717. **u** P.R. Raithby, in "Transition Metal Clusters" (Ed. B.F.G. Johnson), Wiley, New York, 1980, Ch. 2 p. 63. **v** V. G. Albano, D. Braga, S. Martinengo, P. Chini, M. Sansoni and D. Strumulo, J. Chem. Soc., Dalton Trans., 1980, 52. **w** F. Klanberg and E.L. Muetterties, Inorg. Chem., 1966, **5**, 1955. **x** R.C. Burns and J.D. Corbett, J. Amer. Chem. Soc., 1982, **104**, 2804. **y** A. Herschaft and J.D. Corbett, Inorg. Chem., 1963, **2**, 979; R.M. Friedman and J.D. Corbett, Inorg. Chim. Acta., 1973, **7**, 525. **z** A. Arrigoni, A. Ceriotti, R. Della Pergola, G. Longoni, M. Manassero, N. Masciocchi and M. Sansoni, Angew. Chem. Int. Edn. Engl., 1984, **23**, 322. **aa** A. Ceriotti, G. Longoni, M. Manassero, N. Masciocchi, L. Resconi and M. Sansoni, J. Chem. Soc., Chem. Commun., 1985, 181. **bb** G. Ciani, A. Sironi and S. Martinengo, J. Chem. Soc., Dalton Trans., 1981, 519. **cc** A. Ceriotti, G. Longoni, M. Manassero, N. Masciocchi, G. Piro, L. Resconi and M. Sansoni, J. Chem. Soc., Chem. Commun., 1985, 1402. **dd** E.G. Mednikov, N.K. Eremenko, Yu.L. Slovokhotov and Yu.T. Struchkov, J. Organomet. Chem., 1986, **301**, C35.

into e_u and b_{2u}.

In those clusters where a ring of capping atoms exists but no "new" skeletal bonding orbitals are introduced, facile 2-electron electrochemical reduction processes might reasonably be expected.

5.7 Raft Clusters

Raft clusters may be described as a sub-class of bi- (or multi-) spherical clusters, where all of the atoms of the inner and outer spheres lie (in concentric rings) in one plane. Mingos and Evans have identified the LUMO in 90 electron $[Os_6(CO)_{17}(P(OMe)_3)_4]$ [16] as being low lying and of a_2' symmetry (4).[17] In terms of bispherical TSH functions, this orbital may be identified as $3\bar{P}_0^{\pi}$ (as in the case of the tricapped trigonal prism). If this orbital is unoccupied, then a 90 electron cluster results (arising from the 48 electrons characteristic of a triangle and 42 electrons (3 x 14) corresponding to the 14 electrons in metal-carbonyl bonding and metal (d) non-bonding orbitals associated with the outer metal atoms).



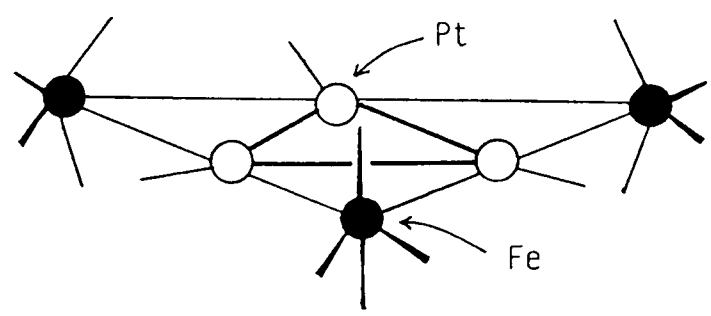
$3\bar{P}_0^{\pi}$ (a_2')

(4)

Occupation of $3\bar{P}_0^{\pi}$ leads to a 92 electron cluster, which is based on a 50 electron triangular unit. Such a 92 electron raft cluster has been

prepared by the reduction of a 90 electron molecule.[20]

Another example of this class of cluster is the platinum-iron raft $[Fe_3Pt_3(CO)_{15}]^{2-}$ **(5)**,[19] which has 86 cluster valence electrons, consisting of 44 electrons for the (inner) $Pt_3(CO)_3$ triangle and 42 electrons (14 from each $Fe(CO)_4$ unit) for the outer ring.

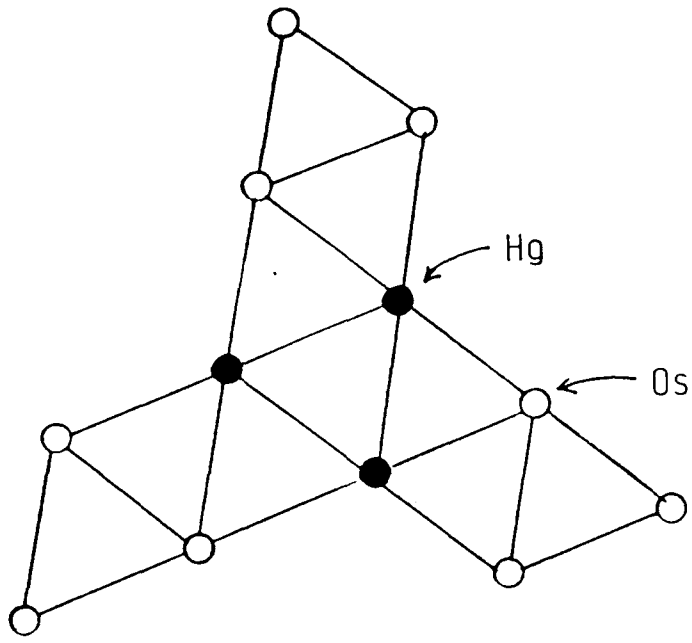


$[Fe_3Pt_3(CO)_{15}]^{2-}$

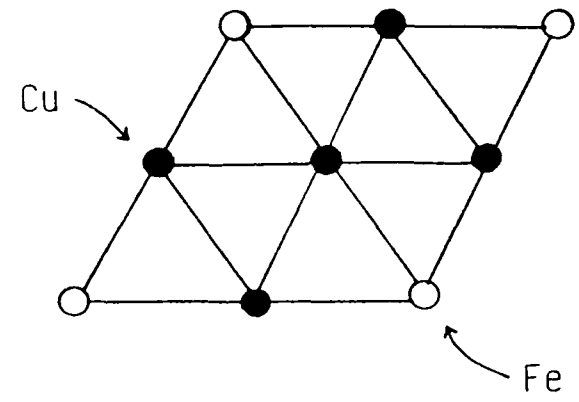
(5)

The characteristic electron count for a Pt_3L_3 triangle is 42, so this cluster has an additional pair of electrons which again reside in the $3\bar{P}_0^{\pi}$ orbital.[17] However, the raft cluster $[Fe_3Cu_3(CO)_{12}]^{3-}$, which has $Fe(CO)_4$ groups bridging a Cu_3 triangle,[20] only possesses 84 cluster valence electrons. This may be explained in terms of the $3\bar{P}_0^{\pi}$ orbital being inaccessible for Cu, because it possesses more (high lying) p^{π} atomic orbital character than in the Pt case, where the terminal CO ligand induces d^{π}-p^{π} mixing.

Extended raft clusters are also known. These clusters may be described in terms of metal atoms which lie on a number of concentric rings, sometimes with a metal atom at the centre (origin) of the ring system. Examples of such clusters are $[Os_3(CO)_{11}Hg]_3$ **(6a)**[21] and $[Cu_5Fe_4(CO)_{16}]^{3-}$ **(6b)**.[20]



$[Os_3(CO)_{11}Hg]_3$



$[Cu_5Fe_4(CO)_{16}]^{3-}$

Metal skeletons of two extended raft clusters

(6a) (6b)

5.8 Bispherical Clusters with Interstitial Metal Atoms and Cluster Units

Particularly interesting examples of bi- and multi-spherical clusters are those molecules in which one cluster unit is completely encapsulated within another cluster polyhedron. Generally, the number of outer sphere atoms is larger than the number of faces of the internal (interstitial) polyhedron. The valence electron counts of such clusters have been rationalised, by Mingos, in terms of the orbitals of the outer sphere (surface) atoms replacing the ligands of the inner sphere (encapsulated) atoms.[22]

In clusters where the tangential L^{π} orbitals of the outer sphere polyhedron are empty, i.e. where radial bonding dominates, the electron count is equal to $(12n_s+\Delta_i)$, where n_s is the number of surface atoms and Δ_i is the electron count characteristic of the interior atom, dimer or

cluster. The simplest example is that of a cluster with a single atom at the centre, such as those found among the cluster compounds of gold.[23] Mingos has shown that these clusters are characterised by either $(12n_s+16)$ or $(12n_s+18)$ cluster valence electrons, depending on whether the outer atoms adopt a toroidal or spherical topology.[24] For larger interstitial units the characteristic electron counts are: dimer 32; triangle 48; linear or bent trimer (with only 2 M-M bonds) 50; tetrahedron 60; butterfly 62; octahedron 86 etc.[20] Examples of molecules which possess one cluster unit within another are presented in **Table 5.5**, along with their electron counts, and examples of the structures adopted by these molecules are illustrated in **Figure 5.14.** Although most clusters obey the $(12n_s+\Delta_i)$ rule, there are a number of exceptions. The cluster $[Pt_{26}(CO)_{32}]^{2-}$, for instance, possesses an encapsulated triangle of metal atoms,[25] but is characterised by $(12n_s+50)$, rather than the predicted $(12n_s+48)$, electrons. As in the case of the raft clusters discussed in **Section 5.7**, the "extra" electron pair resides in an MO which is based on the $\bar{P}\pi$ orbital of the central triangle and which is stabilised by interaction with the outer sphere atoms.

Other high nuclearity clusters are known which possess electrons in excess of the $(12n_s+\Delta_i)$ rule. These are the smaller clusters, i.e. those with a single interstitial atom, where the high ratio of ligands to surface atoms leads to the donation of electron density from the ligands to the outer sphere L^{π} orbitals.[20b] In some cases the L^{π} band is fully occupied and cluster valence electron counts of $(14n_s+2)$ result. Examples of this type of molecule are the centred twinned cuboctahedral cluster $[Rh_{13}(CO)_{24}H_{(5-n)}]^{n-}$ [26] and the centred rhombic dodecahedral cluster $[Rh_{15}(CO)_{30}]^{3-}$ discussed previously.[9]

The occurrence of heterometallic medium and high nuclearity

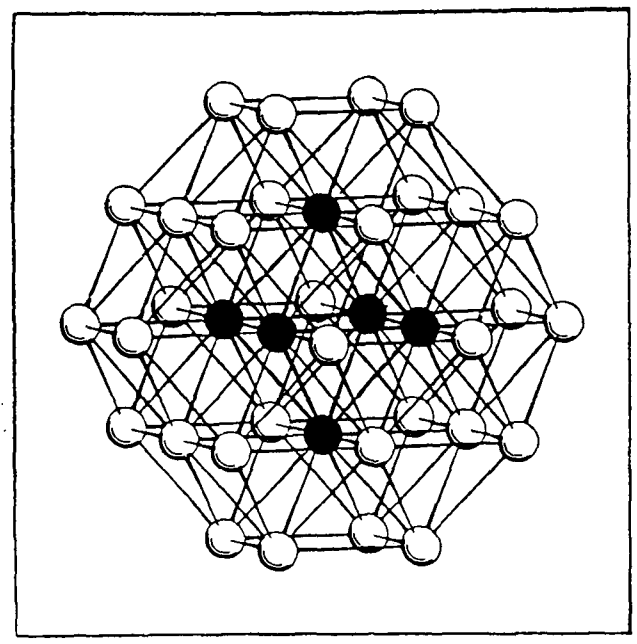
Table 5.5 Examples of high nuclearity cluster compounds where radial metal-metal bonding interactions predominate

Cluster	Ref.	n_i	n_s*	Structure	Electron count	
$[Au_9(PPh_3)_8]^+$	**a**	1	8	b.c.c.	114	
$[Au_{11}I_3(PPh_3)_7]$	**b**	1	10	b.c.c./i.c.p.[j]	138	$(12n_s+18)$
$[Au_{13}Cl_2(PMePh_2)_{10}]^{3+}$	**c**	1	12	i.c.p.	162	
$[Pt_{19}(CO)_{22}]^{4-}$	**d**	2	17	i.c.p.	238	$(12n_s+34)$
$[Rh_{22}(CO)_{35}H_{(5-q-m)}]^{q-}$	**e**	2	20	c.c.p./b.c.c.	(273+m)[k]	
$[Au_{13}Ag_{12}Cl_6(PPh_3)_{12}]^{m+}$	**f**	3	22	i.c.p.	(317-m)	$(12n_s+50)$[l]
$[Pt_{26}(CO)_{32}]^{2-}$	**g**	3	23	h.c.p.	326	$(12n_s+50)$[m]
$[Ni_{38}Pt_6(CO)_{48}H_{(6-n)}]^{n-}$	**h**	6	38	c.c.p.	542	$(12n_s+50)$[n]
$[Pt_{38}(CO)_{44}H_m]^{2-}$	**i**	6	32	c.c.p.	(470+m)[o]	

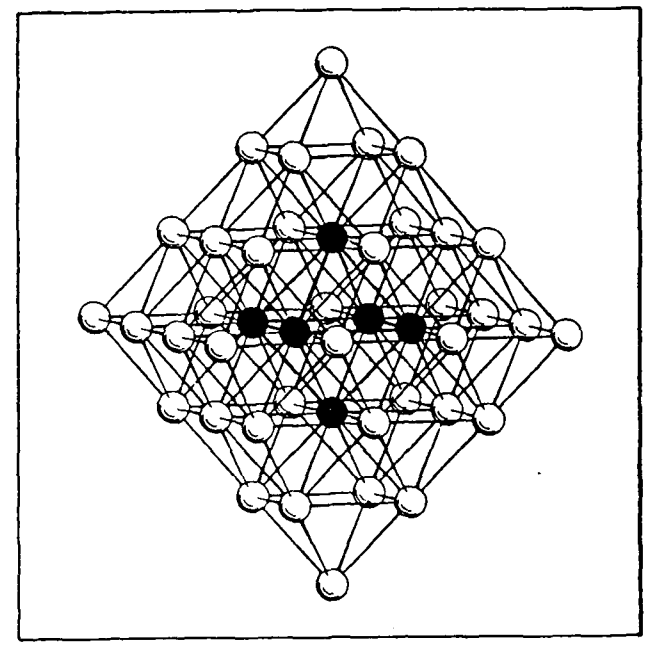
* n_i = number of interstitial (inner sphere) atoms

n_s = number of surface (outer sphere) atoms

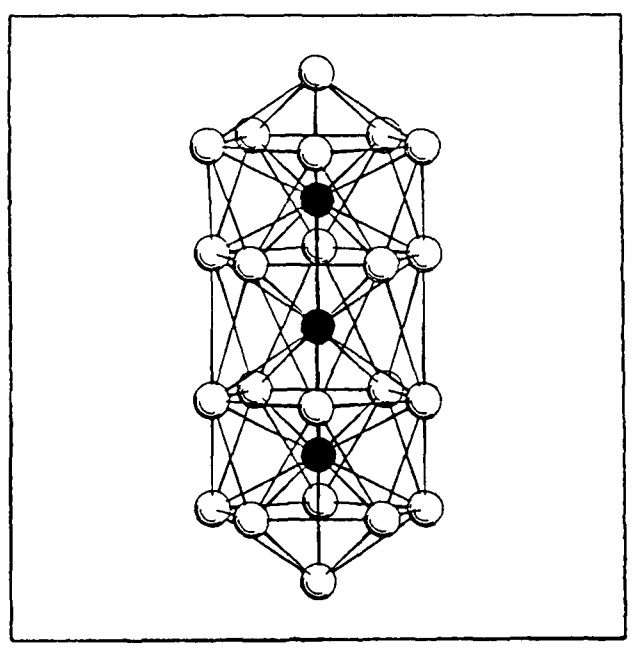
a J.G.M. van der Linden, M.L.H. Paulissen and J.E.J. Schmitz, J. Amer. Chem. Soc., 1983, 105, 1903. **b** J.M.M. Smits, P.T. Burskens, J.W.A. van der Velden and J.J. Bau, J. Cryst. Spectrosc. Res., 1983, 13, 373. **c** C.E. Briant, B.R.C. Theobald, J.W. White, L.K. Bell and D.M.P. Mingos, J. Chem. Soc., Chem. Commun., 1981, 201. **d** D.M. Washecheck, E.J. Wucherer, L.F. Dahl, A. Ceriotti, G. Longoni, M. Manassero, M. Sansoni and P. Chini, J. Amer. Chem. Soc., 1979, **101**, 6110. **e** J.L. Vidal, R.C. Schoening and J.M. Troup, Inorg. Chem., 1981, **20**, 227. **f** B.K. Teo and K. Keating, J. Amer. Chem. Soc., 1984, **106**, 2224. **g** D.M. Washecheck, A. Ceriotti, P. Chini, G. Longoni and L.F. Dahl, personal communication. **h** (n = 4 or 5) A. Ceriotti, F. Demartin, G. Longoni, M. Manassero, M. Marchionna, G. Piva and M. Sansoni, Angew. Chem., Int. Edn. Engl., 1985, **24**, 697. **i** D.M. Washecheck, A. Ceriotti, M.A. Murphy, D.A. Nagaki, P. Chini, G. Longoni and L.F. Dahl, personal communication. **j** i.c.p. = "icosahedral close packing", a term used to denote high nuclearity clusters with 5-fold symmetry (D.M.P. Mingos, Chem. Soc. Rev., 1986, **15**, 31. **k** If m=1 this cluster possesses 274 $(12n_s+34)$ valence electrons. **l** Linear trimeric interstitial moiety. If m=3 this cluster possesses 314 $(12n_s+50)$ valence electrons. **m** Triangular interstitial moiety. **n** Octahedral interstitial moiety. **o** If m=0 this cluster possesses 470 $(12n_s+86)$ valence electrons.



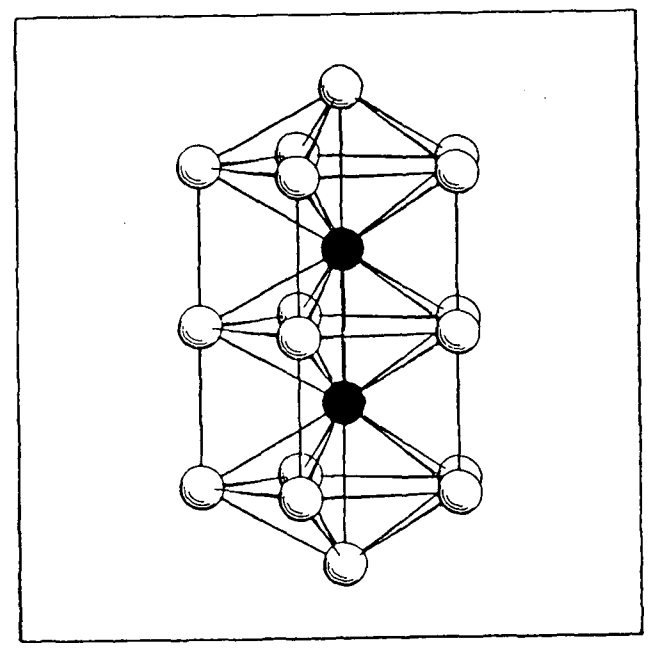
$[Pt_{38}(CO)_{44}H_m]^{2-}$
(c.c.p.)



$[Ni_{38}Pt_6(CO)_{48}H_{(6-n)}]^{n-}$
(c.c.p.)



$[Au_{13}Ag_{12}Cl_6(PPh_3)_{12}]^{m+}$
(i.c.p.)



$[Pt_{19}(CO)_{22}]^{4-}$
(i.c.p.)

Figure 5.14 Examples of high nuclearity bispherical clusters, with interstitial metal atoms and cluster units, where radial metal-metal bonding predominates.

bispherical clusters necessitates the rationalisation of which metal's atoms lie on the inner sphere (i.e. form the kernel of the cluster) and which lie on the outer sphere (i.e. form the surface layer). Dahl has noted that in such clusters the inner sphere atoms are generally those which form the strongest homonuclear metal-metal bonds.[11] The maximisation of strong homonuclear bonds, along with the maximisation of the numbers of all types of metal-metal bonds (i.e. the formation of deltahedral structures), is considered to be the dominant feature which minimises the total energy of the structure. Dahl has used this idea to rationalise the structures of the, above mentioned, Rh_5Ni_6 cluster (**1**) (where the Rh_5 unit forms the cluster kernel),[11] as well as the hexacapped octahedral cluster $[Pd_6Fe_6(CO)_{24}H]^{3-}$ (**3**)[13] and the $[Pt_6Ni_{38}(CO)_{52}H_{(6-n)}]^{n-}$ anions, which (see **Figure 5.14**) possess a Pt_6 octahedral core.[27] Similar arguments, formulated in terms of an inner kernel of atoms of the metal with the higher heat of sublimation and a surface layer of atoms of the metal with the lower heat of sublimation, have been invoked to rationalise the structures of a number of heterogeneous bimetallic catalysts and immiscible alloys.[28]

5.9 Summary

In this Chapter, the L^{σ}, L^{π} and $\bar{L}^{\pi}$ skeletal MO's of bispherical clusters have been derived from those of the constituent spherical polyhedra. It has been shown that the addition of successive spherical shells leads to skeletal MO's with radial, as well as angular, nodes. On deforming bispherical clusters into a spherical topology these radial nodes are converted into additional angular nodes.

In the bispherical extreme, clusters are characterised by an SEP

count which corresponds to the occupation of the bonding MO's of the inner polyhedron and certain orbitals (predominantly localised on the outer sphere), which are lowered due to a bonding interaction between the $\bar{L}^{\pi}$ MO's of the two polyhedra. The number of additional skeletal bonding MO's depends upon the topology of the atoms lying on the outer sphere and the mismatch in symmetry between the L^{π} orbitals of the inner sphere polyhedron and the $\bar{L}^{\pi}$ orbitals of the outer sphere polyhedron. In the case where the outer sphere polyhedral topology is spherical 3 additional orbitals are generally stabilised. These orbitals are $\bar{P}^{\pi}$ if the central poyhedron is 3-connected and $\bar{D}^{\pi}$, $\bar{F}^{\pi}$ etc., if it is a deltahedron. If, however, the topology of the outer sphere atoms is toroidal (planar or puckered rings) only one component of these orbitals is lowered. These concepts have also been applied to the study of planar raft clusters, where again only one additional orbital ($\bar{P}_0^{\pi}$) is stabilised.

A rhombohedral "spherical" cluster lies at the midpoint between the two (omnicapped) bispherical extremes. This cluster is characterised by (n+1) skeletal electron pairs and its molecular orbitals may be correlated with those of the bispherical clusters.

It has been shown that the bispherical cluster methodology may be applied to high nuclearity clusters which have a metal atom or cluster unit, which is completely encapsulated within a larger cluster. It is possible to envisage the extension of this approach to include, as yet unsynthesised, high nuclearity compounds consisting of a cluster, (A), which is completely encapsulated by a second cluster, (B), which in turn is completely encapsulated by a third cluster, (C), and so on. In this way, it should be possible to describe bulk metals as "**polyspherical**

clusters", centred on a single atom in a cubic (b.c.c.), cuboctahedral (c.c.p.) or twinned cuboctahedral (h.c.p.) environment. In two dimensions, infinite rafts of metal atoms may be treated in an analogous fashion.

References for Chapter Five

1. A.J. Stone, Mol. Phys., 1980, **41**, 1339; A.J. Stone, Inorg. Chem., 1981, **20**, 563; A.J. Stone and M.J. Alderton, Inorg. Chem., 1982, **21**, 2297; A.J. Stone, Polyhedron, 1984, **3**, 2051.
2. D.B. Redmond, C.M. Quinn and J.G.R. McKiernan, J. Chem. Soc., Faraday Trans. II, 1983, **79**, 1791; A. Ceulemans, Mol. Phys., 1985, **54**, 161; P.W. Fowler, Polyhedron, 1985, **4**, 2051.
3. For a discussion of graph theoretical aspects of duality see: R.J. Wilson, "Introduction to Graph Theory" (3rd. Edn.), Longman, New York, 1985, Ch.5 p.59. For a discussion of duality in solid geometry see Ref. 4.
4. H.M. Cundy and A.P. Rollett, "Mathematical Models" (3rd. Edn.), Tarquin Pub., U.K., 1981.
5. J.M. Schulman, C.R. Fischer, P. Solomon and T.J. Venanzi, J. Amer. Chem. Soc., 1978, **100**, 2949.
6. K. Wade, J. Chem. Soc., Chem. Commun., 1971, 792; Inorg. Nucl. Chem. Lett., 1972, **8**, 559, 563; Adv. Inorg. Chem. Radiochem., 1976, **18**, 1; D.M.P. Mingos, Nature, Phys. Sci. (London), 1972, **236**, 99.
7. See, for example: W.G.Richards and P.R. Scott, "Structure and Spectra of Atoms", Wiley, London, 1976.
8. R. Mason, K.M. Thomas and D.M.P. Mingos, J. Amer. Chem. Soc., 1973, **95**, 3802; M.I. Forsyth and D.M.P. Mingos, J. Chem. Soc., Dalton Trans., 1977, 610.
9. J.L. Vidal, L.A. Kapicak and J.M. Troup, J. Organomet. Chem., 1981, **215**, C11.
10. See, for example: S.D. Wijeyskera and R. Hoffmann, Organometallics, 1984, **3**, 962.

11. D.A. Nagaki, J.V. Badding, A.M. Stacy and L.F. Dahl, J. Amer. Chem. Soc., 1986, **108**, 3825.

12. L.D. Brown and W.N. Lipscomb, Inorg. Chem., 1977, **16**, 2989; J. Bicerano, D.S. Marynick and W.N. Lipscomb, Inorg. Chem., 1978, **17**, 2041, 3443.

13. G. Longoni, M. Manaserro and M. Sansoni, J. Amer. Chem. Soc., 1980, **102**, 3242.

14. A. Ceriotti, G. Longoni, M. Nanassero, N. Masciocchi, L. Resconi and M. Sansoni, J. Chem. Soc., Chem. Commun., 1985, 1402.

15. E.G. Mednikov, N.K. Eremenko, Yu.L. Slovokhotov and Yu.T. Struchkov, J. Organomet. Chem., 1986, **301**, C35.

16. R.J. Goudsmit, B.F.G. Johnson, J. Lewis, P.R. Raithby and K.H. Whitmire, J. Chem. Soc., Chem. Commun., 1982, 640.

17. D.G. Evans and D.M.P. Mingos, Organometallics, 1983, **2**, 435.

18. J.G. Jeffrey, Ph.D. Thesis, Cambridge University, 1985.

19. G. Longoni, M. Manaserro and M. Sansoni, J. Amer. Chem. Soc., 1980, **102**, 7973.

20. G. Doyle, K.A. Eriksen and D. Van Engen, J. Amer. Chem. Soc., 1986, **108**, 445.

21. M. Fajardo, H.D. Holden, B.F.G. Johnson, J. Lewis and P.R. Raithby, J. Chem. Soc., Chem. Commun., 1984, 24.

22. (a) D.M.P. Mingos, J. Chem. Soc., Chem. Commun., 1985, 1352.
(b) D.M.P. Mingos, Chem. Soc. Rev., 1986, **15**, 31.

23. K.P. Hall and D.M.P. Mingos, Prog. Inorg. Chem., 1984, **32**, 237 and references therein.

24. K.P. Hall, D.I. Gilmour and D.M.P. Mingos, J. Organomet. Chem., 1984, **268**, 275; D.M.P. Mingos, Polyhedron, 1984, **3**, 1289.

25. D.M. Washecheck, A. Ceriotti, P. Chini, G. Longoni and L.F. Dahl,

personal communication cited in Ref. 20b.

26. G. Ciani, A. Sironi and S. Martinengo, J. Chem. Soc., Dalton Trans., 1981, 519.

27. A. Ceriotti, F. Demartin, G. Longoni, M. Manassero, M. Marchionna, G. Piva and M. Sansoni, Angew. Chem., Int. Edn. Engl., 1985, 24, 697.

28. See, for example:J.W.A. Sachtler and G.A. Somorjai, J. Catal., 1983, 81, 77; F.J.C.M. Toolenaar, A.G.T.M. Bastein and V. Ponec, J. Catal., 1983, 82, 35; J.H. Sinfelt, "Bimetallic Catalysts: Discoveries, Concepts and Applications", Wiley, New York, 1983; J.H. Sinfelt, Sci. Am., 1985, 253, 90 and references therein.

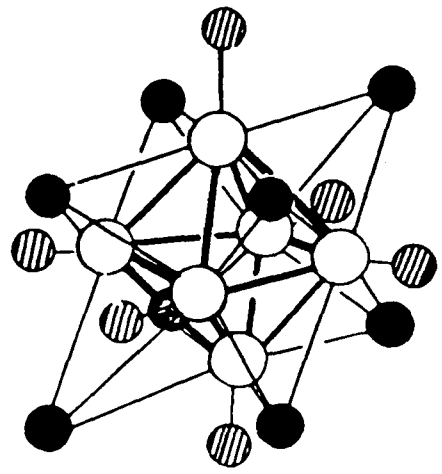
CHAPTER SIX

π-DONOR-BRIDGED TRANSITION METAL CLUSTERS

6.1 Introduction

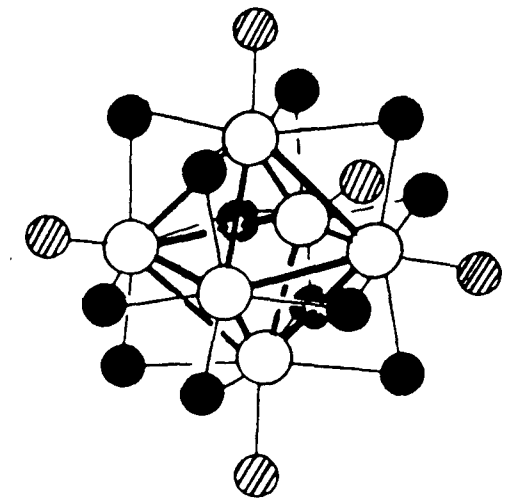
Some of the earliest transition metal clusters to be structurally characterised were those of the early transition metals, with bridging π-donor ligands such as Cl, Br, I, S and OR (R = alkyl).[1] Subsequently, a wide variety of extended metal-metal bonded arrays with bridging chloride and oxide ligands have had their structures determined.[2] The ternary molybdenum chalcogenides known as the "Chevrel Phases", $M_xMo_6X_8$ (M = Pb, Sn, Ba, Au, Cu, Li etc.; X = S, Se, Te),[3] have attracted the attentions of solid state physicists and chemists, since this class of compounds includes both high-temperature and very high-field superconductors.[4] The building blocks of many of these extended arrays are M_6 octahedra with face- or edge-bridging ligands.

The archetypal face-bridged octahedral cluster is $[M_6Cl_8L_6]^{4+}$ **(I)** (M = Mo or W) which possesses a $[M_6(\mu_3\text{-}Cl)_8]^{4+}$ core with 8 face-bridging ligands adopting a cubic arrangement. In $MoCl_2$ the terminal ligands act as bridges between cluster units,[5] but discrete $[Mo_6Cl_{14}]^{2-}$ ions are known, for example in $(NH_4)_2[Mo_6Cl_{14}].H_2O$.[6] The archetypal edge-bridged octahedral cluster is $[M_6Cl_{12}L_6]^{2+}$ **(II)** (M = Nb, Ta), which possesses a $[M_6(\mu_2\text{-}Cl)_{12}]^{2+}$ core with 12 edge-bridging ligands adopting a cuboctahedral arrangement. The six terminal ligands may act as bridges between clusters, as in $[Nb_6Cl_{12}]Cl_2$,[7] although discrete $[M_6Cl_{18}]^{4-}$ ions



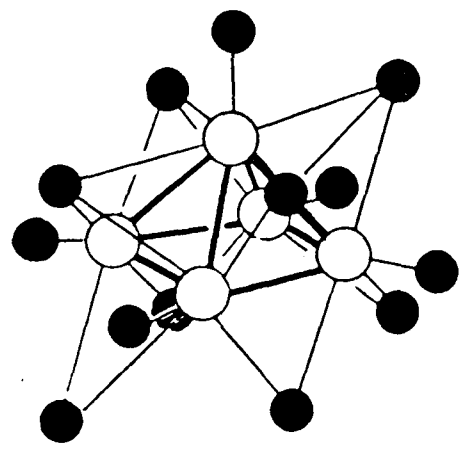
$[M_6Cl_8L_6]^{4+}$ (M-Mo or W)

(I)



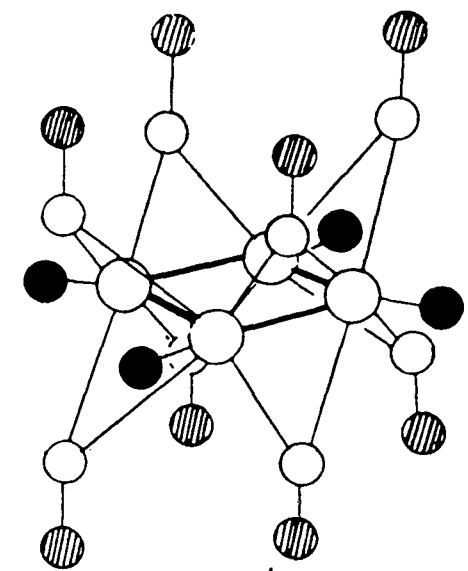
$[M_6Cl_{12}L_6]^{2+}$ (M-Nb or Ta)

(II)



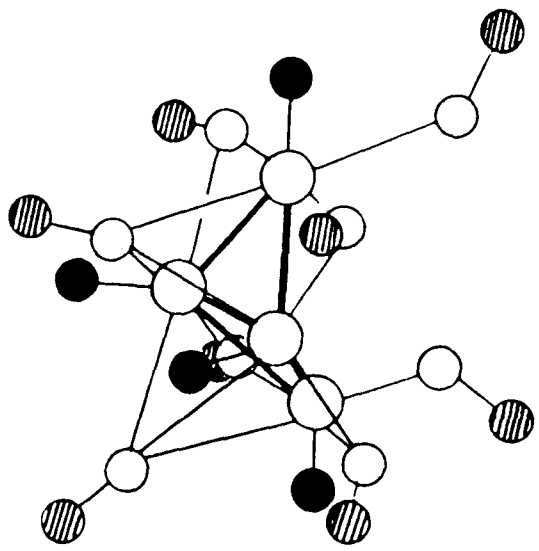
$[Mo_5Cl_{13}]^{2-}$

(III)



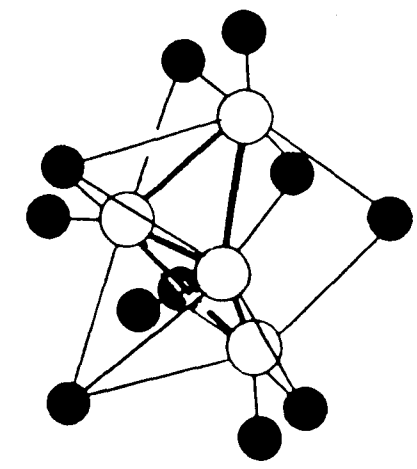
$[Mo_4(OPr^i)_8Cl_4]$

(IV)



$[Mo_4(OPr^i)_8Br_4]$

(V)



$[Mo_4I_{11}]^{2-}$

(VI)

have also been characterised, as in $K_4[Nb_6Cl_{18}]$.[8]

Kettle and others have demonstrated that the bonding in these clusters may be conveniently described in terms of localised bonding schemes.[9] The face-bridged cluster possesses 12 Skeletal Electron Pairs (SEP's), corresponding to the formation of localised 2-centre-2-electron bonds along the edges of the cluster. In contrast the edge-bridged cluster possesses 8 SEP's, corresponding to 3-centre-2-electron bonds localised on the faces of the octahedron. Thus, a complementary relationship exists between the positions of the bridging ligands and the disposition of the localised metal-metal bonds. A semi-empirical molecular orbital treatment, by Cotton and Haas,[10] led to the conclusion that each metal atom in these two clusters uses its valence s and p orbitals for bonding to the terminal and bridging ligands. In addition one of the d^{δ} orbitals (d_{xy} or $d_{x^2-y^2}$) is also required for metal-bridging ligand bonding, so each metal fragment has 4 valence d orbitals from which to form the skeletal bonding and antibonding MO's. A variety of molecular orbital calculations have now been performed on these clusters.[11]

The total cluster valence electron counts for the face- and edge-bridged octahedral π-donor clusters (including those electrons in metal-terminal ligand bonding orbitals) are 84 and 76 respectively[10,11] (although there exist a number of face- and edge-bridged clusters with fewer electrons, such as $[Nb_6I_8(CH_3NH_2)_6]$ (face-bridged, 82e)[12] and $[Zr_6I_{12}]$ (edge-bridged, with some of the edge-bridging ligands acting as terminal ligands towards other clusters, 72e)[13]). These differ from the 86 electron (14n+2) count generally associated with metal carbonyl clusters, on the basis of the Polyhedral Skeletal Electron Pair approach.[14] On the other hand, the localised bonding models, which may

be successfully applied to the π-donor-bridged clusters, are not easily applicable to metal carbonyl clusters.[14a] These obvious differences in electron counts for π-donor and π-acceptor clusters provided the initial stimulus for this theoretical analysis. Furthermore, the two classes of cluster show interesting electronic differences when metal atoms are removed from the octahedral clusters. Metal carbonyl clusters may be classified using the closo, nido and arachno scheme originally developed for the boranes.[14a] This scheme forges a direct link between the polyhedral geometry and the total number of valence electrons, i.e. (14n+2) closo, (14n+4) nido and (14n+6) arachno. This structure-electron count relationship arises because the number of bonding skeletal MO's remains constant in a series of related closo, nido and arachno clusters.[14a] In the class of π-donor-bridged molecules a similar family of clusters has been observed **(III)-(VI)**,[15] but these compounds do not show a similar simple electronic relationship.

The aim of the present analysis is firstly to evaluate the effect of introducing terminal, edge- and face-bridging σ-donor ligands into the bonding scheme developed for a bare octahedral metal cluster. The similarities and differences between π-donor and π-acceptor ligands will then be highlighted by a comparison of related carbonyl and chloride-bridged clusters. Stone's Tensor Surface Harmonic approach[16] is used to describe the nodal characteristics of the MO's of the "naked" metal clusters and the linear combinations of ligand orbitals. In this way the clusters are treated as a series of concentric spheres, on which are placed the metal atoms and the bridging and terminal ligands. The second aim is to investigate the electronic structures of nido and arachno derivatives of the π-donor-bridged octahedral metal clusters, in an

attempt to rationalise existing molecules and predict others. The atomic parameters and cluster bond lengths used in the Extended Hückel calculations are listed in the **Appendix** to this Chapter (**Section 6.9**).

6.2 Naked Octahedral Metal Clusters

Figure 6.1 illustrates the relative energies of the molecular orbitals in a "naked" octahedral Mo_6 cluster. The molybdenum 5s and 5p valence orbitals generate a spectrum of MO's with a large energy spread, so that the completely in-phase combination of metal s orbitals ($S^{\sigma}_{s}(a_{1g})$) actually lies below the d-band. Woolley has pointed out, however, that wide s- and p-bands are not necessarily synonomous with strong metal-metal bonding through the metal s and p orbitals.[17]

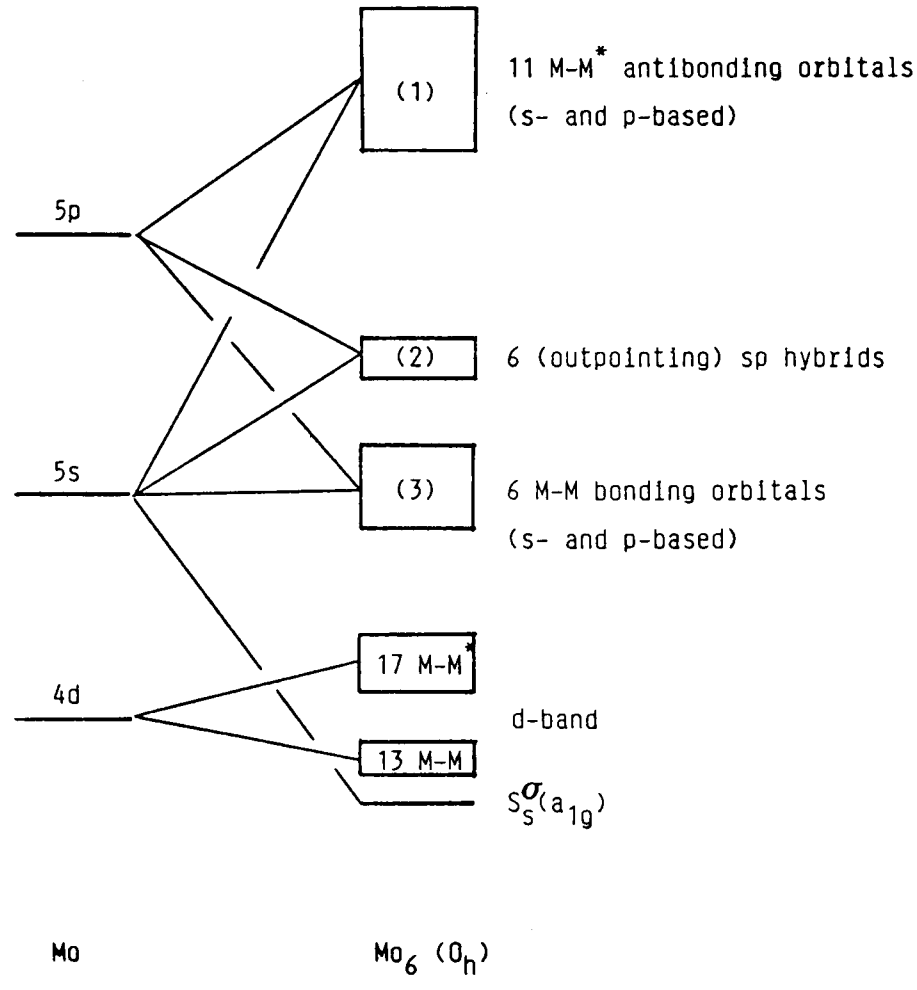


Figure 6.1 Schematic molecular orbital diagram for a "naked" octahedral Mo_6 cluster.

A crucial feature of the MO scheme shown in **Figure 6.1** is the occurrence of 11 strongly metal-metal anti-bonding MO's, viz. $D_{sp}^{\sigma}(e_g)$, P_p^{π}-$P_{sp}^{\sigma}(t_{1u})$, $\bar{P}_p^{\pi}(t_{1g})$ and $\bar{D}_p^{\pi}(t_{2u})$ (set (1) in **Figure 6.1**), which are also unsuitable for metal-ligand bonding due to being inwardly hybridised. These 11 antibonding orbitals, which are present in all octahedral metal clusters, have identical symmetry and nodal properties to the 11 strongly antibonding orbitals of $[B_6H_6]^{2-}$.[18] More generally, it has been established that deltahedral main group and transition metal carbonyl clusters both possess (2n-1) "inaccessible" cluster antibonding MO's.[19] If all of the remaining cluster atom valence orbitals are utilised for metal-metal and metal-ligand bonding, such clusters are characterised by (4n+2) valence electrons (main group) and (14n+2) valence electrons (transition metal).

Since the octahedral π-donor-bridged clusters, e.g. **(I)** and **(II)**, have fewer valence electrons than predicted on the basis of the (14n+2) rule, it can be concluded that such clusters have more than 11 inaccessible orbitals, the additional ones being derived from the metal valence d orbitals. The spectrum of MO's arising from the metal 4d orbitals is relatively narrow (c.a. 4 eV) and contains 13 bonding and 17 antibonding components. The symmetries and TSH labels for these orbitals are given in **Figure 6.2a.** The δ orbitals have been labelled according to whether they are formed by taking linear combinations of $d_{x^2-y^2}$ or d_{xy} atomic orbitals. The former are defined so that their lobes point along the edges, and the latter towards the centres of the faces of the octahedron. It follows that these MO's interact in a highly specific and complementary manner with edge- and face-bridging ligands. The symmetry allowed mixings of the σ, π, and δ components of the d-band are also

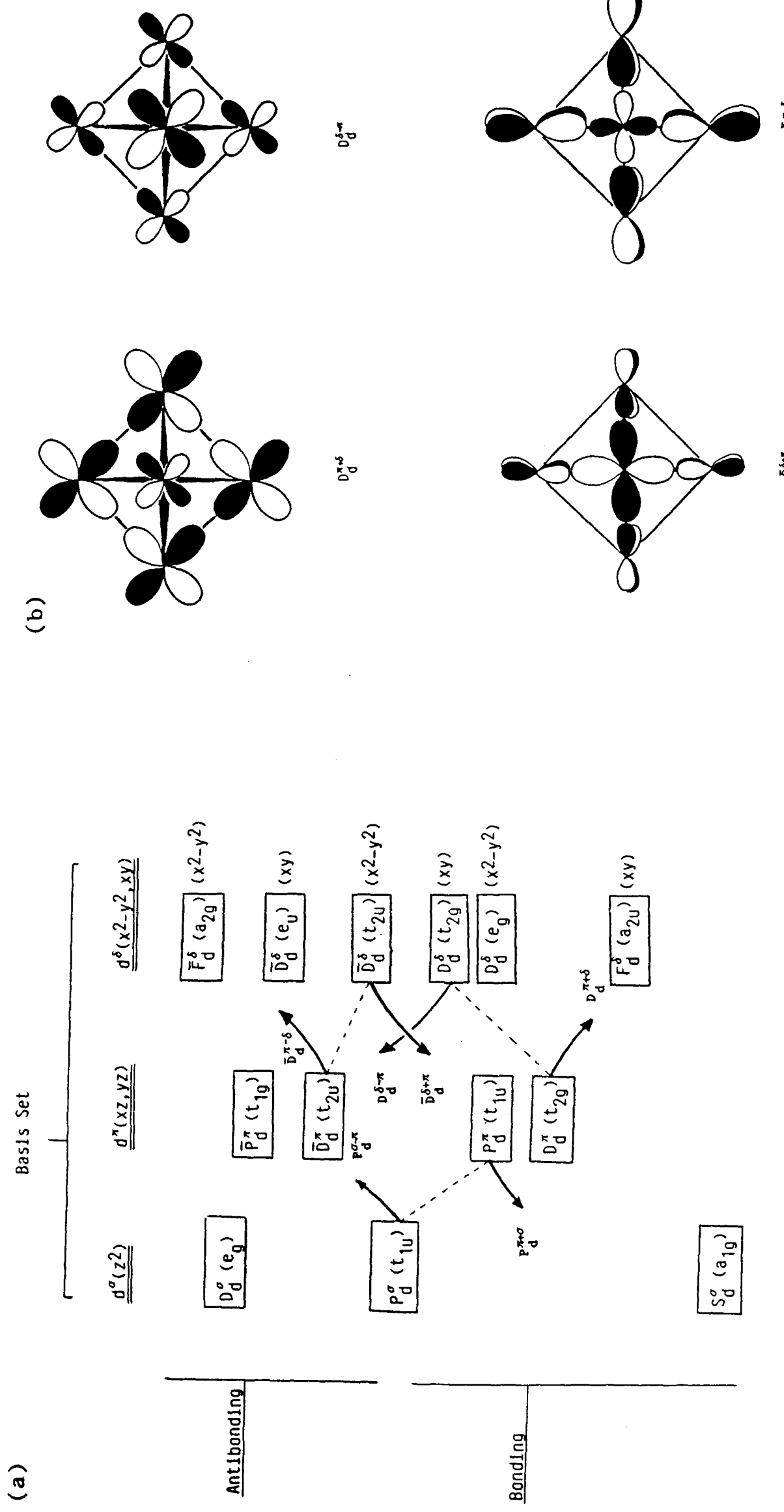
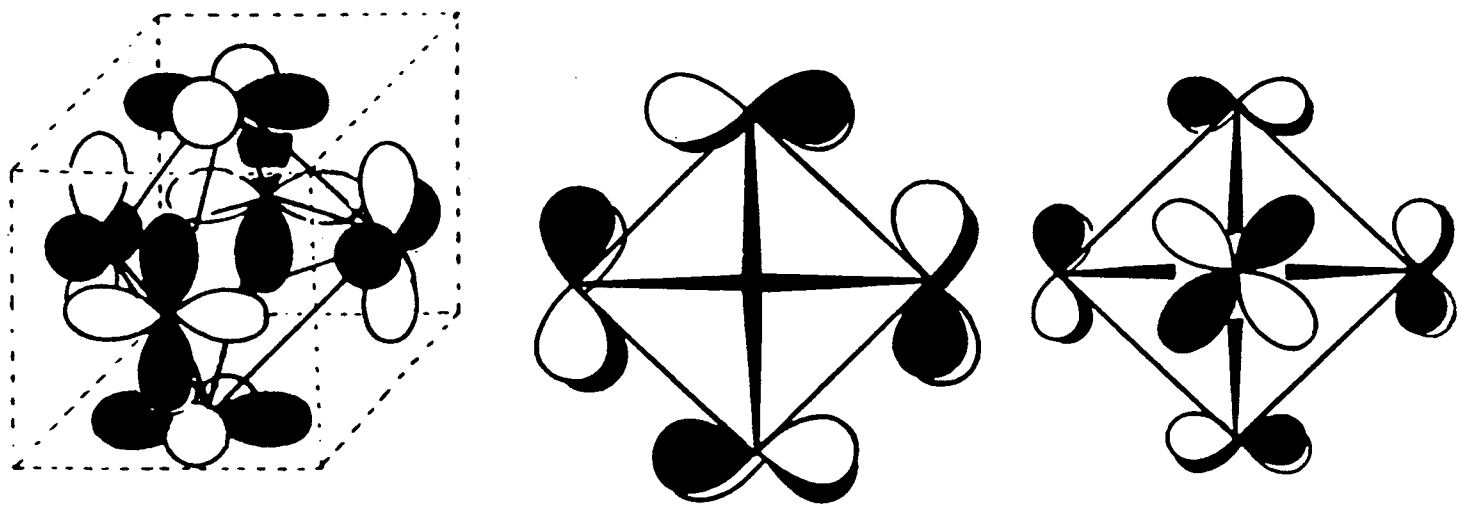


Figure 6.2 (a) Mixing of σ-, π- and δ-type d-band orbitals, of the same symmetry, for a "naked" octahedral Mo_6 cluster. (b) The effect of π/δ mixing on the d-band t_{2g} and t_{2u} orbitals.

indicated. π/δ mixing is particularly important for rationalising the electron counts of the π-donor clusters. As a result of this mixing, illustrated in **Figure 6.2**, the molybdenum $d_{x^2-y^2}$ orbitals only generate one strongly antibonding skeletal MO ($\bar{F}_d^{\delta}(a_{2g})$) (**1**), as the $\bar{D}_d^{\delta}(t_{2u})$ orbitals are stabilised by mixing with the higher lying $\bar{D}_d^{\pi}(t_{2u})$ MO's. In contrast, there are 5 antibonding MO's with predominantly d_{xy} character: $\bar{D}_d^{\delta}(e_u)$ (**2**) and $D_d^{\delta-\pi}(t_{2g})$.



$\bar{F}_d^{\delta}(a_{2g})$ (**1**)

$\bar{D}_d^{\delta}(e_u)$ (**2**)

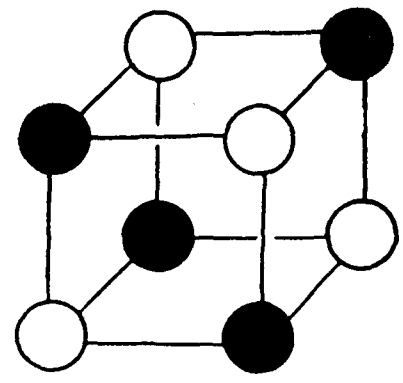
It is these antibonding d^{δ}-based MO's which constitute the additional inaccessible orbitals in π-donor clusters. To understand why this should be so, metal-~~cluster~~ ligand interactions must be considered, starting with the hypothetical clusters $[Mo_6H_{14}]$ and $[Mo_6H_{18}]$ which have bridging hydride ligands capable only of interacting in a sigma fashion with the naked metal cluster MO's.

6.3 Hydrido-Bridged Octahedral Clusters

In $[Mo_6H_{14}]$ and $[Mo_6H_{18}]$ the 6 symmetry adapted linear combinations

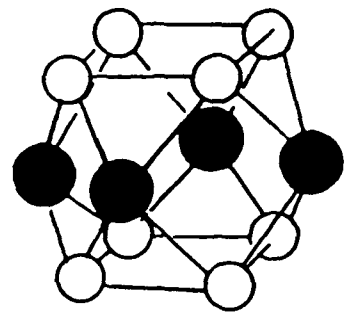
of terminal ligand orbitals correspond to the L^{σ} orbitals of an octahedron: $S_t^{\sigma}(a_{1g})$, $P_t^{\sigma}(t_{1u})$ and $D_t^{\sigma}(e_g)$, where the subscript t denotes a terminal ligand. These orbitals interact primarily with the symmetry-matched set of out-pointing sp^{σ} hybrids (set (2) in **Figure 6.1**). In $[Mo_6H_{14}]$ the 8 face-bridging ligands define a cube and their linear combinations span the representations: $S_x^{\sigma}(a_{1g})$, $P_x^{\sigma}(t_{1u})$, $D_x^{\sigma}(t_{2g})$ and $F_x^{\sigma}(a_{2u})$, where the subscript x denotes a bridging ligand. In $[Mo_6H_{18}]$ the 12 edge-bridging ligands span the representations: $S_x^{\sigma}(a_{1g})$, $P_x^{\sigma}(t_{1u})$, $D_x^{\sigma}(t_{2g}+e_g)$ and $F_x^{\sigma}(t_{2u})$.

Since hydrogen 1s orbitals possess no angular nodes, the linear combinations L_x^{σ} overlap most effectively with cluster MO's which are nodeless across either the edges or the faces of the octahedron. The 7 bonding skeletal MO's derived from the metal s and p orbitals ($S_s^{\sigma}(a_{1g})$ and set (3) in **Figure 6.1**) represent the most suitable match for the bridging-ligand orbitals, but there remain some linear combinations which do not find a match, i.e. $F_x^{\sigma}(a_{2u})$ (3) in $[Mo_6H_{14}]$ and $D_x^{\sigma}(e_g)$ and $F_x^{\sigma}(t_{2u})$ (4) in $[Mo_6H_{18}]$.

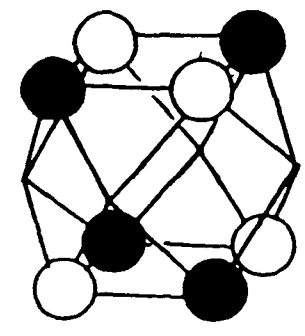


$F_x^{\sigma}\ (a_{2u})$

(3)



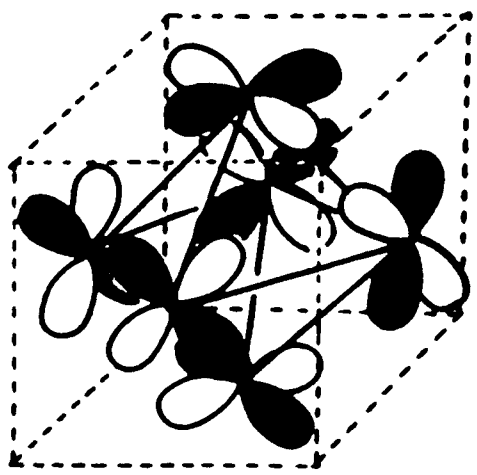
$D_x^{\sigma}\ (e_g)$ (O component)



$F_x^{\sigma}\ (t_{2u})$ (2c component)

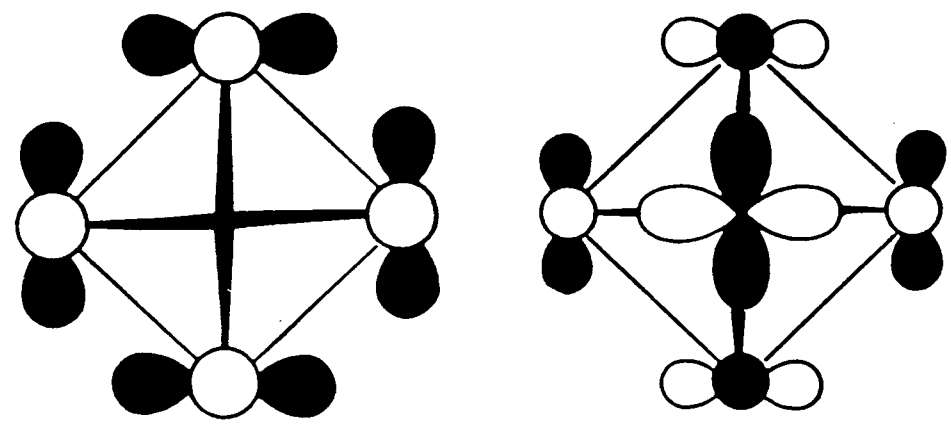
(4)

These linear combinations possess two angular nodes with respect to the cluster vertices and may, therefore, only be matched by metal cluster MO's derived from the d-band, i.e. $F_d^{\delta}(a_{2u}, xy)$ (5) in $[Mo_6H_{14}]$ and $D_d^{\delta}(e_g, x^2-y^2)$ (6) and $\bar{D}_d^{\delta+\pi}(t_{2u}, x^2-y^2)$ in $[Mo_6H_{18}]$.



F_d^{δ} (a_{2u})

(5)



D_d^{δ} (e_g)

(6)

The disposition of the ligands relative to the edges and faces of the octahedron determines whether the L_x^{σ} ligand orbitals interact with linear combinations of d_{xy} or $d_{x^2-y^2}$ orbitals.

The formation of cluster-ligand bonds leaves a d-band of 29 orbitals for $[Mo_6H_{14}]$ (12 bonding and 17 antibonding) and 25 orbitals for $[Mo_6H_{18}]$ (8 bonding and 17 antibonding). If these MO's, together with the cluster-hydrogen bonding orbitals (of which there are 14 and 18 for the face- and edge-bridged clusters, respectively), were completely filled the electron count for both clusters would be 86, i.e. the same as for octahedral metal carbonyl clusters. The net metal-metal bonding in these hydrido-bridged clusters would, however, be negligable, because the occupation of the antibonding part of the d-band cancels out the metal-metal bonding effects of the lower lying MO's. The computed Mulliken overlap populations for these hypothetical 86 electron species (-0.04 for $[Mo_6H_{14}]^{36-}$ and +0.02 for $[Mo_6H_{18}]^{32-}$) confirm this

conclusion. By comparison, the calculated Mo-Mo overlap populations for the 52 electron species, where only the bonding components of the d-band are occupied, are much larger (+0.28 for $[Mo_6H_{14}]^{2-}$ and +0.33 for $[Mo_6H_{18}]^{2+}$).

The arguments developed above have demonstrated that in the 86 electron clusters ($[Mo_6H_{14}]^{36-}$ and $[Mo_6H_{18}]^{32-}$), where the d-band is completely filled, there is no net metal-metal bonding. It is informative, however, to consider the bonding in an alternative hypothetical $[Mo_6H_{18}]^{32-}$ cluster, composed of conical MH_3 fragments. The calculated Mo-Mo overlap population for this species is +0.35, suggesting considerable metal-metal bonding. This marked increase in overlap population is due to important differences in the ways in which terminal and bridging ligands interact with the metal cluster orbitals.

Edge- and face-bridging ligands interact primarily with cluster orbitals which possess a large percentage of s,p and d^{δ} character, because such orbitals have large amplitudes along the edges and faces (i.e. at the ligand sites) of the polyhedron. In $[Mo_6H_{18}]$, composed of conical MoH_3 fragments, the linear combinations of hydrogen 1s orbitals are topologically equivalent to the 6 L^{σ} and 12 $L^{\pi}/\bar{L}^{\pi}$ orbitals of an octahedron. This is because each of the H_3 units give rise to one nodeless (σ-pseudo-symmetry) and two singly-noded (π-pseudo-symmetry) functions. **Figure 6.3** indicates that the ligand L^{σ} combinations interact with the outwardly hybridised cluster L^{σ}_{sp} orbitals in much the same way as that described above for single terminal hydride ligands. In contrast, the ligand L^{π} and $\bar{L}^{\pi}$ combinations interact strongly with the L^{π}_{d} and $\bar{L}^{\pi}_{d}$ MO's of the cluster d-band, because the locations of the ligands now correspond to the positions of maximum amplitude of the metal d_{xz} and d_{yz} orbitals. The L^{π}_{d} orbitals mix with the higher lying L^{π}_{p}

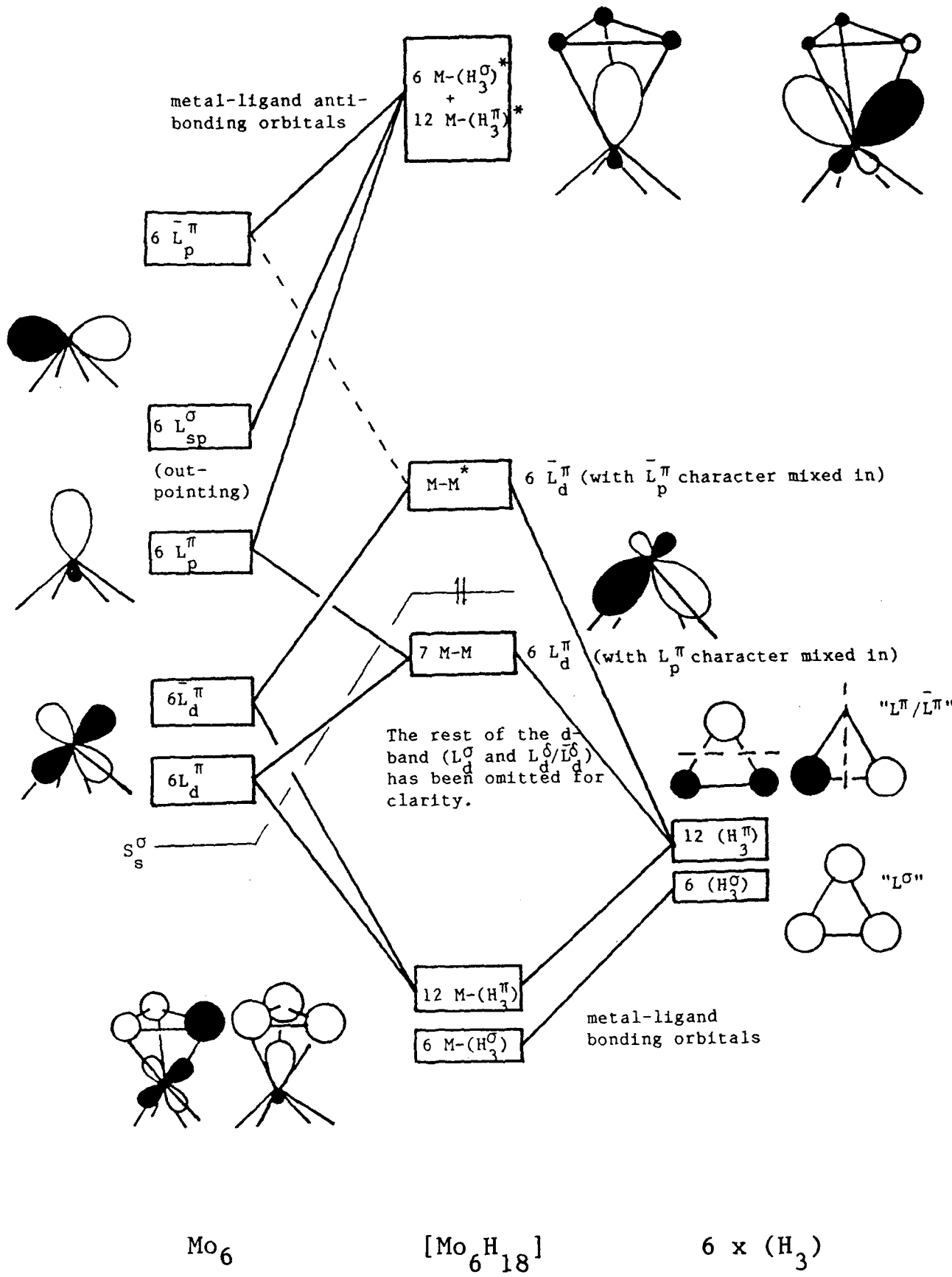


Figure 6.3 Molecular orbital diagram for an $[Mo_6H_{18}]$ cluster made up of conical MoH_3 fragments.

orbitals, thereby mitigating the metal-ligand antibonding character of the former and ensuring that they lie at sufficiently low energy to be occupied. $\bar{L}^{\pi}_{d}/\bar{L}^{\pi}_{p}$ mixing is, however, less effective at stabilising the $\bar{L}^{\pi}_{d}$ orbitals because the $\bar{L}^{\pi}_{p}$ MO's lie at high energy. In consequence, those orbitals with predominantly $\bar{L}^{\pi}_{d}$ character are high lying and unoccupied.

The occupation of all 18 metal-ligand bonding orbitals and the 24 remaining d-band orbitals, together with the low lying $S^{\sigma}_{s}(a_{1g})$ orbital (which is only slightly destabilised by the "S^{σ}" combination of terminal ligand orbitals), results in an electron count of 86 [= 2 x (18+24+1)] for the non-bridged cluster. This 86 electron cluster has a significant degree of metal-metal bonding, for two reasons. Firstly, the metal-metal antibonding $\bar{L}^{\pi}_{d}$ orbitals are unoccupied, and secondly, the strongly metal-metal bonding orbital $S^{\sigma}_{s}(a_{1g})$ is occupied. In the bridged clusters this orbital interacts with the $S^{\sigma}_{x}(a_{1g})$ combination of ligand orbitals. The resulting metal-ligand bonding orbital is mainly localised on the ligands, and consequently, contributes little to metal-metal bonding in the cluster.

The MH_3 fragment is a good model for the $M(PR_3)_3$ and $M(CO)_3$ moieties, if the (quite small) effects of the terminal ligand π-orbitals are neglected. This bonding scheme is, therefore, applicable to 86 electron clusters such as $[Os_6(CO)_{18}]^{2-}$.[20]

6.4 π-Donor- and π-Acceptor-Bridged Octahedral Clusters

The above analysis has indicated that, for purely σ-donating bridging ligands, 86 electron clusters should have minimal metal-metal bonding. There are, however, many octahedral metal clusters, with up to 86 electrons, where the bridging ligands are either π-acceptors (e.g.

CO) or π-donors (e.g. Cl). The metal-metal bonding in such clusters is quite substantial,[21] due to the interaction between the cluster d-band orbitals and the π-symmetry orbitals possessed by the ligands.

In this section, the effect of introducing ligand π-symmetry orbitals into the bonding scheme developed for the hydrido-metal octahedral clusters is discussed. Initially no distinction will be made between π-acceptor and π-donor ligands, so that the symmetry aspects of the problem may be emphasised. Terminal ligands may effectively be treated as σ-donors because π-acceptance or π-donation in terminal sites is generally small compared with that in bridging sites. The effects of σ-donation from terminal and bridging ligands will be qualitatively the same as for the hydride-bridged clusters discussed above.

6.4.1 Face-bridged octahedral clusters

The π-symmetry orbitals of a π-acceptor or π-donor ligand generate linear combinations which match those components of the d-band which are singly noded across the edges or faces of the octahedron. These noded MO's may be identified with the antibonding components of the d-band. In the face-bridged cluster $[Mo_6X_{14}]$, the linear combinations of the 16 ligand π-orbitals are equivalent to the L^{π} and $\bar{L}^{\pi}$ orbitals of a cube ($P_x^{\pi}(t_{1u})$, $D_x^{\pi}(t_{2g}+e_g)$, $\bar{P}_x^{\pi}(t_{1g})$ and $\bar{D}_x^{\pi}(t_{2u}+e_u)$). These ligand orbitals match the symmetries and nodal characteristics of 16 of the 17 antibonding d-band MO's, described above for $[Mo_6H_{14}]$. The only antibonding d-band orbital which does not find a match is $\bar{F}_d^{\delta}(a_{2g}, x^2-y^2)$ (1), which is doubly noded across the faces of the octahedron.

If X is a π-acceptor ligand (e.g. CO), the 16 antibonding d-band orbitals are stabilised by interacting with the acceptor orbitals of the

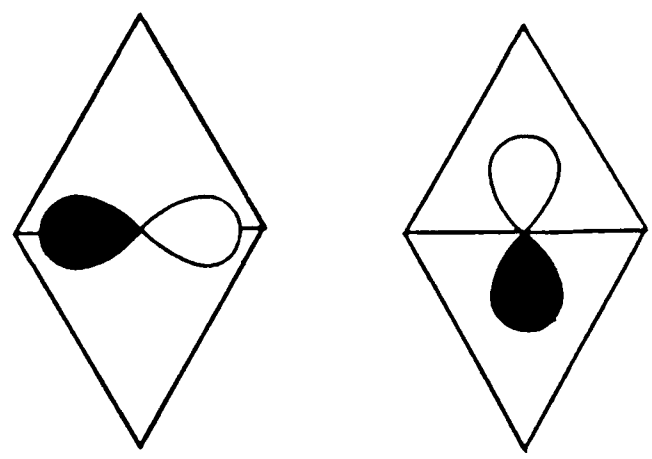
ligand (e.g. the CO π^* orbitals). This results in a partial transfer of electron density from the antibonding part of the d-band to the ligands. The $\bar{F}_d^{\delta}(a_{2g})$ MO alone is not stabilised by back donation and whether it is defined as "inaccessible" or not depends on the inherent width of the d-band. For the later first row transition metals the d-band widths are not very large and consequently this metal-metal antibonding MO is sufficiently low lying to be occupied. Thus, in clusters such as $[Co_6(CO)_{14}]^{4-}$ [22] the a_{2g} MO is occupied and the electron count is 86.[18] In metal carbonyl clusters composed of conical $M(CO)_3$ fragments, the $\bar{F}_d^{\delta}$ MO is stabilised (under the lower symmetry of the molecule) by overlap with a matching linear combination of $\pi^*(CO)$ orbitals. With other arrangements of bridging and terminal ligands, stabilisation of the $\bar{F}_d^{\delta}$ orbital may be achieved in a similar fashion.

If X is a π-donor ligand (e.g. Cl), the 16 linear combinations of Cl $3p\pi$ orbitals lie at lower energy than the d-band orbitals and their overlap leads to a set of 16 metal-ligand bonding orbitals which are mainly localised on the ligands. This represents, in effect, a replacement of 16 metal-metal antibonding d-band orbitals by a matching set of ligand-based orbitals. The $\bar{F}_d^{\delta}(a_{2g})$ MO is unaffected by these interactions and, therefore, the situation is strictly analogous to that described above for π-acceptor-bridged clusters. For an early second row transition metal, such as molybdenum, the d-d overlaps are significantly larger than for Co and $\bar{F}_d^{\delta}(a_{2g})$ is consequently more antibonding, becoming inaccessible. Clusters of this type are, therefore, characterised by 84 rather than 86 valence electrons. The almost complete transfer of electron density from metal-metal antibonding components of the d-band onto the highly electronegative ligands leads to a significant strengthening of the metal-metal bonds relative to the

situation in the hypothetical hydrido-clusters. This is reflected by an increase of the calculated Mo-Mo overlap population to +0.28 for 84 electron $[Mo_6Cl_{14}]^{2-}$. As mentioned above, there is only a partial transfer of electron density, from antibonding d-band orbitals to the ligands, in the carbonyl-bridged clusters. This explains the smaller Mo-Mo overlap population (+0.18) calculated for the hypothetical (84 electron) carbonyl cluster $[Mo_6(CO)_{14}]^{20-}$.

6.4.2 Edge-bridged octahedral clusters

In the edge-bridged $[Mo_6X_{18}]$ clusters the linear combinations of ligand π-symmetry orbitals are equivalent to the L^{π} and $\bar{L}^{\pi}$ orbitals of a cuboctahedron: $P_x^{\pi}(t_{1u})$, $D_x^{\pi}(t_{2g}+e_g)$, $F_x^{\pi}(t_{1u}+a_{2u})$, $\bar{P}_x^{\pi}(t_{1g})$, $\bar{D}_x^{\pi}(t_{2u}+e_u)$ and $\bar{F}_x^{\pi}(t_{1g}+a_{2g})$. In this case, however, the two π-orbitals of the bridging ligands no longer interact with the metal d-band orbitals in an equivalent fashion. The π-orbitals ($\pi_{\parallel}$) lying parallel to the edges of the octahedron **(7a)** overlap more strongly with the metal d orbitals than do those ($\pi_{\perp}$) which are perpendicular to the cluster edges **(7b)**.



(7a) $\pi_{\parallel}$ (7b) $\pi_{\perp}$

The 12 linear combinations of the $\pi_{\parallel}$ orbitals: $P_x^{\pi}/F_x^{\pi}(t_{1u})$, $\bar{P}_x^{\pi}/\bar{F}_x^{\pi}(t_{1g})$,

$D_x^{\pi}(e_g)$, $\bar{D}_x^{\pi}(t_{2u})$ and $\bar{F}_x^{\pi}(a_{2g})$ interact with symmetry-matched antibonding components of the d-band which are also singly noded along the edges of the cluster. The remaining 5 antibonding components of the d-band, $\bar{D}_d^{\delta}(e_u, xy)$ and $D_d^{\delta-\pi}(t_{2g}, xy)$ are unaffected by the ligand $\pi_{\parallel}$ orbitals, but experience a smaller secondary interaction with linear combinations (with matching symmetry characteristics) of $\pi_{\perp}$ orbitals.

If X is a π-acceptor ligand, there is a substantial stabilisation of 12 of the antibonding components of the d-band and a smaller stabilisation of the remaining 5 components. For a late transition metal (where d-d overlap integrals are small and the d-band is, consequently, narrow), occupation of the whole d-band leads to a total valence electron count of 86 and a strengthening of the metal-metal bonding interactions (relative to the hydrido-bridged case) due to partial transfer of electron density from metal antibonding to ligand-based orbitals. The stabilisation of the antibonding components of the d-band makes it even narrower, thereby favouring the 86 electron count. There are, however, no known examples of an all-edge-bridged octahedral metal carbonyl cluster, though it seems reasonable to predict such a structure for the (as yet) unknown species $[Fe_6(CO)_{18}]^{2-}$ (provided that the Fe_6 core is not too small to pack 18 carbonyl ligands around).

If X is a π-donor ligand, the 12 $\pi_{\parallel}$ orbitals lie at significantly lower energies than the cluster d-band so the metal-ligand π-bonding combinations are predominantly localised on the ligands, with 12 of the d-band antibonding orbitals becoming essentially metal-ligand antibonding. The 5 remaining components of the antibonding part of the d-band, $\bar{D}_d^{\delta}(e_u)$ and $D_d^{\delta-\pi}(t_{2g})$, will be inaccessible if the d-d overlap integrals are large, i.e. for an early second or third row transition metal. The inaccessible nature of these orbitals is enhanced by the weak

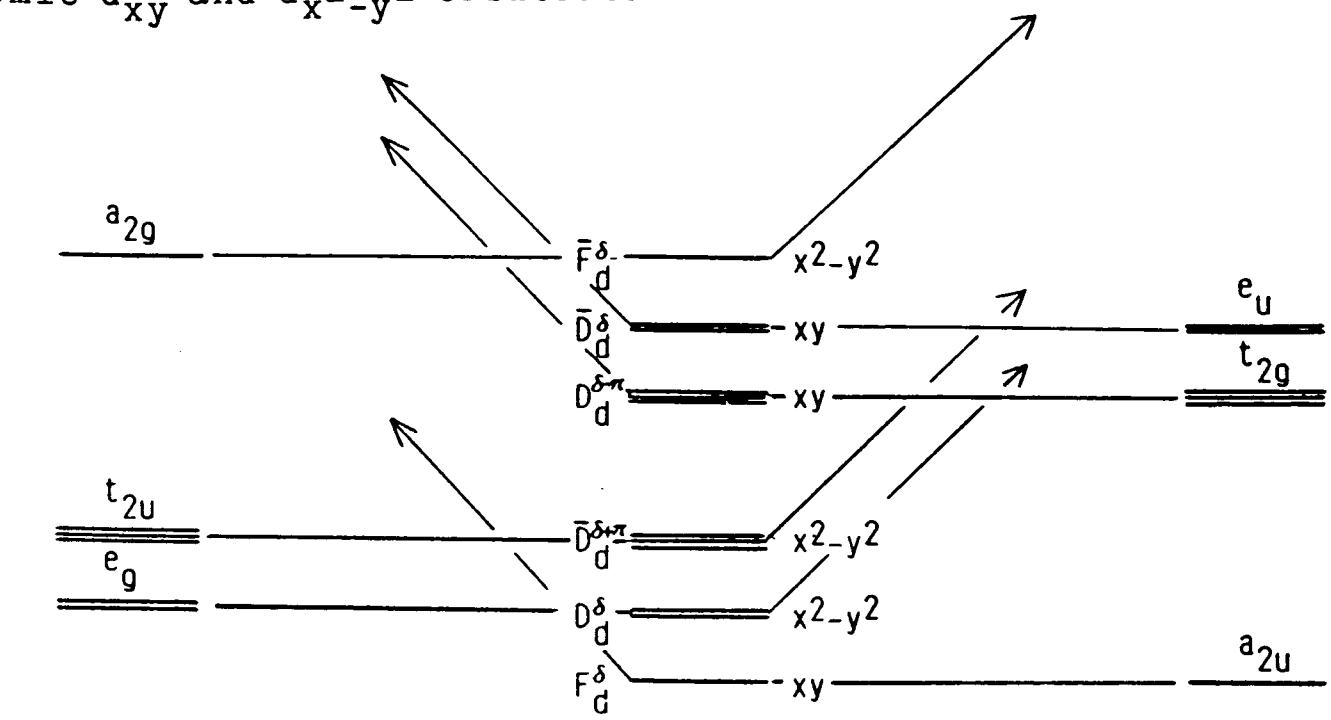
antibonding interactions which they experience with the ligand $\pi_\perp$ orbitals. The presence of these 5 additional inaccessible MO's accounts for the 76 electron count observed, for example, in $[Nb_6Cl_{18}]^{4-}$ The considerably enhanced strength of the metal-metal bonding in such clusters, which again results from the almost complete transfer of electron density from metal-metal (d-band) orbitals onto the ligands (as well as the total non-occupation of 5 cluster antibonding orbitals), is indicated by the high computed Mo-Mo overlap population (+0.34) for the isoelectronic cluster $[Mo_6Cl_{18}]^{2+}$.

6.4.3 Summary

Although it has been customary to discuss the bonding in π-donor and π-acceptor clusters separately, this analysis clearly demonstrates the close relationship between the two types of cluster. In both cases the ligands withdraw electron density from the metal-metal antibonding part of the d-band (i.e. those d-based skeletal MO's which are noded along the edges or across the faces of the octahedron). Both types of cluster have 11 inaccessible orbitals derived from the metal s and p orbitals. For the early transition metals additional inaccessible orbitals arise from the antibonding components of the d-band, because of their greater antibonding character. The number of inaccessible orbitals of this type depends on the positions of the ligands relative to the nodal planes of the metal d_{xy} and $d_{x^2-y^2}$ orbitals.

The detailed analysis presented above has served to emphasise the important role played by the metal d^δ orbitals in determining the total electron count in transition metal clusters. **Figure 6.4** illustrates the relative energies of the naked metal cluster MO's derived from the

atomic d_{xy} and $d_{x^2-y^2}$ orbitals.



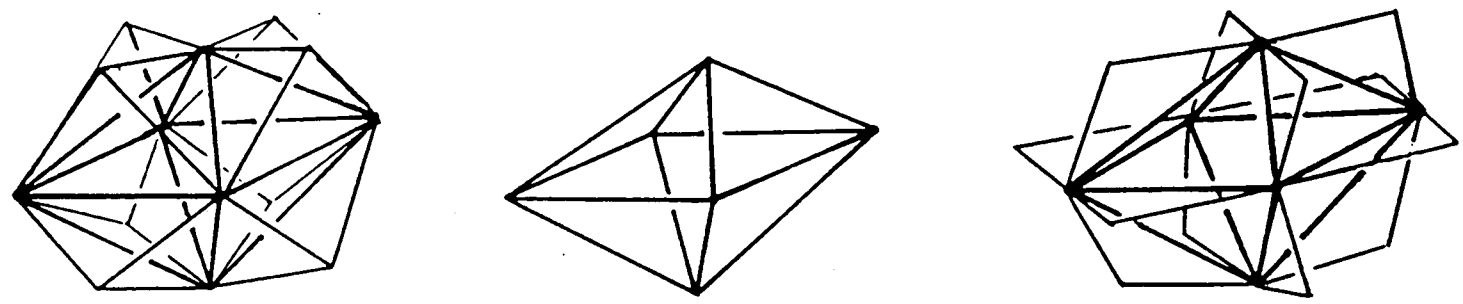


Figure 6.4 Relative energies of the d^{δ}-based MO's of a naked octahedral metal cluster and the complementary way in which they interact with edge- and face-bridging ligands.

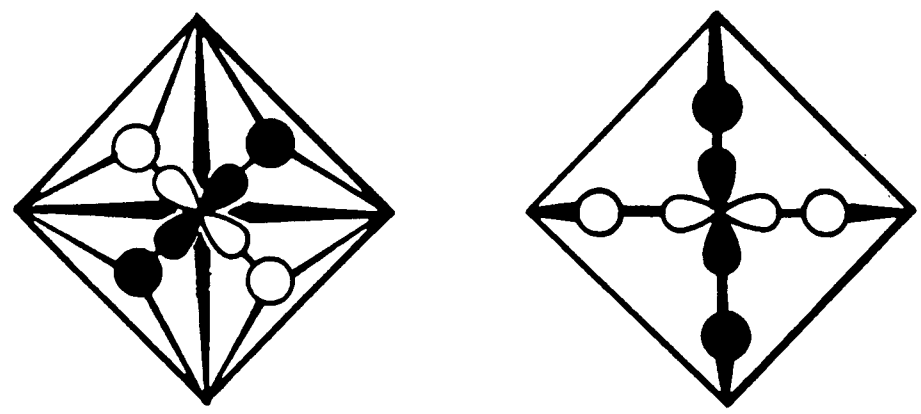
These MO's are inter-related by the Parity Inversion Operation,[16] which rotates each atomic d^{δ} orbital by 45^{o} about a radial vector passing through the atom, thereby transforming d_{xy} into $d_{x^2-y^2}$ and interconverting the cluster L_d^{δ} and $\bar{L}_d^{\delta}$ MO's:

$$\bar{D}_d^{\delta}(t_{2u},\ x^2\text{-}y^2) \xleftrightarrow{\hat{P}} D_d^{\delta}(t_{2g},\ xy)$$

$$D_d^{\delta}(e_g,\ x^2\text{-}y^2) \longleftrightarrow \bar{D}_d^{\delta}(e_u,\ xy)$$

$$F_d^{\delta}(a_{2u},\ xy) \longleftrightarrow \bar{F}_d^{\delta}(a_{2g},\ x^2\text{-}y^2).$$

The Parity Inversion Operation also interchanges the bonding and antibonding character of the cluster MO's, as shown in **Figure 6.4.** Cotton and Haas noted that each metal atom may be regarded as forming localised bonds to the 4 bridging ligands around it.[10] These bonds necessitate the use of one of the d^{δ} pair (xy or x^2-y^2) on each metal atom to form the coordinate bonds, as shown in **Figure 6.5.** The complementary nature of the metal-ligand interactions in edge- and face-bridged clusters is also depicted in **Figure 6.4**



(a) $d_{xy}+\delta(X_4)$ (b) $d_{x2-y2}+\delta(X_4)$

Figure 6.5 Bonding interactions of the d^{δ} atomic orbitals of a metal vertex with δ-symmetry combinations of σ-donor orbitals (X_4) in face-bridging (a) and edge-bridging (b) positions.

Once half of the $L_d^{\delta}/\bar{L}_d^{\delta}$ orbitals have been utilised in this fashion, the spectrum of the remaining orbitals determines the electron count. In the face-bridged cluster there remains only one δ-orbital ($\bar{F}_d^{\delta}(a_{2g})$), which, for an early transition metal is strongly antibonding and inaccessible. In consequence $[Mo_6Cl_{14}]^{2-}$ has a total of 12 inaccessible orbitals and an electron count of: 2 x (9n-12) = 84 (n=6). In the edge-bridged clusters there are 5 high lying antibonding δ-orbitals

($\bar{D}_d^{\delta}(e_u)$ and $D_d^{\delta-\pi}(t_{2g})$) which, for an early transtion metal, are strongly antibonding and inaccessible. For such a cluster, e.g. $[Nb_6Cl_{18}]^{4-}$ there are a total of 16 inaccessible cluster MO's, which results in an electron count of: $2 \times (9n-16) = 76$ $(n=6)$.

Woolley has recently analysed the bonding in clusters possessing the face-bridged $[M_6(\mu_3\text{-}X)_8]$ core (where X is a π-donor or π-acceptor ligand).[23] The conclusions that he has reached are essentially the same as those described above. He agrees that the metal-ligand bonding occurs primarily through the metal s and p orbitals (with the participation of a limited number of d-based orbitals), while metal-metal bonding occurs through the metal d orbitals. In addition he concludes that the HOMO-LUMO gap for the π-donor-bridged clusters is found at the large d-band gap, while the HOMO-LUMO gap for the π-acceptor-bridged clusters (where the d-band is compressed) is found at the s-d gap. Woolley has criticised earlier Extended Hückel treatments of cluster bonding[18] on the grounds that they led to unrealistically narrow d-bands. By using expanded d orbital functions, the calculations discussed in this Chapter yield a a reasonable d-band width of approximately 4 eV for Mo_6.

6.5 Nido and Arachno π-Donor-Bridged Clusters

The structures of several molybdenum clusters, which may be regarded as being derived from the face-bridged $[Mo_6Cl_{14}]^{2-}$ type of cluster, by the removal of one (nido) or two (arachno) metal atoms (along with their associated terminal ligands), have recently been determined, **(III)-(VI)**.[15] The valence electron counts and metal-metal bond lengths of these clusters are summarised in **Table 6.1.** Extended Hückel calculations were performed on $[Mo_nCl_x]$ species (for consistency

Table 6.1 Valence electron counts and metal-metal bond lengths in closo-, nido- and arachno- clusters based on face-bridged $[Mo_6Cl_{14}]^{2-}$

Cluster	Structure	No. of cluster valence electrons	Metal-Metal bond lengths (Å)	Ref.
$[Mo_6Cl_{14}]^{2-}$	Octahedral	84	2.610	6
$[Mo_5Cl_{13}]^{2-}$	Square pyramidal	69	2.602 (a) 2.563 (b)	15a
$[Mo_4(OPr^i)_8Cl_4]$	Square planar	52	2.378	15b
$[Mo_4Cl_{12}]^{3-}$	Rhombic planar (c)	55	2.653, 2.358	15c
$[Mo_4(OPr^i)_8Br_4]$	Butterfly	52	2.515 (d) 2.481 (e) 3.287 (f)	15b
$[Mo_4Cl_{12}]^{3-}$	Butterfly	55	2.552 (d) 2.598 (e) 3.392 (f)	15c
$[Mo_4I_{11}]^{2-}$	Butterfly	55	2.542 (d) 2.669 (e) 3.035 (f)	15d

(a) apical-basal

(b) basal-basal

(c) Mo-Mo-Mo bond angles 99.06° and 80.94°

(d) wingtip-hinge

(e) hinge length

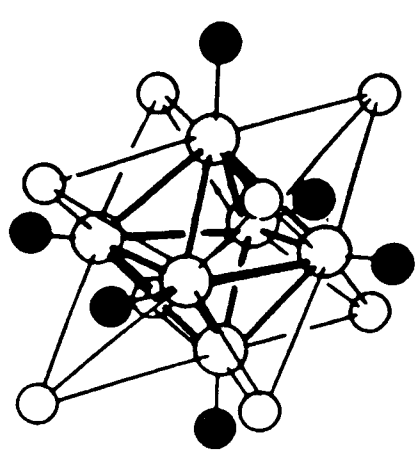
(f) non-bonded wingtip separation

with the work described above) resulting from the removal of Mo-Cl fragments from both $[Mo_6Cl_{14}]^{2-}$ (**Figure 6.6a**) and $[Mo_6Cl_{18}]^{2+}$ (**Figure 6.6b**), though no examples of nido or arachno clusters based on the edge-bridged octahedron have yet been characterised. This section investigates electronic and structural relationships in these molecules and compares their bonding characteristics with those of nido and arachno transition metal carbonyl clusters.

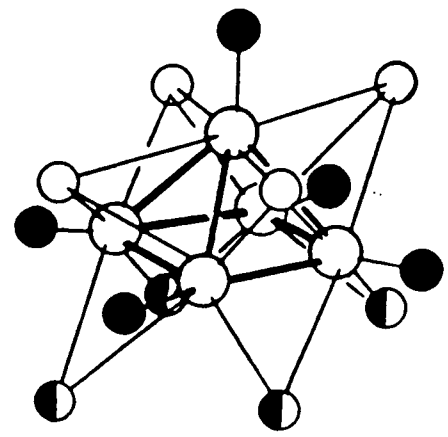
One obvious difference between carbonyl- and π-donor-bridged clusters is the change in the number of electrons, contributed to the cluster, resulting from a modification of the coordination mode of the ligand. For example, the removal of a metal vertex adjacent to a face-bridging chlorine atom (5-electron donor) generates an edge-bridging chlorine (3-electron donor). Similarly the removal of a metal vertex adjacent to an edge-bridging chlorine generates a terminal chlorine (1-electron donor). The carbonyl ligand, however, functions as a 2-electron donor regardless of whether it is in a terminal, edge-bridging or face-bridging coordination mode. Although the loss of metal vertices, illustrated in **Figure 6.6**, alters the coordination number of the individual ligands, their overall cubic or cuboctahedral arrangement around the cluster is retained.

Closo face- and edge-bridged octahedral clusters have 12 and 8 skeletal bonding MO's respectively. They have 7 of these orbitals in common $\{S_d^{\sigma}(a_{1g})$, $P_d^{\pi+\sigma}(t_{1u})$ and $D_d^{\pi+\delta}(t_{2g})$ (though in the face-bridged case this orbital is purely D_d^{π} in character, as the δ-component is utilised in bonding to the bridging ligands)$\}$, which have identical symmetry and similar nodal properties to the 7 skeletal bonding MO's of $[B_6H_6]^{2-}$ and $[Os_6(CO)_{18}]^{2-}$ (a conical $Os(CO)_3$ fragment being isolobal with BH).[24]

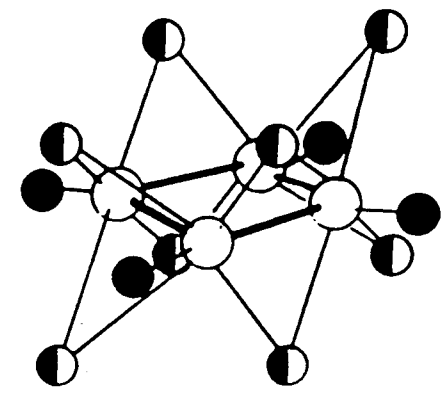
(a)



$[Mo_6Cl_{14}]$

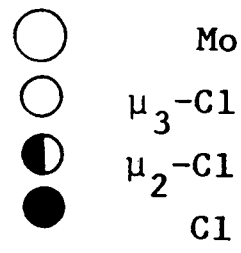


$[Mo_5Cl_{13}]$



square planar

$[Mo_4Cl_{12}]$

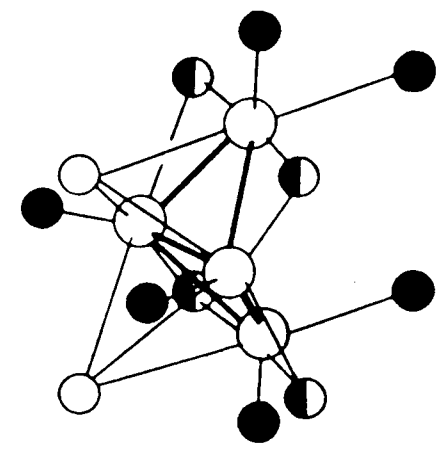


Mo

μ_3-Cl

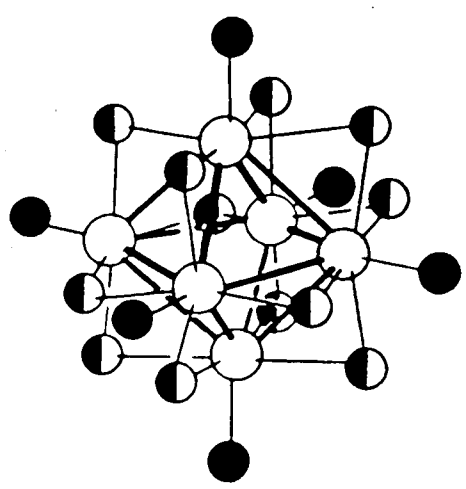
μ_2-Cl

Cl

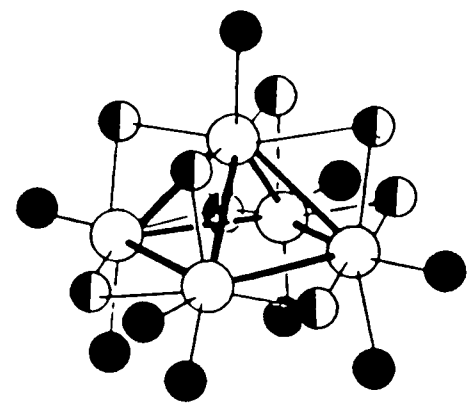


butterfly

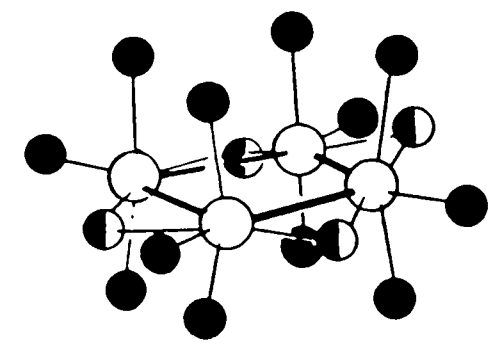
(b)



$[Mo_6Cl_{18}]$



$[Mo_5Cl_{17}]$



$[Mo_4Cl_{16}]$

Figure 6.6 Model <u>closo</u>, <u>nido</u> and <u>arachno</u> chloride-bridged clusters based on (a) $[Mo_6Cl_{14}]^{2-}$ and (b) $[Mo_6Cl_{18}]^{2+}$.

6.5.1 The closo, nido, arachno relationship in main group and transition metal carbonyl cluster chemistry

A previous analysis of the effect of removing a vertex from the octahedral borane cluster $[B_6H_6]^{2-}$ showed that its bonding $D_p^{\pi}(t_{2g})$ orbitals split into a bonding a_1 orbital and an essentially non-bonding e pair (under C_{4v} symmetry), while the S^{σ} and $P^{\sigma+\pi}$ orbitals remain strongly bonding.[14a] On removing a second (trans) vertex, the e pair (now e_g under D_{4h} symmetry) become very slightly antibonding. In the square pyramidal (nido) case the e set may be stabilised by bridging hydrides around the open face, as in $[B_5H_9]$. Square pyramidal transition metal carbonyl clusters achieve stabilisation of the e pair either by interaction with the orbitals of an interstitial atom, as in $[Os_5C(CO)_{15}]$,[25] or those of a capping main group fragment, e.g. $[Os_5(CO)_{15}(\mu_4\text{-}S)]$ [26] and $[Ru_3Rh_2(CO)_{13}(PEt_3)(\mu_4\text{-}PPh)]$.[27] These fragments possess π-symmetry orbitals that can overlap with the frontier e pair of the metal cluster, which are also singly noded on the open face.[28] The e_g pair of orbitals in square planar metal carbonyl clusters, being singly noded on either side of the M_4 plane, are stabilised by two such non-metal capping fragments,[28] as in $[Fe_4(CO)_{11}(\mu_4\text{-}P(p\text{-}tol))_2]$ [29] and $[Ru_4(CO)_{11}(\mu_4\text{-}PPh)_2]$.[30] When the e (or e_g) set of orbitals is occupied, the number of skeletal electron pairs remains constant (i.e. 7) for the series of closo, nido and arachno clusters. There are also several M_4E_2 (E = non-metal) clusters with 8, rather than 7, SEP's, e.g. $[Co_4(CO)_{10}(\mu_4\text{-}PPh)_2]$ and $[Co_4(CO)_{10}(\mu_4\text{-}Te)_2]$.[31] The bonding in these clusters has been studied in detail by Hoffmann et al..[28]

6.5.2 Nido and arachno derivatives of the π-donor-face-bridged octahedral clusters

A comparison of the frontier MO's for octahedral (closo) $[Mo_6Cl_{14}]^{2-}$, square pyramidal (nido) $[Mo_5Cl_{13}]$ and square planar (arachno) $[Mo_4Cl_{12}]$ is presented in **Figure 6.7.** The TSH labels for the MO's of the nido and arachno clusters are those of the bonding MO's, of the octahedral cluster, from which they are derived. The S, P and $D(t_{2g})$ orbitals behave in much the same way as in the borane and metal carbonyl clusters, discussed above, because their nodal characteristics are so similar. The orbitals of real interest, from the point of view of rationalising the electron counts listed in **Table 6.1**, are those derived from the metal d^{δ} orbitals.

When two trans vertices are removed, the HOMO in $[Mo_6Cl_{14}]^{2-}$ $(D_d^{\delta}(e_g))$ generates one strongly antibonding component (b_{1g}), whilst the second component (a_{1g}) remains essentially unperturbed. The former is doubly noded in the M_4 plane and strongly antibonding, since the nodes pass through the metal-metal vectors. In the octahedral cluster, the antibonding nature of this orbital is mitigated by overlap with the in-phase (δ) combination of $d_{x^2-y^2}$ orbitals on the axial atoms, as shown in **Figure 6.8a.** The a_{1g} component of $D_d^{\delta}(e_g)$ has no contribution from the axial atoms and, therefore, its energy is unaffected by the removal of these atoms.

The $\bar{D}_d^{\delta+\pi}(t_{2u})$ orbitals of the octahedron give rise to b_{2u} and e_u components in the square planar (D_{4h} symmetry) cluster. The b_{2u} orbital is strongly antibonding because it is doubly noded in the M_4 plane, but is stabilised in the octahedron by overlapping with the out-of-phase (δ^*) combination of $d_{x^2-y^2}$ orbitals on the axial atoms (**Figure 6.8b**).

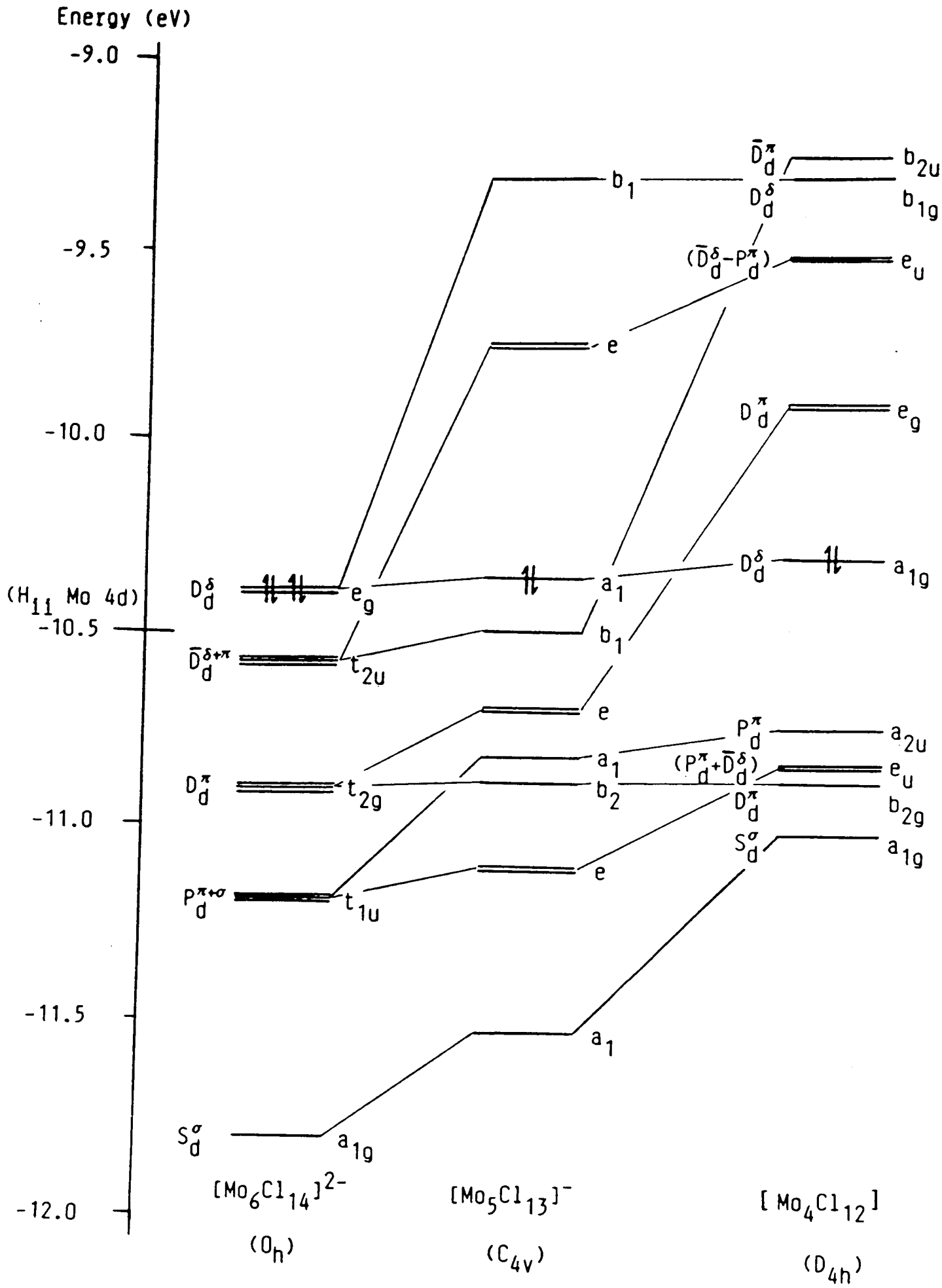
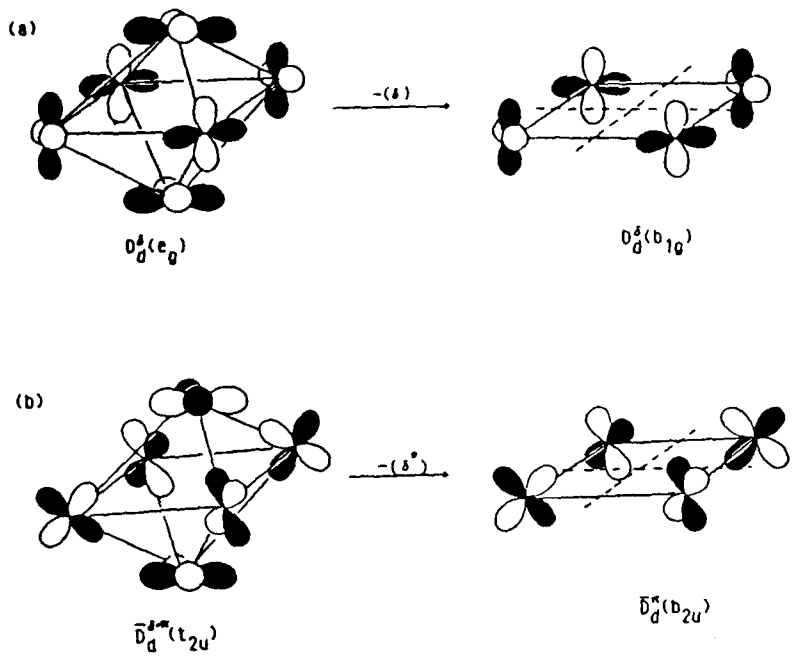
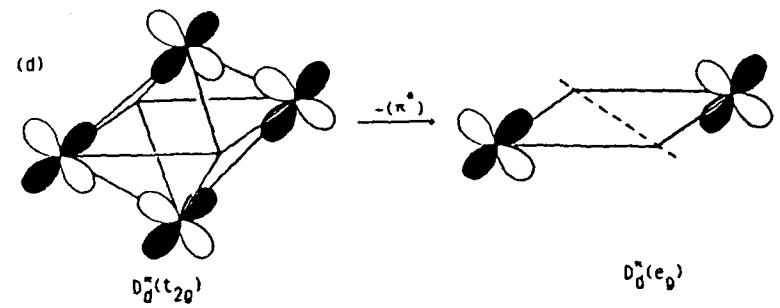


Figure 6.7 Molecular orbital correlation diagram for the removal of one or two (<u>trans</u>) MoCl fragments from $[Mo_6Cl_{14}]^{2-}$.





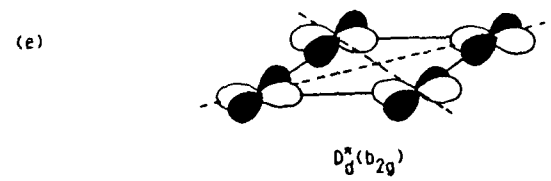


Figure 6.8 Demonstration of the loss of stabilising overlap with in-phase and out-of-phase combinations of (axial atom) d^{π} and d^{δ} orbitals on going from octahedral $[Mo_6Cl_{14}]$ to square planar $[Mo_4Cl_{12}]$.

The e_u orbitals are not as strongly antibonding because they only possess one node in the M_4 plane. In the octahedron these orbitals are stabilised by the in-phase (π) combination of d_{xz} and d_{yz} orbitals on the axial atoms. **Figure 6.8c** illustrates this, together with the change in character of the e_u pair due to mixing with the lower lying $P_d^{\pi+\sigma}(e_u)$ orbitals, which have predominantly π-character. This mixing serves to increase the metal-metal antibonding character of these orbitals.

Figure 6.7 indicates that the removal of two cluster vertices, from the face-bridged octahedron, results in the destabilisation of an e_g pair of orbitals, derived from the $D_d^{\pi}(t_{2g})$ set. As for metal carbonyl clusters, the e_g pair are weakly antibonding due to the single node which they possess in the M_4 plane. In the octahedron these orbitals are stabilised by overlapping with the out-of-phase (π^*) combinations of d_{xz} and d_{yz} orbitals on the axial atoms (**Figure 6.8d**). The remaining component (b_{2g}) derived from the t_{2g} set retains its bonding character on decapping, since it has no contribution from the capping atoms. This orbital is doubly noded in the M_4 plane, but the nodes pass through the metal atoms (**Figure 6.8e**) and consequently impart bonding, rather than antibonding, character.

Inspection of **Figure 6.7** reveals that the square planar cluster possesses 6 d-band bonding MO's (6 of the original 12 bonding MO's of the octahedron having become antibonding on decapping). This leads to the prediction of a 52 electron $[Mo_4Cl_{12}]$ cluster. The isostructural and isoelectronic molecule $[Mo_4(OPr^i)_8Cl_4]$ **(IV)** has been structurally characterised[15b] (an octahedral alkoxide-bridged cluster, $[Mo_6(OMe)_{14}]^{2-}$ is also known).[32] Recently the paramagnetic species $[Mo_4Cl_{12}]^{3-}$ has been reported to have a rhombically distorted planar metal skeleton.[15c]

Calculations by Chisholm et al. have shown that this (55 electron) molecule, if square planar, would have an $(e_g)^3$ configuration (in agreement with the calculations presented above) and a degenerate (^2E_g) ground state.[33] This system is unstable with respect to a Jahn-Teller distortion which results in the observed rhombic cluster geometry, details of which are given in **Table 6.1.**

In the intermediate case of the (nido) square pyramidal cluster (see **Figure 6.7**) the 6 MO's (corresponding to the destabilised orbitals of the square planar cluster) consist of $2b_1$ orbitals and 2e pairs, under the lower (C_{4v}) symmetry of the molecule. Mixing occurs between these orbitals, resulting in the formation of 3 bonding (b_1 + e) and 3 antibonding (b_1 + e) MO's. The bonding combinations have either δ or π contributions from the remaining capping atom which stabilise the doubly or singly noded orbitals respectively. In the antibonding components, these stabilising interactions are absent. Occupation of the 9 bonding d-band MO's leads to the prediction of a stable 68 electron square pyramidal cluster, $[Mo_5Cl_{13}]^-$. The known square pyramidal cluster, $[Mo_5Cl_{13}]^{2-}$ **(III)**, has 69 valence electrons.[15a] These calculations indicate that the additional electron resides in an orbital (one of an e pair) which is singly noded and weakly antibonding in the basal plane of the cluster. This conclusion is in agreement with the earlier Extended Hückel calculations of Meissner and Korol'kov.[34]

Gray has recently reported the electrochemical generation of a series of square pyramidal clusters $[Mo_5X_{13}]^{n-}$ (X = Cl, Br; n = 1, 2, 3), with $(NBu^n_4)^+$ as the counter ion.[35] His findings support the frontier energy level ordering presented above. He has noted that the monoanion is diamagnetic while the dianion and trianion have one and two spin-unpaired electrons respectively. The ground state of the trianion

has been assigned as $^3A_2$, arising from an $(e)^2$ configuration. Gray's studies have shown that the dianions (with a ^2E ground state under C_{4v} symmetry) are not significantly Jahn-Teller distorted, though McCarley has noted a rhombic distortion of the cluster anion in $(NPhEt_3)_2[Mo_5Cl_{13}]$.[36]

Summarising the above results, the octahedral face-bridged cluster is characterised by 12 metal-metal bonding MO's and its nido and arachno derivatives by 9 and 6 MO's respectively (i.e. (3n-6), where n is the number of metal atoms), though the occupation of very weakly antibonding orbitals may also occur. Removing a metal vertex results in the loss of three bonding MO's, while the number of polyhedral edges decreases by four. This means that the ratio of bonding orbitals to edges increases. This is reflected in an increase in the computed metal-metal overlap populations, for the model $[Mo_xCl_{x+8}]^{4-x}$ clusters, on going from closo to nido and then to arachno , as indicated in **Table 6.2.** To back up this theoretical argument, the metal-metal bond lengths of the structurally characterised molybdenum clusters do indeed decrease from closo to arachno, as may be seen from **Table 6.1.** The weakly metal-metal antibonding (roughly non-bonding) nature of the e_g LUMO's of the 52 electron square planar cluster is confirmed by the very small decrease in overlap population on going from $[Mo_4Cl_{12}]$ (52e, overlap popln. +0.44) to $[Mo_4Cl_{12}]^{4-}$ (56e, overlap popln. +0.40). A 56 electron $[Mo_4Cl_{12}]^{4-}$ species has been identified in solution,[28] but has not been structurally characterised.

Table 6.2 Calculated Mo-Mo overlap populations for model clusters based on face-bridged $[Mo_6Cl_{14}]^{2-}$

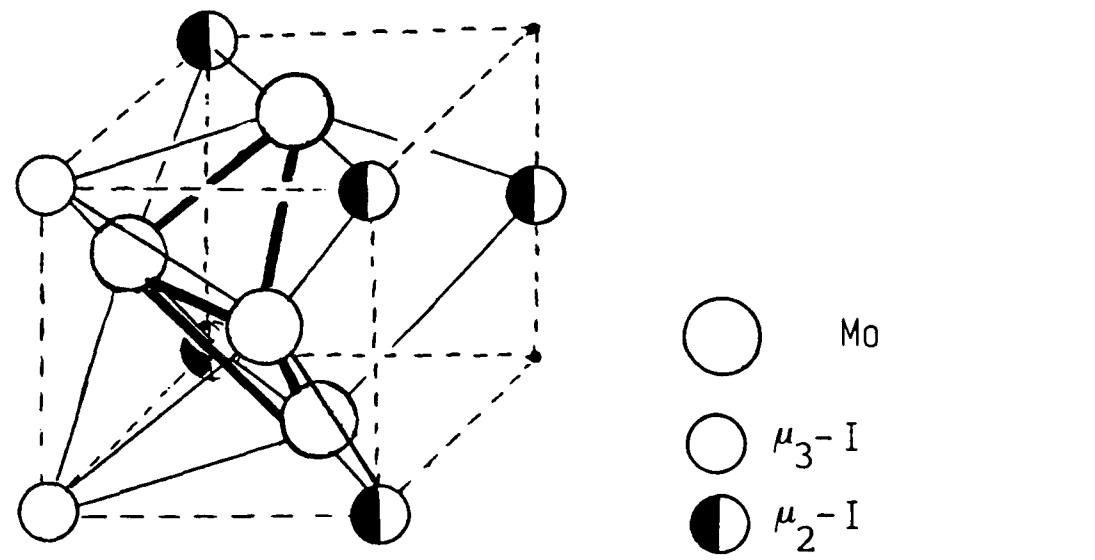
Model cluster	Structure	No. of cluster valence electrons	No. of d band electrons	Calculated Mo-Mo overlap popln.
$[Mo_6Cl_{14}]^{2-}$	Octahedral	84	24	+0.28
$[Mo_5Cl_{13}]^{-}$	Square pyramidal	68	18	+0.29 (a) +0.34 (b)
$[Mo_4Cl_{12}]$	Square planar	52	12	+0.44
$[Mo_4Cl_{12}]^{4-}$	Square planar	56	16	+0.40

(a) apical-basal

(b) basal-basal

6.5.3 Butterfly clusters

The 52 valence electron cluster $[Mo_4(OPr^i)_8Br_4]$ **(V)**[15b] has a "butterfly" (C_{2v}) geometry, which is an alternative arachno geometry derived from the octahedron by the loss of two cis metal atoms. This cluster, like the square planar isopropoxide-bridged molecule, has 12 d band bonding electrons. The metal-metal bonds are also short in this cluster (average 2.50 Å). A 55 electron butterfly cluster, $[Mo_4I_{11}]^{2-}$ **(VI)**,[15d] has also been structurally characterised but it has a slightly different arrangement of bridging ligands. Instead of having 8 ligands arranged in a cubic fashion, it has only 6, with the remaining ligand being located at the midpoint of the edge connecting the "missing ligands" **(8)**. This ligand bridges the wingtips of the butterfly, leading to a smaller wingtip separation (3.035 Å) than that of the 52 electron cluster (3.287 Å).



(8)

Figure 6.9 illustrates the effect of metal-ligand interactions on the frontier orbitals of a bare metal Mo_4 butterfly. In $[Mo_4Cl_{12}]$ and $[Mo_4Cl_{11}]$, with the appropriate wingtip separations, the frontier

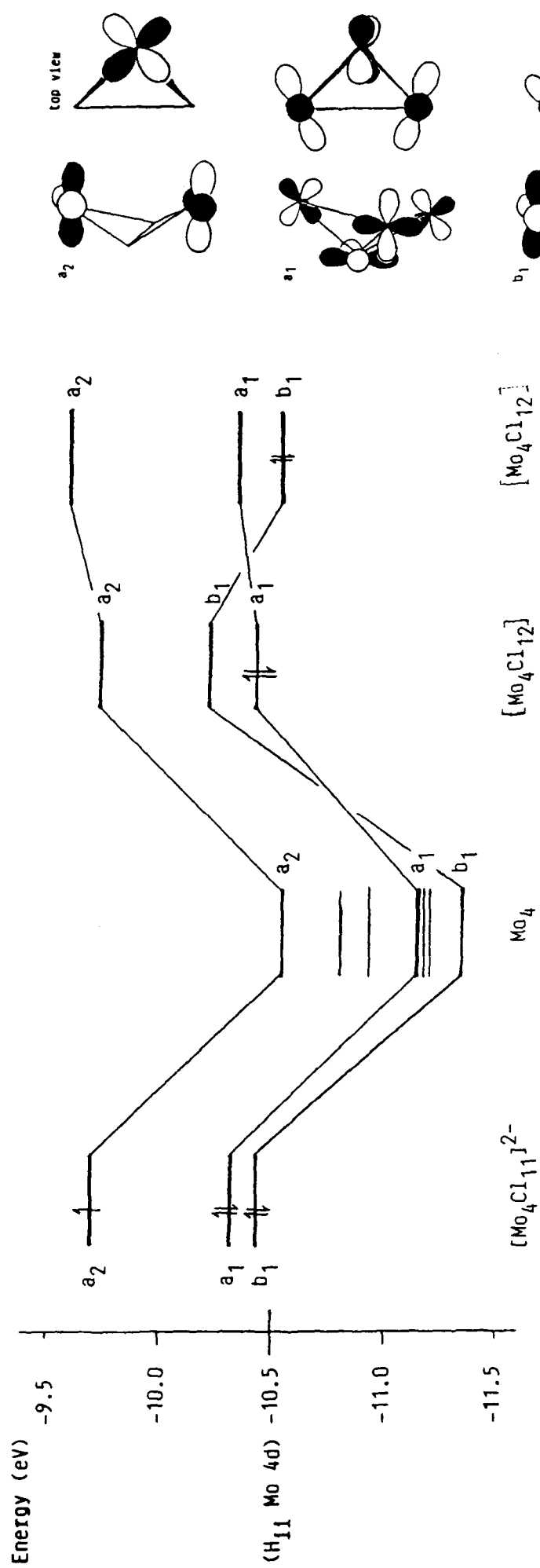


Figure 6.9 Correlation of the skeletal MO's of a "naked" Mo_4 butterfly cluster with those of $[Mo_4Cl_{11}]$ and $[Mo_4Cl_{12}]$.

orbitals of particular interest are those labelled b_1, a_1 and a_2. The b_1 orbital is predominantly localised on the wingtip atoms, with a δ-bonding interaction between them. Consequently, this orbital is stabilised as the cluster is compressed. $[Mo_4Cl_{12}]$, with 12 electrons in the d-band, has the configuration $(a_1)^2(b_1)^0(a_2)^0$, whilst the 15 (d-band) electron $[Mo_4Cl_{11}]^{2-}$ cluster has the configuration $(b_1)^2(a_1)^2(a_2)^1$. The unpaired electron, therefore, resides in an orbital of a_2 symmetry (see **Figure 6.9**) which is weakly antibonding between the wingtip atoms. These results agree qualitatively with an earlier analysis by McCarley.[15d]

Comparing the observed bond lengths in the 52 and 55 electron clusters, the wingtip-hinge distances are very similar (average 2.515 Å for the 52 and 2.542 Å for the 55 electron cluster). There is, however, a significant increase in the length of the hinge bond (2.481 Å in the 52 electron and 2.669 Å in the 55 electron cluster). This is consistent with the occupation, in the latter, of the b_1 orbital (shown in **Figure 6.9**), which has a σ-antibonding component between the hinge atoms.

Recently, a paramagnetic (55 electron) butterfly cluster, $[Mo_4Cl_{12}]^{3-}$, has been structurally characterised, and found to have an identical ligand arrangement to that of **(V)**.[15c] From **Figure 6.9** the predicted electron configuration for this ion is $(a_1)^2(b_1)^2(a_2)^1$. The metal-metal bond lengths (and non-bonded wingtip separations) of the three known butterfly clusters are given in **Table 6.1.**

6.5.4 Nido and arachno derivatives of the π-donor-edge-bridged octahedral clusters

The effect, on the d-band bonding MO's, of removing axial cluster

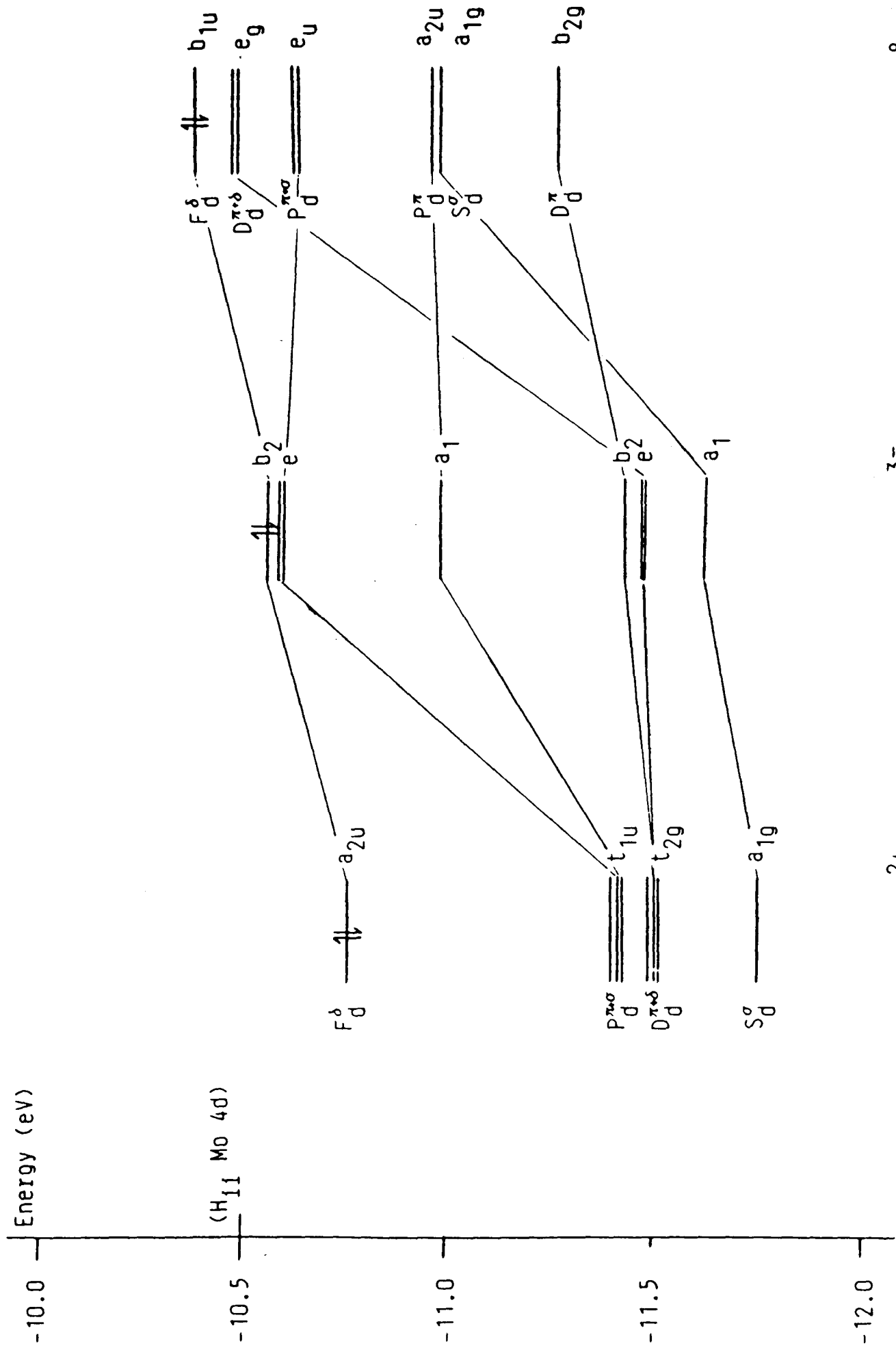


Figure 6.10 Molecular orbital correlation diagram for the removal of one or two (trans) MoCl fragments from $[Mo_6Cl_{18}]^{2+}$.

vertices from the model edge-bridged $[Mo_6Cl_{18}]^{2+}$ cluster is illustrated in **Figure 6.10.** In this case, as may be seen from **Figure 6.10,** the number of bonding skeletal MO's remains constant (i.e. 8) on decapping.

From **Figure 6.10** it is apparent that the $F_d^{\delta}(a_{2u})$ orbital is only slightly destabilised on decapping. This results from the loss of overlap with the out-of-phase (δ^*) combination of d_{xy} orbitals on the axial atoms, as shown in **Figure 6.11a.** This orbital (b_{1u} in the D_{4h} point group) is doubly noded in the equatorial plane, but the nodes pass through the atomic positions, making it bonding even when the axial atoms are removed. The $D_d^{\pi+\delta}(t_{2g})$ orbitals of the octahedron split on decapping to give b_{2g} and e_g orbitals in the square planar cluster. Removing the capping atoms destabilises the b_{2g} component due to the loss of overlap with the in-phase (δ) combination of d_{xy} orbitals on the axial atoms (**Figure 6.11b**). The e_g components are also destabilised as a result of losing the interaction with the out-of-phase (π^*) combinations of d_{xz} and d_{yz} orbitals on the departing axial atoms (**Figure 6.11c**). These orbitals, however, remain sufficiently low lying to be occupied due to π/δ mixing in the square plane. Such mixing is absent in the face-bridged cluster because the δ-component is utilised in bonding to the bridging ligands.

Occupation of the metal-ligand bonding MO's and the 8 d-band bonding MO's leads to predicted electron counts of 66 for the square pyramidal cluster $[Mo_5Cl_{17}]^{3-}$ and 56 for the square planar cluster $[Mo_4Cl_{16}]^{8-}$, though $[Re_4Cl_{16}]^{4-}$ may constitute a more reasonable synthetic goal. Since there is no change in the number of M-M bonding MO's in this series of <u>closo</u>, <u>nido</u> and <u>arachno</u> clusters, they resemble metal carbonyl and borane clusters.[13] The calculated Mo-Mo overlap populations for these clusters (see **Table 6.3**) suggest a strengthening

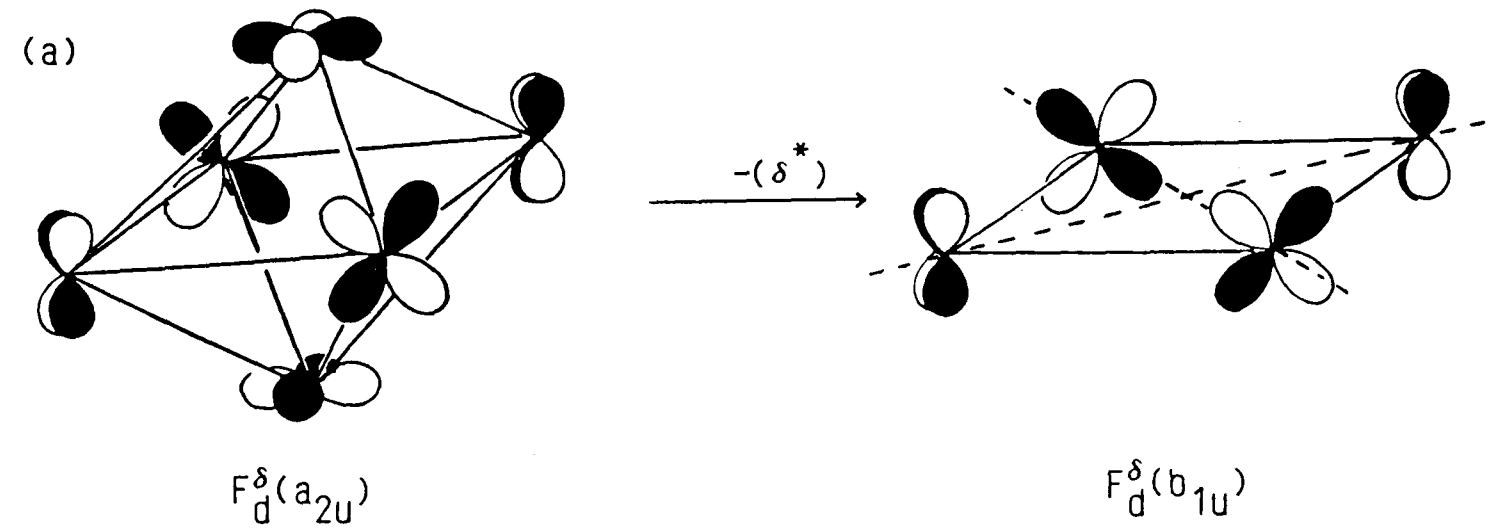


Figure 6.11 Demonstration of the loss of stabilising overlap with in-phase or out-of-phase combinations of (axial atom) d^{π} and d^{δ} orbitals on going from octahedral $[Mo_6Cl_{18}]$ to square planar $[Mo_4Cl_{16}]$.

Table 6.3 Calculated Mo-Mo overlap populations for model clusters based on edge-bridged $[Mo_6Cl_{18}]^{2+}$

Model cluster	Structure	No. of cluster valence electrons	No. of d band electrons	Calculated Mo-Mo overlap popln.
$[Mo_6Cl_{18}]^{2+}$	Octahedral	76	16	+0.34
$[Mo_5Cl_{17}]^{3-}$	Square pyramidal	66	16	+0.35 (a) +0.46 (b)
$[Mo_4Cl_{16}]^{8-}$	Square planar	56	16	+0.58

(a) apical-basal

(b) basal-basal

of the metal-metal bonding as the number of atoms is reduced and the ratio of bond pairs to cluster edges increases.

6.5.5 Summary

Summarising the conclusions described above, face-bridged octahedral (closo) clusters are characterised by 84 cluster valence electrons (of which 24 are in metal-metal bonding orbitals). The removal of an Mo-Cl fragment leads to a decrease of 5 in the total number of metal-chlorine bonding orbitals and the loss of 3 bonding skeletal MO's. This means that the valence electron count drops by 16 for each metal atom removed. Thus, the related nido and arachno clusters possess 68 (18 M-M bonding) and 52 (12 M-M bonding) valence electrons respectively. The loss of an Mo-Cl fragment from the edge-bridged 76 (16 M-M bonding) valence electron octahedral cluster also leads to a decrease of 5 in the number of metal-chlorine bonding ligands, but the number of bonding skeletal MO's is unchanged and the electron count is reduced by only 10. Thus the related nido and arachno clusters are predicted to possess 66 and 56 valence electrons respectively (with 16 electrons in M-M bonding orbitals).

6.6 Localised Treatment of the Bonding in Closo, Nido and Arachno π-Donor-Bridged Clusters

The different behaviour of face- and edge-bridged clusters, on decapping, may be rationalised from a localised bonding viewpoint. As Kettle demonstrated,[9b] the metal-metal bonding orbitals in the edge-bridged octahedral cluster are topologically equivalent to linear

combinations of 8 face-localised 3c-2e bonds. The removal of a cluster vertex leads to the formation of a square pyramidal cluster, with the same number of edges as its precursor had faces. The bonding MO's are topologically equivalent to the 8 edges of the square pyramid, so the bonding may be described in terms of localised 2c-2e bonds. **Figure 6.12** shows how a face-bonding orbital becomes edge-bonding when a cluster vertex is removed.

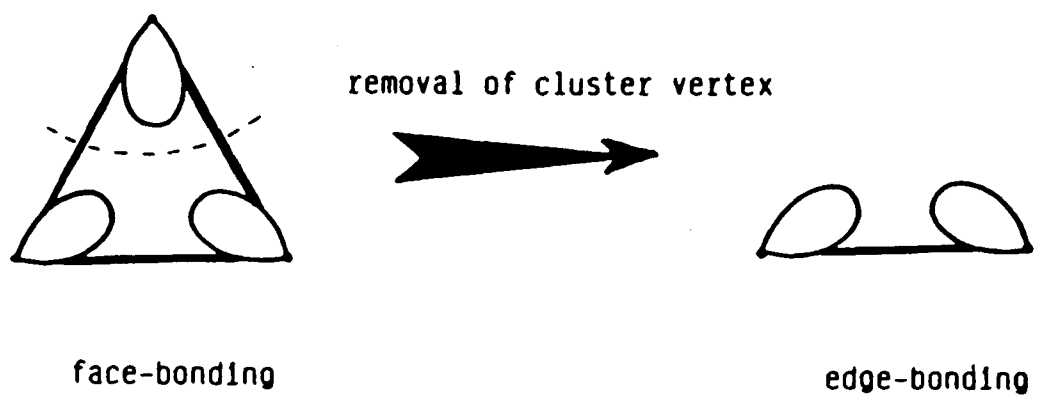
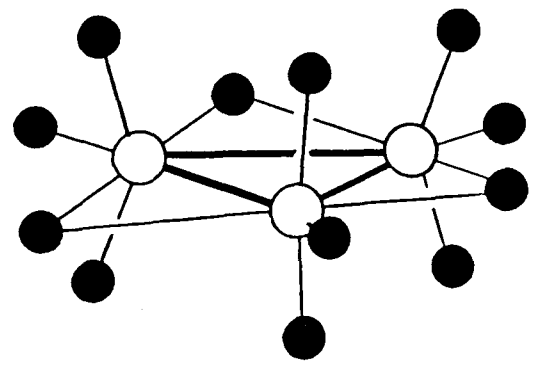


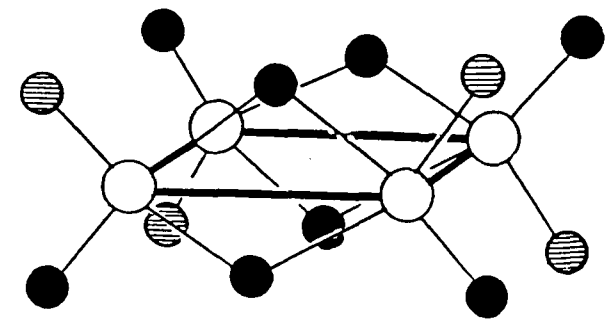
Figure 6.12 Conversion of a localised face-bonding cluster MO into an edge-bonding orbital by the removal of a cluster vertex.

When two <u>trans</u> metal atoms are removed from the octahedron the bonding in the resultant ring cluster may be described in terms of formal double bonds between the metal atoms. An example of such a double bonded cluster is $[Re_3Cl_{12}]^{3-}$ **(VII)**,[37] which has 6 SEP's and may be regarded as an <u>arachno</u> (edge-bridged) trigonal bipyramid. The predicted square planar cluster $[Re_4Cl_{16}]^{4-}$ would possess 8 SEP's. Although no square planar clusters possessing 4 double bonds are known at present, there is a rectangular cluster, $[Mo_4Cl_8(PEt_3)_4]$ **(VIII)**, which has 2 triple bonds and 2 single bonds (i.e. 8 metal-metal bonding orbitals in total).[38]



$[Re_3Cl_{12}]^{3-}$

(VII)



$[Mo_4Cl_8(PEt_3)_4]$

(VIII)

The skeletal bonding in the face-bridged octahedral clusters can be described in terms of 12 edge-localised 2c-2e bonds. The removal of a metal vertex with 4 ($1\sigma + 2\pi + 1\delta$) frontier orbitals leaves 4 out-pointing orbitals on the square face of the square pyramidal cluster. These localised orbitals generate linear combinations with a_1, e and b_1 symmetry, as shown in **Figure 6.13.**

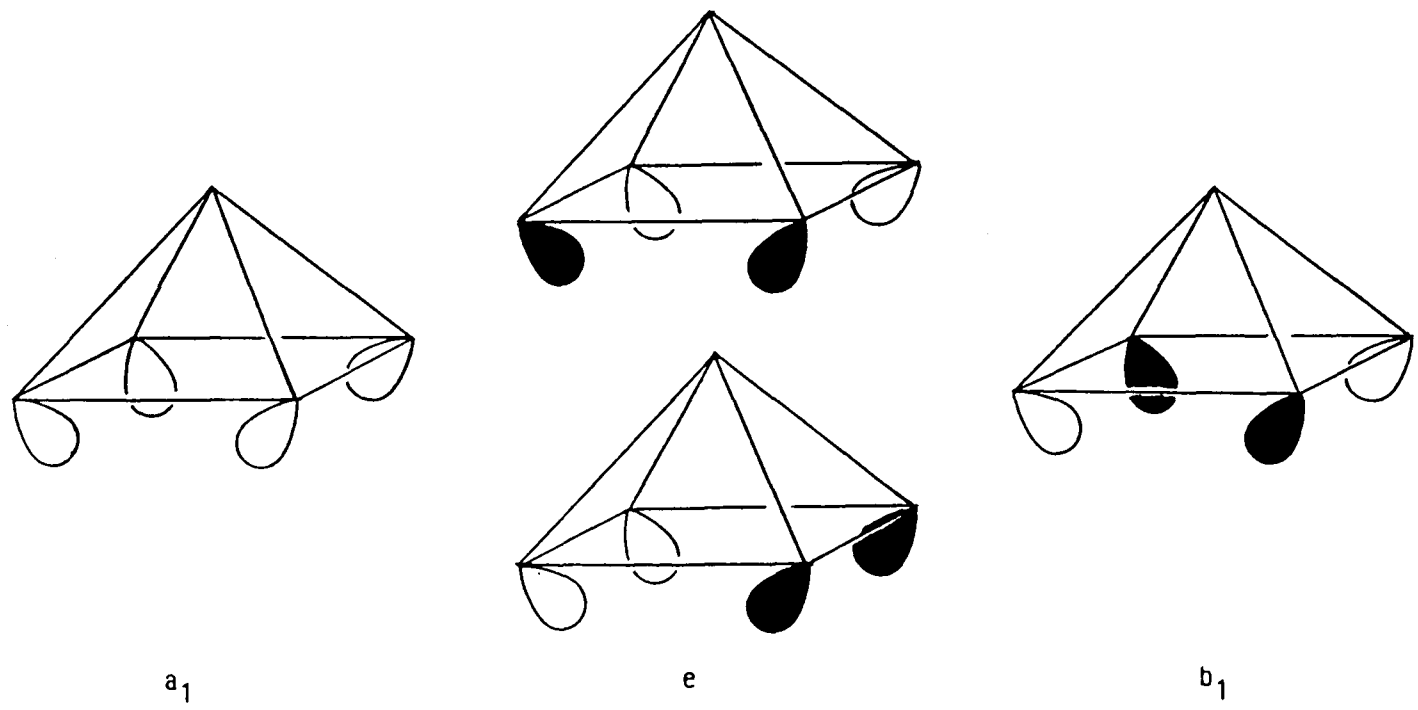


Figure 6.13 Localised orbitals on the square face formed by removing a metal vertex from the face-bridged octahedral cluster.

Since only the nodeless a_1 combination is sufficiently bonding to be

occupied, the overall effect of removing the vertex is the loss of 3 metal-metal bonding MO's. The loss of a second (trans) vertex similarly leads to a decrease of 3 in the number of metal-metal bonding orbitals, though one of the singly noded e pairs may be approximately non-bonding and, therefore, potentially accessible.

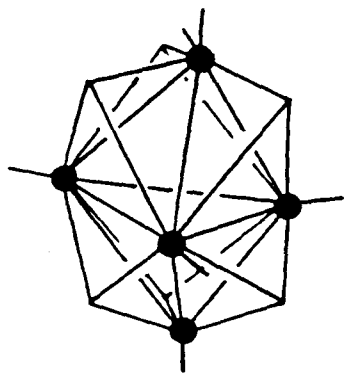
6.7 π-Donor-Bridged Closo Trigonal Bipyramidal Clusters and their Nido and Arachno Derivatives

To complete the studies described in this Chapter, calculations were performed on the families of clusters derived from face- and edge-chloride-bridged trigonal bipyramidal clusters. The predicted structures and electron counts are given in **Figure 6.14.**

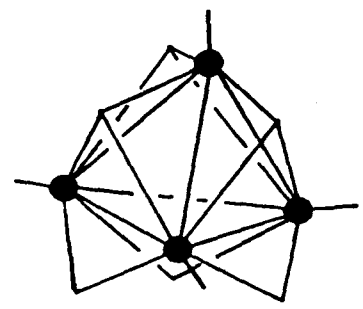
The edge-bridged trigonal bipyramidal (closo) cluster possesses 6 skeletal bonding MO's which are topologically equivalent to the faces of the polyhedron. On removing one or two axial vertices, there is no change in the number of skeletal bonding MO's. This results in a tetrahedral (nido) cluster with 6 edge-localised bonds and a triangular (arachno) species which is doubly bonded. An example of the latter type of cluster is $[Re_3Cl_{12}]^{3-}$ **(VII).**[37]

The face-bridged (closo) trigonal bipyramidal cluster possesses 9 skeletal bonding MO's which are topologically equivalent to the edges of the trigonal bipyramid. The removal of an axial Mo-Cl vertex leads to the destabilisation of 2 skeletal bonding MO's. Thus, as in the case of the clusters derived from the face-bridged octahedral cluster, the number of destabilised MO's is one less than the cluster connectivity of the removed vertex. Alternatively, in a localised sense, only the nodeless combination of out-pointing orbitals on the "open" face is low

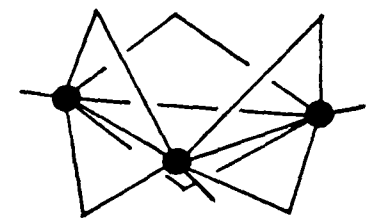
Face-Bridged Clusters



$[Mo_5Cl_{11}]^+$ (or $[Ta_5Cl_{11}]^{4-}$)
(64e, 9 SEP's)

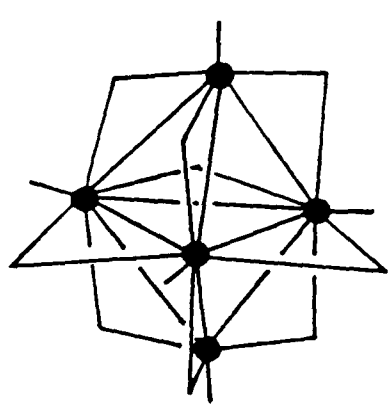


$[Mo_4Cl_{10}]$
(52e, 7 SEP's)

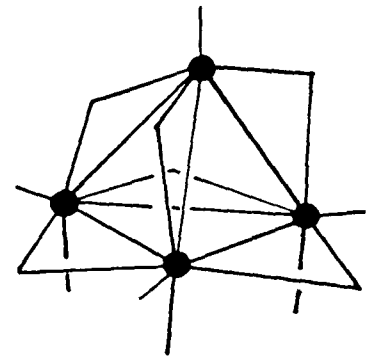


$[Mo_3Cl_9]^-$
(40e, 5 SEP's)

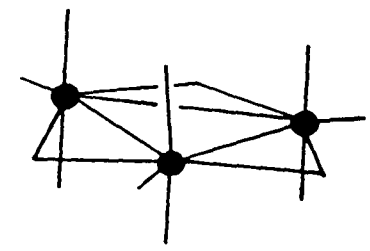
Edge-Bridged Clusters



$[Mo_5Cl_{14}]^{4+}$ (or $[Ta_5Cl_{14}]^-$)
(58e, 6 SEP's)



$[Mo_4Cl_{13}]^-$
(50e, 6 SEP's)



$[Mo_3Cl_{12}]^{6-}$ (or $[Re_3Cl_{12}]^{3-}$)
(42e, 6 SEP's)

Figure 6.14 Structures and postulated electron counts for hypothetical closo edge- and face-bridged trigonal bipyramidal clusters and their nido and arachno derivatives.

lying and accessible. In general terms, a bipyramidal (closo) cluster has e SEP's (e = no. of polyhedral edges, i.e. 9 for a trigonal bipyramid), a pyramidal (nido) cluster has (e+1) SEP's (7 for a tetrahedron) and a ring (arachno) cluster is characterised by (e+2) SEP's (5 for a triangle).

6.8 Related Systems

In this Chapter, the similarities and differences between π-donor and π-acceptor face- and edge-bridged clusters have been emphasised. Those properties which are dependent on the nature of the transition metal, i.e. whether it is early or late in the transition series, have been separated from those which are symmetry or topology dependent.

In addition to the deltahedrally-based structures discussed above, a number of π-donor -bridged clusters have been structurally characterised where the metal skeleton is a 3-connected polyhedron. Such polyhedra include the tetrahedron (also a deltahedron), trigonal prism and cube. Additional types of π-donor-bridged clusters include those with more than one terminal ligand atom per metal atom and also those with a single terminal ligand, such as η^5-C_5H_5, which is a strong π-donor. The purpose of this Section is to outline theoretical treatments of these alternative π-donor-bridged structural types.

The face-bridged tetrahedral clusters $[M_4(\mu_3\text{-}X)_4L_n]$, known as the "cubanes" due to the approximately cubic arrangement of the metal and bridging ligands, have been extensively studied by theoretical[39] and experimental chemists[40] alike. The great interest in cubane clusters stems from structural and electrochemical similarities between certain of these molecules (in particular the Fe-S and Fe-Mo-S cubanes)[40] and

the redox active sites of biologically important electron transfer proteins such as the ferredoxins and nitrogenases.[40b,41] Structural studies have shown that the metal-metal distances in cubane clusters range from non-bonding to quite strongly bonding, depending on the cluster valence electron count.[40]

A number of electron deficient π-donor-bridged clusters are known, e.g. face-bridged $[Nb_6I_8(MeNH_2)_6]$ (with 82 electrons)[12] and edge-bridged $[Zr_6I_{12}]$ (72e).[13] These molecules possess the same basic octahedral skeleton as the 84 and 76 electron species, but many undergo Jahn-Teller distortions which lower the true symmetry from octahedral. Corbett has recently structurally characterised a series of "electron deficient" and "electron precise" octahedral edge-bridged zirconium halide clusters with interstitial main group atoms, e.g. $[Zr_6I_{14}C]$ (14 M-M bonding electrons) and $[Zr_6I_{12}C]$ (16 M-M bonding electrons).[42] An edge-bridged cluster with 16 metal-metal bonding electrons may be regarded as "electron-face-precise" because it possesses 8, i.e. one for every face, 3c-2e bonds. Corbett has also performed Extended Hückel calculations which show that interstitial atoms interact strongly with the d-band bonding MO's of a_{1g} and t_{1u} symmetry,[42b] i.e. S_d^{σ} and $P_d^{\pi+\sigma}$. Interstitial hydrogen has long been known, for example in the octahedral cluster $[Nb_6I_{11}H]$.[43]

There are a number of electron rich sulphide-bridged clusters of the later transition metals, e.g. $[Co_6S_8(PEt_3)_6]^{0,+1}$ (98 or 97e),[44] $[Co_6S_8(CO)_6]$ (98e)[45] and $[Fe_6S_8(PEt_3)_6]^{2+}$ (90e),[46] which possess distorted octahedral structures. High electron counts are possible for these clusters because of the narrowness of their d-bands (due to the contracted nature of the metal d orbitals on the right of the transition

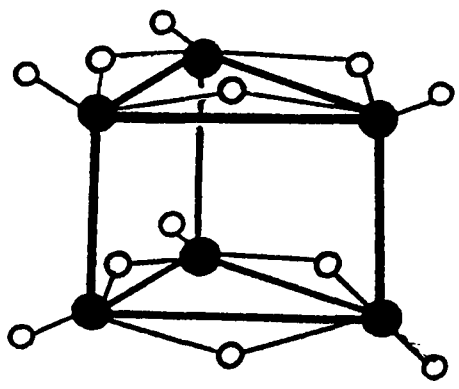
series). It is evident that π-donor-bridged clusters undergo slight distortions upon formal addition or removal of electrons from the "magic number" expected for the cluster (i.e. 84 or 76 for an octahedron). This is also observed in the case of the nido and arachno derivatives mentioned above and should be contrasted with the behaviour of metal carbonyl clusters, where such electronic changes are accompanied by skeletal rearrangements.[14] A likely explanation is that, unlike carbonyl ligands, π-donor -bridging ligands form strong bonds to the metal atoms which would have to be ruptured to deform the cluster skeleton significantly. In other words metal-ligand bonding considerations are very important in holding the cluster together.

Holm has structurally characterised the face-bridged cubic clusters $[Co_8S_6(SPh)_8]^{4-,5-}$,[47] which have the same Co_8S_6 core as that found in synthetic cobalt pentlandite Co_9S_8.[48] The ion $[Co_8S_6(SPh)_8]^{4-}$ possesses 108 valence electrons, of which 56 are in metal d-band orbitals. This electron count is clearly much greater than that required for the formation of edge- or face-localised bonds, suggesting the occupation of a number of non-bonding, or weakly antibonding, d-band cluster MO's.

Bottomley has performed a series of Extended Hückel calculations on deltahedral clusters of the form $[(CpM)_m(\mu_3\text{-}X)_x]$ in order to determine the number of d-band bonding MO's that they possess, to explain trends in metal-metal bond lengths and to predict the occurrence of Jahn-Teller distortions.[49] The octahedral molecule $[Cp_6Ti_6O_8]$ [50] was calculated to have 2 d-band bonding electrons, which must occupy the non-degenerate ($S_d^{\sigma}(a_{1g})$) orbital in order to explain the observed diamagnetism and lack of skeletal distortion. Fowler and Ceulemans have studied this octahedral molecule, along with other bridged transition metal clusters, using Tensor Surface Harmonic theory.[51] For the halide and chalcogenide

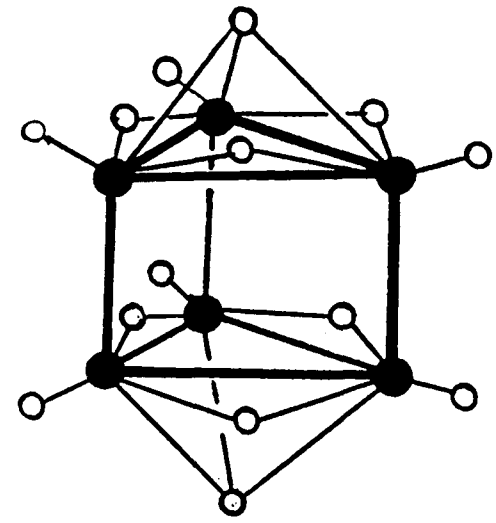
edge- and face-bridged clusters, their energy level orderings and orbital assignments are identical to those presented above.

A series of technicium-halide clusters have recently been characterised, **(IX)-(XI)**, which have structures based on a trigonal prismatic Tc_6 unit with halide ligands bridging the edges of the triangular faces and (in one case) capping these faces.[52]



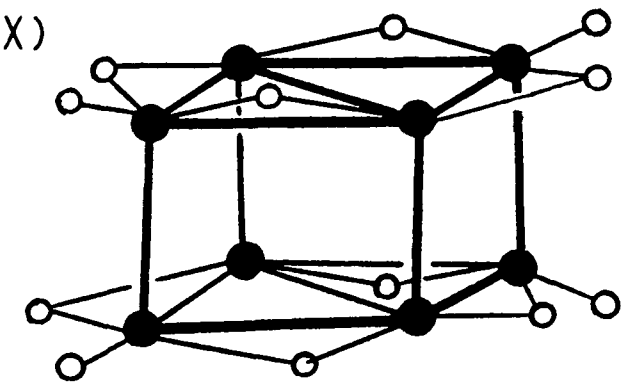
$[Tc_6Cl_{12}]^{2-}$

(IX)



$[Tc_6Cl_{14}]^{3-}$

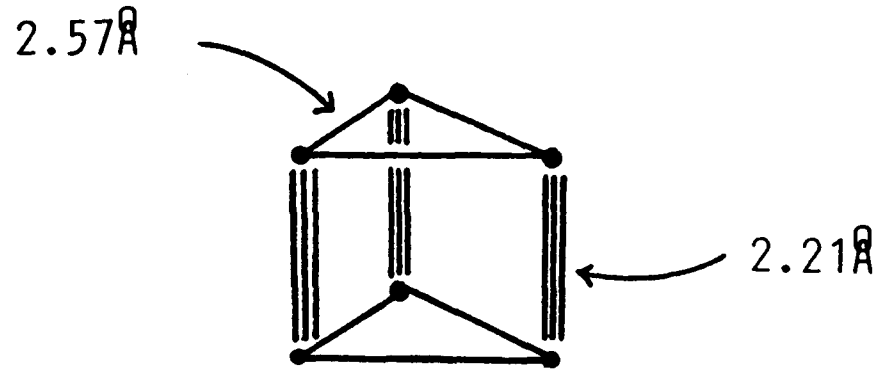
(X)



$[Tc_8Br_{14}]$

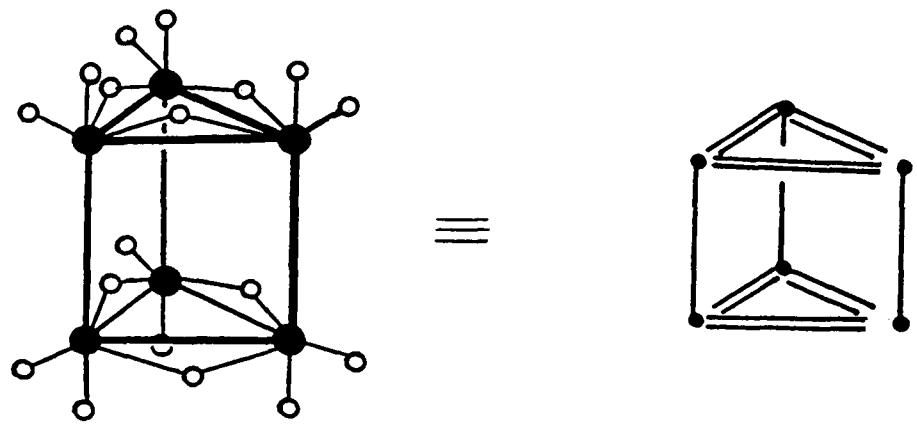
(XI)

Wheeler and Hoffmann have studied the bonding in these clusters, concluding that the 68 electron species $[Tc_6Cl_{12}]^{2-}$ **(IX)** (with 32 metal d-band electrons) may best be regarded in terms of multiple bonding between the two triangular faces of the cluster.[53] This idea is supported by the observed bond lengths **(9)**.[52a]



(9)

The species $[Tc_6Cl_{18}]^{6-}$ has also been postulated.[53] This hypothetical molecule is clearly related to the $[Re_3Cl_{12}]^{3-}$ type of cluster **(VII)**,[37], since it possesses doubly bonded triangular faces **(10)**.

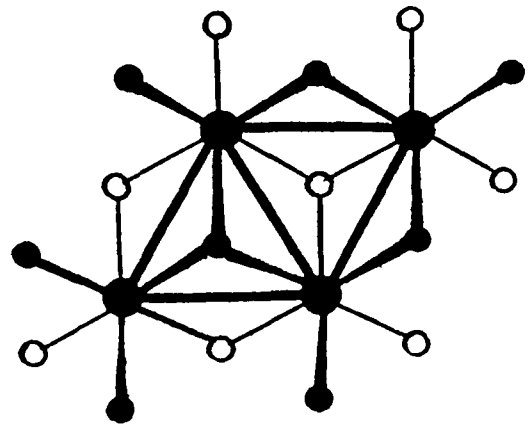


$[Tc_6Cl_{18}]^{6-}$

(10)

Gray has investigated the spectroscopic, electrochemical and photochemical properties of the halide-bridged clusters of molybdenum and tungsten.[35,54] A challenge exists for the theoretical chemist to rationalise such physical properties as the intense luminescence of the octahedral clusters $[M_6Cl_{14}]^{2-}$.[54]

A rapidly enlarging field is the study of extended structures based on halide and chalcogenide-bridged octahedral clusters.[2,3] Notable theoretical studies in this area include the work of Andersen[55] and the tight binding approach (within the Extended Hückel framework) of Hoffmann and Hughbanks.[56] Much of the incentive for this work comes from the superconducting properties[4] of, for example, the Chevrel Phases.[3] There have also been many theoretical treatments of the bonding in trinuclear π-donor-bridged clusters[57] and extended arrays made up of triangular and rhombic units, such as Cotton's treatment of the bonding[58] in $[Ba_{1.13}Mo_8O_{16}]$. This is composed of two symmetrically distinct types of rhombic Mo_4 unit,[59] which are structurally analogous to the discrete rhombic cluster $[W_4(OEt)_{16}]$ **(XII)**, characterised by Chisholm *et al.*.[60]



$[Mo_4(OEt)_{16}]$

(XII)

6.9 Appendix

The molecular orbital calculations described in this Chapter were of the Extended Hückel type, using the weighted H_{ij} formula. The

relevant orbital parameters are summarised in **Table 6.4.**

The following bond lengths were used in these calculations: Mo-Mo, 2.61Å; Mo-H, 1.70Å; Mo-Cl, 2.48Å; Mo-C, 2.06Å; C-O, 1.10Å.

Table 6.4 Extended Hückel parameters

		H_{ii}(eV)	ζ_1[a]	ζ_2[a]	c_1[b]	c_2[b]
Mo	4d	-10.50	4.540	1.900	0.5899	0.5899
	5s	-8.34	1.960			
	5p	-5.24	1.900			
Cl	3s	-26.30	2.033			
	3p	-14.20	2.033			
C	2s	-21.40	1.625			
	2p	-11.40	1.625			
O	2s	-32.30	2.275			
	2p	-14.80	2.275			
H	1s	-13.60	1.300			

Wolfsberg-Helmholz constant k = 1.75

a Slater type orbital exponents

b Coefficients used in double-ζ expansion of contracted d orbitals

References for Chapter Six

1. F.A. Cotton, Quart. Rev. Chem. Soc., 1966, **20**, 389; M.C. Baird, Prog. Inorg. Chem., 1968, **9**, 1 and references therein.
2. J.D. Corbett, Acc. Chem. Res., 1981, **14**, 239; A. Simon, Angew. Chem., Int. Edn. Engl., 1981, **20**, 1; R.E. McCarley, Phil Trans. R. Soc. Lond., 1982, **A308**, 141 and references therein.
3. R. Chevrel, M. Sergent and J. Prigent, J. Solid State Chem., 1971, **3**, 515; R. Chevrel, P. Gougeon, M. Potel and M. Sergent, J. Solid State Chem., 1985, **57**, 25.
4. B.T. Matthias, M. Merezio, E. Corenzwit, A.S. Cooper and H.E. Barz, Science, 1972, **175**, 1465; O. Fischer, Appl. Phys., 1978, **16**, 1; O. Fischer and M.B. Maple (Eds.), Topics in Current Physics: "Superconductivity in Ternary Compounds", Springer-Verlag, Berlin, 1982, **32**.
5. H. Schäfer and H.G. von Schnering, Angew. Chem., 1964, **76**, 833.
6. P.A. Vaughan, Proc. Natl. Acad. Sci., 1950, **36**, 461.
7. A. Simon, H.G. von Schnering, H. Wohrle and H. Schäfer, Z. Anorg. Allg. Chem., 1965, **339**, 155.
8. A. Simon, H.G. von Schnering and H. Schäfer, Z. Anorg. Allg. Chem., 1968, **361**, 235.
9. (a) J.C. Sheldon, J. Chem. Soc., 1960, 1007, 3106; C.D. Grossman, D.P.Olsen and C.H. Duffey, J. Chem. Phys., 1963, **38**, 73; (b) S.F.A. Kettle, Theor. Chim. Acta., 1965, **3**, 211.
10. F.A. Cotton and T.E. Haas, Inorg. Chem., 1964, **3**, 10.
11. L.J. Guggenberger and A.W. Sleight, Inorg. Chem., 1969, **8**, 2041; F.A. Cotton and G.G. Stanley, Chem. Phys. Lett., 1978, **58**, 450; G. Seifert, G. Grossman and H. Müller, J. Mol. Struct., 1980, **64**, 93;

O.K. Andersen, W. Klose and H. Nohl, Phys. Rev. B: Solid State, 1978, **17**, 1209.

12. F. Stollmaier and A. Simon, Inorg. Chem., 1985, **24**, 168.

13. J.D. Corbett, R.L. Daake, K.R. Poeppelmeier and D.H. Guthrie, J. Amer. Chem. Soc., 1978, **100**, 652.

14. (a) K. Wade, J. Chem. Soc., Chem. Commun., 1971, 792; K. Wade, Adv. Inorg. Chem. Radiochem., 1976, **18**, 1. (b) D.M.P. Mingos, Nature Phys. Sci., 1972, **236**, 99; R. Mason, K.M. Thomas and D.M.P. Mingos, J. Amer. Chem. Soc., 1973, **95**, 3802; D.M.P. Mingos, Acc. Chem. Res., 1984, **17**, 311.

15. (a) K. Jödden, H.G. von Schnering and H. Schäfer, Angew. Chem., Int. Edn. Engl., 1975, **14**, 570. (b) M.H. Chisholm, R.J. Errington, K. Folting and J.C. Huffman, J. Amer. Chem. Soc., 1982, **104**, 2025. (c) S. Stensvad, B.J. Helland, M.W. Bakich, R.A. Jacobson and R.E. McCarley, J. Amer. Chem. Soc., 1978, **100**, 6257. (d) B.A. Aufdembrink and R.E. McCarley, J. Amer. Chem. Soc., 1986, **108**, 2474.

16. A.J. Stone, Mol. Phys., 1980, **41**, 1339; A.J. Stone, Inorg. Chem., 1981, **20**, 563; A.J. Stone, Polyhedron, 1984, **3**, 1299.

17. R.G. Woolley, Nouv. J. Chim., 1981, **5**, 219, 227.

18. D.M.P. Mingos, J. Chem. Soc., Dalton Trans., 1974, 133.

19. J.W. Lauher, J. Amer. Chem. Soc., 1978, **100**, 5305.

20. M. McPartlin, C.R. Eady, B.F.G. Johnson and J. Lewis, J. Chem. Soc., Chem. Commun., 1976, 883.

21. J.A. Connor, in "Transition Metal Clusters" (Ed. B.F.G. Johnson), Wiley, New York, 1980, Ch.5 p.345 and references therein.

22. V. Albano, P.L. Bellon and V. Scatturin, J. Organomet. Chem., 1969, **16**, 461.

23. R.G. Woolley, Inorg. Chem., 1985, **24**, 3519.

24. See, for example: R. Hoffmann, Science, 1981, **211**, 995.

25. P.F. Jackson, B.F.G. Johnson, J. Lewis, J.N. Nicholls, M. McPartlin and W.J.H. Nelson, J. Chem. Soc., Chem. Commun., 1980, 564.

26. R.D. Adams, I.T. Horvath, B.E. Segmuller and L.-W. Yang, Organometallics, 1983, **2**, 1301.

27. M.J. Mays, P.R. Raithby and P.L. Taylor, J. Chem. Soc., Dalton Trans., 1984, 959.

28. J.-F. Halet, J.-Y. Saillard and R. Hoffmann, Inorg. Chem., 1985, **24**, 1695.

29. H. Vahrenkamp and D. Wolters, J. Organomet. Chem., 1982, **224**, C17.

30. J.S. Field, R.J. Haines and D.N. Smit, J. Organomet. Chem., 1982, **224**, C49.

31. R.C. Ryan and L.F. Dahl, J. Amer. Chem. Soc., 1975, **97**, 6904.

32. P. Nanelli and B.P.Block, Inorg. Chem., 1968, **7**, 2423; M.H. Chisholm, J. Heppert and J.C. Huffman, Polyhedron, 1984, **3**, 475.

33. M.H. Chisholm and D. Clark, paper presented at the 189th National Meeting of the A.C.S., Miami, FL, April 1985; paper INOR 256 (cited in Ref. 15d)

34. H. Meissner and D.V. Korol'kov, Z. Anorg. Allg. Chem., 1983, **496**, 175.

35. T.C. Zietlow and H.B. Gray, Inorg. Chem., 1986, **25**, 631.

36. R.E. McCarley, unpublished work mentioned in Ref. 35.

37. J.A. Bertrand, F.A. Cotton and W.A. Dollase, Inorg. Chem., 1963, **2**, 1166.

38. R.E. McCarley, T.R. Ryan and C.C. Torardi, Am. Chem. Soc. Symp. Ser., 1981, **155**, 41.

39. See, for example: R.S. Gall, N.G. Connelly and L.F. Dahl, J. Amer.

Chem. Soc., 1974, **96**, 4017; C.Y. Yang, K.H. Johnson, R.H. Holm and J.G. Norman Jr., J. Amer. Chem. Soc., 1975, **97**, 6596; Trinh-Toan, B.K.Teo, J.A. Ferguson, T.J. Meyer and L.F. Dahl, J. Amer. Chem. Soc., 1977, **99**, 408; M. Cook and M. Karplus, J. Amer. Chem. Soc., 1985, **107**, 257; L. Noodleman, J.G. Norman Jr., J.H. Osborne, A. Aizman and D.A. Case, J. Amer. Chem. Soc., 1985, **107**, 3418 and references therein. The synthesis and structural characterisation of a number of molecules, possessing the (slightly puckered) hexagonal prismatic $[Fe_6S_6]^{3+}$ core, has recently been reported (see, for example: M.G. Kanatzidis, W.R. Hagen, W.R. Dunham, R.K. Lester and D. Coucouvanis, J. Amer. Chem. Soc., 1985, **107**, 953).

40. (a) Trinh-Toan, W.P. Fehlhammer and L.F. Dahl, J. Amer. Chem. Soc., 1977, **99**, 402 and references therein; R.H. Holm, Acc. Chem. Res., 1977, **10**, 427, R.H. Holm, Chem. Soc. Rev., 1981, **10**, 455; C.E. Davies, J.C. Green and G.H. Stringer, N.A.T.O. A.S.I. Ser., "Quantum Chemistry: The Challenge of Transition Metals and Coordination Chemistry" (Ed. A. Veillard), Reidel, Dordrecht (NL), 1986, p.413 and references therein. (b) C.D. Garner, in "Transition Metal Clusters" (Ed. B.F.G. Johnson), Wiley, New York, Ch.4 p.265, 1980 and references therein.

41. W.H. Orme-Johnson, Ann. Rev. Biochem., 1973, **42**, 159; W. Lovengerb, "Iron Sulfur Proteins", Academic, New York, 1977, Vol. III; C.D. Garner, S.R. Acott, G. Christou, D. Collison, F.E. Mabbs and V. Petrouleas, Phil. Trans. R. Soc. Lond., 1982, **A308**, 159 and references therein.

42. (a) R.P. Ziebarth and J.D. Corbett, J. Amer. Chem. Soc., 1985, **107**, 4571. (b) J.D. Smith and J.D. Corbett, J. Amer. Chem. Soc., 1985, **107**, 5704.

43. A. Simon, Z. Anorg. Allg. Chem., 1967, **355**, 311.

44. F. Cecconi, C.A. Ghilardi, S. Midollini and A. Orlandini, Inorg. Chim. Acta., 1982, **64**, L47; 1983, **76**, L183.

45. G. Gervasio, R. Rosetti and L. Stanghellini, Inorg. Chim. Acta., 1984, **83**, L9.

46. F. Cecconi, C.A. Ghilardi and S. Midollini, J. Chem. Soc., Chem. Commun, 1981, 640.

47. G. Christou, K.S. Hagen and R.H. Holm, J. Amer. Chem. Soc., 1982, **104**, 1744; G. Christou, K.S. Hagen, J.K. Bashkin and R.H. Holm, Inorg. Chem., 1985, **24**, 1010.

48. V. Rajamani and C.T. Prewitt, Can. Mineral., 1975, **13**, 75.

49. F. Bottomley and F. Green, Inorg. Chem., 1982, **21**, 4170.

50. J.C. Huffman, J.G. Stone, W.C. Krusell and K.G. Caulton, J. Amer. Chem. Soc., 1977, **99**, 5829.

51. A. Ceulemans and P.W. Fowler, unpublished work.

52. (a) P.A. Kuz'min, M.D. Surazhskaya and T.B. Larina, Dokl. Akad. Nauk SSSR, 1983, **271**, 1157; Koord. Khim., 1985, **11**, 1559. (b) P.A. Kuz'min, M.D. Surazhskaya and T.B. Larina, Dokl. Akad. Nauk SSSR, 1982, **265**, 1420; (Engl. Transl.) 1983, **265**, 656.

53. R.A. Wheeler and R. Hoffmann, J. Amer. Chem. Soc., in press.

54. A.W. Maverick and H.B. Gray, J. Amer. Chem. Soc., 1981, **103**, 1298; A.W. Maverick, J.S. Najdzionek, D. MacKenzie, D.G. Nocera and H.B. Gray, J. Amer. Chem. Soc., 1983, **105**, 1878; T.C. Zeitlow, W.P. Schaefer, B. Sadeghi, N. Hua and H.B. Gray, Inorg. Chem., 1986, **25**, 2195; T.C. Zeitlow, W.P. Schaefer, B. Sadeghi, D.G. Nocera and H.B. Gray, Inorg. Chem., 1986, **25**, 2198.

55. See, for example: O.K. Andersen, Phys. Rev. B: Solid State, 1975,

12, 3060; O.K. Andersen, W. Klose and H. Nohl, Phys. Rev. B: Solid State, 1978, 17, 1209.

56. T. Hughbanks and R. Hoffmann, J. Amer. Chem. Soc., 1983, 105, 1150, 3528; T. Hughbanks, Inorg. Chem., 1986, 25, 1492.

57. See, for example: F.A. Cotton, Inorg. Chem., 1964, 3, 1217; Y. Jiang, A. Tang, R. Hoffmann, J. Huang and J. Lu, Organometallics, 1985, 4, 27 and references therein.

58. F.A. Cotton and A. Fang, J. Amer. Chem. Soc., 1982, 104, 113.

59. C.C. Torardi and R.E. McCarley, J. Solid State Chem., 1981, 37, 393.

60. M.H. Chisholm, J.C. Huffman, C.C. Kirkpatrick, J. Leonelli and K. Folting, J. Amer. Chem. Soc., 1981, 103, 6093.

APPENDIX I

TENSOR SURFACE HARMONIC THEORY

AI.1 Introduction

The first stage in the TSH analysis is the assignment of angular coordinates (θ_i, ϕ_i) to each cluster atom (i).[1] This is followed by evaluation of the angular parts of the solutions of the Schrödinger equation for a particle on a sphere[2] (the radial parts can be ignored if the cluster vertices are taken to lie on the surface of a sphere of unit radius):[1]

$$\nabla^2\Psi = -L(L+1)\Psi$$

where $\nabla^2 = (\sin\theta)^{-1}\,(\partial/\partial\theta)\;\sin\theta\,(\partial/\partial\theta) + (\sin^2\theta)^{-1}\,(\partial^2/\partial\phi^2)$.

The solutions of the above equation are the familiar Spherical Harmonics ($Y_{L,M}$).[3] L and M are quantum numbers which are defined such that $L \geq 0$ and $-L \leq M \leq L$ (both L and M are integers). These quantum numbers are analogous to the orbital angular momentum and magnetic quantum numbers obtained in the solution of the Schrödinger equation for the hydrogen atom.[2]

The next stage in the TSH analysis depends upon whether the cluster MO's to be generated are based on atomic orbitals with 0 (σ), 1 (π) or 2 (δ) nodes with respect to a radial vector passing through the atoms (see **Figure AI.1**).

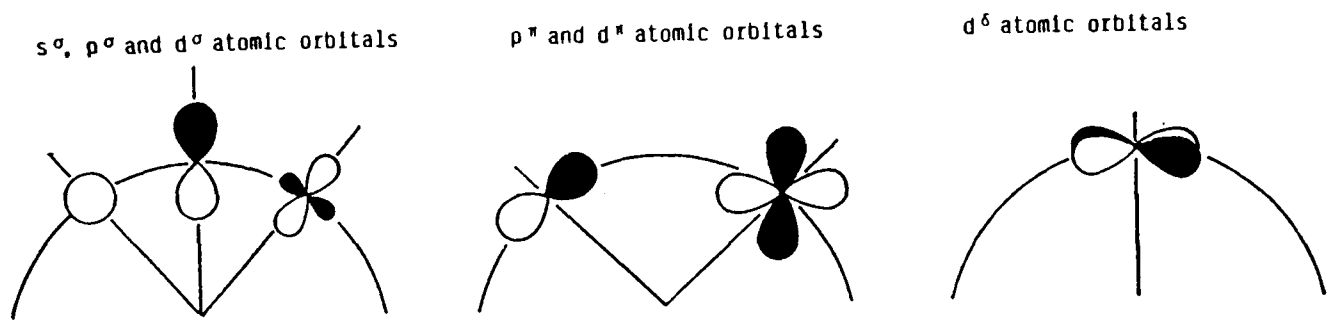


Figure AI.1 σ-,π- and δ-symmetry atomic orbitals used in the construction of cluster MO's.

AI.2 Radial σ-Type Orbitals

For the σ-type cluster wavefunctions, the value of the (Scalar) Spherical Harmonic ($Y_{L,M}$) at each atom position (θ_i, ϕ_i) is taken as the coefficient in an LCAO expansion:

$$\Psi^{\sigma}_{L,M} = \sum_i Y_{L,M}(\theta_i,\phi_i)\sigma_i$$

LCAO coefficients are required to be real numbers, so (for M>0) the real form of the Spherical Harmonics are required:

$$Y_{L,Mc} = \sqrt{2}\{(-1)^M Y_{L,M}+Y_{L,-M}\}$$

$$Y_{L,Ms} = \sqrt{2}i\{(-1)^M Y_{L,M}-Y_{L,-M}\}$$

The subscripts "Mc" and "Ms" refer to the cosine and sine dependence on ϕ which these functions possess:

$$Y_{L,Mc} = \sqrt{2}\, Y_{L,M}(\theta)\cos(M\phi)$$

$$Y_{L,Ms} = \sqrt{2}\, Y_{L,M}(\theta)\sin(M\phi)$$

(this follows from the separation of $Y_{L,M}(\theta,\phi)$ into θ and ϕ components, i.e. $Y_{L,M}(\theta,\phi) = Y_{L,M}(\theta)e^{iM\phi}$).

The σ-type cluster wavefunctions ($\Psi^{\sigma}_{L,Mc}/\Psi^{\sigma}_{L,Ms}$) are generally written as $L^{\sigma}_{Mc}/L^{\sigma}_{Ms}$, where the orbitals are labelled $S^{\sigma}(L=0)$, $P^{\sigma}(L=1)$, $D^{\sigma}(L=2)$, $F^{\sigma}(L=3)$ etc.. For an n-vertex cluster, the first n L^{σ} functions (i.e. those with the lowest L and M values) are chosen, provided that:

(a) they do not possess zero amplitude at all of the cluster vertices and **(b)** they are not merely repeats of earlier MO's.[1]

Examples of the L^{σ} MO's of some small clusters are depicted in **Figure AI.2.**

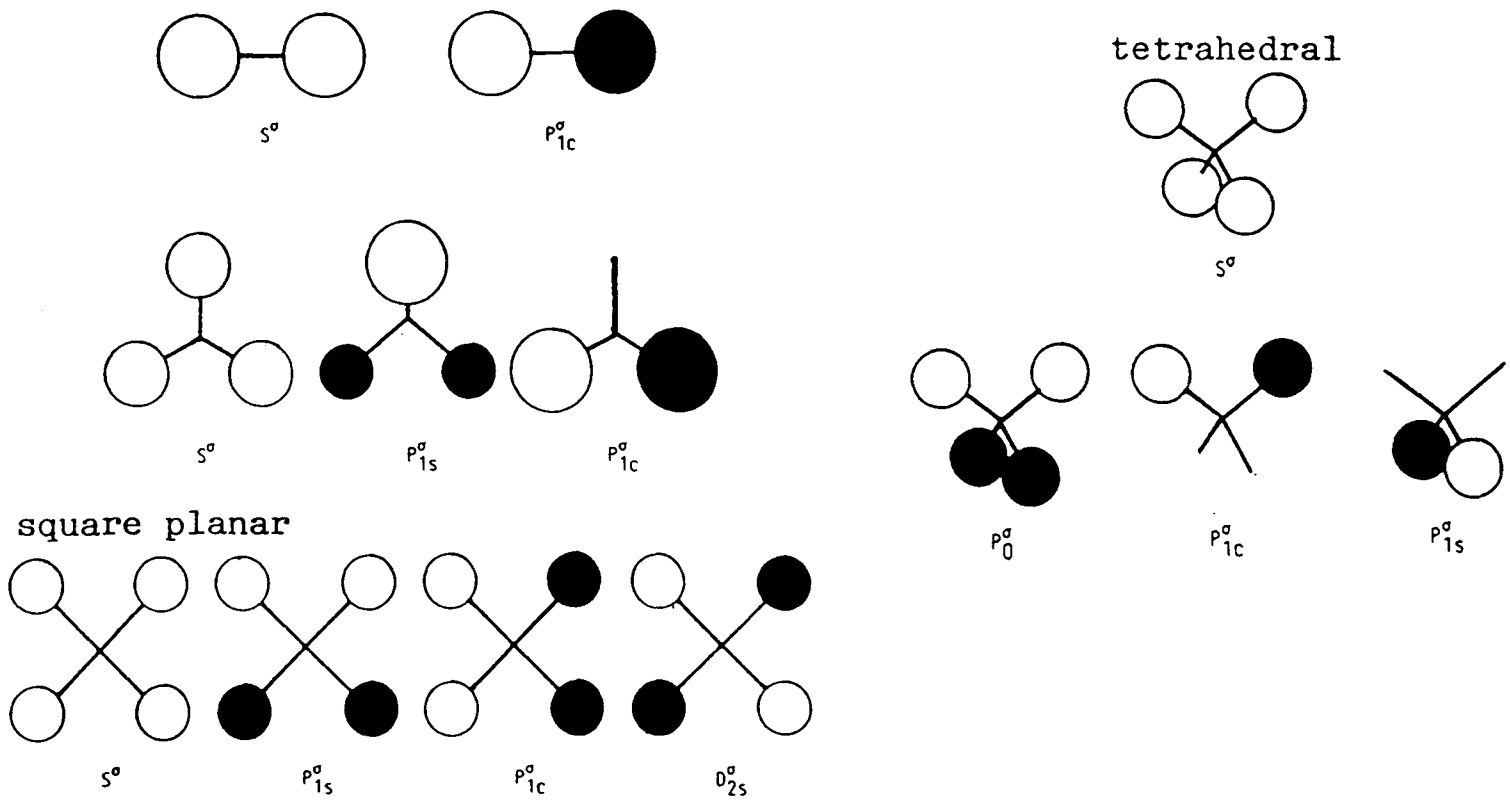


Figure AI.2 L^{σ} MO's for some low nuclearity cluster geometries.

The energies of the L^{σ}_{M} cluster MO's ($E^{\sigma}_{L,M}$) are obtained, via the Variation Principle, as:

$$E^{\sigma}_{L,M} = \frac{\int \Psi^{\sigma}_{L,M}{}^{*} \hat{H} \Psi^{\sigma}_{L,M} \, d\tau}{\int \Psi^{\sigma}_{L,M}{}^{*} \Psi^{\sigma}_{L,M} \, d\tau}$$

where $\hat{H}$ is the effective one electron Hamiltonian of the system. In the original TSH theory, the assumption that the energies of the cluster L^{σ} MO's are reasonably independent of M was made. This leads to a (2L+1)-fold degeneracy for each L manifold. In many cases, however, not all of the (2L+1) components of a given L^{σ} manifold are valid solutions for the cluster. This means that the average energy (E^{σ}_{L}) of the L^{σ} sub-shell cannot be obtained from the simple average ($\sum_{M} E^{\sigma}_{L,M}/(2L+1)$), but instead has to be obtained from the following weighted mean:[1]

$$E^{\sigma}_{L} = \frac{\sum_{M} \int \Psi^{\sigma}_{L,M}{}^{*} \hat{H} \Psi^{\sigma}_{L,M} \, d\tau}{\sum_{M} \int \Psi^{\sigma}_{L,M}{}^{*} \Psi^{\sigma}_{L,M} \, d\tau}$$

This equation may alternatively be written in terms of Spherical Harmonics:

$$E^{\sigma}_{L} = \frac{\sum_{ij} \sum_{M} Y_{L,M}(\theta_i,\phi_i)^{*} Y_{L,M}(\theta_j,\phi_j) H_{ij}}{\sum_{ij} \sum_{M} Y_{L,M}(\theta_i,\phi_i)^{*} Y_{L,M}(\theta_j,\phi_j) S_{ij}}$$

(see **Appendix II** for a discussion of the matrix elements H_{ij} ($= \langle \sigma_i | \hat{H} | \sigma_j \rangle$) and S_{ij} ($= \langle \sigma_i | \sigma_j \rangle$)).

By applying the Spherical Harmonic Addition Theorem,[3] the numerator of the above equation may be written in terms of the angular separation

(ω_{ij}) between each pair of atoms, i and j:

$$= \sum_{ij} [(2L+1)/4\pi] P_L(\cos\omega_{ij}) H_{ij}$$

where $P_L(\cos\omega_{ij})$ is a Legendre Polynomial of the form:

$$P_L(x) = (2^L L!)^{-1} d^L/dx^L \ (x^2-1)^L$$

The next step is to make the simple Hückel approximations: $S_{ij} = \delta_{ij}$; $H_{ij} = \alpha^\sigma (i=j)$, $H_{ij} = \beta^\sigma$ (i,j adjacent) or else $H_{ij} = 0$. The analysis is further simplified by making the approximation that the angular separations of all adjacent atoms are equal (ω). This enables the following equation to be derived:

$$E_L^\sigma = \alpha^\sigma + (2e/n)\beta^\sigma P_L(\cos\omega)$$

where e is the number of edges of the cluster polyhedron (i.e. number of pairs of adjacent atoms) and n is the number of cluster vertices. The energy level scheme for these orbitals is such that the energy increases with the number of angular nodes (i.e. L) of the function, $S^\sigma < P^\sigma < D^\sigma$ etc..[1]

AI.3 Surface π-Type Orbitals

The two p^π (or d^π) atomic orbitals at each cluster vertex (i) behave as a pair of orthogonal unit vectors which are tangential to the surface of the sphere. π_i^θ and π_i^ϕ are defined as π-symmetry orbitals on the ith cluster atom, pointing in the direction of increasing θ and ϕ respectively (see **Figure AI.3**).

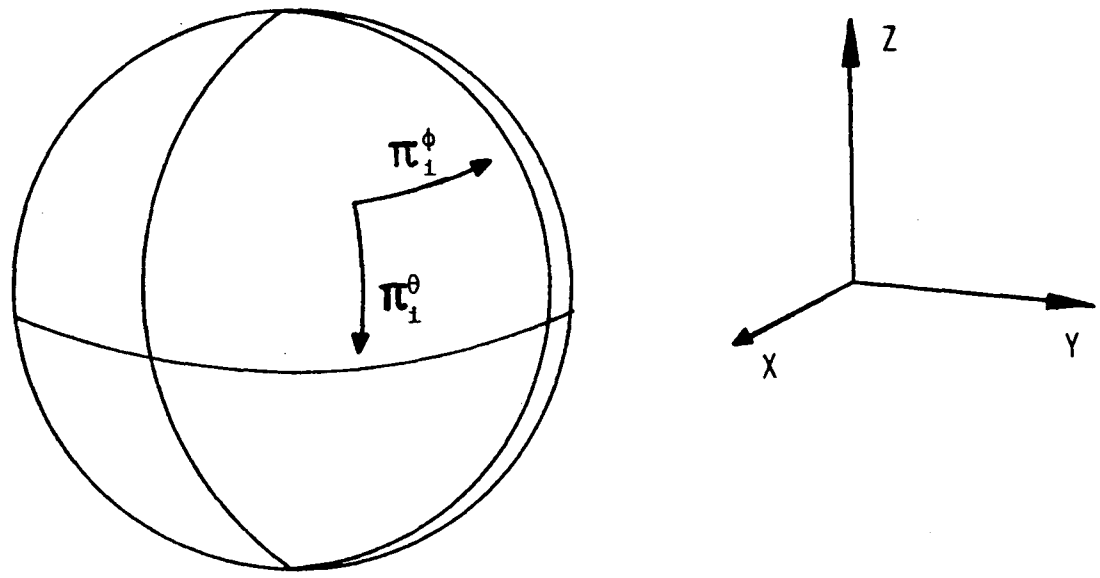


Figure A1.3 Unit vectors on the surface of the cluster sphere

At the poles of the cluster sphere these vectors may be related to Cartesian vectors as follows:

$$\text{North Pole:} \quad (\pi_i^\theta, \pi_i^\phi) = (\pi_i^x, \pi_i^y)$$

$$\text{South Pole:} \quad (\pi_i^\theta, \pi_i^\phi) = (-\pi_i^x, \pi_i^y)$$

Two orthogonal Vector Surface Harmonic functions may be constructed from each Scalar Spherical harmonic (with L>0):

$$\mathbf{V}_{L,M} = \nabla Y_{L,M}$$

$$\bar{\mathbf{V}}_{L,M} = \hat{\mathbf{r}} \times Y_{L,M}$$

where $\nabla = (\partial/\partial\theta) + (\sin\theta)^{-1} (\partial/\partial\phi)$. These functions can be said to possess **even** or **odd parity**, depending on their behaviour under the inversion operator, $\hat{I}$:

$$\hat{I}\, \mathbf{V}_{L,M} = (-1)^L \mathbf{V}_{L,M} \qquad \text{(even parity)}$$

$$\hat{I}\, \bar{\mathbf{V}}_{L,M} = (-1)^{L+1} \bar{\mathbf{V}}_{L,M} \qquad \text{(odd parity)}$$

where the functions $\mathbf{V}_{L,M}$ possess the same (even) parity as the $Y_{L,M}$ functions from which they are derived. Examples of even and odd parity Vector Surface Harmonic functions are depicted in **Figure AI.4.**

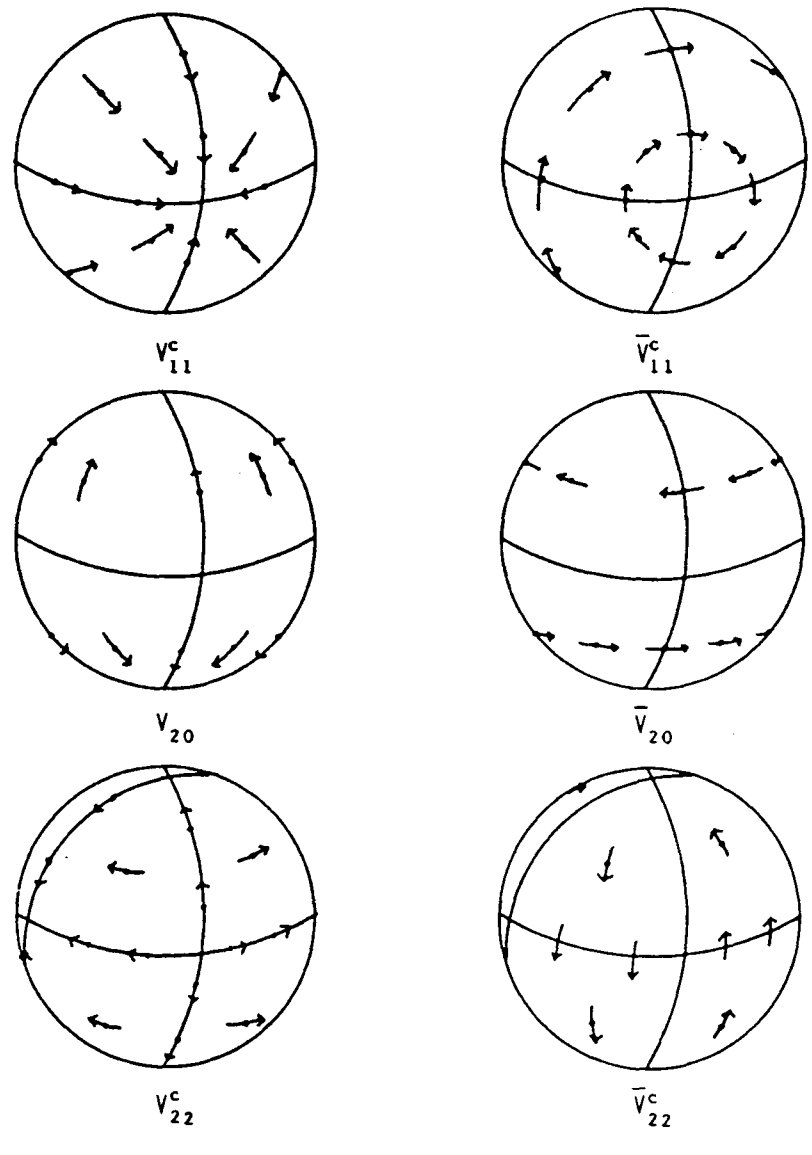


Figure AI.4 Even and odd parity Vector Surface Harmonic functions.

The Vector Surface Harmonic functions may be divided into two orthogonal components which indicate their θ and ϕ dependence:

$$\mathbf{V}_{L,M} = (\mathbf{V}^{\theta}_{L,M}, \mathbf{V}^{\phi}_{L,M})$$
$$\bar{\mathbf{V}}_{L,M} = (\bar{\mathbf{V}}^{\theta}_{L,M}, \bar{\mathbf{V}}^{\phi}_{L,M})$$

where:

$$\mathbf{V}^{\theta}_{L,M} = \bar{\mathbf{V}}^{\phi}_{L,M} = (\partial/\partial\theta)\, Y_{L,M}$$
$$\mathbf{V}^{\phi}_{L,M} = -\bar{\mathbf{V}}^{\theta}_{L,M} = (\sin\theta)^{-1}\, (\partial/\partial\phi)\, Y_{L,M}$$

The even and odd parity functions are related by a 90^{o} anticlockwise rotation of the tangential vectors about the radius vector, at each

point on the sphere. This is known as the Parity Inversion Operation and is described by the operator $\hat{P}$:

$$\hat{P}\ \mathbf{V}_{L,M} = \bar{\mathbf{V}}_{L,M}$$
$$\hat{P}\ \bar{\mathbf{V}}_{L,M} = -\mathbf{V}_{L,M}$$

Cluster π-type wavefunctions are generated by using these Vector Surface Harmonics as the coefficients in an LCAO expansion, with a basis set of π_i^{θ} and π_i^{ϕ} orbitals:

$$\Psi^{\pi}_{L,M} = L^{\pi}_{M} = N \sum_i \mathbf{V}^{\theta}_{L,M}(\theta_i,\phi_i)\pi^{\theta}_i + \mathbf{V}^{\phi}_{L,M}(\theta_i,\phi_i)\pi^{\phi}_i$$

(for M>0 the real forms of the Vector Surface Harmonics ($\mathbf{V}_{L,Ms}/\mathbf{V}_{L,Mc}$) are used).[1] A similar expression may be derived for the $\bar{\Psi}^{\pi}_{L,M}$ ($\bar{L}^{\pi}_{M}$) wavefunctions. As for the L^{σ} functions, the first n non-zero (and non-repeating) L^{π} and $\bar{L}^{\pi}$ functions are used. The L^{π} and $\bar{L}^{\pi}$ MO's of an octahedral cluster are depicted in **Figure AI.5**

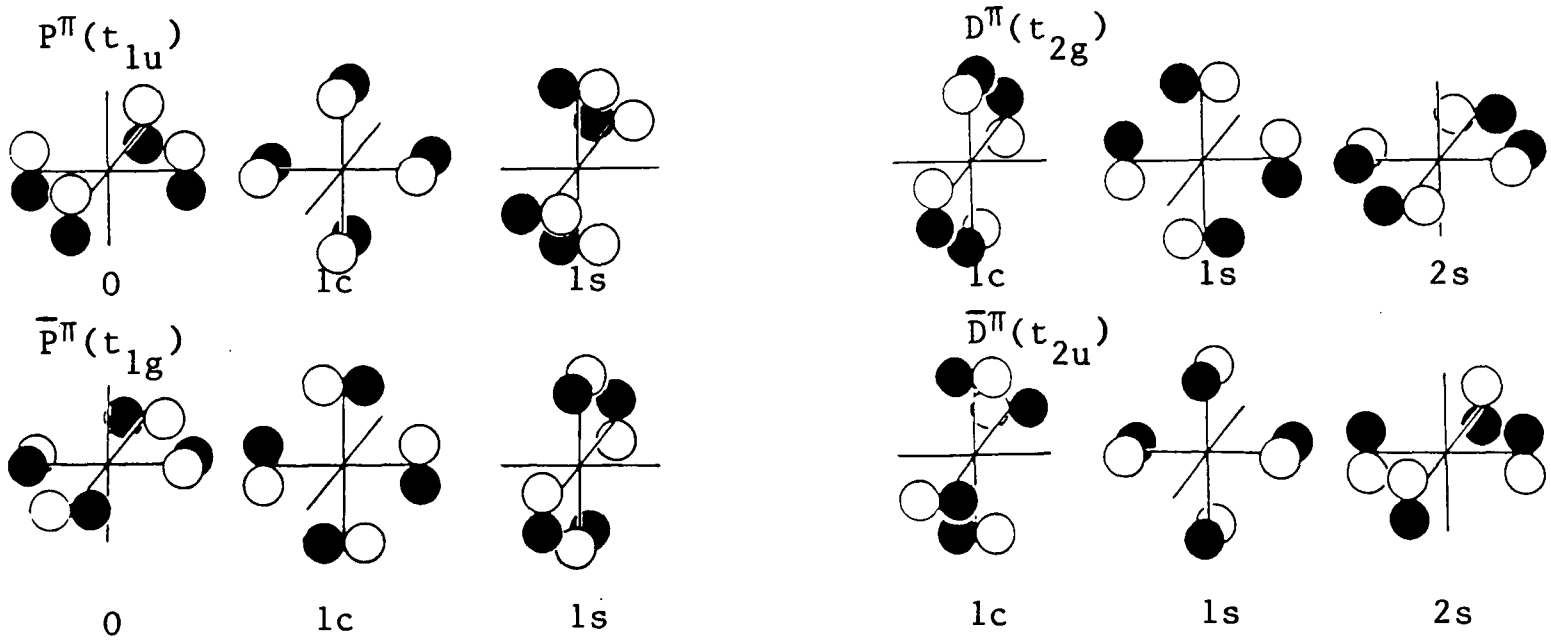


Figure AI.5 L^{π} and $\bar{L}^{\pi}$ MO's of an octahedral cluster.

For these L^{π} and $\bar{L}^{\pi}$ MO's, similar energy expressions may be derived to those obtained for the L^{σ} orbitals:[1]

$$E_L^{\pi} = \alpha^{\pi} + (2e/n) f_L^{\pi}(\omega)$$
$$\bar{E}_L^{\pi} = \alpha^{\pi} + (2e/n) \bar{f}_L^{\pi}(\omega)$$

where $f_L^{\pi}(\omega)$ and $\bar{f}_L^{\pi}(\omega)$ are functions of ω which take account of the fact that there are σ and π components to the overlap between tangential p^{π} orbitals (for cluster MO's composed of atomic d^{π} orbitals, δ overlap must also be included). It is generally found that the L^{π} MO's are bonding and the $\bar{L}^{\pi}$ MO's are antibonding.[1]

AI.4 Surface δ-type orbitals

The surface δ-functions may be treated in an analogous fashion to the π-functions, using the Tensor Surface Harmonics, which are defined as follows:

$$\mathbf{T_{L,M}} = \nabla\nabla Y_{L,M} \qquad \text{(even parity)}$$
$$\bar{\mathbf{T}}_{\mathbf{L,M}} = \hat{r} \times \nabla\nabla Y_{L,M} \qquad \text{(odd parity)}$$

These tensors may be divided into components with $(\theta^2 - \phi^2)$ and $(\theta\phi)$ dependence:

$$\mathbf{T_{L,M}} = \begin{pmatrix} T_{L,M}^{\theta\theta} & T_{L,M}^{\theta\phi} \\ T_{L,M}^{\phi\theta} & T_{L,M}^{\phi\phi} \end{pmatrix} \qquad \begin{aligned} \bar{T}_{L,M}^{\theta\theta} &= -\bar{T}_{L,M}^{\phi\phi} = -T_{L,M}^{\theta\phi} \\ \bar{T}_{L,M}^{\theta\phi} &= \bar{T}_{L,M}^{\phi\theta} = T_{L,M}^{\theta\theta} \end{aligned}$$

The Tensor Surface Harmonics are then used in an LCAO expansion, with a basis set of d^{δ} orbitals at each cluster vertex. These orbitals, $d_{\theta^2-\phi^2}$ and $d_{\theta\phi}$, are defined such that their positive lobes lie along the direction of increasing θ and the line $\theta = \phi$ respectively. At the poles,

they are equivalent to the Cartesian functions $d_{x^2-y^2}$ and d_{xy}.

In this way the cluster wavefunctions $\Psi^{\delta}_{L,M}$ (L^{δ}_{M}) and $\bar{\Psi}^{\delta}_{L,M}$ ($\bar{L}^{\delta}_{M}$) are obtained. These wavefunctions are again related by the Parity Inversion Operation which, in this case, corresponds to a rotation of each d^{δ} component of the MO by 45° anticlockwise about a radial vector passing through the cluster vertex.[1]

The energies of the L^{δ} and $\bar{L}^{\delta}$ orbitals are obtained, in an analogous method to that described above for the L^{σ} and $L^{\pi}/\bar{L}^{\pi}$ MO's, in terms of a function of ω, which takes into account the σ, π and δ components of the overlap between d^{δ} orbitals.

References for Appendix I

1. For mathematical aspects of TSH theory, see: A.J. Stone, Mol. Phys., 1980, **41**, 1339. For applications of the theory, see: A.J. Stone, Inorg. Chem., 1981, **20**, 563; A.J. Stone and M.J. Alderton, Inorg. Chem., 1982, **21**, 2297; A.J. Stone, Polyhedron, 1984, **3**, 2051.

2. See, for example: L. Pauling and E.B. Wilson, "Introduction to Quantum Mechanics", McGraw-Hill, New York, 1935.

3. D.M. Brink and G.R. Satchler, "Angular Momentum", 2nd edn., Oxford University Press, Oxford, 1971.

APPENDIX II

MOLECULAR ORBITAL THEORY AND THE EXTENDED HÜCKEL METHOD

AII.1 Fundamentals of Molecular Orbital Theory

All quantum mechanical descriptions of the electronic structures of atoms and molecules are obtained by solving the **Time Independent Schrödinger Equation** for the system in question:[1]

$$\hat{H}\Psi = E\Psi$$

$\hat{H}$ is the **Hamiltonian Operator** (comprising kinetic and potential energy terms) which acts on the (atomic or molecular) wavefunction (Ψ) to regenerate the wave function multiplied by its energy (E). Equations of this type are known as **eigenvalue equations,** which explains why the wavefunctions and energies are often called **"eigenfunctions"** and **"eigenvalues"** respectively.

For polyelectronic molecules it is not possible to find an exact solution for the Schrödinger equation,[1] since all of the constituent particles are influenced by each other. It is possible, however, to circumvent this **"Many Body Problem"** by making a number of simplifying assumptions.

Nucleus-electron interactions may be simplified by making the assumptions inherent in the **Born-Oppenheimer Approximation.**[2] This approach uses the fact that the atomic nuclei in a molecule are far more massive than the electrons to treat the electrons as moving in an

attractive potential field due to fixed nuclei (i.e. molecular vibrations are ignored).

Electron-electron interactions are simplified by making the **"One Electron Orbital Approximation"** of Hartree and Fock.[3] In this approximation electronic motions are not correlated, but each electron experiences a time-averaged repulsive potential due to the others.

The wavefunction which describes the spatial distribution of an electron throughout a molecule is known as a **Molecular Orbital** (MO). Each MO (Ψ_i) is the eigenfunction of a one-electron Hamiltonian ($\hat{H}_i$):

$$\hat{H}_i \Psi_i = E_i \Psi_i$$

Solutions of this one-electron (Hartree-Fock) Schrödinger equation are generally obtained by first making an initial guess as to the form of the MO's and then applying the **Variation Principle** to refine this initial guess.[1] The important premise of the Variation Principle is that, for any trial wavefunction (Ψ_{trial}) the associated energy (**E**) is always greater than the lowest eigenvalue of the Hamiltonian (i.e. the true ground state energy of the system).

Taking the one-electron Schrödinger equation, premultiplying both sides by Ψ_i^* (the complex conjugate of Ψ_i), rearranging and integrating over all space yields the energy (E_i) as the **expectation value** of the Hamiltonian operator:

$$E_i = \frac{\int \Psi_i^* \hat{H}_i \Psi_i \, d\tau}{\int \Psi_i^* \Psi_i \, d\tau}$$

If the trial wavefunction is expressed in terms of variables (c_1, c_2 ... c_n) then the value of E_i is minimised by altering the values of these

variables until all of the partial differential functions $(\partial E_i/\partial c_n)$ are equal to zero. From the Variation Principle, the set of variables which yield this minimum energy constitute the best approximate wavefunction of the particular functional form originally chosen.

A further simplification, introduced by Roothan,[4] is to write each trial function as a linear combination of known functions ($\phi_1, \phi_2, \ldots \phi_n$), which constitute the **basis set.** If weighting coefficients are introduced, the following expression is obtained:

$$\Psi = c_1\phi_1 + c_2\phi_2 + \ldots\ldots + c_n\phi_n$$

From the Variation Principle, calculating the expectation value of the one electron Hamiltonian for this wavefunction, while constraining the energy to be a minimum, yields the following set of n homogeneous linear equations (**secular equations**):

$$c_1(H_{i1}-ES_{i1}) + c_2(H_{i2}-ES_{i2}) + \ldots\ldots + c_n(H_{in}-ES_{in}) = 0$$

where $i = 1$ to n; $H_{ij} = \langle\phi_i|\hat{H}|\phi_j\rangle = \int\phi_i\hat{H}\phi_j d\tau$; $S_{ij} = \langle\phi_i|\phi_j\rangle = \int\phi_i\phi_j d\tau$. The latter integral reflects the extent of overlap between two orbitals, and is therefore known as the **overlap integral.**

It can be shown that non-trivial solutions to these equations are obtained when the following **secular determinant** is equal to zero:[5]

$$\begin{vmatrix} H_{11}-ES_{11} & H_{12}-ES_{12} & \ldots\ldots & H_{1n}-ES_{1n} \\ H_{21}-ES_{21} & H_{22}-ES_{22} & \ldots\ldots & H_{2n}-ES_{2n} \\ \vdots & \vdots & & \vdots \\ H_{n1}-ES_{n1} & H_{n2}-ES_{n2} & \ldots\ldots & H_{nn}-ES_{nn} \end{vmatrix} = 0$$

Expanding the secular determinant yields a polynomial which is nth-order in E and has, therefore, n solutions. Substituting these E values

back into the secular equations enables the determination of the coefficients, c_n.

In most molecular orbital treatments, molecular wavefunctions are constructed from a basis set of atomic orbitals. This is known as the **Linear Combination of Atomic Orbitals** (LCAO) approach.[6] For polyelectronic atoms, these atomic orbitals are again only approximate functions. The two alternative functional forms of atomic orbitals which are commonly used are the **Slater Type Orbitals** (STO's) and the **Gaussian Orbitals** (GO's). The angular parts of the STO's are identical to those of the hydrogenic orbitals (i.e. the Spherical Harmonics $Y_{lm}(\theta,\phi)$). The radial part of an STO, unlike the hydrogenic orbitals, possesses no nodes:[7]

$$\psi(r) = r^{n-1}\, e^{-\zeta r}$$

where n is the principal quantum number of the orbital and the Slater exponent, ζ , is a function of the nuclear charge (Z), the screening constant (s) and n:

$$\zeta = (Z - s)/n$$

The $e^{-\zeta r}$ dependence of the radial wave function means that, the more electronegative elements, i.e. those with high effective nuclear charges (Z-s) and low principal quantum numbers, possess the more contracted orbitals.

The radial form of the atomic orbitals is often made more realistic by taking linear combinations of STO's. Gaussian orbitals are similar, but have a radial dependence of the form $e^{-\zeta r^2}$.

The various types of molecular orbital calculation,[9] though based on

the same principles, have differing degrees of sophistication and accuracy. Differences in approach can arise at two stages. Firstly a large basis set of atomic functions (e.g. multiple STO functions for each atomic orbital) leads, as mentioned above, to a more realistic representation of the radial part of the atomic orbitals and, hence, a more accurate calculation of the interaction between atomic orbitals. A second source of differences is the form of the Hamiltonian operator. In the more precise **ab initio** methods the integrals H_{ij} are evaluated explicitly, depending on the precise mathematical form of the Hamiltonian. In the more approximate **semi-empirical** methods the form of the Hamiltonian is ignored and the integrals H_{ij} are assigned empirical numerical values, on the basis of spectroscopic data. The advantage of semi-empirical methods is that they require shorter computation times, due to the assumptions made for H_{ij} and the choice of small atomic orbital basis sets, though they obviously lose out on accuracy.

AII.2 The Extended Hückel Method

The molecular orbital calculations described in this Thesis are of the Extended Hückel type. This is an example of a semi-empirical molecular orbital method and is based on simple Hückel theory, which provides an estimate of the energies and approximate forms of the π-MO's of planar unsaturated molecules.[10]

In Hückel theory the secular determinant is considerably simplified by making the following approximations:

$H_{ii} = \alpha$ (**Coulomb Integral**)

$H_{ij} = \beta$ (**Resonance Integral**), when atoms i and j are bonded.

$H_{ij} = 0$, when i and j are not bonded.

S_{ij} (**Overlap Integral**) = 1, when i=j, otherwise S_{ij} = 0.

The energies of the MO's are obtained, from the secular determinant, in the form: $E = \alpha \pm \lambda\beta$, where λ is a function of the geometry and connectivity of the framework atoms. The analysis is further simplified by the choice of a very limited basis set, i.e. only the p atomic orbitals which are perpendicular to the plane of the molecule.

In Extended Hückel theory the basis set includes all of the valence orbitals of the constituent atoms in the molecule.[11] These orbitals are generally STO's of the form:

$$\psi_{n\,l\,m} = r^{n-1}\, e^{-\zeta r}\, Y_{lm}(\theta,\phi)$$

The radial properties of s and p orbitals are quite adequately reproduced by single STO's. For the more contracted valence d orbitals, however, linear combinations of two STO's (**"double-zeta functions"**) are required. These have the following radial form:[12]

$$\psi(r) = r^{n-1}(c_1 e^{-\zeta_1 r} + c_2 e^{-\zeta_2 r})$$

where the coefficients (c_1 and c_2) and orbital exponents (ζ_1 and ζ_2) are defined empirically.

In the Extended Hückel method the overlap integrals, S_{ij}, are evaluated explicitly, since the zero-overlap approach of simple Hückel theory does not yield sufficiently accurate values for the energies of the molecular orbitals.

The elements of the Hamiltonian matrix, H_{ij}, are estimated in the following way. The diagonal terms, H_{ii} (Coulomb integrals), are set equal to the energy (defined as negative), in eV, of an electron in the ith atomic orbital of the isolated atom in a given valence state. These

energies are obtained from experimental data and the values used are known as the **Valence Shell Ionisation Energies** (VSIE's). A VSIE is obtained as the weighted mean of the states arising from a particular valence state configuration.[13]

The off-diagonal terms of the Hamiltonian matrix, H_{ij} (Resonance integrals), are taken to be orbital interaction energies. It is assumed that the interaction between two atomic orbitals is roughly proportional to their overlap and is greater for high energy orbitals than low energy ones. The most commonly used method of evaluating the H_{ij} terms is the arithmetic mean formula of Wolfsberg and Helmholtz:[14]

$$H_{ij} = kS_{ij}(H_{ii} + H_{jj})/2$$

though geometric and reciprocal mean formulae have also been utilised:[15]

$$H_{ij} = -kS_{ij}(H_{ii}.H_{jj})^{0.5}$$

$$H_{ij} = 2kS_{ij}\left\{\frac{H_{ii}.H_{jj}}{H_{ii} + H_{jj}}\right\}$$

Hoffmann has suggested a value of 1.75 for the Wolfsberg-Helmholtz constant k, on the grounds that this value gives the correct value for the rotational barrier in ethane.[11] Most Extended Hückel calculations use a value of 1.75 for k, as generally these calculations are fairly insensitive to the value of k in the region $1.5 < k < 2.0$. Woolley has suggested, however, that k values in the range 2.0 to 4.0 may be more appropriate for d orbitals, as a value of 1.75 leads to an understimation of d-d resonance integrals and d band width for metal clusters.[16]

In this methodolgy the total energy is simply taken as the sum of

the one-electron energies. The absolute value of the energy, therefore, is generally innaccurate, as electron-electron and nuclear-nuclear repulsion terms are neglected. The relative energies of molecules in related conformations or geometries are, however, quite accurately reproduced by this method.

The electron density is partitioned according to the **Mulliken Population** analysis.[17] For a normalised MO, Ψ_j, written as an LCAO:

$$\Psi_j = c_{kj}\phi_k + c_{lj}\phi_l + c_{mj}\phi_m + \cdots\cdots$$

the electron density is proportional to the square of the wave function:

$$\Psi_j^2 = c_{kj}^2\phi_k^2 + c_{lj}^2\phi_l^2 + 2c_{kj}c_{lj}\phi_k\phi_l + \cdots\cdots$$

Since all of the orbitals are normalised, integration over all space yields:

$$1 = c_{kj}^2 + c_{lj}^2 + 2c_{kj}c_{lj}S_{kl} + \ldots$$

Thus, one electron in Ψ_j contributes c_{kj}^2 to the **net atomic orbital electron population** of ϕ_k and $2c_{kj}c_{lj}S_{kl}$ to the **overlap population** between atomic orbitals ϕ_k and ϕ_l.

The **total net atomic orbital population** of ϕ_k, q_k, is obtained by summing over all MO's:

$$q_k = \sum_j n_j c_{kj}^2$$

where n_j is the electron occupation (0, 1 or 2) of MO Ψ_j.

Similarly, the **Mulliken overlap population** for the pair of orbitals ϕ_k and ϕ_l, p_{kl} is obtained by making the summation:

$$p_{kl} = 2 \sum_j n_j c_{kj} c_{lj} S_{kl}$$

The **reduced Mulliken overlap population** between atoms K and L, P_{KL}, is obtained by summing p_{kl} over all of the atomic orbitals on K and L:

$$P_{KL} = \sum_k \sum_l p_{kl}$$

P_{KL} constitutes a two-centre bond order.

The **gross atomic population** (i.e. total electron density) on atom K is obtained by dividing P_{KL} equally between K and L and adding this to the net atomic population of K (= $\sum_k q_k$).

As is the case for orbital and total energies, Mulliken populations are sensitive to the choice of atomic orbital parameters and k. The relative values of the Mulliken populations are, however, reasonably parameter-independent, so that they may be used in a comparitive, if not an absolute, sense. Another limitation of the Mullikan population analysis is encounterd for diffuse orbitals, where there is significant orbital overlap in regions other than the internuclear region.[18]

It is sometimes found that large unrealistic charges are calculated in molecules consisting of atoms with very different electronegativities. This problem which arises because the VSIE values, used in the estimation of H_{ii}, refer to neutral atoms, may be circumvented by the method of **charge iteration.**

The charge iteration method involves a series of Extended Hückel calculations, with the VSIE's for the nth cycle of calculations defined as a function of the atomic charges (q) calculated in the (n-1)th cycle:

$$\text{VSIE}\ (q) = Aq^2 + Bq + C$$

where the parameters A, B and C are obtained from multiconfigurational spectral data on the atoms and their charged ions.[13] The cycles are continued until self-consistent charges result (i.e. differences of less than 10^{-4} e for all atoms between one cycle and the next). Such iterative calculations are known as **Self Consistent Charge and Configuration** (SCCC) calculations.

In certain cases, Extended Hückel calculations have been found to suffer from a defect known as **"counter-intuitive orbital mixing"** (COM).[19] COM (which has also been observed in ab initio calculations) occurs when there are large overlap integrals between orbitals, on different centres, which are widely separated in energy. The orbital mixing which takes place does so in an antibonding fashion, contrary to that expected from perturbation theory, and some MO's possess small antibonding contributions from these orbitals. Although the effect on orbital energies is insignificant, COM results in anomalous Mulliken populations. COM is particularly significant in transition metal complexes with π-acid ligands, such as Cp and CO.

The effects of COM may be minimised by using a modified Wolfsberg-Helmholtz relationship, the **"weighted H_{ij} formula"**. The basis of this approach is the replacement of k (in the equation for H_{ij}) by a new constant k':[19]

$$k' = k + \Delta^2 + \Delta^4(1-k)$$

where $\Delta = (H_{ii}-H_{jj})/(H_{ii}+H_{jj})$. In this way H_{ij} is effectively weighted in favour of the less diffuse orbitals (i.e. those with the most negative H_{ii} value).

AII.3 Description of the Programs used for Performing Extended Hückel Calculations

The Extended Hückel calculations reported in this Thesis were performed using the ICON8 package of FORTRAN computer programs developed by Hoffmann and coworkers.[20]

The input to ICON8, the main calculational program, consists of the cartesian coordinates and orbital parameters (H_{ii}'s, Slater orbital exponents (ζ), and contracted d orbital coefficients (c_1 and c_2) and exponents (ζ_1 and ζ_2)) of the constituent atoms. Optional features include the possibility of performing calculations using weighted H_{ij}'s, charge iteration and non-default (1.75) values of k. If charge iteration calculations are to be performed, values of A, B and C must be specified. The program COORDINATE can be used to convert from polar coordinates (i.e. bond lengths and angles) into cartesian coordinates, suitable for input into ICON8.

The output from ICON8 is completely user controlled, depending on the information required. The input coordinates and parameters may be printed out, as a check. Most of the information is presented in matrix form, and includes the following items: interatomic distances; atomic overlap integrals; wavefunctions; orbital energies and occupations; total energy; overlap populations; reduced overlap populations; charge matrix; reduced charge matrix; total atomic charges and orbital populations.

The **charge matrix** elements (Q_{ij}) correspond to the proportion of the electronic charge for a given MO (normalised to two electrons regardless of the actual orbital occupancy) which may be apportioned to each of its constituent atomic orbitals:

$$Q_{ij} = 2c_{ij} \sum_k c_{kj} S_{ik}$$

where c_{ij} is the coefficient of the ith atomic orbital in the jth MO and S_{ik} is the overlap integral between atomic orbitals ϕ_i and ϕ_k. The reduced charge matrix elements are obtained by summing the values of Q_{ij} over all the orbitals (ϕ_i) of each atom. This gives the proportion of the charge, for each MO, which may be apportioned to a particular atom.

In certain cases it is informative to conceptually divide a molecule into fragments and study the interaction between the orbitals of these fragments. The program FMO transforms the results of an ICON8 calculation from an atomic orbital basis set to a basis set consisting of such fragments. The input for FMO consists of ICON8 calculations on the fragments, as well as the complete molecule.

It is occasionally desirable to study the effect of systematically varying one or more structural parameters (bond length, bond angle or dihedral angle). The program GENERATE produces sets of polar coordinate input decks for COORDINATE, which then creates ICON8 input decks (with the atomic coordinates in cartesian form) for each cluster molecular geometry. ICON8 calculations are then performed for each of these geometries in turn.

References for Appendix II

1. See, for example: L. Pauling and E.B. Wilson, "Introduction to Quantum Mechanics", McGraw-Hill, New York, 1935; A.S. Davydov, "Quantum Mechanics", Pergamon, Oxford, 1965.
2. M. Born and J.R. Oppenheimer, Ann. Phys. (Leipzig), 1927, **84**, 457.
3. D.R. Hartree, Proc. Cambridge Phil. Soc., 1928, **24**, 328; V.A. Fock, Ann. Phys. (Leipzig), 1930, **61**, 126; P.O. Lowdin, Phys. Rev., 1955, **97**, 1474.
4. C.C.J. Roothan, Rev. Mod. Phys., 1960, **32**, 179.
5. See, for example: J.P. Lowe, "Quantum Chemistry", Academic Press, New York, 1978, p.157.
6. R.S. Mulliken, J. Chem. Phys., 1935, **3**, 375.
7. J.C. Slater, Phys. Rev., 1930, **36**, 57.
8. S.F. Boys, Proc. Roy. Soc. Lond., Ser. A, 1972, **10**, 57.
9. See Ref. 5 for a discussion of the various types of MO calculation.
10. E. Hückel, Z. Physik, 1931, **70**, 204; 1931, **72**, 310; 1932, **76**, 628; E. Heilbronner and H. Bock, "Das HMO Modell und seine Andwendung", Verlag, Weinheim, 1968.
11. R. Hoffmann, J. Chem. Phys., 1963, **39**, 1397.
12. J.W. Richardson, W.C. Nieupoort, R.R. Powell and W.F. Edgell, J. Chem. Phys., 1962, **36**, 1057.
13. C.J. Ballhausen and H.B. Gray, "Molecular Orbital Theory", Benjamin, New York, 1965.
14. M. Wolfsberg and L. Helmholtz, J. Chem. Phys., 1952, **20**, 837.
15. W.A. Yerranos, J. Chem. Phys., 1966, **44**, 2207.
16. R.G. Woolley, Nouv. J. Chim., 1981, **5**, 219, 227.
17. R.S. Mulliken, J. Chem. Phys., 1955, **23**, 1833, 1841, 2338, 2343.

18. A. Streitweiser, J.E. Williams, S. Alexandratos and J.M. McKelvey, J. Amer. Chem. Soc., 1976, **98**, 4778; A. Streitweiser, C.M. Berke, G.W. Schriver, D. Grier and J.B. Collins, Tetrahedron Suppl. No. 9, 1981, **37**, 345.

19. H.B. Bürgi, J.H. Ammeter, J.C. Thibeault and R. Hoffmann, J. Amer. Chem. Soc., 1978, **100**, 3686.

20. J. Howell, A. Rossi, D. Wallace, K. Haraki and R. Hoffmann, Quantum Chemistry Program Exchange, 1977, **10**, 344.